Pore structure in blended cement pastes

Mariana Moreira C. Canut

PhD Thesis

Department of Civil Engineering
2012

DTU Civil Engineering
Department of Civil Engineering

Pore structure in blended cement pastes

Mariana Moreira C. Canut

Preface

This thesis is submitted as a partial fulfilment of the requirements of the Danish PhD. degree. The thesis presents the outcome of Project 3 "*Pore structure in blended cement pastes*" one of 15 PhD projects financed through the European Marie Curie Actions Research Training Networks (MC RTNs). The 15 research projects together with a series of six one-week long formal courses formed the MC RTN "Fundamental understanding of cementitious materials for improved chemical physical and aesthetic performance - NanoCem", obtaining information on the cement based materials, which can be exploited using appropriate models. The projects used a common reference base of materials. This provided an unprecedented opportunity to integrate data from a critical mass of multidisciplinary characterisation techniques.

The principal supervisor of the project was the Associated Professor Mette Rica Geiker from DTU Department of Civil Engineering. The academics and industrial co-supervisors and partners were Professor Peter MacDonald from University of Surrey and Doctor Reiner Haerdtl from Heidelberg Cement Group. Visits at University of Surrey were carried out in February and May of 2007 for studies of water in cement based materials by ^{1}H NMR. Visits at Heidelberg Technology Centre were carried out in February 2008 and November 2010 for the characterization of pore structure of cement pastes using mercury intrusion porosimetry (MIP).

Kongens Lyngby, 6th of July 2011

_____
Mariana Moreira C. Canut

Acknowledgements

Abstract

Supplementary cementitious materials (SCMs), such as slag and fly ash, are increasingly used as a substitute for Portland cement in the interests of improvement of engineering properties and sustainability of concrete. According to studies improvement of engineering properties can be explained by a refinement of the pore structure in the paste. Among others, chemical and physical properties of SCMs and curing conditions (moisture and temperature) affect the microstructure of hydrated pastes.

This thesis comprises investigations of pore structure of pastes with and without slag and fly ash, providing a valuable knowledge of SCMs, which is relevant for performance based design of concrete structures. In addition, the thesis provides guidelines for porosity investigations with focus on the applicability of the methods and sources of error.

Pore structure was here determined by several methods, mercury intrusion porosimetry (MIP), low temperature calorimetry (LTC), scanning electron microscopy (SEM) and water desorption. These methods provide information on various pore characteristics (total porosity, pore threshold, pore size distribution etc.) in different size ranges and do therefore to a large extent supplement each other.

Cement pastes (w/b=0.4) with and without slag and fly ash cured at two moisture (sealed and saturated) and temperature (20 and 55ºC) conditions were used to investigate the combined impact of SCMs addition and curing on the pore structure of pastes cured up to two years. Also, the porosity measurements were compared with porosity modelling.

The results of this thesis showed that slag caused a refinement of pores illustrated by a decreased threshold pore size for a given volume for pastes cured saturated at 20ºC for 28 days or more. For the investigated fly ash pastes such impact was not observed. Both, temperature and moisture affected porosity parameters (volume of pores, pore threshold and pore size distribution) of all pastes especially after 28 days of curing. A beneficial effect of high slag addition for pastes cured at high temperature was observed where a reduction of the pore volume and threshold pore size were found when comparing with plain cement paste at the same curing conditions.

The porosity methods MIP, LTC and SEM have been shown to be suitable to characterise pore parameters of the pastes. MIP is a simple and fast method which covers a large range of pore sizes. As complementary information, LTC can be used as it is not required to dry the sample. SEM is relevant as it is a direct method, however different magnifications are required to analyse a large range of pores and a proper sample preparation (impregnation and polishing). Modelling of the capillary porosity based on assumptions of degree of reaction and product densities gave for plain cement pastes results comparable to MIP data.

Key-words: Cement paste, supplementary cementitious materials (SCMs), temperature, moisture, experimental methods, pore structure.

Resumé (in Danish)

Alternative mineralske bindere (SCMs), fx slagge og flyveaske, bliver i stigende grad brugt til delvis erstatning af portlandcement. Dette både for at forbedre betonens ingeniørmæssige egenskaber og for at mindske den miljømæssige belastning. Forbedring af den hærdnede betonens egenskaber forklares ved en mere gunstig porestruktur af cementpastaen. Mikrostrukturen af cementpastaen er bl.a. bestemt af de fysiske og kemiske egenskaber af binderne og hærdeforholdene (fugt og temperatur).

Denne afhandlingen omfatter undersøgelser af porerstrukturen af cementpasta med og uden slagge og flyveakse og giver et vigtige bidrag til kendskabet af effekten af SCMs. Dette har relevans for funktionsbaseret design af betonkonstruktioner. Endvidere giver afhandlingen anbefalinger for porøsitetundersøgelser, specielt fokuseres på metodernes anvendelighed og fejlricisi.

Porestrukturen blev undersøgt vha. flere metoder: Kviksølvporøsimetri (MIP), lavtemperaturkalorimetri (LTC), scanningelectronmikroscopi (SEM) og vanddesorption. Metoderne giver information om forskellige porekarakteristika såsom total porøsitet, karakteristisk porestørrelse og porestørrelsesfordeling. Metoderne supplerer i vid udstrækning hinanden.

Cementpasta med og uden slagge eller flyveaske (w/b=0.4) blev hærdet ved to forskellige fugtforhold (forseglet og vandmættet) og to forskellige temperaturer (20 ℃ og 55 ℃) i op til to år for at undersøge den kombinerede effekt af tilsættelse af SCMs og hærdeforhold på porestrukturen af cementpasta. Derudover blev porøsitetsmålingerne sammenlignet med modellering af totalt porevolumen.

Både temperatur og fugt influerede porøsiteten af pastaerne, specielt efter 28 dages hærdning. Tilsætningen af (den anvendte) slagge resulterede i en forfining af porestrukture illustreret ved en formindsket karakteristisk porestørrelse for et givent porevolumen for pasta hærdet ved 20 ℃ i 28 dage eller mere. Dette kunne ikke konstateres ved anvendelse af flyveaske. En positiv effekt af slaggetilsætning a blev også observeret for paster hærdnet ved høje temepratur, hvor både porevolumenet og den kritisk porestørrelse var mindre i prøver med højt slaggeindhold end i cement pasta uden slagge.

Metoderne MIP, LTC og SEM blev fundet anvendelige til at karakterisere cementpastas porøsitet. MIP er en enkel og hurtig metode, som karakteriserer et stort spektrum af porestørrelser, men der er arbejdsmiljmæssige hensyn at tage. Til yderligere karakterisering anbefales LTC, da denne metode ikke kræver tørrede prøver. SEM er også relevant, da det er en direkte metode. Forskellige forstørrelser er påkrævet for at analysere den store variation af porestørrelser. Anlyse af den fine porestruktur forsætter en høj kvalitet af polerprøverne (imprægnering og polering). Modellering af capillarporøsiteten baseret på antagelse af reaktionsgrad og densitet of produkter gav for almindelige cementpastaer resultater, der var sammenlignelige med resultaterne fra MIP.

Kodeordet: Cementpasta, alternative mineralske bindere (SCMs), temperatur, fugt, eksperimentelle metoder, porestruktur

Table of contents

Appendixes

List of symbols and abbreviations

AFm or $C_3A.CaSO_4.12H_2O$		Monosulfate
Aft or		Ettringite
$Ca_3Al(OH)_6.12H_2O)_2.2H_2O$		
Al_2O_3		Alumina
C_2S		Dicalcium silicate (Beleite)
C_3A		Tricalcium aluminate (Aluminate)
C_3S		Tricalcium silicate (Alite)
CaO, C		Calcium oxide
CH		Calcium hydroxide (Portlandite)
CO_2		Carbon dioxide
C-S-H		Calcium silicate hydrate
C-S-H		Calcium silicate hydrate
K_2O, K		Potassium oxide
KNO_3		Potassium nitrate
MgO, M		Magnesium oxide
NaBr		Sodium bromide
NaO_2, N		Sodium oxide
SO_3, $		Sulfite
SO_4		Sulfate

BSE		Backscattered electrons
CPMG		Carr, Purcell, Meiboom and Gill
DTU		Technical University of Denmark
EPFL		Ecole Polytechnique Fédérale de Lausanne
IUPAC		International Union of Pure and Applied Chemistry
LTC		Low temperature calorimetry
MIP		Mercury intrusion porosimetry
NMR		Nuclear magnetic resonance
SE		Secondary electrons
SEM		Scanning electron microscopy
TI		Danish Technology Institute
XRD		X-ray diffraction
XRF		X-ray fluorescence

b	[g]	Binder
c	[g]	Cement
fa	[g]	Fly ash
PC	[g]	Portland cement
s	[g]	Slag
SCMs	[g]	Supplementary cementitious materials

A_1		Temperature corrections for Calorimeter 1
A_b	[µm²]	Area of black pixels, %
A_p	[m²]	Cross section area of pore
A_s	[m²]	Sample surface area exposed
A_t	[µm²]	Total area of grey scale histogram,%
A_{tp}	[%]	Area of pores,%
d_p	[Pa]	Pressure change
E_i	[V]	Heat flow, differential output of thermopiles
G	[J/mol]	Gibbs free energy
H	[J/mol]	Enthalpy
h		Depth of focus
H_{fus}	[J/kg]	Heat of fusion
m_{Hg}	[g]	Mass of filled mercury
M_l	[g/mol]	Molar mass of the liquid
p	[N/m²]	Pressure
p_0	[N/m²]	Saturated vapor pressure
P_l	[Pa]	Liquid pressure
P_p	[m]	Perimeter of the pore
P_v	[Pa]	Air pressure
p_w	[N/m²]	Pressure applied on mercury to intrude the pore
q	[J]	Heat
R	[J/K.mol]	Universal gas constant
R_b		Body radius
$r_{bulk(MIP)}$	[g/cm³]	MIP bulk density
R_E		Entry radius
r_h	[m]	Hydraulic radius
RH, p/p_o		Relative humidity
r_k	[m]	Kelvin pore radius
r_t	[m]	Total pore radius
r_w	[m]	Pore radius (Washburn Equation),
S	[J/mol.K]	Entropy
S	[m·s$^{-1/2}$]	Sorptivity (the slope of the curve W/A versus. t$^{1/2}$)
S/N		Signal to noise
S_0	[m·s$^{-1/2}$]	Correction for surface effects
S_m	[V/W 10^{-3}]	Calorimeter sensitivity
S_p	[m²]	Surface area of the pores
t	[s]	Time
T_{fp}	[K]	Freezing temperature of the pore liquid
T_1		spin-lattice relaxation time
T_2		Spin-spin relaxation time
T^{bulk}	[s]	Bulk water relaxation time
T_f	[K]	Freezing temperature of the bulk liquid

T_k	[K]	Temperature
T_K	[K]	Temperature, in Kelvin
t_{nf}	[m]	Thickness of adsorbed layer("t-layer") for low temperature calorimetry
$T^{observed}$	[s]	Observed relaxation time
T_s	[ºC]	Temperature in stage
$T^{surface}$	[s]	Surface water relaxation time
tw_{nf}	[m]	Thickness of adsorbed layer for water sorption method
u	[%]	Water content in weight fraction
V	[m³]	Volume filled with liquid,
V_{Hg}	[cm³]	Volume of mercury intruded
V_{ice}	[cm³]	Volume of ice formed
v_m	[m³/mol]	Molar volume
V_{mol}	[m³/mol]	Molar volume adsorbed
V_p	[cm³]	Volume fraction of the pores
V_{pw}	[Fraction]	Volume of pores calculated by water sorption
w	[kg]	Sample weight
$w_{105ºC}$	[kg]	Weight of an oven dried at 105ºC sample
W_a	[m³]	Volume of the absorbed water
$W_{des.}$	[Fraction]	Water content at RH of 100%
$w_{eq.}$		Weight of an oven dried at 105ºC sample
w_{ice-s}	[kg/kg$_d$ $_{105ºC}$]	Mass of ice formed in the stage
w_{ne}	[g/ g$_{cement}$]	Non evaporable water per ignited mass
w_{ps}	[g]	Weight of penetrometer with the sample and mercury (until 0.033 MPa the volume)
w_{pt}	[g]	Weight of penetrometer (sample cell) filled with mercury
w_s	[g]	Weight of dry sample
α	[Fraction]	Degree of hydration
$γ_{s-l}$	[N/m]	Surface tension solid-liquid
$Γ_{v-l}$	[N/m]	Surface tension, vapor –liquid interface
$ΔH_m$	[J/g]	Molar heat ($ΔH = ΔH_{fus} . M_l$)
ε	[m]	Surface layer thickness,
θ	[degrees]	Contact angle between the liquid and the pore wall
$θ_{w-m}$	[rad]	Angle between the pore wall and the meniscus
$ρ_b$	[g/cm³]	Bulk density
$ρ_{Hg}$	[g/cm³]	Density of mercury
$ρ_{ice}$	[g/m^5]	Ice density
$ρ_l$	[g/cm³]	Water density
$σ_{s-l}$	[N/m]	Surface tension, solid-liquid interface

1.   Introduction

The present PhD thesis fits well into the necessities of the actual scenario and perspectives for the future where the overall goal is to achieve sustainable construction producing facilities and infrastructure that meet requirements in a cost-effective manner while minimizing resource depletion of energy and raw materials and optimizing performance throughout their life cycle. The cement industry is one of the responsible for a significant consumption of natural resources and represents a barrier to reduce industrial environmental issues. By substituting supplementary cementing materials (SCMs) for clinker the cement industry has reduced the use of raw materials and thus has lowered CO_2 emission (see e.g. in (Battelle, 2002)). To evaluate the replacement of cement by SCMs, pore structure is often used as it is one of the main parameter that controls strength, transport properties, and durability of hydrated cementitious materials.

Examples of SCMs are slag from iron blast furnaces and fly ash from coal fired power plants. SCMs can have some advantages over pure Portland cement in the end use such as the refinement of the pore structure (Hooton, 1986, Malhotra, 1993). Also, the distribution of cementitious products may be enhanced by SCMs addition due to an improved initial packing and an increased number of nucleation sites. Studies carried out in the past years (Malhotra, 1993, Mehta and Gjorv, 1982, Mehta and Monteiro, 2006, Roy and Idorn, 1982) indicated improvements of strength and durability obtained by the use of SCMs governed by the pore refinement. However, the benefits of the use SCMs may be compromised by their chemical and physical properties, percentage of addition and low early age strength (Al-Amoudi et al., 2004, Chen and Brouwers, 2007, Neuwald, 2005). Investigations carried out by Feldman (1981) showed the effect of SCMs with time using MIP, it was clear that a high percentage of substitution tends to increase the volume of pores of fly ash pastes.

Performed investigations reported in (Bentz, 2007, Lura et al., 2001 , Türkmen et al., 2003, Zhang, 2007) strongly indicate that curing conditions (temperature and moisture) may also play a significant role in the pore structure development of cementitious materials. Hydration reactions proceed more rapidly at higher temperature resulting in a less homogeneous paste. Also, the C-S-H density increase with temperature (Zhang, 2007). Raise in curing temperature may also alter the equilibrium assemblage of the solid cement phases (e.g. Aft and AFm phases) and result in decreased solid volume and increased porosity (Lothenbach et al., 2008). Investigations proposed two effects of high temperature on cement pastes, first an increased porosity is observed and at an ultimate degree of hydration it is reduced (Escalante-Garcia and Sharp 2001). Escalante-Garcia and Sharp (2001) reported a beneficial effect of slag addition in the compressive strength of cement pastes cured at 60ºC, however it was not observed for fly ash pastes. Apparently, little information is available on the impact of curing temperature on the porosity of pastes with slag.

The impact of the moisture conditions on the porosity was dealt with by Bentz and Stutzman (2008). The capillary pore system in cement pastes cured under sealed conditions is likely to de-percolate (become disconnected) earlier than in pastes cured saturated; however a subsequent re-percolation was observed in pastes with low w/c (0.35). On the other hand for saturated curing, the capillary porosity is water filled and accessible to the growing hydration products; therefore at this condition the degree of hydration will be maximized and a refinement of the pore structure is

expected. Earlier findings showed a restricted hydration at relative humidity below 80%, see e.g. Patel et al. (1988).

Various methods (e.g. mercury intrusion porosimetry (MIP), low temperature calorimetry (LTC), scanning electron microscopy (SEM) and water desorption) are available to determine pore structure of cement based material. The methods provide information on varying pore characteristics (pore threshold, pore volume, pore size distribution etc.) in different size ranges (from nm to cm). In general, the methods are indirect which implies that they are based on physical relationships and geometrical models that simplify the complex structure of the pores. Measurements of porosity have showed widely varying values. For instances, Diamond (1971) correlated MIP and water sorption, different curves patterns for pore size distribution were found. Recent investigation (Sun and Scherer, 2010) showed a lower volume of pores for pastes tested by LTC when compared with MIP and gas sorption.

The exact values for porosity parameters given in the literature may be questioned due to the manner of sample preparation, measurement and assessment of the data. It is clear, that there is an urgent need for appropriate specification for porosity measurements to ensure the validity of the data. It should be stress that porosity data using MIP and SEM may be significantly affected by the prerequisite of drying, drying may change the microstructure of cement based materials, see e.g. (Jennings, 2007, Diamond, 2000). Direct oven-drying of specimens tends to collapse the microstructure and removes some of the chemically bound water (Aono et al., 2007, Galle, 2001, Konecny and Naqvi, 1993, Korpa and Trettin, 2006). Villadsen (1992) has found differences curves of pore volume versus pore size curves for MIP and LTC, however when LTC samples were oven dried a good agreement between the data was obtained. Limited impact of drying was found when using solvent exchange (Kocaba, 2009); but the information in the literature is somewhat contradictive (Taylor and Turner, 1987).

In addition to the experimental investigation, thermodynamic modelling can be used to predict the volume of pores of cement with different composition and curing conditions, see e.g. (Atkins et al., 1992, Lothenbach, 2008, Lothenbach et al., 2008). Extended studies by Lothenbach and co-workers (Lothenbach et al., 2008) have shown that it is possible to model the porosity even when different curing conditions are applied. However, some assumptions to simplify the complexities of the cementitious system are made; see e.g. (Lothenbach, 2008). The difficulties increase when SCMs are added; as an example the lack of knowledge of thermodynamic properties of C-S-H at low C/S ratio.

In the present work, the pore structure of SCMs (slag and fly ash) pastes with comparable water to binder volume ratios cured at different conditions (20 or 55ºC; sealed or saturated) for up to two years are investigated. Selected methods for characterizations of porosity were dealt in the present thesis and also reported in the Task 3.1 "Preliminary guidelines for characterization of porosity of cement based materials" (see in (Canut, 2007)). A guideline for porosity measurements and assessment of the results was also prepared as the Task 3.6 and it is also included here (Section 5.9). At the end of this thesis, the correlation between experimental investigations and analytical and numerical modelling is made.

1.1 Objectives

The main objective of the present thesis is to provide information on:

- The impact of SCMs on the porosity development in hydrated cement pastes with SCMs;

- The impact of different curing (moisture and temperature) conditions on the porosity development in hydrated cement pastes;

- Applicability of the selected methods for characterization of porosity in cementitious materials.

Furthermore, the thesis has the aim to provide the reader with guidelines for porosity measurements and assessment of results from the selected methods.

1.2 Scope

The development of the pore structure of cement pastes with and without SCMs (slag and fly ash) cured at different moisture (sealed or saturated) and temperature conditions (20 or 55ºC) for 1, 3, 28, 90 and 720 days were investigated.

The materials were chosen based on their chemical and physicals characteristics; and also they were a common reference base used by other projects part of the Marie Curie Action RTN. The chemical and composition of the material is detailed described in the Section 4.2 of this thesis.

Cement C: CEM I, high C_3S, medium C_3A, high alkali contents
Cement A: white cement high C_3S, low C_3A, low alkali contents (Low Fe and Al content facilitates the modeling of the phases and allow the characterization by NMR)
Slag 1: high amorphous content (typical used composition)
Fly ash 1: less than 10% of CaO, from betuminous coal and normal reactivity (typical used composition)

The main methods to characterize pore structure of cement pastes were:
- Low temperature calorimetry (LTC);
- Mercury intrusion calorimetry (MIP);
- Scanning electron microscope (SEM);
- Water sorption method;

Here, focus was placed on the use of LTC and MIP to characterize pore structure of hydrated cement pastes. LTC has been used to characterize pore structure of saturated pastes (Bager, 1987, Bager and Sellevold, 1986a, Bager and Sellevold, 1986b, Villadsen, 1992); the frozen water (pore solution) within the pores allows the assessment of pore parameters useful for various durability issues (threshold pore size and pore volume).Two equipments are placed at the Department of Civil Engineering at DTU and have an easy access for the project. MIP is a widely used method to characterize pore structure (Canut and Geiker, 2011, Kumar and Bhattacharjee, 2003b, Zhou et al., 2010). The test is simple, fast and less costly when compared to other methods for porosity characterisations, e.g. scanning electron microscopy (SEM) and water sorption. The method seems suitable to illustrate the correlation between the volume of pores and the threshold pore size, i.e. the size of pores providing connectivity.

SEM using backscattered electron imaging is a well-established method to determine pore structure of cement based material. The pore size and total volume of pores can be obtained from the grey histogram from the images. In this thesis, the use of SEM was limited due to the difficulties found in the sample preparation (impregnation and polishing). Samples were then prepared externally (TI –Technologic Institute) to ensure a sufficient quality for image analysis. Moreover, water sorption (desorption and absorption) is used, the experiments have been performed by means of saturated salt solution method (see e.g. (Baroghel-Bouny, 2007b, Baroghel-Bouny, 2007a, Hansen, 1986)). Important pore structure parameters (e.g. pore size and total pore volume) are extracted from the isotherms. Maturity pastes (28, 90 and 720 days) were used due to the long time to acquire results (about one year) and risk of prolonged hydration of the pastes.

Thermodynamic modeling by GEMs was used to get information of the predicted porosity for the pastes, and it is compared with porosity data acquired by the various methods. The modeling was carried out by Lothenbach and De Weerdt (2011) for the cement based materials used in the present thesis.

Additional methods were used, such as:
- Nuclear resonance magnetic (NMR) relaxation;
- Drying methods (evaporable and solvent exchange);
- Capillary suction;
- Autogeneous deformation;
- Thermo-gravimetric analyses;
- Isothermal calorimetry;

Additional methods were explored and used to help on the interpretation of the porosity data obtained by the main methods. ^{1}H NMR relaxation was also planned, however the results acquired during the two visits at University of Surrey showed a variation between the data for similar samples. In addition, difficulties on the interpretation of the water state were found, but they were dealt in the project 4 "*Characterization of cementitious materials by 1H NMR*", see in (Valori, 2009). Solvent exchange and oven drying at 105ºC were carried out to observe the effect of drying in the cement pastes, as MIP and SEM require dried samples. Also, information on the water and solvent porosity was obtained by the drying methods. Capillary suction tests were also carried out with cooperation of a Master student (Larsen-Helms, 2008) to observe the water ingress (sorptivity) on dried pastes. Autogenous deformation was used to observe the volume change of the sealed pastes with and without slag. Moreover, thermo-gravimetric analyses were carried out to observe the carbonation of the samples after water sorption test. Isothermal calorimetry was used to observe the development of hydration of the pastes at 20ºC and 55ºC.

1.3 Outline

The present work is divided in five chapters. Chapter 1 is an introduction of the thesis and it summarizes the intention of writing and the aims. Chapter 2 deals primarily with the impact of the use of SCMs in terms of microstructure. In addition possible impacts of casting and curing conditions on the pore structure are given with focus on the temperature and moisture conditions. Background information was obtained from a literature review and courses carried out during the PhD program. Chapter 3 is divided into two main sections. Section 3.1 deals with the main parameters (e.g. threshold pore size, total pore volume) to characterize the pore structure of cementitious materials, whereas section 3.2 focuses on the methods used to characterize pore structure including their assumptions and limitations. Chapter 4 presents the experimental part of

the project where a detailed description of the materials and tests are given. The following chapter (Chapter 5) provides the results of pore structure for different pastes followed by a discussion based on previous studies found in the literature. In addition, modelling of the porosity of the pastes is given; and correlation between the selected methods and porosity predictions is showed. Also a guideline for porosity characterization using the selected methods is described in Chapter 5. Chapter 6 outlines the most important conclusions of the thesis.

2.   Cement based materials and their porosity

This Chapter contains important information about the chemical-physical properties, main reactions and products of the binders used at the present work: Portland cement (PC) and supplementary cementitious materials (SCMs).

It is also given definitions of a pore space and water in a hydrated cement material. In addition, it is shown the difference in the nomenclature and rage of pore size given in the literature. And a range of pore size is proposed and used at the present work based on the literature from McDonald et al. 2010 and Mindness et. al. 2002.

At the end, this Chapter includes the main impacts of SCMs addition, and casting and curing conditions on the porosity of cementitious materials.

2.1 Portland cement (PC)

Portland cement (PC) clinker consists mainly of four crystalline phases: tricalcium silicate (C_3S); dicalcium silicate (C_2S), tricalcium aluminate (C_3A) and tetracalcium aluminoferrite (C_4AF). Most cement clinkers also contain low amounts (0-3% by weight) of free calcium oxide (CaO), magnesium oxide (MgO) and alkalis (K_2O and NaO_2) (Taylor, 1997). At the final stage of production, clinker is ground with about 4 to 6% of gypsum in order to obtain Portland Cement (PC). Information on the four main phases of Portland cement is given below (Table 2.1).

Table 2.1: Main compounds of the clinker and their characteristics in hydrated cement pastes (Lea, 2004, Taylor, 1997)

Abbreviate name	C_3S	C_2S	C_3A	C_4AF
Technical name	Alite	Belite	Aluminate phase	Ferrite phase
Amount in cement (%)	40-80	0-30	3-15	4-15
Reactivity	High	Low	High	Low
Possible impurities	Al_2O_3, Fe_2O_3, MgO	Al_2O_3, Fe_2O_3, Na_2O, K_2O, SO_3	Fe_2O_3, Na_2O, K_2O, MgO	MgO, SiO_2, TiO_2
Heat of hydration (J/g)	450-500	250	1340	420
Contribution to strength of cementitious materials	High at early ages	High at late ages	High at very early ages	Very low

The composition of Portland cement clinker and cement is usually given with single letters to abbreviate the formulas as shown below:

C = CaO   S = SiO_2 A = Al_2O_3 F = Fe_2O_3 M = MgO
\$ = SO_3 K = K_2O N = Na_2O H = H_2O $\bar{C}$ = CO_2

Cementitious materials are defined as hydraulic materials:

"Hydraulic material has cementing properties. It sets and hardens by chemical interaction with water and is capable of doing so under water (A.C.I. et al., 2004)"

The main compounds of Portland cement, alite (C_3S) and belite (C_2S), reacts with water forming calcium silicate hydrate (C-S-H) and calcium hydroxide (CH). The reaction of alite is as follows (Equation 2.1):

$$C_3S + (3-x+y)H \longrightarrow C_xSH_y + (3-x)CH \qquad \text{(Equation 2.1)}$$

Where x is the C/S ratio, y is the H/S ratio. According to Zhang the C/S ratio varies between 0.8 and 2 (Zhang, 2007). Atkins and Glasser (2002) suggested that C/S ratio is in the limits between 0.85 and 1.70. Neville (2002) reported a C/S ratio of 1.5 when chemical extraction is used and a C/S ratio of 2.0 by thermogravimetric method. Ballonis and Glasser (2008) pointed out that the values measured for C/S may have some errors due to the ions (e.g.alkali, alumina, sulfate) incorporated in C-S-H.

C-S-H (calcium silicate hydrate) has a disordered layer structure: individual layers of calcium oxide (CaO) are formed which are attached by tetrahedral silicate (SiO_4) and hydroxyl group (OH), and the interlayer space is filled with calcium ions and water molecules (Taylor, 1997), see Fig. 2.1. C-S-H is a semi-amorphous product; due to the poor crystalline structure the characterization of its meso-level structure is rather difficult (Balonis and Glasser, 2008, Taylor, 1997). Taylor (1997) divided the C-S-H phases in two imperfect forms of 1.4 nm tobermorite and jennite. Microstructure models were applied to describe the microstructure of C-S-H, see Section 3.1. However, C-S-H structure is still an issue of the studies with hydrated cementitious materials; and it varies according to the literature (Jennings, 1999, Powers, 1960).
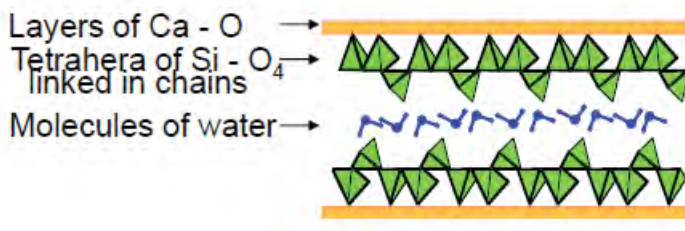
Fig. 2.1: C-S-H structure (analogy with natural mineral torbemorite by (Scrivener, 2010))

Calcium hydroxide (CH, portlandite), one of the main products of cementitious materials hydration, is typically formed as hexagonal crystal plate. CH occupies about 15% of a cement paste. As the hydration proceeds it is possible to observe the formation of CH in the solution of the larger capillary spaces situated in regions from the reaction of the anhydrous cement grains.

Aluminate phases are also presented in hydrated cementitious material. Alumina (Al_2O_3) mainly occurs in C_3A and C_4AF. C_3A plays an important role in the early hydration of the cement pastes. C_4AF reacts much more slowly. The alumina present in the hydration products are mainly in two forms: AFm (Al_2O_3-Fe_2O_3-mono) and AFt (Al_2O_3-Fe_2O_3-tri). AFt phase, known as ettringite, forms

from the reaction of C_3A with the sulfate from the gypsum, see Equation 2.2 and Equation 2.3(Lea, 2004, Taylor, 1997).

$$C_3A + 3C\$ + 32H \longrightarrow C_6A\$H_{32} \qquad\qquad\qquad \text{(Equation 2.2)}$$
or

$$C_3A + 3C\$H_2 + 26H \longrightarrow C_6A\$H_{32} \qquad\qquad\qquad \text{(Equation 2.3)}$$

When the sulfate is fully consumed, ettringite reacts with the C_3A to form monosulfate, see Equation 2.4.

$$2C_3A + C_6A\$H_{32} + AH \longrightarrow 3C_4A\$H_{12} \qquad\qquad\qquad \text{(Equation 2.4)}$$

The stoichiometry of hydration reaction of cement is not precisely known, according to the literature (Atkins and Glasser, 1992, Taylor, 1997, Taylor and Turner, 1987)the amount of water bound in the C-S-H varies with temperature and the water combined by aluminates change over time due to sulfate and carbonate contents.

The hydration process of PC may be divided in five stages, see Fig. 2.2 (Lea, 2004, Taylor, 1997):

I. Initial reaction period. As soon as the anhydrous grain comes into contact with water, soluble components such as alkalis calcium sulfate phases and free lime are dissolved by the surrounding water. The main reaction of this period is the exothermic reaction of C_3A with gypsum. The solution formed increases in pH until a point of super saturation is attained.

II. Dormant or induction period. This period is characterized for the slow and steady reaction which the degree of hydration and microstructure not present relevant changes. The initial set of the paste occurs at the end of this stage.

III. Acceleration period. C_3S and C_3A are accelerated to a high level of activity and maximum reaction is reached. Outer C-S-H starts to form from the reaction of C_3S with water making the strength of the paste increase. C_2S starts to react at lower rate of reaction if compared with C_3S and C_3A. Pore volume starts to decrease with increasing of reactions and decreasing of w/c ratio.

IV. Decelaratory period. The rate of reaction decreases and the reaction get controlled by the diffusion of silicate trough a layer of existing products. Inner C-S-H starts to form on inside of the shell from the continuing hydration of C_3S. Secondary reaction of C_3A takes place and producing long rods of Aft.

V. Final slow reaction. This is a period of steady reaction and decreasing of diffusion process. The deposition of hydrates becomes inhibited by lack of space. From one to three days, C_3A reacts with Aft forming hexagonal plates of AFm. At approximately seven days, inner C-S-H formed is sufficient to decrease the separation of the "shell" and core of the paste. In order it reduces the porosity of the cementitious matrix. And the outer C-S-H becomes more fibrous. The hydration proceed slowly, some of the remaining anhydrous material reacts to form additional inner C-S-H. The ferrite phase appears to remain unreacted.
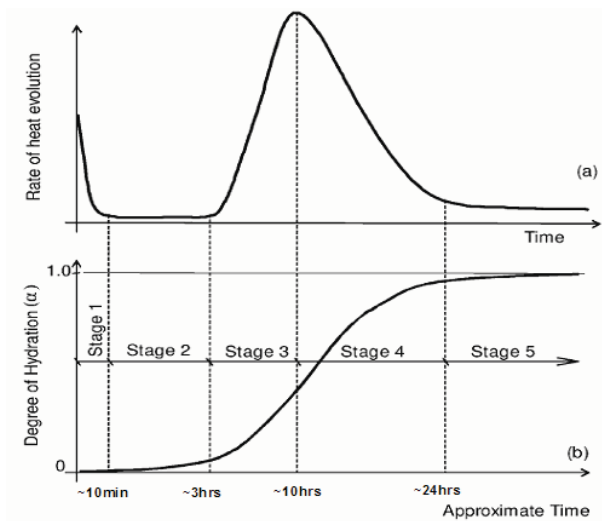
Fig. 2.2: Rate of evolution (a) and degree of hydration of cementitious materials (Byfors, 1980)

2.2 Supplementary cementitious materials

Supplementary cementitious materials (SCMs) are by-products (e.g. slag, fly ash and silica fume) used as partially substitute of PC that takes part in the hydration reaction and thereby make a substantial contribution to the hydration and microstructure of cementitious materials. SCMs may be distinguished through the chemical and physical aspects, see Figs.2.3 and 2.4 and Table 2.2.
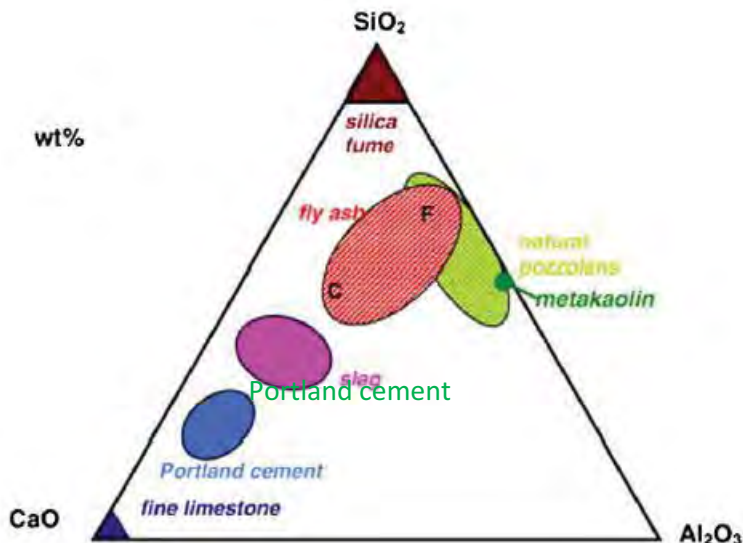
Fig. 2.3: Phase diagram of Portland cement (PC) and SCMs (Scrivener, 2010)

| (a) | (b) | (c) |
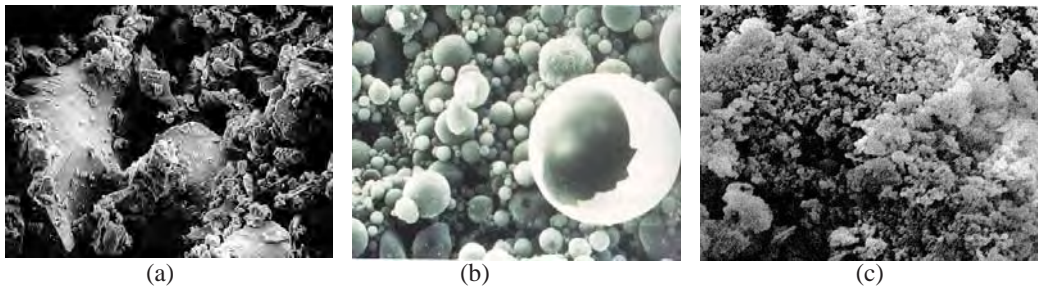
Fig. 2.4: Morphology of (a) slag (2100x), (b) fly ash(1000x) and (c) silica fume (5000x) particles (Kosmatka et al., 2002)

Table 2.2: Classification, composition, density and particle characterization of slag, fly ash and silica fume (Kocaba, 2007b, Mehta and Monteiro, 2006)

Material	Blast furnace slag	Fly ash	Silica fume
Origin	Iron production	Combustion of pulverized coal in electricity power plants	Ferro-silicon alloys and silicon metal manufacture
Reaction classification	Cementitious and pozzolanic	Pozzolanic	Highly active pozzolanic
Composition	Silica, calcium, magnesium, aluminium	Silica, aluminium, calcium and ferrite	Silica in non-crystalline form.
Density	2.6 g/cm³	2.10 to 2.78 g/cm³	2.2 g/cm³
Particle characterization	Particle less than 45 μm with rough texture	Solid spheres of less than 20 μm in diameter (10-15% of particles are larger than 45 μm)	Fine powder of solid spheres of 0.1 μm average diameter

In general, SCMs consist of amorphous glasses which have a higher content of SiO_2 and often Al_2O_3 ,and a lower content of CaO than PC (Kocaba, 2009, Lothenbach et al., 2010, Richardson and Groves, 1997). Glasses from blast furnace slag consists of monosilicate "Q" type like in Portland clinker; and in fly ash glass it is cross-linked silica-tetrahedral, "Q4"type (Fraaij et al., 1989). SCMs may be found as artificial and natural: artificial are the materials such as fly ash and silica fume; and natural or calcined materials (e.g. volcanic, clays) (A.C.I. et al., 2004).

Neuwald (2005) suggested a definition of SCMs according to the reaction they undergo: hydraulic materials react directly with water to form cementitious compounds, while pozzolanic materials react with calcium hydroxide (CH) in the presence of moisture to form compounds possessing cementitious properties, see Fig. 2.4. According to Kocaba (2009) slag may be considered as a latently hydraulic rather than pozzolanic due to its C/S ratio is higher than the other pozzolans, see Fig 2.5. According to ACI "Cement and Concrete Terminology" SCMs may be defined as:

"Inorganic material such as fly ash, silica fume, metakaolin, or ground-granulated blast-furnace slag that reacts pozzolanically or hydraulically.(A.C.I. et al., 2004)"
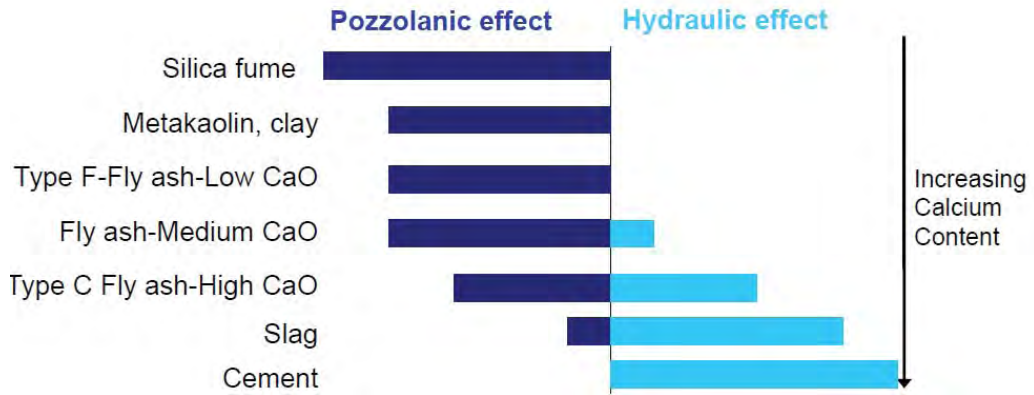
Fig. 2.5: Pozzolanic and hydraulic effect; and calcium content after (Scrivener, 2010)

Studies concluded that the SCMs reaction is activated by hydroxyl ions of the pore solution from PC hydration (Cook, 1986, Takemoto and Uchikawa, 1980, Roy and Idorn, 1982). When activated the blast furnace slag dissolves whereas the fly ash decompose through the break of silica structure (Si and OH group). As a result of the fly ash decomposition, the ions (SiO_4^{-4} and H_2O^{2+}) absorb Ca^{2+} from Portland cement hydration. Slag only has to be activated (latent hydraulic), while fly ash needs also lime (pozzolanic). The activation of slag occurs at relatively low pH's (e.g. less than 12), while fly ash needs a pH of more than 13 (Fraaij et al., 1989, Taylor, 1997) .The alkalinity is build up over the first few days; therefore the amount of reaction of SCMs is negligible in this period. The reaction of the silica from SCMs with the CH from cement (known as secondary reaction) is represented by the Equation 2.5.

$$xCH + yS + H \quad \longrightarrow \quad C_x\text{-}S_y\text{-}H \qquad \qquad \text{(Equation 2.5)}$$

During the secondary reaction, SiO_2 from SCMs reacts with CH forming additional C-S-H phase. The consumption of CH is observed for cement with fly ash and silica fume; for slag blends it is less clear see e.g. (Kocaba, 2009, Lothenbach et al., 2010). The additional C-S-H phase is significantly different to C-S-H in PC; a tobermorite-like structure has been proposed (Lothenbach et al., 2010, Richardson, 2008). The C-S-H formed by SCMs has a lower content of C/S ratio (about 1.2 or less) if compared with Portland cement hydrates (Kocaba, 2007b). The formation of a C-S-H with low C/S leads to an increased uptake of aluminum in the C-S-H. Richardson and Groves' (1997) studies using NMR spectroscopy and analytical TEM found aluminum in the bridging sites in the silicate chains (Richardson, 2008). The disappearance of monosulfate phase is also reported in the literature (Lothenbach et al., 2010). Moreover, differences in diffusion characteristics of the C_3A and C-S-H are noticed during the SCMs reaction; C_3A is formed away from the SCMs while the C-S-H phases are found at the surface of the SCMs. This mechanism is called diffusion-controlled dissolution, and it is described by some authors (Cook, 1986, Taylor, 1997, Roy and Idorn, 1982). Richardson and Groves (1997) reported that at low degree of reaction of SCMs is possible to observe at the "inner" product and the "outer" product of C-S-H between the clinker and the grains of SCMs. However later, around the SCMs particles it is possible to see rims with different grey level due to the high level of intermixed phases (e.g. alumina) (Kocaba, 2009,

Richardson and Groves, 1997). Studies (Lothenbach et al., 2010) pointed out that there is an interaction between the hydration of the clinker and SCMs, and it may compromise the measurements of the degree of reaction of these two components separately .

A volume change of the products by SCMs addition is also reported in the literature and it may have an impact in the mechanical properties and durability of material. Adopting the following densities (see Table 2.3) it is possible to estimate the volume changed of solid contents due the reaction of SCMs (Equation 2.6 and 2.7).

Table 2.3: Densities of the reactant and products of the SCMs reaction (Lea, 2004)

Products of SCMs reaction	C_3S	C-S-H*	CH	S
Density	3.17 g/cm³	1.90 g/cm³	2.23 g/cm³	2.20 g/cm³

*the same density for C-S-H product was adopted for the calculation of the molar volume

$1C_3S + 0.75H \longrightarrow 1.25C\text{-}S\text{-}H + 0.69CH; \Delta V_{solids} = 1.94$ cm³/mol of C_3S (Equation 2.6)

$0.69CH + 0.19S + 0.75H \rightarrow 1.31C\text{-}S\text{-}H^*; \Delta V_{solids} \sim 1.25$ cm³/mol of CH   (Equation 2.7)
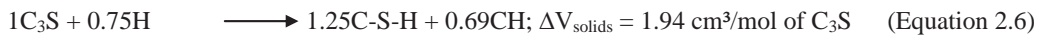
An extra solid volume (C-S-H) of about 1.25 cm³/mol has been estimated from the reaction of the SCMs (Equation 2.7). The increase of solid volume of C-S-H may result in the reduction of capillary pores volume whereas the volume of gel pores may increase. Studies of chloride ingress and microstructure development with SCMs suggested a decrease of threshold pore size (Diamond, 1999, Martys and Ferraris, 1997, Zhang, 1998).

In addition to the refinement of the pore sizes, the volume previously occupied by the consumed CH is filled in by C-S-H. The decrease of CH may lead to an improvement of the mechanical properties of the cement based materials (Hooton, 1986, Mehta and Monteiro, 2006, Stefanovic et al., 2007). High amount of portlandite in cement pastes is reported to cause instability of concrete when it is exposed to acid solution as well as high temperatures. Hooton (1986) and Mehta (1981) also found that the reduction of CH improves the sulfate and chloride resistance of hardened pastes.

Filler effect is also a contributing factor of SCMs (Gutteridge and Dalziel, 1990, Lange et al., 1997). Gutteridge and Parrott (1976) found out that inert materials blended with cement have a significant effect on their reaction. The first few days where no SCMs reaction occur the changes in hydration kinetics are dominated by the filler effect. Two main mechanism of filler effect were suggested: 1) SCMs particles fill the voids between the cement grains resulting in the immobilization of the water; and 2) SCMs act as nucleation sites for C-S-H growth which may increase the volume of solid decreasing the pores (Gutteridge and Dalziel, 1990, Gutteridge and Parrott, 1976).

As previously discussed, a high porosity for SCMs hydrated pastes at early age is expected when low degree of reaction is observed. This is even more evident for pastes with high percentage of cement replacement. Studies with SCMs have showed that it often reduces the rate of the hydration heat in cementitious materials (Mehta, 1986, Taylor, 1997).

Delay of the hydration reaction has also been associated with the type and amount of blend. Fly ash seems to have a more impact on the delay of hydration than slag (Stefanovic, 2007). Investigations

by Stefanovic (2007) showed an example of the reacting rate of fly ash, the concentration of CH is used as a parameter of the progress of hydration reaction, see Fig. 2.6. As observed, it takes over seven days (stages VI and VII) for the starting of the fly ash reaction. As opposite to that, studies with silica fume pastes showed no delay in the hydration degree when compared with plain Portland material, this may be due to the high surface area of silica fume particles, see e.g. (Mehta and Gjorv, 1982, Radjy et al., 1986, Sellevold and F.F., 1983). The curing conditions has also an impact in the reaction rate (Geiker, 1999, Taylor, 1997, Zhang, 2007). At temperatures lower than 15ºC the reaction are more slower; at high temperatures (from 30ºC) the opposite is observed (Zhang, 2007). The effective period of strength contribution also is affect by the delay in the hydration process of slag and fly ash, see Fig. 2.7 (Mehta, 1986).
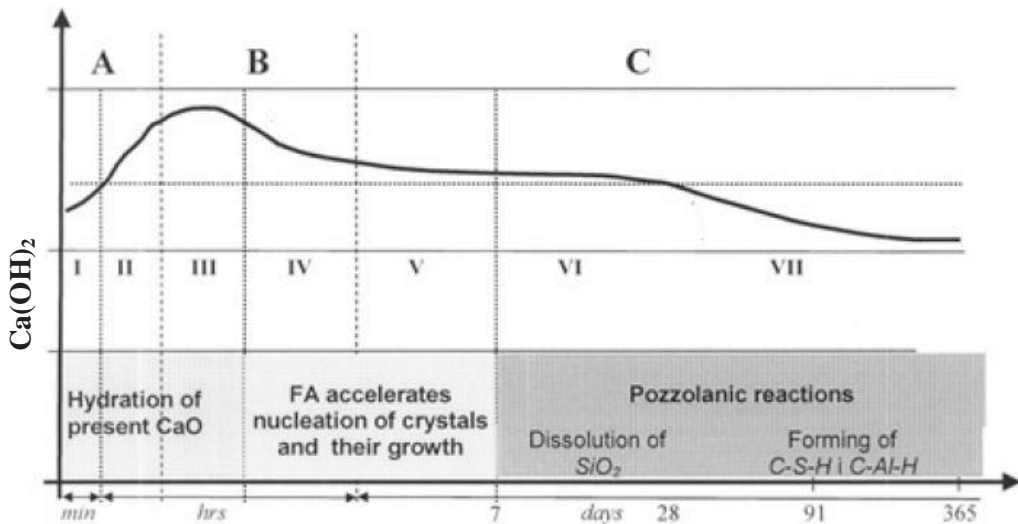

Fig. 2.6: Hydration of PC with fly ash (FA) addition (Stefanovic et al., 2007)
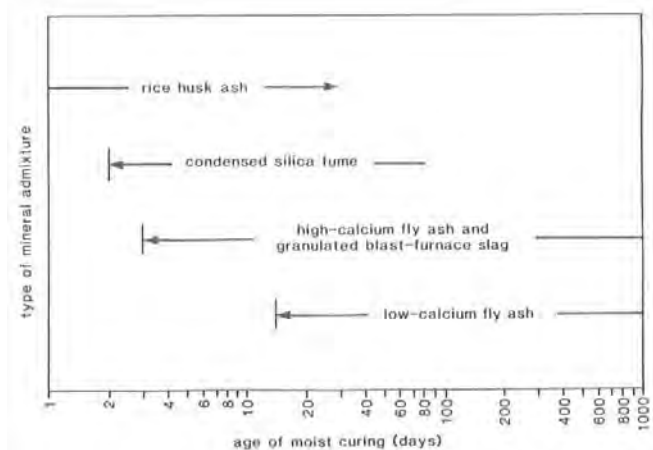
Fig. 2.7: Age of strength contribution from various mineral admixtures (Mehta, 1986)

In terms of sustainability, great benefits of the use of SCMs in the civil construction have been reported (Hooton, 1986, Malhotra, 1993, Mehta and Gjorv, 1982). Replacement of cement by SCMs seems to be a viable solution for the cement industry to minimize the release of carbon dioxide (CO_2), save energy as well reduces the raw material extraction. In the Table 2.4 is shown the percentage of saving with the use of slag and fly ash, the data is given by "*Slag Cement Association*" (SCA) and it is based on percentage of Portland cement systems compared with systems containing slag or fly ash (SCA, 2003). The percentage of the cement replacement may vary according to the application and it may change the final properties of the material, see Table 2.5.

Table 2.4: Environmental benefits comparison of slag and fly ash addition (SCA, 2003)

Environmental benefit (substitution rate for PC)	Slag (35%)	Slag (50%)	Fly ash (20%)
Carbon dioxide emission saving*	30%	43%	17%
Energy saving*	21%	30%	14%
Reduction in extracted material*	5%	7%	3%

* Percentage based on 100% of PC systems compared with system containing slag and fly ash substitution

Table 2.5: Ranges of mixture percentages for SCMs by Slag Cement Association (Slag Cement Association, 2007)

Application	Slag cement	Fly ash	Silica fume
General concrete	25-50%	10-30%	0-10%
High performance	35-65%	15-30%	5-15%
Mass	50-80%	25-50%	0-10%
Precast, block	20-50%	10-30%	0-15%

In the next section an overview of ground granulated blast furnace slag and fly ash is outlined. First a short description of the by-product generation is given followed by chemical and physical properties of the SCMs. Then the hydration products of the SCMs and their possible effects on the microstructure are described.

2.2.1   Ground granulated blast furnace slag

Ground granulated blast furnace slag is a by-product from iron production. It consists primarily of silica, calcium, alumina and magnesium. Higher content of CaO is found in the slag compared to others SCMs that gives the material a particular characteristics in the hole of SCMs. Kocaba (2009) refers to slag as a latent hydraulic material, with a few pozzolanic characteristics. In the process of iron manufacture the blast furnace slag is formed at 1350-1550ºC. To obtain a material with cementitious properties, the slag (molten) is rapidly cooled to a temperature below to 800ºC. This process minimizes the crystallization of the material. The treated product (dried and ground) contains particles of less than 45 µm and 95% of glass and is called ground granulated blast furnace slag or slag (Taylor, 1997, Mehta and Monteiro, 2006). The true density of slag measured by helium picnometry is about 2.6g/cm³ (Kocaba, 2007b).

The slag modified the composition of hydrates: C-S-H has typically a Ca/Si content of about 1.2 and Al/Ca content around 0.19 (Kocaba, 2009). It is also reported that the slag favored the hydration of the ferrite phase (Kocaba, 2009). Phase assemblage calculations carried out by Lothenbach et al. (2010) showed comparable results for cement pastes blended with slag, fly ash

and silica fume: reduction of portlandite, formation of C-S-H with a lower C/S ratio and consumption of monocarbonate, see Fig. 2.8. However, lack of knowledge of thermodynamic properties of C-S-H at low C/S ratio, moreover instability of the phases may give wrong information of the predicted material. It is important to stress that thermodynamic modelling must be combined with experimental data. Kocaba (2009) reported that no large decrease of CH was found in slag pastes even after one year of curing.
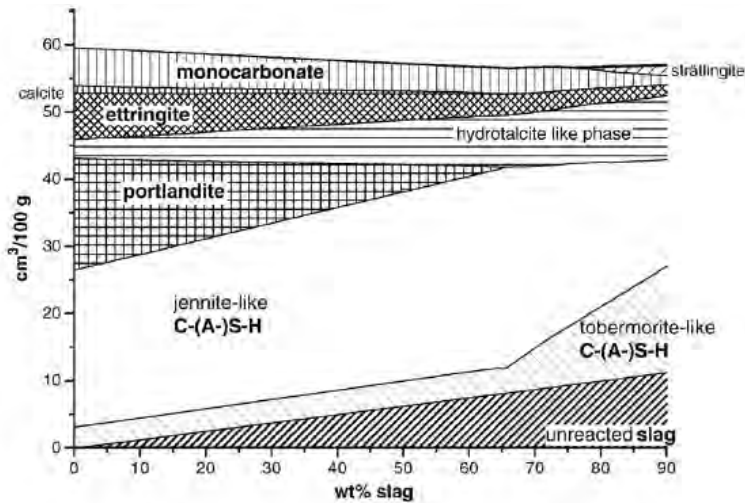
Fig. 2.8: Modeling of assemblage phase in hydrated slag pastes (Lothenbach et al., 2010)

Studies using transmission electron microscopy (TEM) showed that with a limited increasing of slag in the blend, the microstructure of the outer product becomes less fibrilar and more foil like. It is suggested that it decreases the connective and the volume of the pore system (Taylor, 1997). Kocaba (2007) and Roy and Idorn (1982) reported a slower and lower heat released for slag cement at normal temperatures, which provides a higher porosity and may compromise the compressive strength in slag systems at early age, see Fig. 2.9.

1 - Dissolution of materials and formation of ettringite;
2 - Induction period, increase in calcium concentration;
3 - Rapid formation of CH and C-S-H;
4 - Reformation of ettringite;
5 - Formation of monosulfate.
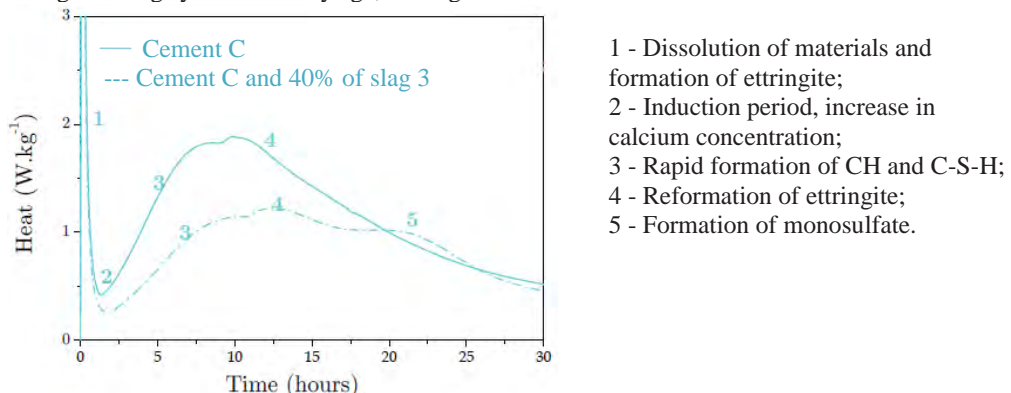
Fig. 2.9: Heat liberation for plain cement paste and with 40% of slag addition (Kocaba, 2007b)

Also the dissolution process is influenced by the slag addition (shift and shape of the peaks), see Fig. 2.9. Roy and Idorn (1982) observed less chemical shrinkage at early age for pastes with 50% of slag substitution cured at room temperature which indicates a slower rate of reaction of the slag (Fig. 2.10).
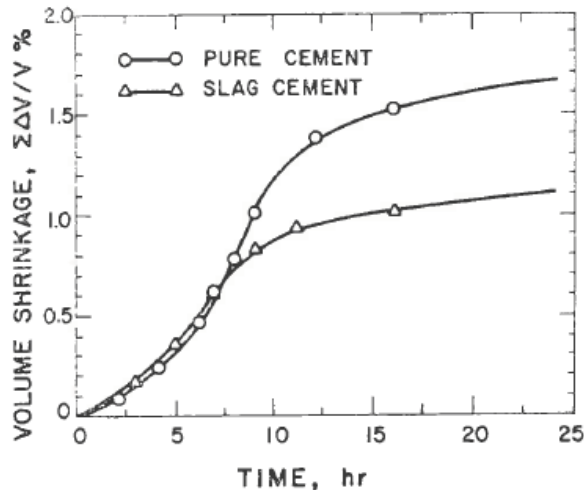
Fig. 2.10: Chemical shrinkage of plain cement paste and 50% of slag substitution at room temperature (Roy and Idorn, 1982)

2.2.2   Fly ash

Fly ash is a pozzolanic by-product from the combustion of pulverized coal in electricity power plants, an amorphous constituent (glass) of coal molten formed through rapid cooling. Fly ashes solidify forming particles with spherical shape in the range of 1 to 100 µm. The true density of fly ash is approx. from 2.10 to 2.78 g/cm³. The density of fly ash is suggested to be rather difficult to determine due to the presence of hollow spheres and spongy aspects (Haerdlt, 2008, Taylor, 1997).

The chemical composition of fly ash is mostly glass containing mainly silicate, alumina and ferrite. The CaO content of the fly ash may vary: less than 10% of CaO (from betuminous coal) and 15 to up to 40% of CaO (sub-bituminous or lignites). ASTM C618-08a (2008) classify the fly ash type by the CaO content as: Class F-fly ash with low amount of CaO and Class C-fly ash with high amount of CaO. The high calcium fly ash is in general more reactive because it contains most of the calcium in the form of reactive crystalline compounds (Mehta and Monteiro 2006). As the Class F-fly ash is the most abundant and used, the following discussion focus on this type of fly ash.

According to the literature (Lea, 2004, Taylor, 1997), fly ash products closely resemble C-S-H produced by the hydration of the Portland cement. However as described previously (Section 2.2), the reaction from fly ash does not start at early age. Fly ash reaction only starts when the pH of the pore solution (alkali hydroxide) becomes about 13, and according to Neville (2002) this can be as long as one week or even more. Haerdtl (2008) suggested that even after 28 days the degree of reaction from fly ash systems is in the range of 10%. Stefanovic (2007) studies observed that the low activity of fly ash lies in two factors: (1) the surface layer of the glassy phase of the fly ash particles is dense and chemically stable and (2) internal Si–Al glass chains are difficult to disintegrate in order to allow activity. Lothenbach et al (2010) reported a considerable error in the

thermodynamic calculation of fly ash systems caused by a high amount of alumina content in the system and coupled with a potentially high aluminium uptake in C-S-H. Their model for fly ash found destabilization of portlandite and the formation of additional C-S-H with a decreased Ca/Si ratio. Also a decrease of ettringite and an increase of AFm content due to the high amount of Al_2O_3(alumina) and low amount of sulphate (SO_4).

Studies have showed (Bijen, 1996, Hooton, 1986), the decrease of chemical ingress into concrete with fly ash, this suggest the beneficial effect of fly ash addition on the performance of reinforced concrete structures. Among others Stefanovic et al. (2007) pointed out certain disadvantage of fly ash addition, such as that the compressive strength of fly ash paste decreases with increasing fly ash content. It is important to keep in mind that effect of SCMs, such as fly ash depends on the type and amount of material added, as well age, curing conditions and etc., see e.g. (Malhotra, 1993).

2.3 Pores and water in cement based materials

The reaction of cement with water leads to the setting and hardening of a porous cementitious material. Some of the water is a constituent of the new solids produced by chemical reactions, and the other part of the water is free movement in response to changes in ambient conditions and it is an index to the degree of porosity of the hardened paste (Powers and Brownyard, 1947). Table 2.6 shows the difference in the used nomenclature for water and pores found in hydrated cementitious materials.

Table 2.6: Type of water and pores of cementitious materials (Feldman, 1981, Jennings, 1999, Lea, 2004, Mehta and Monteiro, 2006, Mindness et al., 2002, Powers and Brownyard, 1947, Taylor, 1997, McDonald et al., 2010)

Type of water	Type of pores
Non-evaporable water, chemically bound water, structural water,	-
Gel water, evaporable water	Gel pores, interlayer space of C-S-H, nanopores, micropores, intra C-S-H gel , inter C-S-H gel
Physically adsorbed water, gel water , part of evaporable water	
Capillary water, free water, part of evaporable evaporable water	Capillary pores, capillary cavity, mesopores
-	Air voids, entrapped air, entrained air pores

2.3.1   Pores in cement based materials

Pores are the spaces, empty or filled by pore solution, in the hydrated cementitious materials (Westermarck, 2000). Various types of pores may be observed in a porous solid, as showed in the Table 2.7 and Fig. 2.11.

Table 2.7: Pore classification in cement based materials

Pore definition	Characteristics	Illustrated in
Open pore	Communicates with the surface	Fig.3.1a)
Ink-bottle pores	Entry smaller than the actual pore size (Nielsen, 1970)	Fig. 3.1b)
Closed pores	No communication with the surface	Fig.3.1c)
Open-ended pore	Voids or space between particles (Westermarck, 2000)	Fig.3.1d)
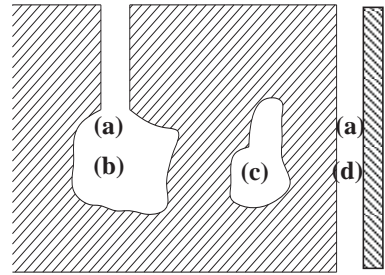
Fig. 2.11: Pore types: (a) open pore; (b) ink bottle pore; (c) closed pore; (d) open ended pore (Westermarck, 2000)

The classification of the pores is a challenge due to the complex and interconnected nature of the pore network in cement pastes. A typical pore size distribution for hydrated cement encompasses a large range of pore sizes, from about cm to as small as nm in diameter. A standard classification of the pore size for cement based materials has not been established yet, so it is possible to find difference in the nomenclature and range of pores size, see Fig. 2.12.
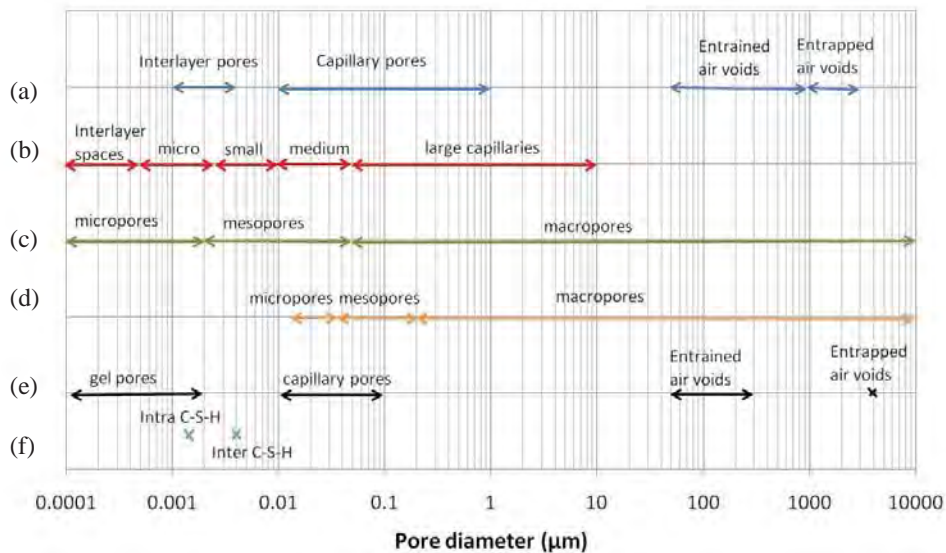
Fig. 2.12: Range of pores and nomenclature by (a) Powers and Brownyard; (b)(Mindness et al., 2002)(c) IUPAC (1998), (d)Mindness et al. (2002); (e) Mehta and Monteiro (2006); (f) (McDonald et al., 2010)

In the present work, capillary and gel pores are divided into (McDonald et al., 2010, Mindness et al., 2002).

- Gel pores ≤0.004 µm;
- Small capillaries 0.004 to 0.010 µm;
- Medium capillaries 0.010 to 0.050µm;
- Large capillaries 0.050 to 10 µm.

2.3.1.1 Gel pores, interlayer spaces in C-S-H, micropores, nanopores

Interlayer space in C-S-H, gel pores or micropores may be defined as: *" the gel porosity in the intrinsic part of the C-S-H"* (Mindness et al., 2002).

According to Powers (1975) the gel pores size is about 0.002 to 0.004 µm of diameter. Feldman and Sereda (1968) suggested that the width of the gel pores may vary from 0.0005 to 0.0025 µm. In a series of papers McDonald and co-workers have proposed 0.004 µm for inter C-S-H gel and 0.0015 µm for intra C-S-H gel (McDonald et al., 2005, McDonald et al., 2010).

Gel pores may contribute to about 26% to 28% of paste porosity and it is reported to have a little or no impact on the strength and permeability (Powers and Brownyard, 1947). Also, Odler and Robler (1985) suggested that the pores with the radius less than 0.010 µm have a negligibly impact on the strength of the cement pastes. However, the pores in the gel range may influence the drying shrinkage and creep (Mehta and Monteiro, 2006, Mindness et al., 2002).

2.3.1.2 Capillary pores, macropores, mesopores

Capillary pores, macropores or mesopores may be defined as the spaces not taken up by cement or hydration products (Mehta and Monteiro 2006). The term "capillary pores" is here used to define this type of pores. *Capilla*, comes from Latin and it means hair, it is used for small pores that only a single hair can fit (Dictionary, 2010). Mindness et al.(2002) divides the capillary pores in larger capillary (0.050 to 10 µm), medium capillary (to 0.010 to 0.050 µm) and small capillary pores (0.0025 to 0.010 µm). According to them capillary pore is one which capillarity effects may occur (e.g. meniscus, ionic diffusion).

Studies by Pores and Brownyard (1947) showed that the capillary pores do not begin to be filled below about $0.45p_s$ (saturation pressure). Capillary pores depend on initial separation of cement particles, which is controlled by the w/c ratio. Studies reported that capillary pores are direct related to the strength and durability issues (Hooton, 2010 (in press), Nilsson, 2002).

2.3.1.3 Air voids

According to Mehta and Monteiro (2006), air voids are generally spherical and they are usually divided in entrained (50 to 200 µm) and entrapped (approx. 3 mm) air voids. Entrapped air is the empty pores formed during the mixing and casting process. Entrained air is air purposely entrained by the addition of admixtures to the cement mixture (Mehta and Monteiro, 2006). It is generally accepted that entraining air in concrete improves its frost resistance (Powers, 1975).

2.3.2   Water in cement based materials

Water, essential for the reaction of cement and SCMs, is introduced during the process of mixing the cement paste, mortar or concrete. The state of the pore water depends on the size of the pores and the ions in solution. The present work uses "evaporable" for water removed by standard drying using oven at 105ºC and "non-evaporable" for water removed from105 to 1050ºC.

2.3.2.1 Non evaporable water

Non evaporable water is a constituent of the solid material in the paste (Powers and Brownyard, 1947). This water may be removed at low relative humidity or at high temperatures. Some authors (Jensen and Hansen, 1999, Powers and Brownyard, 1947) suggested the measurement of the non-evaporable water may be determined as the relative mass loss between 105ºC and 1050ºC. Powers' Model (1960) determined that the non-evaporable water for a fully hydrated cement paste is equivalent to 0.23g/g cement reacted.

Taylor and co-workers (Taylor and Turner, 1987) recommended drying at 11% RH to find chemically bound water which the interlayer water is part. According to them, in contrast with the chemically bound water, the procedure of "non evaporable water" is not a measure of chemically bound water, as much water from the interlayer space is lost under this conditions.

2.3.2.2 Gel water

Powers and Brownyard (1947) defined the gel water as the water is that contained in the pores of the C-S-H gel. Gel water can be divided into: adsorbed and interlayer water (Mehta and Monteiro, 2006). Mehta and Monteiro (2006) suggested that adsorbed gel water can be removed when hydrated cement paste is dried to 30% RH and interlayer below 11%RH.

According to Powers and Brownyard (1947) the weight of gel water in a saturated paste is equal to 4Vm, where Vm is the weight required to form a complete mono adsorbed layer on the solid phase (measured by BET). In Powers' model the gel water is 0.19g/g cement reacted (Powers and Brownyard, 1947). It is suggested that this water does not affect the strength but its removal may cause creep and drying shrinkage (Kurtis, 2007, Mehta and Monteiro, 2006).

2.3.2.3 Capillary water, free water

The sum of capillary water and gel water is termed evaporable water, which may be removed from the cement based materials using oven at 105°C (Powers, 1960). A large range of methods are described in the literature to remove the evaporable water, for instances "D-drying", P-drying, solvent exchange (Thomas and Jennings, 2008).

The evaporable water may also be represented by the water held in a paste as a function of the relative vapor pressure, see Fig. 2.13.

According to Powers and Brownyard (1947), capillary water is held in larger pores by capillary forces and it can be represent by desorption isotherm in equilibrium with RH of 40 to 100%, see Fig. 2.13. Mehta and Monteiro (2006) suggested that the water in large pores of >0.050 µm is mobile whereas the water in small capillaries is considered immobile at 20°C and saturated conditions.
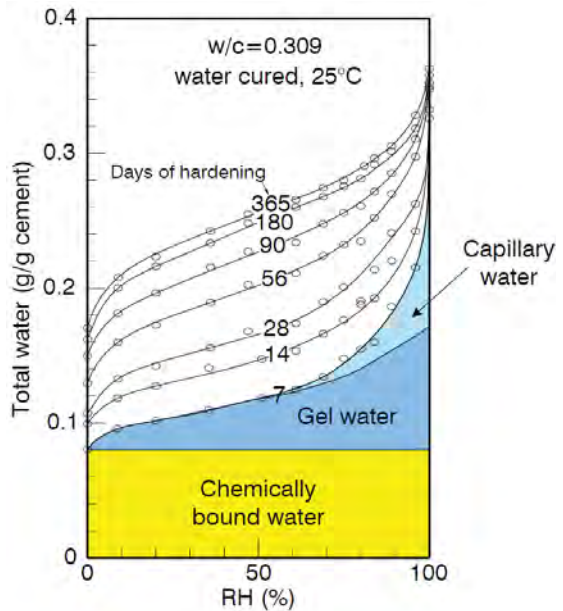
Fig. 2.13: Separation of water into gel water and capillary water ((Jensen, 2010b) after (Powers and Brownyard, 1947))

2.4 Impact of SCMs on the pore structure

The use of SCMs as substitute of cement has been reported as a tool to refine the pore structure of cement paste. From the previous discussion (Section 2.1 and 2.2), it is clear that changes in the microstructure are expected with the use of SCMs. During the literature review it was observed some difficulties to give detailed information of the effects of SCMs addition on cement pastes. A more complex system is found when SCMs is added, and it still missing information of the "new" C-S-H formed at low C/S ratio and with some ions incorporated such as K, Na, Al. Data in the literature, also showed a more complex kinetic for SCMs and some limitations to predict their phases, see in (Lothenbach, 2008, Lothenbach and De Weerdt, 2011). These difficulties may also reflect on the interpretation of the microstructure of SCMs materials, where new type of products are formed e.g. C-S-H (density, colour, shape, aspect). For this reason a review of the effect of SCMs on the pore structure of the hydrated cementitious paste showed is given here. The data will be further compare with the data acquired in the present work.

Feldman (1981) reported the effect of SCMs addition for pastes with 35% of fly ash and 70% of slag cured saturated and at a w/c ratio of 0.45 for 1,3,7,14,28, 90, 180, 360 and 540 days by MIP (Fig. 2.14). Further information was not given by the author (i.e. method of drying, the grain size of the material).

The threshold pore size and pore volume were acquired by the Fig. 2.14 by Feldman (1981) and illustrated in the Fig. 2.15. The threshold pore size is acquired by two tangents in the intrusion curve versus pore size (further details in the Section 3.3.2): Portland cement (o), Portland cement and 35% of fly ash (□) and Portland cement and 70% of slag (Δ) (Fig. 2.12). The pore threshold size was calculated through the Washburn Equation, see section 3.3.2. It was assumed: contact angle of 141° and surface tension liquid-solid of 485N/m². These values were suggested by a contact from Heidelberg Cement and they are in the range suggested by some authors (Cook and Hover, 1991, Diamond, 1999, Kumar and Bhattacharjee, 2003b). The percentage of the intruded mercury multiplied by the bulk density of the material give the porosity of the samples. However the bulk densities of the materials were not given. Thus, it was assumed that the intruded volume may represent the total porosity even knowing that this is not true.
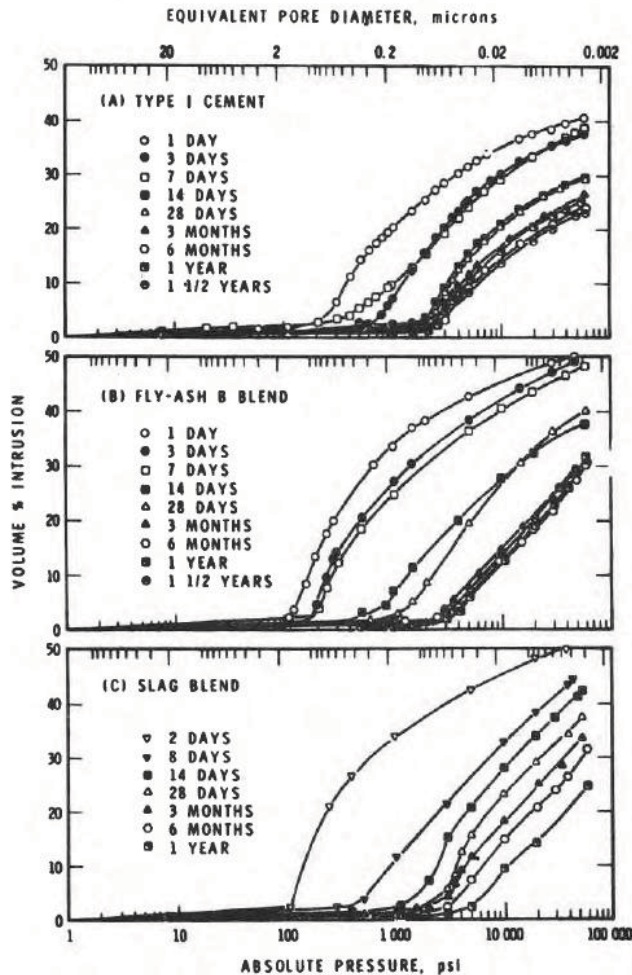
Fig. 2.14: Intrusion volume (%) versus pressure (psi) of cement pastes with addition of 35% fly ash and 70% slag, w/c ratio of 0.45 (Feldman, 1981)
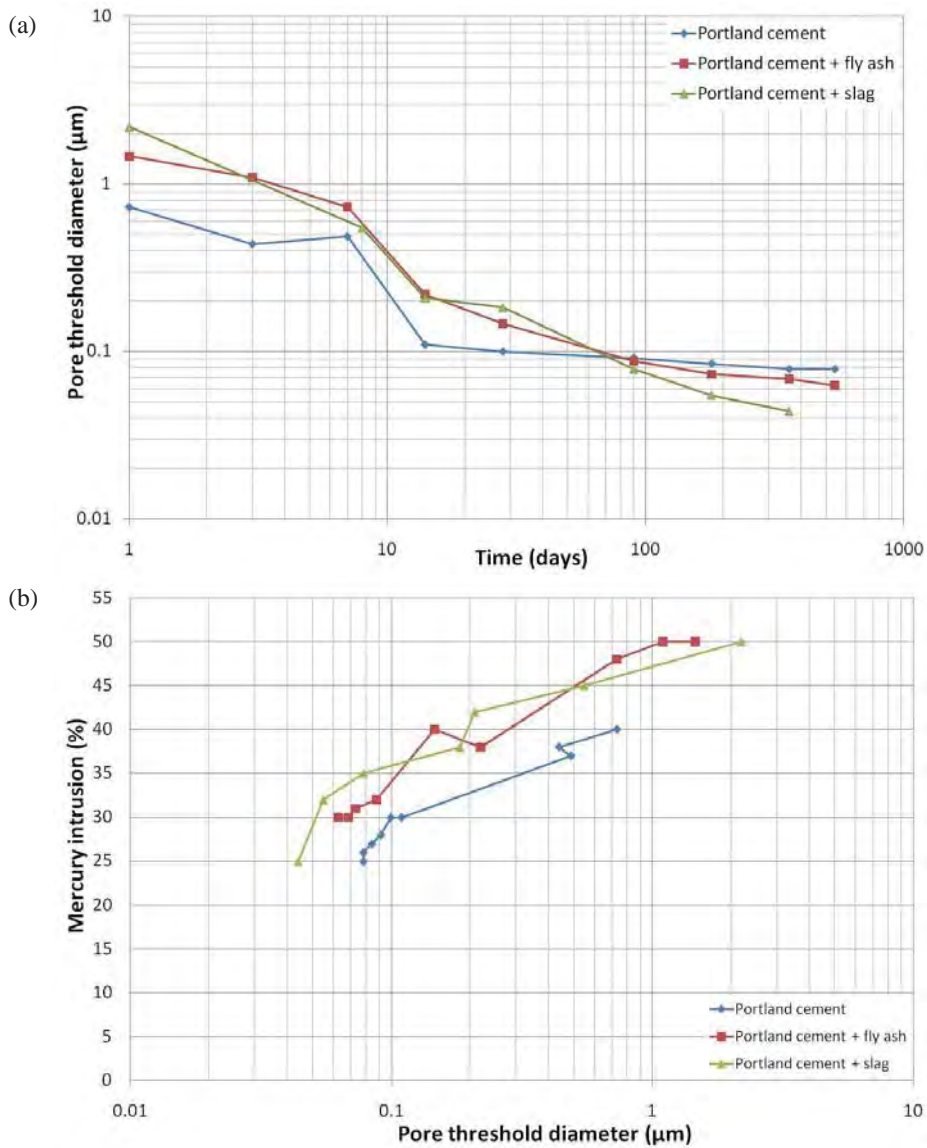
Fig. 2.15: (a) Threshold pore size diameter (µm) in function of time (days) and (b) volume
of mercury intruded (%) versus diameter (µm) for selected pastes (data from Feldman 1981)

Fig. 2.15(a) shows a lower threshold pore size for the SCMs (slag and fly ash) pastes after 28 days
when compared with plain cement pastes. However, a higher percentage of mercury intruded was
noticed for the fly ash pastes when compared with plain cement pastes, see Fig. 2.15(b). This is in
agreement with the data here presented, see Section 5. 2.

Among others Villadsen (1992) studied cement pastes with 20% of fly ash addition at w/c ratio of 0.4 by low temperature calorimetry (LTC), see Fig. 2.16. The test was undertaken for cement pastes older than 80 days. The samples were rotated in the first 16 hours after casting followed by saturation with lime water and curing at room temperature. Rotation of the samples is not recommended since the sedimentation of the particles is a factor which may not stop after 16 hours; and it may also change the pore structure of the pastes (see e.g. in (Mohr and Hooda, 2010)). The ranges of pores (e.g. 0 to -20°C percolated capillary pores) are given in the literature (Bager and Sellevold, 1986a, Lindgreen et al., 2006).
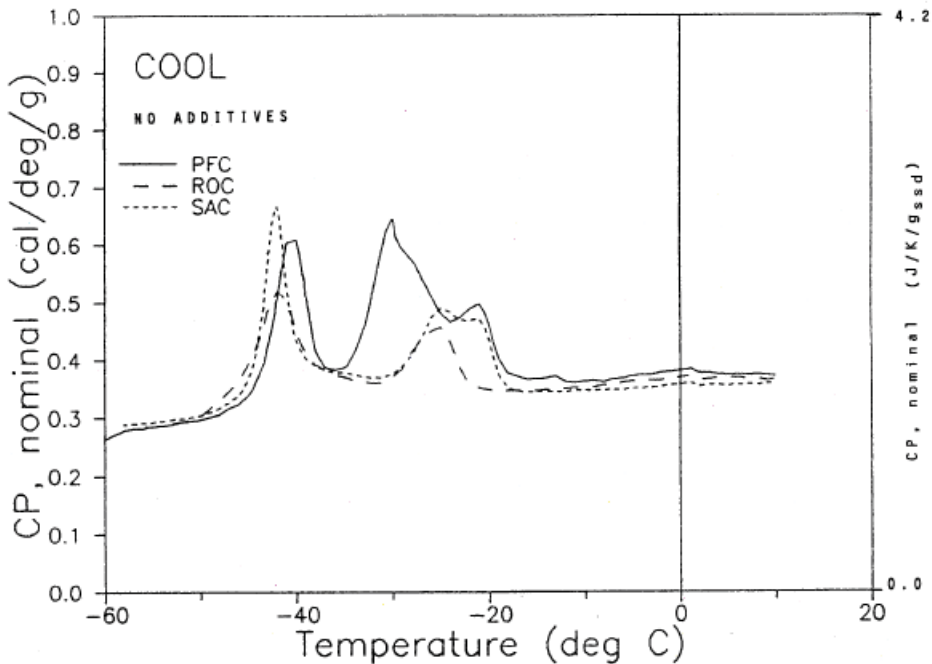
Fig. 2.16: Freezing curve for cement paste with fly ash (PFC), Rapid hardening cement (Roc) and sulfate resistance cement (SAC) (Villadsen, 1992)

In the Fig. 2.16, it is possible to observe that the peak in the range of large percolated capillary pores (0 to -20°C) was not observed for old samples (over 80 days). This may be due to larger pores becoming disconnected (de-percolated) at old ages. A higher peak of frozen pore solution is observed in the range of -20 to -35°C (gel range) for cement paste with fly ash (PFC) if compared with rapid hardening cement (Roc) and sulfate resistance cement (SAC). It may be explained by the fly ash reaction, where extra volume of C-S-H is formed.

The desorption and adsorption isotherms for cement pastes with and without slag (50% and 85% of addition), fly ash (50% of addition) and silica fume (10% of addition) cured saturated for 4 and 18 months using dynamic water sorption are given by Belie et al. (2010), see Fig. 2.17. The water/binder ratio varied from 0.33 to 0.50. Super-plasticizer (polycarboxylate) was used for some mixes, identified by SP. The samples were crushed in particles of 0.5 to 1 mm. The time to reach

equilibrium was around two weeks. The water content mass was expressed by the percentage of the sample mass in dry state (i.e. 3% of RH).
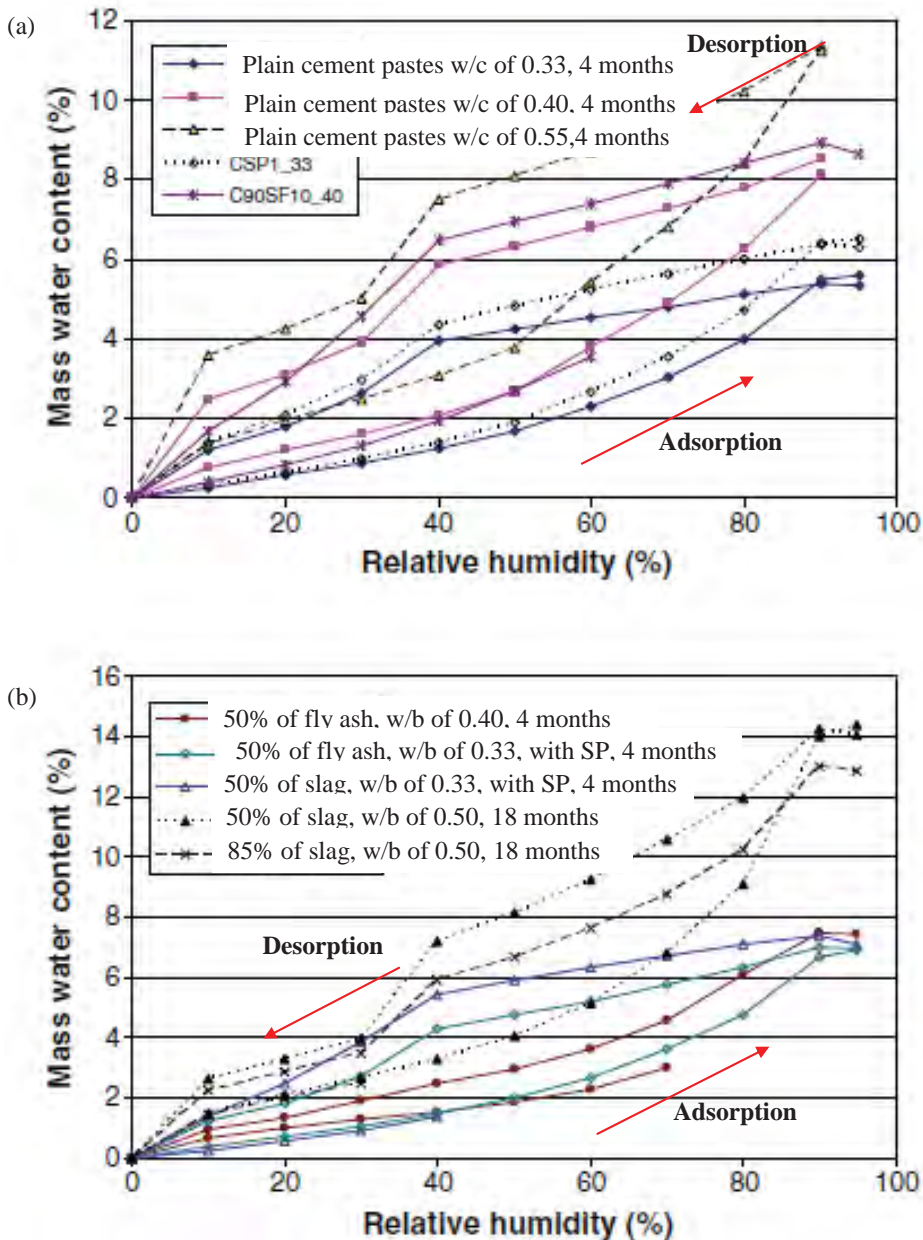
Fig. 2.17: Isotherms for (a) plain cement pastes and with silica fume addition(b) pastes with slag and fly ash addition (Belie et al., 2010). Legend was modified for a better identification of the curves

By the sorption isotherms it is possible to observe a slightly decreased porosity for SCMs pastes cured for 4 months, see Fig. 2.17. It is important to say that carbonation was found in the samples, specially the samples with fly ash (Belie et al., 2010). Carbonation may change the pore structure of the pastes.

The autogenous shrinkage for concrete with and without slag cured sealed at 20ºC for 28 days and w/b ratio of 0.45 is illustrated in the Fig. 2.18 (Darquennes et al., 2011). Three types of cement were used and identified by: CEM I- plain cement pastes, CEM III/A – 42% of slag addition and CEMIII/B- 71% of slag addition. Lower value of autogenous shrinkage for plain cement concrete is observed at 28 days when the time zero of the test is after setting of the pastes; see Fig. 2.18(b). The author used as the time-zero the final setting time of the concrete (about 10 hours). High values of autogenous shrinkage found for the concrete with slag may indicate that the material is more susceptive to cracking (Darquennes et al., 2011, Darquennes et al., 2009, Jensen and Hansen, 1999, Jiang et al., 2005).
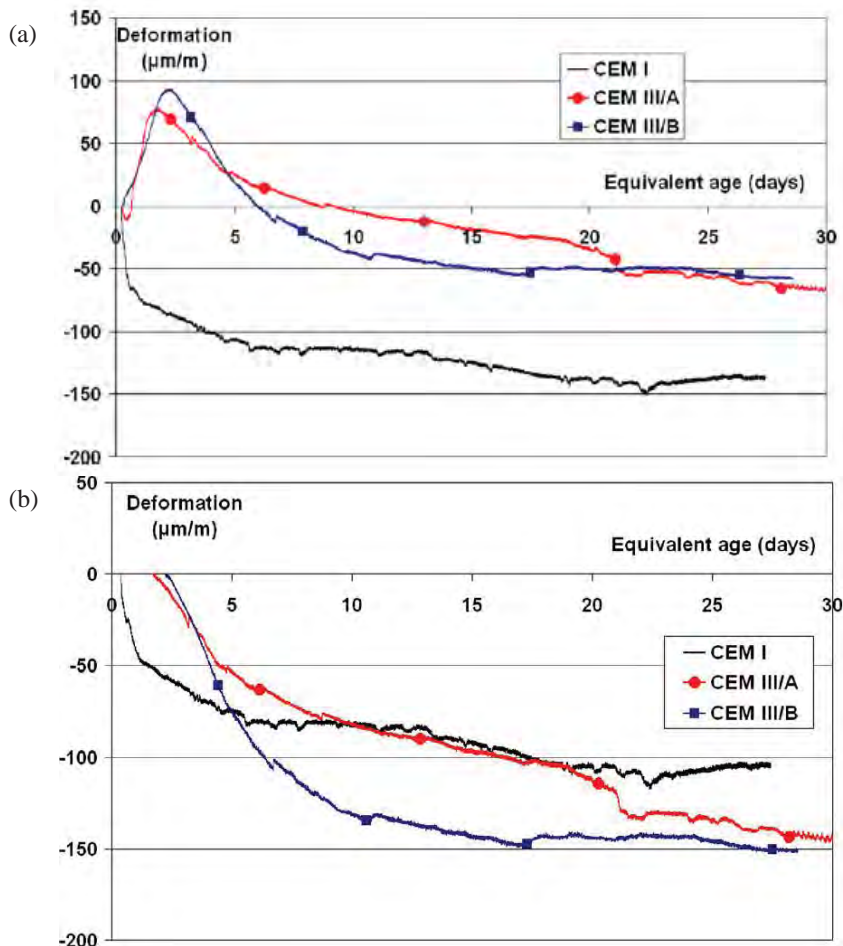
Fig. 2.18: Autogenous shrinkage of the concrete with and without slag cured sealed at 20ºC for 28 days (Darquennes et al., 2011) (a) time-zero initial setting; (b)time-zero final setting

The graph for diffusivity versus time for pastes with 25% of fly ash addition is illustrated in the Fig. 2.19(Bijen, 1996). Further details about the paste and test procedure were not given by the author. Decreased diffusivity found for fly pastes may indicate a more compact and less porosity structure, which has a major beneficial effect with respect to the protection of reinforcement against chloride-initiated corrosion. According to Bjen (1996) the effect of the SCMs on the pore structure is rather reflected in the diffusivity of ions, and not so much in the permeability.
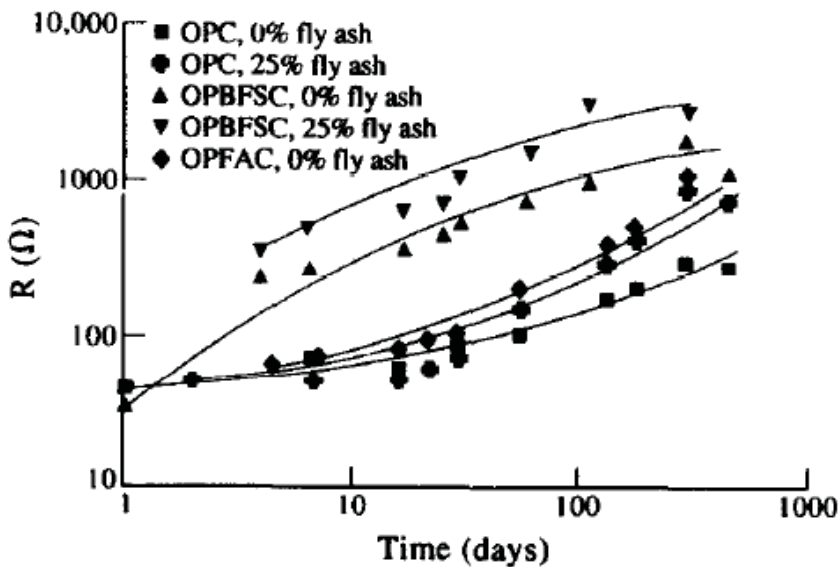
Fig. 2.19: Ohmic electrical resistance of concrete with and without fly ash: OPC = CEM I, OPBFSC = CEM III (Bijen, 1996)

Experiments carried out by Marsh and Day (1985) for plain cement and with 43% of fly ash pastes cured saturated (by weight) at different temperatures (20, 35, 50, 65 and 80ºC) at water/binder ratio of 0.47 using evaporable water (oven at 105ºC) are given in the Fig. 2.20. The total porosity is related to the evaporable water loss. The plain pastes showed a decrease in total porosity with time. However, the blended pastes showed first a reduction and then an increase of the total porosity. The author explained that fact based on the conversion of portlandite to a porous calcium silicate hydrate (pozzolan reaction) (Marsh and Day, 1985). This in contraction of what is expected for pastes with SCMs where an increase of the volume of solids and decrease of the pores is observed, see in (Atkins et al., 1992, Chen and Brouwers, 2007, Fernandez- Altable, 2010).
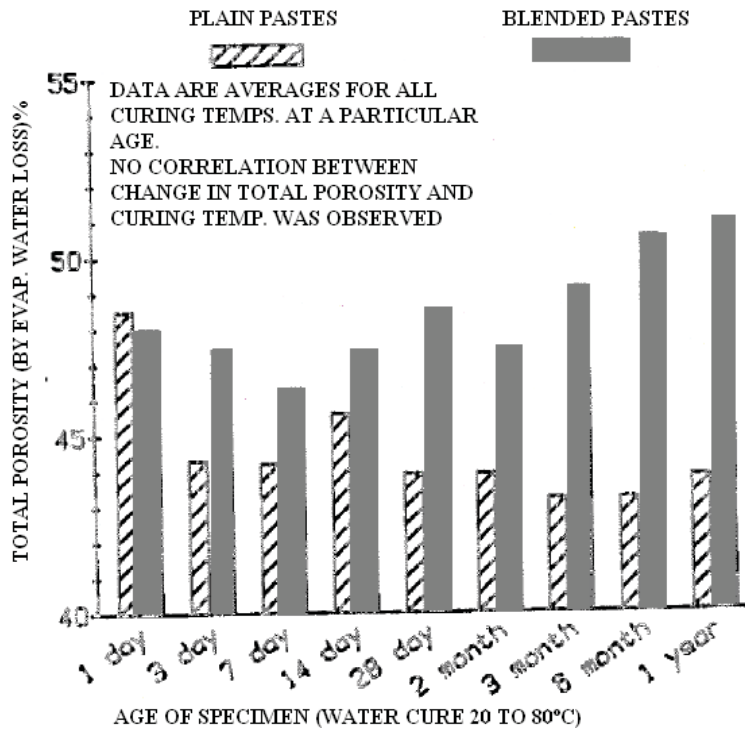
Fig. 2.20: Total porosity for plain and blended cement pastes (Marsh and Day, 1985)

Predictions of hydration for cement pastes with and without slag addition cured saturated; assuming w/c=0.5 and 70% of degree of hydration of slag was conducted by Chen and Brouwers (2007).

Fig. 2.21 shows that the C-S-H is the dominant phase and it is slightly increased with slag addition. Also with the increase of slag addition the amount of capillary pores is increased, especially with 50 to 100% of slag addition.
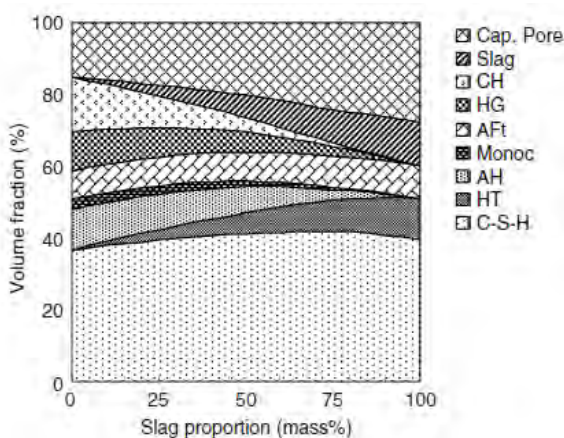
Fig. 2.21: Prediction of hydration products in slag blended
cement paste (Chen and Brouwers, 2007)

2.5 Impact of casting and curing conditions on the pore structure

2.5.1 Mixing

Time and intensity of mixing may have an impact in the rheological properties, homogeneity and consequently the pore structure of cement based materials (Brown et al., 1990, Macaulay et al., 2002, Yang and Jennings, 1995).

Williams et al. (1999) suggested that agglomerated network of cementitious material may be broken as shear rate of mixing is increased. Yang and Jenning (1995) investigated cement paste at low and high mixing intensity and it was found that low speed mixer results in a high agglomeration of the grains as large as mm size, whereas at high speed the agglomerates are eliminated.

2.5.2 Temperature

A heat source is already presented in the exothermic reactions during the hydration of cementitious materials. In addition, a combination of factors (e.g. hot weather, accumulated heat of hydration or steam curing) may lead to a raise in temperature during the curing of cement based materials. Hot weather for instance, have adversely influence on the behavior of cementitious materials mostly reported as the increase in the rate of hydration (Goto and Roy, 1981, Zhang, 2007). Thomas and Jennings (2008) suggested that the effect of temperature is not evident to samples cured at up to 40ºC. As cementitious materials are considered as a poor conductor of heat, the heat dissipation is much slower than the heat release in its mass. Elevated curing temperature is also used for the precast concrete industry to accelerate curing providing an early strength and fast de-mold of the building materials.

Studies have showed that curing temperature has an impact on the pore structure of cement based materials (Goto and Roy, 1981, Lea, 2004, Zhang, 2007, Kjellsen et al., 1990a). Like most chemical reactions, cement hydration proceeds more rapidly with increasing temperature. With rapid hydration, the cement products are diffused to a significant distance from the cement grain resulting in heterogeneous distribution of the solid phases. Moreover, C-S-H density and hydrated products of the cement paste varies with the increase of temperature. Jennings (2007) suggested a lower density of C-S-H structure for cement pastes cured at 20ºC analyzed by angle neutron scattering (SANS) when compared with pastes cured at increased temperature (60ºC). In agreement with Jennings studies, Zhang (2007) reported the increase of C-S-H density for pastes cured at high temperature observed by SEM, see Fig. 2.22(a).

Raise in curing temperature may also alter the equilibrium assemblage of solid cement phases. Particular examples are AFt and AFm phases which are strongly related to the curing conditions (moisture and temperature) of the hydrated products, as the ettringite is more stable than monosulfate at ambient temperatures. At temperature above 50ºC monosulfate is increasingly formed from ettringite and monocarbonate, see Fig. 2.22(b). Lack of ettringite during initial curing can lead to a delayed ettringite formation (DEF) known as an expansive agent of cement based materials. Changes of hydrated products may results in a decrease of volume of solids and an increase of porosity (Lothenbach et al., 2008, Thomas et al., 2003).

(a)
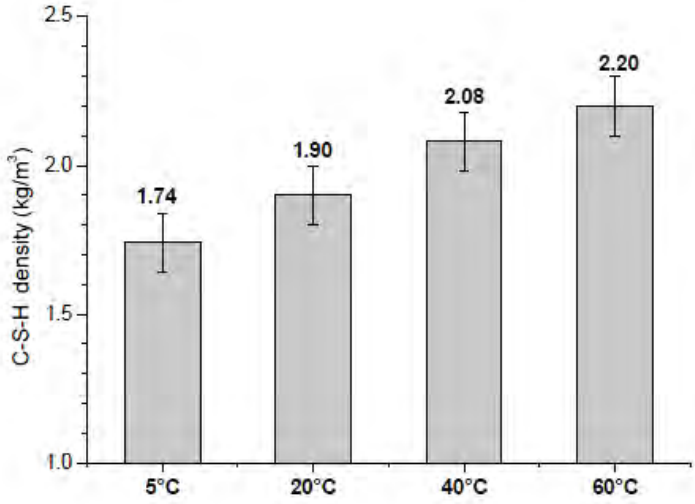
(b)
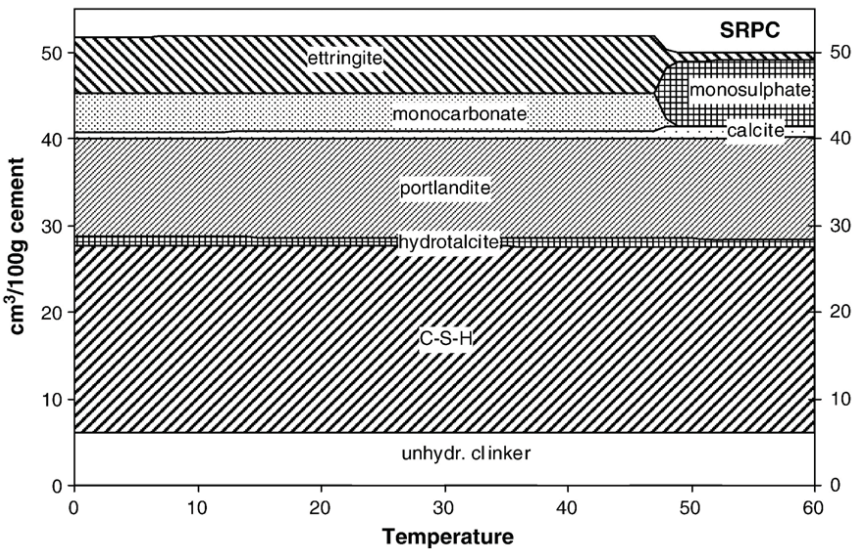
Fig. 2.22: (a) Density of C-S-H cured at different temperatures for cement pastes (Zhang, 2007) and (b) varying reaction products due to the increase of curing temperature (Lothenbach et al., 2008)

Fischer and Kuzel (1982) findings show that curing conditions (moisture and temperature) have an impact on the AFm phases, see Table 2.8. Fig. 2.23(a) shows the degree of hydration of the cement pastes at varying curing temperature (5, 20, 40 or 60ºC) and w/c ratio of 0.4 determined by SEM (Zhang 2007). It is possible to observe a high difference in the degree of hydration for pastes cured at varying temperature at early age; however this effect is not so evidence for pastes cured at later ages. In agreement with data showed by Zhang (2007), Haha et al. (2009) found similar data for degree of hydration for cement pastes cured at 20 and 85ºC at later ages (28, 90 and about 5 years), see Fig. 2.23(b).

Table 2.8: AFm phases at different curing conditions (RH and temperature) (Fischer and Kuzel, 1982)

Composition	Relativity humidity (%)	Temperature (ºC)
C_4AH_{19}	>88	25
C_4AH_{13}	11-81	25
C_4AH_{11}	25	40
$C_4AC_{0.5} H_{11}$	*	35
C_4ACH_8	*	95
C_4ACH_6	*	130

*value not given.

| (a) | (b) |
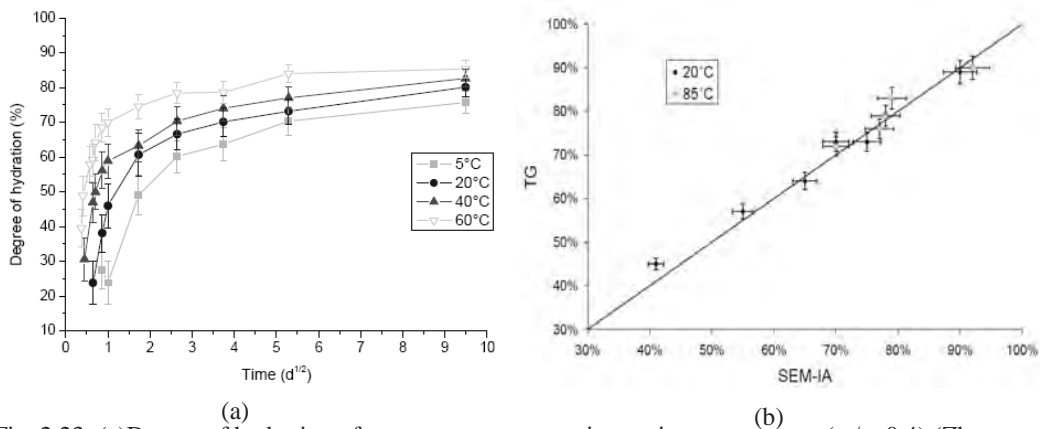
Fig. 2.23: (a)Degree of hydration of cement pastes at varying curing temperature (w/c=0.4) (Zhang, 2007) and (b)degree of hydration for cement pastes tested by SEM and TG (Haha et al., 2009)

Investigation with cementitious hydrated materials cured at high temperature have shown the coarsening of the pore structure parameters, e.g. (Escalante-Garcia and Sharp, 2001, Vodák et al., 2004, Zhang, 2007). Roy et al (1982 , 1993) investigations on the effect of temperature on the pore structure of cement pastes containing 60% of slag substitution cured at 27, 45, 60 or 90ºC and varying w/b ratio (0.3, 0.4, 0.5 or 0.6) by MIP are shown in the Fig. 2.24(a). It is important to emphasize that the degree of hydration of the pastes cured at varying temperature was not determined. At curing temperatures of 60ºC a similar or slight reduction of the pore volume is possible to observe for pastes cured for 14 days. At 28 days a great impact of the curing temperature is observed for pastes cured with w/c ratio of 0.4. For the others, a sharp impact was not noticed. Investigation carried out by Kjellsen (1990a) for plain cement pastes hydrated at 5°C , 20°C , and 50°C at the same degree of hydration (70%) and w/c ratio of 0.50 tested at mercury intrusion porosimetry (MIP) showed that increasing the curing temperature results in increased porosity, see Fig. 2.24(b). No information was given by the author on how the degree of hydration was determined. Haha et al. (2009) found a larger porosity for pastes cured at 85ºC when compared with pastes cured at 20ºC observed by SEM images, see Fig. 2.25.

Experiments conducted by Bentur and Berger (1979) on alite cement pastes by MIP showed a larger threshold pore size for pastes cured at 65ºC when compared with similar samples cured at 4ºC and

Experiments conducted by Bentur and Berger (1979) on alite cement pastes by MIP showed a larger threshold pore size for pastes cured at 65ºC when compared with similar samples cured at 4ºC and 25ºC. Cao (1995) and Kjellsen (1990b) reported for plain cement pastes with a w/c ratio of 0.5 cured at elevated temperatures tested by scanning electron microscopy (SEM) that a coarser and interconnected pore structure is found for pastes cured at high temperature. Verbeck and Helmuth (1968) studies of mechanical properties showed a decreased strength of cement based materials cured at high temperature.

(a)   (b)
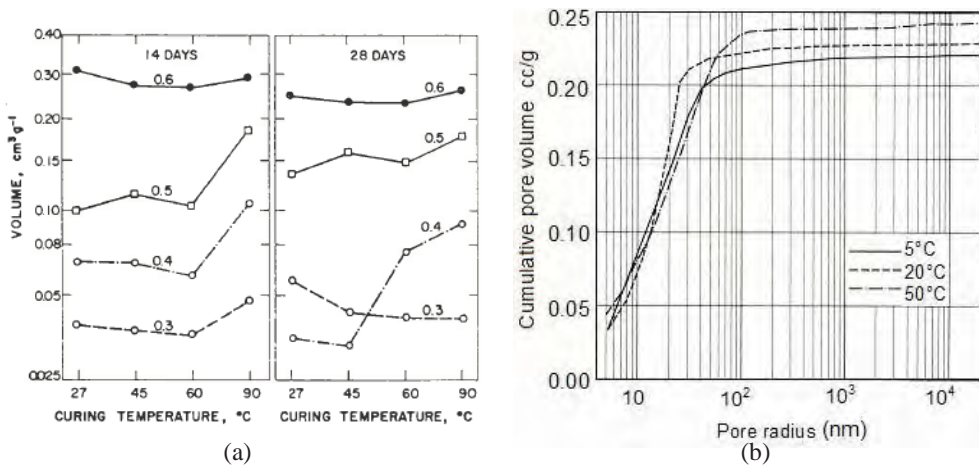
Fig. 2.24: (a) Volume of pores for cement paste with 60% of slag addition at different temperatures and w/c ratios of 0.3 to 0.6 by MIP (Roy et al., 1993)and (b) Cumulative pore size distribution at MIP of cement paste hydrate at 5°C, 20°C and 50°C with a degree of hydration of 70% Kjellsen (1990a).
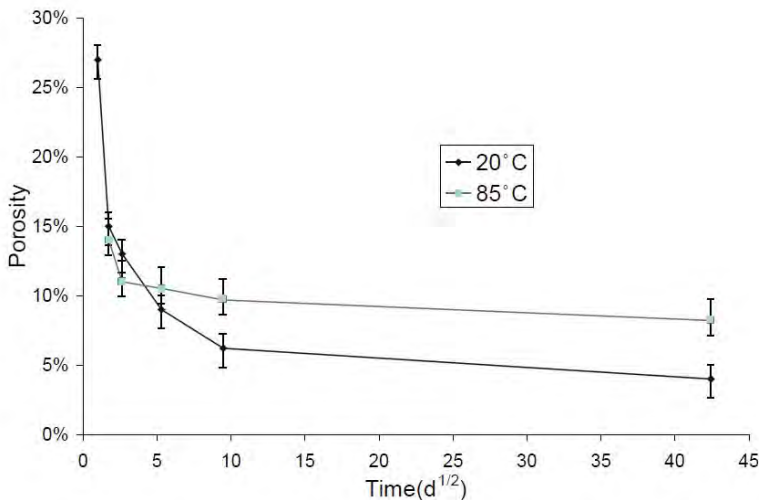
Fig. 2.25: Porosity data determined by SEM versus time for cement pastes cured saturated (Haha et al., 2009).

2.5.3　Moisture

The moisture content of cement based materials depends on several factors: constituents, water/ cement (w/c) ratio, relative humidity, and the size of the elements (Canada, 2006, Hedenblad, 1997).

Physical-chemical properties of the cement based materials such as particle size and use of aggregates may change the moisture content of the hydrated products. Materials with a higher specific surface area requires larger amount of water to hydrate. Furthermore, the water/cement (w/c) ratio of the pastes may be explored in the context of moisture. Samples with a lower w/c ratio may have excess of remaining unhydrated cementitious grains. On the other hand, high w/c ratio may lead to bleeding, high porosity and weak compressive strength. An optimum w/c ratio for the hydration of the grains and workability of the specimens may be given for each mix, improving therefore the engineering properties.

Relative humidity (RH) of the environment, the amount of water vapor in a gaseous mixture of air and water, is an important key regarding to moisture of the cementitious materials. The evaporation rate from a cementitious material is strongly influenced by the relative humidity. Freshly cast cementitious materials have an abundance of water, but as drying progresses from the surface inward and hydration of the products proceeds, the relative humidity of the paste may change. The amount of unhydrated products is increased by low relativity humidity; cementitious materials must have over 80% (approx.) of relative humidity to proceed the hydration (Hedenblad, 1997). Studies carried out by Griesel and Alexander (2001) showed the influence of relative humidity in PC concrete exposed to a RH from 50% to 65%, and it was possible to observe that microstructure did not change significantly. However, for concrete cured at 82% RH, significant improvements in the microstructure were noticed.

According to Bentz and Stutzman (2006), cement pastes cured under sealed conditions will self desiccate creating a coarse capillary pores, see Fig. 2.26. On the other hand for saturated curing, the capillary porosity is water filled and accessible to the growing hydration products therefore at this condition the degree of hydration will be maximized and smaller empty pores will be formed.

(a) saturated　　　(b) sealed
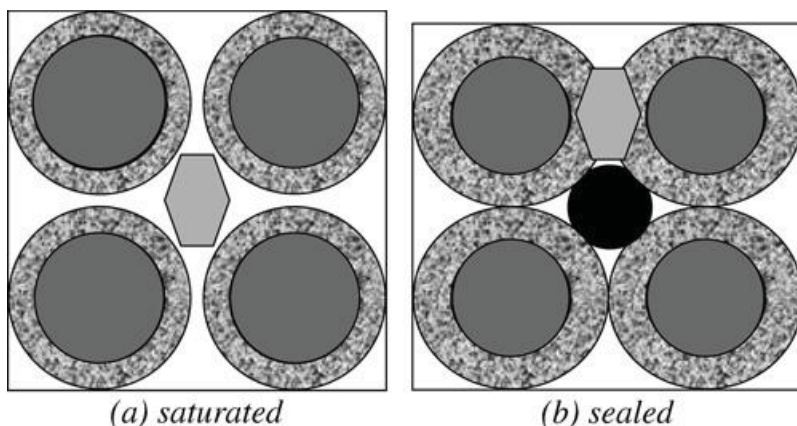
Fig. 2.26: Particle model for cement paste at (a) saturated and (b) sealed conditions for hydrating cement past. Dark gray is unhydrated cement grains, textured and light gray are hydration products, white is water-filled porosity, and black is empty pores (Bentz and Stutzman, 2006).

Bentz and Stutzman (2006) observed large capillary pores for pastes cured sealed when compared with saturated pastes analyzed by SEM. Furthermore, for sealed and re-saturated pastes de-percolated capillary pores (absence of the peak at -15ºC) were noticed by low temperature calorimetry (LTC).

Studies carried out with saturated and sealed concrete with 0%, 8% and 16% of silica fume addition, cured at 20ºC for 90 days show similar results of strength for both conditions of curing: dry cured and wet cured, see Fig. 2.27.
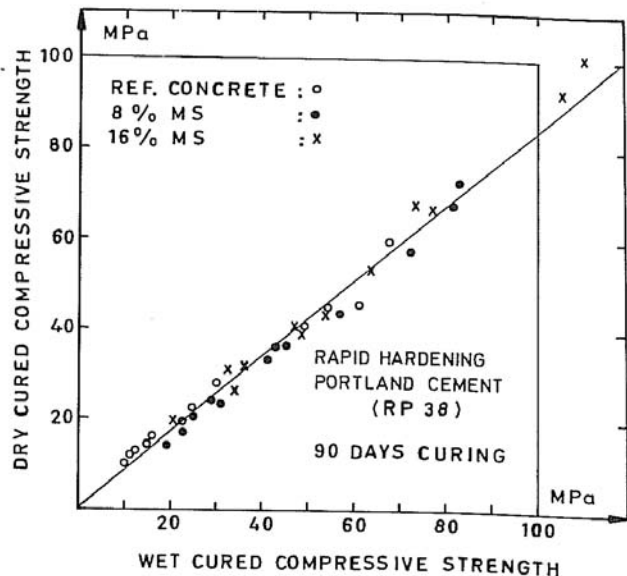
Fig. 2.27: Compressive strength for concrete with silica fume additions (8 and 16%) at sealed or saturated conditions (Sellevold and Radky, 1983).

2.5.4   Bleeding

Bleeding is the appearance of water on the top of the cement paste before it has set. This phenomenon is reported as a problem due to the alteration of homogeneity and water/cement ratio of the pastes in order to affect the engineering properties of cementitious materials.

Bleeding is a result of sedimentation, which may reduces de original spaces separating the particles (Powers, 1939b). The solid particles are separated from another far enough to permit some movement where the cementitious grains in suspension move downward. The final product of bleeding is a non uniform concentration of grain, where a layer of complete "*sedimentation zone*" is formed at the bottom whereas a layer of fluid appears on the top. Therefore, bleeding has an impact on the overall porosity; higher in the top part (bleeding) and lower in the bottom (Geiker, 1983, Maia et al., 2008).

Some mitigating methods may be applied for bleeding samples such as use of salts, superabsorbent polymer (SAP) and rotation of the sample after casting. The effect of use of some salt solutions was reported by Powers (1939a) where the relative bleeding rate was measured for different types of salt solutions (LiCl, KCl and NaCl), different values were found depending on the degree of salvation and adsorbability of the salts. The incorporation of superabsorbent polymer (SAP) particles in the cement-based material is also known as water filled control which may prevent bleeding of the samples. The method of rotation of the samples right after the casting is reported by some authors (Bager and Sellevold, 1986b, Villadsen, 1992), and it is used to reduce the sedimentation of the particles providing a more homogeneous paste. However, the use of rotation during the sample preparation may change the pore structure of the hydrated materials.

2.5.5   Entrapped air voids (air voids)

Entrapped air voids are irregular and small bubbles (about 3 mm) distributed through the cement paste (Mehta and Monteiro, 2006). The presence of air voids in cement paste is a result of mixing and placing of the cement paste and as a capillary pore it may change the pore structure of the cement based materials (Mehta and Monteiro, 2006). Often, entrapped air voids are measured through saturation of the paste at different levels or image analysis. By saturation of samples, vacuum saturation and pressure saturation methods are applied, see e.g. (Laugesen et al., 1997).

The volume of air voids is reported as about 2% of the volume of the material, according to the literature (NTBuild-368, 1991) this amount do not give marked change in its properties. The entrapped air voids in cement pastes at varying w/c ratio were investigated by Corr et al. (2002) and Rashed and Williamson (1991). A thin "shell" of paste was observed surrounded the entrapped air voids. Varying the water cement ratio of the pastes at high w/c ratio the air void "shells" were porous, while at low w/c ratio the "shells" were filled by hydration products.

2.5.6   Leaching

Leaching is the loss of calcium and soluble salts of the cement pastes to the environment. When cement based material is in contact with solution, ionic transfers occur between the external water and the pore solution which is a basic solution. The variation in the chemistry of pore solution leads to a dissolution of cement hydration products. Portlandite is the first mineral to be dissolved followed by C-S-H (Kamali et al., 2008). CH dissolution and the decalcification of C-S-H may increase the porosity of the surface layers of concrete. Leaching of calcium may also affect the core of the material and may have a negative influence on the engineering properties of concrete structures.

Leaching tests are mostly carried out by measurements of CH, pore solution content and porosity parameters, see in (NTEnvir002, 1995). In order to avoid leaching a limited amount of water is used for the saturated curing. Also, calcium hydroxide saturated solution instead of water is used for the curing under saturated conditions (Kocaba, 2009).

Marchan et al. (2001) studies found significant effect of CH dissolution on the diffusivity of hydrated cement paste using a hydration and microstructure development model. Carde and Fracois (1997) suggested that progressive decalcification of cement based materials leads to an increase in the porosity of cement paste by leaching. Van Gerven et.al (2007) reported that the small capillary pores diminish (<0.1 µm) and the larger capillary pores increases (>0.1 µm) when leaching takes place in cement pastes with 30% of flue gas cleaning residue tested by MIP. The measurements were undertaken after 225 days of leaching in an acidified leachant solution (distillated water and HNO_3). These results are in agreement with findings reported by Garboczi and Bentur (1996) and Kumar and Bhattzcharjee (2003a).

2.6 Impact of conditioning on the pore structure

2.6.1   Drying

Conditioning in form of drying is required as a first step when using some of the techniques for pore structure characterization (e.g. MIP and SEM). Different methods generates very unlike surface area and consequent pore structure for the cement pastes (Korpa and Trettin, 2006).

According to Korpa and Tretin (2006), the water present in the gel pore is more strongly bound and it can be removed by drying of the pastes. However, stresses related to surface tension of the receding water menisci generate a collapse of some of the fine pores of the pastes when oven drying is applied (Galle, 2001, Korpa and Trettin, 2006). Possible effects of drying on the cement based material are summarized in Table 2.9. Some of the drying methods usually used for cementitious materials are described with more details below.

Table 2.9: Effect of drying methods on hydrated cementitious materials (Galle, 2001, Korpa and Trettin, 2006, Scrivener, 1997, Taylor and Turner, 1987)

Drying methods	Possible effects on hydrated cementitious materials
Oven drying	Destructive effect on the microstructure, blurring the fine morphology of the hydrate phases and inducing micro-cracking.
Vacuum drying, D-drying and P-drying	May not remove all the water from the gel pores and prolonged vacuum collapse C-S-H structure
Freeze drying	Generate ice microcrystal in larger pores and compressive stresses in the finer porosity.
Solvent exchange	Dehydration of C-S-H and ettringite

Possible detrimental effects of drying may lead to a change on pore structure of pastes (Galle, 2001, Korpa and Trettin, 2006, Scrivener, 1997, Taylor and Turner, 1987). Roper (1966) studies of drying cement pastes at varying RH divided the drying mechanisms into four regions: 1) Drying to 90% RH produces relatively small shrinkage. Water is lost from large pores with associated small capillary stress; 2) drying down to 40% RH produces greater shrinkage for the amount of water lost, and this is attributed to smaller capillary pores and gel pores that are associated with larger stress; 3) a region between 40% and 20% RH showed relatively small shrinkage that is attributed to loss of adsorbed water; 4) drying from 20 to 0% RH is accompanied by loss of interlayer water, causing irreversible collapse in the structure (Roper, 1966). Jennings (Jennings, 2007) also showed that drying to 40% RH causes low density C-S-H structure to collapse and large shrinkage occurs.

Bager and Sellevold (1986) investigated the effect of drying of cement pastes at different RH using low temperature calorimetry, see Fig. 2.25. The re-saturation was undertaken by the increase of RH stepwise by water sorption and then vacuum saturation was applied.

A large peak in the range of capillary pore (0 to -20ºC) is observed for dried pastes from RH of 0.83 to 0.11; see Fig. 2.28 curves numbered from 4 to 8. They suggested a de-percolation of the pore structure for these pastes due to drying at RH lower than $0.83p/p_o$.
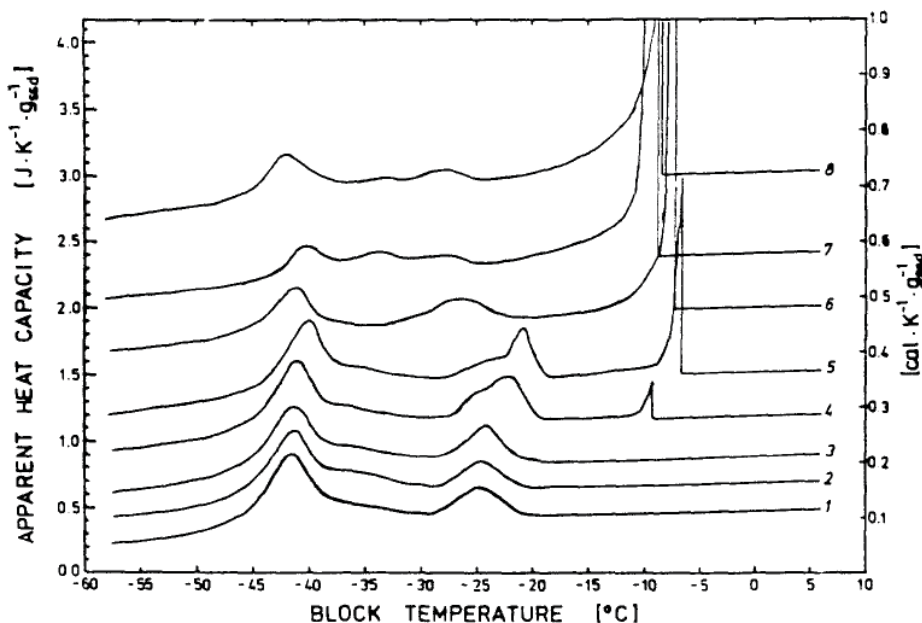
Fig. 2.28: Apparent heat capacity curves for cement pastes water/cement ratio of 0.4. Virgen samples (1), dried and re-saturated samples: p/p_o=0.97(2); p/p_o=0.92(3); p/p_o=0.83(4); p/p_o=0.75(5); p/p_o=0.58(6); p/p_o=0.33(7); p/p_o=0.11(8) (Bager and Sellevold, 1986b).

Oven drying

Oven drying is a widely used method to remove evaporable or non-evaporable water; however it is claimed to cause damage on the pore structure of the pastes(Beaudoin et al., 1998, Feldman and Beaudoin, 1991, Korpa and Trettin, 2006). A decomposition of some cement hydrated products with the increase of the temperature may also be observed (Table 2.10).

Table 2.10: Temperature of the decomposition of cement pastes phases (Taylor, 1997)

Compound	Temperature that the decomposition starts
Ettringite	60°C
Gypsum	80°C
C-S-H	<105°C

Feldman (1986) showed a larger volume of pores for fly ash pastes cured saturated at 35ºC for 1, 7 and 28 days dried by oven at 105ºC when compared with solvent exchange, see Fig. 2.29(a). For plain cement pastes the difference may be noticed for pastes cured saturated at 35ºC for 1 day, after 2 months of curing the curves seems to become similar (Fig. 2.29(b)). This suggested that drying may have different effects for plain cement and blended paste. In addition, great difference in drying by oven and solvent were found for the blended paste, where a coarser pore structure is found for oven drying. For that reason, organic solvent is suggested to be used on drying of cement pastes as it is a more gentle method.

(a)

(b)
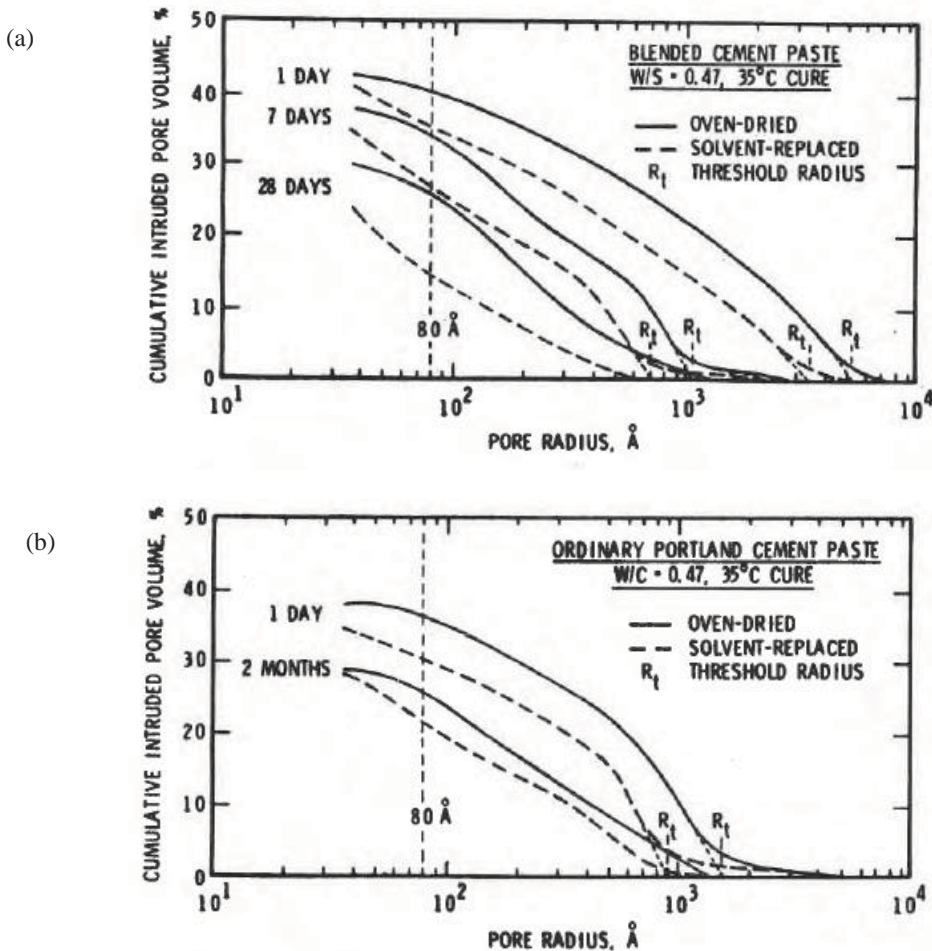
Fig. 2.29: Cumulative intruded pore volume (%) versus pore radius (Å): (a) for blended cement paste cured at 35ºC oven dried (full line) and solvent replaced (broke line) and (b) for plain cement pastes (Feldman, 1986b)

Solvent exchange

A large variation of organic solvents can be used for drying cement materials such as methanol, isopropyl or isopraponol, and acetone.

Some authors (Beaudoin et al., 1998, Feldman and Beaudoin, 1991) claimed that methanol may react with cement hydration products during the exchange process. Others (Parrot et al., 1980) reported that the pores of the pastes where the water has been removed by methanol were closed as a result of capillary tensions developed at relative humidities between 40% and 70%.

Taylor and Turner (1987) found different proportions of drying of C_3S by methanol, acetone and isopropyl alcohol. For C_3S pastes dried using methanol retained equilibrium with atmosphere of about 29.5%RH; for acetone 31%RH and isopropyl 32%, see Fig. 2.30 (Taylor and Turner, 1987). Korpa and Trettin (2006) emphasized that drying by solvent do not remove the gel water.

Studies with isopraponol indicate no reactive between solvent and the solids of cement paste (Beaudoin et al., 1998, Feldman and Beaudoin, 1991, Kocaba, 2009). But the literature is somehow contractive. Expansion of the pastes using isopraponol as a drying method were found by Beaudoin et al.(2000), especially for C-S-H with C/S of 1.6. Moreover, investigations (Beaudoin et al., 1998, Taylor and Turner, 1987) demonstrated that most solvents tend to be strongly adsorbed on the pore walls and cannot be entirely removed from the pastes.
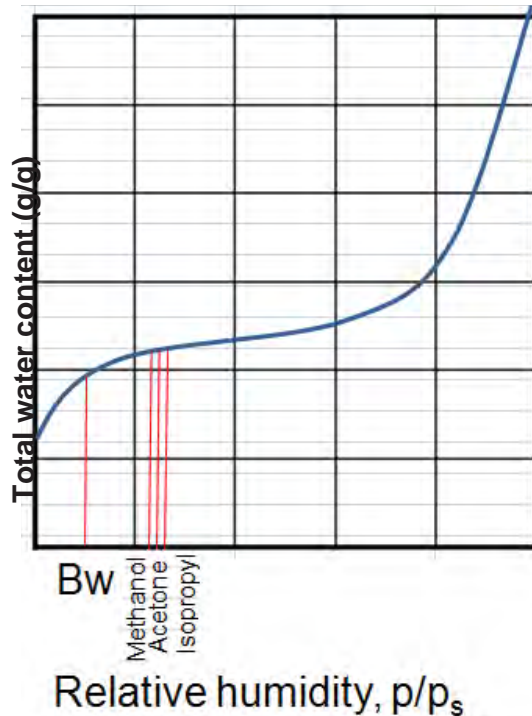
Fig. 2.30: RH of different drying methods applying solvent liquids (after(Taylor and Turner, 1987))

2.6.2 Carbonation

Carbonation may be defined as a liquid phase reaction of carbon dioxide (CO_2) with aqueous hydroxide and cations to produce carbonates. In cement based materials, carbonation results primarily in the conversion of portlandite ($Ca(OH)_2$) to calcite ($CaCO_3$), according to the Equation 2.8.

$$Ca^{+2} + 2OH^- + CO_2(aq) \longrightarrow CaCO_3 + H_2O \qquad \text{(Equation 2.8)}$$

C-S-H is also subject to carbonation at long term attack, which is decomposed into calcium carbonate and an amorphous silica gel as observed in the Equation 2.9.

$$C\text{-}S\text{-}H + HCO_3^- \longrightarrow CaCO_3 + SiO_2(gel) + H_2O \qquad \text{(Equation 2.9)}$$

Those reactions are accompanied by the neutralization of the cement matrix by the conversion of alkaline constituents to carbonates. A drop of pH from water pore water is expected normally associated with the dissolution of portlandite in non-carbonated cement (Gervais et al., 2004, Neville, 2002).

Carbonation may be measured by measurement of pH of the pore solution or by the methods which identifies the amount of calcite of the cement phases (e.g. thermo analysis, X-ray diffraction).

Roy et al. (1999) found significant carbonation for concrete expose to 52 to 75% of RH after eight or sixteen weeks in chambers with carbon dioxide (6% of volume). From 75%RH, a decreased carbonation depth was found. Ngala and Page (1997b) studies showed the influence of carbonation in the pore structure of cement pastes exposed to an atmosphere of 65% RH containing up to five percent by volume of carbon dioxide for several weeks. It was pointed out that the total porosity of cement paste measured by MIP and water desorption was reduced when exposed to carbonation and the capillary pores increased slightly. Dewaele et al.(1991) reported a reduced pore structure due to the carbonation as a consequence of the increase in solid volume expected when portlandite is converted to calcium carbonate.

2.6.3   Re-saturation

Re-saturation may be performed to obtain similar/comparable initial saturation conditions for samples cured at sealed conditions. Also, it is largely used to fill up air voids of saturated pastes, see e.g. (Laugesen et al., 1997 and Larsen-Helmes, 2008). Several ways of sample saturation are applied in cementitious materials (e.g. capillary suction, vacuum saturation, pressure saturation, salt solutions) as given in the Table 2.11.

Re-saturation of concrete has been investigated by Laugesen et al. (1997). They showed that vacuum saturation method applied for two days result in only half of the absorption obtained by capillary suction after 14 days. Experiments of re-saturation with concrete samples at higher w/c ratio (0.45 w/c) were also carried out; however, it absorbed less than half of the moisture lost during the drying. The conclusion obtained through the studies is that generally sample re-saturation is slow and the original water content (before drying) is not reached (Laugesen et al., 1997). Parrot et al. (1980) suggested that re-saturation of dried alite pastes using salt solution (water desorption) at varying RH (7% to 97%) increased the accessibility of the water, however the original condition is not reached. Some regions that were originally filled with water seem to become empty and inaccessible to water after drying (Parrot et al., 1980).

Table 2.11: Methods for sample saturation in cementitious materials

Method	Samples	Sample description	Procedure	Reference
Vacuum saturation	Concrete cylinder slices	Ø100x20 mm	Samples are evacuated (for 3 hours) then supplied with water. After submersion of 10 hours the weight is recorded.	(NTBuild-368, 1991)
Capillary suction	Concrete and mortar	Ø100x20 mm	Samples cured for 28 days are placed in oven at 40ºC for 7 days. Then, the sample is placed in a vessel with a water level of 1 mm. Weight is recorded at fixed intervals	(NTBuild-368, 1991)
	Concrete	Ø80x30 mm	Samples are placed in isopropanol, and then dried by vacuum for at least 1 day. The samples are exposed to water at a height of 1 mm. Weight is record at fixed intervals.	(Lamberet, 2005, Zhang, 2007)
Pressure saturation	Concrete cylinder		Samples are placed in a cylinder pressure filled with water and a pressure of 15MPa is applied for 24 hours	(Henrichsen et al., 1997)
Salt solutions	Cement paste	Ø from70 to 110 mm; or 20 to40 g	Samples are kept in desiccators with a salt solution at give RH under vacuum until it reaches equilibrium.	(Baroghel-Bouny, 2007a)
	Pastes	22.6 Ø and 2-3 mm of thickness		(Villadsen, 1992)
	Powder	150 to 250 μm, 1 gram		(Powers and Brownyard, 1947)
	Powder	< 2 mm		(Kjeldsen, 2002)

Bager and Sellevold (1986) studies used sorption at varying relative humidities as a re-saturation method for cement pastes, see procedure below (Table 2.12). The age of the samples were not given by the author.

Table 2.12: Saturation procedure for cement pastes adopted by Bager and Sellevold (1986b).

Step	Time	Method of saturation
1	4 days	Placed over a NaBr solution (0.58 p/ps) in desiccators
2	4 days	Placed over a KNO_3 solution (0.92 p/ps) in desiccators
3	1 day	Placed over a water at atmospheric pressure
4	7 days	Placed over a water at saturated vapour pressure
5	1 day	Immersed in water at atmospheric pressure
6	2 days	I immersed in water at vapour pressure
7	2 days	Immersed in water at atmospheric pressure

3 Porosity characterization

This section deals with the porosity characterization of cementitious hydrated materials. How should a pore space be defined? What is the borderline between the types of pores? How can we classify them? They were some of the questions raised during this work; and they may not have a simple answer. The pore characteristics (e.g. threshold pore size, total pore volume) are also described in this section. Pore structure models used in the literature are presented here to give a better idea on how complex the pore structure is and possible ways to describe it. Finally, methods to measure porosity such as low termperature calorimetry (LTC), mercury intrusion porosimetry (MIP), scanning electron microscopy (SEM) are here described.

3.1 Models for porous cement based materials

Microstructure

Microstructure models are often used to idealize representations of the complex pore network in the hydrated materials (Feldman and Sereda, 1968, Jennings, 1999, McDonald et al., 2010, Mehta and Monteiro, 2006, Mindness et al., 2002, Powers and Brownyard, 1947). Both, Powers and Jennings (Jennings, 1999, Powers, 1960) have suggested a granular model for C-S-H, proposing two kinds of this material with different porosity and density, see Fig. 3.1. Whereas others (Feldman and Sereda, 1968, Mehta and Monteiro, 2006, Mindness et al., 2002), proposed sheets with disorganized structure which are focused on the internal structure of the glanular module.

The differences in the microstructure models are based on the considered C-S-H structure, see Fig. 3.1. Jennings (1999) based the model on the nitrogen surface experiments, he suggested a globule structure which pack together to form two types of C-S-H gel: high density (1,670 kg/m³) and low density (1,400 kg/m³). According to McDonald et al. (2010) two types of water are presented in the C-S-H structure; intra C-S-H sheets and inter C-S-H particles. Powers (1960) recognized that the inner and outer products might differ in porosity, but considered that the hydration product would tend towards a uniform porosity.

It should be stressed that the borderline between water sheets of C-S-H and chemically bound water is not clear. McDonald and co-workers (2010), Ballonis and Glasser (2008) reported difficulties to distinguish between bound and free water in cement based materials.

(a)

C - Capillary pores

(b)

x - Interlayer water
o – Adsorbed water

(c)

C - Capillary water
I - Interlayer water
P - Physically adsorbed

(d)

P - Capillary water
M - Micropore
I - Interlayer pore

(e)

N₂ inaccessible pore

(f)

IntraC-S-H she
po

InterC-S-H gel
pore
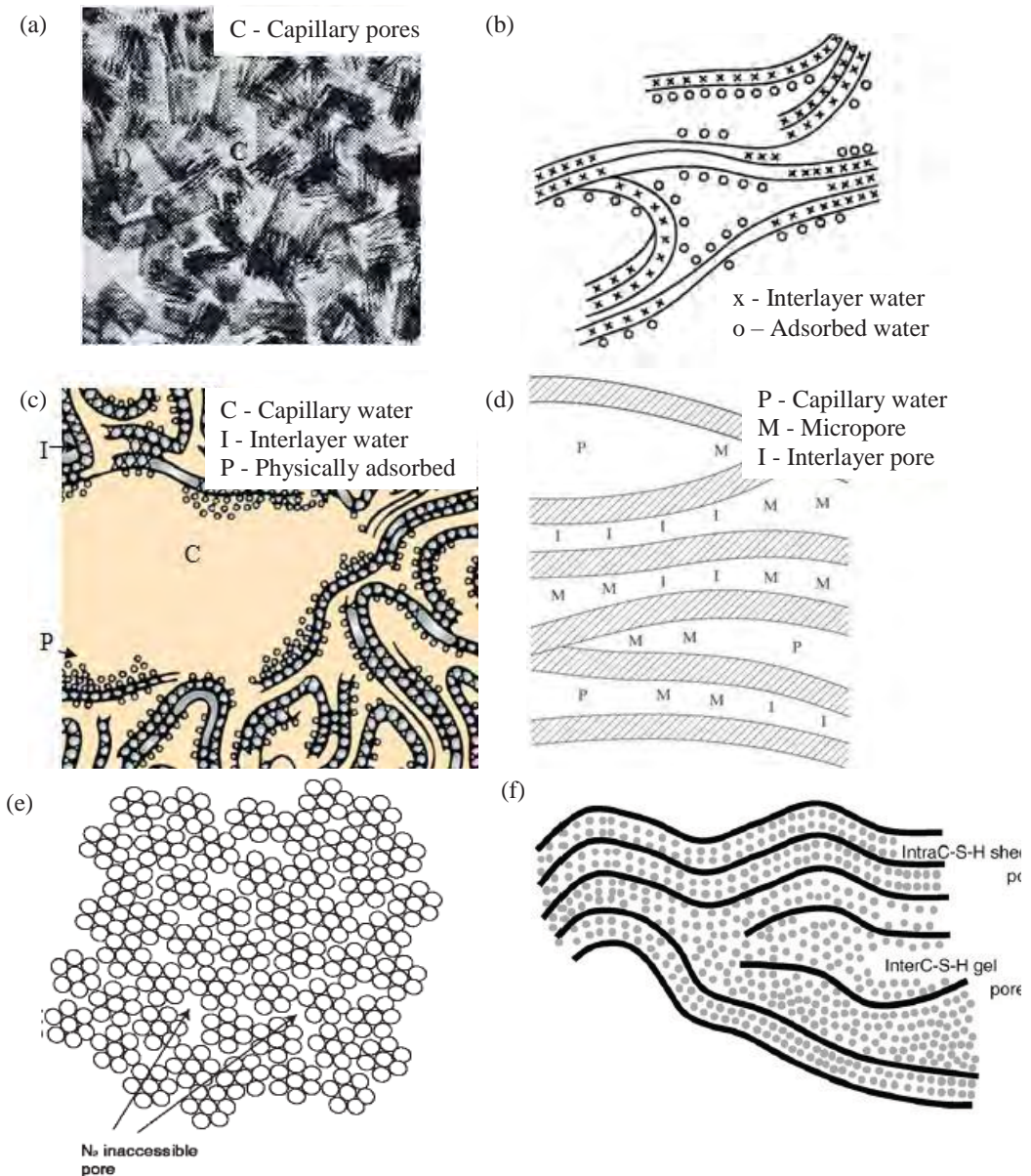
Fig. 3.1: Models used for C-S-H structure: (a) Powers (1960); (b) Feldman and Sereda (1968); (c)Mehta and Monteiro (2006) 4); (d)Mindness et al.(2002); (e) Jennings (1999); (f) McDonald et al.(2010)

Information on the microstructure and accurate measurements to correlate microstructure and pore size are still missing to fulfil questions raised in the past years. Is the pore system change between inner and out C-S-H? Intra C–S–H sheet pores and inter-C–S–H particle gel pores? Progress in the study of pore structure by electron microscopy and other methods along with mathematical

modelling of microstructure has begun to provide answers to these and similar questions (Gallucci et al., 2010, Gallucci et al., 2007, Lothenbach, 2008, Richardson, 2008). Moreover, recent studies with ^{1}H NMR relaxation revealed new findings for the size of C-S-H gel, see in (McDonald et al., 2010).

Despite a great number of models and studies, pore structure formation in hydrated cementitious materials is not fully understood. Pore structure is very complex and it changes according to the physics and chemical properties of the cement replacement by SCMs and curing conditions, which makes it difficult to model and describe it in detail. The present study, once more, has the aim to give contributions for the pore structure characterization of hydrated cement pastes by different methods. The overview of the porosity measurements will allow a better understanding of the complex structure of pores.

Predictions of porosity development

Current literature presents a series of potential models to predict the evolution of the pore structure system and the microstructure of cement based materials (Lothenbach et al., 2008, Chen and Brouwers, 2007, Atkins et al., 1992)

Power's model is still a powerful tool to predict the evolution of the pore structure, and in some extend it also evaluates the effects of different w/c ratios, age and degree of saturation on the pore structure. This model divides the hydrated paste in un-reacted cement, hydration products, gel water, capillary water and pores, see Fig. 3.2. However, Powers' model is used only for plain cement paste cured at 20ºC and it is based on assumptions (e.g. cement has the same chemical and physical properties that the one Powers and Brownyard proposed). An extension of Powers' model using silica fume was proposed by Bentz et al. (2000). At present, modeling based on

Fig. 3.2: Powers' model ((Jensen, 2010b) after (Powers and Brownyard, 1947))

thermodynamic approaches is available to predict phase assemblage of cementitious materials (see e.g. (Lothenbach et al., 2008, Chen and Brouwers, 2007, Atkins et al., 1992)). These models predict the solid and solution chemistry of plain cement or blended cements hydrated materials for use in equilibrium modeling.

3.2 Pore parameters characteristics

Porosity of hardened paste is likely to be misleading unless the term is properly qualified. This section proposes the characterization of the porosity according to the pore characteristics of pore threshold, pore size and pore volume, see Fig. 3.3.

<table>
(a)	(b)	(c)
</table>
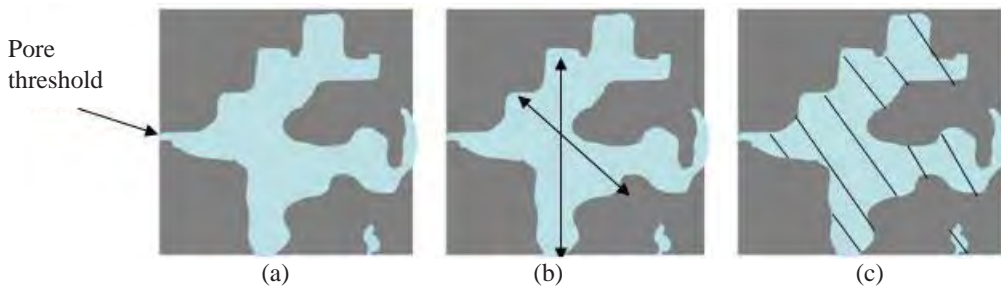
Fig. 3.3: Pore characteristics: (a) pore threshold; (b) pore size and (c) pore volume

3.2.1 Threshold pore

Threshold pore is related to pore connectivity (Fig. 3.3(a)). It is defined as the minimum diameter of channels that are essentially continuous ("percolated") through the sample (Winslow and Diamonds, 1970). The threshold pore size is considered relevant for the assessment of the resistance to transport of substance in the material (Hooton, 1986, Nilsson, 2002) .

3.2.2 Pore size

Pore size may be defined as the size of the empty or spaces filled with water of hydrated cementitious materials (Fig. 3.3(b)). Radius of a pore is often measured by direct (SEM) or indirect methods (e.g. MIP and LTC). One way to estimate the average size of a pore radius is through the stereological theory, as hydraulic pores (r_h), see Equation 3.1. The stereological theory is often used for image analysis of micrographs from scanning electron microscopy (SEM), it uses a three-dimensional structure based on a two-dimensional plane, see in (Dehoff and Russ, 2000).

$$r_h = \frac{2 \cdot A_p}{P_p}$$

(Equation 3.1)

Where
r_h Hydraulic radius, m
A_p Cross section area of pore, m²
P_p Perimeter of the pore, m

For indirect methods assumptions and theoretical equations are used to determine the size of pores radius. For instances the pore size measured by LTC, where the Kelvin Equation is applied to estimate the curvature radius *r*. See Section 3.3 for further details.

3.2.3 Pore volume

Pore volume is the total fraction of spaces: empties and/or filled by pore solution (Fig. 3.3(c)). The pore volume may be given as total pore volume, effective pore volume and filled pore volume, as given in the Table 3.1.

Table 3.1: Pore volume: total, effective and filled porosity

Pore volume		
Total pore volume	**Effective pore volume**	**Filled porosity**
Includes both open and closed pores (Haynes, 1973a, Haynes, 1973b)	Fractional volume of open and interconnected pores with respect to the bulk (total) volume of the material.	Fractional volume of filled pores (e.g. by water, by mercury) with respect the bulk (total) volume of the material
☐Measured volume	☐Measured volume	☐ Measured volume

In the calculation of volume of pores, the density of the material is used (Table 3.2), for example for mercury filled porosity the volume of pores may be determined by (Equation 3.2):

$$V_p = m_{Hg}/\rho_{Hg}$$ (Equation 3.2)

Where

V_p	Volume of pores, cm³
m_{Hg}	Mass of filled mercury, g
ρ_{Hg}	Density of mercury, g/cm³

Table 3.2: Different types of density of the materials (Atkins, 1997)

True density (ρ_{true})	**Apparent density ($\rho_{ap.}$)**	**Bulk density (ρ_{bulk})**
Density of the material excluding all the pores and voids. Related to the total volume of pores	Density of the material including some portion of the pores and voids	Density of the material including all pores and voids

3.3 Methods to characterize pore structure

This section deals with selected methods used to characterize pore structure in cementitious materials. The selected methods for this work are low temperature calorimetry (LTC), mercury intrusion porosimetry (MIP), scanning electron microscopy (SEM) and water sorption.

According to Powers and Brownyard (1947), the total pore space in a saturated system may be measured by the total evaporable water. However, the determination of pores may be more complex than they thought and do not always yields the same value, especially if it involves removal or addition of water. Drying is reported as a factor which may damage the pore structure of cement based materials (Bager and Sellevold, 1986b, Espinosa and Franke, 2006, Korpa and Trettin, 2006, Parrot et al., 1980). Methods to characterize pore structure are generally based on physical relationships and geometrical models that simplify the complex structure of the pores. Hence, the data may provide an erroneous picture of the pore system of cement based materials. In addition, no

single technique can adequately characterize all of the important components of the pore system covering the large range of pore sizes (from a few nanometres to tens of micrometers), see Fig. 3.4.

For those reasons, the reader must be aware when comparing porosity data from varying methods. In an attempt to clarify and limit the errors in the interpretation of pore structure data this section has the aim to point out their limitations and the assumptions of the methods here used. Furthermore, procedures of the selected methods are given in the Appendixes (X to XIII) and guidelines containing information on how to measure the porosity is given at the end of this work (Chapter 5).
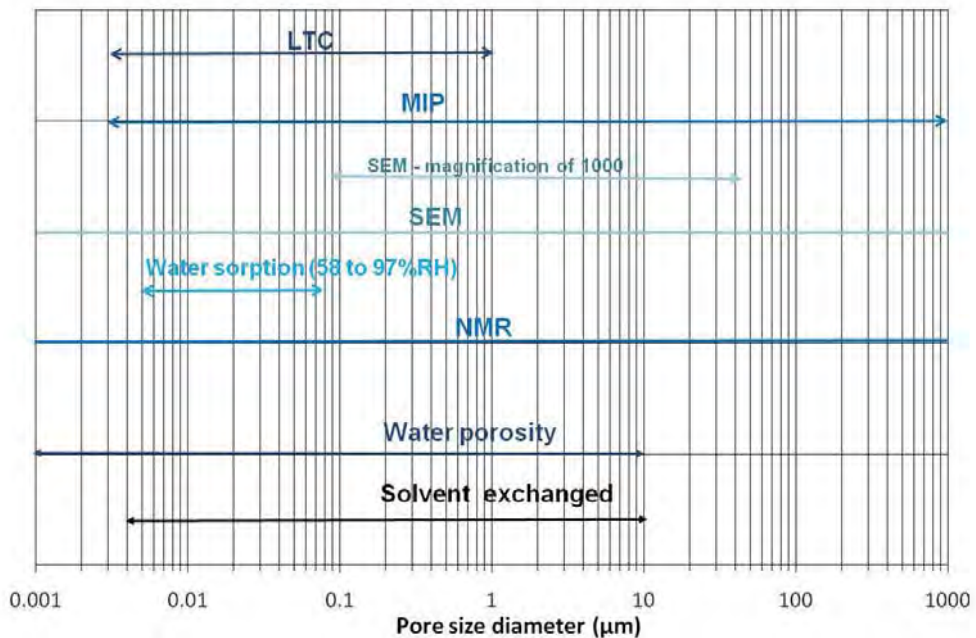
Fig. 3.4 : Range of pore size diameter of different tests: LTC from 0.003 to approx. 1 µm (Sun and Scherer 2010); MIP from 0.003 µm to 1000 µm (Diamond, 1999, Micrometrics, 2000); SEM depends of the magnification of the images; H_2O sorption from 0.005 to 0.075 µm (58 to 97%RH); ^{1}H NMR (McDonald et al., 2005); water porosity range of gel and capillary water and solvent porosity the range of capillary pores

3.3.1 Low temperature calorimetry (LTC)

Low temperature calorimetry (LTC) is a test method used to characterize the pore structure of saturated cement based materials. The test determines important pore structure parameters, e.g. pore thresholds (connectivity), pore size distribution and total volume of pores which are relevant for the assessment of mechanical properties and durability of the materials. The range of detectable pore size is related to the temperature and it may vary according to the references; from about 0.004 µm

to 0.080 µm in diameter based on Kjeldsen and Geiker studies (2008), 0.004 µm to 0.1 µm according to Sun and Scherer (2010) and up to 0.400 µm from Aligizaki (2006).

The use of a virgin sample (non-dried) is a great benefit of LTC since drying may change the pore structure of cement materials (1986b, Beaudoin and Tamtsia, 2004, Parrot et al., 1980), and it is in contrast to the other methods currently used to characterize porosity of cementitious materials (e.g. mercury intrusion porosimetry (MIP), scanning electron microscopy (SEM)).

Several investigations have been made to measure the amount of ice formed within the pores of cement based materials (Bager, 1987, Fagerlund, 1973, Bager and Hansen, 2000, Bager and Sellevold, 1986a, Bager and Sellevold, 1986b, Fridh, 2005, Kjeldsen and Geiker, 2008, Powers, 1945, Scherer et al., 2007). First, Powers and Brownyard (1947) determined the amount of ice formed from measured volume change. Later on, studies based on heat flow measurements have been reported. Fagerlund (1973) was apparently the first to propose to use the Kelvin Equation to determine the pore size distribution of cement pastes from freezing point depression. Brun et al. (1977) suggested a comparison of the melting and freezing curves from LTC to deduce the shape of the pores (cylindrical or spherical). Sellevold, Fontenay and Bager (Bager, 1984, Fontenay and Sellevold, 1980, Sellevold and Radjy, 1976) described the fundamentals of pore structure of cementitious materials by LTC. Bager and Sellevold reported ice formation in cement pastes with varying moisture content (Bager, 1987, Bager and Sellevold, 1986a, Bager and Sellevold, 1986b). They pointed out the importance of the moisture history for samples tested using LTC. Villadsen's investigations on ice formation in both virgin and dried/re-saturated pastes showed that LTC and MIP are comparable when similar samples (dried) are used (Villadsen, 1992). A series of studies carried out at Technical University of Denmark investigated possibilities and limitations of LTC (Bager and Hansen, 2000, Kjeldsen and Geiker, 2008). Kjelsen and Geiker (2008) reported significant differences in the equilibrium of the temperature between block (measured) and sample, moreover supercooling was found even when ice nucleation agent (AgI) was added on the top of the samples. Current literature showed that two-cycling experiment limits the amount of supercooling where the first cycle creates enough nucleation sites for the ice growth and the second cycle where the measurements are made (Sun and Scherer, 2010).

In the present work, LTC was used to determine pore threshold size, cumulative pore volume and pore size distribution of cementitious pastes with or without SCMs cured at different curing conditions (moisture and temperature).

Limitations and assumptions of LTC have been reported in the literature (Bager, 1984, Kjeldsen and Geiker, 2008, Sun and Scherer, 2010, Villadsen, 1992), for instances non-thermal equilibrium of the sample, freezing point depression and supercooling. Due to that, correction of the block temperature needs to be done for LTC measurements. Calculation of the baseline has been a common concern for the measurements of volume of ice formed; see e.g. Johannesson (2010).

3.3.1.1 Principle of LTC

Low temperature calorimetry (LTC) characterizes the pore structure of cement based materials by measurements of heat flow during the cooling and heating of the water or ice (pore solution) within the pores.
The test is based on the solidification process of the pore solution. The internal energy of a closed system changes either by adding or removing heat to the system, or by the system performing

compression or expansion, and it may be expressed by Gibbs and Thomson Equation 3.3 (Atkins, 1997).

$$dG = H - dT \cdot S_l \qquad \text{(Equation 3.3)}$$

Where

G	Gibbs free energy, J/mol
H	Enthalpy, J/mol, $H = v_m \cdot d_p$
T_k	Temperature, K
S_l	Entropy, J/mol.K

Therefore, the free energy following a change of state, from an initial temperature (T_o) and initial pressure (p_o) to the temperature (T) and pressure (p) assuming that no chemical reaction occur. And it can be calculated by Equation 3.4.

$$G(T,p) = G_l(T_o, p_o) - \int_{T_o}^{T} S \cdot dT + v_m \cdot d_p \qquad \text{(Equation 3.4)}$$

Where

v_m	Molar volume, m³/mol
d_p	Pressure change, Pa

At the transition point between solid and liquid extra energy is required (e.g. heat of fusion).The entropy of the system (liquid-solid) in a constant pressure will change by the amount of ΔS (see Equation 3.5).

$$\Delta S = \frac{\Delta H_{fus}}{T} \qquad \text{(Equation 3.5)}$$

Where

H_{fus}	Heat of fusion, J/g; $\Delta H_{fus} = H_l - H_s$

The vapour pressure of a material in thermodynamic equilibrium over a curved surface with radius r differs from that over a plane surface, and it is given by the Kelvin Equation (Equation 3.6), see Fig. 3.5. The curvature of the solid meniscus between liquid and ice lowers the free energy of the liquid within the pores and induces a depression of the freezing point (the triple point) (Feldman and Sereda, 1970, Hansen et al., 2000).

$$ln\frac{T}{T_o} = \frac{-2 \cdot M_l \cdot \sigma_{s-l}}{\Delta H_s \cdot \rho_{ice} \cdot r_k} \qquad \text{(Equation 3.6)}$$

Where

r_k	Kelvin pore radius , m
M_l	Molar mass of the liquid, g/mol
γ_{s-l}	Surface tension solid-liquid interface, N/m
ΔH_s	Specific heat capacity ($\Delta H_s = \Delta H_{fus} \cdot M_l$), J/g
ρ_{ice}	Ice density, g/m³

T_f Freezing temperature of the bulk liquid, K
T_{fp} Freezing temperature of the pore liquid, K

The relationship between the heat (q) that is removed or added, and the change in temperature (ΔT) is given by the Equation 3.7.

$$q = C_{pa} \cdot \Delta T \text{, J /kg} \qquad\qquad\qquad \text{(Equation 3.7)}$$

Amount of heat flow (Ei) consumed and temperatures (T) are measured by LTC, in order to obtain the apparent heat capacity (C_{pa}), see Equation 3.8. A and S_m are instrument dependent.

$$C_{pa} = \frac{dq}{dt} \cdot \frac{1}{A_1} \cdot \frac{1}{w} \text{, J/(}^\circ\text{C·kg)} \qquad\qquad \text{(Equation 3.8)}$$

Where

$$\frac{dq}{dt} = \frac{E_i}{S_M} \cdot \Delta t \text{, J}$$

E_i Heat flow, differential output of thermopiles, V

S_m Calorimeter sensitivity, V/W 10^{-3}; $58.845 + 0.03642 \cdot T_c - 0.000454 \cdot T_c^{\,2}$, (for Calorimeter 1 at DTU)

t Time, s

A_1 ($A = -0.355 \cdot 10^{-6} \cdot T_c - 0.00093$ during cooling; and $A = 0.001147$ during heating), (for Calorimeter 1 at DTU)

w Sample weight, kg.
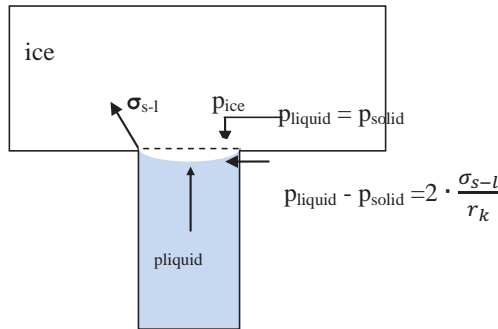
Fig. 3.5: Ice formation in the pores

3.3.1.2 Calculation of porosity characteristics

Volume of pores

A baseline is necessary to be established for the calculation of the amount of ice formed. The baseline will separate the phase change from the heat flow from the unfrozen water and the solid component. Examples of baseline calculation proposed by Johannesson (2010) and Sun and Scherer (2010) are given in the Appendix X. The heat consumed or released at different stages (ΔC_{pa}) can be converted to the correspond amount of ice by Equation 3.9.

$$w_{ice} = \frac{\Delta C_{pa}}{\Delta H_{fus} \cdot \Delta T_s} \qquad \text{(Equation 3.9)}$$

Where

w_{ice-s}	Mass of ice formed in the stage, kg/kg$_{d\ 105°C}$
H_{fus}	Heat of fusion, J/kg;
T_s	Temperature in stage, °C

In order to obtain the volume of ice formed (V_{ice}), the mass of ice formed (w_{ice}) is divided by the density of the ice (r_{ice}), see Equations 3.10 and 3.11. The density of the ice is used in the calculation based on the recent considerations made by Sun and Scherer (2010).

$$V_{ice} = \frac{w_{ice}}{\rho_{ice}}, \text{cm}^3 \qquad \text{(Equation 3.10)}$$

Where

$$\rho_{ice} = (0.9167 - 2.053 \cdot 10^{-4} \cdot T - 1.357 \cdot 10^{-6} \cdot T^2) \cdot 10^{-3}, \text{kg/cm}^3 \qquad \text{(Equation 3.11)}$$

The volume of the sample (V_s) is obtained dividing the amount of dried sample at 105°C ($w_{105°C}$) by the bulk density of the sample, see Equation 3.12. The bulk density of the sample can be obtained by MIP measurements ($r_{bulk(MIP)}$). The result of cumulative volume of pores (fraction): total volume of ice by volume of dried sample (cm³$_{ice}$/cm³$_{105°C}$).

$$V_s = \frac{w_{105°C}}{\rho_{bulk\,(MIP)}}, \text{cm}^3 \qquad \text{(Equation 3.12)}$$

Pore size

Freezing point depression is dependent on the radius of the menisci and hence of the pore radius and may be quantified from the Equation 3.6 (Kelvin Equation), see Equation 3.13.

$$r_K = \frac{-2 \cdot M \cdot \sigma_{s-l}}{\Delta H_s \cdot \rho_{ice} \cdot \ln\left(\frac{T}{T_o}\right)} \qquad \text{(Equation 3.13)}$$

The non-freezable adsorbed water is called "t-layer", t_{nf}. Values for t-layer vary in the literature (Fagerlund, 1973, Sun and Scherer, 2010). Sun and Scherer (2010) reported values from 1.0 to 1.2

nm for t-layer.The radius of the pore is the sum of the thickness of the adsorbed layer and the Kelvin radius, see Equation 3.14 and Fig. 3.6.

$r_t = r_k + t_{nf}$, m   (Equation 3.14)
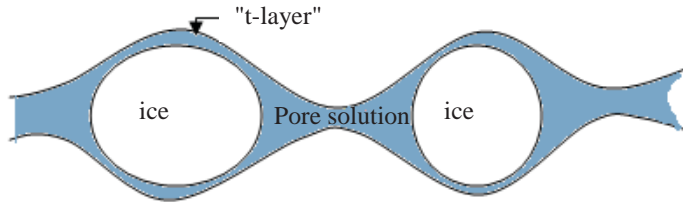
Fig. 3.6: Solid-liquid phases in a pore system with partially frozen pore solution

3.3.1.3 Parameters and values used for the calculations

Special attention is given to the parameters selected for calculation of pore size and volume of pores, as they vary from reference to reference contributing to the scatter of pore size and amount of ice formed values found in the literature (Bager and Sellevold, 1986a, Fagerlund, 1973, Sun and Scherer, 2010, Villadsen, 1992).

Results of pore size and pore volume reported from LTC data are largely dependent on the parameters used as well as the values of these parameters, e.g. surface tension, heat of fusion and density.

Apparently, values for surface tension are not well established in the literature; see Table 3.3. Studies also do not agree in which water transition phases (e.g. liquid-gas or liquid-solid) should be applied for the pore calculation of LTC data. Investigations have considered the interface between liquid and ice crystal σ_{s-l} for freezing curves (Blachere and Young, 1972, Villadsen, 1992, Williams, 1967). While, others have used the interface between liquid and vapour (σ_{l-g}) (Kubelka and Wenzel, 1931, Powers and Brownyard, 1947). The use of different interfaces has a significant impact on the pore size distribution curves, see Fig. 3.7. It is important to notice that more energy is necessary during the process of freezing water than melting of ice.

An extensive discussion of the effect of different meniscus existing inside a porous material, on the freezing point is given in (Defay et al., 1966, Sun and Scherer, 2010). Defay et al. (1966) pointed out that there are three possibilities for the meniscus when a porous materials freezes: 1) ice and liquid are exposed to the water vapour phase; 2) pore liquid is in contact with both the ice and vapour; and 3) ice is in contact with both vapour and pore liquid. According to the reference, they correspond to a different depression of freezing point and thus to different pore size (Defay et al., 1966).

The heat of fusion, or the thermal energy required to change water from solid to liquid state, is temperature dependent and varies from reference to reference; see Table 3.3. Assumptions are made for the heat of fusion values found in the literature, for instances that both ice and water are at atmospheric pressure; however this is not true after the water starts to freeze. Also, according to

studies the heat of fusion of pore water may be several percentage lower that the heat of fusion of free pure water (Bager and Sellevold, 1986a).

Density of water and ice are used to calculate pore size and volume of pores and it also varies according to the references (Table 3.3) (Hansen et al., 2000, Sun and Scherer, 2010, Powers and Brownyard, 1947, Villadsen, 1992). Water density is used by Hansen et. al (2000) and Villadsen (1992). However, investigations have been carried out using ice density (Sun and Scherer, 2010).

In Fig. 3.8, the scatter of values found in the literature is illustrated graphically. It is possible to observe a large difference in the pore size between the adopted parameters according to the references (Bager and Hansen, 2000, Fagerlund, 1973, Sun and Scherer, 2010, Villadsen, 1992). Sun and Scherer (2010) parameters and values used for calculation of pore size are based on Brun et al. (1977) and they are applied at the present work. The parameters and values used for pore size calculation are carefully reviewed and described in a recent paper by Sun and Scherer (2010).
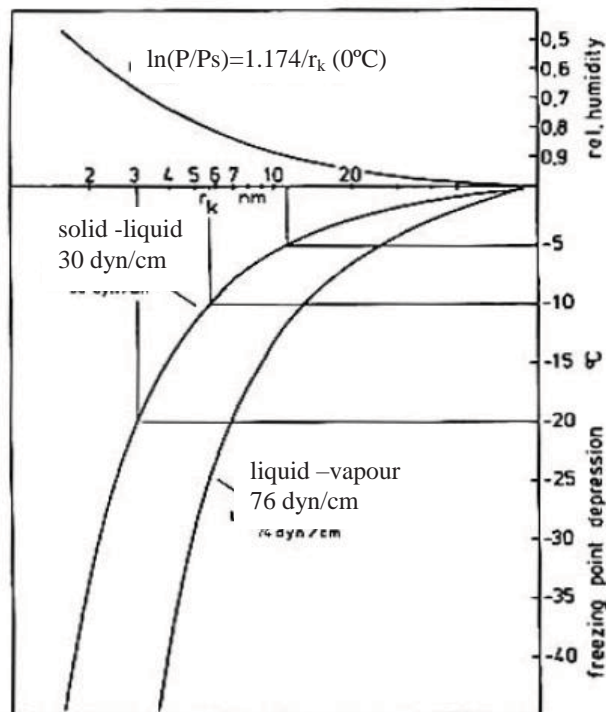
Fig. 3.7: Solid-liquid and liquid-vapour interface for Kelvin pore radius, (Bager and Sellevold, 1986a)

Table 3.3: Equations or values used for pore size calculation from LTC data

References	Surface tension (N/m)		Heat of fusion (Δh_f) (J/g)		Density (ρ) (kg/m³)		t-layer (m)
	$\sigma_{l\text{-}g}$ (liquid-gas)	$\sigma_{s\text{-}l}$ (solid-liquid)	Melting	Freezing	ρ_l (liquid)	ρ_{ice} (ice)	
(Dorsey, 1954)	$(75.64 - 0.1391T - 0.00003T^2)\cdot10^{-3}$				$1000 - 0.26\Delta T$ [1]		
(Everett and Haynes, 1965)**		0.030*					
(Dufay et al., 1966)**	0.0757 at 0°C	0.022 at 0°C					
(Blachere and Young, 1972)**		0.040*					
(Morioka et al., 1973)**		0.042*					
(Fagerlund, 1973)		$30.5(1\text{-}0.93\cdot10^{-2}.\Delta T).10^{-3}$ [2]		333.7-2 ΔT			$19.7(273.2\text{-}T)^{-1/3}$
(Brun et al., 1977)		$0.0409+3.9\cdot10^{-4}\Delta T$	$-332 -5.56.10^{-2}\cdot\Delta T^2-7.43\Delta T$	$-332 - 0.155\Delta T^2- 11.39\Delta T$		$916.7 - 2.053$ $\cdot10^{-1}T - 1.357$ $\cdot10^{-3}T^2$	$8\cdot10^{-10}$
(Bager, 1984)			$334 + 2.2\Delta T$ [3]	$334 - 2.2\ \Delta T$ [3]	$1000 - 0.26\Delta T$ [1]		$19.7(273.2\text{-}T)^{-1/3}$ [4]
(Villadsen, 1992)		0.030*	$334 + 2.2\Delta T$ [3]		1000		$19.7(273.2\text{-}T)^{-1/3}$ [4]
(Bogdana, 1996)	0.0756 at 0°C						

(reference)						
(Hansen et al., 2000)				1000		
(Lide, 2005)	0.0756 (at 0°C); 0.0764 (at -5°C); 0.077 (at -8°C); 0.02024 (-35°C)					
(Fridh, 2005)**		$334 + 2.2\Delta T$ [3]				
(Kjeldsen and Geiker, 2008)	$30.5(1-0.93\cdot10^{-2}\Delta T)10^{-3}$ [2]	$334 + 2.2\Delta T$ [3]	$334 - 2.2\Delta T$ [3]	$1000 - 0.26\Delta T$ [1]		$19.7(273.2-T)^{-1/3}$ [4]
(Sun and Scherer, 2010)	$0.0409+3.9\cdot10^{-4}\Delta T$ [5]	$333.8 + 1.79T$ ***; 332.4 ****	332.4		$916.7 - 2.053\cdot10^{-1}T - 1.357\cdot10^{-3}T^2$ [5]	$1\cdot10^{-9}$ to $1.2\cdot10^{-9}$

* Assumption where the used temperature is not given

** Do not calculate pore size

***Cylindrical pore melting from the side

****Cylindrical pore melting from the end

(1)(Powers and Brownyard, 1947)
(2) (Hesstvedt, 1964)
(3) (Radjy and E.J., 1972)
(4)(Fagerlund, 1973)
(5)(Brun et al., 1977)
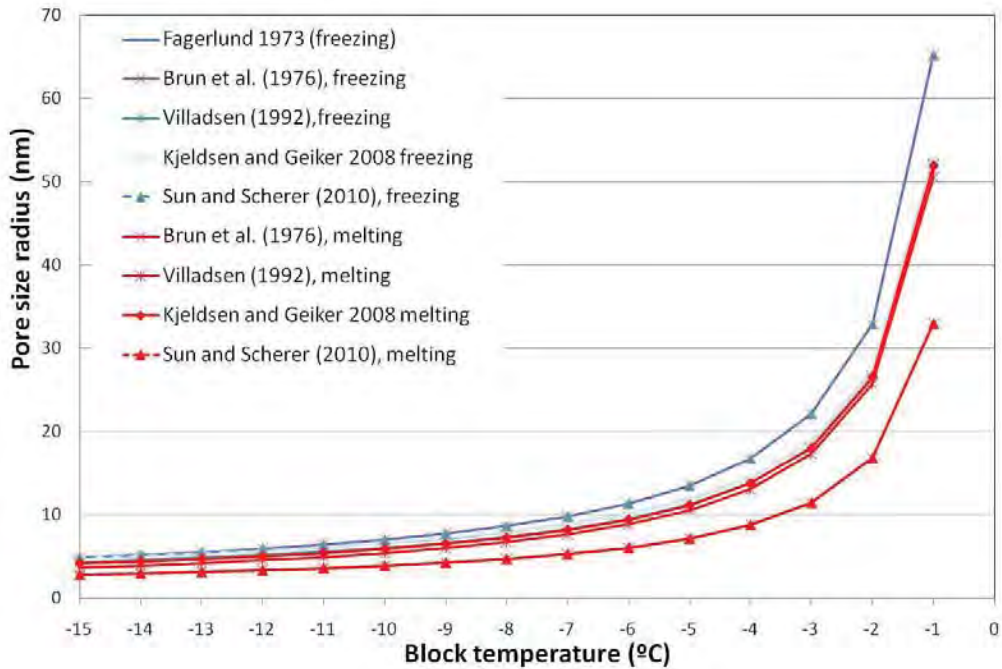
Fig. 3.8: Pore size calculation using Equation 2.8(Kelvin equation) and parameters given in the Table 2.5. Range from 0 to -15ºC

3.3.1.4 Interpretation of the results

Pore structure of cement based materials during cooling and heating process are illustrated in the Figs. 3.9 and 3.10. Assuming A the pore with a larger radius, B and D pores with the same radius and C is the pore with smaller radius; it is possible to analyse freezing and thawing curves of LTC. The freezing front in a saturated cement based materials is assumed to start from the larger to the smaller pores, see Figs. 3.9(a) and 3.9(b). As pointed out by Sun and Scherer (2010), during the cooling process when the temperature is low enough to enter the smaller pore (C), it can also enter in the pore D, see Fig. 3.9(d). This is the so called "ink bottle" effect. As C and D pores do not have the same radius ($r_D > r_C$) and they freeze at the same time, the pores of r_D are reported as the same size of r_C. This may be a matter to be considered for the determination of the pore size distribution by cooling curves. Therefore the melting curve is suggested to be used for pore size distribution calculation.

The heating curve is illustrated in the Fig. 3.10(b) where the pore C is the first to melt complete followed by Pore B and D. At about 0ºC, the pore solution should be melted.

Cooling
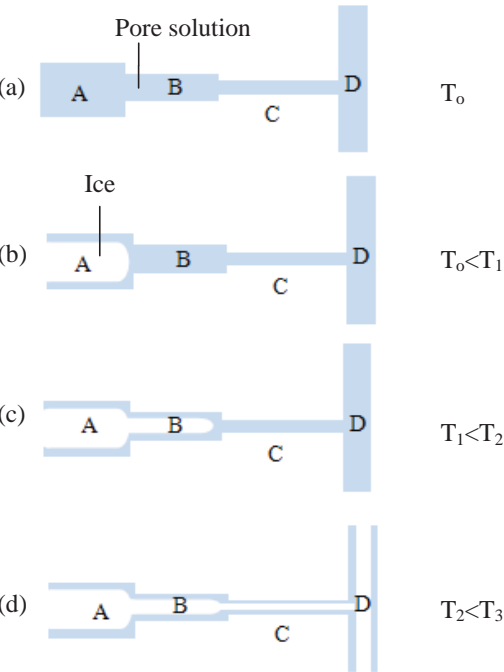
Heating

Fig. 3.9: Scheme of pore structure submitted to cooling (a) saturated pore structure; (b) initial freezing; (c) T is low enough to enter the pore B, but not C; (d)Pore C and D freeze at the same (different sizes)(after Sun and Scherer, 2010)
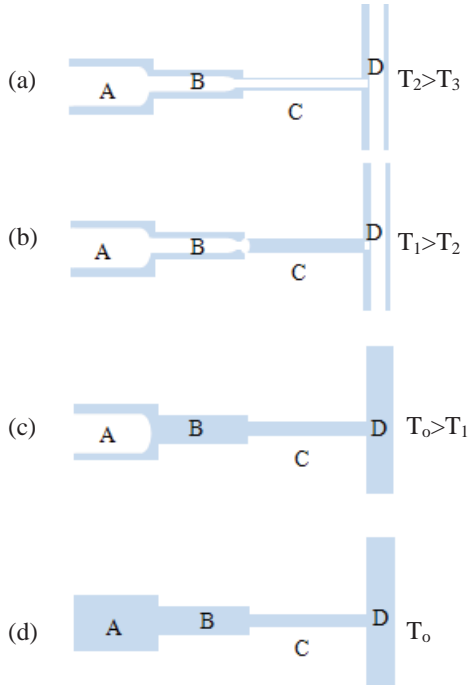
Fig. 3.10: Scheme of pore structure submitted to melting (a) ice formed (b) pore C melts first; (c) Pore B and D melts at the same time $r_B = r_D$; (d) pore A is the last to melt (after Sun and Scherer, 2010)

Well defined peaks for cement paste are found for the cooling curves given by LTC. The peaks are classified (percolated capillary pores, gel pores and etc.) according to the temperature ranges, see Table 3.4. It is claimed that below -50ºC no bulk ice is formed (Fridh, 2005, Bager and Sellevold, 1986a, Wittmann, 1973). Setzer and Zech (1988) reported a freezing of an adsorbed water film at about -90ºC.

Table 3.4: Range of the temperature of freezing curves for pore classification by different authors (Bager and Sellevold, 1986b, Lindgreen et al., 2006, Snyder and Bentz, 2004).

Pore size classes	Temperature interval		
	Snyder and Bentz (2004)	Bager and Sellevold (1986a)	Lingreen et al (2006)
Bulk water	-	-	0 to –10ºC
Percolated capillary pores	-20ºC	-10 ºC	0 to –10ºC
Inter LD and HD gel pores	-30ºC	-25ºC	Around –25ºC
Inter globule pores in LD gel	-45ºC	-45ºC	Around –40ºC

According to the literature (Fridh, 2005, Sun and Scherer, 2010), freezing curve involves two phenomena: freezing point depression and supercooling of water, while melting curve only involves freezing point depression. Also, the curvature of the interface between the ice and liquid during freezing is dependent on the entry radius (R_E), while during the melting is controlled by the body radius (R_B), see Fig. 3.11 (Sun and Scherer, 2010). Therefore, freezing curves may be used to determine: (1) pore threshold size (peak start), (2) and accumulated amount of pores see Fig. 3.12 and Table 3.5. Whereas, melting curve is used to determine the pore size distribution (Fig. 3.12(3)).

Table 3.5: Pore structure parameters from the LTC curves.

Pore structure parameter	Acquired from
Pore size	Block temperature using Kelvin Equation
Pore threshold	Start of the peaks from freezing curves, Fig. 3.12(1)
Total amount of pores	Area from the freezing curves, Fig. 3.12(2)
Pore size distribution	Area from the melting curves versus block temperature from the melting curves. Calculate pore size from the Kelvin Equation
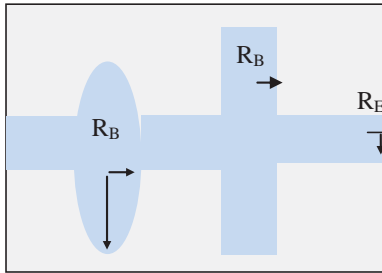
Fig. 3.11: Scheme of pore curvature interface: entry radius (R_E) and body radius (R_B) in cementitious materials (after Sun and Scherer, 2010)
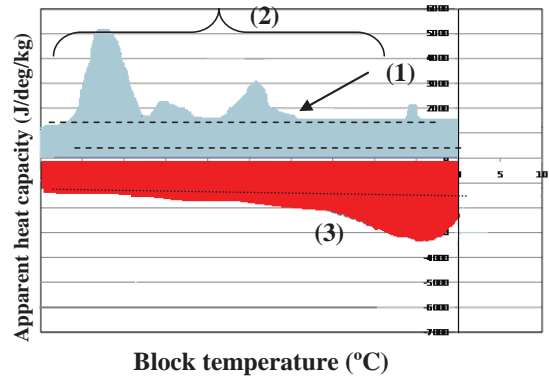
Fig. 3.12: Pore characteristics from LTC curves: 1)pore threshold; 2) volume of ice (g_{ice}/kg_{sample}); 3) pore size distribution (amount ice versus temperature (pore size calculated by Kelvin Equation)

3.3.1.5 Matters of consideration

There are a number of factors and assumptions which may have an impact on the LTC data, see Table 3.6. They are divided in two parts: experimental and calculation; some of them were investigated in the present project as it is shown in the Table 3.6.

Table 3.6: Matter of consideration: experimental and calculation

Nr.	Matter of consideration	Investigated by the Project
	Experimental	
1	Liquid transport takes place during freezing (migration)	
2	Sample temperature	x
3	Supercooling	
4	Damage of the sample due to freezing	
5	Rates of cooling and heating	x
6	Degree of sample saturation	x
7	Reference cell (dried sample or empty)	x
	Calculation	
8	Parameters and values for Kelvin Equation	
9	Pores are cylindrical	
10	Water properties are applied for pore solution (freezing point depression)	
11	Pore size in the range from 0 to -10ºC	

Experimental
Liquid transport takes place during freezing (migration)
It is assumed that water (pore solution) freezing starts at the larger pores progressing to the smaller pores. Fridh (2005) and Sun and Scherer (2010) reported that during the freezing the water may move from the narrower to the larger pores (air voids) depending on the connectivity of the pores. Also some of the water may be expelled from the sample (Brun et al., 1977, Fridh, 2005, Sun and Scherer, 2010). The water expelled from the sample may provide a layer of ice on the outer surface of the sample which is in equilibrium with the surrounding vapour. During the thawing the expelled water will not be part of the sample´s bulk which may lead to errors in the pore size values acquired for the pore size distribution curves.

Sample temperature
Lack of temperature equilibrium between block (measured) and sample cell may disturb the values found for pore size by LTC. Studies (Kjeldsen and Geiker, 2008) with bulk water showed that as freezing and melting take time and the temperature continuously changes in the calorimeter the equilibrium between the block and the sample is not obtained. It was also noticed that the equilibrium is dependent on the applied rate of freezing and thawing. At a lower freezing rate (e.g. 1.2ºC/h) a more accurate temperature is registered due to the thermal equilibrium between the block (calorimeter) and the sample (Wittmann, 1973, Kjeldsen and Geiker, 2008). Studies carried out with bulk water at varying rates of cooling and heating suggested a correction of the pore size values based on the thermal equilibrium of up to 2ºC behind (Kjeldsen and Geiker, 2008). It is important to emphasize that the difference between block temperature and sample cell is largely dependent on the equipment set-up and sample size. Thus, it may have to be analyzed individually for each set-up.

Supercooling
When the temperature reaches about 0ºC bulk ice starts to melt, but for ice to form from pure water, the temperature must drop to about -30ºC (Weeks & Ackley 1986). This phenomenon is called supercooling and is caused by the lack of nucleation sites for ice crystal growth. AgI (silver iodide) or biological materials have been used to create nucleation sites in order to limit the amount of

supercooling (Kjeldsen and Geiker, 2008). Kjeldsen and Geiker (2008) reported supercooling of bulk water when higher rates (e.g. 3.3ºC/h and 15ºC/h) of freezing and thawing are used even when AgI is used. Sun and Scherer (2010) suggested the use of two cycling experiments to avoid supercooling , where the first cycle creates enough nucleation site for the ice formation.

Damage of the sample due to freezing
Investigations by Fridh (2005) with concrete samples (w/c ratio of 0.40 and 0.60) indicated that ice formation is accompanied by an immediate expansion of the samples. Powers showed that bulk water expands 9% when it freezes. In 1945, Powers reported that cementitious materials are not a closed vessel and it always contains enough air filled space to accommodate the increase in water volume caused by freezing (Powers, 1945). Later on, Powers advanced his hypothesis and suggested that the destructive stresses during the freezing were produced by the flow of displaced water to the freezing sites, therefore osmotic pressure develops (Powers and Brownyard, 1947). First the paste tends to shrink as the water is drawn from the unfrozen to frozen pores, followed by the expansion after diffusion has filled the pores. The use of entrained air bubbles was suggested to prevent the development of osmotic pressure in frozen cement pastes (Powers, 1975). Sun and Scherer (2010) pointed out that the stress exerted on the porous host by ice is about ten times less than exerted by mercury at MIP in a similar pore size.

Rates of cooling and heating
As reported previously in this section (Supercooling), LTC results may substantially be affected by the applied rates of cooling and heating. Findings showed an impact of freezing and melting rates of ±1.2 ºC/h; -3.3ºC/h +4.1ºC/h ; ±15ºC/h for bulk water (Kjeldsen and Geiker, 2008). It was noticed that when higher rates (e.g.15ºC/h) were applied the thermal equilibrium between block and sample cell was not acquired and supercooling was observed (Kjeldsen and Geiker, 2008). Also, at an increased rate it is expected to attain more damage of the material (Bager and Sellevold, 1986a). Rates of 3.3ºC/h (freezing) and 4.1ºC/h (heating) have been used for LTC studies and they are reported to give reliable equilibrium of temperature for samples of 50x15Ø mm (Bager, 1987, Bager and Hansen, 2000, Bager and Sellevold, 1986a, Bager and Sellevold, 1986b).

Degree of sample saturation
It is recommended that sealed samples are re-saturated before testing by LTC, since the test is based on the water freezing of the samples. Vacuum saturation or water sorption methods are largely used to re-saturated cementitious samples (Baroghel-Bouny, 2007a, Bager, 1987, Bager and Sellevold, 1986b), however if the sample is not fully saturated it will have an impact on the results of LTC.

Reference cell
At LTC measurements two cells are used; sample cell and reference cell. The output from the calorimeter is proportional to the difference between the heat flow from the sample cell and reference cell. At the reference cell, a dried sample (Fridh, 2005) or no sample (Bager and Sellevold, 1986b, Kjeldsen and Geiker, 2008) is normally used. Difference in the reference cell may lead to a variation of the baseline and consequently the calculated amount of frozen ice.

Calculations
Parameters and values used for the Kelvin Equation
This topic is discussed in details in the section 3.3.1.3

Pores are cylindrical
The Kelvin Equation is applied to determine the LTC pore size, considering that the pore shape is cylindrical. It is known that the pore structure of the cementitious materials is complex compared to

many other porous materials. This complex structure is formed by pores at different shape and size spread out in the cement paste. The difficulties to established a pore shape for cement based materials may be noticed in the melting curves, Fig. 3.13 where the pore C is the first to melt completely leaving a hemispherical interface in pore B and a cylindrical interface in pore D. Pore B and D show different interfaces because of the difference in their connectivity (Sun and Scherer, 2010), see Fig. 3.13.
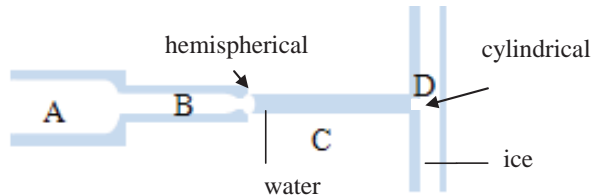
Fig. 3.13: Hemispherical and cylindrical shape of pore during the melting

Water properties are applied for pore solution (freezing point depression)
Pore solution is also a factor which may have an impact on the results of LTC. During freezing of the pore solution, the ions of the solution (NaCl) are expelled from the ice front, which may cause an increased salinity of the remaining pores. Increased salinity may result in freezing point depression (Fagerlund, 1973). Kjeldsen and Geiker (2008) suggested an initial freezing point depression of 1 to 2ºC due to the salt in the water within the pores of cement based materials. Also, the values of surface tension used may induce errors, as the pore solution is salinity the interface is not smooth but spiked. Investigations (Weeks and Ackley (1986)) also showed that ice crystals grow separated by small non-freezing areas, this fact may change the chemical energy of the solution.

Pore size in the temperature range from 0 to -10ºC
In the range of temperatures from 0 to -10ºC, it is possible to observe that a small difference in temperature leads to significant change in pore size calculated by the Kelvin Equation. The variance in pore size calculated from the Kelvin Equation (Equation 3.15) is shown in the Fig. 3.17 and Table 3.9. However, for the temperature range between -10 and -55ºC, the variance in pore size is small.

Table 3.7: Difference in pore size values due to 1ºC of temperature difference (based on Sun and Scherer (2010) calculation)

Temperature range (ºC)	-1 to -2	-2 to -3	-3 to -4	-4 to -5	-5 to -6	-6 to -7	-7 to -8	-8 to -9	-9 to -10
Difference in pore size (nm)	32.34	10.78	5.39	3.23	2.16	1.54	1.15	0.90	0.72
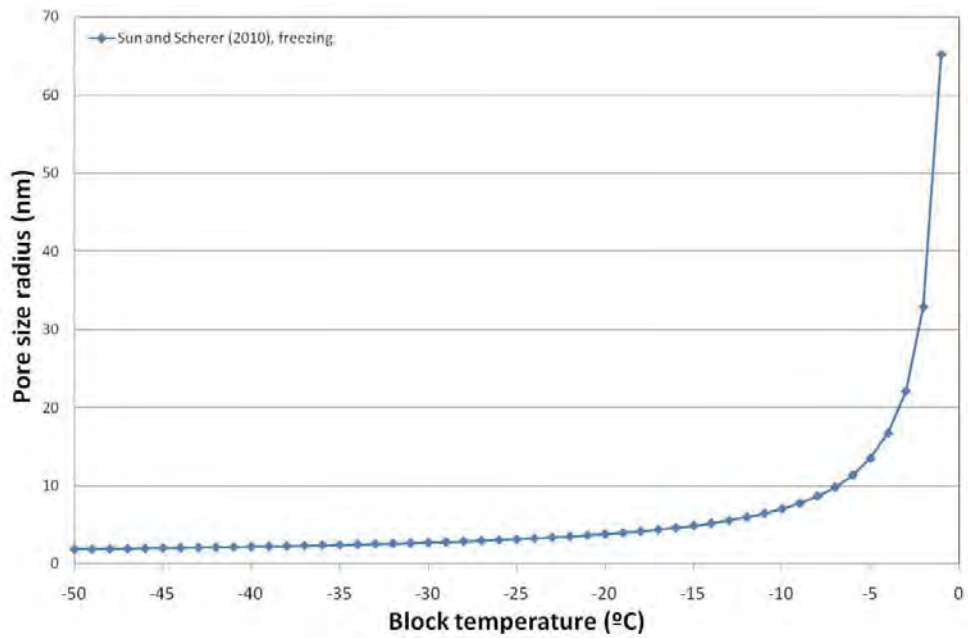
Fig. 3.14: Pore size versus block temperature using Equation 11 and parameters and values given in Sun and Scherer 2010

3.3.2   Mercury intrusion porosimetry (MIP)

Mercury intrusion porosimetry (MIP) may be used for porosity characterization of cement-based materials, e.g. (Day and Marsh, 1988). The range of pore diameters measured by MIP is from 0.003 µm (pressure = 414 MPa) up to 1000 µm (Micrometrics, 2000). The method provides information on the volume of accessible pores and the threshold pore size, i.e. the size of pores providing connectivity. The threshold pore size is considered relevant for the assessment of the resistance to transport of substance in the material.

In 1921, Washburn (1921) pointed out the relation between pressure and pore size by the so-called Washburn Equation. Later on, a survey of the method as applied to cement systems and some data were given by Winslow and Diamond (Winslow and Diamonds, 1970). Since then a significant amount of work with MIP for characterization of the porosity in cement materials has been undertaken (Bager and Sellevold, 1975, Cebeci and Received June 4, 1980, Day and Marsh, 1988, Diamond, 2000, Kumar and Bhattacharjee, 2003b, Rigby and Fletcher, 2004, Winslow and Liu, 1990, Zhou et al., 2010).

MIP is simple, fast and less costly when compared to other methods for porosity characterisations, e.g. scanning electron microscopy (SEM) and water sorption. When comparing porosity data the size of pores measured should be kept in mind; MIP provides information on a large range of pores (from gel to capillary), but capillary condensation methods not. One topic of concern is that dried sample are required for MIP and that drying may change the microstructure of cement based materials, see e.g. (Jennings, 2007). Limited impact of drying was found when using solvent exchange (Kocaba, 2009). Another topic to be considered is that according to Bager (Bager and Sellevold, 1975)the size of the tested material has an impact on the intrusion curve. However, he found only minor differences for grain size larger than 0.5 mm. Finally, the high pressure applied in MIP might cause a compaction of the gel, which may increase the measured total volume of pores.

3.3.2.1 Principle of MIP

Non-wetting mercury is forced into the porous material at incremental pressures; at each step the intruded volume is measured. When a non-wetting liquid is in contact with a solid, the liquid surface develops a characteristic contact angle ($\theta > 90º$) due the cohesion forces between liquid and material surface, see Fig. 3.15(a) and 3.15(b). As a consequence of the non-wetting behaviour of mercury, a higher pressure is needed to obtain intrusion in smaller pores.
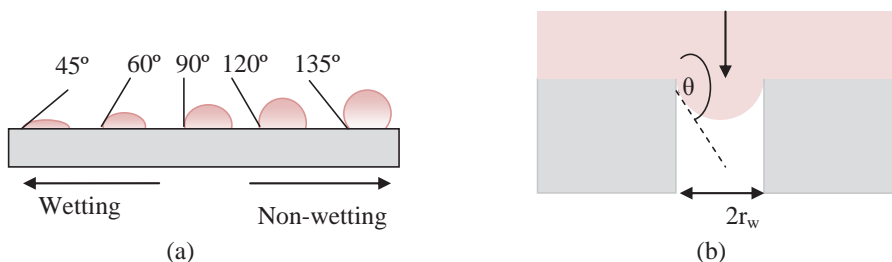
Fig. 3.15: (a) Contact angles for various for wetting and non wetting liquids.
And (b) intrusion of mercury into a pore (after La Scala 2000)

3.3.2.2 Calculation of pore characteristics

The pressure (p_w) required to force a non-wetting fluid into a circular cross-section capillary of radius r_w is given by the Washburn equation (Equation 3.14).

$$r_W = \frac{-2 \cdot \gamma_{s-l} \cdot cos\theta}{p_w} \qquad \text{(Equation 3.14)}$$

Where:

r_w Pore radius (Washburn Equation), m;
γ_{s-l} Surface tension solid-liquid, N/m;
θ Contact angle between the liquid and the pore wall, degrees;
p_w Pressure applied on mercury to intrude the pore, N/m².

The bulk density of the sample is determined from Equation 3.15, assuming that no intrusion of mercury into the sample occurs at 0.033 MPa (Micrometrics, 2000)).

$$\frac{w_{pt}}{\rho_{Hg}} = \frac{(w_{ps} - w_s)}{\rho_{Hg}} + \frac{w_s}{\rho_{bulk}} \qquad \text{(Equation 3.15)}$$

Where

w_{pt} Weight of penetrometer (sample cell) filled with mercury, g
w_s Weight of dry sample, g
w_{ps} Weight of penetrometer with the sample and mercury (until 0.033 MPa the volume), g
ρ_{Hg} Density of mercury, 13.5 g/cm³
ρ_{bulk} Bulk density of sample; g/cm³

The volume of pores was calculated using Equation 3.16.

$$V_p = V_{Hg} \cdot \frac{\rho_{bulk}}{w_s} \qquad \text{(Equation 3.16)}$$

Where

V_p Volume fraction of the pores, cm³
V_{Hg} volume of mercury intruded, cm³

Two important pore structure parameters can be extracted from the cumulated pore volume versus pore diameter graphs; threshold pore size and total pore volume, see Fig. 3.16. The threshold pore size is the size of pores providing entry to the pore network, i.e. connectivity, and it is one of the parameters controlling transport properties of the paste. Threshold pore sizes may be acquired from the intersection of the two tangents to the curve of cumulative pore volume versus pore size. The total pore volume compares to a broad range of pores and may be related to the mechanical properties of the paste. The total pore volume is the highest cumulative pore volume intruded.
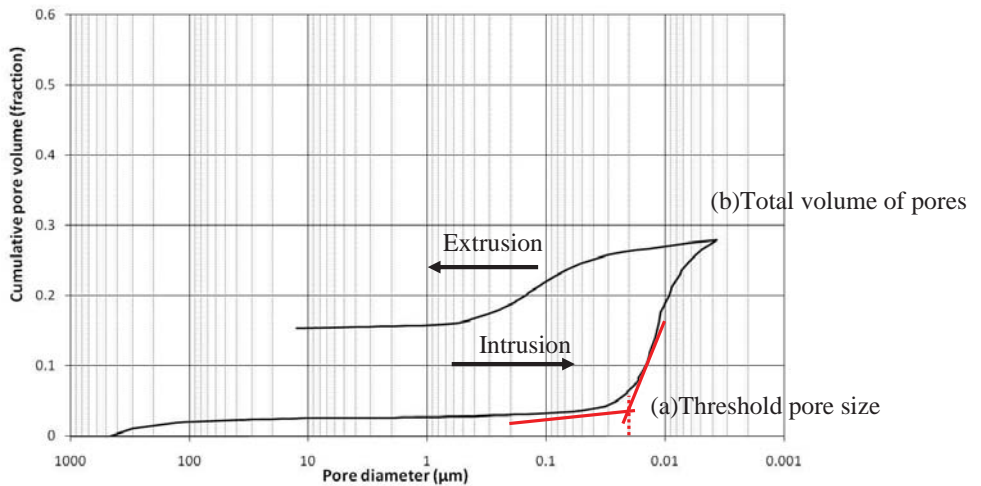
Fig. 3.16: Pore characteristics: (a)threshold pore size and (b)total volume of pores) acquired from
the intrusion curve of MIP

3.3.2.3 Matters of consideration

As reported for previous studies, some factors and assumptions may lead to a wrong interpretation
of the MIP results, see Table 3.8. Many of these factors and assumptions were already dealt with by
others (Diamond, 2001, Diamond, 2000, Villadsen, 1992).

Table 3.8: Matters of consideration for the use MIP test

Matter of consideration for MIP test	Investigated by the Project
Pores are cylindrical	
Dried sample is requested	X (LTC)
Effect of inkle bottles and closed pores	
Sample size	
Pressure applied	
Values for contact angle	
Surface tension values	
Environmental	

Pores are cylindrical
Washburn equation assumes cylindrical pores, which does not represent the pore structure of
cement-based material.

Dried sample is requested
Possible detrimental effects of drying may lead to a modified pore structure (Bager and Sellevold,
1986b, Espinosa and Franke, 2006, Korpa and Trettin, 2006, Beaudoin and Tamtsia, 2004, Parrot et
al., 1980). Hardened cement paste dried using different methods (e.g. oven at 105 °C, isothermal
smooth at 22°C and 4 kPa , solvent exchanging) showed differences in total pore volume curves,

see Fig. 3.17 (Rubner and Hoffmann, 2006). Higher amount of pores and threshold pore size is found for oven dried pastes indicating the coarser of the pore structure. Isopropanol replacement followed by evacuation has been reported to cause the last damage in cementitious paste (Kocaba, 2009, Korpa and Trettin, 2006). This topic is reviewed with more detail in the Section 2.6.1.
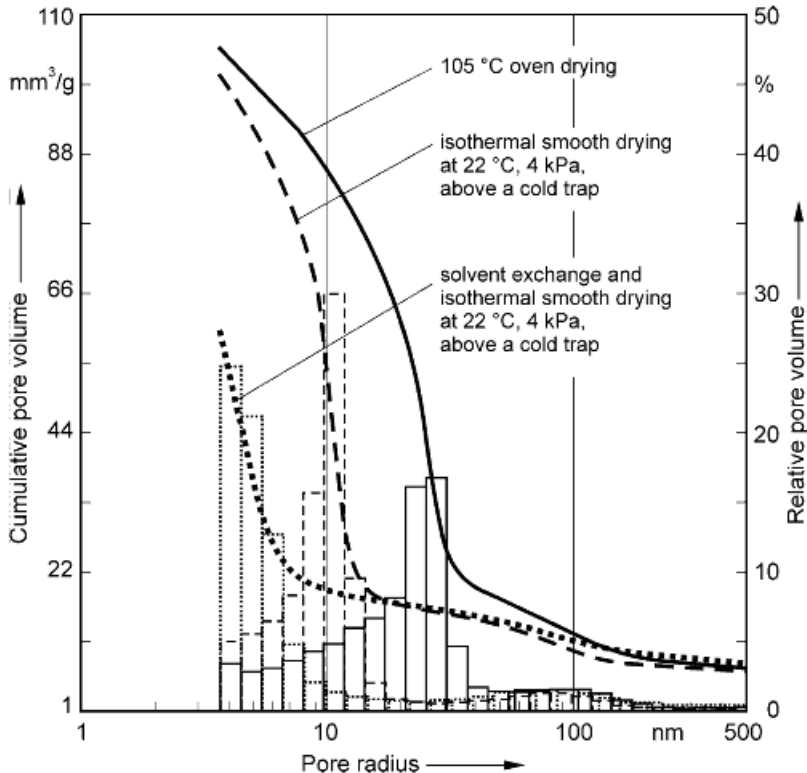
Fig. 3.17: MIP for samples at varying drying conditions: a) oven 105ºC; b) drying at 22ºC and 4kPa; c) solvent exchange and drying at 22ºC and 4kPa (Rubner and Hoffmann, 2006)

Effect of inkle bottles and closed pores
MIP does not measure the real pore size distribution, but that of pore-entry sizes (threshold pore size)(Cook and Hover, 1993, Feldman and Sereda, 1968). If large pores can be entered only through small pores, they will be registered as small pores (ink bottle effect).

Also closed pores are not revealed in mercury intrusion curve because they do not have direct contact with the external surface (Rigby et al. 2002; Nielsen 1970).

Sample size
Bager and Sellevold (1975) studies claimed a possible effect of sample size due to restricted ingress of mercury within the pores. He found changes in the curves of cumulative intrusion versus pore radius for samples smaller than 0.5 mm (Bager and Sellevold, 1975), see Fig. 3.18.
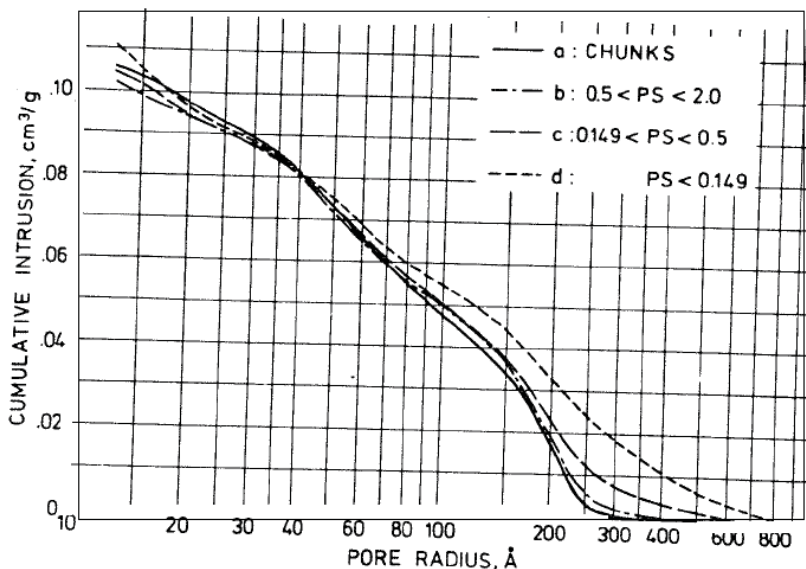
Fig. 3.18: Cumulative volume of pores for pastes at varying particle size (in mm) (Bager and Sellevold, 1975)

Pressure applied

Mercury may penetrate the sample by breaking trough pore wall and damaging the pore structure (Cook and Hover, 1991). Investigation reported damage of the pores for cementitious pastes trough the high pressure applied by MIP(Feldman, 1984). The data is also affected by the rate of pressure applied on the samples(Kumar and Bhattacharjee, 2003a).

Values for contact angle and surface tension values

The accuracy of the results depends on the adopted values of: a) contact angle between the mercury and the material; and b) surface tension of mercury (Diamond, 2000, Kumar and Bhattacharjee, 2003a, Park and Ihm, 1990). According to studies (Cook and Hover, 1991, Rigby and Edler, 2002, Salmas and Androutsopoulos, 2001), the contact angle depends on the nature of the sample and the purity of the mercury. Drying method may change the contact angle; when a more aggressive method is used, a lower contact may be used to calculate the pore size by MIP see Fig. 3.19.
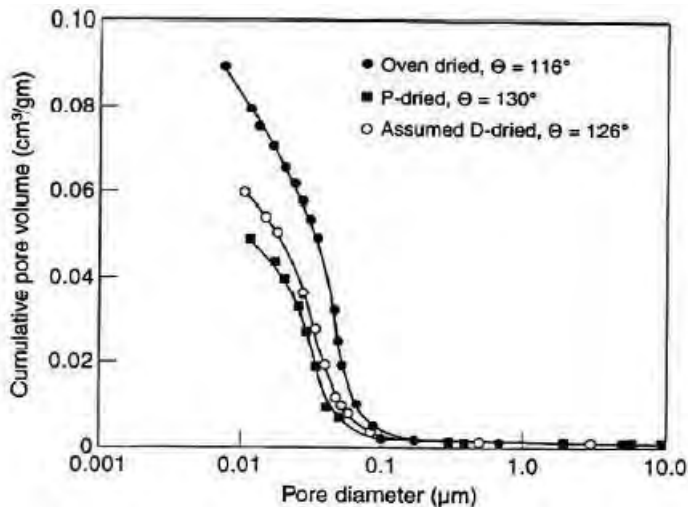
Fig. 3.19: Cumulative pore volume (cm³/gm) versus pore diameter (µm) for pastes dried using:
oven dried,P-dried and D-dried by MIP (Yassin, 2010)

Cook and Hover (1993) observed that the contact angle values may vary from 117º to 175º. Villadsen (1992) reported the difference in pore radius using different values of contact angle (117º and 140º), see Fig. 3.20. It is possible to observe that the curve of volume of pores versus pore radius is shifted, lower values for pore size is found when the angle of 117º is used in the Washburn Equation.
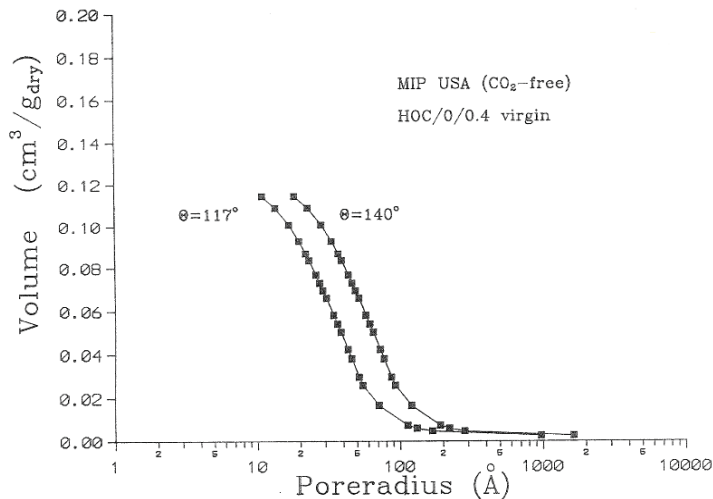
Fig. 3.20: Volume of pores (cm³/g_{dry}) versus pore radius (Å) by MIP using contact angle of 117º and 140º (Villadsen, 1992)

Studies pointed out, difficulties in the measurements of the surface tension liquid-solid and it also should be stress that it may vary with temperature. In the case of mercury, the literature reports variances from 484.2×10^{-7} MPa at 25°C to 472×10^{-7} MPa at 50°C (Cook and Hover, 1991).

Environmental
Mercury is a heavy metal considered as an excrementally dangerous material. Mercury has to be handle very carefully using special safety equipment (glasses, gloves, suction cabin, etc.), as it can be absorbed into the body, and cause irreversible damage to the nervous and metal system of the users. MIP is reported as a non-environmental friendly test, for being a test which uses mercury in large amount.

3.3.3   Scanning electron microscopy (SEM)

Scanning Electron Microscopy (SEM) is widely used to characterize materials (e.g. cement paste microstructures) using high-resolution image. Images obtained by SEM using backscattered electron reproduce a difference in the brightness and contrast which may reflect in the different phases and the pores of hydrated cementitious material. Also changes in morphology of the cement based materials due to the curing conditions (temperature) are possible to be observed by SEM.

The primary reason for developing electron microscopes was to improve the resolution of optical microscopes (Michler, 2008). The understanding of electron wavelength and its lenses in the 1930s resulted in 1931 in the creation of the first transmission electron microscope (TEM) (Jakob, 2011). In 1937, Von Ardenne showed a prototype of a SEM (Von Ardenne and Beischer, 1940). Further SEM development occurred in 1951, when Charles Oatley and his colleagues obtained the first SEM images at Cambridge University. Since then there have been great improvements in the electron microscopes (see e.g. (Oatley et al., 1965)). Scrivener and Pratt (1983) were the pioneers on the quantification of porosity of cementitious materials using the grey scale histogram from backscattered electron (BSE) imaging (Scrivener and Pratt, 1983). At the present, SEM is been widely used for porosity characterization of cement based material.

SEM is based on the emission of electrons onto the surface of a sample to generate signals, and therefore an image is formed. The key to produce a quality SEM image is an understanding of the equipment´s parameters (accelerating voltage, probe current, working distance) and their impact on the image. There are no standard or defined values applied for these parameters, as they are related to the type of sample used, magnification, area scanned and type of detector used. Also, they are to some extend dependent on each other.

SEM using backscattered electron has been used to determine the pore structure of cementitious materials (Jensen, 2010a, Kocaba, 2009, Scrivener, 1989). The different energy levels of the emitted backscattered electrons will reproduce a difference in the brightness and contrast on the image. For a plain cement paste sample the darkest parts (black) are the pores, the middle part of the gray scale represents the hydrated phase and the lightest gray levels are unhydrated cement grains. When used for porosity characterization, SEM has advantages over other methods, as they can provide a direct "view" with a high local resolution of the studied material. Other methods (e.g. MIP and LTC) for the porosity assessment are based on theoretical equations and assumptions. Moreover, SEM has a large depth of field, which allows a large amount of the sample to be in focus. The combination of higher magnification, larger depth of field, greater resolution, and compositional information makes SEM widely used equipment. However, to optimize the images for porosity determination, preparation of the sample is required (e.g. drying, polishing). Drying of

cement based materials may change the microstructure of the pastes (Korpa and Trettin, 2006). Moreover, polishing is time consuming and requires some experience from the user (Jensen, 2010a). For the SEM analysis, many parameters have to be set to acquire a reliable SEM image, such as working distance, bean size.

3.3.3.1 Principle of SEM

Image formation

The schematic diagram with the main parts of a scanning electron microscope is presented in Fig. 3.21. SEM microscope can be divided into several sections with different vacuum levels. The highest vacuum is obtained at the electron gun section and it is decreasing going down the column to the specimen chamber. An electron beam is generated in the very top of the microscope's column. There are two types of electron sources: tungsten thermionic gun and field emission gun (Fig. 3.21(a)).

When a steady stream of electrons is generated, it is passing through the condenser lenses (one or more) which adjust the beam current that impinges on the specimen while the objective lens determines the final size of electron beam. The scan coils control the beam scanning across the specimen

Fig. 3.21: SEM overview (Hansen et al., 2000)

(Fig. 3.21(b)). As the electron beam traces over the specimen, it interacts with the specimen and as a result the electrons can be backscattered or they can generate secondary electrons (Goodhew et al., 2000, Michler, 2008). Moreover some of the electrons can be absorbed or pass through the specimen (Fig. 3.21(c)).

The signal (electron emitted) from the surface is registered by different detectors (e.g. backscattered and secondary electron) (Fig. 3.21(d)). The detector counts the number of electrons given off from each point of the samples surface. The intensity of the emitted electron signal is displayed as brightness on a cathode ray tube (CRT). By synchronizing the CRT scan to that of the scan of the incident electron beam, the CRT display represents the morphology of the sample surface area scanned by the beam. The electron beam and CRT spot are scanned to a monitor; see Fig. 3.21(e). (Goodhew et al., 2000, Yao and Wang, 2005).

Electron interaction with atom of the sample

For a better understanding of the SEM, it is important to know the nature of the possible interactions between the primary electron (PE) beam and the atom. PE are charged particles and so they interact strongly with the electrically charged particles of the atoms in the sample (Hansen et al., 2000, Michler, 2008). When this electron beam reaches the sample, the electrons are scattered

many times (multiple scattering) before they are deflected into different ways. The interaction between the electron and the sample´s atoms may be inelastic, elastic or electromagnetic radiation. Inelastic and elastic interactions are commonly used for the characterization of cement based materials (Table 3.9).

Table 3.9: Inelastic and elastic interaction between electron and atom

Interaction	Inelastic	Elastic
Definition	Some of the energy of the primary electron is lost during the interaction	No energy is lost during the interaction
Illustration (Hansen et al., 2000)		

The area where the elastic or inelastic interaction takes place is called the "interaction volume" (Fig. 3.22(a)). The size of the interaction volume depends on the electron's energy and the atomic number of the sample. For an element with lighter atomic number (for instances Al), the penetration depth of the primary electrons is higher than that observed for a heavier atomic number. Monte Carlo methods are normally used for simulation in order to obtain a statistical picture of the movement of the electrons in the interaction volume, where path simulations of the sample are possible to be observed (see e.g. (Horsewell, 2010)).

Emitted lower-energy electrons resulting from inelastic scattering are the secondary electrons (SE). Secondary electrons can be formed by inelastic collisions which results in the emission of low-energy electrons from near the sample's surface. They are collected on a SE detector (scintillator) which is positively charged to improve the signal to noise ratio (S/N). SE is abundant and they are used to give topological and morphological information of the sample. Scrivener (1989) suggested the use of SEs to analyze rough surfaces of cement based materials, such as a cracked sample. High-energy electrons resulted from an elastic collision of an incident electron, typically with a sample atom's nucleus, are referred to as backscattered electrons (BSE). The energy of BSE will be comparable to that of the incident electrons. These high-energy electrons can escape from areas deeper than secondary electron, so surface topography is not as accurately resolved as for secondary electron imaging, see Fig. 3.22(b). BSE are highly influenced by atomic number of the sample, which is responsible for the phase contrast of the image (Gallucci 2007). For that reason, BSE have been used in the past years to characterize porosity on the cement based materials.

<table>
(a)	(b)
</table>
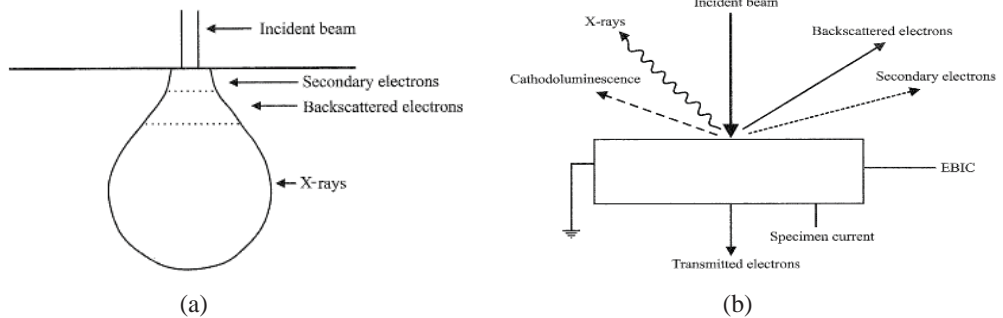
Fig. 3.22: (a) Interaction volume and (b) signals from the sample (Goodhew et al., 2000)

3.3.3.2 Characterization of porosity by backscattered electrons image

Backscattering electron image has been successfully used in the characterization of the pore structure of cementitious materials (Kocaba, 2009, Scrivener and Pratt, 1983). The reproduced contrast and brightness of the backscattered images enable them to have different colors representing different substance in the material. For cement paste impregnated with epoxy, the porosity represented by the black pixels and the microstructure is illustrated by different grey levels (e.g. brighter grey for anhydrous), as seen in the Fig. 3.23 (a).

The importance of the sample preparation may not be underestimated when representative images are required. The sample preparation (drying, impregnation, polishing and coating) are essential to the quality of the images. First of all the sample has to be dried, as SEM operates under a vacuum. Epoxy impregnation is an important step because pores that are filled with epoxy will appear black in the backscattered image, allowing a segmentation of porosity from the hydration products. A flat polished sample is required for the optimization of topographical variations and overlap of the features on the grey scale (Lee and Jacobsen, 2010, Scrivener and Pratt, 1983, Wong et al., 2006). The polishing is largely depend on the hardness and type of material used therefore its procedure may vary according to the type of material used. Coating is also necessary to prevent charge build up from the primary electrons.

Segmentation of the different phases on the image is also an important issue for image analysis of cement based material. Scrivener (Scrivener, 2004) suggested the segmentation of phases of cementitious hydrated phases and porosity by "thresholding" the image at the minimum in the histogram, see Fig. 3.23(b). Scrivener (2004) suggested that the color of the C-S-H may vary according to the temperature and use of SCMs. Higher temperature leads to a denser C-S-H with lower micro-porosity so a lighter gray appearance in the histograms. During image capture, the brightness and contrast setting are adjusted that all peaks can be seen in the histogram.

(a)   (b)
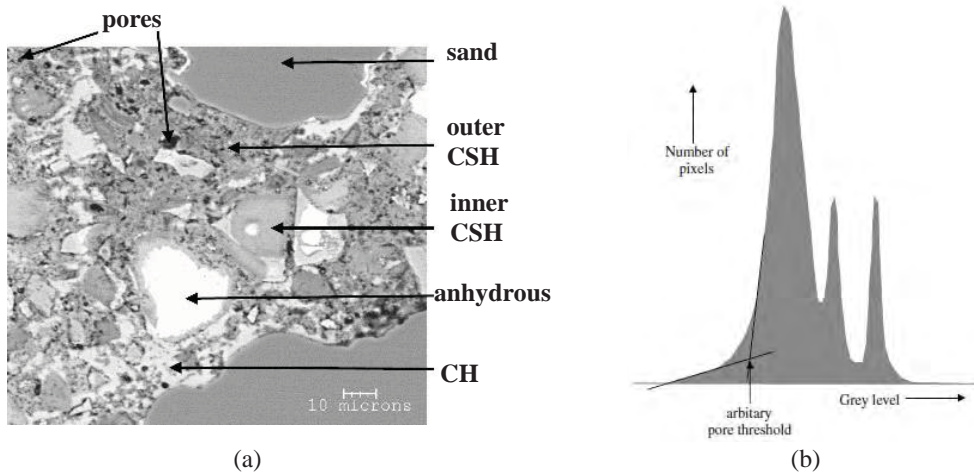
Fig. 3.23: (a) Pores and main product of cementitious hydrated pastes and (b) "thresholding" of the grey scale histogram(Scrivener, 2004)

For the quantification of the area of pores is necessary to know the magnification of the image, from that it is possible to calculate the size of each pixel (eg. magnification of 800 =0.375мm pixel size). To reduce the noise produced by imperfections in the image, a median filter may be applied in the image. Once the porosity is isolated, the total area of pores can be calculated, see Equation 3.17

$$A_{tp} = \frac{A_b}{A_t}$$ (Equation 3.17)

Where

A_{tp}	Total area of pores, fraction
A_b	Area of black pixels, μm^2
A_t	Total area of grey scale histogram, μm^2

3.3.3.3 Matter of consideration

Parameter for the image acquisition

One of the main challenges to imagining is to use appropriate parameters (e.g. working distance, accelerating voltage, probe size, etc.) and values to acquire a sharp and noiseless image with optimum contrast and brightness. Examples of images applying different parameters and values are given in the Appendix XIX. Contamination of the image is also reported here. The images were taken in SEM practical classes for the course "Electron Microscopy and Analysis for Materials Research" carried out at DTU. The material used was zeolite, the images were obtained by secondary electron detector using SEM. Sample preparation was not undertaken. Technical terms used for SEM analysis are described in the Appendix XII.

Plane of a 3D structure

Scrivener (2004) has listed some important limitations of measurement by SEM. She pointed out the influence of the plane of two-dimensional (2D) section of a three dimensional structure, as given in the Fig. 3.27:

(a)

- Sections trough cement grains and aggregates will not generate a real image so the thickness of features will be overestimated (Fig. 3.24(a));
- Connectivity of a 3D structure cannot be deduced from 2D sections (Fig. 3.24(b)).

(b)
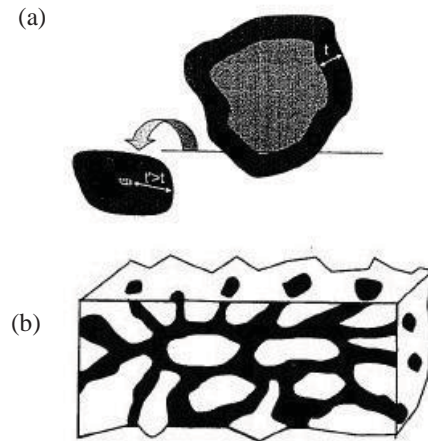
Fig. 3.24: SEM limitation (Scrivener 2004)

Sample preparation

Polishing is reported as a challenge in the characterization of pore structure by SEM (Jensen, 2010a, Scrivener and Pratt, 1983). Sample preparation for SEM may be divided in impregnation, polishing and coating of the sample. Jensen (2010) reported that the depth of epoxy intrusion at old cement pastes is small and it gives problem in the polishing of the samples. Also problems with polishing and coating were faced by the author (Jensen, 2010a).The polishing of the samples has to reach a level where the pores are impregnated with epoxy and no epoxy on the surface of the sample is seen, see Fig. 3.25.

From the literature review and experience from the author, it was possible to observe that a procedure for polishing of cement paste is difficult to be established. Polishing depends on several parameters as epoxy intrusion depth, polish equipment, mix design of the paste, age and etc.

Polishing level
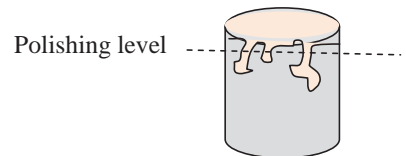
Fig. 3.25: Polishing of cement paste

Segmentation of the grey scale histogram

The segmentation method will influence the porosity result; and one should always consider this for the comparison of the data.

The difficulties in the segmentation of the porosity area is illustrated by examination of the colors around a borderline of a single pore, see Fig. 3.26. The pore edge is not exactly divided over one or two colors but several grey scale colors before reaching a steady state. This may have an impact on the computation of the amount of pores measured by SEM.
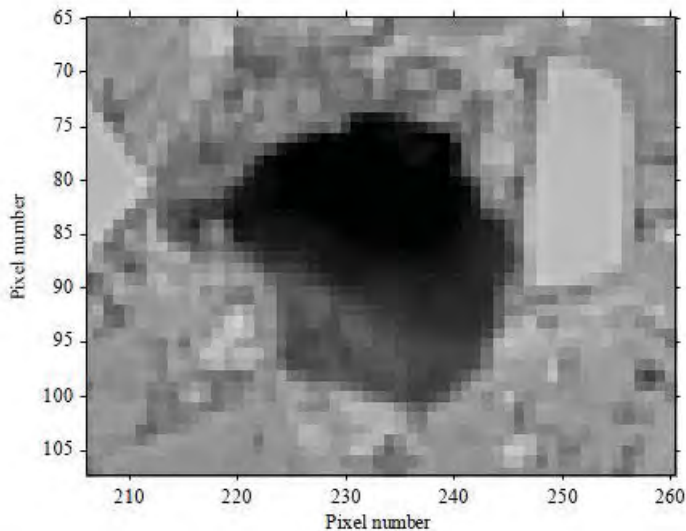
Fig. 3.26: Non defined boundaries for a pore observed at a high magnification (Jensen, 2010a)

3.3.4 Water sorption (desorption-adsorption) method

Water sorption is used to determine the state of water of cement pastes using saturated salt solution method on powder or thin samples. The study of the relationship between water content and vapor pressure for hardened paste at constant temperature may give important information of the water held on the paste and at some extend it can be related to the porosity. In addition, the vapor content of the concrete pores will have a strong influence on the transport properties of the hydrated cementitious materials moisture flow and the moisture flow direction (Nilsson, 2002).

In 1916, Langmuir proposed a model involving a thermodynamic equilibrium to predict the fraction of solid surface covered by an adsorbate as a function of its gas pressure (Langmuir;J.I., 1916). After that, Gibbs' studies in thermodynamics explained the adsorption of gas molecules on a surface of the samples; later on, he deduced the equation for free adsorption, the so-called "Gibbs adsorption isotherm" (Gibbs, 1993). The thermodynamic equilibrium between liquid and its vapor in a capillary pore leads to the relation between vapor pressure and capillary radius and thus to the theory of the capillary condensation. This is given by the Kelvin Equation (Atkins, 1997, Atkins et al., 1992, Broekhoff, 1969). German studies were apparently the first to examine the relation between water content and vapor pressure for hardened paste at constant temperature (Jesser, 1927). In their studies, larger samples (25.4x25.4 mm) cured for 3 days were used. He reported difficulties to interpret the results which may be due to the size and age of the samples. Powers and Brownyard (1947) have shown different methods to measure water held in hydrated cementitious materials, such as high-vacuum apparatus, air-stream and desiccators with salt solution. It was observed, that the rate of absorption in an air-filled desiccators is less than that in vacuum or air stream. This suggested the possibility that the exposing time was not enough. At the past years, some studies with isotherm of cement based materials have been reported in the literature (Baroghel-Bouny, 2007b, Baroghel-Bouny, 2007a, Espinosa and Franke, 2006, Nilsson, 2002).

Studies carried out by Baroghel-Borny (2007a, 2007b) showed that a saturated salt solution method is particularly suitable to concrete samples and to the study of their pore characteristics. The method is mentioned by the standard prEN-ISO12571 (1999). The method provides information on the pore system in the size range 0.005 (about 50%RH) to 0.075 µm (97%RH) in diameter. According to Powers and Brownyard (1947), capillary condensation starts to take place at about 40% of relative humidity. However, the pore volume may be measured for all ranges of RH. From the isotherm curves it is possible to have the apparent pore size distribution curves and also the specific surface area of the samples. However, according to the literature the specific surface area from water sorption method is higher than other methods, for instances gas sorption by N_2 and it should be extract from adsorption curves. The method has an advantage of not requiring dried samples; in addition the method is based on a simple procedure and cheap set-up. Many studies related to the durability of materials applied data from water sorption isotherms (see for example (Nilsson, 2002))). Nevertheless, few data are available for hydrated cementitious materials. This may result from the fact that the experiments can be time-consuming and require very accurate testing procedure and experimental conditions.

3.3.4.1 Principle of water sorption method

At different RH, the porous materials desorb or absorb water vapor to its accessible surfaces and pores. In the Fig. 3.30(a), the adsorbed and capillary water are illustrated. The water content spontaneously changes until equilibrium between the water held in the specimen and the outside water vapor is reached (Powers and Brownyard, 1947).

The establishment of equilibrium involves a change in moisture content of the sample, for the nature of the hardened paste is such that at a given temperature the relationship between vapor pressure of the water in the hardened specimen and the water content is represented by a smooth curve. A sorption isotherm describes the equilibrium of the sorption of a material at a surface at constant temperature; see Fig. 3.30(b). According to Powers and Brownyard (1947) the taking up of moisture from the atmosphere is called "adsorption", and the reverse is called "desorption". The processes in general without specifying the direction of moisture change is called "sorption".

(a)   (b)
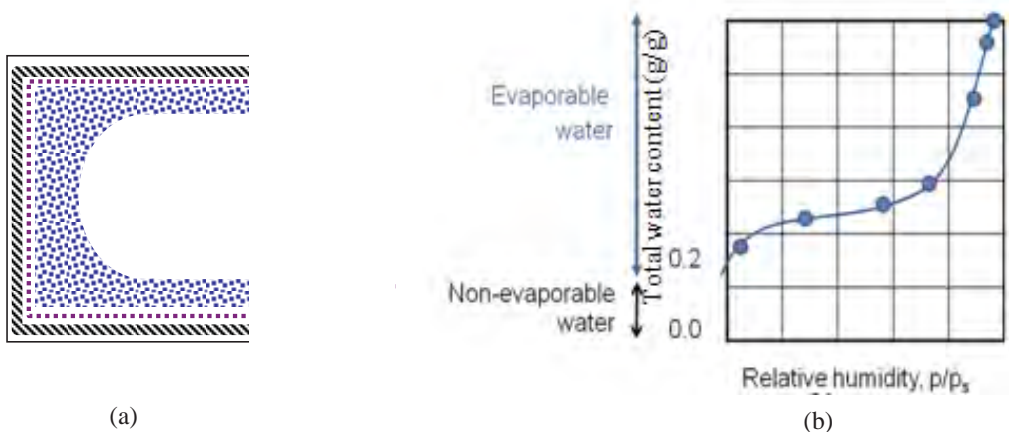
Fig. 3.27: (a) Adsorbed (pink) and capillary condensed water (blue) in the pore and (b) sorption
curve for cement pastes at varying relative humidity (after (Hansen, 1986))

3.3.4.2 Calculation of the pore characteristics

A meniscus exists between liquid and vapor in capillary condensed liquid. The curvature of the meniscus lowers the free energy of the pore liquid and induces a decreased vapour pressure. This effect can be quantified by use of the Kelvin equation for the capillary condensed water (Equation 3.18).

$$r_K = \frac{-2 \cdot V_m \cdot \gamma_{v-l}}{R \cdot T \cdot \ln \cdot (p/p_0)}$$
(Equation 3.18)

Where:

r_K	Kelvin pore radius, m
γ_{v-l}	Surface tension, vapor –liquid interface, N/m
V_m	Molar volume, m³/mole
p	Pressure, N/m²
p_0	Saturated vapor pressure, N/m²
T_K	Temperature in Kelvin, K
R	Universal gas constant, J/(Kmole)

A layer of increasing thickness adsorbs to cement paste at increasing RH. The thickness of the adsorbed layer can be described by Halsey equation for the thickness of the adsorbed t-layer (Equation 3.19) (Halsey, 1952). A water mono layer of 0.0003 µm was suggested by Hagymassy et al. (1969).

(Equation 3.19)

$$tw_{nf} = d_l \cdot \left[\frac{-5}{\ln \cdot (RH)} \right]^{\frac{1}{3}}$$

Where

tw_{nf}	Thickness of adsorbed layer("t-layer") for water sorption method, m
d_l	Average thickness of a single layer of adsorbed molecules, m

Equilibrium water content in weight (u), u, is determined by dry weight (oven at 105ºC), $w_{105ºC}$, and the weight in equilibrium, $w_{eq.}$, for a given relative humidity (RH), see Equation 3.20.

$$u = \frac{w_{eq.} - w_{105ºC}}{w_{105ºC}}, \text{fraction}$$
(Equation 3.20)

The volume of pores (V_{pw}) is deduced from the water content at RH of 97% ($W_{des.}$), see Equation 3.21 (Baroghel-Bouny, 2007a).The apparent bulk density is the measure using a dried material (e.g. density find for MIP).

$$V_{pw} = \frac{W_{.des} \cdot \rho_{bulk}}{\rho_l}, \text{fraction}$$
(Equation 3.21)

3.3.4.3 Matters of consideration

Cylindrical pore shape
or water sorption method, the pores are assumed to be cylindrical by the Kelvin Equation (Equation 3.20), however it should be kept on mind that may have an impact on the data.

Hysteresis
The different liquid–vapour interface during capillary condensation and capillary evaporation leads to a pronounced hysteresis by simple pore geometries. Indeed some researchers came to the conclusion that the existence of so-called "ink-bottle pores" causes a significant hysteresis between capillary condensation (absorption) and evaporation (desorption) (Espinosa and Franke, 2006).Others, associated hysteretical behaviour of the hydrated cementitious materials with the degree of liquid water saturation (Baroghel-Bouny, 2007b).

Slow method
The method is slow when salt solution desiccators are used. Typically, months of exposition on evacuated salt solution desiccators are needed to reach the weight equilibrium. Weight equilibrium depends on the size of the specimen, the RH gradient, the hygral history and type of sample (Baroghel-Bouny, 2007a). To save time, other methods have been used on the determination of sorption isotherms, see for instances dynamic sorption (Johannesson and Janz, 2002, Powers and Brownyard, 1947).

Experimental conditions
Very accurate experimental conditions (temperature, relative humidity) are required for water sorption testing in hydrated cement materials. The desiccators with varying salt solutions need to be placed in water bath at constant temperature (e.g. 20ºC) and level during the whole testing (up to one year). The pressure is assumed to be equal to the atmospheric pressure during the experiment.

Weighing of the samples
The test is based on the weight measurements of the samples. Therefore a very accurate scale and weighing procedure is required for the test, detailed procedure is given in the Appendix XIII.

Carbonation of the samples
Carbonation was reported in the literature as a fact which may change the pore structure of crushed cement pastes (Belie et al., 2010, Thomas et al., 1996, Van Gerven et al., 2007). Carbonation may occur in aqueous phase by the action of carbonate/bicarbonate ions migrating within the pore solution after dissolution (Belie et al., 2010). According to Belie et al. (2010) a high level of carbonation (i.e. 60 to 70% of CH) was found for crushed pastes after a 3-month curing period. For pastes with 50% of fly ash, a higher level of carbonation was found when compared with cement pastes.

Sample size
There is no standard size for samples used to water sorption measurements. Current literature (Bakhshi and Mobasher, 2011) comparing cement pastes in powder and slices have showed an increased in the cumulative moisture loss for samples with high specific surface (powder). Studies with mortar at varying size using water absorption also showed the effect of sample size, where a smaller samples showed greater absorption values (Cobanoglu et al., 2009). Among others, Johannesson (2002) reported similar results for calcareous sandstone at different size (grains (0.1-0.2 mm), discs of 10 mm and 25 mm) tested using different sorption methods. However, different

methods may also have an impact in the data, see in (Belie et al., 2010). Moreover, Baroughel-Bouny (2007a) investigations with cement pastes in powder and concrete in slice concluded that the sample size does not influence the data of isotherms curves, however different materials (cement and mortar) were used. Few data concerning this topic was found in the literature.

Effect of pore solution on the relative humidity

Ions dissolved on the pore solution may affect the relative humidity of the desiccators (Mjornell, 1994, Hedenblad, 1993). Measurements carried out by Mjornell (1994) showed a decreased of RH of about 1% for synthetic pore solution analyzed by ICP (Inductively Coupled Plasma). This effect is not significant and it may not be taken to account in the porosity measurements.

Risk of continued hydration

Continuous hydration may occur when samples for water sorption are exposed to high relative humidity (Baroghel-Bouny, 2007a, Mikhail and Abo-El-Enein, 1972). According to Hansen et al. (2000), at relative humidity exceeding 60% only mature cement pastes may be studied due to the possibility of re-hydration of eventual anhydrated grains in the samples. This problem in commonly described in the literature and it should be limited with maturity samples older than 3 months.

Risk of shrinkage and swelling

Shrinkage and swelling may perturb the pore structure of pastes exposed at different RH. According to studies carried out by Roper (1966), at high relative vapor pressure shrinkage may occur and it is caused by capillary tension stress. At low relative humidity, a slight swelling of the paste was observed and during the removal of the last amounts of evaporable water a substantial shrinkage of the paste is reported (Roper, 1966).

3.3.5   Additional methods

3.3.5.1 ^{1}H NMR relaxation

^{1}H NMR nuclear spin relaxation provides information about the state of water within the pore in cement based materials (McDonald et al., 2006, McDonald et al., 2005).

The water state may be determined by the relaxation time of the hydrogen nuclei within the water molecule. Two relaxation times are generally measured by NMR: T1, the spin-lattice relaxation time, and T2, the spin-spin relaxation time.

Pore size

T1 and T2 times differ for chemically bound hydrogen, hydrogen adsorbed onto surfaces, and hydrogen in water confined to small pores. From the exchange between the pore-bulk and pore-surface molecules, average relaxation times are obtained for bulk water and adsorbed water (McDonald 2006) (Equation 3.22). According to (McDonald et al., 2005), the liquid in the bulk have a longer relaxation time than in molecules temporarily adsorbed onto the surface (Fig. 3.28). On the other hand, bound water has almost no mobility and exhibits a short T2 (~10 μs) relaxation time. Equation 3.22 can be used to find the volume of water within the pores.

$$\frac{1}{T_{1,2}^{\ observed}} = \frac{1}{T_{1,2}^{\ bulk}} + \frac{\varepsilon \cdot S_p}{V} \frac{1}{T_{1,2}^{\ surface}} \quad \text{(Eq.3.22)}$$

ε	Surface layer thickness, m
S_p	Surface area of the pores, m²
V	Volume filled with liquid, m³
$T^{observed}$	Observed relaxation time, s
T^{bulk}	Bulk water relaxation time, s
$T^{surface}$	Surface water relaxation time, s
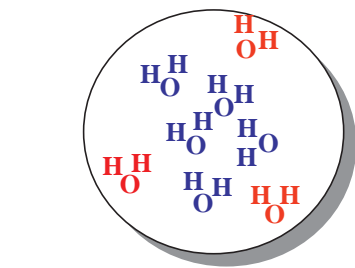
H₂O -surface molecules
H₂O – bulk molecules

Fig. 3.28: Water molecules relaxation (Valori, 2007)

The measured relaxation time of water in a pore may be related to pore size. Assuming the pores are spherical $S/V=3/r_p$, where r_p is the pore radius (Equation 3.21). The approximately scale to measure the pore size filled with water through the T_2 relaxation time is showed in Fig. 3.29.
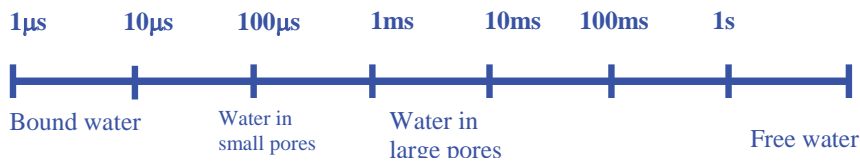
Fig. 3.29: Pore size by T_2 relaxation time (afterValori, 2007)

Pore size distribution (filled with water)
The pore size distribution may be obtained from the distribution of the relaxation rates presented by a liquid filled porous medium (McDonald 2005). Trough one-dimension (T_1 and CPMG (Carr, Purcell, Meiboom and Gill) pulse sequence) and two-dimension inverse Laplace transform (T_1-T_2 and T_2-T_2) it is possible to determine the relative amount of water populations which have different relaxation time. It is important to observe that T_2 values are influenced by several factors including: presence of paramagnetic materials, temperature, magnetic field, etc (McDonald et al., 2006, McDonald et al., 2005). A calibration model is applied to correlate the relaxation time with pore size distribution of cementitious materials (Fig. 3.30) (Valori, 2007).
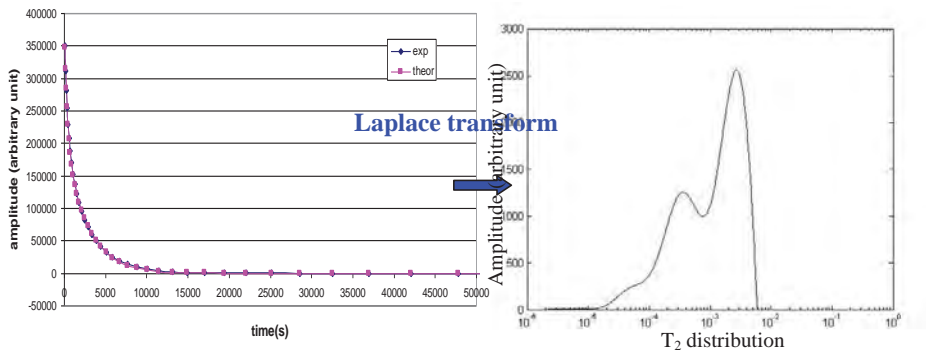
Fig. 3.30: Pore size distribution obtained by CPMG in white cement paste (own data)

State of water

NMR relaxation time is also performed to investigate the state of water in cement based material, see Table 3.10:

Table 3.10: Information of water state given by experiments with NMR relaxation

Experiments	Information on
T_2 echo amplitude	Proportional amount of mobile water as determined by the curves
Quad echo	Total bound, total evaporable water (confined and free water)
CPMG echo train (amplitudes of the curves)	Total evaporable water
T_2 (measured from CPMG)	Pore size
T_2xT_2	Water exchange between the pores, see Fig. 3.31
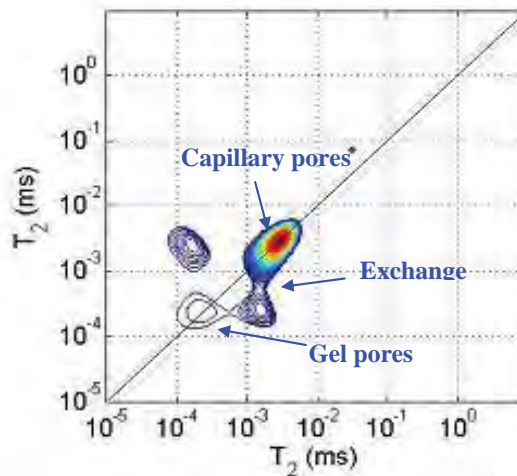
Fig. 3.31: T_2xT_2 relaxation time in white cement paste (own data)

3.3.5.2 Drying methods

Drying is required for some methods to measure porosity of hydrated cementitious materials (Diamond, 2001, Gallucci, 2007a, Rarick et al., 1996). Moreover, water and solvent porosity have been used to acquire the volume of pores of hydrated cementitious materials, see in (Feldman, 1986b). Here, oven drying at 105ºC and solvent exchange methods are used and described in the following sections.

3.3.5.3 Oven drying

Determination of the evaporable water and non-evaporable water of cementitious materials may be carried out through temperature criterion: evaporable water is the weight loss from ambient temperature to 105ºC and non-evaporable water is the weight loss from 105ºC to 1000ºC. The weight change is then compared to a "dry state", here the dry state is define as the weight of the sample at 105ºC.

In the Table 3.11, several methods to determine evaporable and non-evaporable water in cementitious hydrated materials are described according to the literature (Atlassi, 1993, Jensen et al., 1999, Powers and Brownyard, 1947, Zhang, 2007)

Errors may be introduced during the sample preparation and weighing of the sample for determination of evaporable water. For instances, samples may be exposed to differing ambient atmospheres containing more or less humidity and carbon dioxide (Atlassi, 1993). Moreover, the temperature has also an impact in the weight measurements. The accuracy of the scale should also be included, the precision of 0.0001 is recommended for the tests.

According to the literature, the computation of non-evaporable water by temperature involves also the loss of ignition of about 0.2g/g (Powers and Brownyard, 1947). This assumption may introduce some errors on the data for non-evaporable water. The relation of the total amount of non-evaporable water and the degree of hydration is also well known by Powers and Brownyard (1947) studies. Atlassi (1993) suggested that pastes with SCMs gives a questionable relation of non-evaporable water and degree of hydration. SCMs reacts with $Ca(OH)_2$ in order to form C-S-H, however what happens with the hydroxyl water is still not sharp. Is it formed a new product or is it converted to evaporable water? Sellevold et al. (1982) showed less non evaporable water in a mix with silica fume than in one with the same water/binder ratio without silica fume; however it does not mean that the hydration degree is higher in silica fume pastes. To clarify the questions regarding to cement hydration and the pozzolanic reaction, Atlassi (1993) studies propose to determine the total non-evaporable water content directly by X-ray diffraction or Si NMR.

Table 3.11: Methods used in the literature to determine evaporable and non-evaporable water in cementitious materials

Material	Amount	Size	Determine	Method	Duration	Reference
Mortar	1 g (approx.)	35-100 mesh	Evaporable water	$Mg(ClO_4)_2$ solution in vacuum desiccators	7 days	(Powers and Brownyard, 1947)
			Non evaporable water	Furnace 1000ºC	15 min (approx.)	
Cement pastes	1000 g	<1 mm	Evaporable water	Oven 105ºC	1 hour	Lab B (DTU)
			Non evaporable water	Furnace 1000ºC	1 hour	
Clinker mineral pastes	2 grams (approx.)	370m²/kg	Evaporable water	Submerge in acetone (approx.1 hour) then heat by oven at 105ºC for 1 h	2 hour	(Jensen et al., 1999)
			Evaporable water	Vacuum drying with a rotary pump for 1 h	1 hour	(Jensen et al., 1999)
Cement paste and mortar	Not given	Not given	Non evaporable water	TG from 100 to 1100°C at the rate of 10°C/min	100 min	(Zhang, 2007)
Cement paste, mortar and concrete	5-6 grams	Not given	Evaporable water	TG from 20 to 105ºC at the rate of 10°C/min.		(Atlassi, 1993)
			Non evaporable water	TG from 105 to 975ºC at the rate of 10°C/min.		
Cement paste	Not given	10x40Ø mm	Evaporable water	D-drying water vapor pressure of $5x10^{-4}$ Tor	Until constant weight.	(Koster and Odler, 1986)
		10x40Ø mm	Evaporable water	Acetone is used	Not given	
		Central part of 10x40Ø mm	Non evaporable water	Heat until 800ºC		

Solvent exchange
The method is based on the replacement of pore water by an organic solvent in order to decrease the relative humidity (RH) and stop the hydration of the pastes. Isopropyl alcohol or isopropanol is considered one of the gentlest alcohol to dry cement based materials (Beaudoin et al., 1998, Feldman and Beaudoin, 1991, Kocaba, 2009). The density of the isopropyl alcohol is about 0.78g/cm³ and the water is about 1g/cm³, then the porosity may be calculated (Kocaba, 2006).

3.3.5.4 Capillary suction method

Capillary suction is a widely used method for information of transport of water and durability hydrated cementitious materials (Nielsen, 2001, Prat, 2007, Winslow et al., 1994).

The method is simple and non-costly, and it is based on the determination of the evolution in the ingress of the water into a specimen as a function of time, see detailed information on the standard (prEN-ISO12571, 1999). Water ingress may occur due to the pressure gradient between the water within the pores and the air, negative pressure for liquid and positive for air (Nilsson, 2002). A dried cement paste is used to accelerate the process of capillary suction (relative humidity is around 50 percent).

The water mocules will bind together due to hydrogen bounds, in multiple layers of liquid. The thinnest and smallest pores gets complete saturated first since the liquid layers on the surfaces has lesser distance to unite. If the humidity increases the larger pores will gradually be saturated as well. This continues until the equilibrium between the surrounding atmospheric air and the material.

Experiments conducted has shown that there seems to exist intervals of the capillary suction rate, see Fig. 3.32 (NTBuild-368, 1991) . An initial wetting of the surface will cause a weight gain when the paste comes into contact with water (higher slope of the curve, see Fig. 3.32). Hereafter different rates occur until either a steady state achieves or a complete saturation of the material is attained.
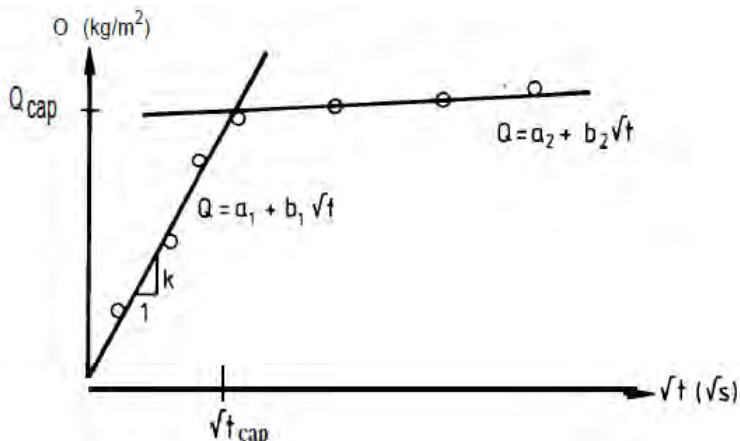
Fig. 3.32: Weight gain versus time for capillary suction method (NTBuild-368, 1991)

Data from the literature showed that capillary suction test has been successfully used for mortar and concrete (Martys and Ferraris, 1997, prEN-ISO12571, 1999, Zhang, 2007). However, the use of cement pastes may need a longer expose time to water to fully re-saturate the sample as less porous is found for cement pastes compared with concrete and mortar.

Pore size
A concave coherent surface (meniscus) of water forms within the saturated pores. The meniscus formation is caused by the surface tension of water as well as the hydrophilic surface of the pore surface; see Fig. 3.33. At the formed meniscus inside a porous material exists a hydrostatic negative pressure, thus the pore size can be determined by the Equation 3.23.

$$p_v = p_L - \frac{2 \cdot \sigma \cdot \cos\theta}{r}$$

(Equation 3.23)

Where

P_l	Liquid pressure, Pa
P_v	Air pressure, Pa
θ_{w-m}	Angle between the pore wall and the meniscus, rad
σ_{v-l}	Surface tension vapour-liquid interface, N/m
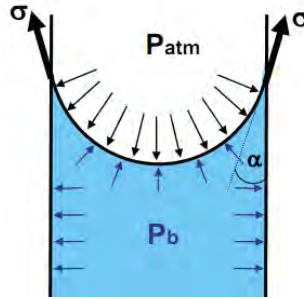
Fig. 3.33: Meniscus formed in a saturated pore (after (Brunauer et al., 1967))

Sorptivity
The total water uptake is given by the Equation 3.24 (Martys and Ferraris, 1997).

$$\frac{W_a}{A_s \cdot \rho_l} = S_w \cdot \sqrt{t} + S_0$$

(Equation 3.24)

Where

W_a	Volume of the absorbed water, m³
A_s	Sample surface area exposed, m²
t	Time,s
S_w	Sorptivity (the slope of the W/A versus. $t_{1/2}$),g/ m²·s$^{1/2}$
S_0	Correction for surface effects, m·s$^{-1/2}$

3.3.5.5 Autogenous deformation

Autogenous phenomena is related to the autogenous deformation and autogenous relative-humidity change (Jensen and Hansen, 1995, Jensen and Hansen, 2001).

Autogenous deformation is defined as the "*bulk deformation of a closed, isothermal, cementitious material system not subjected to external forces*"(Jensen and Hansen, 2001). Autogeneous deformation may be represented by the self-desiccation shrinkage and/or expansion during the hydration of cementitious materials. Setting shrinkage is the first part of the shrinkage curve (Fig. 3.34) where the internal volume reduction of the material can be converted to a bulk deformation of the system. After that, drying of the pastes occurs (self-desiccation), see Fig. 3.34(b).

Self-desiccation of pastes leads to a decline in its autogenous relative humidity (RH) and therefore results in autogenous shrinkage. This is especially seen at early age structure or sealed curing. One of the negative effects of autogenous deformation is to cause micro-cracking and it also may be related with continuous crack patterns find in hydrated cementitious materials (Jensen and Hansen, 1999).
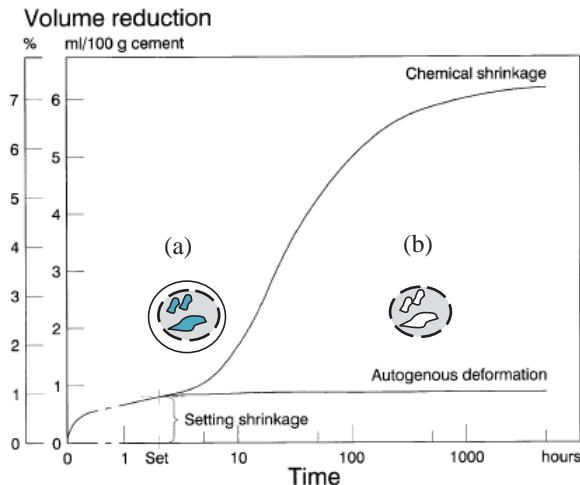
Fig. 3.34: Example of chemical shrinkage and autogenous deformation for cementitious materials (after (Jensen and Hansen, 1999))

Autogenous deformation have been determined in different ways (Jensen and Hansen, 1995, Jiang et al., 2005). Linear measurement of autogenous is standardized method and performed by placing the cement paste in a rigid mould with low friction (ASTM-C1698–09, 2009). The length change of the cement paste is recorded by a displacement transducer at the end of the specimen.

Evolution of autogenous deformations is expressed from the time-zero as the time when stresses appears, see in (Tazawa and Miyazawa, 1995). The autogenous deformation curves for slag pastes show expansion and shrinkage of the pastes, and this may reflects on the cracking of slag pastes, see in (Darquennes et al., 2011). It should be stressed that changes in time-zero can modify the conclusions that larger autogenous shrinkage is found for slag pastes (Darquennes et al., 2011).

3.3.5.6 Thermal analyses: thermo gravimetric (TG) and differential thermogravimetry (DTG)

Thermal analyses experiments based on the heating of the sample and an inert reference under identical conditions (e.g. rate, temperature, pressure) are used to determine the decomposition of the phases and locate the ranges corresponding to the phases of hydrated products of cementitious materials (Hansenb and Panea, 2005, Khoury, 1992, Ruiza et al., 2005, Kocaba, 2007b, Zhang, 2007).

TG analysis simultaneously measures the weight loss due to the decompositions, while trough the first derivative of TG (DTG) is suggested to identify the phase compounds of the cement pastes by endothermic and exothermic reactions, see Fig. 3.35. The following ranges of temperature are suggested for the analysis of the decomposition of the hydrated cementitious materials (Taylor, 1997):

- - 30 to 105ºC: Evaporable water and a part of the bound water are consumed.
- - 110 to170ºC: Decomposition of gypsum, ettringite and the loss of water from part of the carboaluminate hydrates take place
- - 180 to 300ºC: Loss of bound water from the decomposition of the C-S-H and carboaluminate hydrates undergoes
- - 425 to 550ºC: De-hydroxylation of the portlandite (CH)
- - 600 to 800ºC: De-carbonation of calcium carbonate

As described, the loss of bound water from C-S-H mainly occurs from 180 to 300ºC. However, some of the water loss from C-S-H may also occur later, which complicates the evaluation of its total amount of water trough thermal analyses (Mackenzie and Mitchell, 1961, Panea and Hansen, 2005, Shimada and Young, 2001). Calcium hydroxide decomposition is at about 425 to 550ºC and amorphous calcium carbonate (calcite) in the range of 600 to 800ºC. Carbonation may be measured by the amount of amorphous calcium carbonate (Belie et al., 2010, Ngala and Page, 1997a).
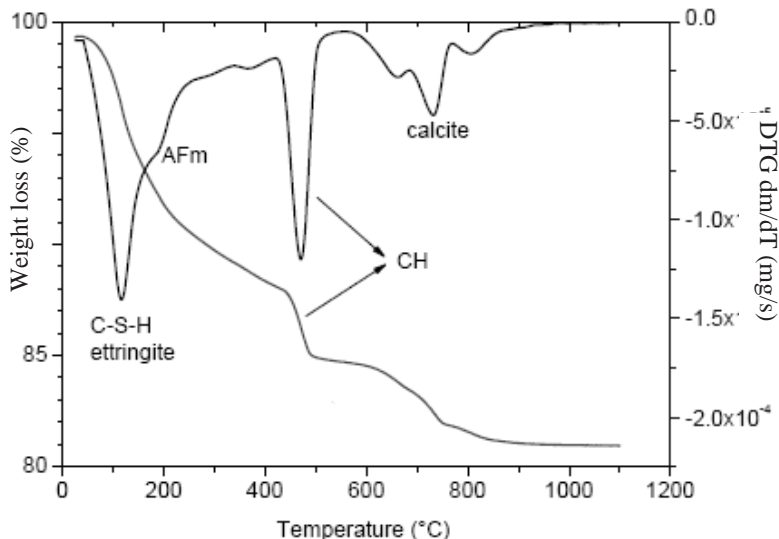
Fig. 3.35: TG and DTG curve for hydrated cement paste (Zhang 2007)

3.3.6   Comparison of methods

The characterization of the pore structure also become difficult due to the uncertainties associated to the methods of porosity characterization. The interpretation of data provided by individual techniques based on different assumptions and principles are reported as a barrier to characterize the pore structure of hydrated cementitious materials (Diamond, 1971, Villadsen, 1992, Yassin, 2010). This section is based on the literature review of the data for similar samples applying different methods of porosity characterization.

Day and Marsh (1988) compared the results between the solvent exchange and water porosity; and solvent exchange and mercury porosity for cement pastes with 0, 30 or 50% of fly ash, and 10% of silica fume addition (by weight) cured saturated at room temperature for 7, 28 and 90 days at w/c

ratio of 0.47. In addition, samples cured at 35ºC for three months were used for solvent exchange and water porosity tests (marked in the Fig. 3.36 as Δ35). The water porosity was calculated through the difference between the weight of water-saturated and oven-dried at 105ºC. Solvent exchange porosities were calculated from the change in the sample weight, knowing the specific gravities of the initial pore fluid (approx. 1g/cm³) and the alcohol used (methanol 0.7871g/cm³ and isopraponol 0.7811g/cm³). The mercury porosity was based on the fraction of the bulk volume of specimen intruded by mercury at a maximum pressure of 414 MPa; assuming 140° for contact angle and 480 mN/m for surface tension.

The results showed that the water porosity method gives a higher porosity than solvent exchange; see Fig. 3.36(a). A good agreement between the results of alcohol exchange and mercury porosity was found see Fig. 3.36(b).
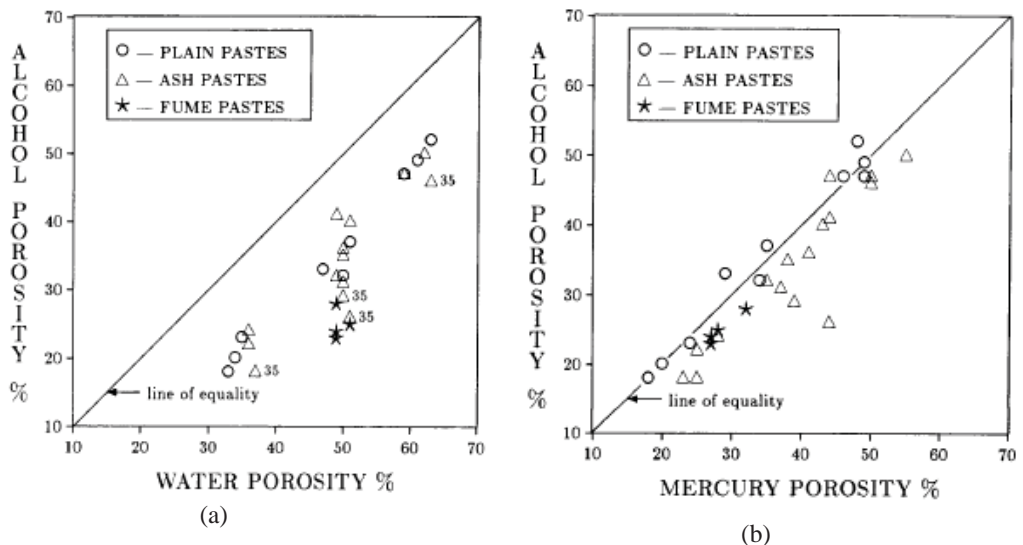
Fig. 3.36: (a)Alcohol porosity (%) versus water porosity (%) and (b) alcohol porosity (%) versus mercury porosity (%) for blended pastes at 7, 28 and 90 days and w/c ratio of 0.47 cured at room temperature (Day and Marsh, 1988)

Also, studies pointed out that the total porosity of fly ash pastes measured by helium turned out to be lower than plain Portland cement, see Fig. 3.37 (Feldman, 1986a). The author suggested that some of the pores of fly ash pastes may be not accessible by helium (Fig. 3.37(a)). He also demonstrated that high pressure applied by mercury intrusion caused damage on the pore structure of the fly ash pastes. Fig. 3.37(b) shows a higher threshold pore size for the second intrusion curve of MIP. This fact was not so evidence for plain cement pastes, (Feldman, 1986a). Sun and Scherer (2010) compares MIP, gas sorption (nitrogen) and LTC for mortar without entrained air, see Fig. 3.38. LTC (black curves) seems to give a lower volume of pores, according to the author the pores may not freeze in the smaller pores.

(a)
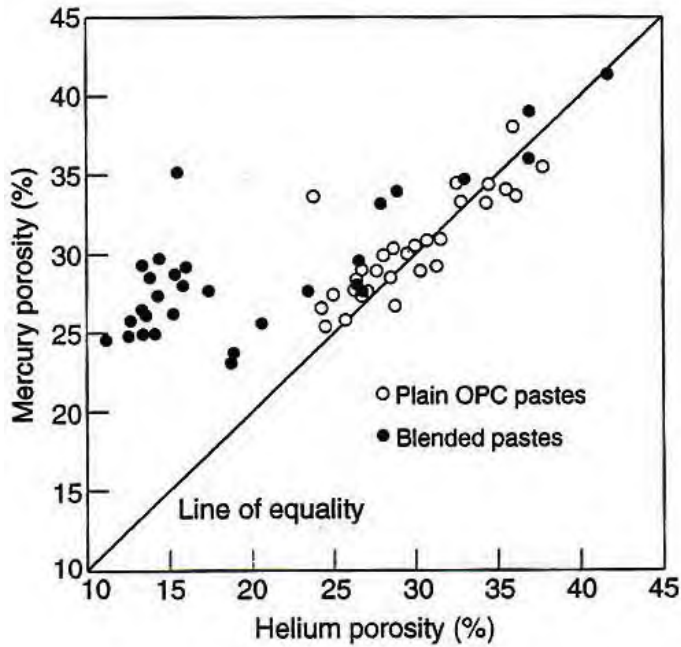
(b)
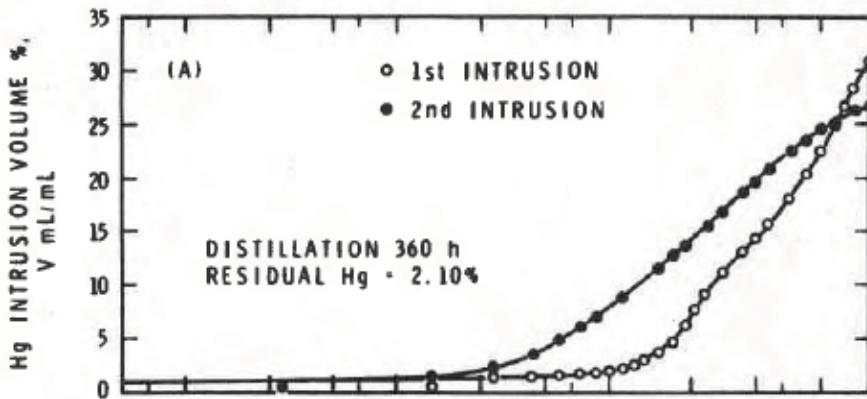
Fig.3.37: (a) MIP versus helium porosity (%) (Feldman, 1986b) and (b) MIP curves for fly ash paste:1st and 2nd intrusion (Feldman, 1986b)
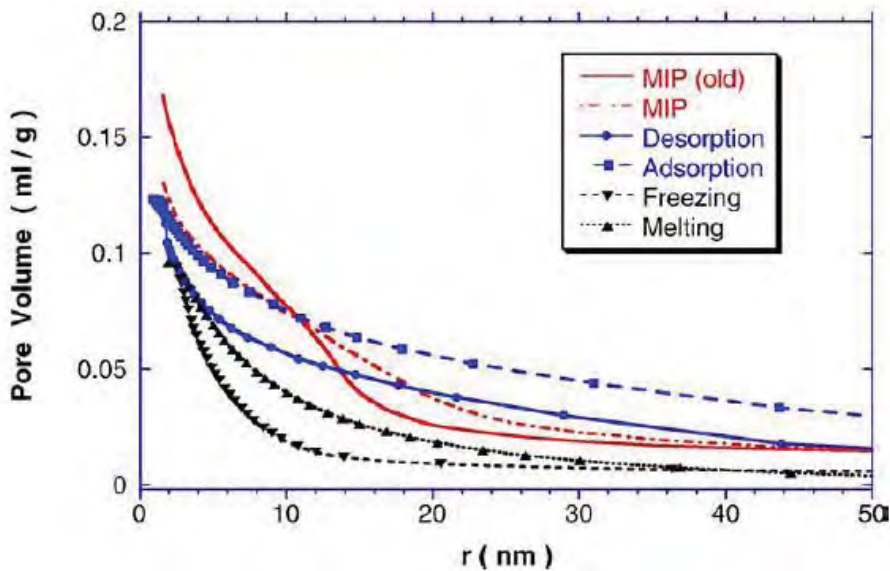
Fig.3.38: Pore volume versus pore radius for mortar for MIP (red line), gas sorption (blue line) and LTC (black line) (Sun and Scherer 2010)

Comparison of porosity methods was also reported by Villadsen (1992) using white cement pastes cured saturated at room temperature for at least 86 days and water/cement ratio of 0.40 (by volume). He used nitrogen sorption; MIP and LTC for test similar samples, see Fig. 3.39. For MIP, different equipments (LBM and USA)) and drying conditions of the samples (methanol and CO_2 free) were evaluated. LTC was carried out using samples at different drying conditions: virgin (Fig. 3.39(a)) and dried and re-saturated (Fig. 3.39(b)). The re-saturation was carried out using vacuum saturation.

(a)

(b)
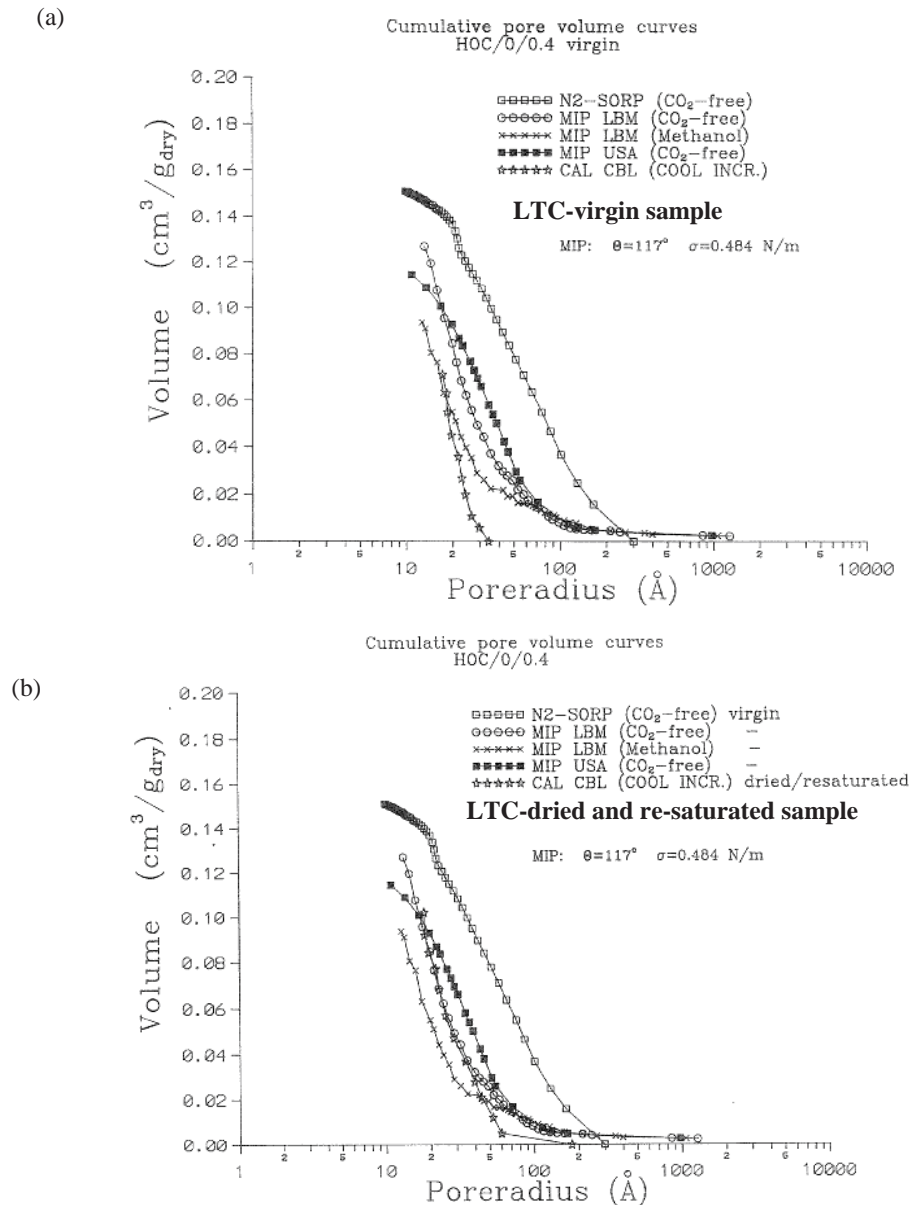
Fig. 3.39: Cumulative volume of pores (cm³/g dry) for: nitrogen sorption; MIP measured at LBM; MIP measured at LBM using methanol; MIP measured at USA; LTC using(a) virgin sample and (b) dried and re-saturated sample (Villadsen, 1992)

Fig. 3.39(a) shows a shift between the patterns of the curves for varying methods, where lowest values of pore volume are represented by the LTC curve. It may indicate that some of the water not freeze. This is also in agreement with data showed by Sun and Scherer (2010). It is also possible to

observe that the curves of pore size distribution for different methods are not similar. All the variables analysed by the author (equipment, sample preparation) affected somehow MIP data, see Fig. 3.39. When the samples from LTC were dried and re-saturated, a good accordance of MIP and LTC results was found (Fig. 3.39(b)).

Among others, Diamond (1971) found different curves of pore size distribution for similar hydrated cement pastes measured by nitrogen sorption (based on capillary condensation) and MIP. MIP showed coarser pore parameters than nitrogen sorption. The author also calls attention to the range of pores measured by capillary condensation methods (e.g. water sorption, LTC), which are very small pores to represent the pore structure of a cement paste.

Diamond and Leman (1995) studies discussed MIP and SEM (magnification of 400 and 1200) data for cement pastes cured saturated at 1 and 28 days with w/c of 0.4, see Figs. 3.40(a) and 3.40(b). They call attention to the inconsistency of the results when the methods are compared, see Fig. 2.43. Both methods requires drying of the samples however the data showed different trends when MIP and SEM are compared. MIP may underestimate the content of larger pores (about µm) and overestimate the pores in the range of sizes below of approx. 0.1 µm, and it is due to the "ink-bottle effect, see in (Diamond and Leeman, 1995).
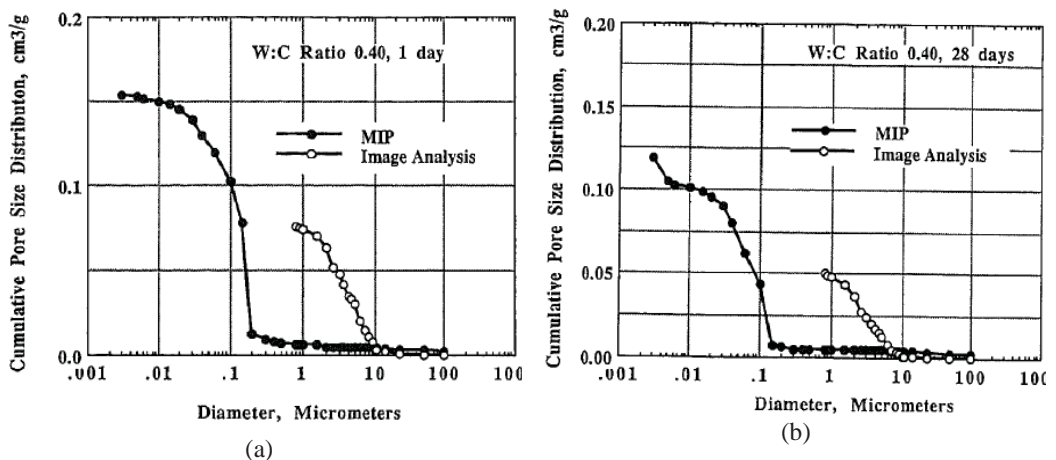
Fig. 3.40: MIP and SEM for cement pastes, w/c of 0.4 cured saturated for (a) 1 day and (b) 28 days (Diamond and Leeman, 1995)

Unfortunately, pore structure is difficult to measure accurately, and different techniques have given widely varying values. The differences may be related to the different assumptions and principles used to obtain values for pore size. It is also known that some of the methods analysed here (i.e. MIP, water sorption) may overestimate the volume of smaller pores due to the bottlenecks in the pores system. The sample preparation is also a matter to be considered, as showed by Villadsen (1992) that with similar sample submitted to similar preparation (oven dried at 105ºC) had comparable data for MIP and LTC. It is important to call attention for the urgent necessity of specifications for porosity measurements. Differences in sample preparation, measurement and assessment of data may introduce errors in the results of porosity. To draw clear conclusions about

porosity of the hydrated cementitious materials still a challenge. In any case, it is important to consider what part of the pore structure are being asses for the used method and how relate that to the properties of interest.

4 Experimental

The present section covers the experimental investigation of the project. Firstly, an overview of the experimental program is given (Section 4.1). Then, the characteristics (e.g. chemical and physical properties) of the constituent materials and the methods of casting and curing are described, see Section 4.2. Section 4.3 and 4.4 describes the testing covering sub-sectioning of samples, pre-conditioning and short procedure of techniques applied. Detailed procedure of the test methods are given in the Appendixes (VII to XV).

4.1 Overview of experimental program

Cement paste samples were used for investigation of the impact of SCMs and curing conditions (temperature and moisture) on the development of porosity. The overview of the investigations is given in the Table 4.1. The detailed plan for the project covering materials, curing conditions and techniques for porosity characterisation are summarized in Table 4.2.

Samples identification includes information on cement type, SCM (type and amount), age, and moisture condition during curing (s for sealed and w for saturated), and curing temperature. For example: C_s40_28s20 is a sample made from 60% cement C + 40% slag and cured for sealed (s) at 20°C for 28 days.

Table 4.1: Overview of constituent, curing conditions and methods.

Materials		Curing conditions			Procedures
Cement	**SCMs**	**Temperature ($^\circ$C)**	**Moisture**	**Duration (maturity days)**	
A C	Slag: 40 and 70% Fly ash: 15 and 30%	20 55	Saturated Sealed	1 3 28 90 720	LTC MIP SEM Water sorption NMR Evap. and non-evap. water Capillary suction Isothermal calorimetry Thermogravimetry Solvent exchange Autogenous deformation

Table 4.2: Investigations, number of samples tested

Material	Methods	Cured saturated 20°C Days						Cured saturated 55°C Days (maturity days)				Cured sealed 20°C Days					Cured sealed 55°C Days (maturity)			
		1	3	7	28	90	720	0.69 (3)	6.45 (28)	20.7 (90)	165.6 (720)	1	3	28	90	720	0.69 (3)	6.45 (28)	20.7 (90)	165.6 (720)
A	LTC	1	1		1	1	1		1	1	1			1	1			1	1	
	MIP	2	2		2	2	2	2	2	2	2			2	2	2		2	2	2
	SEM				1															
	Water sorption				1									1			1			
	NMR	1																		
	Evap. and non evap. water		1											1	1			1	1	
	Capillary suction																			
	Autog.deformation																			
	Isothermal cal.																			
	Thermogravimetry																			
	Solvent exchange			1																
C	LTC		1		1	1	1		1	1	1			1	1			1	1	
	MIP		2		2	2	2	2	2	2	2	2	2	2	2	2		2	2	2
	SEM		1		1															
	Water sorption				1	1	1							1				1		
	NMR	1																		
	Evap. and non-evap. water		1		1	1	1	1	1	1	1			1	1			1	1	
	Capillary suction		1		1															
	Autogenous deformation											2	2	2	2					
	Isothermal cal.											2	2	2			2	2		
	Thermogravimetry								1											
	Solvent exchange	1			1	1														

Table — Experimental program (number of specimens per method, curing condition, temperature and age).

Header grouping: **Cured saturated** [20°C: Days 1, 3, 7, 28, 90, 720 | 55°C: Days (maturity days) 0.69(3), 6.45(28), 20.7(90), 165.6(720)] and **Cured sealed** [20°C: Days 1, 3, 28, 90, 720 | 55°C: Days (maturity) 0.69(3), 6.45(28), 20.7(90), 165.6(720)].

Material	Methods	1	3	7	28	90	720	0.69 (3)	6.45 (28)	20.7 (90)	165.6 (720)	1	3	28	90	720	0.69 (3)	6.45 (28)	20.7 (90)	165.6 (720)
C_s40	LTC	1	1		1	1	1	1	1	1	1	2	2	1	1			1	1	1
	MIP	2	2		2	2	2	2	2	2	2	2	2	2	2	2	2	2	2	2
	SEM		1		1	1	1				1					1				1
	Water sorption	1			1	1	1					2	2	1				1		
	NMR	1	1									2	2							
	Evap. and non-evap. water	1	1		1	1	1	1	1	1	1	2	2	1	1			1	1	
	Capillary suction		1		1															
	Autog. deformation											2	2	2	2		2			
	Isothermal cal.											2	2	2	2		2	2		
	Thermogravimetry								1											
	Solvent exchange		1		1	1	1													
C_s70	LTC	1	1		1	1	1	1	1	1	1	2	2	1	1			1	1	1
	MIP	2	2		2	2	2	2	2	2	2	2	2	2	2	2	2	2	2	2
	SEM		1		1	1	1				1			1		1				1
	Water sorption	1			1	1	1					2	2	1				1		
	NMR	1	1									2	2							
	Evap. and non-evap. water	1	1		1	1	1	1	1	1	1	2	2	1	1			1	1	
	Capillary suction		1		1															
	Autog. deformation											2	2	2	2		2			
	Isothermal cal.											2	2	2			2	2		
	Thermogravimetry								1											
	Solvent exchange		1		1	1														

Material	Methods	Cured saturated										Cured sealed								
		20°C						55°C				20°C					55°C			
		Days						Days (maturity days)				Days					Days (maturity)			
		1	3	7	28	90	720	0.69 (3)	6.45 (28)	20.7 (90)	165.6 (720)	1	3	28	90	720	0.69 (3)	6.45 (28)	20.7 (90)	165.6 (720)
C-f15	LTC	1	1		1	1	1	1	1	1	1			1	1	2		1	1	
	MIP	2	2		2		2	2	2				2	2	2	2	2	2	2	2
	SEM																			
	Water sorption													1				1		
	Evap. and non-evap. water	1	1		1	1	1	1	1	1	1			1	1			1	1	
	Capillary suction																			
	Autog.deformation																			
	Isothermal cal.											2	2	2			2	2		
	Thermogravimetry																			
	Solvent exchange																			
C-f30	LTC	1	1		1	1	1	1	1	1	1			1	1	2		1	1	
	MIP	2	2		2		2	2	2				2	2	2	2	2	2	2	2
	SEM																			
	Water desorption													1				1		
	Evap. and non-evap. water	1	1		1	1	1	1	1	1	1			1	1			1	1	
	Capillary suction																			
	Autog. deformation																			
	Isothermal cal.											2	2	2			2	2		
	Thermogravimetry																			
	Solvent exchange																			

4.2 Materials

4.2.1 Constituent of materials

The chemical composition and the density of the constituent materials are listed in Table 4.3. The cements A and C; and the SCMs s01 and f01 were received in August of 2007 from Aalborg Portland Cement and EPFL and stored in sealed containers of 30 litres at DTU. Accumulative particle size distributions for cements A and C, and the SCMs slag and fly ash were analyzed in connection with NanoCem Core Project 4 (Kocaba, 2007a), data is given in the Fig. 4.1.

Table 4.3: Main oxides and densities of the constituent materials (Kocaba, 2009, Le Saout, 2007)

Id.	Type of material	Density (g/cm³)	Main oxides concentration (XRF)									
			SiO_2	Al_2O_3	Fe_2O_3	CaO	MgO	SO_3	K_2O	Na_2O	TiO_2	P_2O_5
			(%)	(%)	(%)	(%)	(%)	(%)	(%)	(%)	(%)	(%)
A	white cement	3.14	24.68	2.11	0.43	68.67	0.58	1.82	0.06	0.17	0.05	0.45
C	Grey cement	3.18	21.01	4.63	2.60	64.18	1.82	2.78	0.94	0.20	0.14	0.40
s01	slag	2.6	36.61	12.21	0.85	41.59	7.18	0.63	0.28	0.18	0.35	0.01
f01	fly ash	2.2	50.30	25.5	9.10	4.90	2.40	1.00	3.60	1.10	1.0	0.60
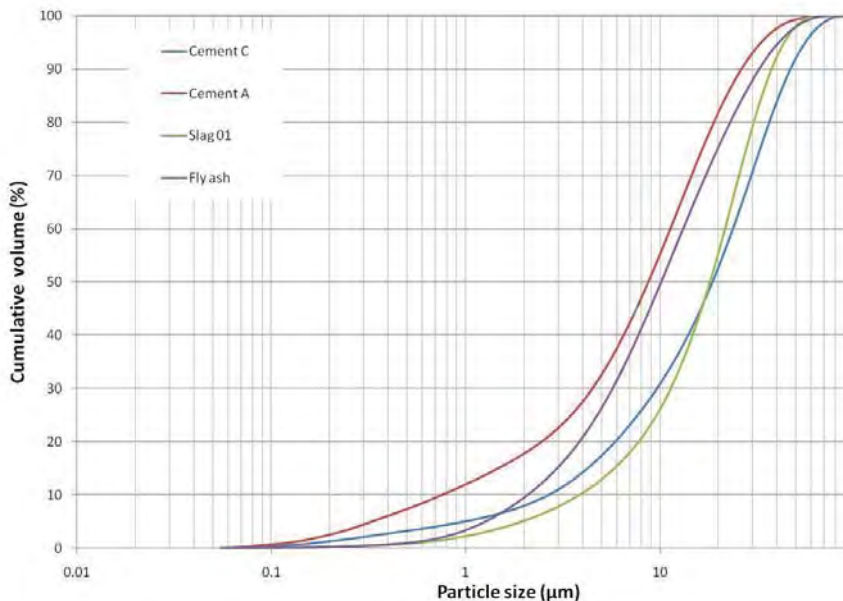
Fig. 4.1: Particle size distribution for cements A and C, and the SCMs S01 and F01 (Kocaba, 2007a)

Data on the degree of hydration measured by SEM and X-ray diffraction (XRD) for cement pastes cured saturated at 20°C for 1, 3, 28, 90 and 360 days, water cement ratio of 0.4 are given in Table 4.4 (data from NanoCem Core project 4 (Kocaba, 2008)). According to Kocaba (2008a) the degree of slag reaction is approx. 20% after 28 days curing at 20°C. Fernandez-Altable (2010) measured the degree of hydration of the slag at 90 days for the same mix design and composition, see Table 4.5. Degree of hydration using a different type of cement at w/c ratio of 0.4, cured saturated at 20ºC or 60ºC for 3, 28 and 90 days may be seen in the Table 4.6 (Zhang, 2007).

Table 4.4: Degree of cement hydration for selected samples cured saturated at 20°C (Kocaba 2008)

Material	Test	Cured saturated at 20°C				
		Days				
		1	3	28	90	360
A	SEM	46.1 ± 2.8	61.6 ± 2.8	79.6 ± 2.3	86.6 ± 2	-
	XRD	41.7 ± 3	65.0 ± 3	75.8 ± 3	86.0 ± 3	87.2 ± 3
C	SEM	48.0 ± 5.2	57.6 ± 4.6	69.5 ± 4.7	76.6 ± 3.4	-
	XRD	58.6 ± 3	67.1 ± 3	72.4 ± 3	84.1 ± 3	93.4 ± 3
C_s40	SEM	-	61.1 ± 6.3	81.5 ± 3.0	86.6 ± 2.3	-
	XRD	55.6 ± 3	58.7 ± 3	81.7 ± 3	83.1 ± 3	-

Table 4.5: Degree of hydration of slag (%) analyzed by XRD and SEM (Fernandez- Altable, 2010).

Sample id.	Curing conditions	Degree of hydration of slag(%)
		90 days
C_s40 (40% of slag)	20ºC, saturated	67%
C_s70 (70% of slag)	20ºC, saturated	40%

Table 4.6: Degree of hydration of cement pastes cured at different temperature (Zhang, 2007)

Material	Curing conditions	Degree of hydration of cement pastes (%)		
		3 days	28 days	90days
Cement paste	Saturated, 20ºC,	61	72	78
Cement paste	Saturated, 60ºC	75	84	86

The development of heat of hydration for pastes was measured using thermal calorimeter for pastes with and without slag and fly ash cured at 20ºC or 55ºC, see Appendix XIV. The cumulative heat evolution curves of pastes blended with slag and fly ahs at 20ºC or 55ºC over a period of 120 hours are also given in the Appendix XX. The effect of slag and fly ash addition can be seen in the shape and the pattern of the curves of heat flow versus time, see Appendix XX.

4.2.2 Paste compositions

Pastes with initial water/solid volume ratio at 1.26 (corresponds to w/c=0.40 for cement A) were prepared. The proportions are given in Appendix II. The procedures for bleeding methods are given in the Appendix V. Due to bleeding the obtained w/b was lower in all pastes except pastes from

cement A, see Table 4.7. The measurements of bleeding are described in Appendix V. The method which gave more reliable results were based on the measurements of the height of pastes in plastic moulds after casting and 2 hours later (named as Method 3, see Appendix V).

Table 4.7: W/b ratio for cement pastes before and after bleeding

Mix	Sample (after casting)		Sample (after bleeding)	
	w/b	Water to solid volume	w/b	Water to solid volume
		cm^3		cm^3
C	0.40	1.26	0.36	1.16
		1.26	0.36	1.16
C_s40	0.43	1.26	0.40	1.15
		1.26	0.40	1.17
C_s70	0.46	1.26	0.43	1.18
		1.26	0.43	1.18
C_f15	0.42	1.26	0.38	1.13
		1.26	0.39	1.16
C_f30	0.45	1.26	0.40	1.12
		1.26	0.40	1.12
A	0.40	1.26	0.40	1.26
		1.26	0.40	1.26

4.2.3 Mixing, casting and curing of paste and mortar

The mixing and casting of the pastes were undertaken as described in detail in the Appendix III. For mixing, an electronic mixer and custom made paddle (diameter of 44.5 mm) were used. The water was added to the cement mix and mixed for 3 minutes at the speed of 500 rpm. After that, the mixing was stopped for 2 minutes and mixed for 2 more minutes at 2000 rpm. All samples were cast in plastic moulds with lids; the sizes are given in Table 4.8.

Table 4.8: Size of moulds (approx.)

Method	Sealed curing	Saturated curing
LTC	65x15 Ø mm	73x23 Ø mm
NMR	50x8 Ø mm	73x23 Ø mm
Others	73x23 Ø mm	73x30 Ø mm

Curing was undertaken at 20ºC and 55ºC for the periods given in Table 4.9. The curing time at 55°C was estimated assuming a activation energy at 33.5 kJ/mol for all pastes and using Equations 4.1 and 4.2 (Hansen and Pedersen, 1977).

$$M = \int_0^t H(T)dt \qquad \qquad \text{(Equation 4.1)}$$

$$H(T) = exp\left[\frac{E_a}{R}\left(\frac{1}{293} - \frac{1}{273+T}\right)\right] \qquad \qquad \text{(Equation 4.2)}$$

Table 4.9: Duration of curing

Temperature (ºC)	Time (days)					
20	1	3	28	90	360	720
55	0.23±	0.69	6.45	20.7	82.9	165.6

Curing was either undertaken sealed or saturated; possible bleeding water was removed in the first two hours after casting (beginning of the set of the pastes). The moisture conditions are briefly described in Table 4.10; further information is given in Appendix III. All samples were kept in the laboratory at approximately $20^{°}$C for 2 hours, after that they were transferred to water baths to control the curing temperature and to restrict evaporation and ingress of CO_2.

Table 4.10: Moisture curing conditions

Curing condition	Abbreviation	Procedure
Saturated	_w	After 2 hours the samples were placed in water baths. All pastes, except pastes with cement A, had sufficient bleeding water to stay saturated for 24 maturity hours. After 1 day the sample was removed from the mould and placed in slightly larger container and covered by saturated calcium hydroxide solution.
Sealed	_s	Possible bleeding water was removed after 2 hours.

4.2.4 Heterogeneity of samples

Bleeding was observed for all pastes, except the pastes with cement A, as described in the previous section. The corrected w/b and water/solid ratios are given in Table 4.7.
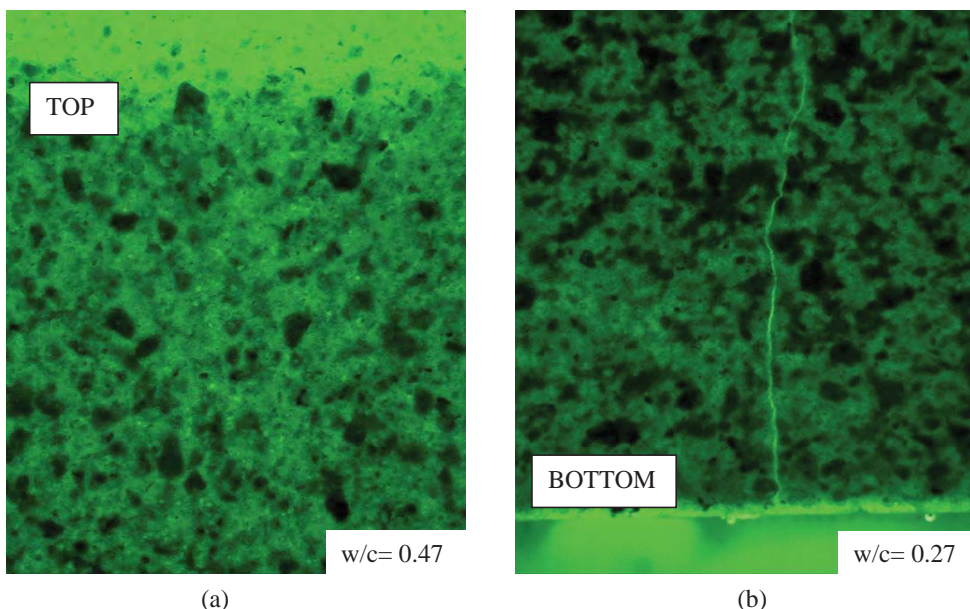
Fig. 4.2: Thin section of the (a) top and (b) bottom of plain cement pastes cured saturated with bleeding cured at 20ºC sample C at 28 days (1.34 mm wide)

Due to the bleeding it is expected that the solid concentration is reduced in the upper part and increased in the lower part of the samples. The heterogeneity of a sample C cured saturated for 20ºC for 28 days was determined by thin section analysis. In the Figs. 4.2(a) and 4.2(b), plain cement pastes showed less than 5 mm of the upper (Fig. 4.2(a)) and lower part (Fig. 4.2(b)) exhibit a capillary porosity different from the remaining sample.

4.2.5 Entrapped air voids of the pastes

The volume of air voids was measured by vacuum saturation and pressure saturation, see Appendix IX. The method of vacuum saturation and pressure saturation are described in the Appendix IX and it is according to the standard NTBuild-368 (1991). The results showed a maximum of approx. 2 % of air voids for cement C_f30 (30% of fly ash). The size of the air avoids were from 1 to 2.5 mm. The measurements of entrapped air voids are given in the Table 4.11. The impact of air voids on the porosity measurements are shown in the Table 4.12.

Table 4.11: Volume fraction of air voids in the cement pastes at 28 days cured sealed at 20ºC

Sample id.	Total volume of the sample (cm³)	Weight (g)		Air voids (fraction)
		Vaccum saturation	**Pressure saturation**	
A_28s20	42.77	20.21	20.33	0.27
	33.54	19.52	19.60	0.25
C_28s20	41.38	22.74	23.15	0.99
	35.09	19.25	19.78	1.53
C_s40_28s20	43.43	19.81	20.09	0.65
	37.85	19.25	19.54	0.78
C_s70_28s20	41.09	18.70	18.93	0.58
	41.99	20.08	20.26	0.44
C_f15_28s20	41.41	18.46	18.76	0.71
	48.68	22.70	23.13	0.88
C_f30_28s20	35.97	16.46	16.69	0.66
	36.88	16.86	17.09	0.61

Table 4.12: Possible effect of entrapped air voids in the porosity results by selected methods

Methods	Possible effect of air avoids
LTC	No effect as saturation of the air voids is not expected
Water desorption	No effect as the samples were crushed to grin size 150 to 250 µm
MIP	Small effect, as the samples were crushed to grain size 5 to 10 mm
SEM	Air voids are not taken in account
Isoproponal exchange	No effect as saturation of the air voids is not expected

4.3 Testing

4.3.1   Subsection of the samples

Samples for MIP, SEM and water sorption were cast in plastic moulds of 70x30 Ø mm (sealed) or 70x22Ø mm (saturated) and cut in slices as showed in the Fig. 4.3(a). The upper and the bottom part of the sample (approx. 15 mm) were discharged to avoid the effect of bleeding in the samples. Samples for LTC were cast in plastic moulds of 65x15 Ø mm of height; and NMR 50x8 Ø mm; see Fig. 4.3(b). No subdivision of the samples for NMR and LTC was undertaken.

(a)   (b)
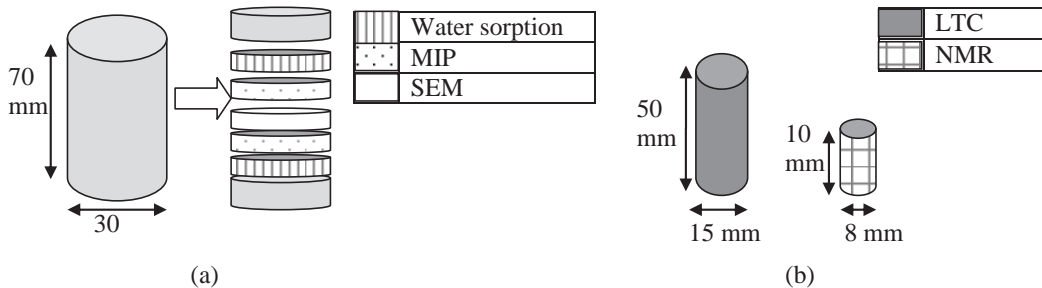
Fig. 4.3: (a) Slices used for water sorption (stripes), MIP(dots) and SEM(white) and (b) samples for LTC and NMR respectively

4.3.2   Drying of the samples (solvent exchange)

Samples for MIP, SEM and capillary sorption were dried by solvent exchange according to the procedure given in the Appendix XVIII in this way also the hydration was stopped. The slices were placed in isopropyl alcohol (isopraponol) for 7 days (5 mm approx), recommended by Kocaba (2006). The isopraponol was subsequently evaporated by placing the samples in vacuum for 24 hours. Dried samples were stored in desiccators with silica gel under vacuum.

4.3.3   Procedures

4.3.3.1   Low temperature calorimetry -standard procedure

Low temperature calorimetry studies were carried out using Calorimeter Calvet, Model: BT 2.15, from Setaram. Two instruments were used for the measurements named as: Calorimeter 1 and Calorimeter 2.Procedure for LTC is given in the Appendix X.

LTC was performed on non-dried samples to characterize threshold pore size, total pore volume and pore size distribution.

Cement pastes were wiped in a moist tissue (distillate water) in order to obtain a saturated surface dried (SSD) sample, and then weighed (accuracy of 0.0001 g). Therefore the sample was placed in the sample cell; AgI (approx. 0.01 grams) was sprinkled upon the top of the sample to facilitate ice crystallization during the cooling. The sample was introduced into the calorimeter using a metallic bar, see more details in the Appendix X. In the present study, an empty reference was used and the baseline was calculated based on the calculation described in the Procedure for LTC (Appendix X).

The calorimeter (LTC equipment) measures the differential heat flow by means of thermocouple detectors connected in series. The calorimeter operates either isothermally or in a constant

temperature gradient. Inside the calorimeter, there is a block which contains two identical and symmetrical cells: (1) sample cell and (2) reference cell, see Fig. 4.4. The large numbers of thermocouples effectively integrates temperature differences over the entire cell surface (except for top and bottom) which may give reliable results of the samples (Setaram, 2005).
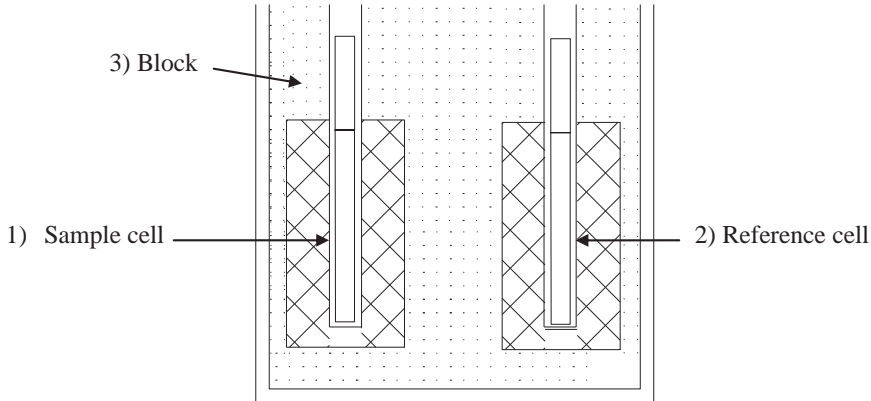
Fig. 4.4 : Sketch of the Calorimeter inside: 1) sample cell, 2) reference cell and 3)block

Tests were carried out with cooling rates of 3.3ºC/h and heating rates of 4.1 ºC/h, in the range of temperature from 20ºC to -55ºC. The temperature of -55ºC was chosen because it is assumed that no crystalline ice forms below that (Bager and Sellevold, 1986a). Freezing and thawing rates were chosen based on literature review and previous tests carried out at DTU (Bager and Hansen, 2000, Kjeldsen and Geiker, 2008). To cool down the samples to such low temperatures, a controlled temperature forcing system called Thermojet was used (Thermojet TM Precision Temperature Cycling System, Model: THJ-TC1, from FTS).

After LTC, the sample was weighted and placed in the oven at 105ºC and then 1000ºC in order to determine respectively the amount of evaporable and non-evaporable water through weight loss measurements. The procedure for determination of evaporable and non-evaporable water is given in Appendix VII.

4.3.3.2 Assessment of the data

The final data of LTC is collected through the computer and analysed and discussed trough graphics and values. Pore size and pore volume are calculated according with section 3.3.1. The parameters used for LTC calculations are given in the Table 4.13. The values and parameters used for determination of pore size are according to Sun and Scherer (2010).

Graphs of apparent heat capacity versus block temperature are used for a qualitative analysis of the data and type of pores, see Table 4.14. The amount of ice formed is calculated and convert to pore volume, see more details in the Section 3.3.1 and Appendix X.

Table 4.13: Parameters used for the pore size determination.

Description	Symbol	Adopted value	Unit
Heat of fusion of ice	ΔH_{fus}	333.8 + 1.79.T * 332.4 **	J/g_{ice}
Surface tension liquid-solid	$\sigma_{l\text{-}s}$	$0.0409 + 3.9.10^{-4}\Delta T$	N/m
Density of the liquid	ρ_l	$916.7 - 2.053 \cdot 10^{-1}T - 1.357 \cdot 10^{-3}T^2$ (Brun et al., 1977)	Kg/m³
Freezing temperature of the pore	T_o	273	K
Molar mass of the liquid	M	18.10^{-3}	Kg/mol

*melting by the side
**freezing

Table 4.14: Range of temperature for the porosity studies

Temperature ranges	0 to -20ºC	-20 to -38ºC	-38 to -50ºC
Pore classes	Large and medium capillary percolated pores	Small capillary percolated pores	Small capillary percolated and de-percolated capillary pores and air voids

4.3.3.3 Low temperature calorimetry – Measurement procedure and analysis of data

Additional tests were carried out to evaluate limitations and assumptions made by LTC, see Table 4.15. Also, tests with drying and re-saturated samples were carried out to determine possible changes of the microstructure of cementitious paste due to drying methods (solvent and oven at 105ºC). Parts of the standard procedure described above were changed (Table 4.15) and it is given with more details in the following Table.

Table 4.15: Procedures for tests of interpretation of LTC data

Additional tests	Changes from the "Standard Procedure"
Number of cycling of freezing and thawing	1st cycle: Cooling from 20 ºC to -20ºC followed by heating to -0.5ºC, (rate of 15ºC/h). 2nd cycle: cooling from -0.5 to -55ºC followed by heating until 20ºC (rate of 15ºC/h).
Reference (dried sample or empty as reference)	Use a dried sample (oven at 105ºC) in the reference cell.
Determination of sample temperature	Distillate water was used at varying rates: ±1.2ºC/h; -3.3ºC/h and 4.1ºC/h; ±15ºC/h;
Calculation of the baseline	No changes
Accuracy of the test (repetition)	No changes

Number of cycling of freezing and thawing
Studies reported that using two cycles experiments may create enough nucleation sites for ice to growth, therefore the amount of supercooling is limited (Sun and Scherer, 2010). In order to evaluate that, two cycles experiments were carried out with sample C cured saturated at 20ºC for

720 days. The samples used were 15Øx50 mm. AgI (approx.0.010 grams) was also used to limit supercooling.

- 1st cycle – The samples were submitted to cooling from 20 ºC to -20ºC followed by heating from -20ºC to -0.05ºC, using a rate of 15ºC/h;

- 2nd cycle: cooling from -0.05 to -55ºC followed by heating until 20ºC using a rate of 15ºC/h.

Reference (dried sample or empty as reference)
Investigations of porosity in cementitious materials have used dried sample as reference for LTC (Fridh, 2005). LTC is usually performed using an empty reference cell, thus the baseline is calculated, see Sun and Scherer (2010).

To evaluate the use of dried sample as reference, two similar cement pastes cured saturated at 55ºC for 28 maturity days were used. However one of the samples was dried using oven at 105ºC (see procedure in the Appendix VII). The saturated sample (virgin) was placed in the sample cell (1); and the oven dried sample was placed in the reference cell (2). The size of the samples was 55x15Ø mm and about 0.010 grams of AgI was used to limit supercooling.

Determination of sample temperature
Thermal non-equilibrium between block (measured) and sample cell is been reported as a factor which may influence the size of the pores determined by LTC (Bager and Sellevold, 1986a, Kjeldsen and Geiker, 2008). The gap between block and sample temperature may show a delay of heating and cooling equilibrium in temperature, especially when higher rates are applied. To evaluate that, 0.5 and 1 gram of distillate water at varying rates of cooling and heating (±1.2 ºC/h; -3.3ºC/h and +4.1ºC/h; ±15ºC/h) from 20ºC to -15ºC followed by heating from -15 ºC to 20ºC were tested by LTC.

The amount of 0.5 and 1 gram of water were chosen based on the amount of freezable water from the cement pastes previously tried and it may varies according to the age and materials used, see Table 4.16. About 0.010 grams of AgI, as AgI is insoluble in water it may be used to create nucleation site in distillate water (Wikepedia, 2010).

Due to the small amount of sample tested (0.5 and 1 gram of water) two bronze cylinders were introduced: one in the sample cell (1), and other in the reference cell (2). The cylinder of the sample cell (1) is used to improve the contact of the sample with the thermal couples located around the sample cell (Fig. 4.5(a)). Therefore, the thermal couples will better detect changes in temperature of the water, see Fig. 4.5(b). The cylinder in the reference cell is used to obtain thermal equilibrium between sample cell and reference cell. Both cylinders have approximately the same mass (Table 4.17).

Table 4.16: Amount of freezable water for the cement pastes cured saturated at 20ºC for 1, 3, 28, 90 and 720 days.

Sample Id.	Age	Volume of ice ($g_{\cdot ice}/kg_{sample105ºC}$) 0 to-20ºC (percolated capillary range)	weight$_{105ºC}$ (kg)	Volume of ice fraction(cm³/cm³) 0 to-20ºC (percolated capillary range)
C_1w20	1	82.64	0.012	0.99
C_s40_1w20	1	161.22	0.012	1.93
C_s70_1w20	1	222.59	0.012	2.67
C_3w20	3	22.67	0.012	0.27
C_s40_3w20	3	76.54	0.012	0.91
C_s70_3w20	3	49.56	0.012	0.59
C_28w20	28	3.98	0.012	0.04
C_s40_28w20	28	4.56	0.012	0.05
C_s70_28w20	28	4.23	0.012	0.05
C_90w20	90	1.90	0.012	0.02
C_s40_90w20	90	3.68	0.012	0.04
C_s70_90w20	90	2.57	0.012	0.03
C_720w20	720	2.45	0.012	0.03
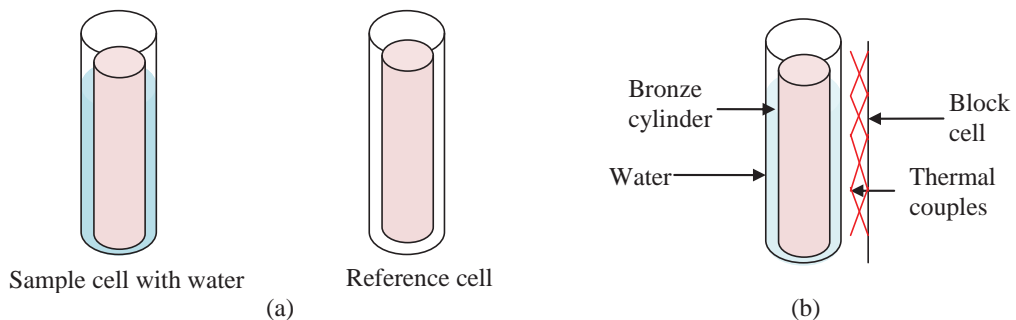
Fig. 4.5 : (a) Sample cell and reference cell with bronze cylinder and (b) set up around the sample cell

Table 4.17: Weight of bronze cylinders added in the reference and sample cell

Bronze cylinder	Reference cell	Sample cell
Weight in grams	77.1314	77.3765

Determination of the baseline calculation
Three methods of baseline calculation were analysed (Bager, 1984, Johannesson, 2010, Sun and Scherer, 2010). The "Standard procedure for LTC" was followed (see Appendix X).

Accuracy of the test
To observe the accuracy of the results, selected samples were tested three times and twice. The "Standard procedure for LTC" was followed (see Appendix X).

4.3.3.4 Mercury intrusion porosimetry (MIP)

MIP was performed using the equipment Autopore IV- 9500 from Micrometrics at Heidelberg Cement. The early age (1 and 3 maturity days) pastes were cast in Heidelberg Cement. Samples at 28, 90 and 720 maturity days were cast at Technical University of Denmark (DTU). The pastes were tested during the visits at Heidelberg Cement in the period of July 2007, January and February 2008 and November 2010. Due to the amount of samples and time consuming in travelling and testing, Heidelberg Techonology Centre provided a technician to carried out test for some of the samples cured for 28 and 90 maturity days.

The samples were solvent dried using isopraponol and evacuated following the procedure given in Appendix VIII. After that, the samples were crushed in pieces from 5 to 10 mm (approx.) and tested. MIP is undertaken by intruding mercury into the porous material at incremental pressures; at each step the intruded volume is measured. The detailed procedure for MIP is given in the Appendix XI. The parameters adopted for MIP are: mercury contact angle of 141°, surface tension solid-liquid of 485×10^{-7} MPa and mercury density of 13.50 g/cm³. The parameters adopted were suggested by users of MIP at Heidelberg Cement and they are in the range of values given in the literature (Diamond, 1995, Feldman, 1986). Repetition of the tests was done and the results seem to have a good reliability.

4.3.3.5 Assessment of the data

The final data is collected trough the computer and analyzed and discussed trough graphics and values. The pore threshold size is calculated based on the pressure value obtained by the Washburn equation (see Equation 3.17).The total porosity is measured when the volume of mercury measured is reached at the highest pressure and it is given by the Equation 3.19.

Curves of cumulated pore volume versus pore diameter illustrate the intrusion and extrusion curves of MIP (Appendix XVIII). The threshold pore size is determined from the intersection of the two tangents to the curve of cumulative pore volume versus pore size, and the total pore volume is the highest cumulative pore volume measured.

The treated data are here illustrated in graphics of cumulative pore size versus threshold pore size for cement pastes with and without SCMs at varying curing conditions and age.

4.3.3.6 Scanning electron microscopy (SEM)

SEM was performed on dried samples to determine the pore size distribution and the total pore volume. The samples were cast at Technical University of Denmark (DTU). Impregnation, polishing and analyses of samples at 3 and 28 maturity days were carried out at EPFL on March of 2008 with the support of Emmanuel Gallucci. The samples at 720 days were impregnated and polished at Technologic Institute (TI) on January 2011 and the test was carried out at DTU.

For the sample preparation carried out at EPFL the procedure was (see detailed procedure in the Appendix XII):
- Drying by solvent (isopraponol) and evacuated;
- Impregnate with epoxy resin;
- Polish using several steps;
- Coating using carbon.

After the sample preparation, the sample is placed in the microscope vacuum column. The air is pumped out of the column and an electron gun is activated. The emitted electrons from the sample are collected by a backscattered electron detector and amplified. By this way, an electronic image of the sample is produced with different grey scales. The magnification of 1000 was used to acquire the images. The detailed procedure for SEM is given in the Appendix XII.

Assessment of the data
The images were treated by image analysis program ImagAna developed by Jensen (2010a). The threshold pore size was acquired manually by analysing all the grey histograms from the images. The program Ipiwin 4 was used for some of the samples.

4.3.3.7 Water sorption method

Water sorption tests were undertaken on non-dried samples to characterize the pore size distribution and pore volume of the samples at different relative humidities, see Table 4.18. The samples were cast at DTU. The tests were undertaken at DTU in the period from March 2008 to February 2011.

Table 4.18: Saturated salt solution for humidity control

Saturated salt solution	mbar	Equilibrium humidity (%)
LiCl	4	11
$MgCl_2$	10	33
NaBr	17	59
NaCl	23	75
KBr	25	83
KNO_3	29	92
K_2SO_4	31	97

The samples were crushed to grain size from 150 to 250 µm. Slices of 30x20Ø mm were also used to observe the impact of sample size in the samples. Crushing was undertaken in a glove box and a system with bubbling calcium hydroxide saturated solution was set up inside the glove chamber to provide high relative humidity and low CO_2 content to avoid drying and carbonation of the samples during sample preparation. The samples were weighted to approximately 1 gram (0.0001 precision) in weighing glasses and placed in desiccators with seven different salt solutions to provide various relative humidity. The desiccators were evacuated and placed in water bath at 20ºC. The weight change of the samples was measured every two to four weeks. The detailed procedure for water desorption is given in Appendix XIII and in the standard prEN-ISO 12571 (1999).

Assessment of the data
Samples were weighted in a digital scale (0.0001 precision) and recorded in a computer program (BathMonitor.vi). More details see Appendix XIII.

When equilibrium (constant weight ±1%) was obtained the samples were dried at 105ºC to determined the remaining amount of evaporable water followed by drying at 1000ºC to determine the amount of non-evaporable water, see Appendix VII. A ''oven dried at 105ºC'' reference state was chose for the water content calculations of water desorption and adsorption.

4.3.3.8 Other methods

4.3.3.6.1 Nuclear magnetic resonance (NMR) relaxation
The mixes for NMR were cast at University of Surrey during the second visit in May of 2007. The cement pastes were weighted and placed in a small tube (approximately 20 mm of diameter) inside the magnetic field at Benchtop ^{1}H NMR relaxation. The signal produced which is the characteristic from the pore liquid of the samples is recorder and analysed. The test parameters are given in Appendix XVI.

Drying methods
Oven drying
To determine the effect of size and amount of sample during the drying the average of the weight of three samples was used. Cement paste with 40% of slag addition and without slag cured saturated at 20ºC for 3 days were used at varying sizes (powder, slices of 5x 30Ø mm, and 55x15Ø mm). They were submitted to oven drying at 105ºC for 1, 3 and 10 days followed by oven dried at 1000ºC for 1, 4 and 24 hours. The amount of samples used is given in the Table 4.19. Detailed procedure for evaporable and non evaporable water is given in the Appendix VII.

Table 4.19: Amount of cement pastes in powder, slices of 0.5x3Ø cm and 5.5x1.5Ø cm

Sample id	Amount of samples (g)		
	Powder (particles < 5 mm)	Slices of 5x30 Ø mm	Slices of 55x15 Ø mm
C_1	1.9425	2.4149	12.4589
C_2	1.5071	2.6128	14.5669
C_3	1.8605	1.7863	15.1354
C_s40_1	1.7324	2.0789	13.8682
C_s40_2	2.991	2.5112	14.5991
C_s40_3	1.4734	2.5316	-

Solvent exchange
The hydrated samples were cut in slices of approximately 5 mm and submerged in isopropyl alcohol for seven days (volume of solvent 50 times the volume of the water in the sample). Subsequently, the samples were placed in desiccators with silica gel and dried under vacuum for one day. Procedure for solvent exchange is given in the Appendix VIII.

Vacuum saturation
Hydrated samples were placed in desiccators with water and vacuum was applied for 24 hours. Detailed procedure for vacuum saturation is given in the Appendix IX.

Capillary suction
Capillary suction method were carried out following the standard pr EN-ISO12571 (1999). Adjustments were made to limit the amount of evaporation of the water and they are described in the Appendix XV.

Autogeneous deformation
Measurements of autogenous deformation were carried out by measurement of linear deformation of the cement pastes with and without slag cured sealed at 20ºC.

Linear measurement of autogenous deformation was performed by placing the cement paste in a corrugated mould. The length change of the cement paste is recorded by a displacement transducer at the end of the specimen, see details in (Jensen and Hansen, 2001, Jensen and Hansen, 1995). The test procedure and calculation are given in the standard ASTM –C1698-09 (2009) .

As the samples supposed to be in a sealed state, the bleed water from the samples was removed after 2 hours of casting in the corrugated mould. A siring was used to remove the water and the moulds were sealed again with a black tape around it. The amount of water removed from the samples is given in the Table 4.20.

Table 4.20: Amount of bleed water removed from the pastes for autogenous deformation test

Sample	Amount of bleed water removed (ml)
C	15.5
C_r	13
C_s40	18
C_s40_r	16.2
C_s70	13.5
C_s70_r	12.5

Thermo gravimetric analyses
A Stanton Redford STA- 781 equipment was used for thermo-gravimetric analysis (TG) and differential thermo analysis (DTA) pastes of cement C with and without slag cured sealed at $55^{\circ}C$ for 6 days and subsequently tested at 11 and 97% RH. The samples were oven dried at $105^{\circ}C$ for 24 hours before the test.

The tests were carried out to determine the non-evaporable water and the amount of Portlandite and calcite from the hydrated products of the cement pastes with and without slag. The samples were tested in June of 2008 at University of Aberdeen by Magdalena Ballonis (Marie Curie Project 1, (Balonis, 2010)). Thus they were packed in sealed containers and sent by mail to University of Aberdeen. For testing the samples were placed into a platinum crucible in the thermal analyser. The observed temperature ranges were between 20ºC to 1000ºC; the rate of heating was 10 ºC/min. All measurements were done in nitrogen atmosphere. Corundum was used as reference material for the analysis.

The instrument simultaneously record thermo-gravimetric weight changes (TG) together with during the heating. Differential values of mass and temperature (DTG) are calculated. Moreover, the difference in thermal behaviour between the sample and reference material (corundum) (DTA) is acquired.

Isothermal Calorimetry
Isothermal calorimetry was carried out during the second visit at Heidelberg Cement (January 2008). For that the equipment TAM Air Isothermal – Thermometric was used for studying of the hydrated of the cement pastes with and without slag and fly ash at different temperatures (20ºC and 55ºC).

The pastes were cast and placed in proper sealed glass containers (ampoule). After that the samples are placed in the calorimeter at a desired set temperature. The detailed procedure is given in the Appendix XIV.

5 Results and discussion

This Chapter presents the main results and discussion of the thesis. The chapter is divided into sections according to the methods used:
- 5.1 Low temperature calorimetry (LTC)
- 5.2 Mercury intrusion porosimetry (MIP)
- 5.3 Scanning electron microscopy (SEM)
- 5.4 Water sorption
- 5.5 H NMR relaxation
- 5.6 Autogenous deformation
- 5.7 Drying methods
- 5.8 Estimated porosity

In the section 5.9, porosity data for similar samples acquired by different method is compared and the applicability of the methods is discussed. A guideline for porosity measurement and assessment of the data is also given.

For some of the methods (i.e. LTC, water sorption), extra tests were carried out to illustrate the applicability of the method. And the impact of SCMs and curing conditions was analysed.

Porosity data for pastes with and without SCMs cured at varying conditions and age are here presented and discussed. An overview of the range of the pores and pore structure parameters measured by the used methods is given in the Table 5.1. The nomenclature used for the pores is illustrated in the Fig. 5.1, it is according to McDonald (2010) and Mindness et al.(2002).

Table 5.1: Range of pores and pore structure parameters measured by varying methods

Method	Range of pores measured in diameter (approx.)			Pore structure parameters
	Measured pore	t-layer	Total size of pore	
LTC – melting curve	0.001 (at -55ºC) to 1.30 (at -0.05ºC) µm*	0.001 µm*	0.003 to 1 µm	Threshold pore size, total pore volume and pore size distribution
MIP	0.003 to 1000 µm**		0.003 to 1000 µm**	Threshold pore size and total pore volume
SEM	0.009 to 40 µm (magnification of 1000)		0.009 to 40 µm (magnification of 1000)	Total pore volume
Water sorption	0.004 (58%RH) to 0.075 (97%RH) ***	From 0.0004 to 0.001 µm***	0.005 to 0.075 µm	Total pore volume and pore size distribution
NMR	All ranges			Not measured
Water porosity	Water saturated pores			Volume of pores filled by water
Solvent porosity	Solvent exchanged pores			Volume of pores exchanged by solvent

*(Sun and Scherer, 2010), **(Quantachrome, 2007), ***(Halsey, 1952)
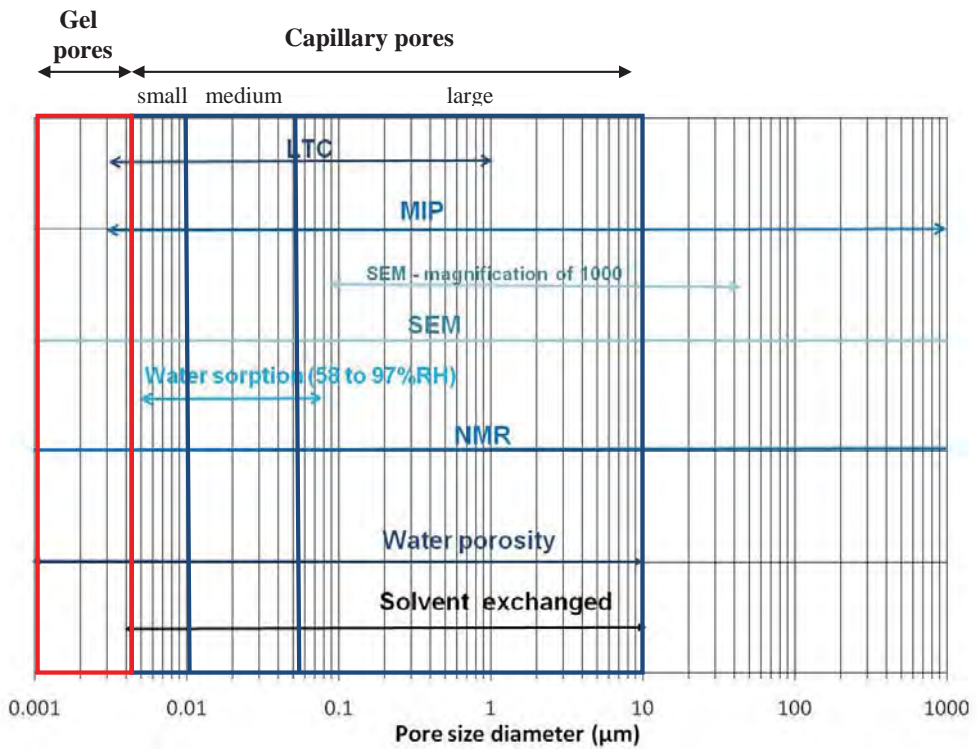
Fig. 5.1: Adopted pore size nomenclature: gel (d<0.004 µm); small capillary (0.004<d<0.01 µm); medium capillary (0.01<d<0.05 µm) large capillary (0.05<d<10 µm) (McDonald et al., 2010, Mindness et al., 2002)

5.1 Low temperature calorimetry (LTC)

Pore parameters such as threshold pore size diameter, total volume of pores containing freezable water and pore size distribution can be determined by LTC. The max. threshold pore size is determined from the start of the first peak in the freezing curve. The pore size is calculated from the block temperature by the Kelvin Equation, see Appendix X and section 3.3.1. The total volume of ice is the total mass of ice frozen in the freezing curve multiplied by the bulk density of MIP. The melting curve of LTC represents the pore size distribution. It should be stressed that the pore size at same temperature is different for melting and freezing curves, see Table 5.2. Typically when dealing with cementitious materials, the porosity of interest is given in volume. For that, bulk density from MIP measurements was used. However, it is important to stress that MIP bulk density was calculated for solvent dried samples and the ice formed by LTC is calculated per gram of dried sample using oven at 105ºC. Thus, MIP bulk density may give lower values of bulk density than oven dried as the solvent release less water from the samples than oven at 105ºC. This was the best estimation of the amount of pores in volume and it allows the comparison with other porosity methods. The parameters and calculation for pore size were based on Sun and Scherer (2010). The following ranges of temperature were used to characterize the pores, see Table 5.2.

Table 5.2: Range of temperature, nomenclature and pore size used for LTC.

Range of temperature	Used nomenclature	Pores from melting curves (Kelvin radius +t-layer) in diameter	Pores from freezing curves (Kelvin radius +t-layer) in diameter
-0.05 to -20ºC	Large and medium capillary pores*	0.005 to 1 µm	0.008 to 2 µm
-20 to -38ºC	Small capillary	0.004 – 0.005 µm	0.005 to 0.008 µm
-38 to -50ºC	Gel pores and de-percolated	0.003 -0.004 µm	0.004 -0.005 µm

*For freezing curves only large and medium percolated capillary pores

The results and discussion of LTC are divided into:
- Part I (5.1.1 and 5.1.2), Measurement procedure and analysis of data (section 5.1.1). This part analyse possible errors introduced by the measurement procedure and analysis of LTC data. Some of the errors were already dealt in the literature (Johannesson, 2010, Kjeldsen and Geiker, 2008, Sun and Scherer, 2010). Based on the results obtained here, it is applied a correction of the block temperature of -3ºC (see section 5.1.2).

- Part II (5.1.3), Impact of SCMs and curing conditions on the pore structure of cement pastes determined by LTC. Pore threshold size, total amount of pores with freezable water and pore size distribution parameters are determined for cement pastes with and without SCMs at different curing conditions and age.

5.1.1   Measurement procedure and analysis of data

This part evaluates critical points of LTC which may affect the porosity data, such as:
- 5.1.1.1 Number of cycling of freezing and thawing;
- 5.1.1.2 Reference (dried sample or empty as reference);
- 5.1.1.3 Determination of sample temperature;
- 5.1.1.4 Calculation of the baseline;
- 5.1.1.5 Accuracy of the data;

5.1.1.1 Number of cycling for LTC test

Two cycling tests is suggested by Sun and Scherer (2010) as a way to increase the nucleation sites in the samples and limit the amount of supercooling. Apparent heat capacity versus block temperature curves for similar sample using one or two cycle experiments are given in the Fig. 5.2.
- 2 cycling applying the rate of 3.3ºC/h and 4.1ºC/h (full line)
- 1 cycling applying the rate of 3.3ºC/h and 4.1ºC/h (broken line)
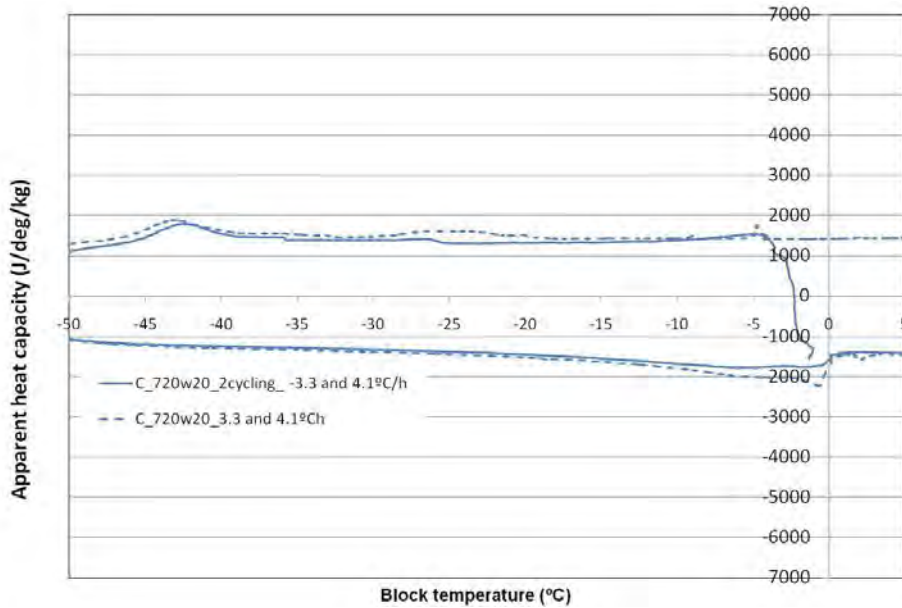
Fig. 5.2: Apparent heat capacity (J/deg/kg) versus block temperature (ºC) for sample: 2 cycling plain cement paste cured saturated at 20ºC for 720 days

The impact of two-cycles could not be observed for samples cured for 720 days, a good agreement between the curves for samples tested using one and two cycling with the rate of -3.3ºC/h and +4.1ºC/h is shown in the Fig 5.2. For young samples (3 days) the impact may be more pronounced as a large peak is found in the range of percolated capillary pores (0 to -20ºC).

It is suggested by Sun and Scherer (2010) for the increase of nucleation sites, that the sample reaches temperatures of about -20ºC and then heating until -0.5ºC (first cycle) followed by the second cycling from -0.5 to -55ºC and heating to 20ºC. However, difficulties were experienced to control the sample temperature. Two reasons can be pointed out: problems to control maximum and minimum temperature of the cycles when using large samples (55x15 mm) at the rate of -3.3 and +4.1ºC/h and non equilibrium between the block temperature (measured) and sample.

For those reasons, only one-cycle was used with the rate of 3.3ºC/h for cooling and 4.1ºC/h for heating.

5.1.1.2 Reference

The calorimeter used for the tests has two identical cells: sample cell (placed the sample) and reference cell (placed the reference). The final data is the difference in the heat flow response from both, reference and the sample. Dried sample or empty reference have been used for LTC measurements, see e.g. (Bager and Sellevold, 1986a, Johannesson, 2010). The use of different references may have an impact in the LTC data. To illustrate that, apparent heat capacity versus block temperature curves were prepared for cement paste C cured saturated at 55ºC for 6.45 days (28 maturity days) using either: 1) an empty reference cell; or 2)dried sample as reference, see in the Fig. 5.3. The mass fraction of ice formed per dried sample versus block temperature curves are given in the Fig. 5.4.
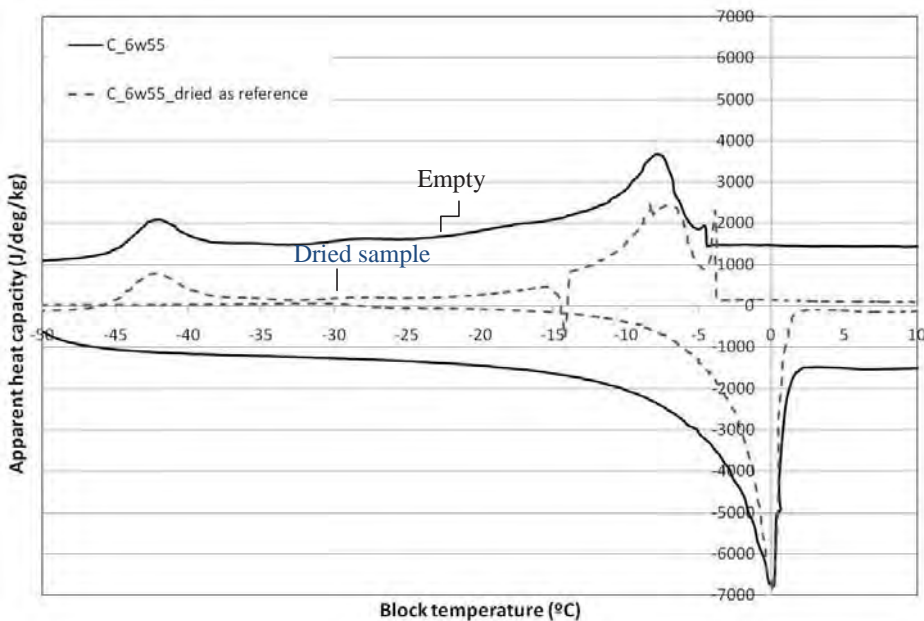
Fig. 5.3: Apparent heat capacity (J/deg/kg) versus block temperature (ºC) for cement pastes cured saturated at 55ºC for 6 days (28 maturity days) using: Empty reference cell (full line); Dried sample as a reference cell (broken line)
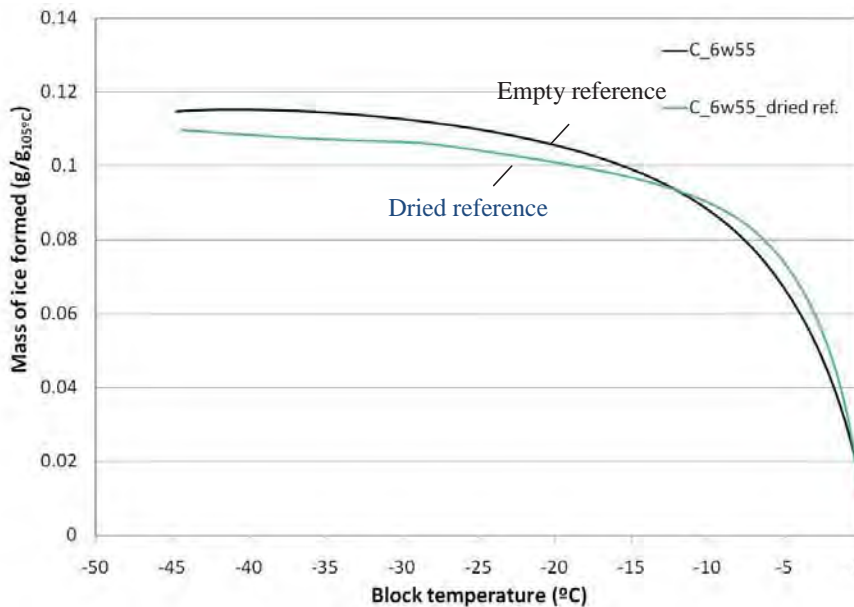
Fig. 5.4: Mass of ice formed ($g/g_{105°c}$) versus block temperature (°C) for cement pastes cured saturated at 55°C for 6 days (28 maturity days) using: Empty reference cell (black); Dried sample as a reference cell (blue)

The gap observed between the curves for (1) empty reference cell and (2) dried as reference is basically the baseline (Fig. 5.4). The difference in the baseline for dried and non dried sample may be corrected by the baseline calculation. A point where no ice formation takes place (e.g. 0°C) is chosen and it is subtracted from the apparent heat capacity curve, see for instances Sun and Scherer (2010). Even with that correction, a slight higher mass fraction of pores was found when an empty reference cell was used, see Fig. 5.4.

Based on the test procedure and data showed above, it was chosen to carry out experiments using an empty reference cell.

5.1.1.3 Determination of sample temperature

Non equilibrium of temperature between the block (measured) and sample may introduce errors in the calculation of pores size from LTC curves. Distillate water was tested to evaluate the sample temperature, as pure water should melt in about 0°C. Apparent heat capacity versus block temperature curves were prepared for 0.5 and 1 gram of distillate water (corresponding the amount of water frozen in young and old samples) using different rates of cooling and heating (±1.2°C/h; -3.3°C/h and 4.1°C/h; ±15°C/h), see Fig.5.5(a) and 5.5(b) respectively. The total volume of ice formed is given in the Fig.5.5 (b) and Fig. 5.6(b).

(a)
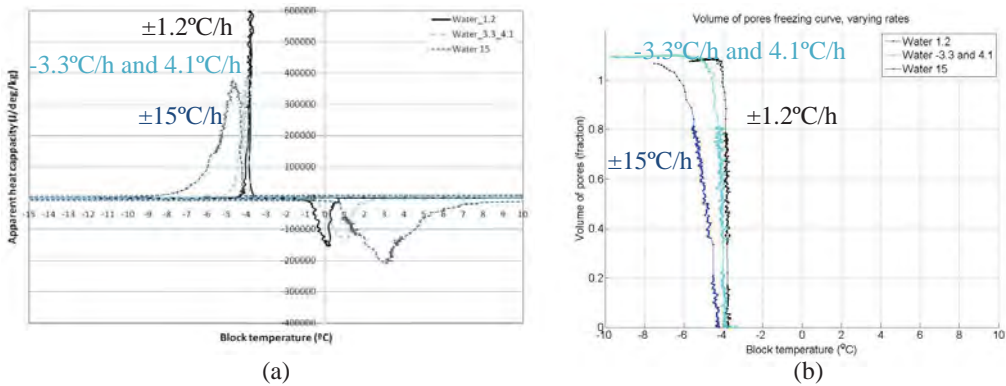
Fig. 5.5 : a) Apparent heat capacity (J/deg/kg) versus block temperature (ºC) and a)cumulative amount of ice versus block temperature for 0.5 grams of water at varying cooling and heating rates: ±1.2ºC/h (black line); -3.3ºC/h and 4.1ºC/h (light blue line); ±15ºC/h(dark blue line)

(a)   (b)
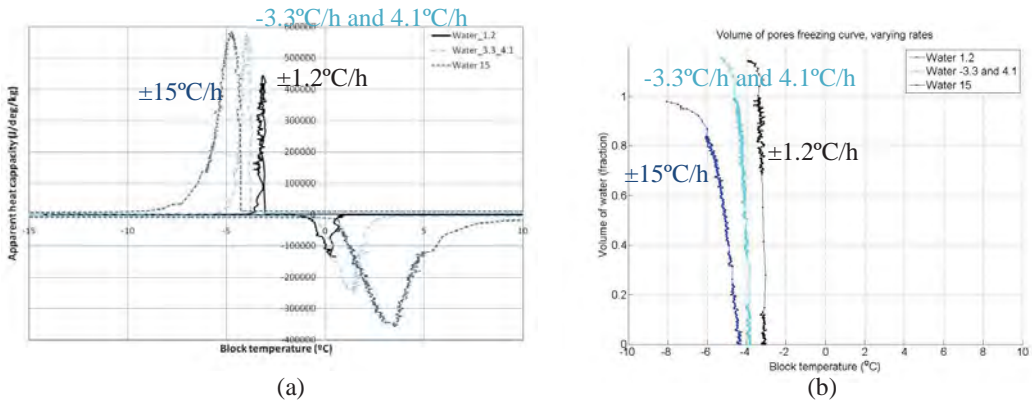
Fig. 5.6: a) Apparent heat capacity (J/deg/kg) versus block temperature (ºC) and b) cumulative amount of ice versus block temperature for 1 gram of water at varying cooling and heating rates: ±1.2ºC/h (black line); -3.3ºC/h and 4.1ºC/h (light blue line); ; ±15ºC/h(dark blue line)

Peaks were found at different position and shape according to the applied freezing and melting rates (Fig. 5.5(a) and 5.6(a)). It was observed thin peaks for the rate of ±1.2ºC/h and -3.3 and 4.1ºC/h it indicate a better thermal equilibrium between the block (measured) and sample cell temperature, see Fig. 5.5. It was also observed that more than 100% of the water was frozen from 0 to -10ºC, except for 1 gram of water at the rate of 15ºC/h. An volume expansion due to the ice formation of about 10% was found in the literature (Powers and Brownyard, 1947).

Peak maximum and peak start values for cooling and thawing curves at different rates are given in the Table 5.3 and illustrated in the Fig. 5.7.

Table 5.3: Peak max and peak start for 0.5 grams and 1 gram of water applying varying rates of freezing and heating

Water at the rates of	Correction for freezing		Correction for heating	
	Peak max.	Peak start	Peak max.	Peak start
0.5 grams of water				
±1.2ºC	+4	+3.7	-0.1	+1.2
-3.3 and +4.1ºC/h	+4.3	+4	-0.8	+0.6
±15ºC/h	+4.8	-+4.3	-2.9	-0.7
1 gram of water				
±1.2ºC	+3.1	+3.0	-0.3	+1.0
-3.3 and +4.1ºC/h	+4.0	+3.7	-1.1	+0.3
±15ºC/h	+4.7	+4.3	-3.1	-0.6
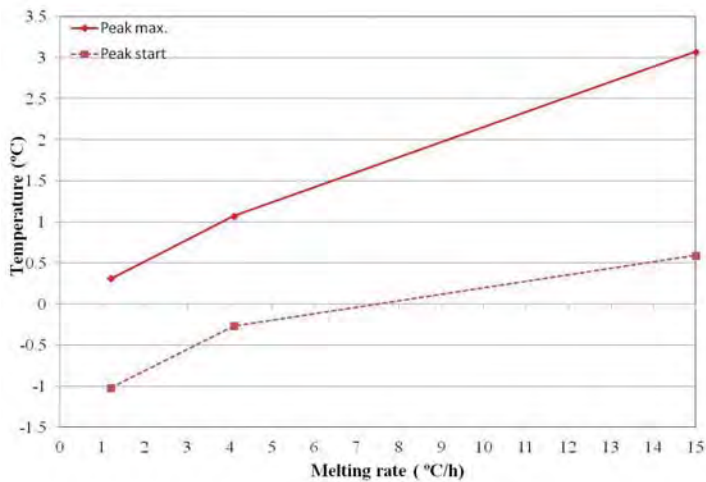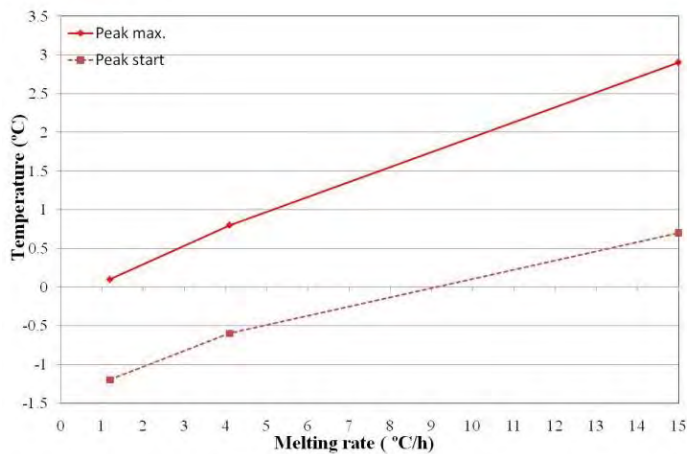
Fig. 5.7: Peak max. and peak start versus melting rate at heating for (a) 0.5 grams and (b) 1 gram of water at varying freezing and cooling rates

The heating rate had a function variation with the start peak and the peak max., as shown in the Figs. 5.7 (a) and 5.7(b). As ice nucleation does not take place in the melting curves, the equilibrium in temperature between block and sample is chosen to be analysed by the melting curves. For that, the peak max from the melting curve for bulk water should be at 0ºC (melting temperature of water). A correction of temperature of -1ºC (from -0.8 to -1.1ºC) is proposed when the freezing rates of -3.3ºC/h and 4.1ºC/h are applied, see Table 5.3. Sellevold and Bager (1980) found differences of 0.4 and 0.8ºC between sample temperature and reference block using a rate of - 3.3ºC/h and 4.1ºC/h. It is important to emphasize that this correction may be different when other equipment and samples with different water content are used.

5.1.1.4 Calculation of the baseline

Calculation of the baseline is a matter of concerning for the data of LTC (Johannesson, 2010). The difficulties arise when the prediction of how much heat goes into the sample and how much goes into forming ice is assumed (Johannesson, 2010). The baseline is meant to separate the heat flow from unfrozen water and solid (cement paste) from the ice formed at varying temperatures. Bager and co-workers (Bager, 1984, Le Sage de Fontenay and Bager, 1980) adopted a calculation method based on the incremental method, see Fig. 5.8. The amount of ice is calculated by ranges where a liner portion of the curve just before freezing is extended down to the next point of the range, see Fig.5.8. The amount of ice in the interval (i.e. 0 to -10ºC) is multiply by the specific heat capacity of the ice (0.5cal/g/ºC) at zero degrees, see Fig. 5.8. Hence the reduction of Cp as a function of decreasing temperature is obtained.
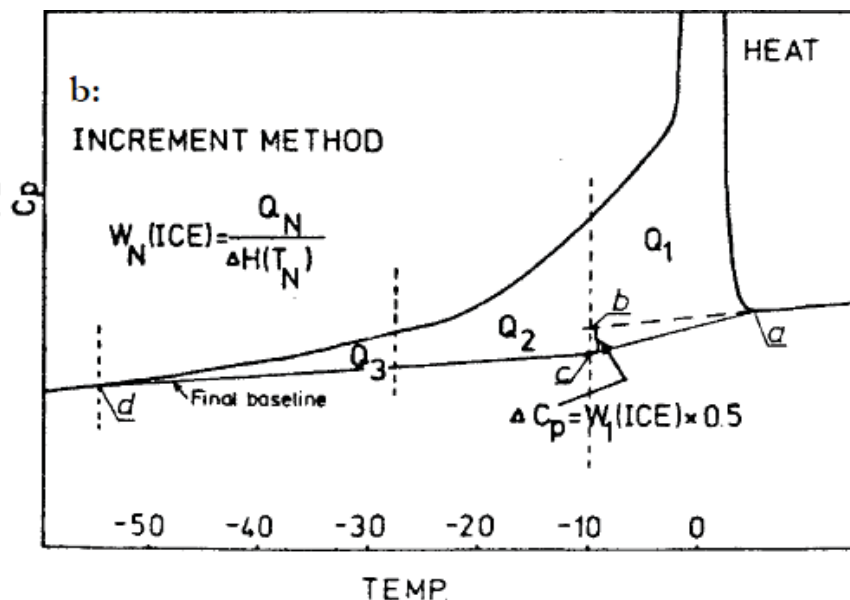
Fig. 5.8: Baseline calculation proposed by Bager (1984)

Johannesson (2010) has used the principle that the total accumulated heat must go back to its initial value after a completed cycle. The method proposed by him assumed that the total required energy to convert all water to ice or vice verse is the mean value of A+B, see Fig.5.9. The calculation of the baseline was carried out by a Matlab script and it is given in the Appendix XVII.
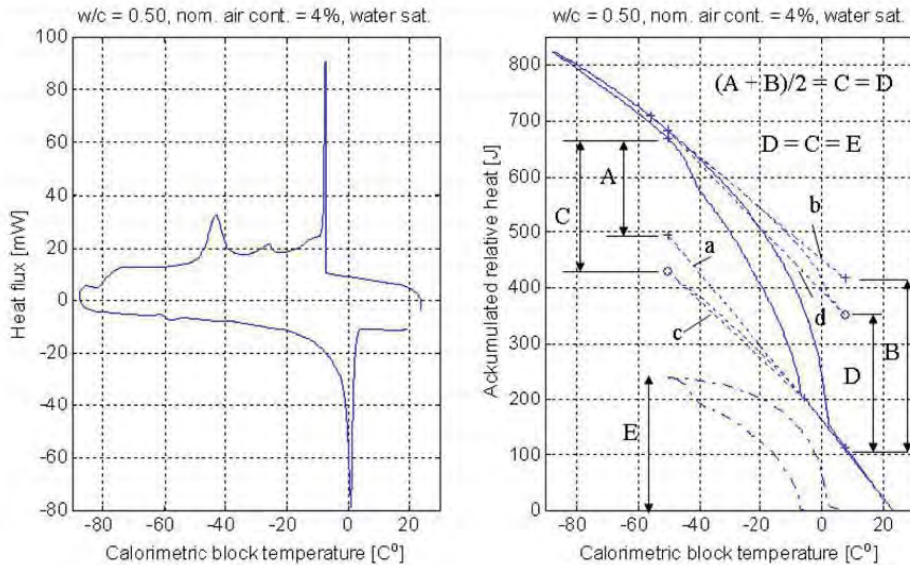
Fig. 5.9: Baseline calculation proposed by Johannesson (2010)

Sun and Scherer (2010) also have proposed a calculation of baseline for LTC based on the contributions of the heat capacity of ice and liquid and the heating rate, see in Sun and Scherer (2010).

To illustrate the baseline calculation proposed by Bager (1984), Johannesson (2010) and Sun and Scherer (2010) the apparent heat capacity and cumulative mass of ice formed versus block temperature for pastes with and without slag cured saturated at 20ºC for 90 days are given in the Figs. 5.10, 5.11 and 5.12. The parameters used by Sun and Scherer (2010) were adopted for the calculation.
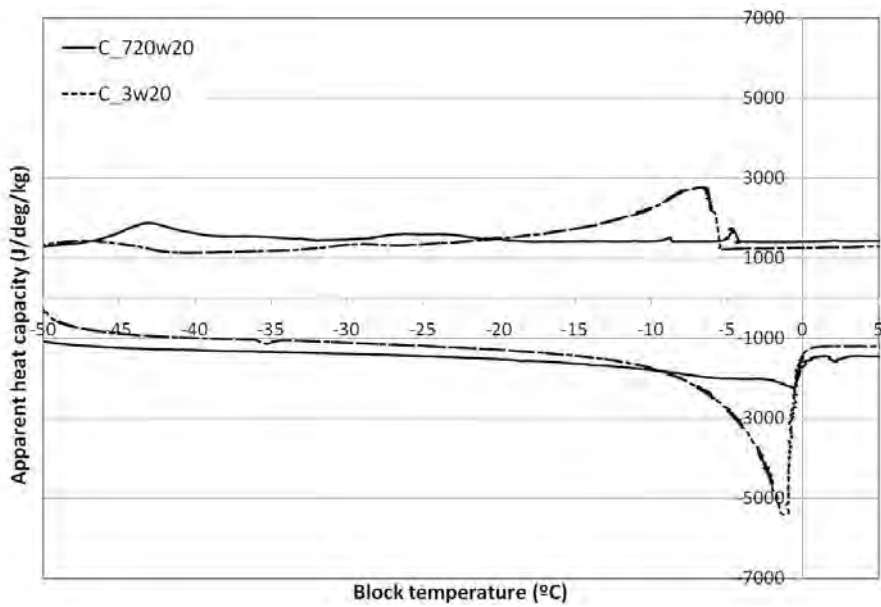
Fig. 5.10: Apparent heat capacity versus block temperature for pastes with and without slag cured
saturated at 20ºC for 3 (broken line) and 720 (full line) days
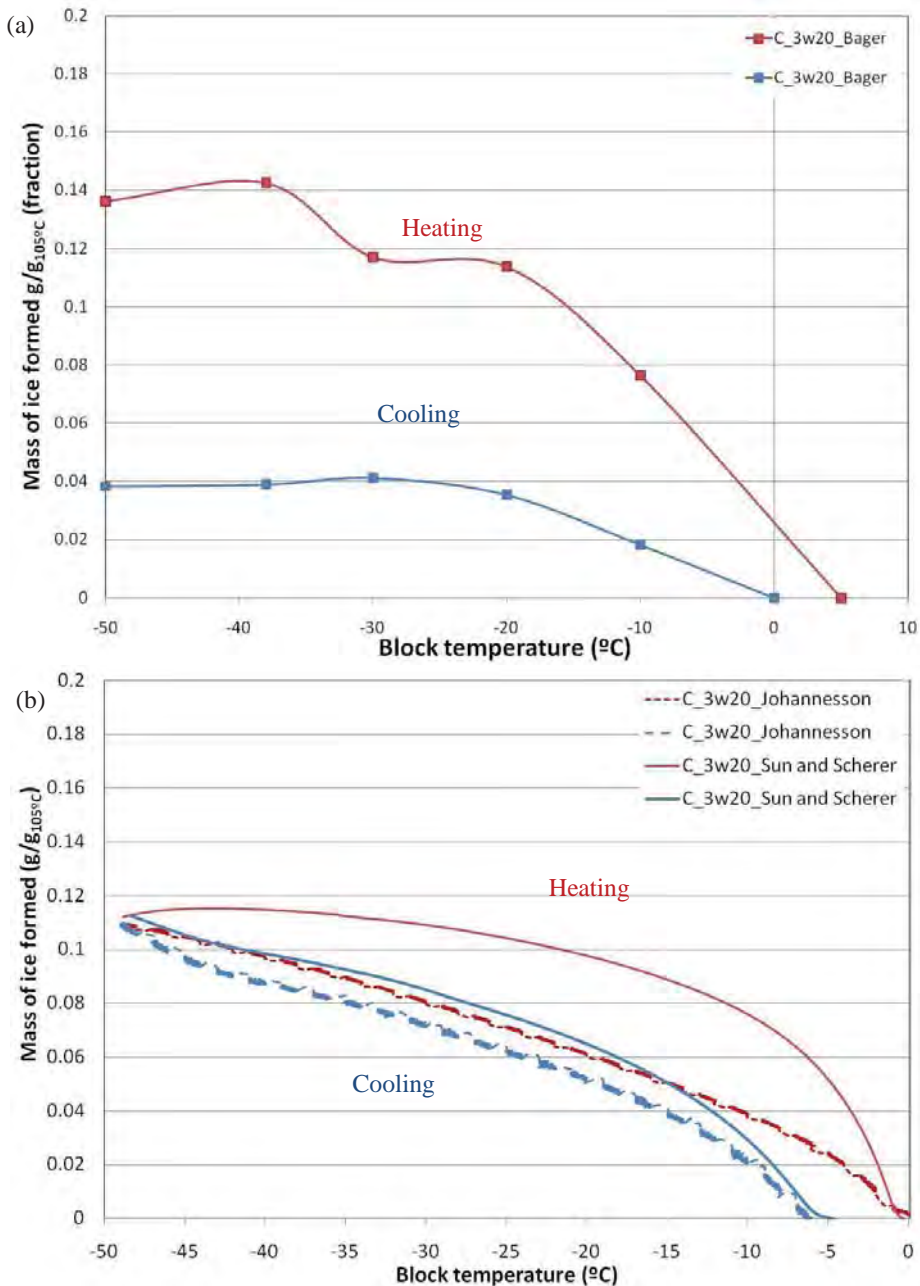
Fig. 5.11: Mass of ice formed ($g/g_{105°C}$)versus block temperature (°C) for freezing and heating curves for cement paste cured saturated at 20°C for 3 days. Calculation of the baseline proposed by (a)Bager (1984); (b) Johannesson (2010) (broken line), and Sun and Scherer (2010) (full line)

(a)

(b)
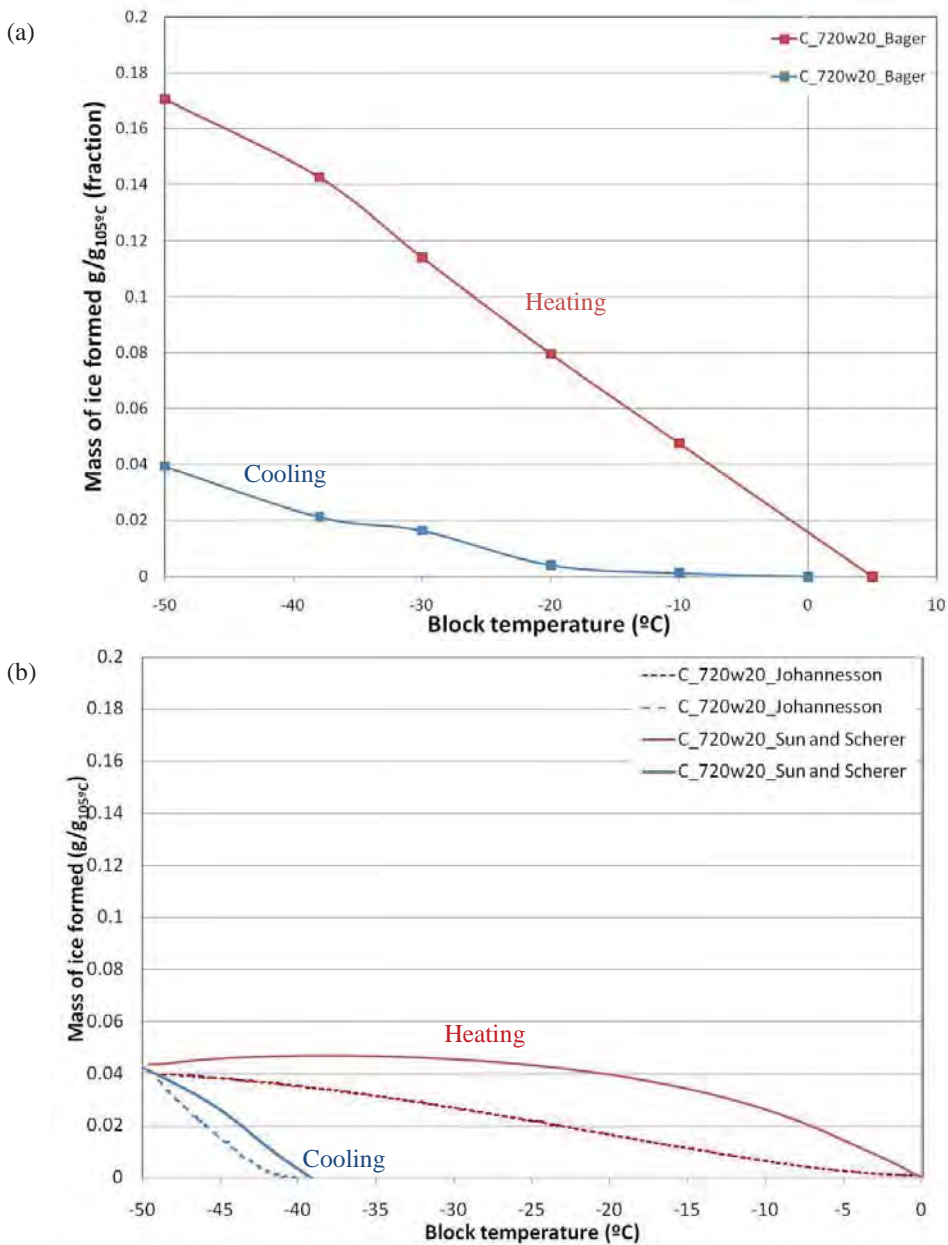
Fig. 5.12: Mass of ice formed (g/g$_{105°C}$) versus block temperature for cement paste cured saturated at 20ºC for 720 days. Calculation of the baseline proposed (a)Bager (1984) and (b) Johannesson (2010) (broken line) and Sun and Scherer (2010) (full line)

Based on the graphics above the method proposed by Sun and Scherer (2010) performed in a manner acceptable for the purposes of the present work. Moreover the following reasons are valuable to consider:

- Bager (1984) method showed a significant discrepancy between the volume of pores calculated by freezing and meting.
- Johannesson (2010) and Sun and Scherer (2010) method calculates continuously the volume of ice formed. Bager (1984) calculation is based on the intervals of ice formed.
- Johannesson (2010) method assumes that is formed half water and half ice, this may underestimate the amount of ice formed in some areas and overestimate in others.

5.1.1.5 Accuracy of the data

The lack of time and larger number of samples tested did not allow the repetition of the test using similar samples. However the accuracy of the data was here evaluated for some samples. Curves of apparent heat capacity and cumulative mass of ice formed versus block temperature for similar samples are shown in the Fig. 5.13 and 5.14.

(a)   (b)
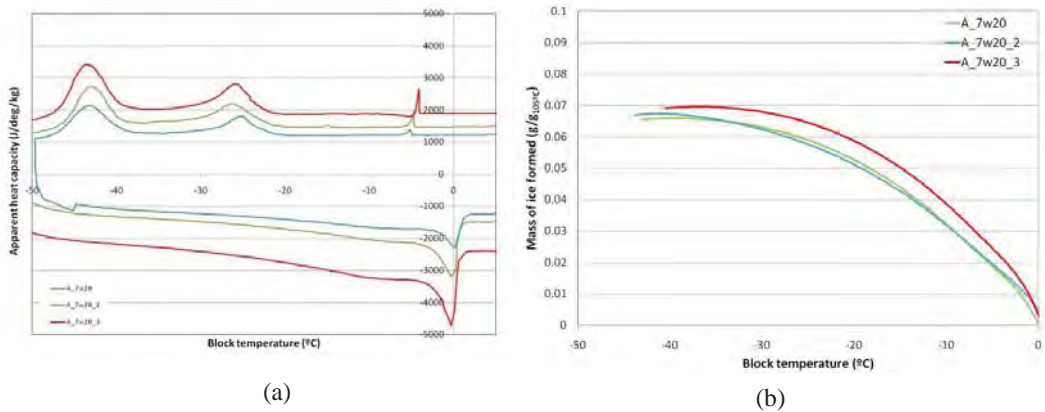
Fig. 5.13: (a) Apparent heat capacity (J/deg/kg) versus block temperature (ºC) and (b) cumulative mass of ice formed versus block temperature for cement paste A cured saturated at 20ºC for 7 days (baseline changed for comparison)

(a)   (b)
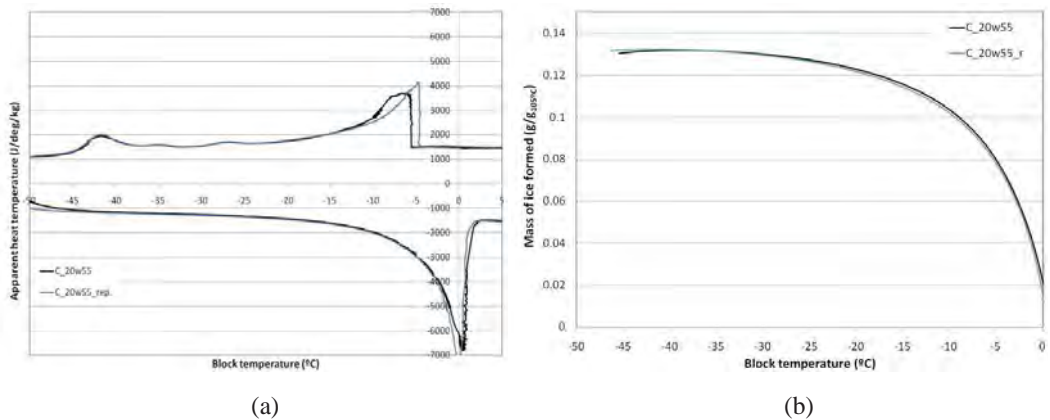
Fig. 5.14: (a) Apparent heat capacity (J/deg/kg) versus block temperature (ºC) (b) cumulative mass of ice formed versus block temperature for cement paste cured saturated at 55ºC for 90 maturity days

The pattern of apparent heat capacity versus block temperature curves showed variance in the first peak (range from 0 to -20ºC), see Figs. 5.13(a) and 5.13(b)). The discrepancy in the position of the first peak for similar samples may leads to a large difference in the threshold pore size calculated from the block temperature, as shown in the Section 3.3.1. Also it may have an impact on the total mass of ice formed, see Fig. 5.13(b).

The difference in the first peak in the range of large and medium capillary pores (0 to -20ºC) and the cumulative pore volume curves may be related to some bulk water on the surface of some samples while others have dried surface. The SSD (sample surface dried) weight is used for the weight measurements, where the sample is dried in a wet tissue and the weight is measured. Weight measurements of a sample submitted several times to SSD showed a small and not representative difference between the recorded weights, see Appendix XVII. In addition, about 2% of the total water content (evaporable water) was lost between the weighing of the sample and the end of the test (approx. 48 hours). The sample is weighted in sealed glass containers and placed in a sealed sample cell inside the calorimeter, however some water may evaporates. It is important to keep in mind that samples tested by LTC are small, and a small extra amount of water added in the sample may reflect in changes of the overall weight.

For a more realistic pore characterization by LTC, it is suggested a qualitative analysis of the pores by the range formed in the freezing curves (e.g. percolated large capillary in the range from 0 to -10ºC), as used by references (Bager and Sellevold, 1986a, Fridh, 2005, Villadsen, 1992). Also the characterization of the pore by pore size distribution curves by melting curves.

5.1.2   Correction of LTC data (proposed based on the interpretation of LTC)

Block temperature measured by LTC may need to be corrected due to the non thermal equilibrium (section 5.1.2), supercooling and freezing point depression (according to (Kjeldsen, 2002, Villadsen, 1992). Proposal for corrections are given in the Table 5.4.

According to the Table 5.4, a correction of -3ºC (sample temperature + freezing point depression) is proposed for the block temperature values acquired by LTC. The temperature correction has an impact in the pore size, larger threshold pore size is found when the block temperature is corrected (Fig. 5.15). The impact is even more pronounced for samples cured up to 28 days, where the first threshold pore is placed in the range of 0 to -10ºC.

Table 5.4: Corrections for LTC results

Issue	Correction of sample temperature
Sample temperature	$T_{sample} = T_{block}$ -0.8ºC (0.5 grams of water) $T_{sample} = T_{block}$ -1.1ºC (1 gram of water)
Supercooling	Varies according with the sample (type and age). It was not consider here.
Freezing point depression due to the pore salt solution	$T_{sample} = T_{block}$ -2ºC (Kjeldsen and Geiker, 2008) $T_{sample} = T_{block}$ -1 to -2ºC (Villadsen, 1992)
Total	$T_{sample} = T_{block}$ -3ºC
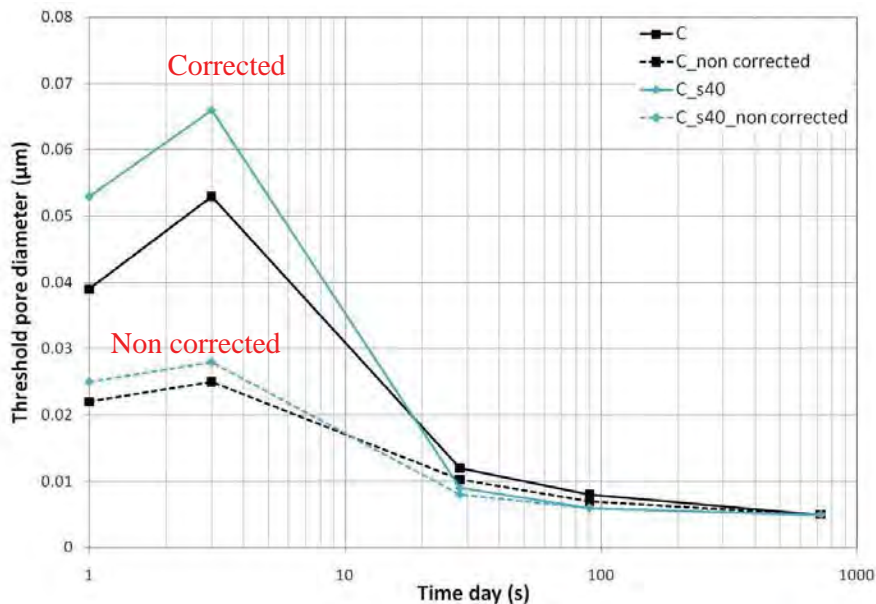
Fig. 5.15: Corrected (full line) and non corrected (broken line) threshold pore diameter (µm) from freezing curve versus time (day(s)) for sample without and with 40% of slag cured saturated at 20ºC

5.1.3 Impact of SCMs and curing conditions on the porosity development by LTC

Apparent heat flow curves versus block temperature for pastes with and without slag and fly ash cured saturated at 20ºC for 3 days are illustrated in the Figs. 5.16, 5.17, 5.18 and 5.19. All the graphics were plotted in the same scale to allow comparison between the data. Two scales where used for samples at 3 days where a much larger peak of apparent heat flow was found. The apparent heat flow versus block temperature for paste with and without slag and fly ash of samples cured

saturated at 20ºC for 1 day is given in Appendix XVII. Baseline was calculated based on Sun and Scherer (2010). The pore size distribution curves are given in the Appendix XVII.
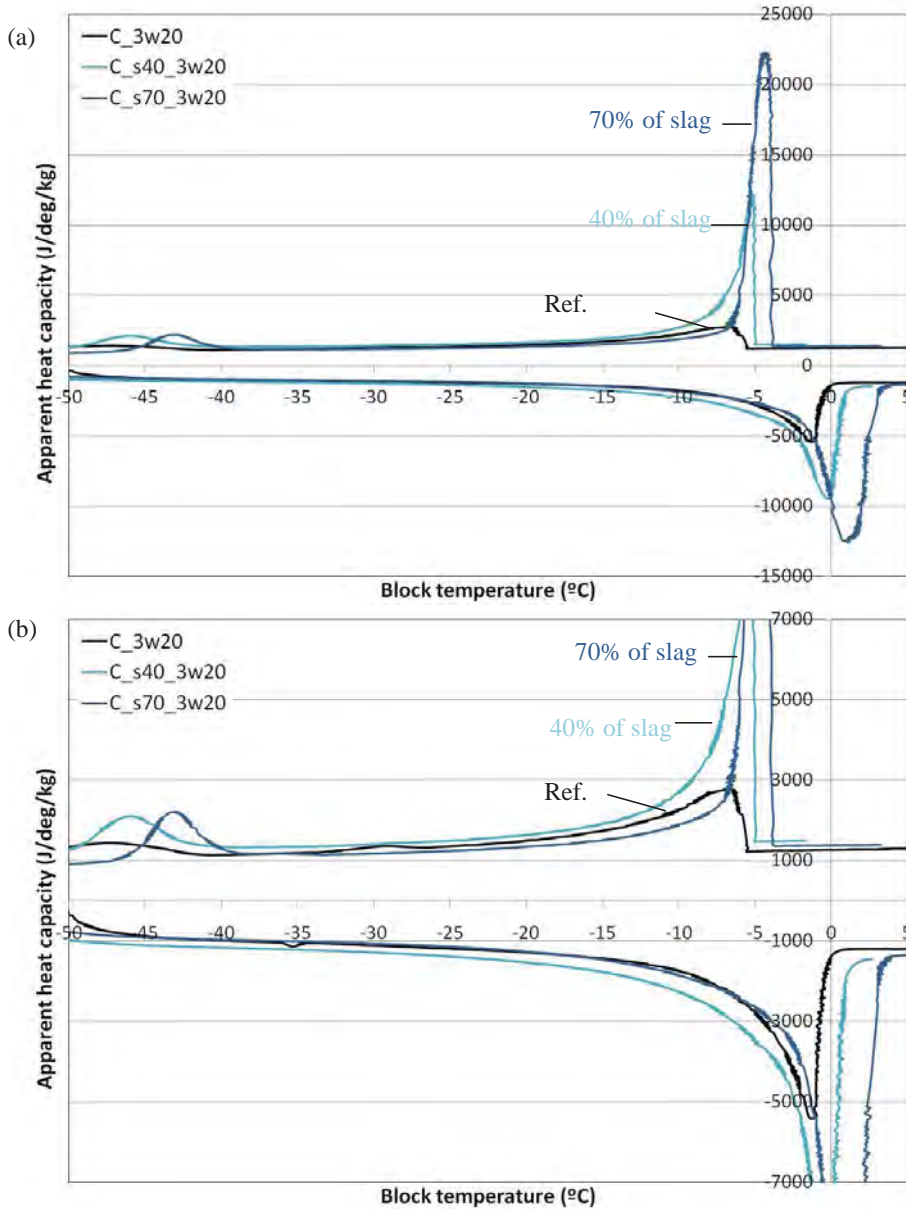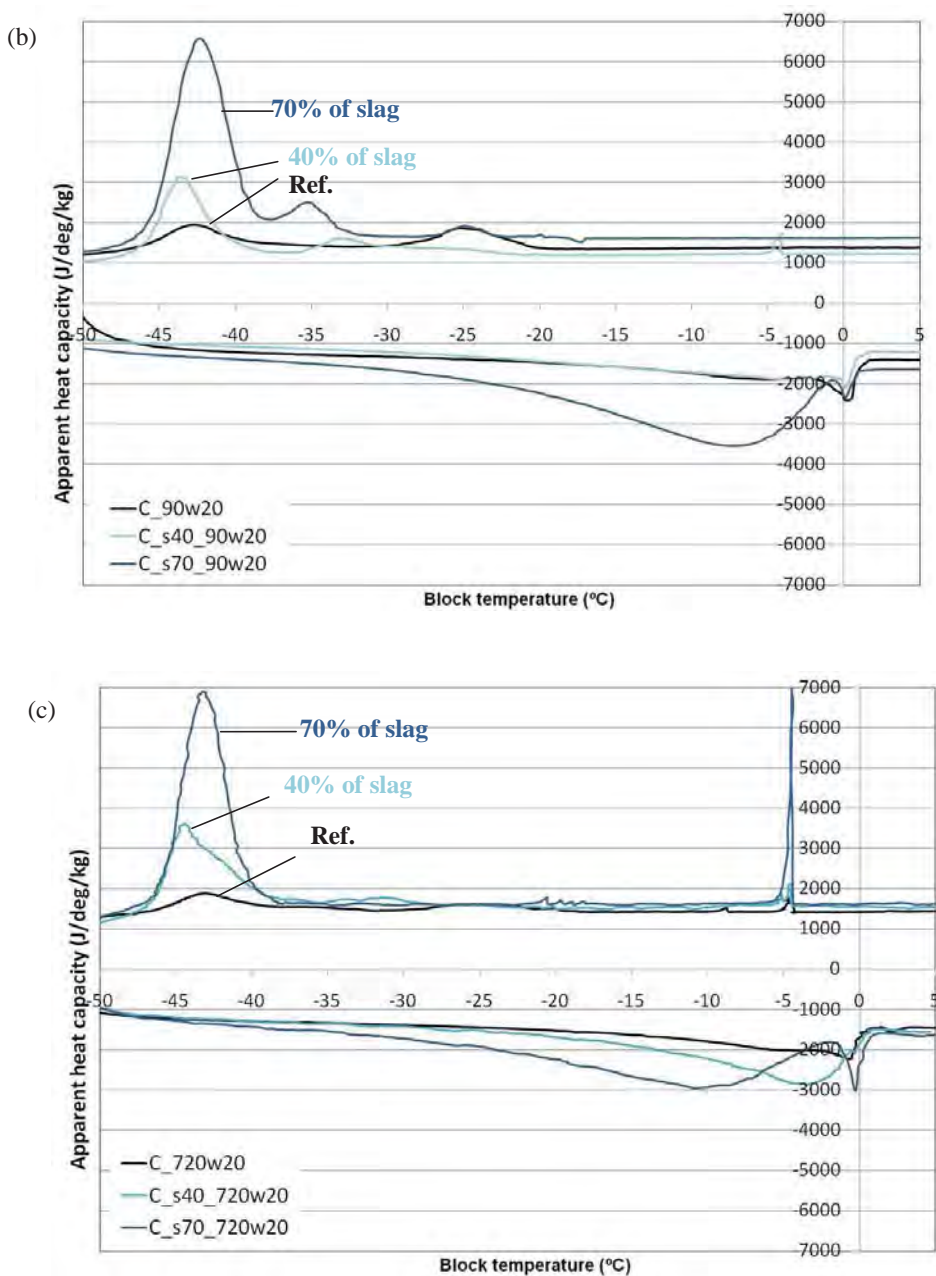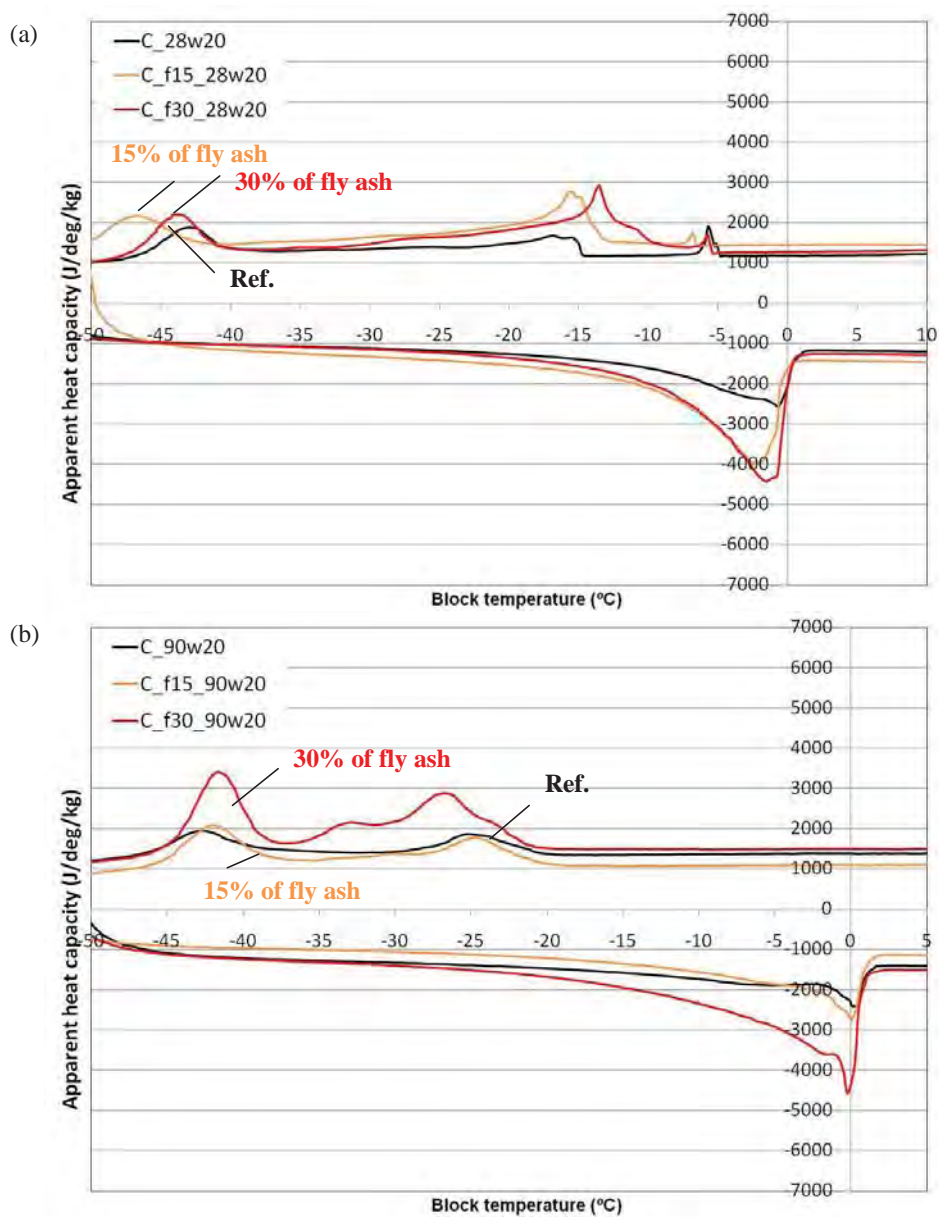

Fig. 5.16: Apparent heat capacity (J/deg/kg) versus block temperature (ºC) of pastes with and without slag cured saturated at 20ºC for 3 days (a) at different scale and (b) the same
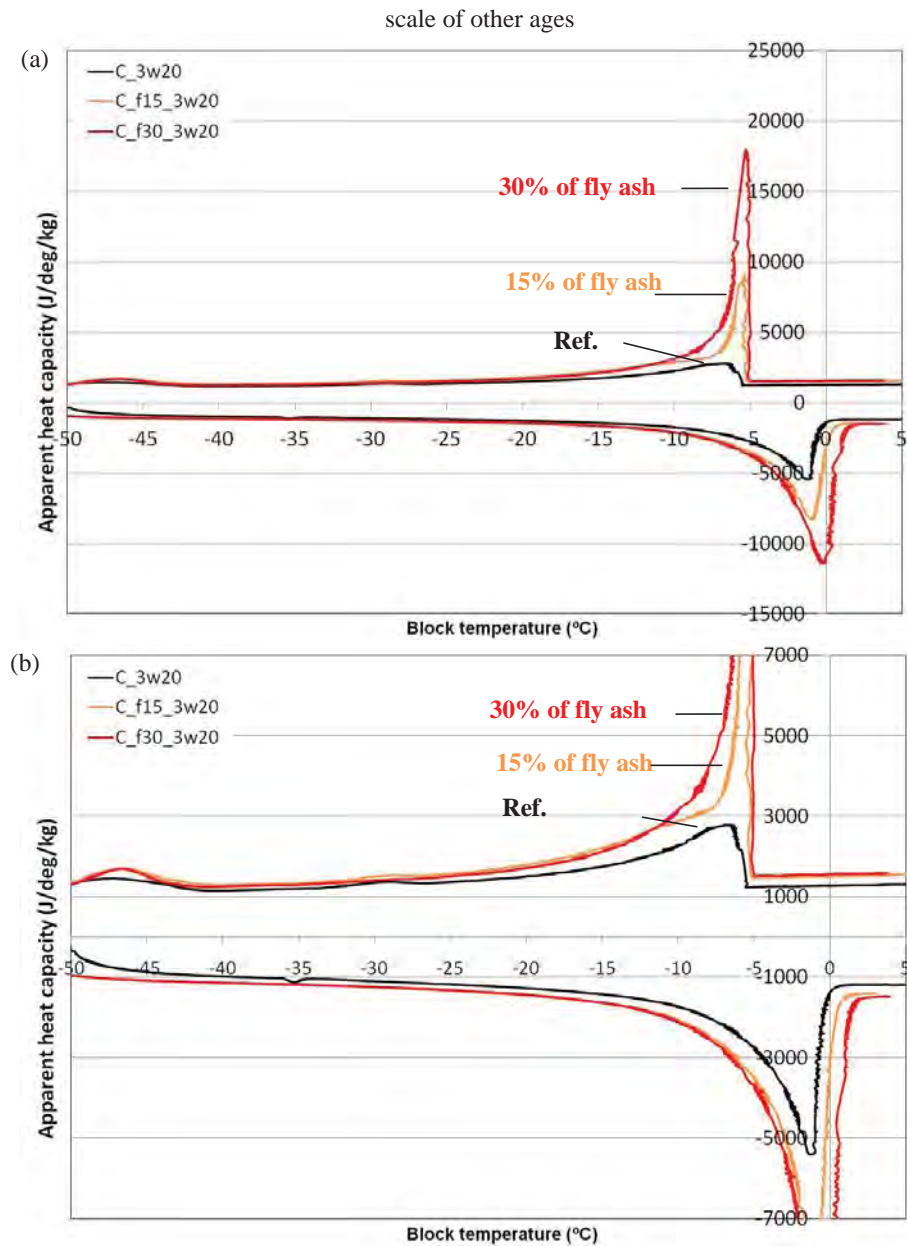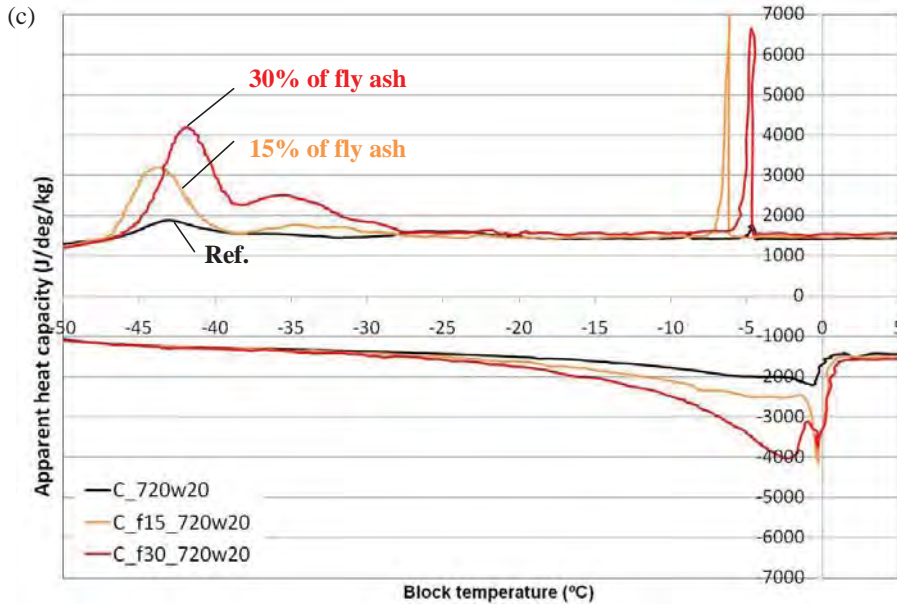
scale of other ages

Fig. 5.17: Apparent heat capacity (J/deg/kg) versus block temperature (ºC) of pastes with
and without fly ash cured saturated at 20ºC for 3 days (a) at different scale and b) the same
scale of other ages

Fig. 5.16 and 5.17 shows large peaks in the range 0 to -20ºC for the pastes with SCMs cured for 3 days when compared with plain cement pastes. This indicate a coarser percolated capillary porosity and it may be due to the low degree of reaction of the slag and fly ash at early age, see e.g. in (Feldman, 1981, Hooton, 1986, Roy and Idorn, 1982). Peaks in the range from -38 to -50ºC were observed to develop at 3 days, and slight larger peaks were found for SCMs than for plain cement paste. This may indicate the start of smaller pores formation and also a different porosity for cement pastes with slag and fly ash. The peaks in the range of -38 to – 50ºC are also due to the de-percolated porosity as pure water freeze at approximately -38ºC rather than 0ºC (Atkins, 1997).

Apparent heat flow curves for pastes with and without slag cured saturated at 20ºC for 28, 90 and 720 days are illustrated in the Fig. 5.18. The effect of fly ash addition for pastes cured saturated at 20ºC for 90 and 720 days is illustrated in the Fig. 5.19.

A refinement of the pore structure for all the pastes is seen from 28 to 720 days of curing time, where the pores move from the range of 0 to -20ºC to lower temperature. In general, it seems that a new family of pores is formed for pastes with SCMs addition. For this new family, a refinement of threshold pores and a higher volume of pores in the range from -20º to -50ºC is seen (Fig 5.18). These peaks may be due to an extra amount of small pores formed by slag reaction. As previous discussion, the peaks in the range of about -40ºC or lower temperature may be also due to closed pores (de-percolated). Studies of improved resistance of aggressive chemicals such as chlorides and sulphate also show less permeability for concrete with SCMs (Bijen, 1996, Hooton, 1986, Malhotra, 1993). Thin peaks in the range of large capillary pores (0 to -10ºC) were observed for some of the slag and fly ash pastes, see Fig. 5.18(c) and 5.19(c). The best explanation for the appearance of these peaks in old sample is that some free water may be on the surface of the samples.
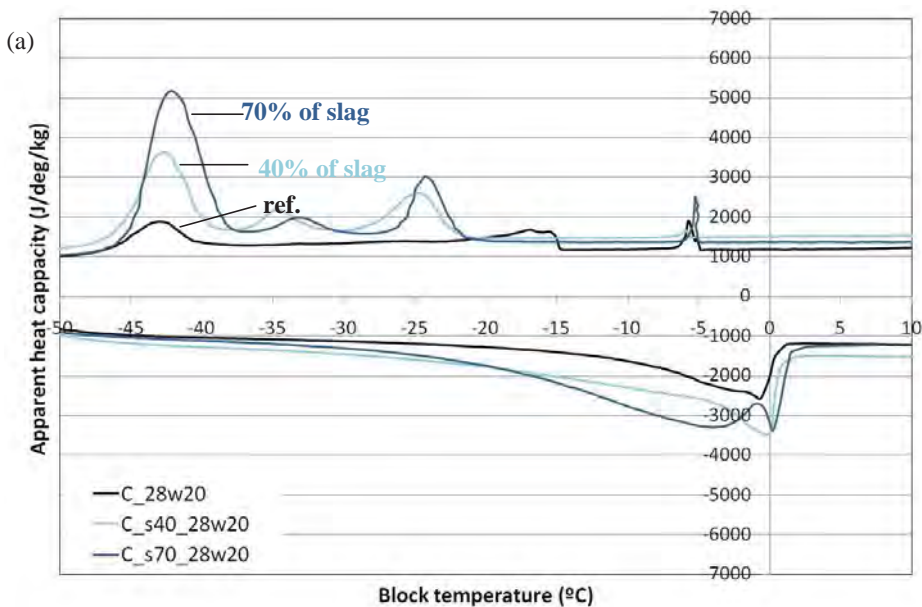
Fig. 5.18: Apparent heat capacity (J/deg/kg) versus block temperature (ºC) of pastes with and without slag cured saturated at 20ºC for (a)28 days, (b) 90 days; and (c)720 days

(a)

(b)

Fig. 5.19: Apparent heat capacity (J/deg/kg) versus block temperature (ºC) of pastes with and without fly ash cured saturated at 20ºC for a) 28 days, b)90 days and c)720 days

The threshold pore size corrected and non-corrected, and volume of ice formed during freezing are given in the Table 5.5 and illustrated in the Figs.5.21 and 5.22. As described in the Section 5.1.2, a correction of -3ºC in the block temperature is proposed. The thin peaks appeared in the range from 0 to -5ºC were not considered as a pore, but water on the surface of the samples, see e.g. samples cured for 720 days.

Table 5.5: Non corrected and corrected threshold pore size, volume of pores for pastes cured saturated at 20ºC for 3, 28 and 90 and 720 days

Sample id.	Time (day(s))	Pore threshold size diameter				Non freezable water (fraction)	Total volume of pores (fraction)
		Non corrected		Corrected			
		(ºC)	(μm)	(ºC)	(μm)		
C_3w20	3	-5.5	0.025	-2.5	0.053	0.13	0.22
C_s40_3w20	3	-5	0.028	-2	0.066	0.08	0.29
C_s70_3w20	3	-4	0.034	-1	0.131	0.09	0.36
C_f15_3w20	3	-5	0.028	-2	0.066	0.11	0.26
C_f30_3w20	3	-5	0.028	-2	0.066	0.08	0.32
C_28w20	28	-15	0.010	-12	0.012	0.17	0.11
C_s40_28w20	28	-21.5	0.008	-18.5	0.009	0.18	0.15
C_s70_28w20	28	-21.5	0.008	-18.5	0.009	0.15	0.24
C_f15_28w20	28	-13	0.011	-10	0.014	0.16	0.11
C_f30_28w20	28	-9	0.016	-6	0.023	0.18	0.16
C_90w20	90	-22.5	0.007	-19.5	0.008	0.16	0.10
C_s40_90w20	90	-32	0.006	-29	0.006	0.19	0.12
C_s70_90w20	90	-33	0.006	-30	0.006	0.10	0.24
C_f15_90w20	90	-21	0.008	-18	0.009	0.17	0.13
C_f30_90w20	90	-20	0.008	-17	0.009	0.10	0.20
C_720w20	720	-40	0.005	-37	0.005	0.16	0.10
C_s40_720w20	720	-38	0.005	-35	0.005	0.15	0.15
C_s70_720w20	720	-38	0.005	-35	0.005	0.12	0.22
C_f15_720w20	720	-31	0.006	-29	0.006	0.15	0.19
C_f30_720w20	720	-28	0.006	-25	0.007	0.14	0.23

Fig. 5.20(a) shows a decrease of the threshold pore size and volume of pores with time for all the pastes from 1 to 28 days. After 28 days, an increased amount of de-percolated capillary and gel pores is formed for pastes with SCMs and it is reflected in the total volume of pores (Fig. 5.20 and 5.21). Also, the baseline calculation may have an impact in the data, as observed in the section 5.1.1.4. It seems that a better overview of the pores is observed when a semi-quantitative analysis is done by the peaks of apparent heat capacity versus block temperature.

In addition, cracks were found for slag pastes cured for 720 days by SEM, the crack formation may be responsible for the increase of the total porosity given by LTC. The amount of freezable water was obtained by the value of water content (measured by evaporable water tests) subtracted by the amount of ice formed, see Fig.5.22. A large amount of water (about 30 to 80%) does not freeze, and it varies with age and material used. The increased amount of non freezable water may indicate an increased of the specific surface area for samples at old ages (90, 720 days), except for pastes with 70% of slag and 30% of fly ash. According to the literature, evidence of freezing of an adsorbed water film was found at approx. -90ºC by Withwann (1973). For the LTC tests, it was possible to reach the minimum temperature of -55ºC using the set up provided at DTU.
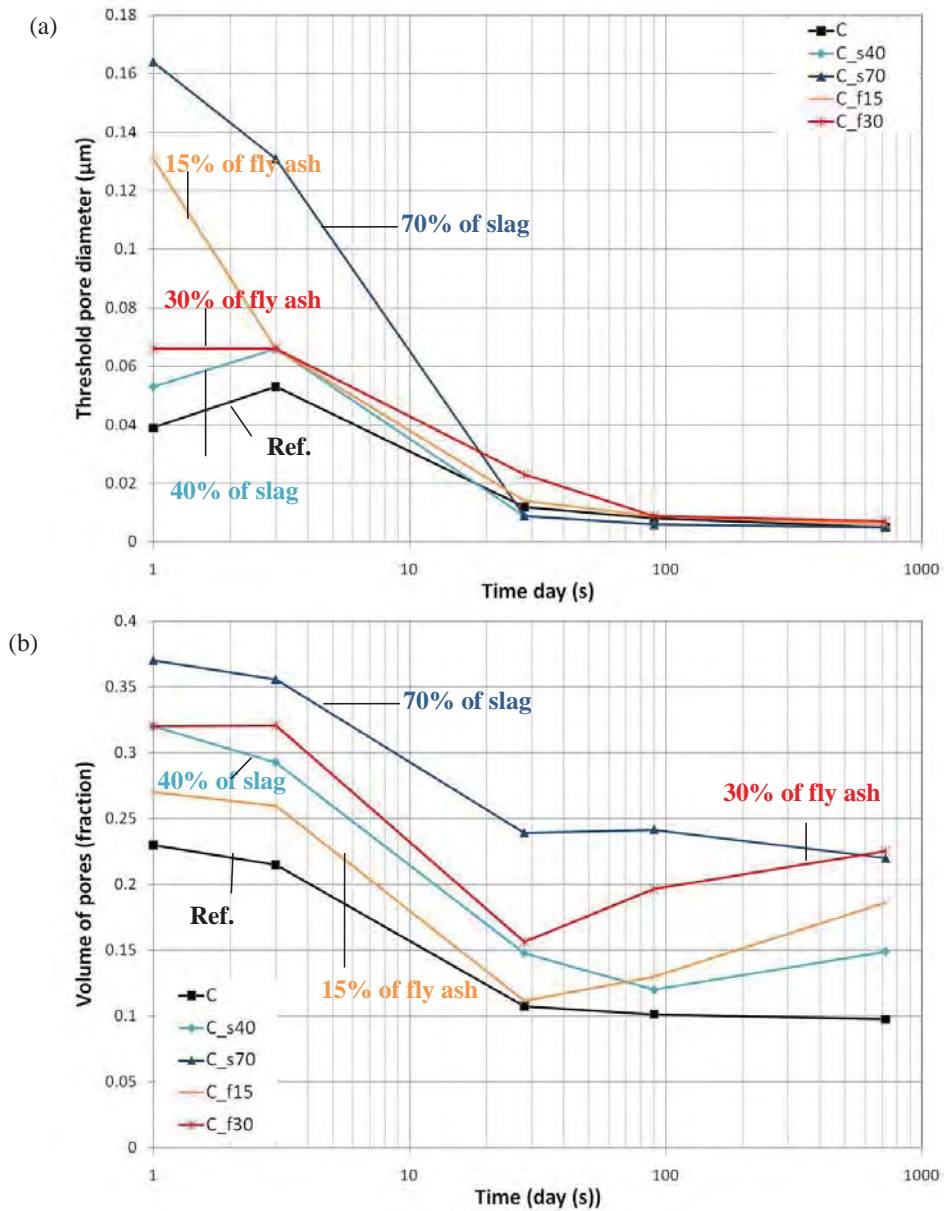
Fig. 5.20: (a) Threshold pore diameter (µm) versus time (day(s)) and (b) total pore volume (fraction) versus time (day(s)) for cement pastes with and without slag and fly ash cured saturated at 20ºC for 1, 3, 28 and 90 days
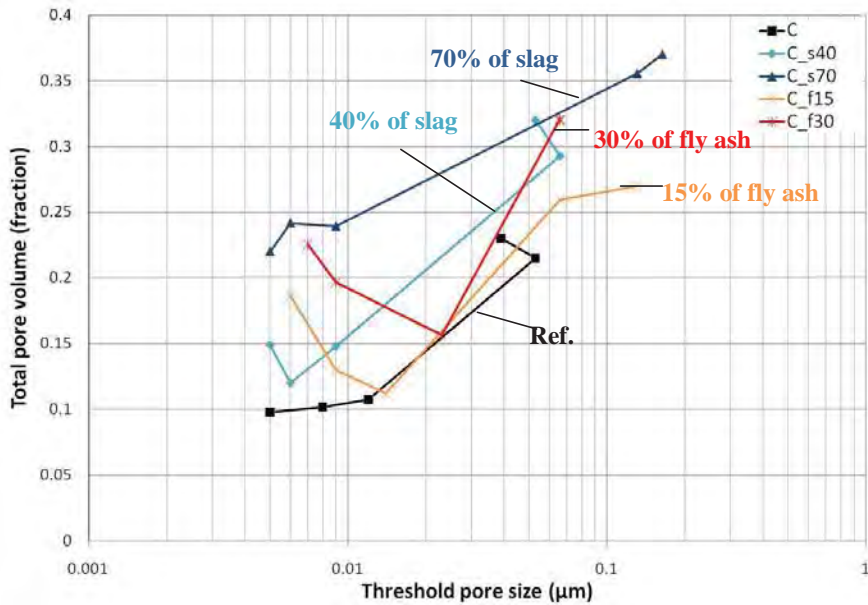
Fig. 5.21: Threshold pore diameter (µm) versus total volume of pores (fraction) for cement pastes with and without slag and fly ash cured saturated at 20ºC for 1, 3, 28 and 90 days
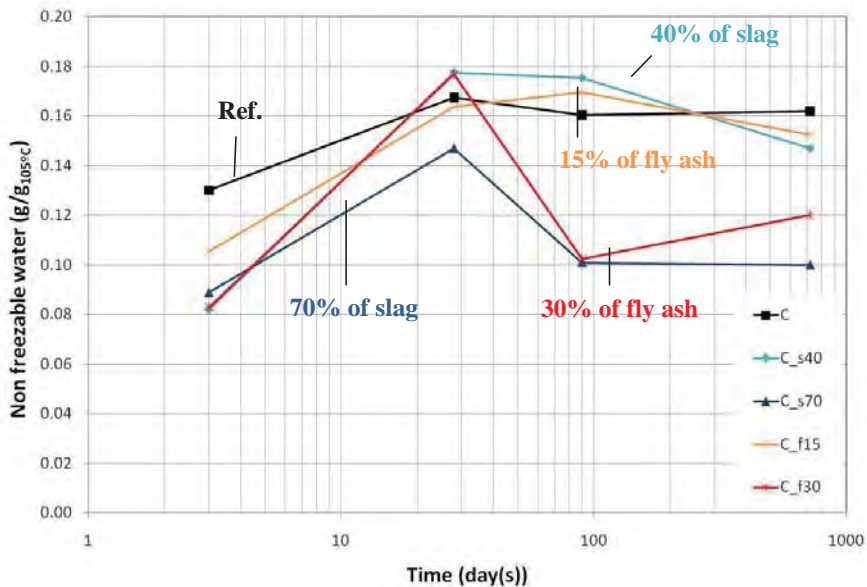

Fig. 5.22: Non freezable water versus time for pastes with and without slag cured saturated at 20ºC for 1, 3, 28, 90 and 720 days

The impact of temperature on the pastes with and without slag cured saturated at 55º or 20ºC for 28, 90 and 720 maturity days is illustrated by the curves of apparent heat capacity versus block temperature, see Fig. 5.23, 5.24 and 5.25. The impact of temperature is also shown for fly ash paste, see Figs. 5.26 and 5.27. The degree of hydration of the pastes was not taking into account.

In general larger peaks were found for pastes cured at high temperature which indicates a coarser porosity; see Figs. 5.23 (a), 5.24(a) and 5.25(a). Lothenbach et al. (2007) explained the increased pore volume by a combination of increased density of the C-S-H and different products formed at high temperature. Another important observation is that the effect of curing temperature is more pronounced for plain cement pastes than slag and fly ash pastes; see Figs. 5.23 to 5.27. Studies (Escalante-Garcia and Sharp, 2001, Ramlochan et al., 2004) have also highlighted a beneficial effect of the slag addition at high temperature. In an important study, Escalante-Garcia and Sharp (2001) shows higher compressive strength for pastes with 60% of slag addition cured at 60ºC than for plain cement pastes. The beneficial effect of the slag addition for pastes cured at high temperature is also showed by MIP, see section 5.2.
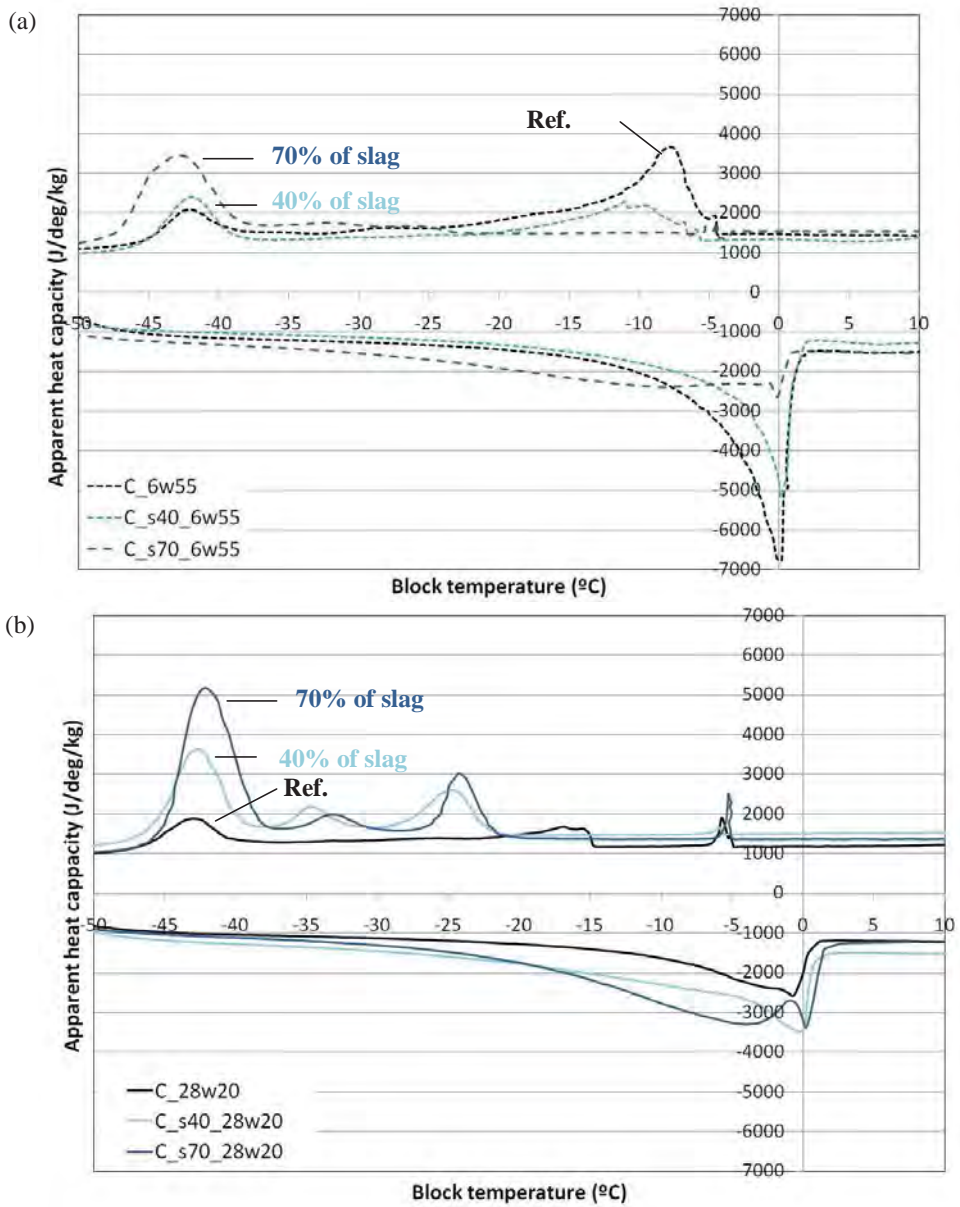
Fig. 5.23: Apparent heat capacity (J/deg/kg) versus block temperature (ºC) pastes with and without slag cured saturated at (a)55ºC for 6.45 days (28 days maturity) and (b)20ºC for 28 days

(a)

(b)
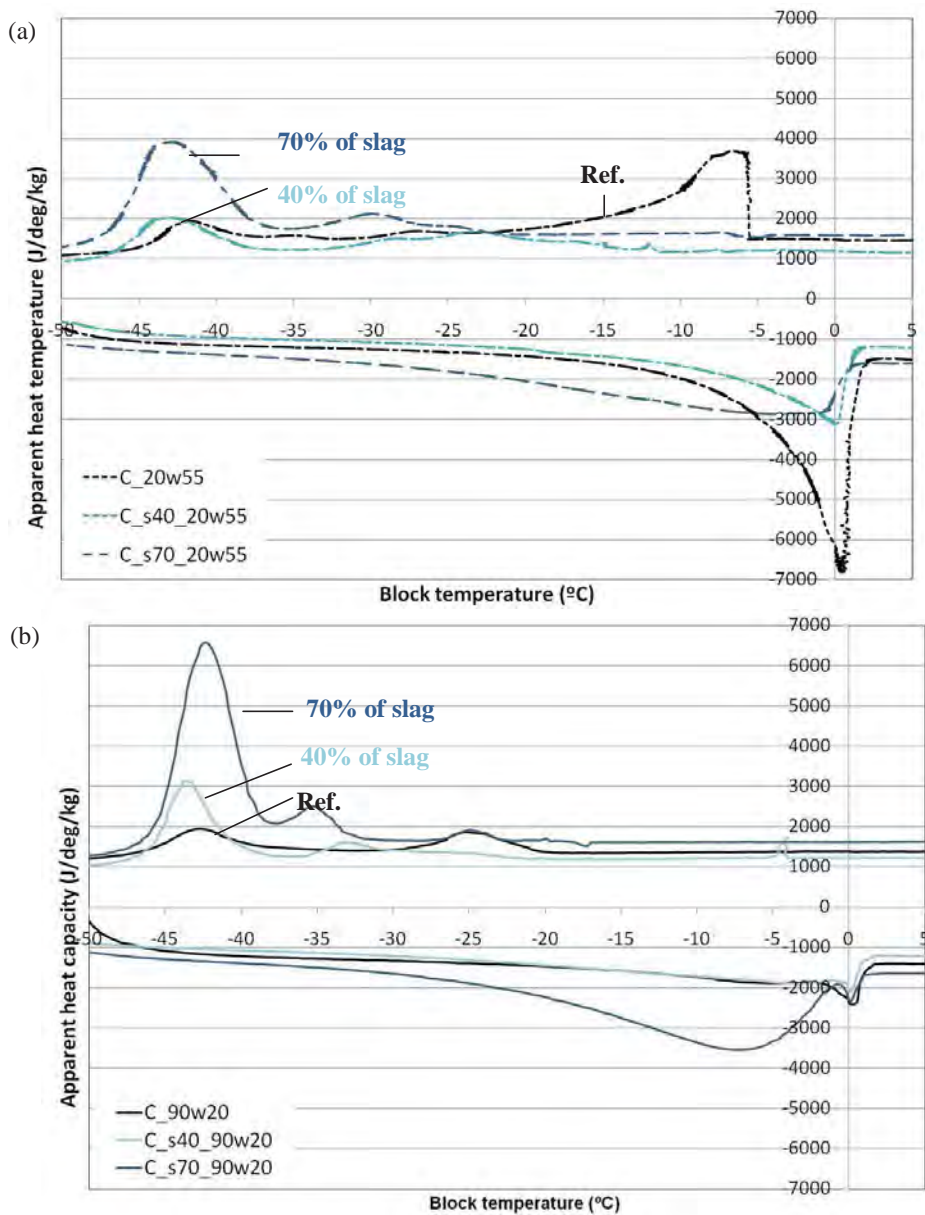
Fig. 5.24: Apparent heat capacity (J/deg/kg) versus block temperature (ºC) pastes with and without slag cured saturated at a) 55ºC for 20.7 days (90 days maturity) b) 20ºC for 90 days
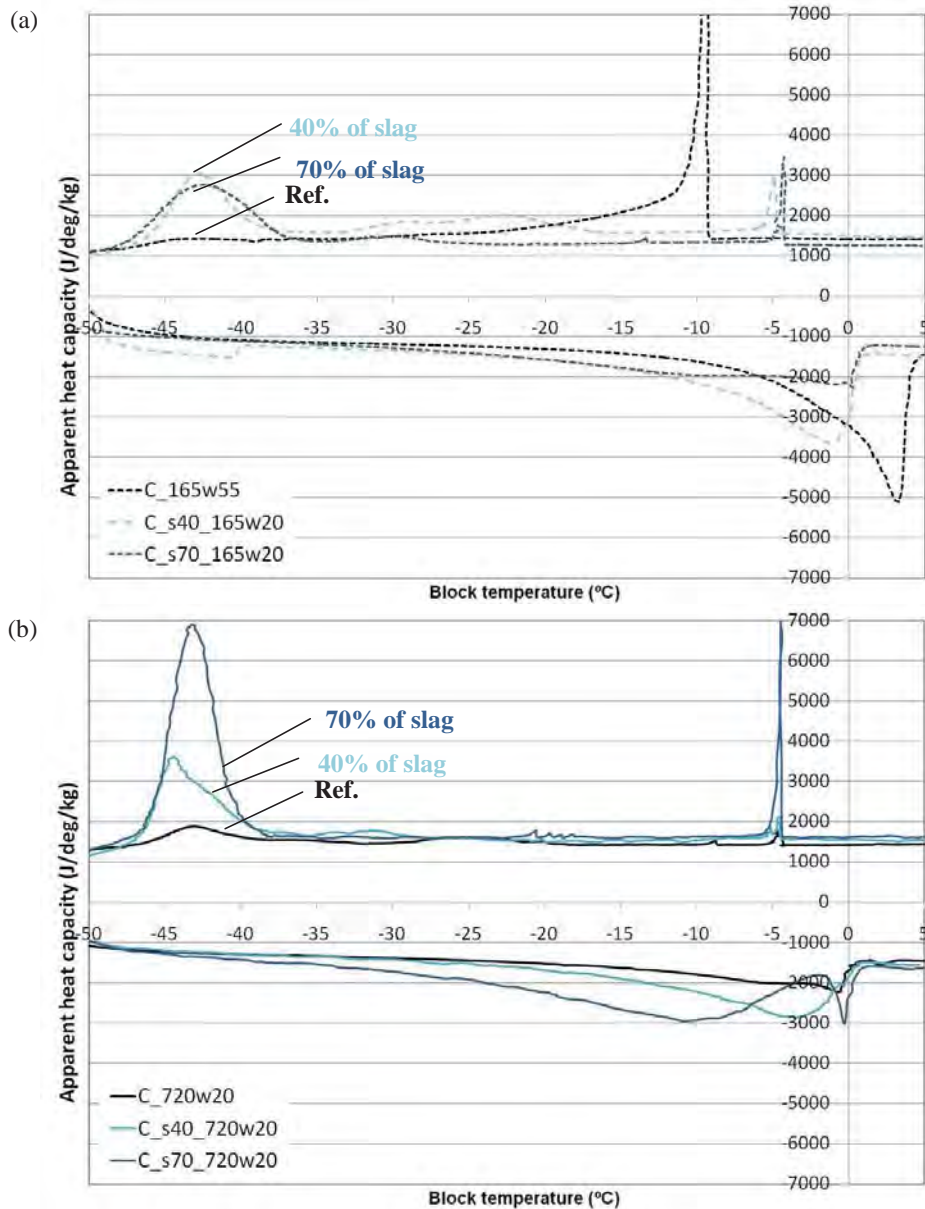
Fig. 5.25: Apparent heat capacity (J/deg/kg) versus block temperature (ºC) pastes with and without slag cured saturated at a) 55ºC for 165 days (720 days maturity) b) 20ºC for 720 days

(a)

(b)
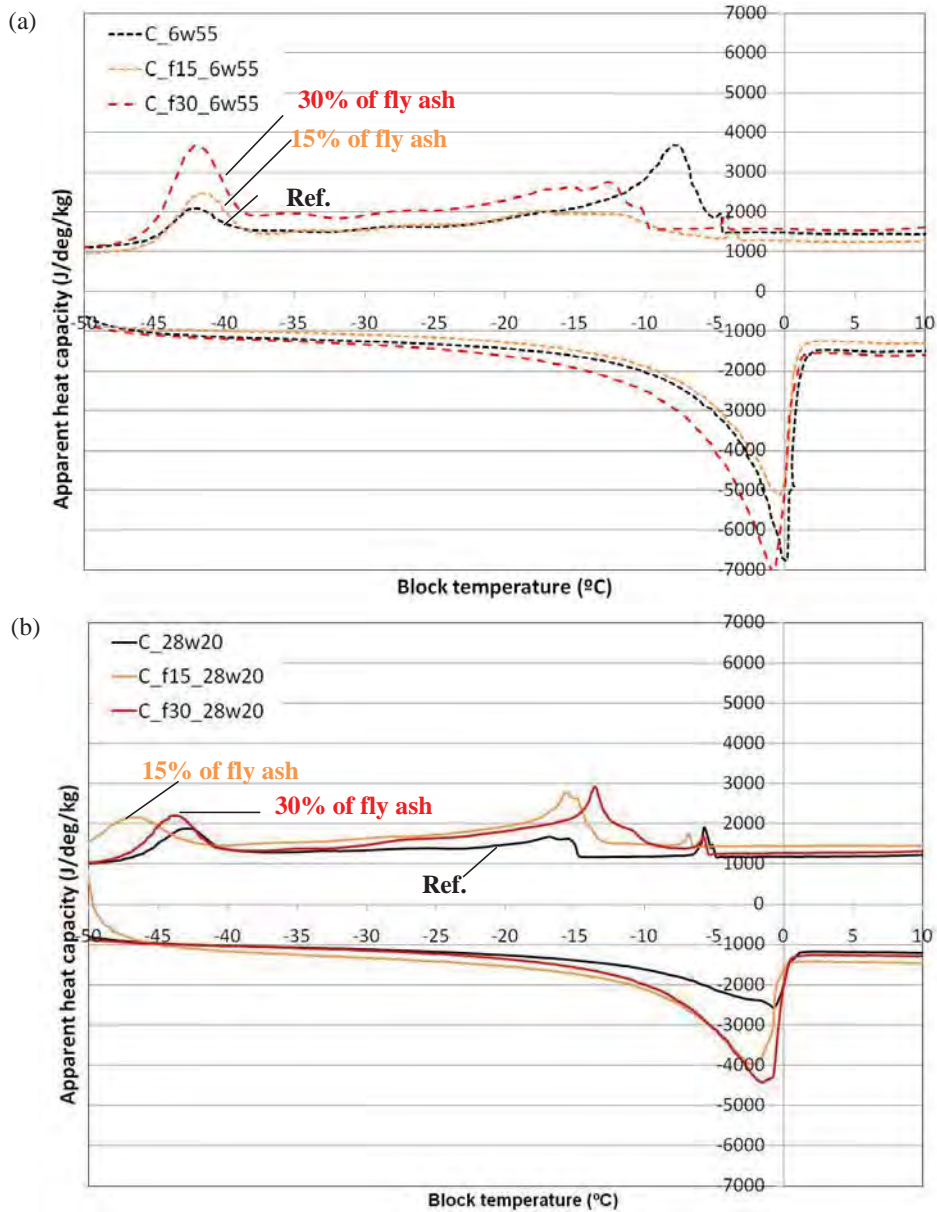
Fig. 5.26: Apparent heat capacity (J/deg/kg) versus block temperature (ºC) pastes with and without fly ash cured saturated at a) 55ºC for 6.5 days (28 days maturity) b) 20ºC for 28 days.
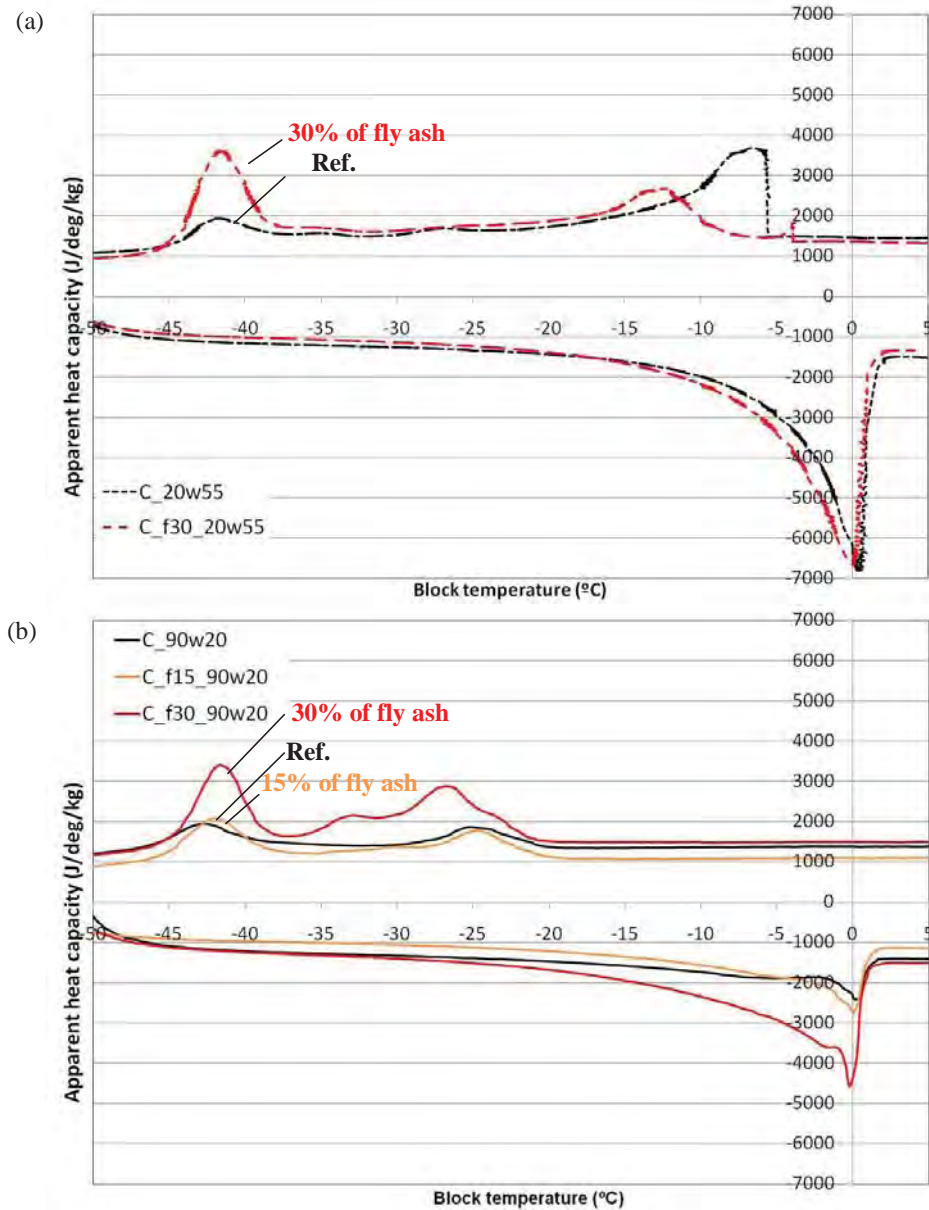
Fig. 5.27: Apparent heat capacity (J/deg/kg) versus block temperature (ºC) pastes with and without fly ash cured saturated at a) 55ºC for 20.7 days (90 days maturity) b) 20ºC for 90 days

The threshold pore size total volume of pores formed during freezing for pastes with and without slag and fly ash cured saturated at 55ºC for 28, 90 and 720 days are given in the Table 5.6 and

illustrated in the Figs. 5.28 and 5.29. In the Fig. 5.30, the correlation between volume of pores and threshold pore size for pastes with and without slag and fly ash cured saturated at 55 or 20ºC is graphically illustrated.

The impact of temperature in the pastes with and without SCMs should be resumed in two facts:
- Larger threshold pore size and volume of pores for pastes cured at 55ºC when compared with pastes cured at 20ºC. Except pastes with 70% of slag;
- The beneficial effect of the slag addition, where a lower pore volume and threshold pore size is found for slag pastes when compared with plain cement pastes at 55ºC, see Fig. 5.23(a), 5.24(a) and 5.25(a). This effect is even more pronounced for pastes with 70% of slag.

Table 5.6: Threshold pore size diameter (µm) and total volume of pores (fraction) formed during freezing for pastes with and without SCMs cured saturated at 55ºC for 6.5 (28 days maturity) and 20.7 days (90 days maturity)

Sample id.	Time (day(s))	Pore threshold diameter (µm)				Non freezable water (fraction)	Total volume of pores (fraction)
		Non corrected		Corrected			
		(ºC)	(µm)	(ºC)	(µm)		
C_6w55	28	-4.0	0.034	-1.0	0.131	0.15	0.22
C_s40_6w55	28	-5.0	0.028	-2.0	0.045	0.15	0.13
C_s70_6w55	28	-27	0.006	-24	0.007	0.11	0.17
C_f15_6w55	28	-7.5	0.019	-4.5	0.030	0.16	0.16
C_f30_6w55	28	-10	0.015	-7.0	0.020	0.12	0.25
C_20w55	90	-5.5	0.026	-2.5	0.053	0.06	0.23
C_s40_20w55	90	-14	0.010	-11	0.013	0.12	0.12
C_s70_20w55	90	-25	0.007	-22	0.008	0.15	0.19
C_f30_20w55	90	-8.0	0.018	-5	0.028	0.06	0.22
C_6w55	720	-8	0.018	-6	0.028	0.15	0.22
C_s40_6w55	720	-17	0.009	-14	0.011	0.12	0.21
C_s70_6w55	720	-32	0.006	-29	0.006	0.15	0.17
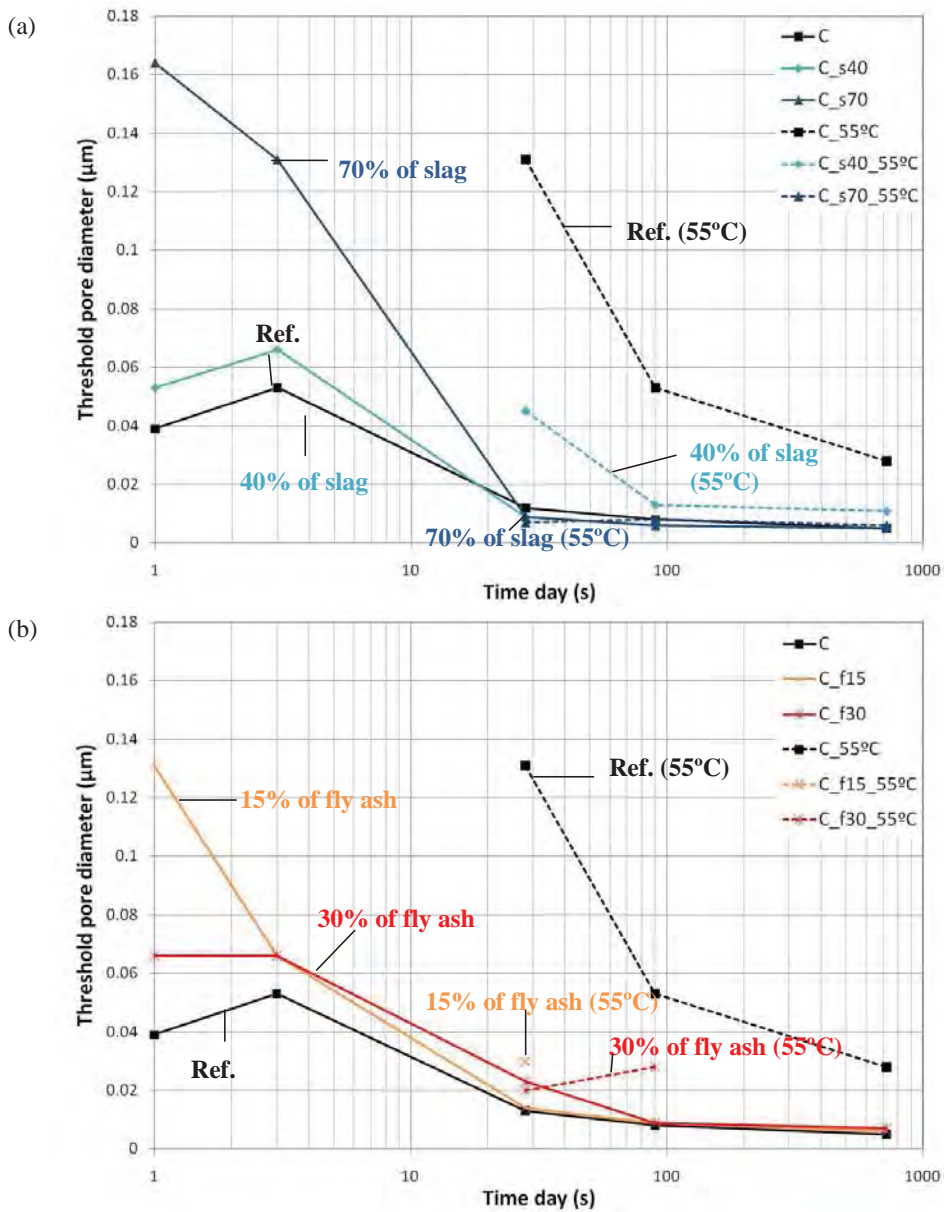
Fig. 5.28: Threshold pore diameter (µm) versus time (day(s)) for (a) pastes with and without slag and (b) pastes with and without fly ash cured saturated at 20°C (full line) and 55°C (broken line) for 28 and 90 maturity days

(a)

(b)
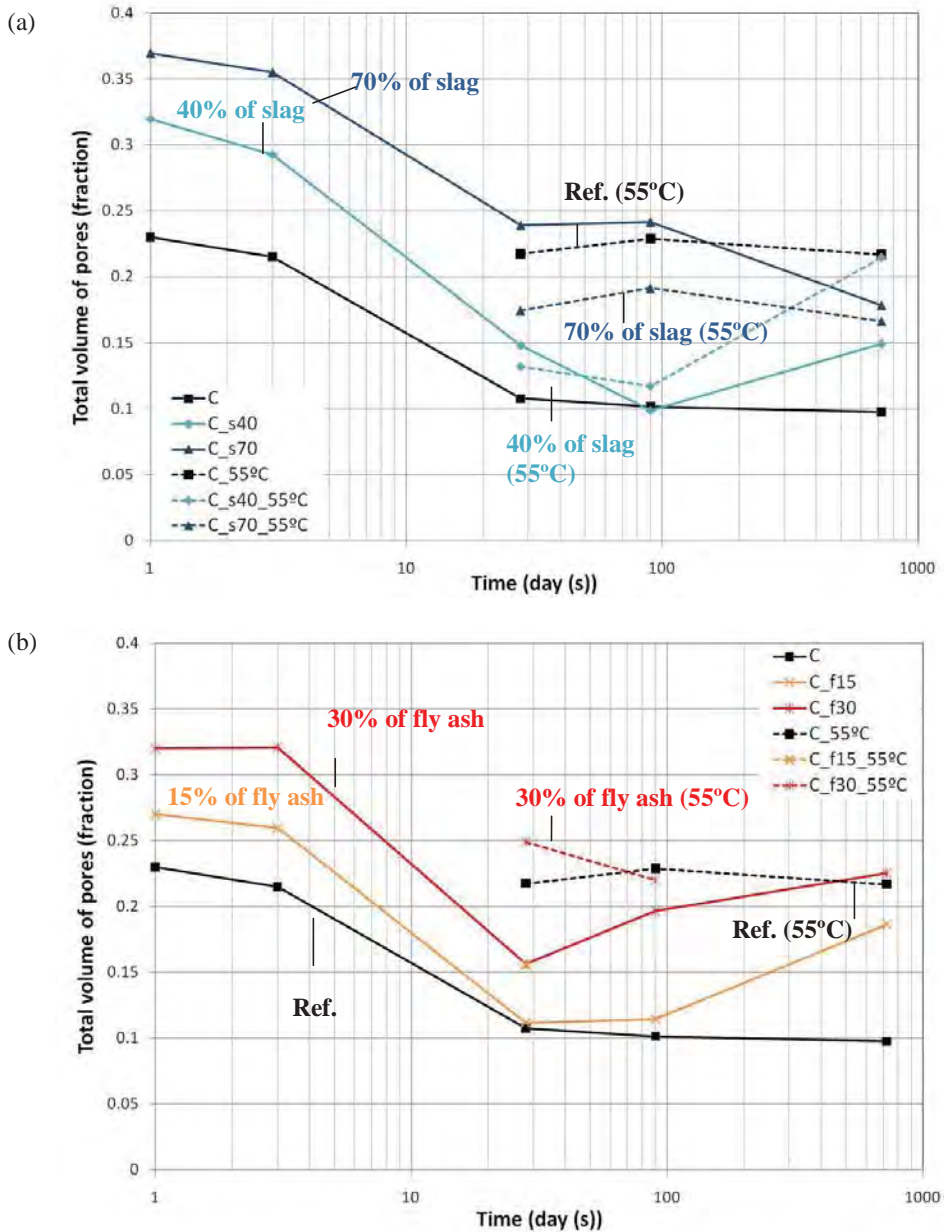
Fig. 5.29: Total pore volume (fraction) versus time (day(s)) for pastes (a) with and without slag and (b) with and without fly ash cured saturated at 20ºC (full line) or 55ºC (broken line) for 28 and 90 maturity days
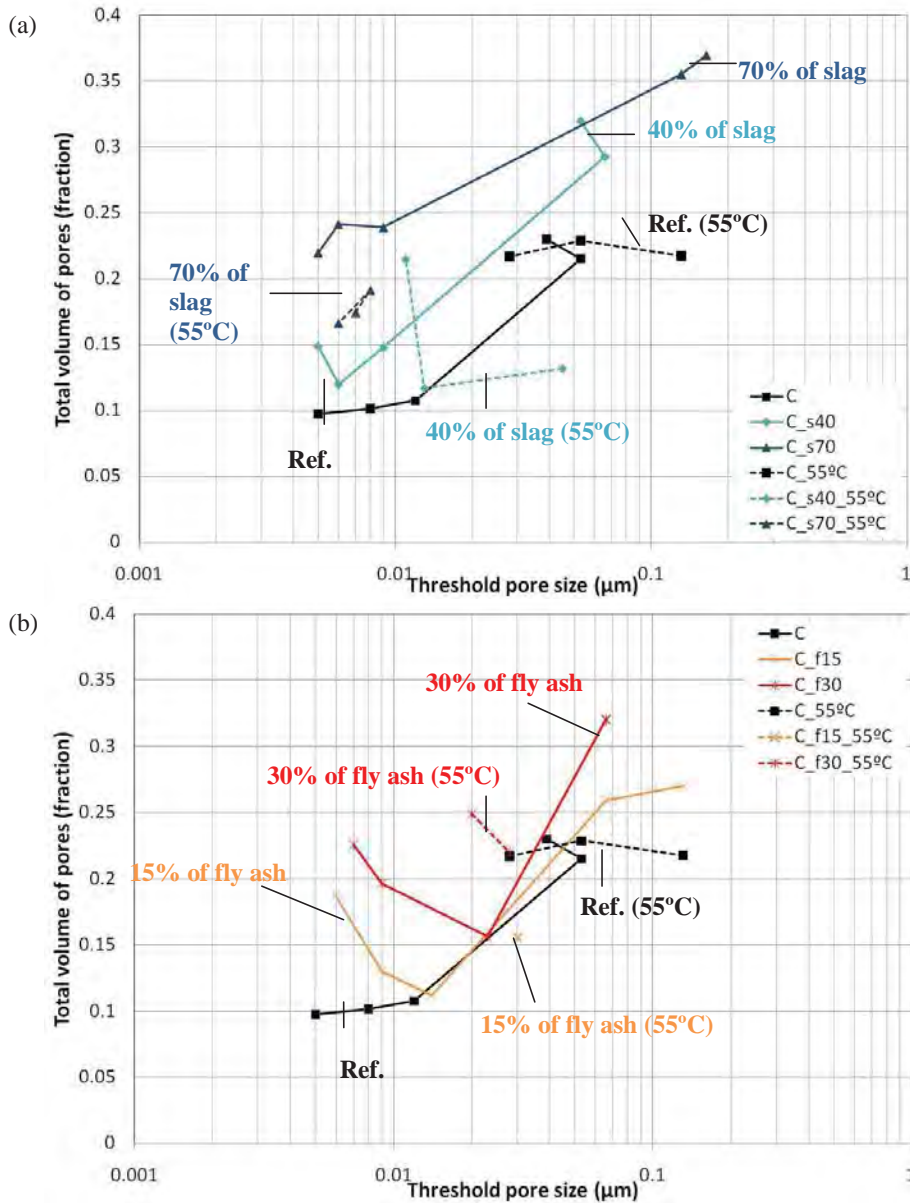
Fig. 5.30: Total pore volume (fraction) versus threshold pore size diameter (µm) for pastes (a) with and without slag and (b) with and without fly ash cured saturated at 20ºC (full line) or 55ºC (broken line) for 28 and 90 maturity day

Example of the possible impact of the curing conditions on pastes with and without slag cured sealed, with bleed water and saturated at 55ºC for 6.5 days (28 maturity days) is illustrated in the Fig. 5.31. The samples with bleed water and sealed were re-saturated using vacuum saturation for 24 hours, the method of re-saturation is described in the Appendix IX. The impact of moisture condition investigated by LTC was not related to the pore structure due to uncertainness related to the degree of re-saturation of the samples.

Fig. 5.31(a) shows a shift of the first peak during freezing for plain cement paste cured sealed, with bleed water and saturated. The shift of the peaks indicated a change in the pore structure for pastes cured at varying curing conditions. For the other samples tested this effect was not so evidence, see for instance pastes with 40% of slag addition in the Fig. 5.31(b).

(a)

(b)
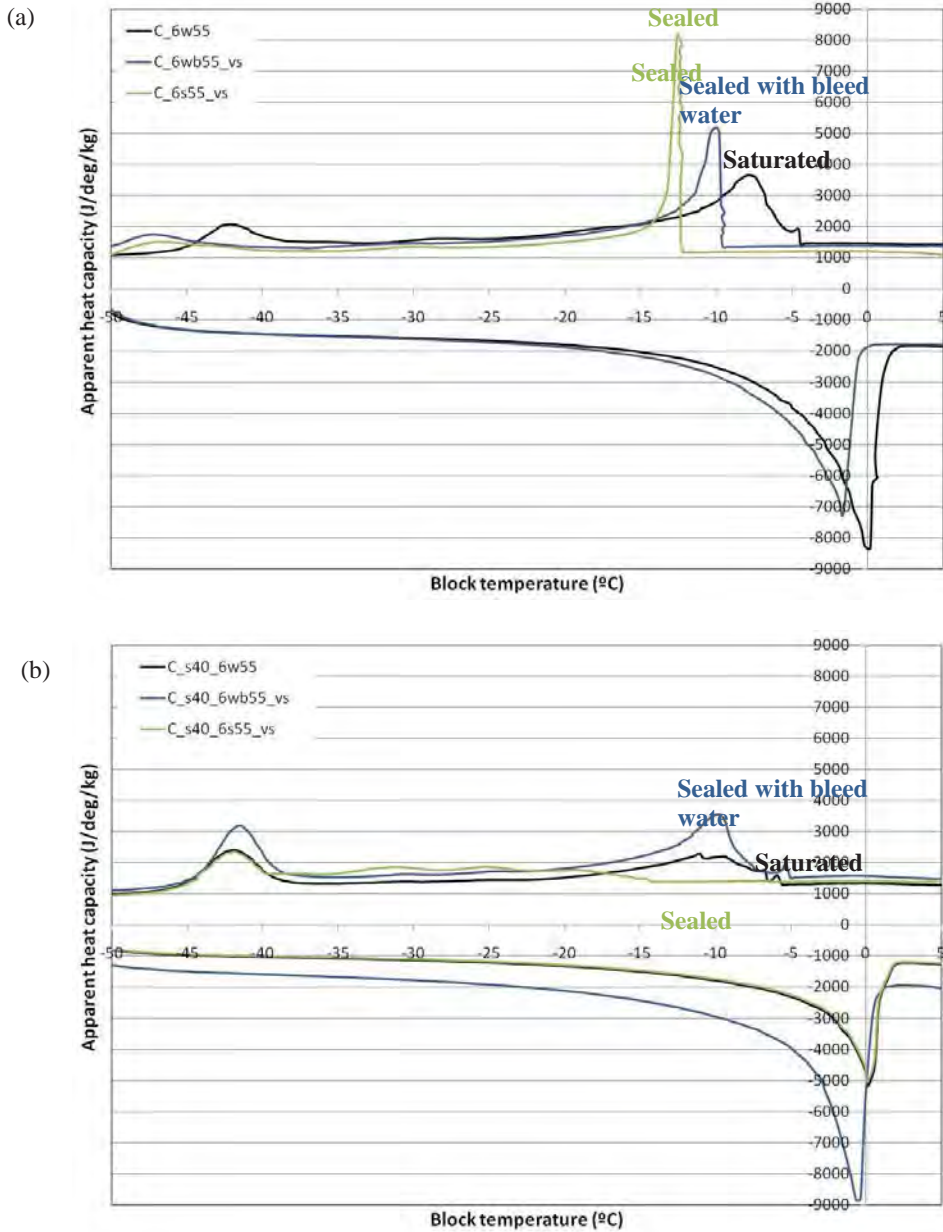
Fig. 5.31: Apparent heat capacity (J/deg/kg) versus block temperature (ºC) for pastes (a) plain cement and (b) 40% of slag addition cured at 55ºC for 6.5 days (28 maturity days) at varying moisture conditions.

The overall results showed that LTC seems suitable to illustrate the pore structure of saturated cement pastes. However in assessment of LTC data, the parameters applied for Kelvin Equation, baseline calculation have to be carefully considered. It is recommended a semi quantitative analysis of the pores by the curves of apparent heat capacity versus block temperature. Moreover, a correction of the block temperature may be necessary based on the non equilibrium between sample and block temperature and freezing point depression due to ions in the pore solution. Also findings here described, showed that the moisture content of the sample is a key for the test, and the re-saturation may interfere in the results of LTC.

5.2 Mercury intrusion porosimetry (MIP)

The threshold pore size and total volume of pores were determined by intrusion curves of MIP. They were calculated according to the Appendix XI. Bulk density of the pastes was also calculated based on the data of MIP, see Appendix XI. Each data point is the average of two measurements on samples from the same batch; the minimum and maximum values are illustrated by an error bar. Intrusion and extrusion curves of MIP are given in the Appendix XVII. The overview of the experimental plan for MIP is given in the Table 4.4.

Threshold pore diameter and total pore volume versus time for slag and fly ash pastes cured saturated at 20ºC are illustrated in the Fig. 5.32. Comparing the pastes, it is possible to observe that smaller threshold pore size for slag pastes cured for more than 28 days, whereas the total intruded pore volume is larger for pastes with slag than for plain cement paste for saturated curing up to 720 days at 20ºC.This is in agreement with observations of improved resistance to ingress of e.g. chloride ions, see e.g. (Hooton, 1986).

(a)

(b)
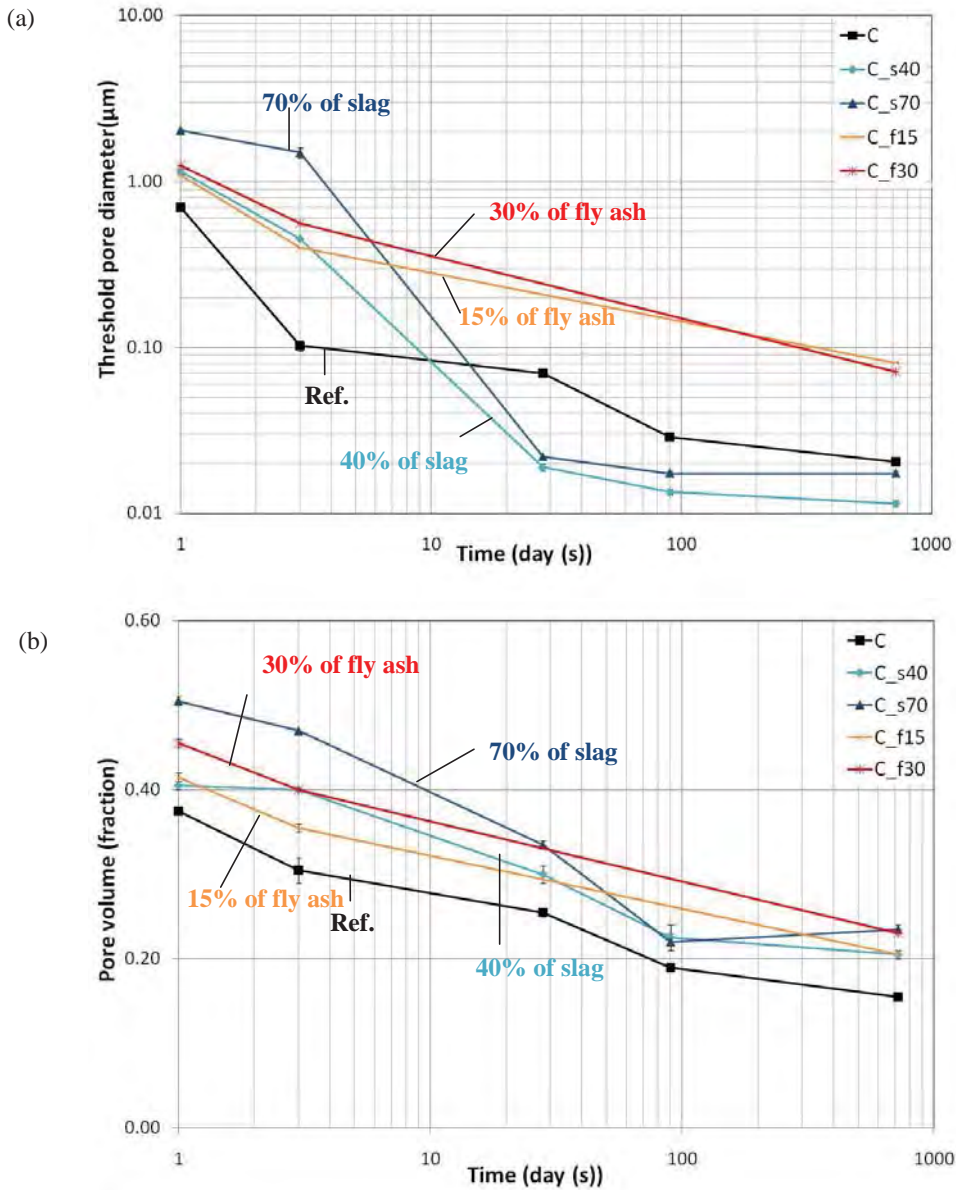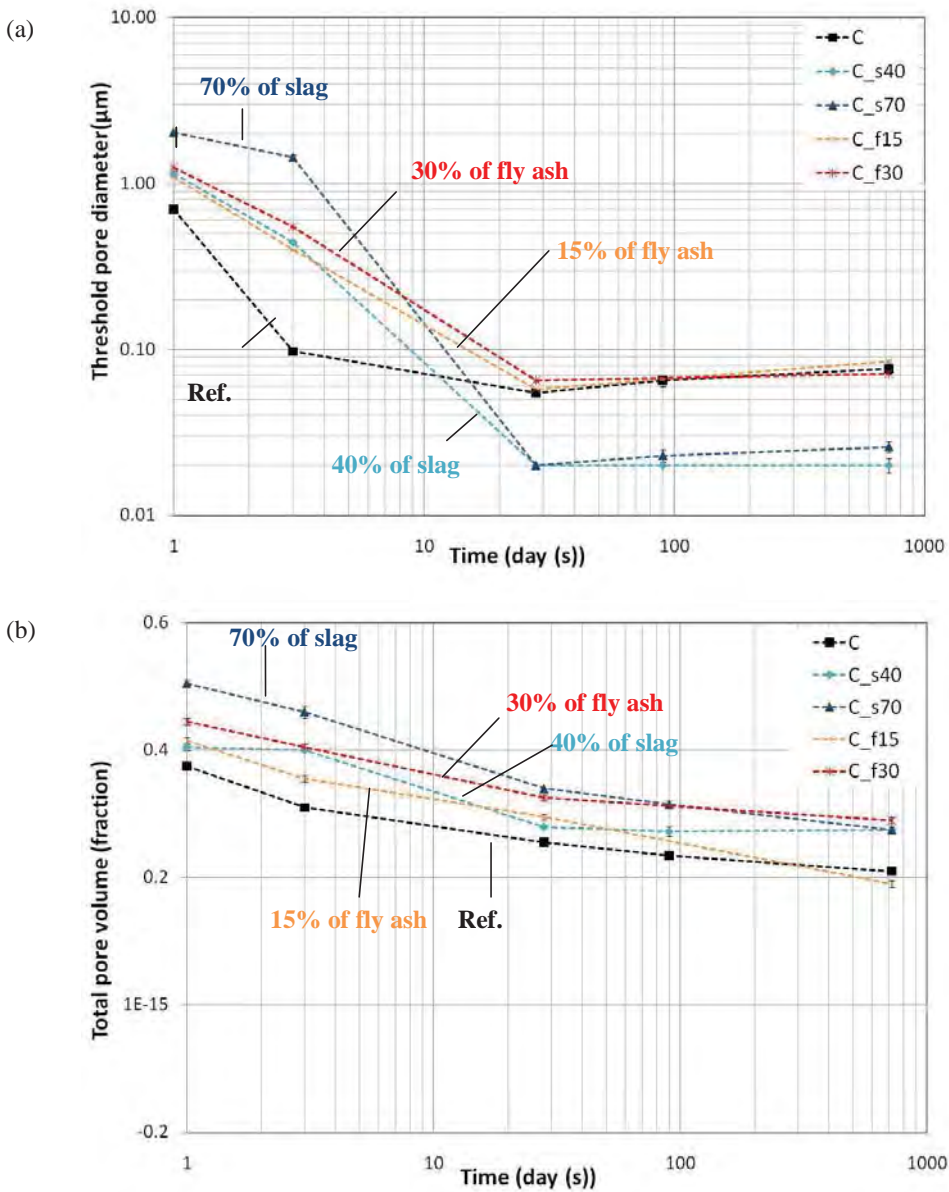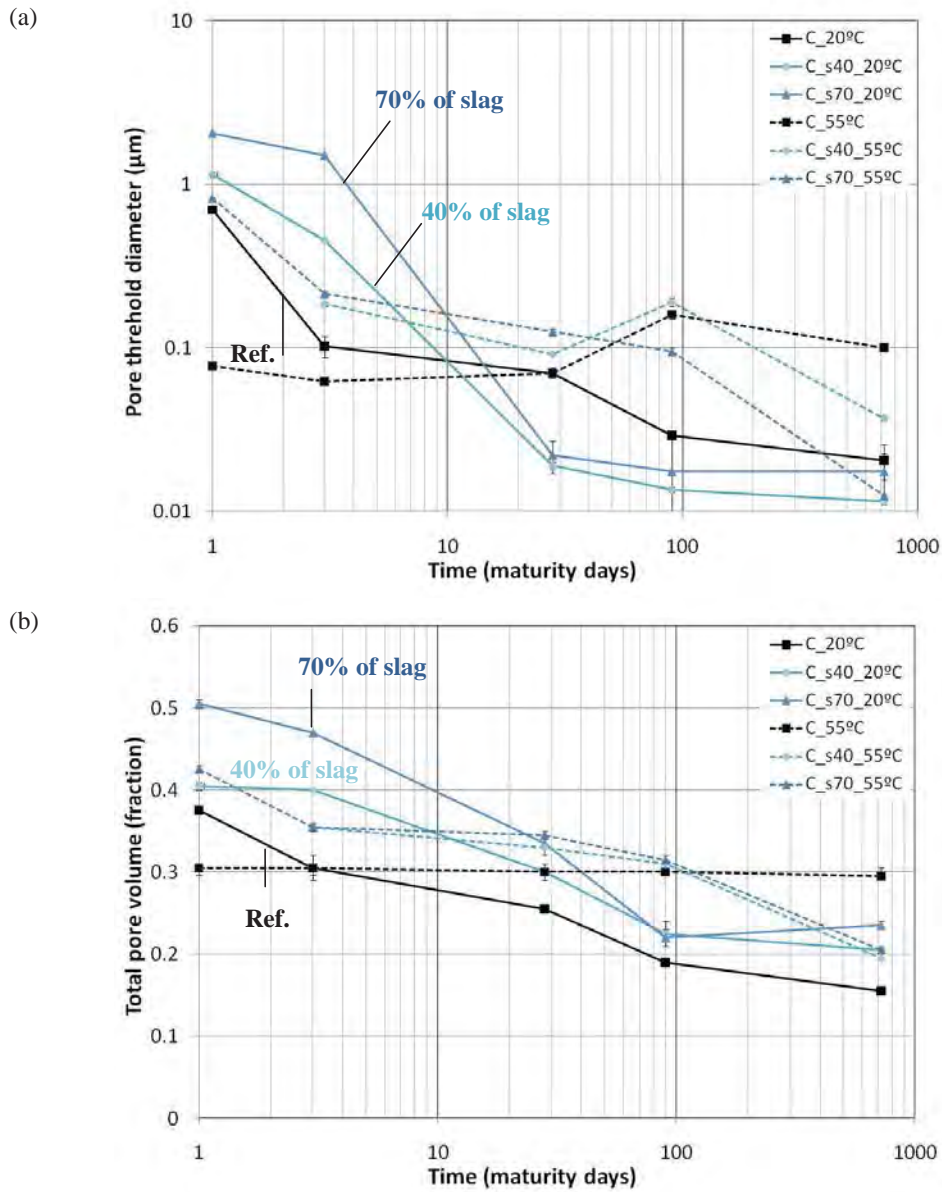

Fig. 5.32: (a) Threshold pore diameter versus time and (b)total pore volume versus time for cement pastes with and without slag cured saturated at 20°C for 1, 3, 28, 90 and 720 days and fly ash cured saturated at 20°C for 1, 3 and 720 days

Derivative curves of the pore volume versus pore diameter for slag pastes cured saturated at 20ºC for 1, 3 and 28 days are illustrated in the Fig. 5.33. The curves indicate a possible refinement of the pore structure with time. It is important to emphasize that MIP does not give true values of pore size due to the effect of "ink bottle" (Diamond, 1971, Diamond, 1995).
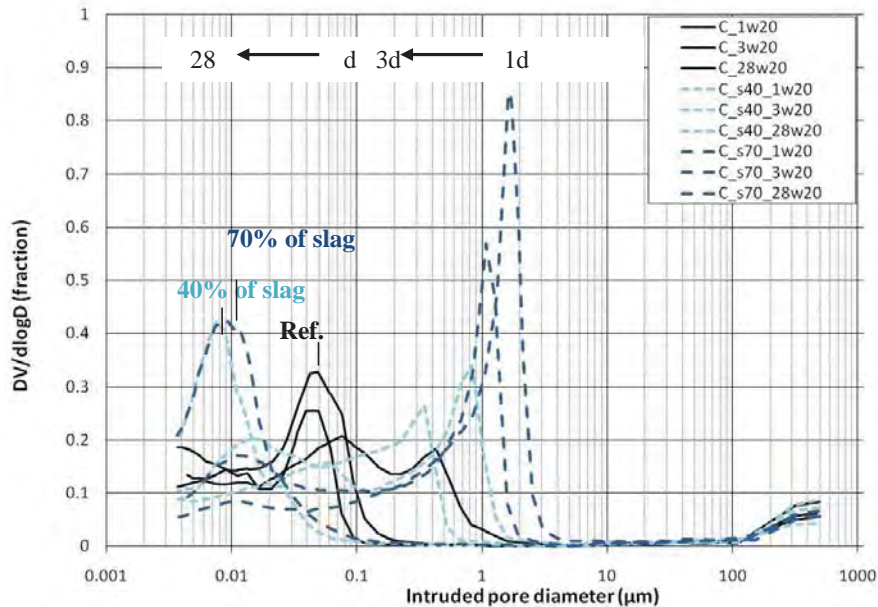
Fig. 5.33: Differential of pore volume versus intruded pore diameter for cement pastes with and without slag cured saturated at 20ºC for 1, 3 and 28 days

The effect of SCMs addition for sealed pastes cured at 20ºC for 1, 3, 28, 90 and 720 days is graphically illustrated in the Fig.5.34.

For samples cured sealed at 20ºC a measurable reduction in the pore threshold size was observed for the slag pastes when compared to plain cement paste with similar pore volume (Fig.5.34(a)). Studies also found evidences to support that, see in e.g. (Feldman, 1984, Malhotra, 1993). Plain cement and fly ash pastes showed similar values of threshold pore size and volume of pores for 720 days, except the volume of pores of 30% of fly ash addition paste. The comparison of curing conditions (sealed and saturated) will be dealt further in this section.

Fig. 5.34: (a) Threshold pore size versus time and (b) total pore volume versus time for cement pastes with and without slag and fly ash cured sealed at 20ºC for 1, 3, 28, 90 and 720 days

The effect of slag addition and curing condition (temperature and moisture) are illustrated in the Figs. 5.35, 5.36, 5.37 and 5.38. To illustrate the possible pore refinement without taking into account the degree of reaction of the binders, graphs of threshold pore size versus time, pore volume versus time were prepared, see Fig. 5.39. Graphic of the correlation between total intruded pore volume and threshold pore size is given in the Fig. 5.40.

(a)

(b)

Fig. 5.35: (a)Threshold pore diameter and (b) total pore volume versus time for cement pastes with and without slag cured saturated at 20ºC (full lines) and 55ºC (broken lines) for 1, 3, 28, 90 and 720 days
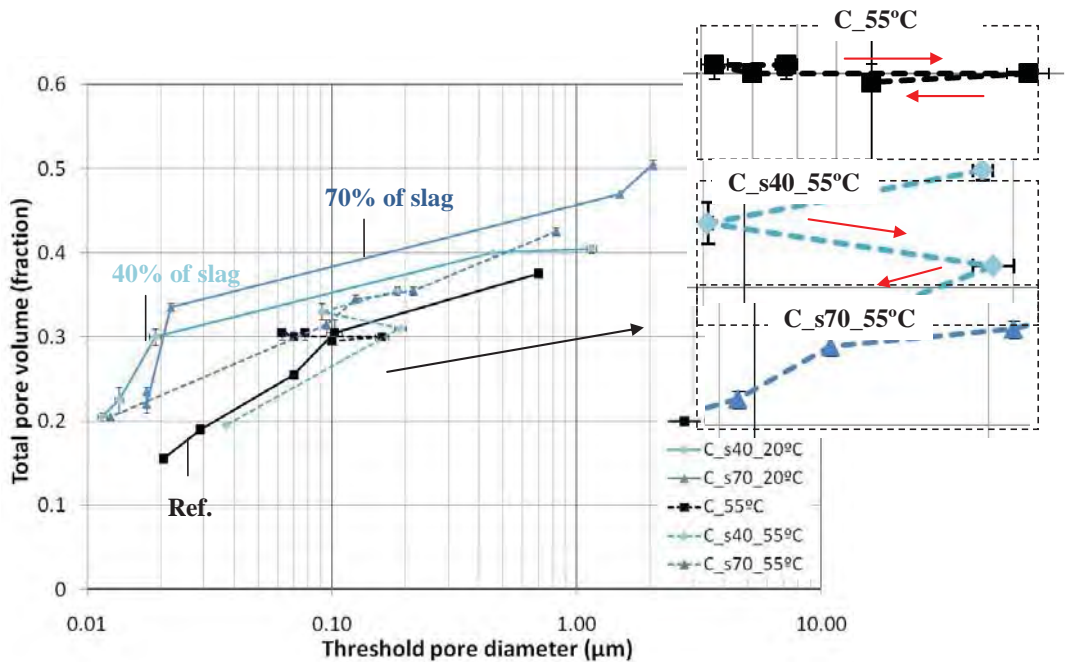
Fig. 5.36: Total pore volume versus threshold pore diameter (determined by MIP) for cement pastes with and without slag cured saturated at 20ºC (full lines) and 55ºC (broken lines) for 1, 3, 28, 90 and 720 days. The arrows illustrate increasing curing time

Assuming comparable degree of reaction of the cement paste cured for 28 maturity days at 20 and 55ºC, an increased pore threshold size and total pore volume was found for plain cement pastes cured at 55ºC when compared with 20ºC, see Fig. 5.35 and 5.36. Similar observations of increased total pore volume have been made by e.g. Zhang (2007) and Kjellsen (1990a). Lothenbach et al (2008) explained the increased pore volume of cement pastes by a combination of increased density of the C-S-H and different reaction products (e.g. monosulfate on the expense of ettringite). The slag pastes show, however, a different trend; where are decreased pore volume is observed at increased curing temperature (55ºC). Also a lower threshold pore size is found for paste with 70% of slag. The refinement of the pores indicate a positive impact of high curing temperature on the transport properties of slag concrete compared to concrete from Portland cement. This is also supported by microstructure and mechanical studies with slag pastes cured at high temperature (Escalante-Garcia and Sharp, 2001, Ramlochan et al., 2004). The slag benefits here reported are also in agreement with data showed by LTC, see section 5.1.3.

For pastes cured sealed the impact of temperature is given in the Fig.5.37 and 5.38. After 28 days curing at 55ºC, an increased threshold pore size is observed for pastes with 40% and without slag, indicating coarsening of the porosity or formation of cracking. For pastes cured sealed at 55ºC the beneficial effect of slag was observed, as a similar volume of pores was found for pastes cured at 20 and 55ºC.
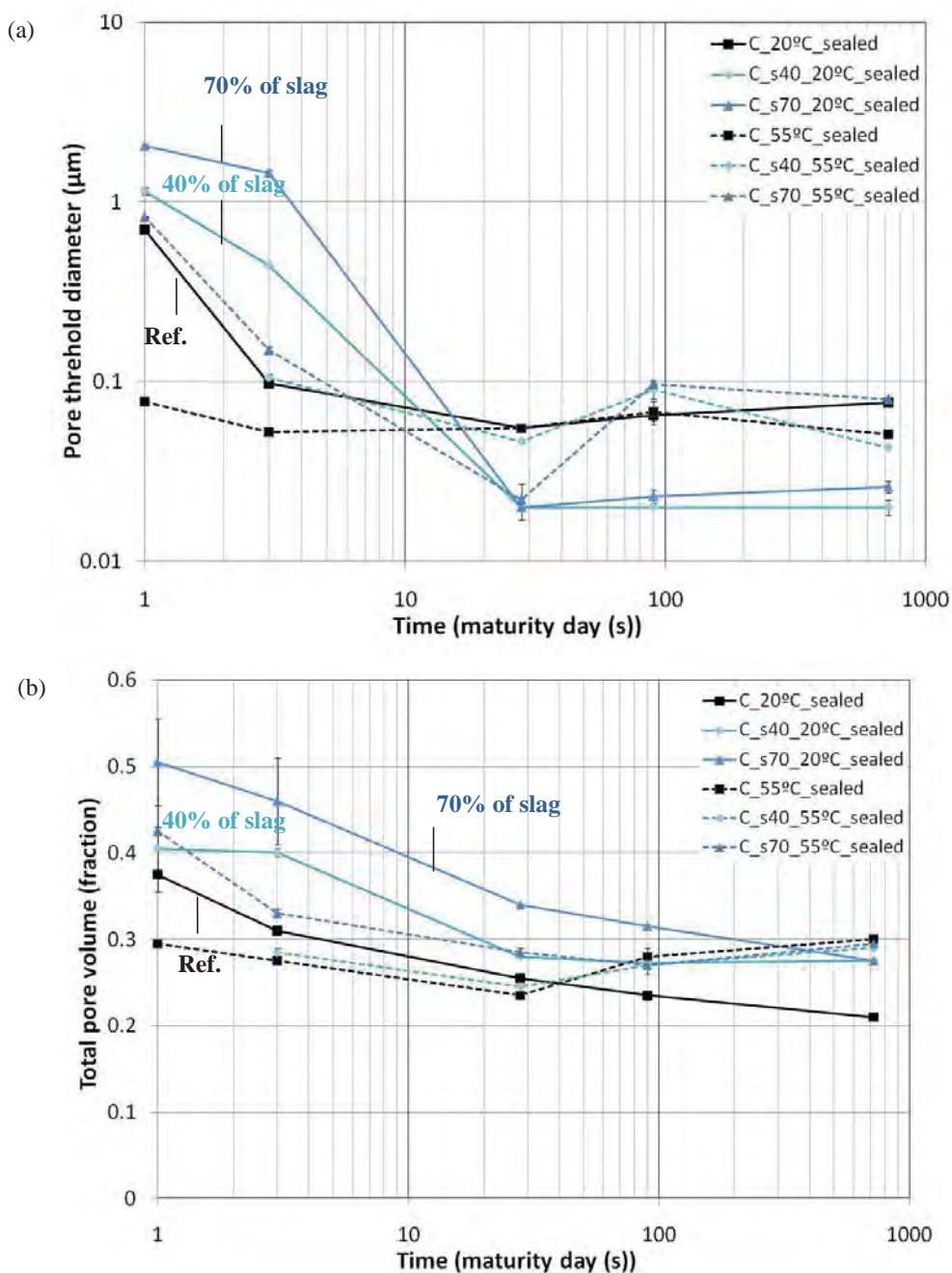
(a)

(b)

Fig. 5.37: (a)Threshold pore diameter and (b) total pore volume versus time for cement pastes with
and without slag cured sealed at 20°C (full lines) and 55°C (broken lines) for 1, 3, 28, 90 and 720
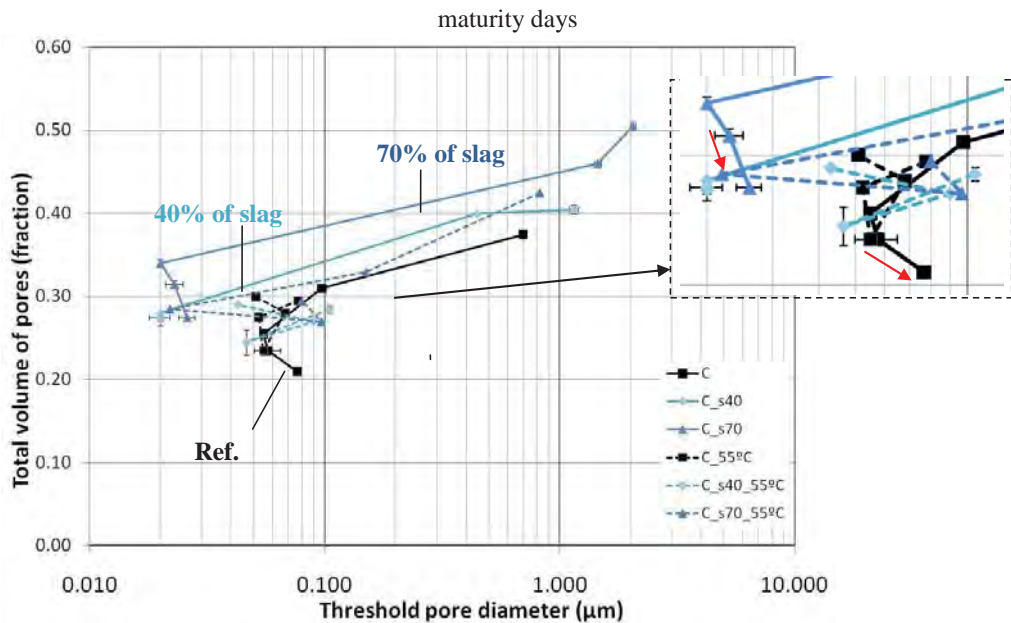
Fig. 5.38: Total pore volume versus threshold pore diameter (determined by MIP) for cement pastes with and without slag cured sealed at 20ºC (full lines) or 55ºC (broken lines) for 1, 3, 28, 90 and 720 maturity days

The effect of moisture conditions (sealed or saturated) is illustrated in the graphs of threshold pore diameter and total volume of pores versus time, see Fig. 5.39 and 5.40. Also, the correlation between total intruded volume and threshold pore size is given in the Fig.5.41.

No major impact on the pore structure characteristics were observed for pastes with slag cured saturated or sealed for 1, 3 and 28 days. After 28 days, the pore structure parameters were increased for pastes with and without slag. Comparable threshold pore size were found for fly ash pastes cured sealed and saturated.

Self desiccation of the sealed samples may explain the coarsening of the pore structure of the pastes with and without slag cured after 28 maturity days. According to Bentz (1999), when external water is unavailable, empty porosity will be created within the cement paste, influencing its microstructure. He found out that self-desiccation are clearly evident as the microstructure formed under sealed curing contains many large capillary pores and large grains of unhydrated cement (Bentz, 1999). Also re-percolation seemed to occur for all the pastes cured after 28 maturity days see Fig. 5.41(a) and it is also reported by Bentz and Stutzman (2008). They show that the capillary pore system in cement pastes cured under sealed conditions is likely to re-percolate.
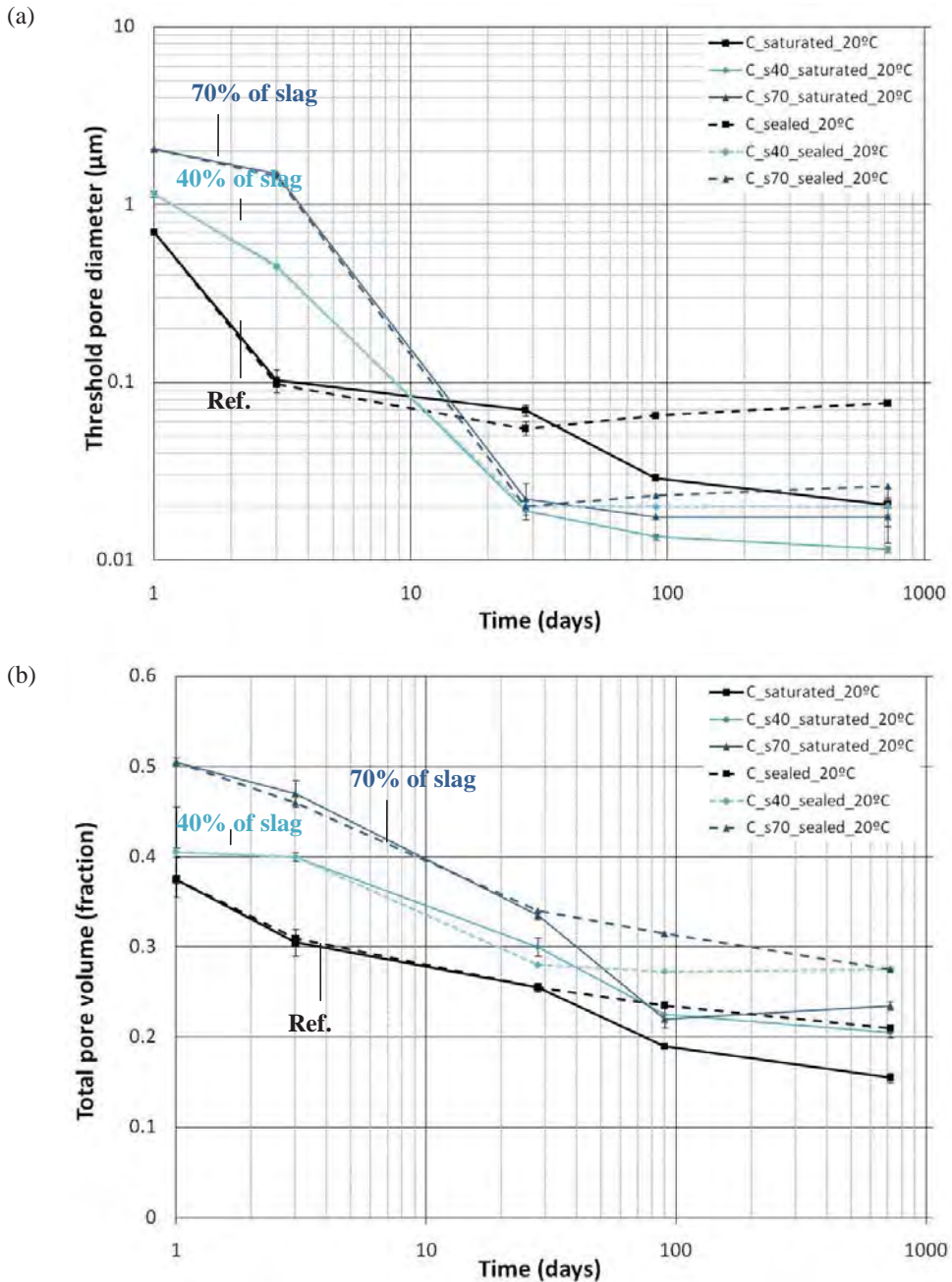
(a)

(b)

Fig. 5.39: (a)Threshold pore diameter versus time (b) Total pore volume versus time for cement pastes with and without slag cured saturated (full lines) and sealed (broken lines) 20ºC for 1, 3, 28, 90 and 720 days
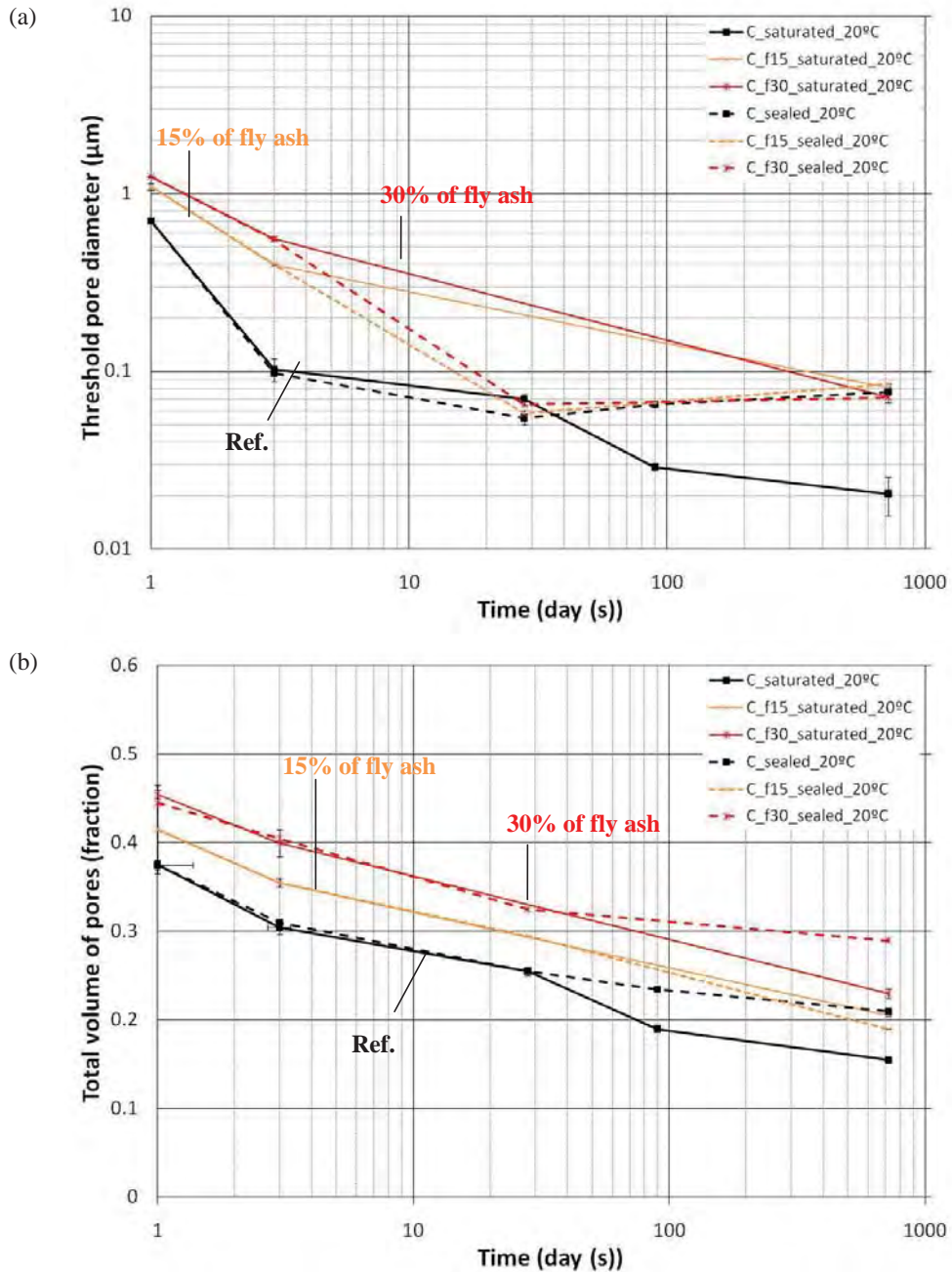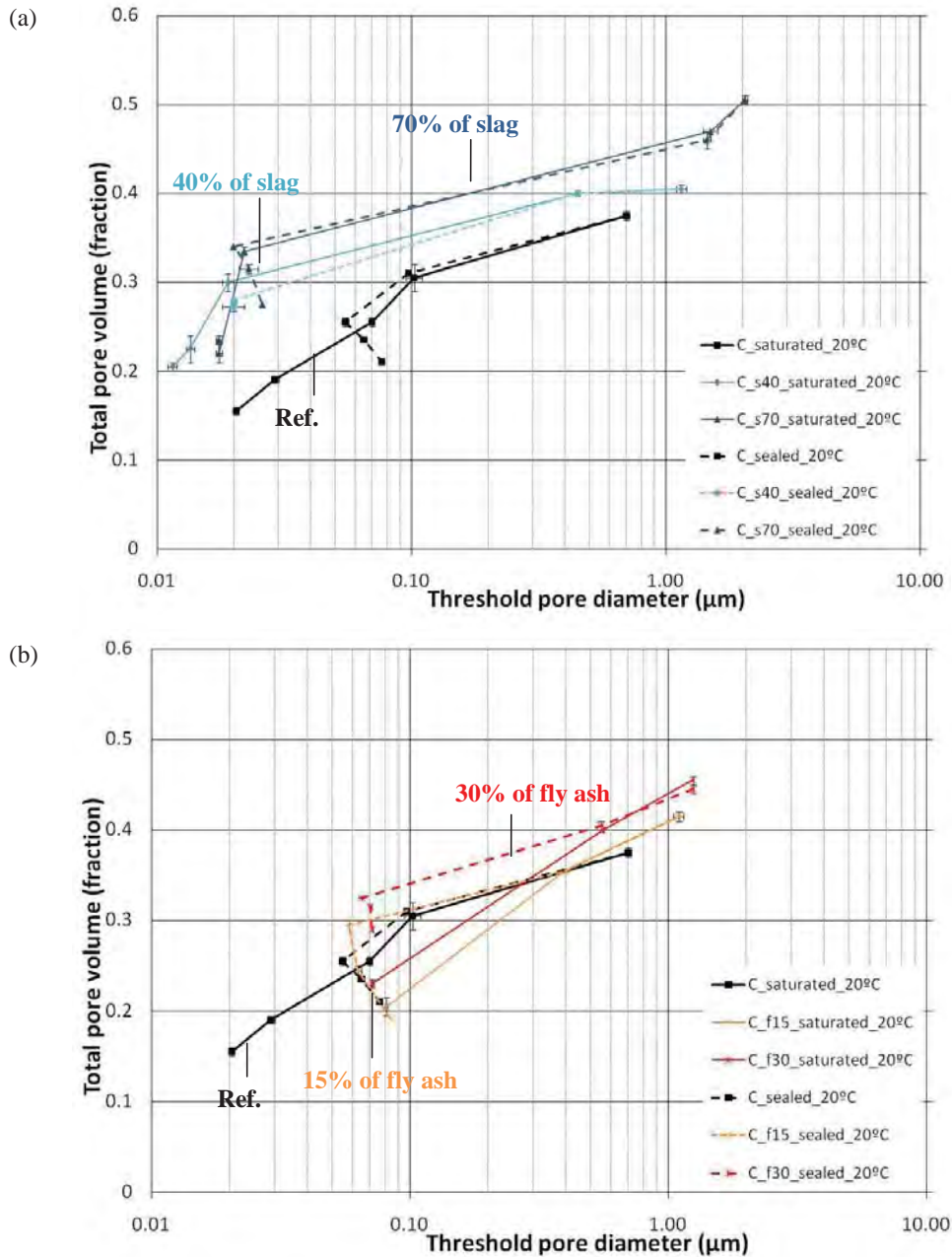
Fig. 5.40: (a)Threshold pore diameter versus time (b) Total pore volume versus time for cement pastes with and without fly ash cured saturated (full lines) and sealed (broken lines) 20ºC for 1, 3, 28, 90 and 720 days

Fig. 5.41: Total pore volume versus threshold pore diameter (determined by MIP) for: (a) cement pastes with and without slag cured saturated (full lines) and sealed (broken lines) at 20ºC for 1, 3, 28, 90 and 720 days and (b) cement pastes with and without fly ash cured saturated (full lines) and sealed (broken lines) at 20ºC for 1, 3, 28 and 720 days

Considering the data here reported, MIP seems suitable to illustrate the porosity of hydrated cementitious materials. Good accuracy between the data was also observed for similar sample tested. The method is fast, simple and non costly and provides information on the maximum size of the connected pores and the total volume of a large range of pores. It is important to keep in mind that the pore size acquired from the pressure values (by Washburn Equation) should be used only for the threshold and not for pore size distribution due to the ink bottle effect. Moreover, MIP data seems to be in agreement with studies carried out with cementitious hydrated materials, taking this into account the method can be used for comparing hydrated cementitious materials using different materials and curing conditions.

In the assessment of MIP data the impact of preconditioning the sample, the test conditions, the range of pore sizes measured as well as the assumptions made in the data analysis should be taken into account. Also, the high pressure used for the intrusion of mercury intrusion may perturb the pore structure (Diamond, 2000, Feldman, 1986a). One questionable point about MIP is the use of a dangerous heavy metal for the analysis. The users should avoid any contact with mercury, for that special cares are necessary: use of gloves and protection glasses for handling the mercury, clean the penetrometer filled with mercury inside a suction chamber and discharge the mercury in special places.

5.3 Scanning electron microscopy (SEM)

SEM images were used to determine:
- Morphology;
- Degree of hydration of plain cement pastes;
- Volume of pores

An average of 100 images (average) at 1000 magnification was used, see procedure in the Appendix XII. The program *Ipwin 4* and ImagAna (Jensen, 2010a) were used to treat the images and acquire porosity data. Pores are identified by the black pixels of the images and at 1000 magnification each pixel is equivalent to approximately 0.30 µm (image size= 3044 µm and amount of pixels =1024). The overview of the experimental plan for SEM is given in the Table 4.2.

The pore structure of fly ash pastes were not investigated at the present work by SEM. It was observed empty spaces (black pixels) in the interior of the fly ash particles and it may overestimate the volume of pores measured by SEM, see Fig. 5.42.
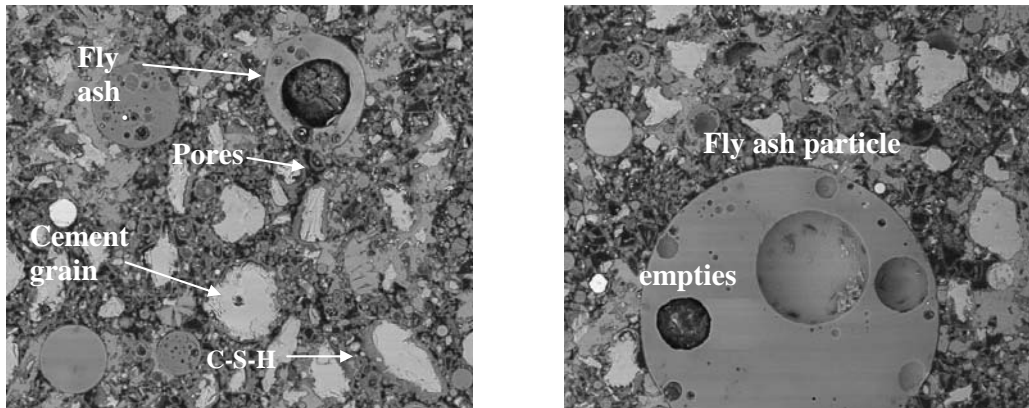
Fig. 5.42: Morphology of the cement paste with 15% of fly ash cured saturated at 20ºC for 3 days; empty spaces within the fly ash particles (imagine width =3044 µm)

Images of the pastes with and without slag cured saturated at 20ºC for 3 and 28 days are given in the Fig.5.43. The impact of moisture and temperature conditions was also analysed by SEM for cement pastes with and without slag cured for 720 maturity days, see Fig. 5.44 and 5.45. Areas in the pastes with air voids and cracks were not taken into account for image analysis.

Anhydrate grains, C-S-H, C-H and pores are part of the main products formed by the pastes which are possible to identify by the grey scale histogram from the images. Grey level differences between the different hydration products, for instances ettringite, monosulfate, are too small and rather difficult to be individually distinguished by image analysis (Scrivener, 2004). C-S-H (light grey) may be observed around the cement grains for plain cement pastes cured saturated at 3 days, see Fig. 5.44(a). In contrast, little amount of inner C-S-H and high amount of non reacted slag particles and pores was noticed for the slag pastes at early age (3 days), see Figs. 5.43(b) and 5.44(c). With the developing of the microstructure with time is possible to observe an increased amount of C-S-H (Fig.5.44). This may indicate the start of the slag reaction and a lesser porosity for pastes with slag cured over 28 days when compared with 3 days. In addition, rims (darker layer) around slag grains are possible to be observed see Fig. 5.44(b) and (c). According to the literature it may be due to magnesium concentration (Kocaba, 2009, Richardson and Groves, 1997). Also for a slag paste is it possible to observed zones of blocked pores, see Figs. 5.43(e), 5.43(f), 5.44(b) and 5.44(c). Investigations reported (Chini et al., 2003) that pore system becomes discontinuous as results of the SCMs reaction and blocked pores may appear in the paste. MIP results also showed a decreased of the threshold pore size for a given intruded volume for pastes with SCMs, see section 5.2.

The effect of moisture conditions on the morphology of the pastes could not be observed by the SEM, see Fig. 5.44. For the temperature conditions, a denser C-S-H is formed and a lighter appearance in BSE images is observed see Fig.5.45. This was also described in the literature, see in (Scrivener, 2004).

Optical microscope images were used to illustrate the crack patterns on the pastes, see Fig. 5.46 and 5.47. After the impregnation of the samples cured for 720 days with epoxy, cracks were observed. This is especially observed for pastes with slag cured saturated and sealed at 20 or 55ºC for 720 maturity day. For samples cured at high temperature, the amount of cracks seemed to be limited or

extinguished (Figs.5.46 (c) and 5.46(f)). The change in moisture content during the hydration may cause pastes to shrink or swell that may induces to cracking formation (ACI224R-01, 2001). Autogenous deformation measurements carried out for pastes with and without slag cured sealed at 20ºC suggested that slag pastes tends to expand during the curing to up to one month and then shrinkage, see section 5.6. This may explain the cracks in the slag pastes cured sealed and saturated at 20 and 55ºC. According to ACI224R-01 (2001), drying occurs no uniformly from the surface towards the paste core, shrinkage creates internal tensile stresses near the surface and compression in the core.
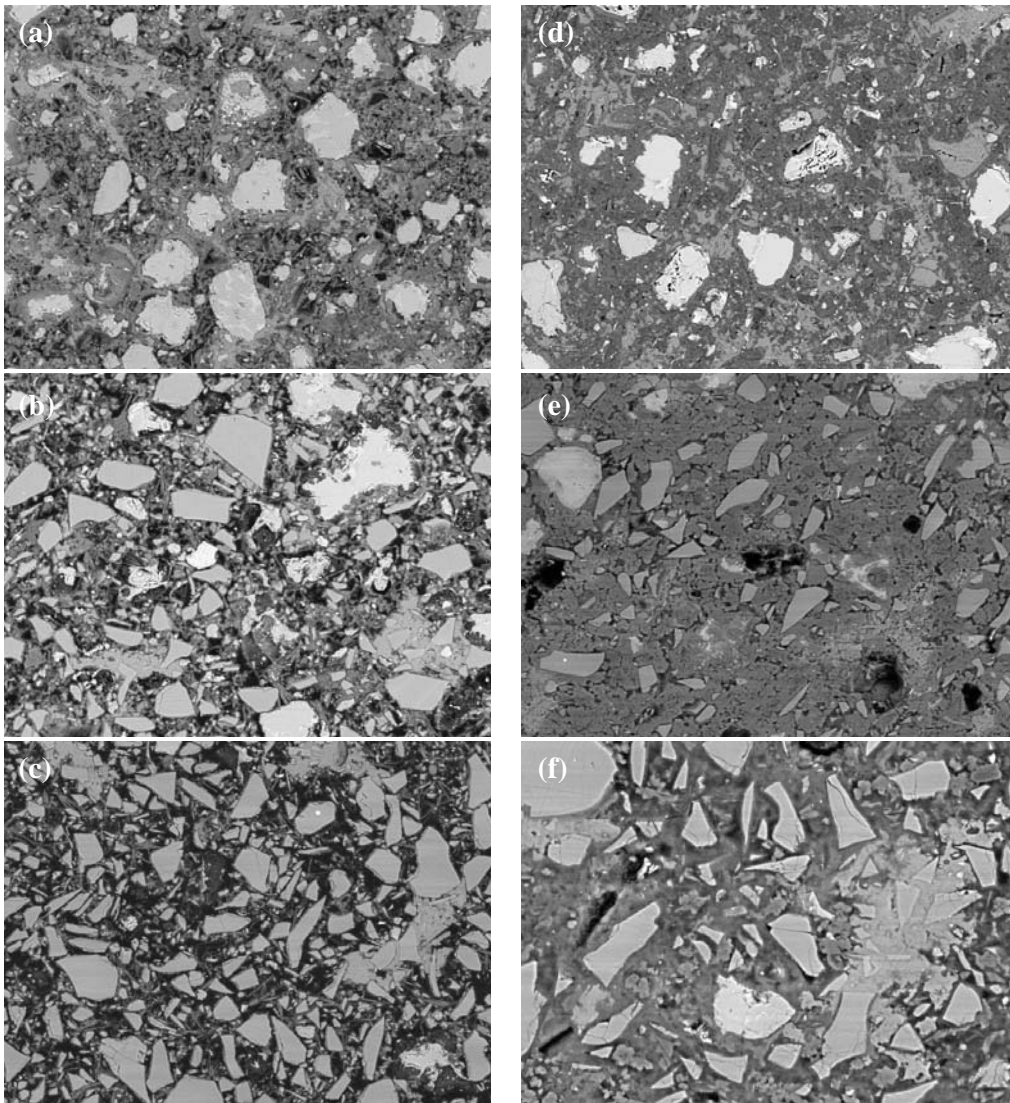
Fig. 5.43: Morphology of cement pastes cured saturated at 20ºC a) plain cement pastes cured for 3 days; b) with 40% of slag cured for 3 days; c) with 70% of slag cured for 3 days and d) plain cement pastes cured for 28 days; e) with 40% of slag cured for 28 days; f) with 70% of slag cured for 28 days (image width =3044 µm)
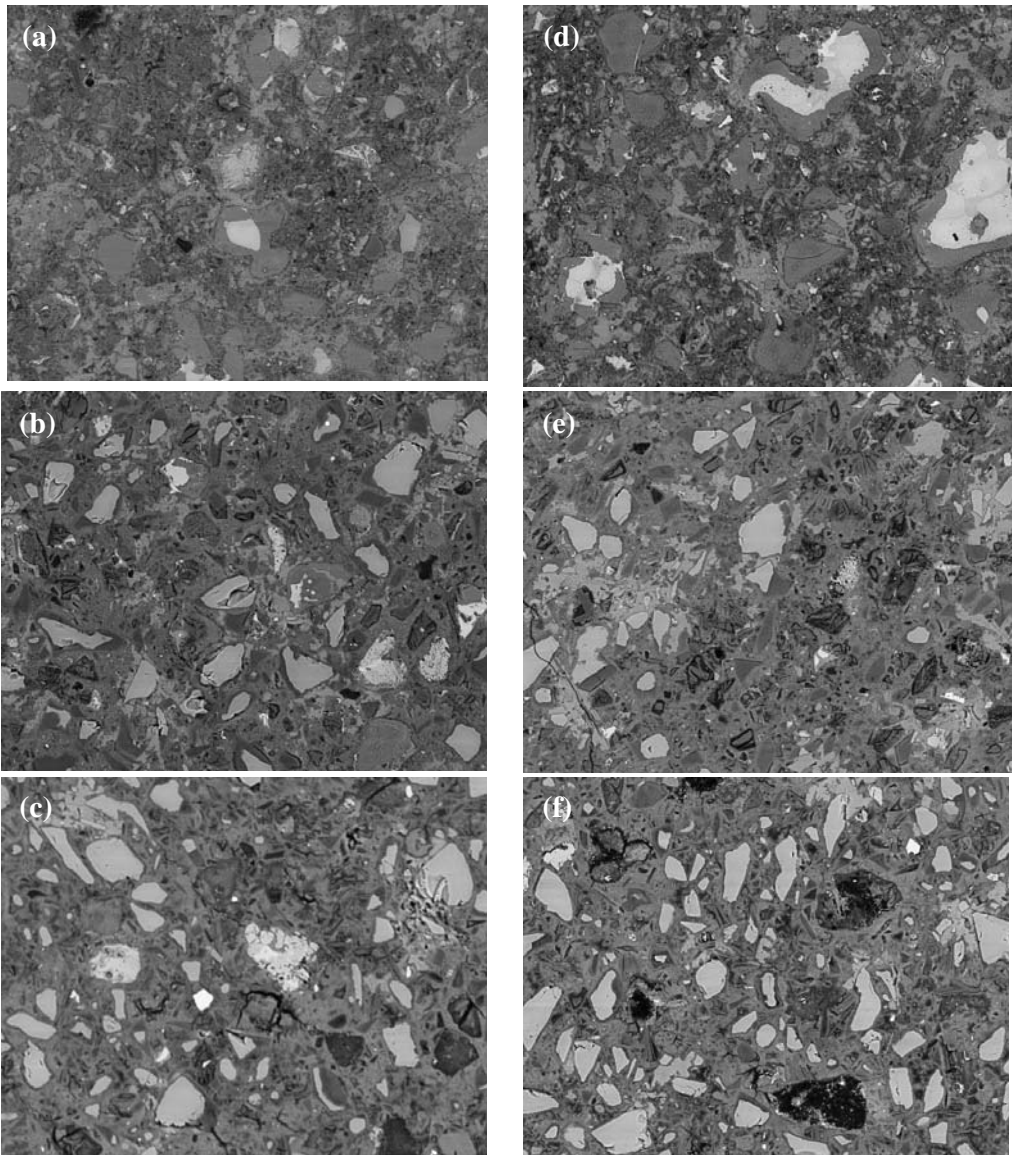
Fig. 5.44: Morphology of cement pastes cured saturated and sealed at 20ºC for 720 days a) plain cement pastes cured saturated; b) with 40% of slag cured saturated; c) with 70% of slag cured saturated and d) plain cement pastes cured sealed; e) with 40% of slag cured sealed; f) with 70% of slag cured sealed(image width =3044 µm)
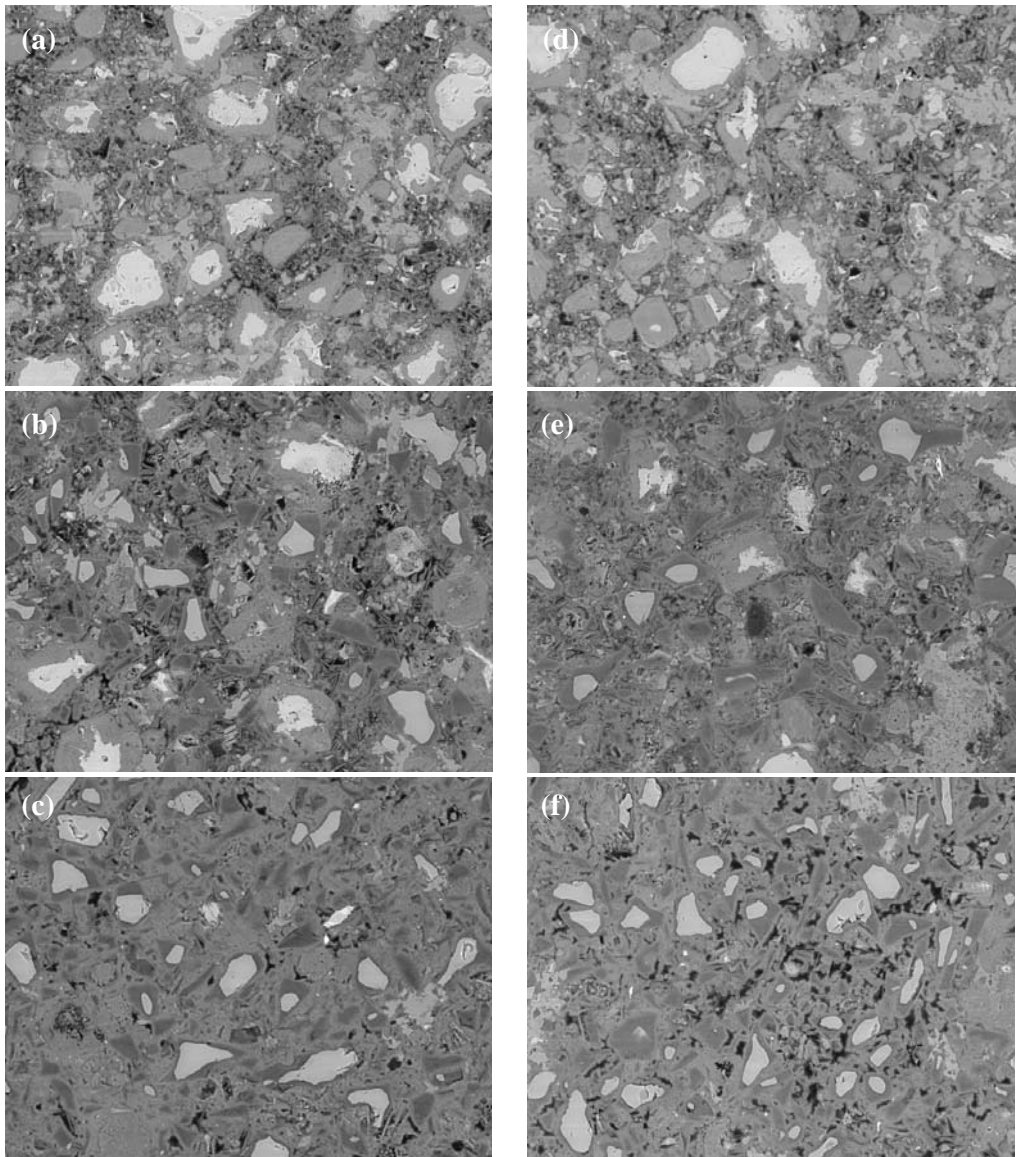
Fig. 5.45: Morphology of cement paste cured sealed and saturated at 55ºC a) plain cement pastes cured saturated; b) with 40% of slag cured saturated; c) with 70% of slag cured saturated and d) plain cement pastes cured sealed; e) with 40% of slag cured sealed; f) with 70% of slag cured sealed(image width =3044 µm)
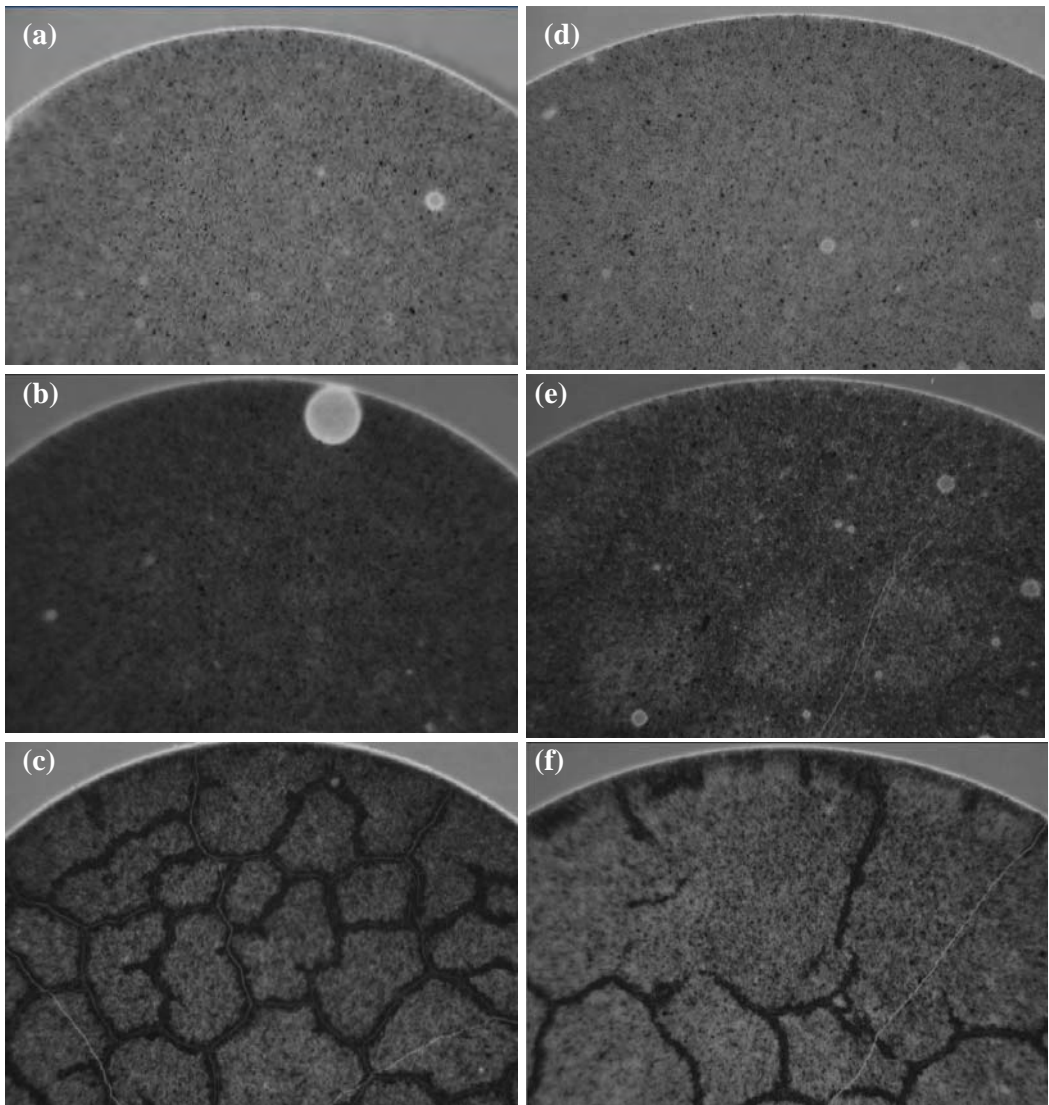
Fig. 5.46: Optical microscope images for pastes cured saturated and sealed at 20ºC for 720 days (a) plain cement paste cured saturated; (b) 40% of slag cured saturated; (c) 70% of slag cured saturated (d) plain cement paste cured sealed; (e) 40% of slag cured sealed; (f) 70% of slag cured sealed, magnification of 8x
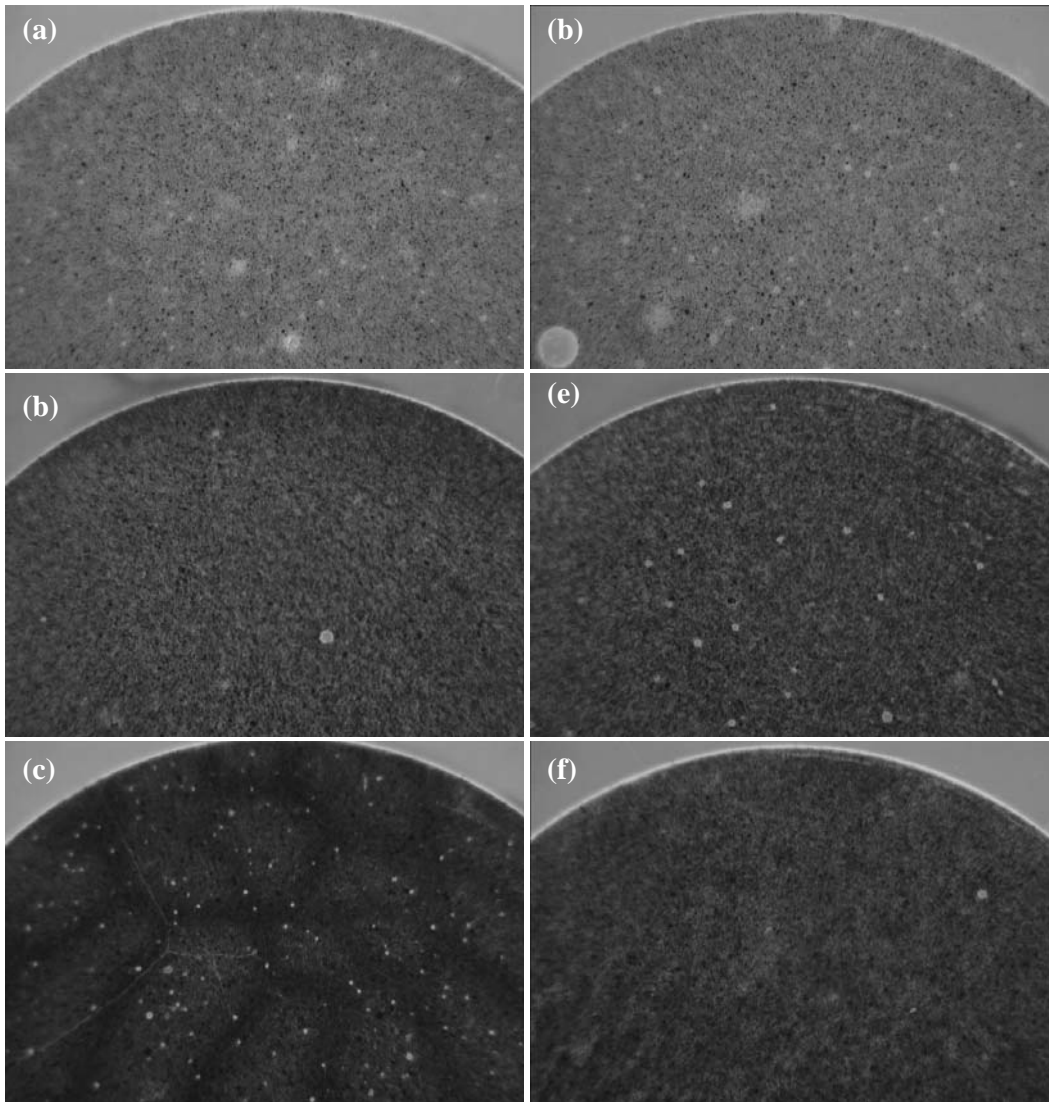
Fig. 5.47: Optical microscope images for pastes cured saturated and sealed at 55ºC for 720 days (a) plain cement paste cured saturated; (b) 40% of slag cured saturated; (c) 70% of slag cured saturated (d) plain cement paste cured sealed; (e) 40% of slag cured sealed; (f) 70% of slag cured sealed, magnification of 8x.

Automatic threshold of the images was carried out using ImagAna and Ipwin4, however the data was not reliable, see Fig. 5.48. The automatic "thresholding" is obtained by a computer script based on the tangent of the first peak presented in the grey level histogram; see in Jensen (2010). However, the first peak of the grey scale histogram sometimes is located in the range of the pores, example is given in the Fig. 5.49(a) where a high peak at the range between 0 and 50 pixels (pores)

is observed for slag paste cured for 3 days. Thus "thresholding" of the pores should not be acquired by the tangent from the C-S-H peak (see Fig. 5.49(b)). In this case, the program Ipwin4 was used to acquire the threshold pore size, see Fig. 5.50.
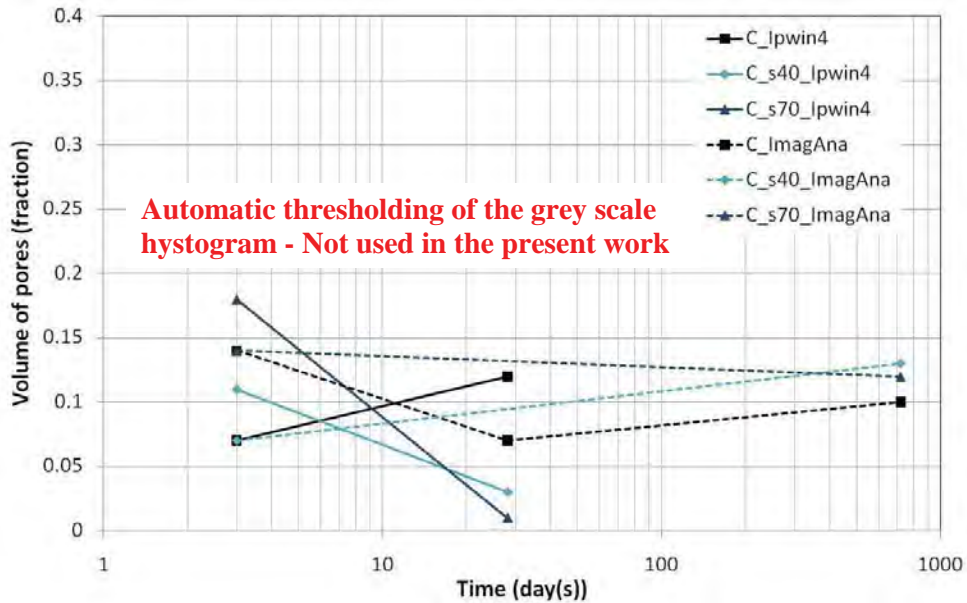

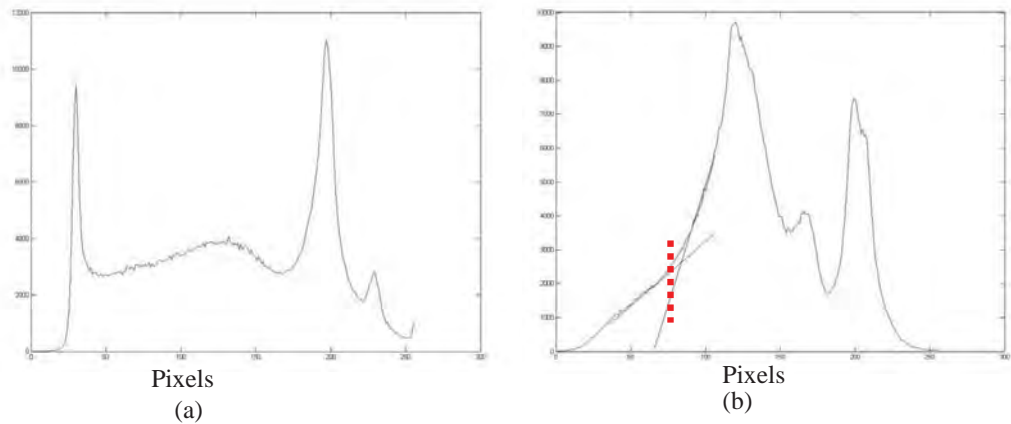Fig. 5.48: Volume of pores (fraction) obtained by automatic "thresholding" of the grey histogram

Fig. 5.49: Grey level histogram for (a) paste with 40% of slag and (b) plain cement pastes cured saturated at 20°C for 3 days
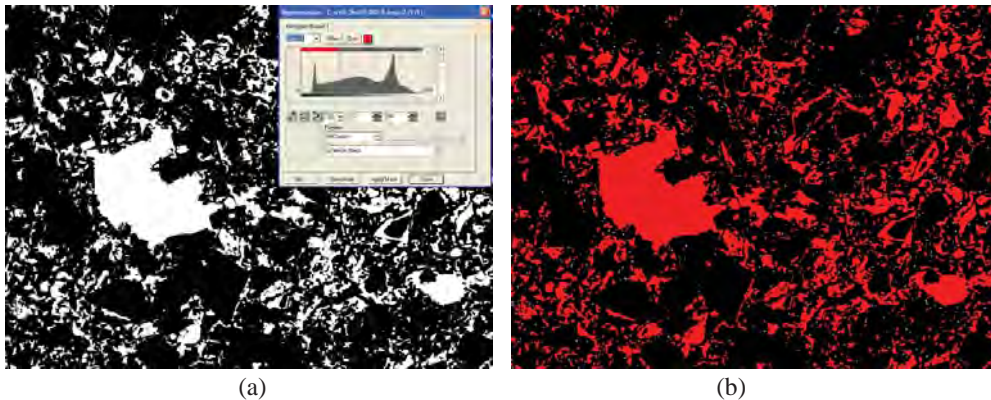
(a)   (b)

Fig. 5.50: Threshold pore size by Ipwin4 for image 13 of paste with 40% of slag cured saturated at 20ºC for 3 days

The pore volume for the pastes obtained by the manual threshold of pores from the grey scale histogram is given in the Table 5.7 and Fig. 5.51(b). The decrease of the volume of pores with time (3 to 720 days) was possible to observe for pastes cured at 20ºC. The impact of SCMs for pastes cured at 720 days could not be observed, however the SEM at magnification of 1000 characterize a limited range of pores. A finer porosity (gel pores) can be found beyond the range measured by SEM at 1000x, for that a higher magnification is necessary (e.g. 2000x). Combining varying magnification a broad range of pores can be analyse and a better overview of the porosity is acquired.

The effect of the moisture and temperature are graphically illustrated in the Fig. 5.51. Higher volume of pores was observed for pastes without and with 40% of slag cured at high temperature or sealed when compared with saturated curing at 20ºC. This fits well with data showed by Haha et at (2009) where plain cement pastes cured at 85ºC showed a larger capillary than pastes cured at 20ºC. The pore structure for hydrated pastes cured at high temperature tends to collapses towards a denser C-S-H and larger pore structure, while paste cured at 20ºC forms a low density CSH gel structure with a wider range of gel pore size (Haha et al., 2009, Jennings, 2007, Zhang, 2007). The coarsening of the pore structure of sealed pastes may be due to the self desiccation where micro-cracks may be observed, see e.g. (Jensen et al., 1999, Vodák et al., 2004). No mayor impact on the porosity was observed for with 70% of slag cured at varying conditions (moisture and temperature) for 720 maturity days, sees Fig. 5.52. This confirm the positive impact of the slag at high temperature indicates a positive impact of high curing temperature on the mechanical properties concrete with high percentage of slag addition. This is in agreement with MIP and LTC data showed in the previously sections (5.1 and 5.2).

The degree of hydration of plain cement pastes was obtained by the sum of hydrated products compared to the overall volume of the paste, see Table 5.7. The data is in agreement with Kocaba (2009), where similar cement pastes were used. For slag pastes, the degree of hydration was not given. The C-S-H formed by slag reaction is lighter (less dense) than the C-S-H formed by cement reaction and it may be computed as an unhydrated products. Further analysis by SEM needs to be undertaken to establish a limit between the unhydrated grains of cement and slag and C-S-H from

slag pastes. Degree of hydration for plain cement paste and 40% of slag were then obtained by NanoCem Project 4 (Kocaba, 2009).

Table 5.7: Volume of pores (fraction) for pastes with and without slag cured saturated or sealed for 20ºC or 55ºC for 3, 28 and 720 maturity days

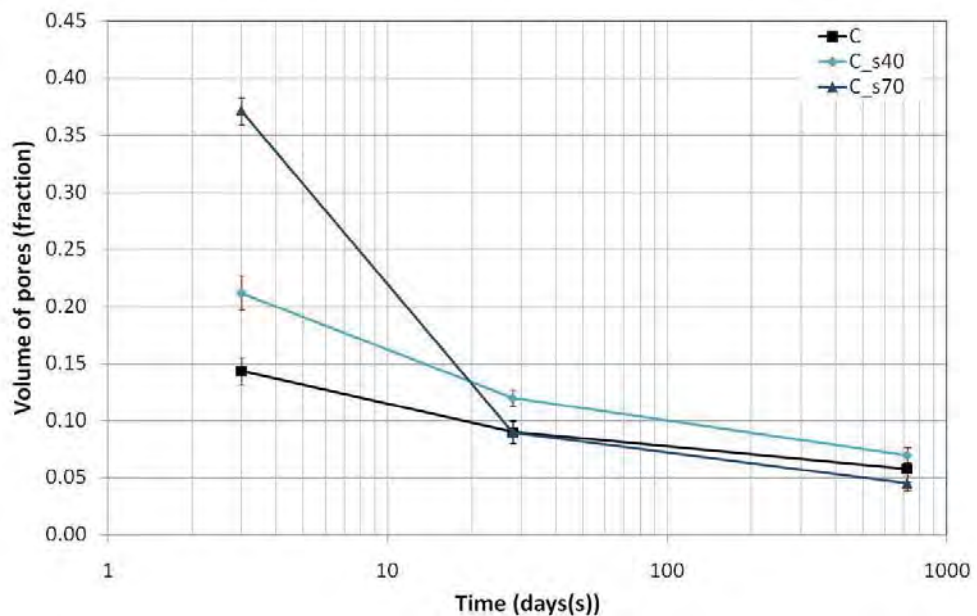| Sample id.	Age	Curing conditions	Volume of pores		Degree of cement hydration		Amount of cracks
	(Maturity days)	(Moist., temp.)	(fraction)	Std. deviation	(fraction)	Std. deviation	
C	3	Sat, 20ºC	0.14	0.02	0.60	0.07	No
	28	Sat, 20ºC	0.09	0.02	0.72	0.09	No
	720	Sat, 20ºC	0.06	0.02	0.84	0.02	Few
	720	Seal, 20ºC	0.08	0.02	0.78	0.07	Few
	720	Sat, 55ºC	0.10	0.01	0.78	0.22	No
	720	Seal, 55ºC	0.09	0.01	0.85	0.06	No
C_s40	3	Sat, 20ºC	0.21	0.03	-	-	No
	28	Sat, 20ºC	0.12	0.01	-	-	No
	720	Sat, 20ºC	0.07	0.01	-	-	Moderate
	720	Seal, 20ºC	0.09	0.01	-	-	Moderate
	720	Sat, 55ºC	0.09	0.02	-	-	Moderate
	720	Seal, 55ºC	0.09	0.02	-	-	Moderate
C_s70	3	Sat, 20ºC	0.37	0.02	-	-	No
	28	Sat, 20ºC	0.09	0.02	-	-	No
	720	Sat, 20ºC	0.05	0.01	-	-	Large
	720	Seal, 20ºC	0.06	0.01	-	-	Large
	720	Sat, 55ºC	0.06	0.01	-	-	Few
	720	Seal, 55ºC	0.06	0.01	-	-	Few

Fig. 5.51: Volume of pores obtained by manually "thresholding" of the grey histogram for pastes cured saturated at 20ºC for 3, 28 and 720 days. Stand. deviation between s given by error bars
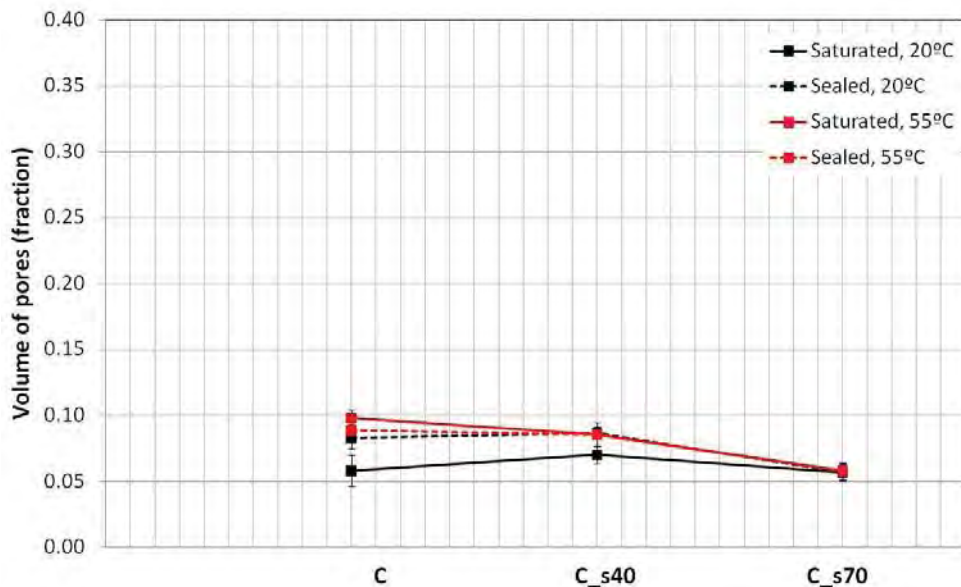

Fig. 5.52: Volume of pores obtained by manually place of the threshold of the grey histogram for pastes cured saturated at 20ºC or 55ºC for 720 maturity days. Stand. deviation between 50 images is given by error bars

SEM showed to be suitable for characterizing of the pore structure of hydration cementitious materials; at the magnification of 1000 the test provides information on the total volume of pores in the range between about 0.1 and 30 µm. The time-consuming and lack of appropriated equipment makes the sample preparation a challenge. The sample preparation is essential to obtain reliable images at SEM. Also the time needed to acquire the images (about 100 at 1000 magnification) cannot be underestimated. Moreover, parameters applied for image acquisition (e.g. working distance, accelerating voltage, probe size) have an effect on the quality of the image. The adjustment of the brightness and contrast of the images is also important to obtain a realistic grey level histogram where the phases are not lost or summarize. It is important to point out that the gray scale histogram from the images has to be carefully "thresholding" otherwise the volume of pores can be dramatically under or overestimated. It is recommended the use of other magnifications to cover a larger range of pores of cement based materials. For instances, the use of 2000 magnification to analyzed gel pores but more images (approx. 4000) are necessary to have an realistic porosity data. Due to time restraints further work using SEM was not overtaken.

5.4 Water sorption method

Water sorption method allows the assessment of the volume of pores and pore size distribution of the pastes based on measurements of sample weight at selected relative humidity (RH). The pore size and volume of pores were calculated for each studied RH, according to the section 3.4 and Appendix XIII. In order to allow a direct comparison, the water contents are expressed in percentage per unit of dried mass using oven at 105ºC. The volume of pores were calculated using the bulk density of MIP, the use of dried bulk density is suggested by Baroghel- Borny (2007a, , 2007b). Graphics of volume of pore versus pore size for pastes with and without slag are given in the Appendix XXI. The overview of the experimental plan for water sorption is given in the Table 4.2.

First, possible errors introduced by the sample preparation or analysis were discussed here:
- Impact of the relative humidity on the pastes (5.4.1)
- Sample size (powder and slice) (5.4.2)
- Possible carbonation of the pastes in powder(5.4.3)

Then, the impact of SCMs and different moisture and temperature conditions on the pore structure of the selected pastes were analysed by water sorption. Sorption isotherms were used to determine the total volume of pores and pore size distribution for selected cement pastes. Also graphics with weight change versus time are given. According to Olson and Jennings (2001) a monolayer of water is formed in about 11%RH and multi-layers from 11% to 50%RH. According to Powers and Brownyard (1947) adsorption in multilayer, without capillary condensation occurs in the pore network for RH between 30 and 40%. At approx. 50% RH water starts to condensate in the pores (Olson and Jennings, 2001). Thus the pore size was calculated for RH higher than 50%.

For the determination of the gel pores content, the RH of 33% was chosen, this value is between the 11% and 59% and it should maximize the amount of water that could be adsorbed by the C-S-H and avoid any value of condensation. And total pore volume was calculated using the ranges of RH from 0 to 97%. Sorption isotherms were divided in 3 ranges of relative humidities, see Table 5.8.

Table 5.8: Ranges of relative humidities, pore size, nomenclature and pore volume used for water sorption measurements.

RH (%)	Pore size (diameter);			Nomenclature of pores	Ranges of pore volume
	Kelvin Pore size (diameter)	t-layer	Total diameter		
<33%	<0.002 µm (not taken to account)	0.0004	0.003 µm	Gel pores	0 to 33%RH
33% to 59% RH	0.002 <d< 0.004 µm	0.0005	0.003<d<0.005	Gel pores and small- medium capillary	33 to 59%RH
59% to 97%RH	0.004 µm <d<0.075 µm	0.001	0.005<d<0.077	Large capillary	59 to 97%RH

5.4.1   Impact of the relative humidity on the pastes

Prolonged exposure of the samples at high relative humidity (e.g. 92% and 97%) may result in additional hydration of the cement pastes. In order to illustrate that, graphics of weight change versus time were plotted for plain cement pastes with and without slag and fly ash cured sealed at 55ºC for 6.5 days (28 maturity days), stored in evacuated desiccators at 11, 92 and 97% RH for 3 months (approx.), see Fig. 5.53.
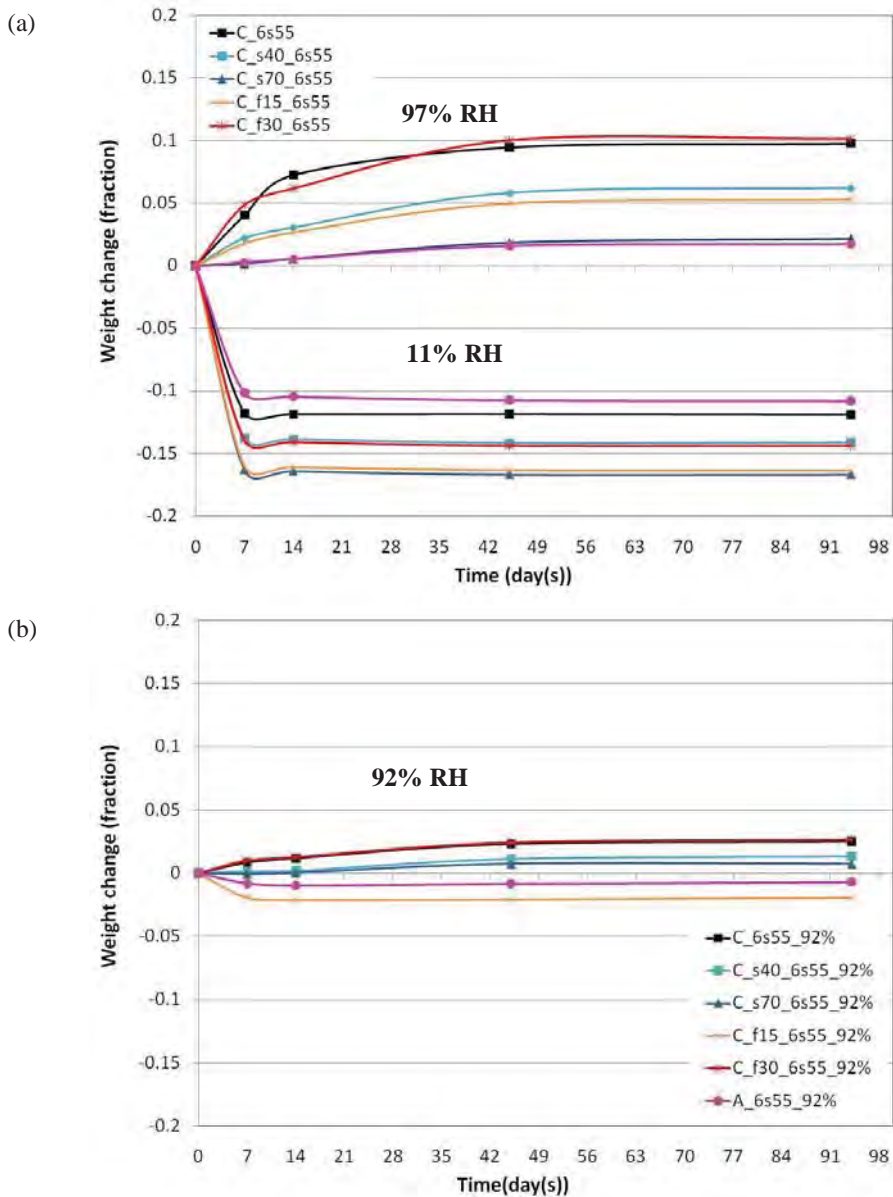
(a)

(b)

Fig. 5.53: Weigh change (fraction) versus time (day(s)) for samples with and without slag and
fly ash cured sealed at 55ºC for 6.45 days expose to (a) 11 and 97% RH and (b) 92% RH

For the pastes exposed at low relative humidity (11%) a weight lost was observed and the
equilibrium was reached after be stored for 3 months in desiccators. The hydration of the sample is
stopped when expose to a low RH (e.g. 11%) (Powers, 1960) (Fig. 5.53(a)).

A continuous weight gain was observed for samples exposed to salt solution at high relative humidity (e.g. 92 and 97%RH), it may be due to prolonged hydration of the pastes (Baroghel-Bouny, 2007a, Carlier et al., 2009, Roper, 1966) (Fig. 5.53). The weight change varies according with the type of the material and relative humidity, see Fig. 5.52. Also the expose time, as the pastes were gaining weight with time. Cement paste with high substitution of slag and fly ash showed a higher weight change at 97%RH.

Consistent with the hypothesis of continuous hydration, an increased amount of non evaporable water for pastes exposed to 97%RH was also found, and it was not observed at 11%RH (Table 5.9). It indicated a possible prolonged hydration of the samples. Jensen et al. (1999) reported also adsorption of water in cement pastes expose at a high RH. Powers studies suggested that hydration of cement pastes continues at 90% RH (Powers, 1960). However, Baroguel-Bouny (2007a) assumed that cement hydrated pastes cured for long periods (over 6 months) and subsequently exposed to high relative humidity do not rehydrate. This was not observed in the present studies, where a prolonged hydration was observed even for pastes with and without slag cured saturated at 20ºC for 720 days. Those were exposed for approx. 7 months in total. After two months of exposure at 92 and 97%RH was observed a progressively weight gain, see Fig.5.54.

Table 5.9: Non evaporable for cement pastes with and without slag cured sealed at 55ºC for 6.45 days (28 maturity days) expose and exposed at 11% and 97%RH for 3 months.

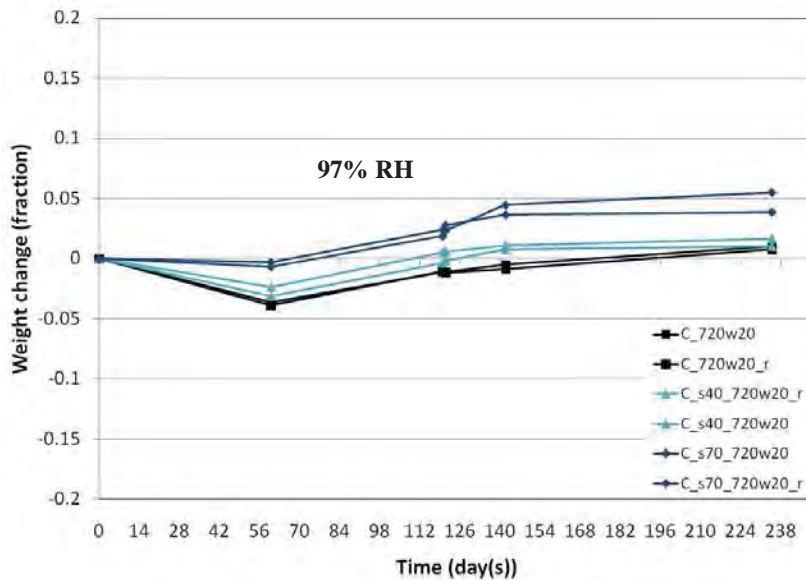| Sample id.	Non evaporable water (W_n) ($g/g_{105ºC}$)		
	About 70% RH (measured using oven at 1000ºC)	After expose to salt solution for 3 months (measured using thermogravimetric analyses)	
		11% RH	97% RH
C	0.13	0.14	0.16
C_s40	0.14	0.14	0.17
C_s70	0.14	0.14	0.18

Fig. 5.54: Weigh change (fraction) versus time (day(s)) for pastes with and without slag cured saturated at 20ºC for 720 days expose to 92% RH after approx. 7 months

From the above observations, it is possible to conclude that the pastes exposed to high RH were not in equilibrium. This may overestimate the total pore volume measured by water sorption and should be taken account in the interpretation of the data. To limit the amount of the prolonged hydration it is suggested to use old samples (over 3 months) and observe the development of the weight change over time.

According to the literature (Diamond, 1999, Jensen et al., 1999, Persson and Fagerlund, 2002), a changed microstructure may also be observed for cementitious pastes exposed at different RH. Jensen et al. (1999) studies suggest that C_3A can hydrate at lower humidity (75%RH) rather than C_3S and C_2S, see Fig. 5.55. The hydration of C_3A at low RH may form different cement products (e.g. C_3AH_6 (hydrogarnet)). Moreover, self desiccation may be found for cement pastes expose to low RH (<75%) and it may disturb the pore structure of the pastes (Diamond, 1999, Jensen et al., 1999, Persson and Fagerlund, 2002). To conclude this section it possible to say that self desiccation at low RH, prolonged hydration at high RH may affect porosity data from water sorption.

	Time (days)	Exposure RH (%)						
		23	43	66	75	85	95	98
C$_3$S	1	0	0	0	0	0	0	0
	3	0	0	0	0	0	0	0
	7	0	0	0	0	0	0	1
	14	0	0	1	0	0	1	12
	30	0	0	1	1	1	4	29*
	90	0	0	2	1	2	33*	36
	365	0	1	3	1	4	72	67
C$_2$S	1	0	0	0	0	0	0	0
	3	0	0	0	0	0	−0	0
	7	0	−2	1	0	0	0	0
	14	0	0	0	0	0	0	1
	30	0	0	1	0	2	1	5
	90	0	0	1	0	0	1	15
	365	0	1	1	1	1	16	49
C$_3$A	1	0	0	0	0	2	6	8
	3	0	0	0	0	6	18	23*
	7	0	0	0	1	16	30*	36
	14	0	0	0	6	26	35	40
	30	0	0	1	18	28*	37	44
	90	0	0	3	24	33	41	48
	365	0	0	8	28*	45	52	61

*Studied by SEM.

Fig. 5.55: Degree of hydration of C$_3$S,C$_2$S and C$_3$A after expose to varying relative humidity (Jensen et al., 1999)

5.4.2 Impact of sample size

To show the impact of sample size on the data of water sorption, plain cement pastes in two sizes were used: powder (150 to 250 µm) and slice (30x22Ø mm) cured saturated at 55ºC for 28 maturity The weight change at 92% RH and sorption isotherms are possible to be observed in the Figs. 5.56 and 5.57.

Weight change at 92%RH for cement pastes in powder and slice is illustrated in the Fig. 5.58. Larger weight change was found for pastes in powder. Apparently, after two months expose at high relative humidity it is possible to notice a weight gain, this is more clear for samples in powder (Fig. 5.56).

The cement pastes in powder showed a larger amount of water desorbed (0 to 86%RH) and adsorbed (92 to 97%RH) than for cement pastes in slices, see Fig.5.57. This may indicate that the creation of new surfaces due to the crush of the sample in powder (higher specific surface area) leads to a higher sorption of water. According to Baroguel-Bouny (1994), crushing may expose anhydrated cement grains, and at a high RH a possible hydration of these grains may occur. Studies (Bakhshi and Mobasher, 2011) with cement pastes in powder and slices also have showed an increased in the cumulative moisture loss for samples with high specific surface area. In addition, carbonation may take place when crushing the sample or expose to oven for drying leading to a

higher porosity of the pastes. Moreover, loss of some of the samples in powder may happen when the samples are evacuated within the desiccators or due the drying at oven 105ºC

Investigations by meaning of water sorption (Hansen, 1963, Olson and Jennings, 2001, Baroghel-Bouny, 1994) suggested the use of samples in powder for testing cement pastes by water sorption. Also the time of testing to reach the weight equilibrium is minimized by the crushing of samples. Bakhshi and Mobasher (2011) suggested that the degree of evaporation is lower for larger samples and the equilibrium may not be obtained. For further tests here presented samples in powder (150 to 250 μm) were used. A glove cabin with high relative humidity (about 92%) was used during the crushing of the sample to limit the amount of evaporation of water and carbonation (see Appendix XIII).
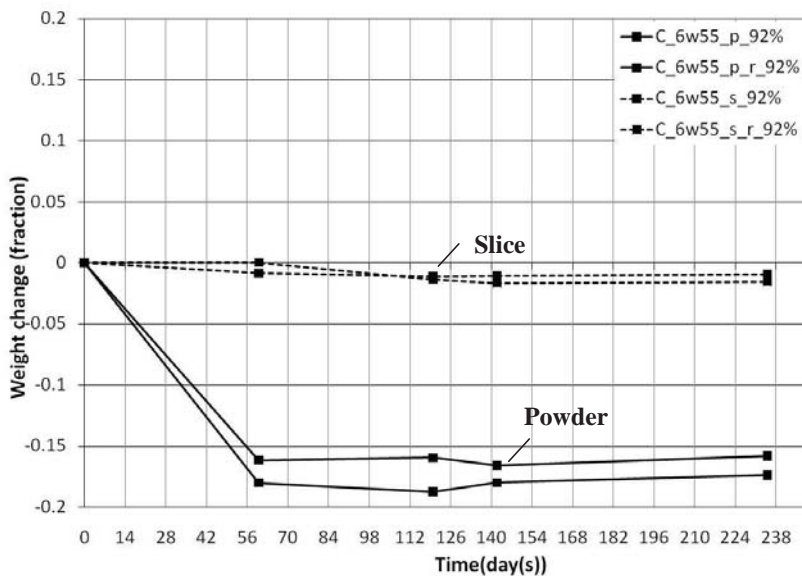
Fig. 5.56: : Weigh change (fraction) versus time (day(s)) for samples with and without slag and fly ash cured sealed at 55ºC for 6.45 days expose to 92% RH
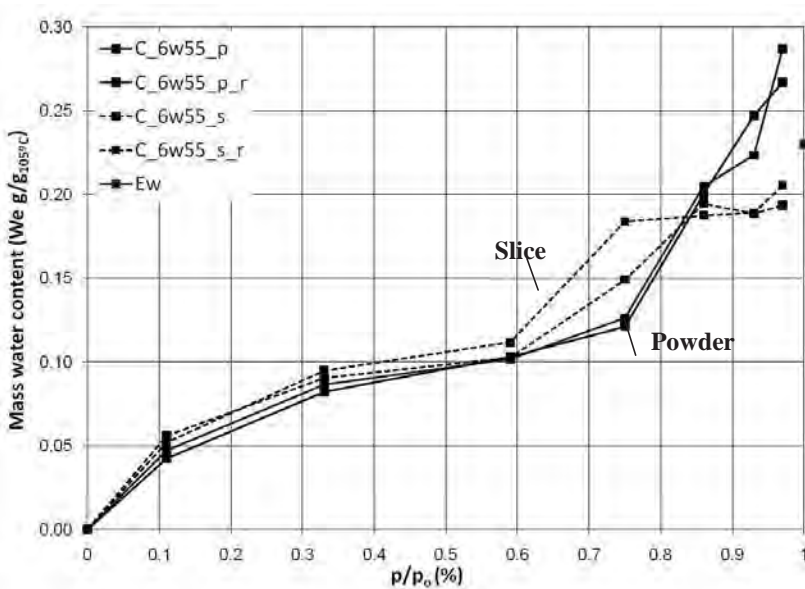
Fig. 5.57: Mass water content (gH_2O/g$_{105°C}$) versus relative humidity (%) for plain cement pastes in powder (full line) and slices (broken line) cured saturated at 55°C for 28 maturity days

5.4.3   Possible carbonation of the sample in powder

Cement pastes for water sorption were crushed in powder inside a glove cabin at high relative humidity (about 92%RH) to limit the amount of carbonation. However, the samples were kept a long time (between 4 to 17 months) in desiccators to reach the required RH. Furthermore, they were dried using oven at 105°C (dried as state) after the test and the drying process may also contributes for the carbonation of the cement pastes, see e.g. (Thomas et al., 1996, Van Gerven et al., 2007).To illustrate a possible carbonation of the samples exposed to 11% and 97%RH, thermal analysis was carried out after the water sorption test (and drying at 105°C) for pastes with and without slag cured saturated for 28 maturity days see Fig. 5.58.

A possible conclusion to be draw from the Fig. 5.58 is that some carbonation takes place in the samples. The weight loss in the range from 600 to 780°C is about 2% for samples expose to 11% and 97% and it may be due to carbonation of the samples. For a better evaluation of the carbonation, a test of a non exposed sample (non carbonated) would be necessary for the data comparison, moreover additional methods may be used; for instances measurement of the pore solution PH, X-ray diffraction).
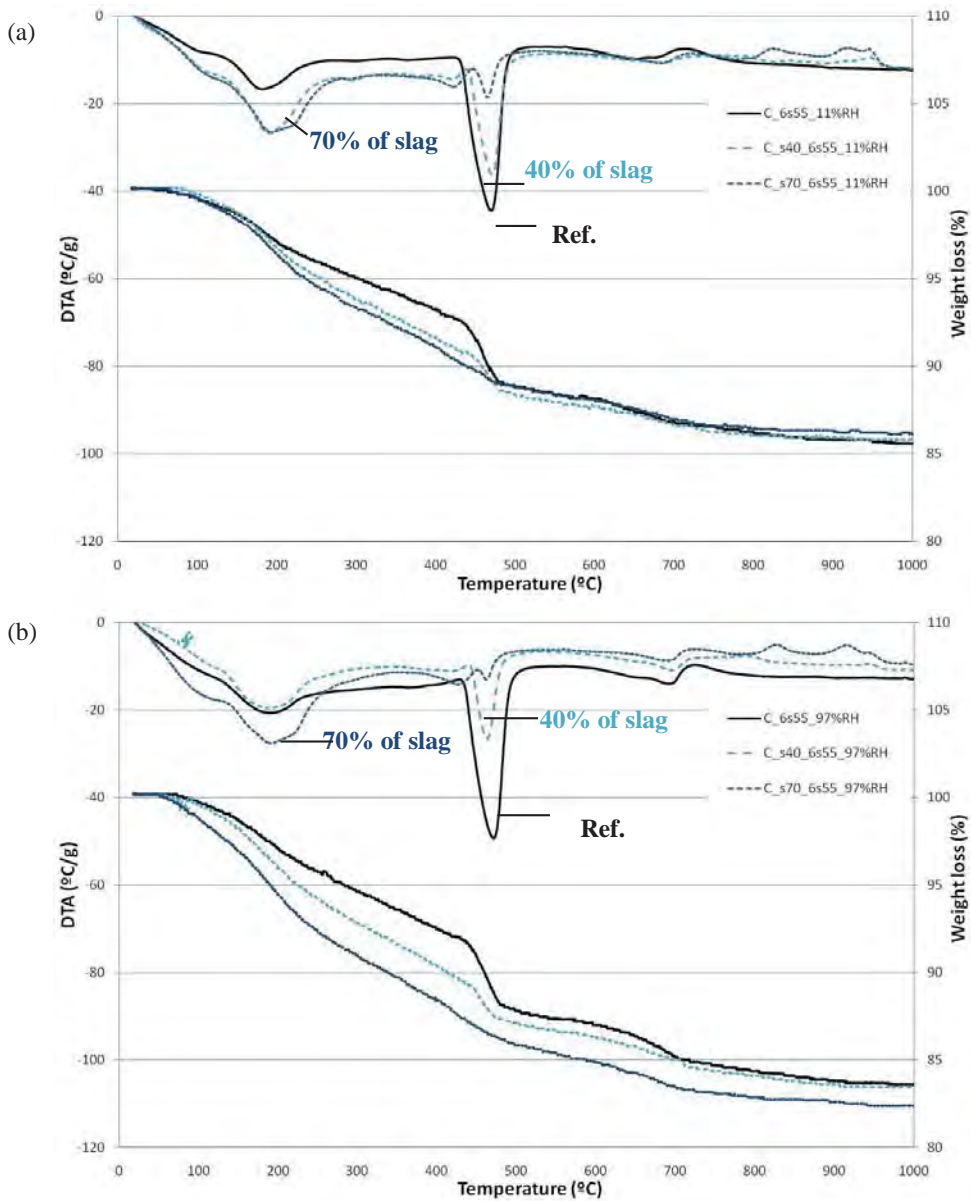
Fig. 5.58: DTA versus temperature for pastes with and without slag cured sealed at 55ºC for 6.5 days (28 maturity days) expose at (a)11%RH and (b)97%RH

5.4.4   Impact of SCMs and curing conditions on the porosity by water sorption

The impact of slag on the pore structure is illustrated by sorption isotherms for pastes with and without slag cured saturated at 20ºC for 28, 90 and 720 days, see Fig. 5.59. The pastes cured for 28 days were expose for approx. 7 months (31/03/2008 to 20/10/2008), 90 days were expose for about 17 months (19/11/2008 to 16/04/2010) and 720 days were expose for approx. 7 months (18/06/2010 to 10/02/2011) at varying RH. At high relative humidity (92% and 97% RH) adsorption of water was observed for most of the pastes by the progressively weight gain. Adsorption is represented in the graphics of mass water content versus RH (p/p_0) by red arrows. Evaporable water measured by oven at 105ºC for samples at 50x15Ø mm (LTC size) is represented in the graphics by square (□) for plain cement pastes; quadrilateral (◊) for pastes with 40% of slag addition and triangle (Δ) for pastes with 70% of slag addition. In general, lower values of mass of water content were found for evaporable water, when compared with 97%RH. For the discussion of this method, few data of cementitious materials tested by water sorption were found in the literature.

*Less than 33% RH (pores smaller than 0.003 μm in diameter- gel pores)*
An increase of water desorbed in the range from 0 to 33%RH with curing time (28 to 720 days) for cement pastes with and without slag is shown in the Fig. 5.59. This indicates the increase of the hydrated products with time. The amount of water desorbed in this range is part of the water adsorbed on the surface of the C-S.H gel. According to Olson and Jennings (2001), water monolayer is formed between 0 and 11%RH and multi-layers may be seen from 11 to 50% RH. Belie et al. (2010) also showed an increased amount of pores in this range for cement pastes with 50% of slag and fly ash addition cured saturated for 18 months when compared with 4 months.

33% to 59% RH (pores between 0.003 and 0.005 μm in diameter- gel pores and small medium capillaries)
This range represents the water adsorbed in the surface; moreover part of the capillary condensations in larger pores starts to take place in this area. A linear behavior is observed for pastes cured for 28 and 90 days. According to Baroguel- Borny (2007a) it can be the deduced that this is the range where the water amount adsorbed is proportional to the C–S–H amount. Fig. 5.58 shows a larger amount of water desorbed by the pastes with slag in this range. This is also in agreement with the LTC results, see Section 5.1. Gel pores of C-S-H; they also indicated an increase of the amount of hydrated products

More than 59% (pores larger than 0.005 μm – medium and large capillary pores)
Larger volume of water desorption (0 to 86%RH) adsorption (92 to 97%RH) was found for cement pastes with slag when compared with plain cement pastes, except for 28 days (Fig. 5.59). For pastes cured from 28 to 720 days was not possible to observe a reduction of the volume of pores. It may be due to the adsorption of water of the samples exposed to relativity humidity above 86% where a continuous hydration was observed. This is also outlined in the literature (Baroghel-Bouny, 2007a).
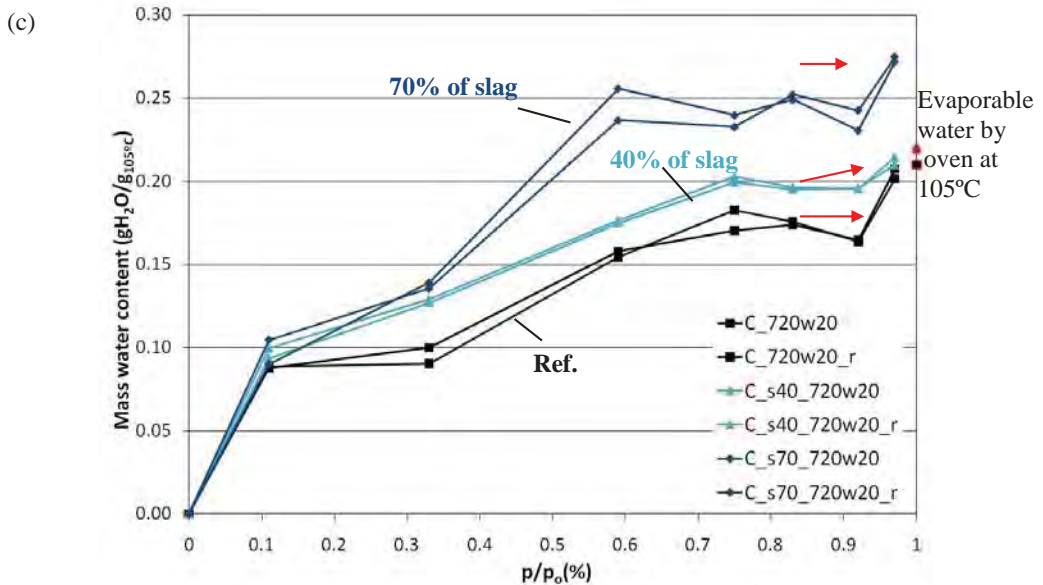
(a)

(b)

(c)
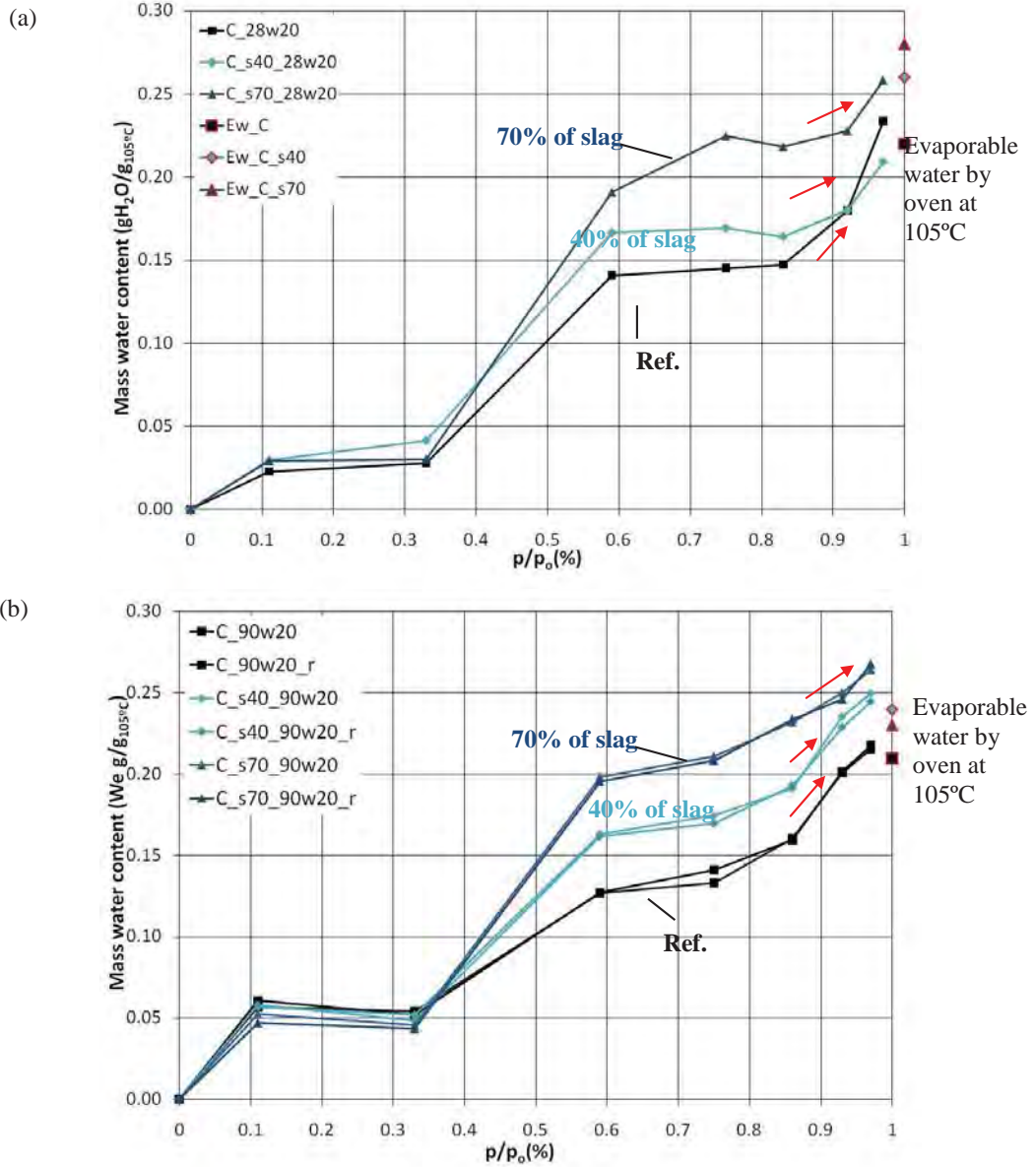
Fig. 5.59: Mass of water content ($gH_2O/g_{105°C}$) versus relative humidity (%) for pastes with and without slag cured saturated at 20ºC for (a) 28, (b) 90 and (c) 720 days. Red arrows indicate adsorption of water

In the Table 5.10, it is possible to observe the amount of mass of water content and volume of pores for the range of 0 to 33% of RH and the range of 0 to 97%RH (total) for pastes cured saturated at 20ºC for 28, 90 and 720 days. The total volume of pores was calculated using the bulk density found for MIP (see Appendix XII) and illustrated in the Fig. 5.62.

Table 5.10: Mass of water content and total mass of water content; and volume of pores at different RH ranges (0 to 33%RH and 0 to 97%RH) for pastes with and without slag cured saturated at 20ºC for 28, 90 and 720 days

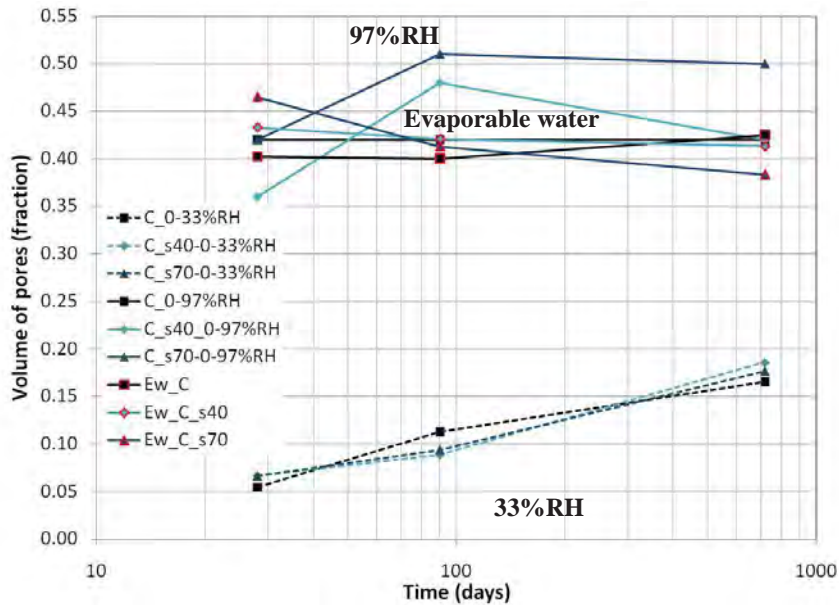| Sample id.	Age (days)	Mass water content from 0 to 33%RH ($gH_2O/g_{105°C}$)	Mass water content from 0 to 97%RH ($gH_2O/g_{105°C}$)	Volume of pores from 0 to 33%RH (fraction)	Volume of pores from 0 to 97%RH (fraction)	Evaporable water (fraction)
C	28	0.03	0.24	0.05	0.42	0.22
C	90	0.06	0.22	0.12	0.42	0.21
C	720	0.16	0.21	0.32	0.42	0.21
C_s40	28	0.04	0.21	0.07	0.36	0.26
C_s40	90	0.05	0.25	0.09	0.47	0.24
C_s40	720	0.18	0.23	0.33	0.43	0.22
C_s70	28	0.04	0.26	0.07	0.42	0.28
C_s70	90	0.05	0.27	0.09	0.51	0.22
C_s70	720	0.13	0.27	0.46	0.50	0.22

Fig. 5.60: Pores in the range of 0-97% and 0-33% for pastes with and without slag cured saturated
at 20ºC for 28, 90 and 720 days

Comparable data of volume of pores was found for plain cement pastes cured at 28, 90 and 720 days. For slag pastes an increased of volume of pores was observed, see Table 5.10 and Fig. 5.60. For pastes with 40% of slag an increase at 90 days and decrease at 720 days of volume of pores was found. It may be due to the long period of expose for pastes cured saturated for 90 days. The increase of the C-S-H products from the slag reaction may induce to an increase of gel pores for slag pastes, as observed in the Fig. 5.60.

The impact of SCMs on the pore structure of the pastes cured sealed at 20ºC for 28 days is also illustrated by sorption isotherms, see Fig. 5.61.
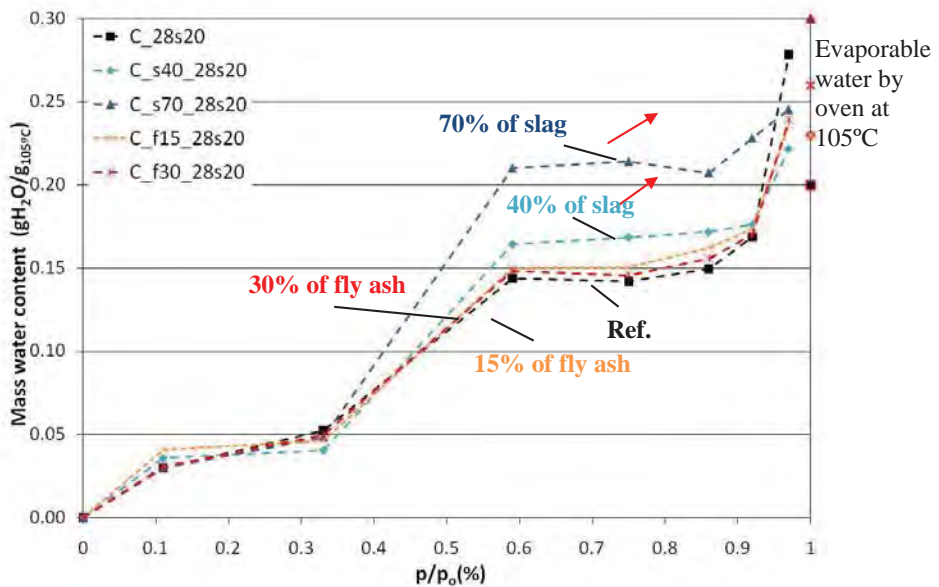
Fig. 5.61: Mass of water content ($g/g_{105°C}$) versus relative humidity(%) for pastes with and without slag and fly ash cured sealed at 20ºC for 28 days

Slag pastes showed larger desorption of water at the range of 59 to 86%RH than pastes with and without fly ash. Moreover, the curves shows a large increase of the mass of water content for plain cement pastes from 92 and 97%RH see Fig. 5.61. As mentioned previously, a re-hydration for the pastes expose at high relative was observed and the equilibrium in weight was not reached.

5.4.5   Impact of curing conditions on the porosity by water sorption

The impact of temperature was also determined by water sorption isotherms for pastes with and without slag and fly ash cured sealed at 20ºC or 55ºC for 28 maturity days, see Fig. 5.62. The amount of mass of water content and volume for pastes cured sealed at 20 or 55ºC for 28 maturity days is given in the Table 5.11. The correlation between volume of pores by water sorption and evaporable water (oven at 105ºC) and type of materials is given in the Fig. 5.63.

Fig. 5.62 show a reduction of the pores in the range of 0.003 to 0.005 µm (33 to 55% RH) for all the pastes cured at high temperature. In general, higher total of water content at 97%RH was observed for cement paste with and without slag cured at 55ºC, when compared with 20ºC. Comparable values of evaporable water were found for pastes cured at 20 and 55ºC. The values of evaporable water were lower than values obtained by water sorption at 97%RH.
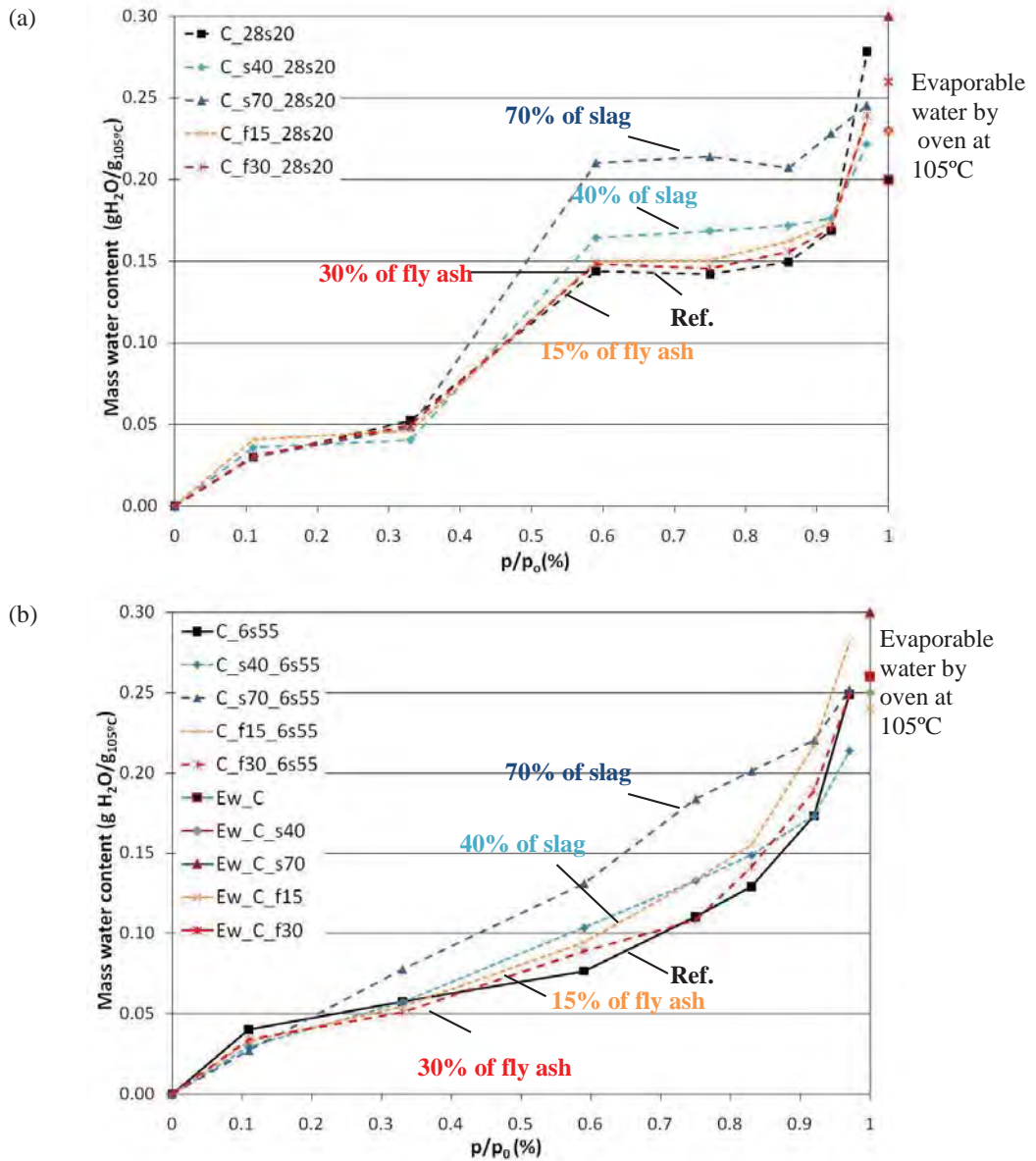
Fig. 5.62: Mass of water content ($gH_2O/g_{105°C}$) versus relative humidity (%) for pastes with and without slag cured sealed at (a) 20°C or (b) 55°C for 28 maturity days

Table 5.11: Mass of water content; volume of pores at varying ranges of RH for pastes with and without slag cured sealed at 20 or 55°C for 28 maturity days.

Sample id.	Curing temperature (°C)	Mass water content from 0 to 33%RH (gH$_2$O/g$_{105°C}$)	Mass water content from 0 to 97%RH (gH$_2$O/g$_{105°C}$)	Bulk density (g/cm³)	Volume of pores from 0 to 33% of RH (fraction)*	Volume of pores from 0 to 97% of RH(fraction)*
C	20	0.05	0.28	1.82	0.09	0.51
C_s40	20	0.04	0.22	1.69	0.07	0.37
C_s70	20	0.05	0.24	1.66	0.08	0.40
C_f15	20	0.05	0.24	1.68	0.08	0.40
C_f30	20	0.05	0.24	1.6	0.08	0.38
C	55	0.06	0.25	1.84	0.11	0.46
C_s40	55	0.06	0.22	1.76	0.11	0.39
C_s70	55	0.08	0.25	1.78	0.14	0.44
C_f15	55	0.05	0.29	1.64	0.08	0.48
C_f30	55	0.05	0.25	1.77	0.09	0.45

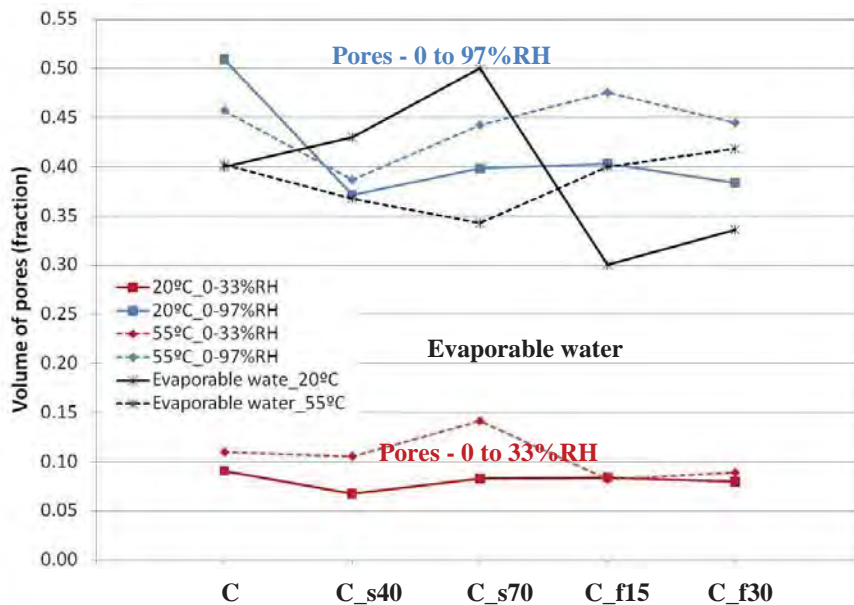*Mass of water content multiplied by the bulk density (found by MIP)

Fig. 5.63: Volume of pores in the range of 0 -97%RH (blue line) for pastes with and without SCMs cured saturated at 20°C or 55°C (broken line) for 28 maturity days; Volume of pores in the range of 0 -33%RH (red line); Evaporable water measured by oven at 105°C (black line)

The impact of moisture conditions was observed by the sorption isotherms for pastes with and without slag cured sealed and saturated for 20ºC (Fig. 5.64). This is possible to observe that the impact of moisture is not so clear for paste cured for 28 days. This was also observed for MIP studies with sealed or saturated pastes, see Section 5.2. For slag pastes a larger amount of water content was found in the range of from 11% to 59% RH for pastes cured under sealed conditions.
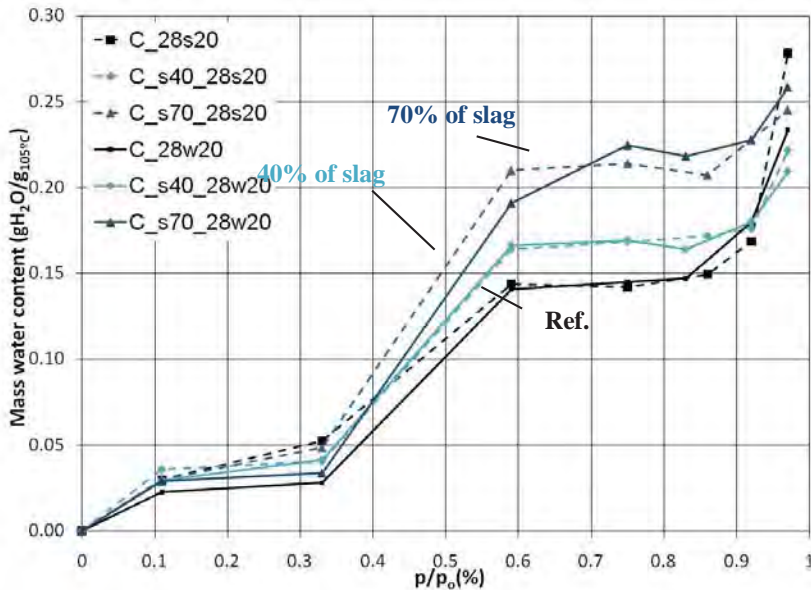

Fig. 5.64: Mass of water content ($gH_2O/g_{105ºC}$) versus relative humidity (%) for pastes with and without slag cured saturated (full line) or sealed (broken line) at 20ºC for 28 days

Table 5.12: Mass of water content; volume of pores at varying ranges of RH for pastes with and without slag cured saturated or sealed at 20ºC for 28 days.

Sample id.	Moisture	Mass water content) - 0 to 33%RH ($g_{H2O}/g_{105ºC}$)	Total mass water content - 0 to 97%RH ($g_{H2O}/g_{105ºC}$)	Bulk density (g/cm^3)	Volume of pores - 0 to 33% RH (fraction)*	Volume of pores - 0 to 97% RH (fraction)*
C	Saturated	0.03	0.24	1.82	0.05	0.44
C_40	Saturated	0.04	0.22	1.69	0.07	0.37
C_70	Saturated	0.04	0.26	1.66	0.07	0.43
C	Sealed	0.05	0.28	1.81	0.09	0.51
C_40	Sealed	0.04	0.23	1.69	0.07	0.39
C_70	Sealed	0.05	0.25	1.66	0.08	0.42

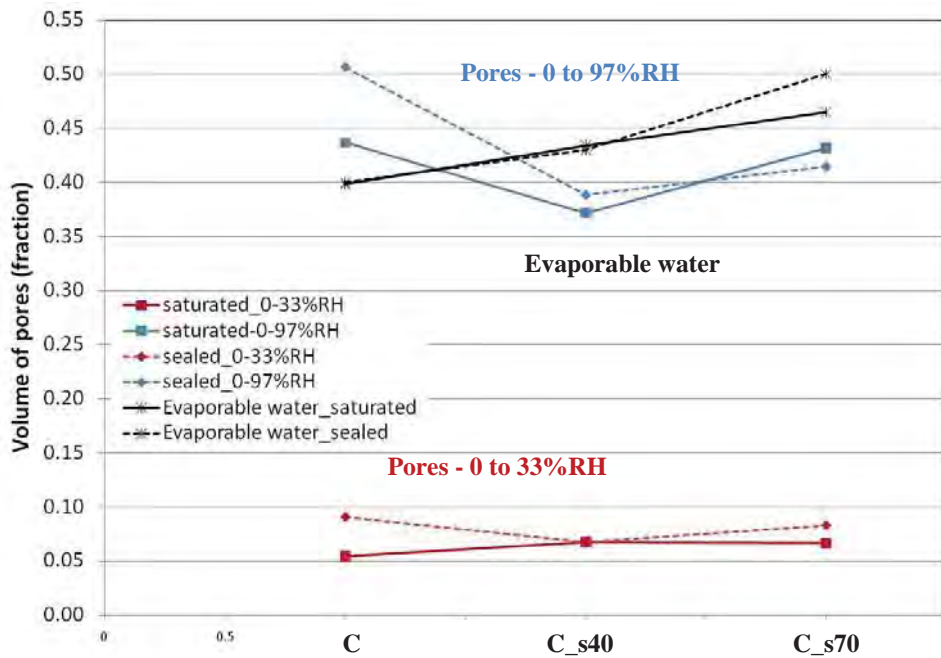*Mass of water content multiplied by the bulk density (found by MIP)

Fig. 5.65: Volume of pores in the range of 0 -97%RH (blue line)for pastes with and without slag cured saturated or sealed (broken line) at 20ºC for 28 days; Volume of pores in the range of 0 - 33%RH (red line); Evaporable water measured by oven at 105ºC (black line)

Information on the water state related to the pore structure may be extracted from isotherms curves of water sorption. As observed, experimental errors (e.g. carbonation, weight loss, temperature) may mislead the data acquired by the sorption isotherms. Matured samples should be tested to limit the continuous hydration of the pastes at high relative humidity. The sample preparation and test procedure are carried out by varying steps: e.g. cut or crushing the samples, weighing of the glasses and samples, place the samples in desiccators, evacuate the desiccators, place desiccators in the water bath. These steps make the method extensive. Long time is also required for acquiring data: monthly measurements during almost a year.

For sample preparation it is suggested the use of samples in slices to avoid possible carbonation, loss of material and continuous hydration of the cement pastes. Loss of the material may also occur during the weight measurements and evacuation of the desiccators. Sample weight should be carefully obtained and recorded, special attention may be given for the proper evacuation and sealing of the desiccators with salt solutions, see more detail in the procedure given in the Appendix XIII. Temperature and RH should be controlled during the entire period of testing, e.g. changes in the bath temperature may affect the equilibrium of RH inside the desiccators.

It is valuable to consider another method for sorption in hydrated cementitious e.g. dynamic sorption where fast data may be obtained.

5.5 **1H NMR relaxation**

NMR relaxation was carried out to observe the state of water in plain cement pastes. The use of the method was part of the project plan however difficulties to have a reliable data and interpretation of the results were experience during the two visits in the University of Surrey. Further details and data for NMR relaxation were carefully given in the MC-RTN Project 4 (Valori, 2009). Overview of the plan for NMR relaxation test is given in the Table 4.2. The parameters used for the test in given in the Appendix XVI.

The Figs. 5.66 and 5.67 shown $T_2(ms) \times T_2(ms)$ relaxation time for cement pastes "A" (white cement) and "C"(grey cement) saturated at 20^oC for 1 and 3 days.
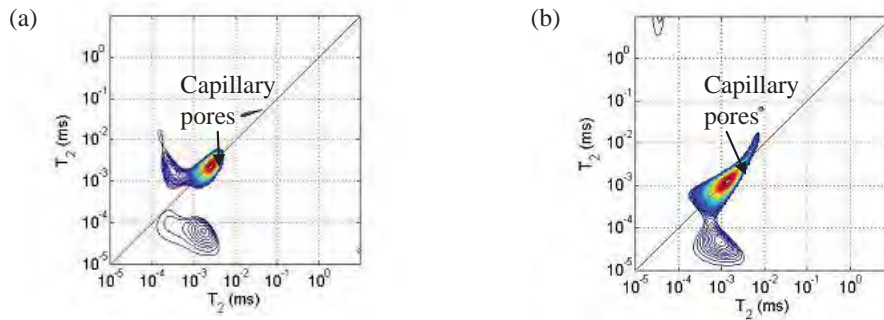
(a)   (b)

Fig. 5.66: $T_2(ms) \times T_2(ms)$ relaxation time for cement paste "A", cured saturated at 20^oC for (a)1 day and (b) 3 days, storage time of 3000 ms

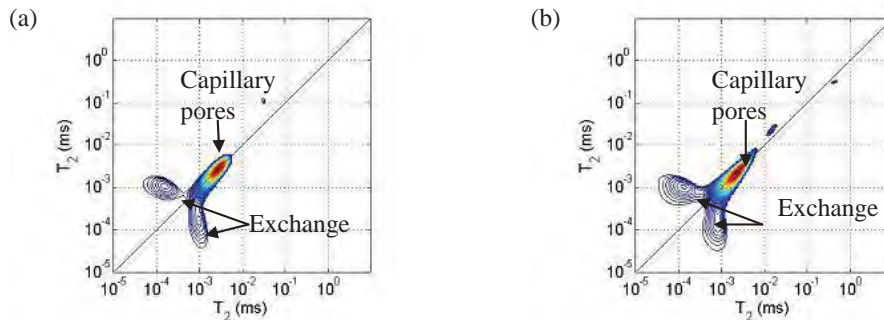(a)   (b)

Fig. 5.67: $T_2(ms) \times T_2(ms)$ relaxation time for cement paste "C", cured saturated at 20^oC for (a)1 day and (b) 3 days, storage time of 3000ms

For cement paste "A" cured saturated for 1 and 3 days, the curves for gel pores and connectivity were not noticed in the results (MacDonald 2006). However for plain cement paste "C" cured saturated for 1 and 3 days two symmetrical (approx.) curves indicated the connectivity of the pores, see Fig. 5.67. The results showed that NMR relaxation may be applied for the water studies in grey cement (cement "C") even though its iron content is higher than the iron content of white cement (cement "A"). The paramagnetic contents may disturb the magnetic field from the NMR (McDonald et al., 2006, McDonald et al., 2005).

The state of water within the pores for plain grey cement paste cured saturated at 55°C for 6.5 days (28 days of maturity) is shown in the Fig. 5.68.The signal obtained from the sample was not suitable (trembled peak) to get information on the water state, as showed in the Fig.5.68(a). It may be due the water be consumed by the hydration products for pastes cured for 28 maturity days.
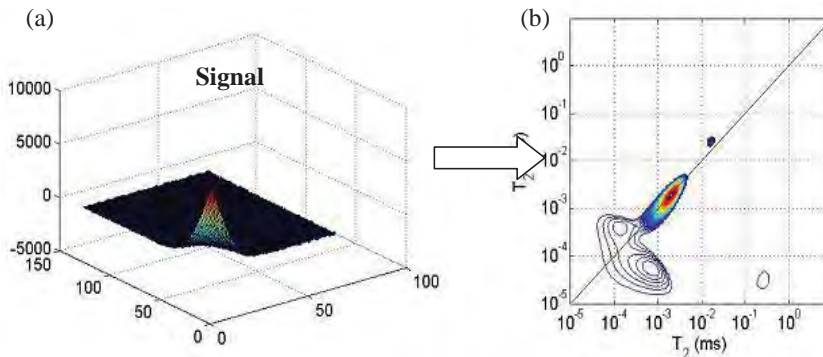

Fig. 5.68: T_2(ms)xT_2(ms) relaxation time for cement C, cured saturated at 55°C for 6.5 days (28 maturity days), storage time of 3000ms

Further information of the accuracy and calibration of the test and pore size range measured is given in the MC Project 4 "*Characterization of cementitious materials by ^1H NMR*"(Valori, 2009).An extended series of papers have also explored the water state in cementitious hydrated materials by NMR relaxation (McDonald et al., 2006, McDonald et al., 2005, McDonald et al., 2010).

5.6 Autogenous deformation

The aim of autogenous deformation measurements was to observe the deformation of the pastes cured sealed with and without slag. It may also explain the cracking of the pastes cured for 720 days found by SEM (see section 5.3).

Autogenous deformation is given by deformation versus time graphics for cement pastes with and without slag cured sealed (without bleeding water) at 20ºC, see Fig. 5.69. The bleed water was removed from the moulds with a siring, see section 4.6. However different amount of water were removed, this may explain the difference trend of the curves for similar samples. The method is standardized by ASTM C-1698 (2009). The standard suggests the time zero as the time after setting of the paste. The test was carried out for 4320 hours (approx.6 months). The time zero of the test was chosen to be 24 hours after casting of the samples.
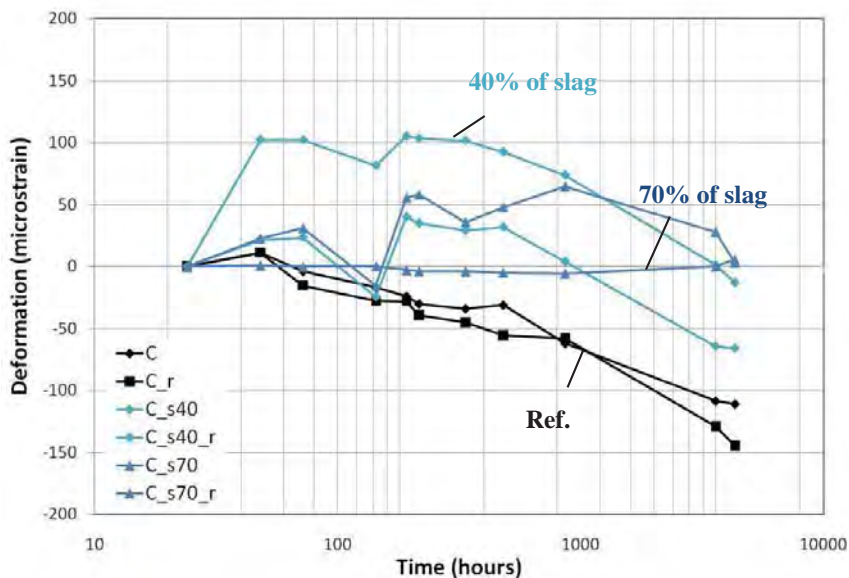
Fig. 5.69 : Deformation (µ/m) versus time (hours) for cement pastes with and without slag cured sealed (without bleed water) at 20ºC

For slag pastes, expansion was observed up to one month of curing, followed by a shrink of the pastes from 1 to 6 months of curing. At the end of six months, a less shrinking from the pastes with slag was observed when compared with plain cement pastes (Fig. 5.69). However the expansion and shrinkage causing volume change of the pastes may lead to the cracking of the pastes. This is also showed by (Darquennes et al., 2011). Cracking of pastes with slag cured saturated or sealed at 20ºC for 720 days was observed by SEM, see section 5.3. Plain cement pastes seemed to have a limited amount of cracks, see section 5.3.

5.7 Drying methods

Drying of cement pastes by oven at 105ºC (evaporable water) and solvent exchange was carried out to determine:

-   Impact of drying on the pore structure of pastes with and without slag;
-   Porosity characterization, water and solvent filled porosity.

Drying of the pastes was here evaluated by measurements of weight loss and freezing of the pores solution by LTC. Also re-saturation methods were used here, including capillary suction, vacuum saturation and pressure saturation. Drying and re-saturation of the pastes with and without slag cured saturated at 20ºC for 28 days are illustrated by the weight change curves see Fig. 5.70. The pastes were cut in the middle (two pieces); the bottom (b) and top (t) were tested. The impact of the bleeding on the top and sedimentation on the bottom could be observed. The samples size was approximately 30x22Ø mm after cutting.
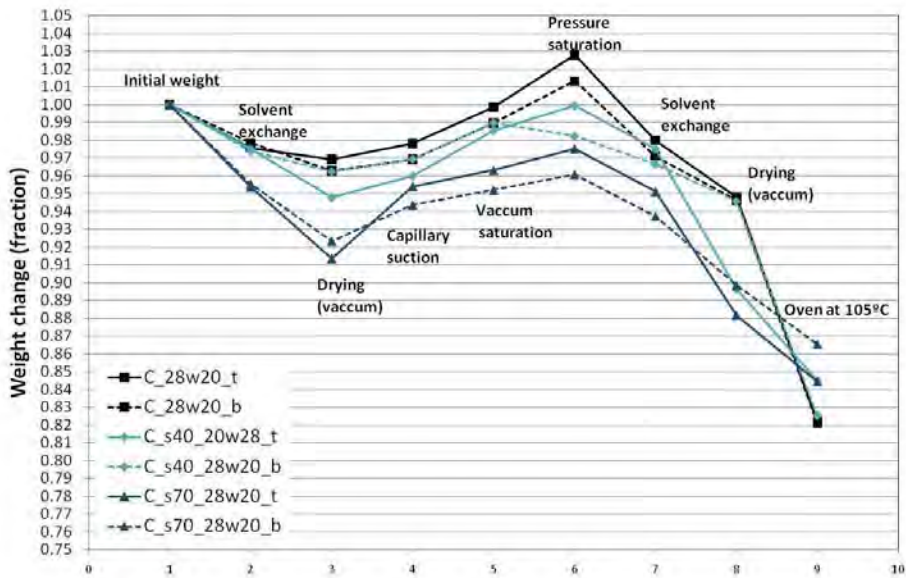
Fig. 5.70 : Weight change versus drying (2-5 and 7-9)and re-saturation (4-6) steps for cement pastes with and without slag cured saturated at 20ºC for 28 days. Top (full line) bottom (broken line)

By the overview of the methods was possible to observe different impacts of dying and re-saturation on pastes with and without slag, see Fig. 5.70. A higher amount of water was removed from the pastes with slag when solvent exchange was used when compared with plain cement pastes (Fig. 5.70). It is suggested in the literature (Belie et al., 2010, Bijen, 1996, Lothenbach et al., 2010) that different products are formed for slag pastes which may cause the difference in drying and re-saturation of the pastes. Capillary saturation method carried out for 72 hours seemed to not fully re-saturate the pastes at the size of 30x22Ø mm. Problems with the method were faced, see section 5.7.4. Pressure saturation assumed to fill the air voids of the pastes, the Fig. 5.70 indicated that larger amount of air voids were found for plain cement pastes. It was also noticed a larger amount of weight change for oven drying at 105ºC when compared with solvent exchange followed by dying in vacuum.

More information on drying and re-saturation methods is given in the following section: 5.7.1 oven drying; 5.7.2 solvent exchange and 5.73 comparison of drying methods.

5.7.1   Oven drying

Oven drying at 105ºC is often used to determine the evaporable water of hydrated cementitious materials. However the size of the samples and time of exposure at oven 105ºC may have an impact in the data of evaporable water, as discussed in the following section (5.7.1.1 Effect of sample size on the oven drying). The evaporable water acquired by oven at 105ºC can be expressed into water porosity of hydrated cementitious materials, see section 5.7.1.2. Data of water porosity were compared to other porosity methods see section 5.9.

5.7.1.1 Effect of sample size and time of exposing at oven 105ºC

The effect of sample size (powder, slice of 5x30Ø mm or 55x15Ø mm) on the time to reach the weight equilibrium was observed for drying using oven at 105ºC (evaporable water) and furnace at 1050ºC (non evaporable water), see Fig. 5.71. Three similar samples for each sample size were used. For pastes dried at oven at 105ºC, the expose time was 1, 3 or 10 days. For pastes dried at furnace at 1050ºC, the expose time was 1, 4 or 24 hours. The Table with the weight change for pastes in powder and slices is given in Appendix XXII.

The weight loss for evaporable water was to some extend influenced by the size of the samples, where the pastes in powder had an average higher values of weight loss than larger samples, see Fig. 5.71. According to studies (Atkins, 1997, Bakhshi and Mobasher, 2011) a large specific surface area is preferable for providing large sorption capacity. The small size of the grains in powder means a greater specific surface area. The section 5.4.1 described the effect of sample size for water sorption test. Moreover, loss of powder during oven and furnace drying measurements may happen and/or carbonation due to the crush of the sample to powder and exposure at oven (Gervais et al., 2004, Parrot and Killoh, 1984). Atlassi (1993) suggested that after longer periods of exposition at oven at 105ºC a continuing slow loss of water can be registered. No information on sample, loss of water and time was given by the author. Moreover, errors introduced by the measurements (e.g. equilibrium, accuracy of the scale) change in the relative humidity and temperature of the room may influence in the weight see e.g. in (Atlassi(1993), Fridh(2005)).

As shown in the Fig. 5.71, the equilibrium in weight was partly obtained after three days of drying using oven at 105ºC and four hours at 1050ºC. Deviations due to sample size and errors in the measurements were suggested by previous discussion. To limit the errors, it is recommended to use samples in slices exposed for longer period: at least 3 days to determine evaporable water and 4 hours for non evaporable water.
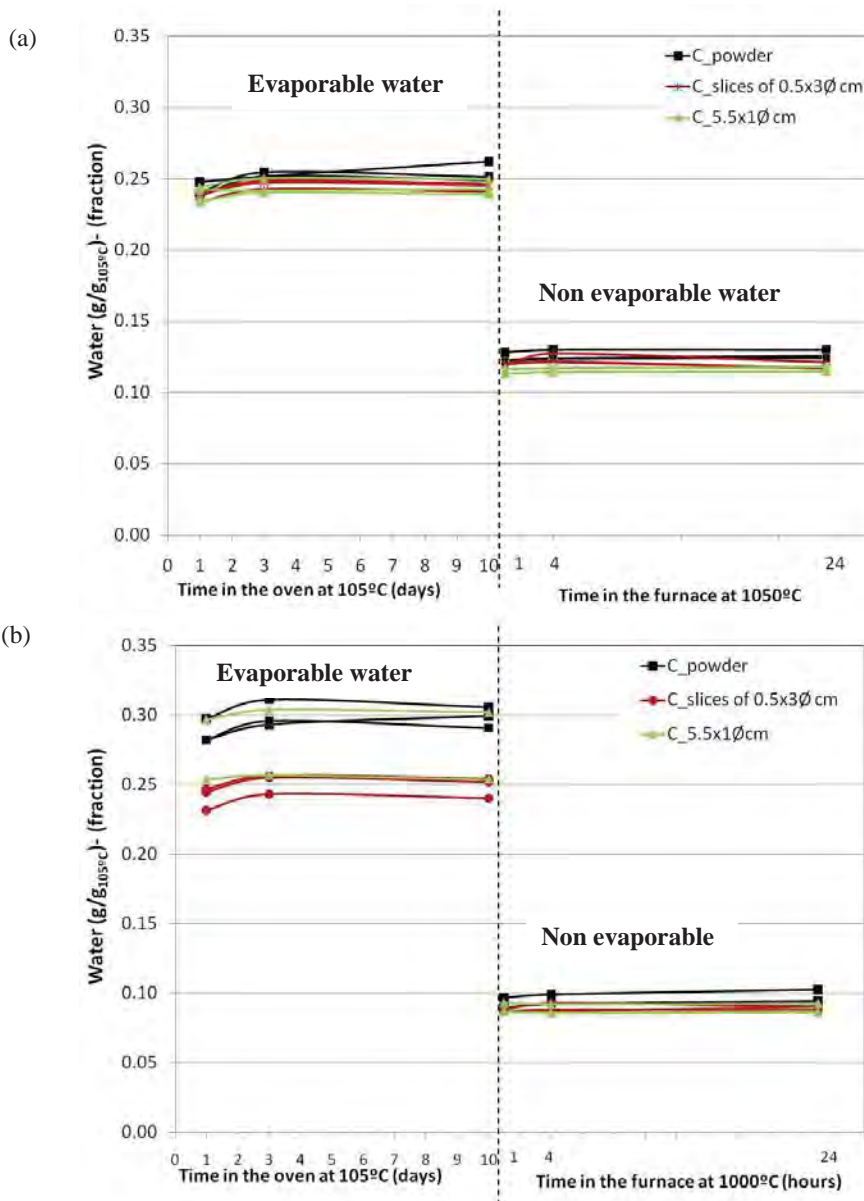
Fig. 5.71: Amount of water ($g/_{g105°C}$) versus time (days and hours) for: (a) cement paste and (b) cement paste with 40% of slag addition cured saturated at 20°C for 3 days: powder (black); slice of 0.5x3Øcm (red) and slice of 5.5x1Ø cm (green)

5.7.1.2 Water porosity

Water porosity measurements for cement pastes with and without slag and fly ash cured saturated (full line) or sealed (broken line) at 20ºC are shown in the Fig. 5.72. The volume fraction of water porosity was obtained by the value of evaporable water (at oven 105ºC) multiplied by the bulk density given by MIP. Data of evaporable and non evaporable water are given in the Appendix XXII.The sample size was 55x15Ø mm (sample size for LTC). The impact of temperature conditions was also observed for pastes with and without slag and fly ash cured saturated at 20 or 55ºC for 1, 3, 28 and 90 maturity days, see Fig. 5.72(b).

The water porosity for pastes sealed and saturated showed a volume of about 0.45. Slightly increase and decrease of the volume of water were observed for pastes cured from 1 to up to 720 days.

For samples cured at high temperature, a lower volume of pores was obtained for slag when compared with plain cement pastes. Differences in hydrated product of slag formed at high temperature may explain that. According to investigations with cement pastes carried out by Marsh and Day (1985), there is no correlation between curing temperature and total porosity measured by evaporable water.

Water porosity is not suggested for porosity measurement of hydrated cementitious materials. The porosity measured using water as a displacement is often higher than using other liquids (e.g. isopraponol and mercury) (Marsh and Day, 1985, Krus et al., 1997). According to Krus et al. (1997) the gel pores in the hardened cement paste takes the water during absorption which leads to change in microstructure by the hygric expansion of these pores. In addition, drying at oven 105ºC may dehydrate some of the cement products (e.g. ettringite) and collapse the microstructure of pores, see in (Aono et al., 2007, Galle, 2001, Korpa and Trettin, 2006). Moreover experimental errors (e.g. sample size, time of exposing at oven 105ºC) may have a high impact on the data of water porosity, as showed in the section 5.7.1.1. Carbonation may also take place for samples dried in the oven leading to a change in microstructure, see e.g. (Belie et al., 2010, Ngala and Page, 1997a)
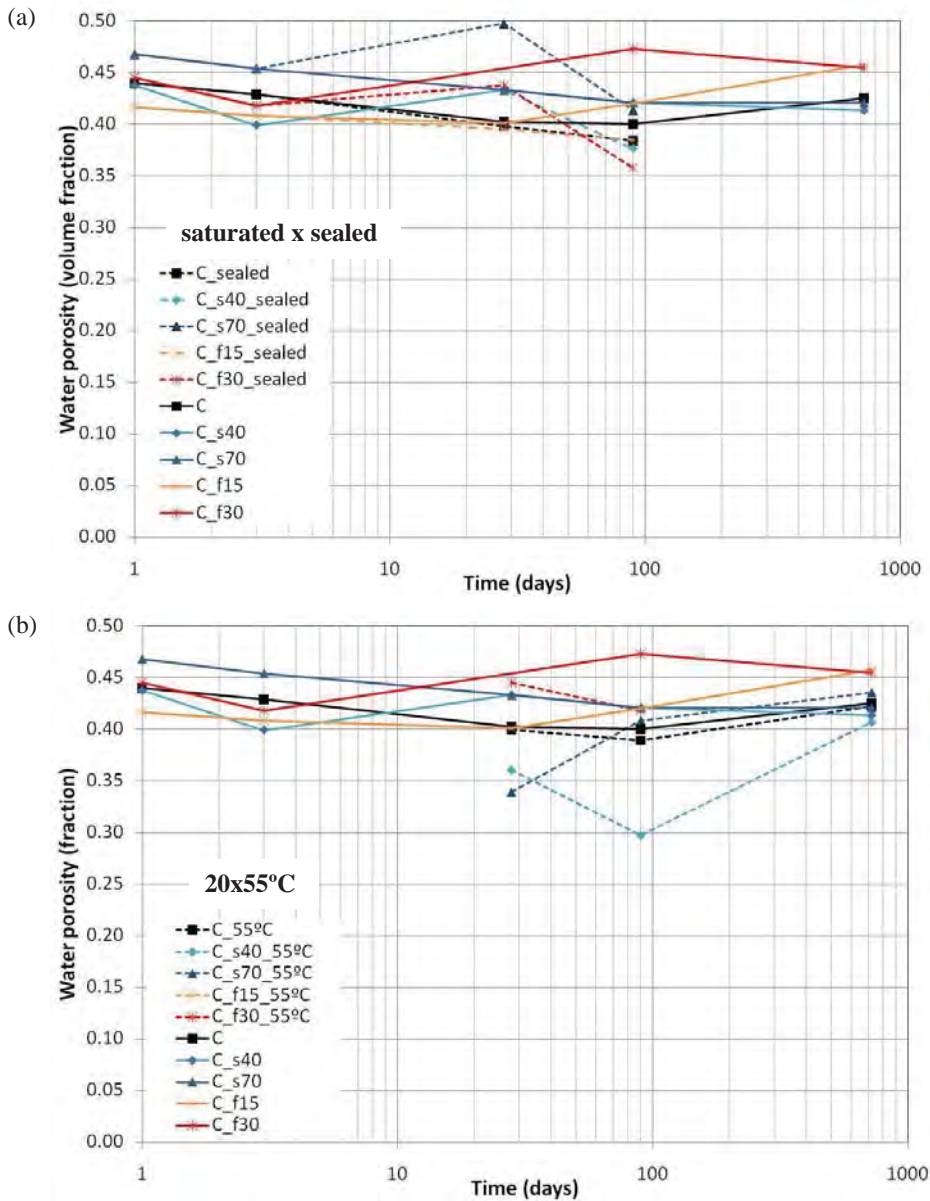
Fig. 5.72: (a) Water porosity versus time (days) for cement pastes with and without slag and fly ash cured (a) saturated (full line) or sealed (broken line) at 20ºC for 1, 3, 28, 90 and 720 days (b) saturated at 20ºC (full line) or 55ºC (broken line) for 1, 3, 28, 90 and 720 maturity days

5.7.2 Solvent exchange

Tests with isopraponol were carried out by manual measurements using a glass sealed container for the measurements for cement pastes with and without slag cured sealed at 55ºC for 90 maturity days (Fig. 5.73). The expected weight change is represented by the red line. Only about 3% of weight change was observed for the pastes; see Fig. 5.73. The samples exposed to isopropyl alcohol and weighted manually during five days and divided in three: bottom (b), middle (m) and top (t) (sample size of approx. 2x2.2Ø mm). At the first day it was possible to observe a decrease of the weight, as the density of isopraponol is lower (about 0.78 g/cm³) than the water (about 1 g/cm³) this fact is expected during the exchange of water to solvent within the pores of the pastes. From the second day the weight change of the pastes was increased. A larger decreased is expected with time (see red line in the Fig. 5.75), but it was not observed. In general, it is possible to conclude that only about 20% of the water was exchanged by the solvent.

Porosity measured by solvent versus time for pastes with and without SCMs cured sealed or saturated for 28 and 90 days is graphically illustrated in the Fig. 5.74. It was possible to observe a higher porosity for pastes with SCMs when compared with plain cement paste. The weight change is illustrated in the following section.
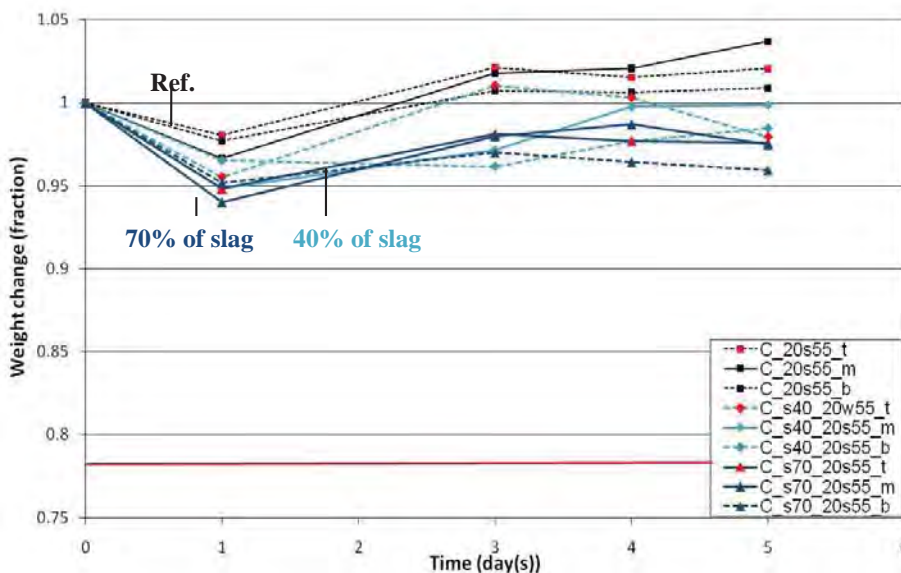

Fig. 5.73: Weight change (fraction) versus time (day) for cement pastes with and without slag cured saturated at 55ºC for 90 maturity days. Bottom (b)-broken line, middle (m)-full line and top (t) – broken line and red marks
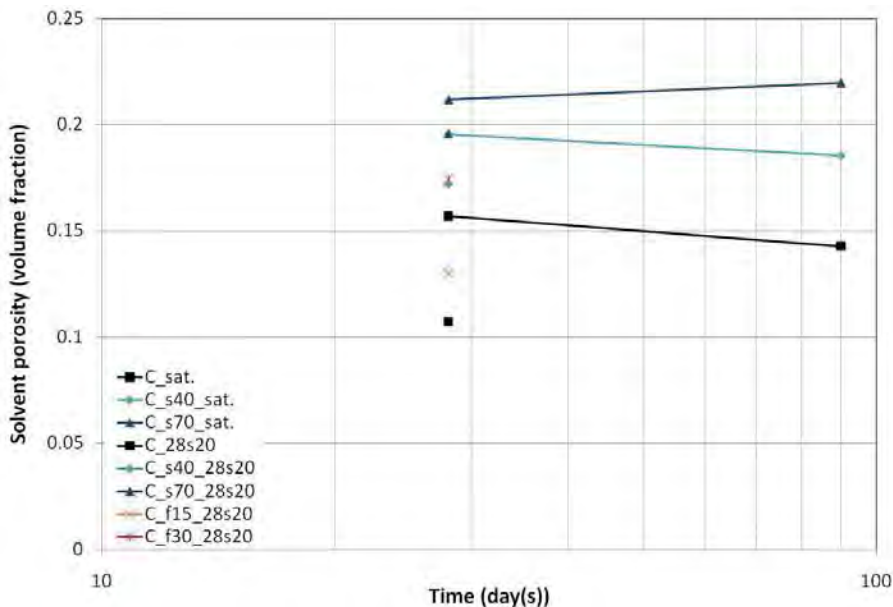
Fig. 5.74: Porosity measured by solvent exchange (volume fraction) versus time for sample with
and without SCMs cured saturated or sealed at 20ºC for 28 and 90 days

Investigation with cementitious materials have showed that low amount of water is released when solvent is used (Feldman, 1986a, Korpa and Trettin, 2006). According to Korpa and Trettin (2006) the water from gel pore is more strongly bound and can be only removed by drying the paste. Moreover an expansion followed by a slight contraction is found for cement pastes dried with isopraponol alcohol (Beaudoin et al., 2000). This may also contributes for the change in microstructure. However, the use of solvent isopraponol is considered a gentlest way of drying and stop of the pastes hydration (Beaudoin et al., 2000, Beaudoin and Tamtsia, 2004, Kocaba, 2009). According to Gallucci (Gallucci, 2007b) the hydration of the hydrated cementitious materials stops when the relative humidity is below 75% (approx.) and it may be obtained before 7 days of exposition in isopropanol.

5.7.3   Comparison of drying methods

The weight change of cement pastes submitted to drying using oven at 105ºC and solvent exchange is illustrated in the Figs. 5.75 and 5.76. The data is an average of three measurements.

Drying by oven or solvent has two different impacts on the cement pastes. As illustrated in the Fig. 5.75 and 5.76, drying using solvent released less water from the sample than oven drying. This is in agreement with Feldman (1986) and Korpa and Trettin (2006). For oven dried samples, Simada and Yang (2001) and Kocaba (2009) suggested an dehydration of the ettringite at about 70ºC by thermogravimetry analyses. This may be the reason of the increased weight loss for oven dried pastes. Moreover, a collapse of the C-S-H pore structure for pastes oven dried at 105ºC is reported in the literature (Day and Marsh, 1988, Galle, 2001, Konecny and Naqvi, 1993, Korpa and Trettin,

2006). Errors during the weight measurements have also to be taken into account, as reported by the Section 5.7.1.1.

Cement pastes with slag also showed a higher weight loss for solvent exchange and oven at 105ºC when compared with plain cement pastes, see Fig. 5.76. It may be due the different products formed and/or different degree of hydration of the cement pastes with slag (Chen and Brouwers, 2007, Malhotra, 1993, Roy and Idorn, 1982).

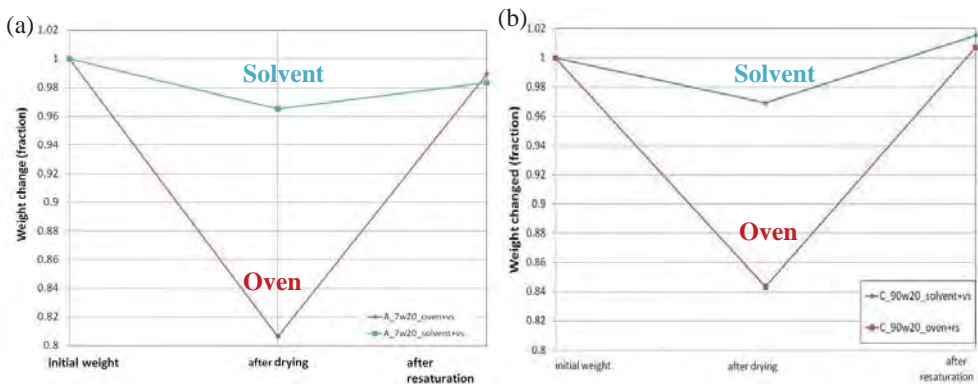Fig. 5.75: Weight change for cement pastes dried by solvent exchange and oven at 105ºC and re-saturated (a) plain cement paste "A" cured saturated at 20ºC for 7 days and (b) plain cement paste "C" cured saturated at 20ºC for 90 days. Average of three measurements
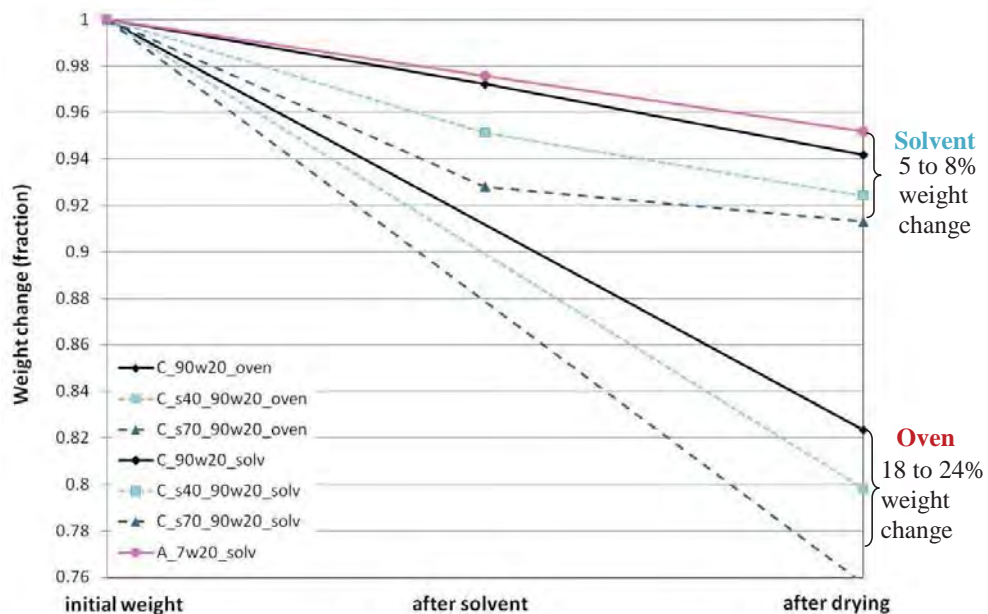

Fig. 5.76: Weight change for sample with and without slag cured saturated at 20ºC for 90 days after: solvent exchanged and vacuum dried; and oven dried at 105ºC

The use of solvent exchange for drying and stop hydration of the hydrated cementitious materials is proposed. However, porosity data from solvent exchange may not be comparable to any of the methods. It seems that the fully exchange of water by isopropanol does not occur even when vacuum drying is applied. And for oven drying, the microstructure is damage and water may be removed from some of the cementitious hydrated compounds.

5.7.3.1 Possible change of microstructure of the pastes due to drying by solvent exchange or oven at 105ºC

Apparent heat capacity versus block temperature curves from LTC were used to evaluate possible changes in the microstructure of pastes dried by oven at 105ºC and solvent exchange, see Fig. 5.77 and 5.78. The plain cement pastes were cured saturated at 20ºC for seven days: (1) virgin; (2) oven/solvent dried and re-saturated; (3) oven dried at 105ºC/solvent dried, see Figs. 5.78 and 5.79. The pastes were first dried and then re-saturated by vacuum re-saturation. Procedure for vacuum saturation method is given in the Appendix IX.

The apparent heat capacity versus block temperature curves show a difference pattern of the curves for dying (oven and solvent) and re-saturated pastes. This indicated a change of the pore structure of the pastes; see Fig. 5.77 and 5.78. For pastes oven dried at 105ºC and re-saturated, a larger peak at percolated capillary pores range (0 to -20ºC) is showed when compared with virgin pastes (non dried sample). This may be caused by the coarsening of pore structure when drying by oven at 105ºC and it is supported by the literature (Yurtdas et al., 2006, Konecny and Naqvi, 1993, Korpa and Trettin, 2006, Galle, 2001).

Solvent dried and re-saturated pastes shows no peaks of frozen water in the range of small capillary pores (-20 to -50ºC), see Fig. 5.78(2). As expected, tor pastes dried using oven dried at 105ºC and solvent exchange no freezable water was observed see Fig. 5.77(3) and 5.78(3).

Fig. 5.77: Apparent heat capacity (J/deg/kg) versus block temperature(ºC) for plain cement paste
"A" cured saturated at 20ºC for 7 days (1) virgin (2) dried using oven at 105ºC and then re-saturated
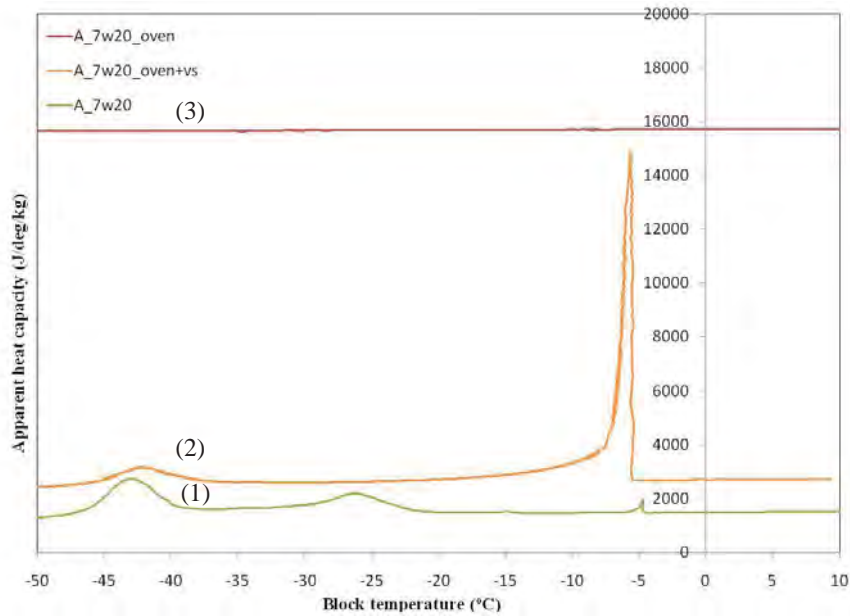by vacuum re-saturation (3)dried using oven at 105ºC (baseline changed for comparison)
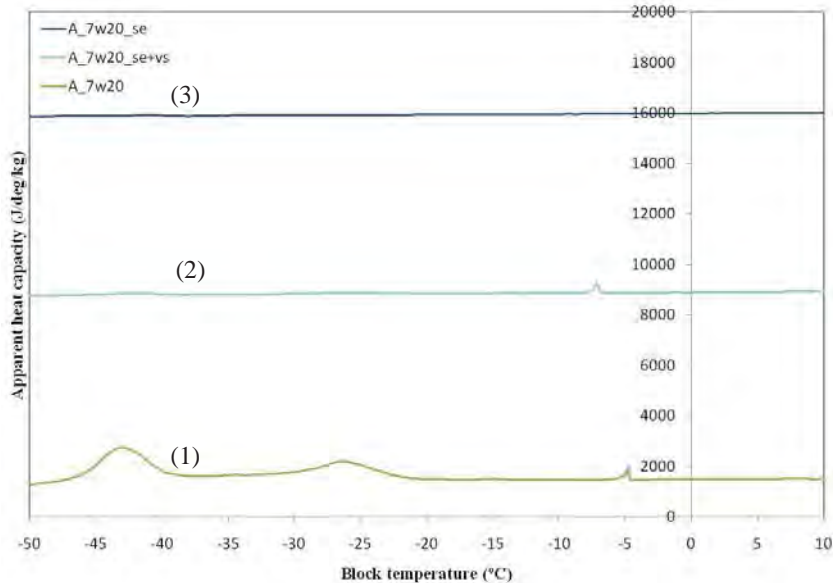

Fig. 5.78: Apparent heat capacity (J/deg/kg) versus block temperature (ºC) for paste A cured
saturated at 20ºC for 7 days (1) virgin (2) dried using solvent and then re-saturated by vacuum re-
saturation (3) dried using solvent (baseline changed for comparison)

Based on the previous results, a longer saturated period of 20 days was carried out with plain cement paste cured saturated at 20ºC for 90 days, see Figs. 5.79. The graphic shows that even with a longer period of re-saturation the paste dried with isopraponol present a lower amount of freezable water, than virgin pastes, see Fig.5.79. It may indicate that either the gel pores from the pastes exposed into solvent may not be water re-saturated or there was some solvent left in the gel pores limiting the freezing of the water within the pores. A reaction of the solvent with the hydrated products is suggested by low weight change (about 5 to -8%) observed in the section 5.7.2 for pastes dried with solvent. Studies undertaken using isopropanol (Beaudoin et al., 1998, Feldman and Beaudoin, 1991, Kocaba, 2006) indicate no reactive between solvent and the solids of cement paste ; but the information in the literature is somewhat contradictive (Taylor and Turner, 1987).

In the Table 5.13, the freezing temperature for isopropyl alcohol according with the concentration is given. Delay on the freezing should occur if there is any isopropanol left within the pastes. Sun and Scherer (2010) used solvent dried followed by oven dried at 60ºC and re-saturation for testing cementitious materials by LTC, the porosity was higher for dried sample when compared with virgin. However, the effect of drying by oven has to be carefully observed as it may perturb the pore structure of the pastes. The underlying reason of the effect of drying using isopropanol on the cement pastes is not completely understood and it may need some extra studies to be explained.
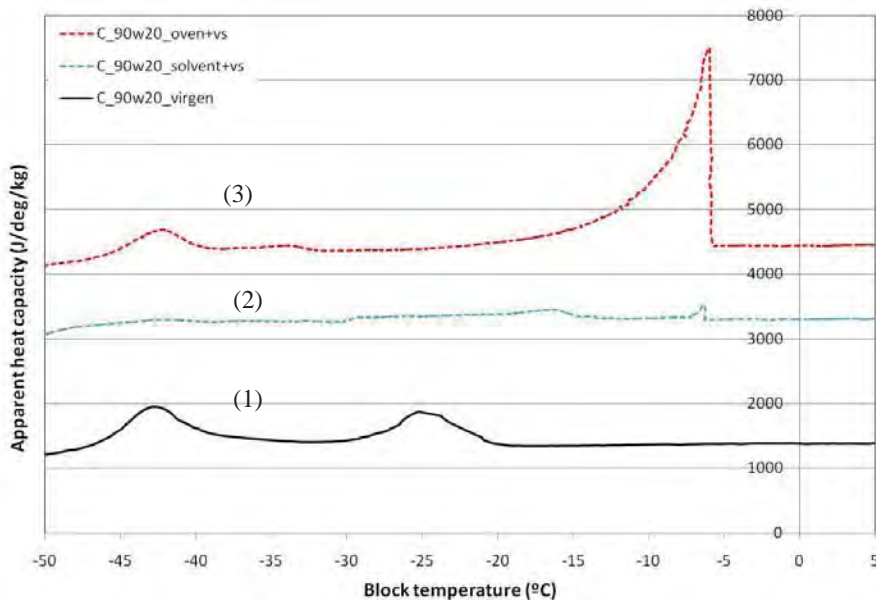

Fig. 5.79: Apparent heat capacity (J/deg/kg) versus block temperature (ºC) for paste C cured saturated at 20ºC for 90 days: (1) non dried sample, (2) dried using isopraponol and then re-saturated by vacuum re-saturation and (3) dried using oven at 105ºC and then re-saturated by vacuum re-saturation (baseline changed for comparison)

Table 5.13: Freezing temperature of isopropyl alcohol (Toolbox, 2009)

Isopropanol concentration (% by volume)	0	10	20	30	40	50	60	70	80	90	100
Freezing temperature (ºC)	0	-4	-7	-15	-18	-21	-23	-29	-37	-57	-73

5.8 Estimation of pore structure

Estimation of porosity is often used to illustrate the porosity of cementitious of materials based on: (a) the volume fraction of the cement, SCMs and water used, (b) degree of hydration of the cement and SCMs, (c) density of the materials and products. For that, information on the raw and hydrated material should be acquired and correctly used. For porosity here estimated, the degree of hydration of some of the cement pastes and slag were acquired using SEM carried out by Kocaba (2009) and Fernandez-Altable (2010), see Table 5.14. Other values for degree of hydration and density of the products were estimated based on the literature review and MIP data. Data for fly ash pastes was assumed to be like slag pastes, even knowing that it is not the case. For other pastes, the degree of hydration was assumed as showed in the Table 5.14. The density of the cement and slag in powder were measured by helium picnometry and the water is assumed to be 1g/cm³, see Table 5.14(Kocaba, 2009).

The curves of estimated pore volume versus time for cement pastes with and without slag and fly ash are illustrated in the Fig. 5.80. The pores estimated here are the capillary pores. The overall data show a lower volume of plain cement paste from 1 to 720 days if compared with system with slag and fly ash. This is also observed by MIP and it is described in the section 5.2. After 90 days of curing, a slight reduction was observed for all the pastes. It should be kept on mind that the data is sensitive to the values of degree of hydration and density of products. Estimation of the porosity using the volume fraction of materials, degree of hydration and density of the materials and products may be used to illustrate the porosity of the pastes, however variance from the real value are expected as the hydration of cementitious materials is such complex and involves many heterogenic hydrated products.

Table 5.14: Degree of hydration of the pastes and SCMs for estimation of porosity for cement pastes

Sample id.	Degree of hydration of the cement – α (fraction)				
	1 day	**3 days**	**28 days**	**90 days**	**720 days**
C	0.40	0.61*	0.72*	0.77*	0.83*
C_s40	0.45	0.62*	0.82*	0.86*	0.90*
C_s70	0.48	0.65	0.84	0.88	0.92
C_f15	0.45	0.61	0.70	0.82	0.88
C_f30	0.45	0.61	0.72	0.86	0.90
SCMs	Degree of hydration of the SCMs – α (fraction)				
	1 day	**3 days**	**28 days**	**90 days**	**720 days**
40% of slag	0.00	0.10	0.40	0.67**	0.75
70% of slag	0.00	0.10	0.20	0.40**	0.55
15% of fly ash	0.00	0.10	0.20	0.65	0.75
30% of fly ash	0.00	0.10	0.20	0.60	0.70

*(Kocaba, 2009)

**(Fernandez- Altable, 2010)

Table 5.15: Used density for the materials for estimation of porosity for cement pastes

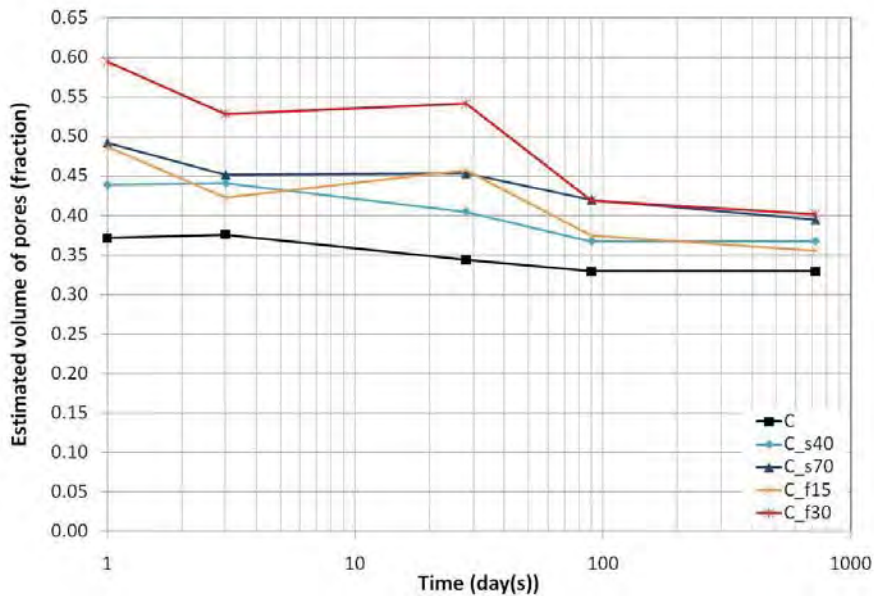| **Material**	**Density (g/cm³)***	**Density of the products (g/cm³)**
Cement	3.15	1.70 (1 to 3 days) and 2.00 (28 to 720 days)
Slag	2.60	1.55(1 to 3 days) and 1.70 (28 to 720 days)
Fly ash	2.20	1.55 (1 to 3 days) and 1.70 (28 to 720 days)
Water	1	1

*(Kocaba, 2009)

Fig. 5.80: Estimated volume of pores (fraction) for pastes with and without slag and fly ash cured
saturated at 20ºC for 1, 3, 28, 90 and 720 days

To compare with the porosity estimated at the present work, the porosity based on the thermodynamics predictions by GEMS (Geochemical modeling codes) was used. They were carried out by Barbara Lothenbach and Klartje De Weerdt for the pastes used at the present work: systems with and without slag at w/c ratio of 0.4 cured saturated at 20ºC for 0 to about 1000 days. Details are given in (Lothenbach, 2008). Combining thermodynamic modeling with a set of kinetic equations which described the dissolution of the clinker, it was possible to predict quantitatively the amount of hydrates as a function of the time of hydration. It is important to point out that some problems were experienced by the modeling: Fig. 5.81(b) and (c) shows some instabilities for the slag systems. Furthermore, after about 60 days hemicarbonate should form but GEMS did not predict it.

The volume of C-S-H and the pores (gel, capillary and total) predicted by GEMS are illustrated in the graphic below, see Fig. 5.82. Gel pores are assumed to be about 35% of the volume of C-S-H. As expected a reduction of the capillary and an increase of the gel pores is observed with time for predictions made for the threes systems (Fig. 5.82). Fig. 5.81(b) and 5.81(c) shows the higher amount of gel pores for pastes with slag than plain cement pastes. Larger total volume of pores was found for pastes with slag addition when compared with plain cement paste.
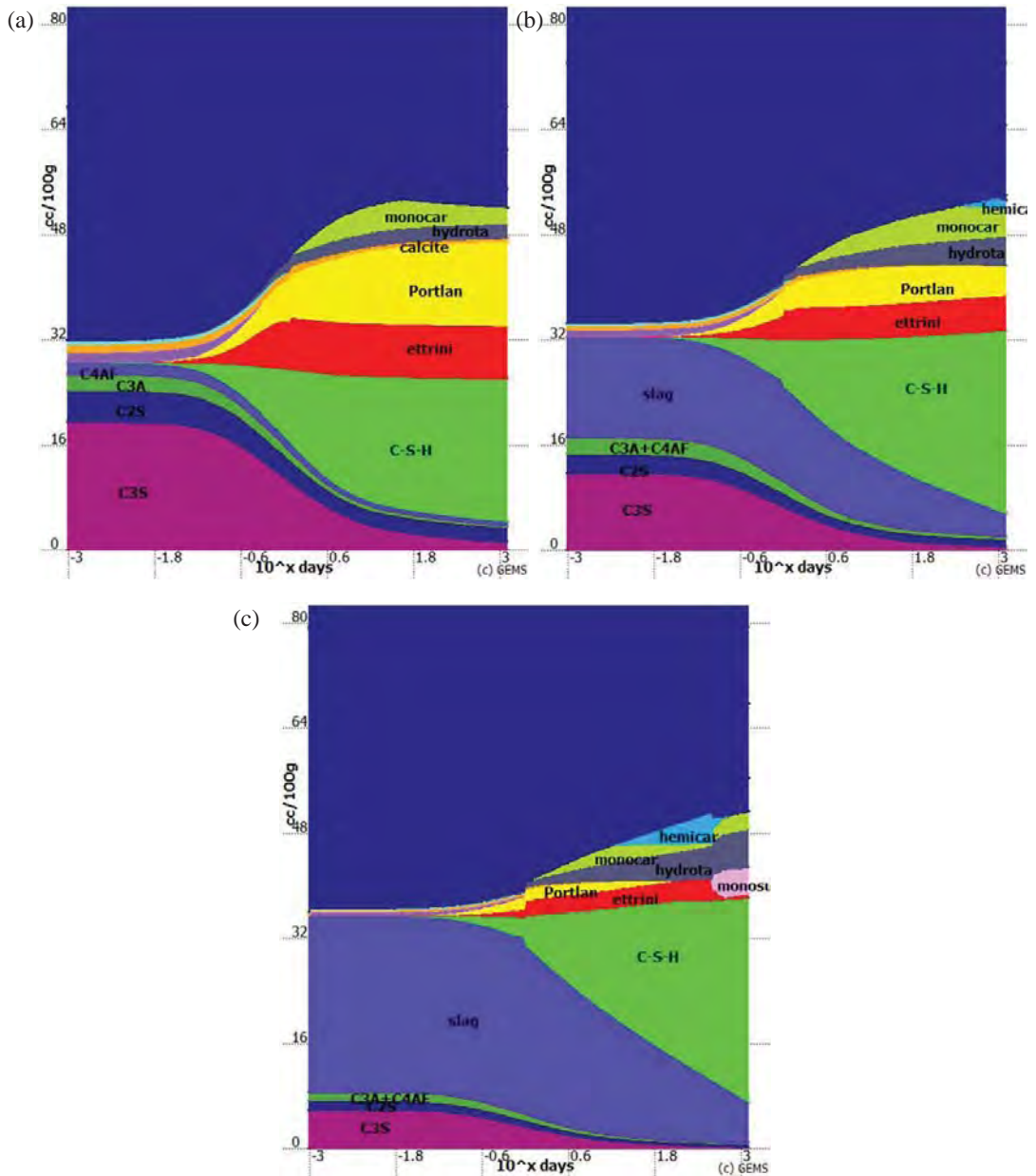
Fig. 5.81: Predicted development of the porosity by GEMs in volume ((cm³)/100g of unreacted cement)versus predicted time (day(s)10ˣ) (a) plain cement paste, (b) cement paste with 40% of slag and (c) cement paste with 70% of slag (Lothenbach and De Weerdt, 2011)

Fig. 5.82: Volume (cm3/100g) of C-S-H and pores predicted by GEMS for systems at w/c ratio of 0.4 cured saturated at 20ºC for about 1000 days (a) plain cement pastes, (b) cement paste with 40% of slag and (c) cement paste with 70% of slag (Lothenbach and De Weerdt, 2011)

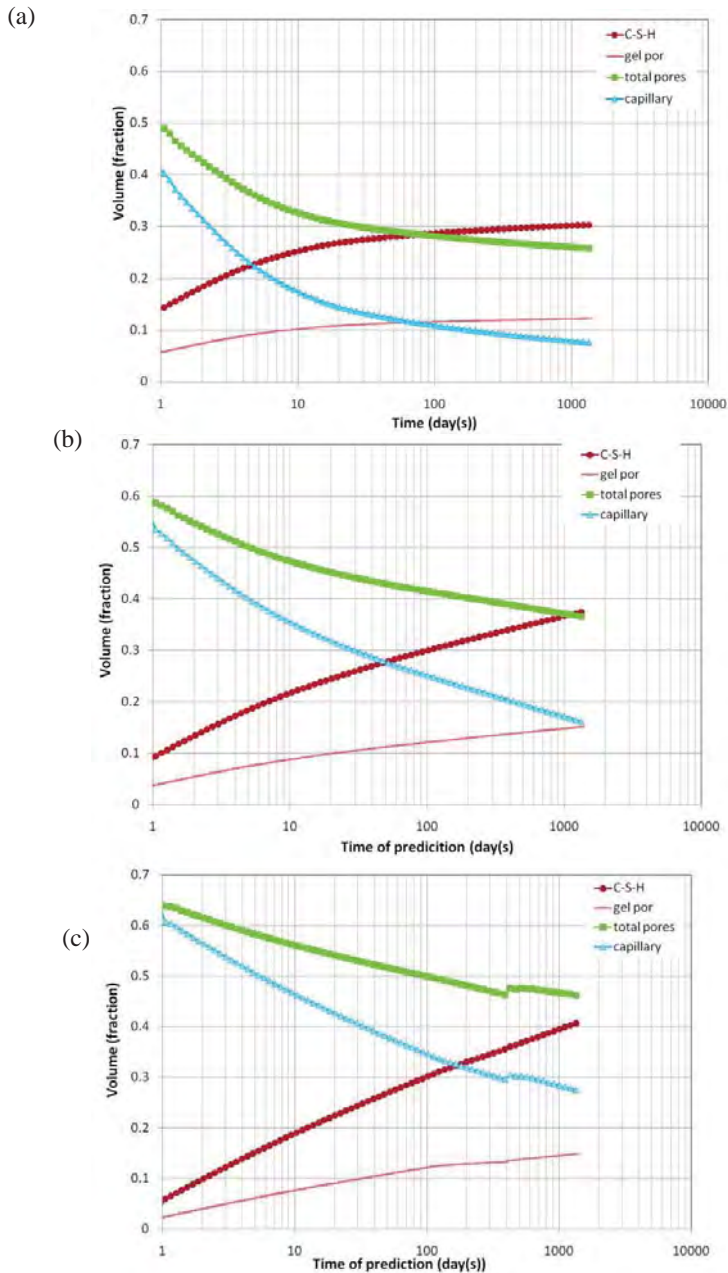It seems that modeling of the assemblage phases of hydrated cementitious is possible. However, the data has to be carefully interpreted as some instabilities and omission of some of the hydrated products may occur.

The comparison between GEMs and estimated porosity is illustrated in the Fig. 5.83. Fig. 5.83 shows lower values for porosity for slag pastes estimated than the predicted by GEMs. It seems that the plain cement paste had a better agreement. In general it seems easier to estimate and predict the porosity for plain cement paste. When slag or fly ash is added, the complexity of the system increases and the estimation and prediction may not give reliable values.
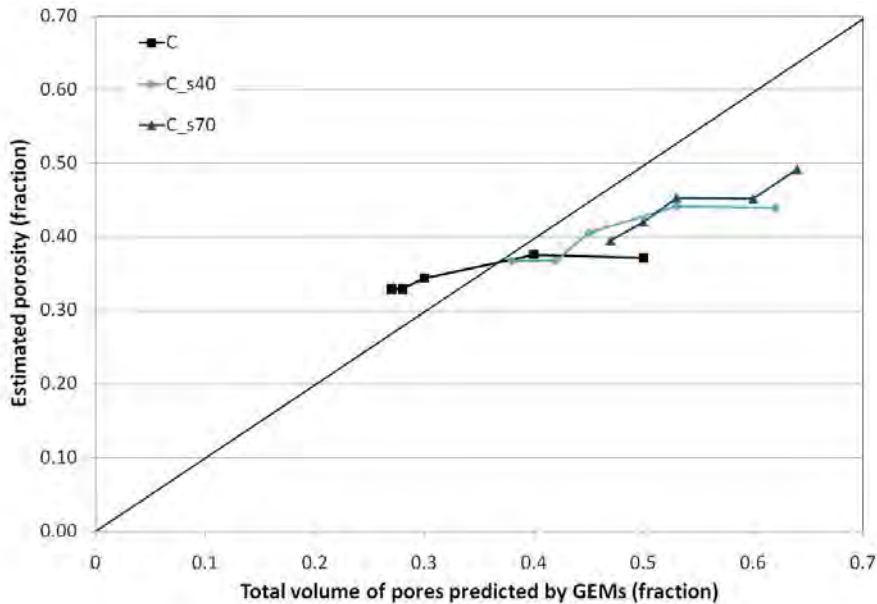

Fig. 5.83: Total volume of pores estimated versus total volume of pores predicted by GEMs in volume fraction for similar pastes cured saturated at 20ºC for 1,3, 28, 90 and 720 days

5.9 Comparison of methods

Comparison of the methods is here illustrated by the volume of the pores given by different methods. With the possibility of data comparison by various methods extra information can be gained. The overview of the methods compared, sample age and curing conditions are given in the Table 5.16. Similar samples (material, moisture and temperature) were used to compare different porosity methods.

One difficulty with comparing the results of techniques is that different principles and assumptions are made for the porosity determination. For instances, the Kelvin Equation use parameters (e.g. surface tension, density, heat of fusion) to calculate the pore size of the pastes. Apparently, the parameter's values are not well established in the literature and may give large difference on the porosity data (Bager and Sellevold, 1986a, Fagerlund, 1994, Sun and Scherer, 2010). When comparing porosity data the size of pores measured should be kept in mind that the methods give

information on different range of pores. Also, drying may affect the pore structure and it is required for MIP and SEM. Recent investigations carried out by Sun and Scherer (2010) found different curves for mortars tested using MIP, LTC and gas sorption. Similar observations were made by Villadsen (1992) and March and Day (1985) when methods were compared, concluding that a widely varying values are found for different methods.

Table 5.16: Overview of the comparison of the methods

Comparison of volume of pores	Age (days)	Curing conditions (moist., temp.)	Fig.
LTC x MIP	1,3,28,90 and 720	Sat, 20ºC	5.84(a)
LTC x SEM	3, 28 and 720	Sat, 20ºC	5.84 (b)
LTC x Water sorption	28, 90 and 720	Sat, 20ºC	5.84 (c)
LTC x Estimated porosity	1,3, 28, 90 and 720	Sat, 20ºC	5.84 (d)
MIP x SEM	3, 28 and 720	Sat, 20ºC	5.85 (a)
MIP x Water sorption	28, 90 and 720	Sat, 20ºC	5.85 (b)
MIP x Estimated porosity	1,3, 28, 90 and 720	Sat, 20ºC	5.85 (c)
SEM x Water sorption	28 and720	Sat, 20ºC	5.86(a)
SEM x Estimated porosity	3, 28 and 720	Sat, 20ºC	5.86 (b)
Water sorption x Estimated porosity	28, 90 and 720	Sat, 20ºC	5.87
Water porosity x Solvent porosity	28 and 90	Sat and seal, 20ºC	5.88
Water porosity x Estimated porosity	1,3, 28 and 90	Sat, 20ºC	5. 89
Predicted by GEMS x LTC, MIP and SEM	Varied	Sat, 20ºC	5.90

Comparison between porosity measurements obtained by LTC and other methods (MIP, water sorption) using similar samples is shown in the Fig. 5.84. The porosity estimation was calculated using parameters (density of the products, degree of hydration) based on the literature and estimations, some deviation of the real porosity is expected. Exploring LTC data was possible to see that a large amount of water (30 to 80% approx.) not freezes by LTC. It is also important to say that some of the ice may not entre in the small pores. Moreover it is assumed that the sample is fully saturated, but it may not be the case. Some of the water lost from the weighing of the sample to the end of the test (about 2%) may affect the total volume of ice measured by LTC. Also the baseline calculation show differences when three methods used in the literature are applied see section 5.1.1.4.

Comparison between total volume of pores given by MIP and other methods are illustrated in the Fig. 5.85. Problems associated with the required drying treatment of samples from MIP and SEM samples were discussed in detail in the section 5.7. Based on the literature, it seems that the porosity is changed even when a more gentle method like solvent is used. A large range of pores is measured by MIP and it can be reflected in the higher total volume of pores measured when compared with LTC and SEM. The compress of the hydrated solid products reported by Diamond (2000) and damage of the pore structure due to the pressure applied by MIP have also to be considered when porosity is compared. According to Scherer et al. (1995) the pressure of mercury intruded is ten times higher than the freezing stresses when ice is formed.

The correlation between the data of SEM and other methods is given in the Fig. 5.86. Sample preparation for SEM analysis has to be carefully done and it requires some experience and special equipments (see more detail in the Appendix XII). SEM may clearly reveal the amount of pores of

the pastes; however a large range of magnification is required for the analysis a larger porosity range (e.g. from gel to large capillary). In the analysis of the data, the way (position and program used) of "thresholding" the pore area in the grey scale histogram may affect the amount of pores.

The total volume of pores from water sorption seems to be overestimated if compared with other methods, see Fig. 5.87. In the section 5.4 was observed that sample preparation have a high impact in the data of water sorption, for samples in powder carbonation was observed. The porosity was not measured for the whole hygroscopic range, but only from 0 to 97%RH. Difficulties to acquire the equilibrium in weight for samples exposed at high RH were observed, it may be due to a continuous hydration of the samples. Comparison of methods reported in the literature also point out a higher porosity is found when water is used as a displacement, see e.g. (Marsh and Day, 1985, Krus et al., 1997).

Water porosity measured by oven at 105ºC versus solvent exchange curves are graphically represented in the Figs. 5.88. As observed in the section 5.7.3, the porosity measured by oven at 105ºC is higher than solvent porosity. Relatively lower values for porosity measured by solvent exchange were observed and it is also reported in the literature (Feldman, 1987, Marsh and Day, 1985). Apparently there is some isopropanol left in the sample or the water is not fully exchanged by isopropanol.

Modeling of the pastes carried out by GEMs was also compared with other porosity methods (LTC, MIP and SEM), see Fig. 5.89. A good agreement between the predictions by GEMs and MIP data was observed, especially for plain cement paste.

(a)
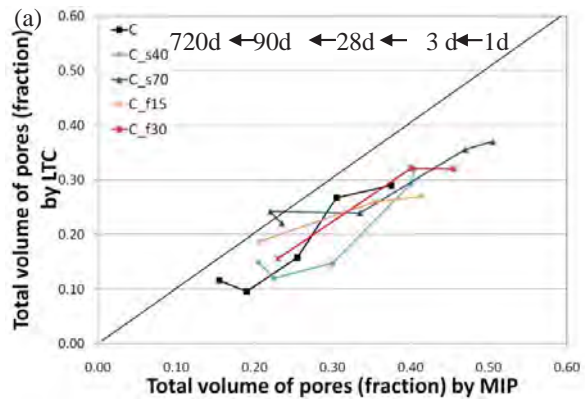
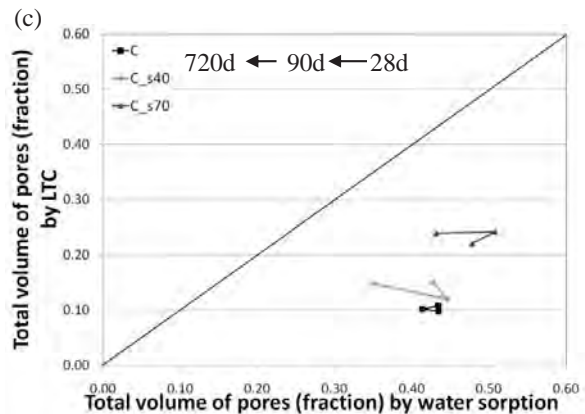| Main remarks: Higher porosity MIP |
|---|
| -Solvent exchange method applied for MIP may remove some of the non freezable water |
| -Water in small pores does not freeze |
| -Inaccuracy of the baseline calculation by LTC |
| -For old fly ash samples a better agreement between LTC and MIP is observed. |
| -Compression of the solid products by MIP |

(b)
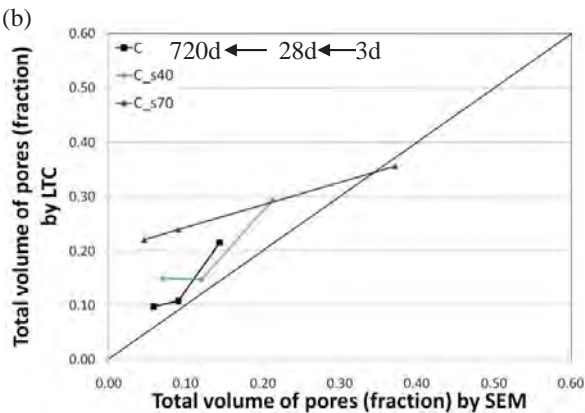
Main remarks: Higher porosity for LTC
-Different range of pores measured by LTC and SEM. SEM using the magnification of 1000x, measures the large capillary pores.
-Water in small pores does not freeze
-Inaccuracy of the baseline calculation by LTC

(c)

Main remarks: Higher porosity for water sorption
-Possible carbonation and continuous hydration observed for samples tested by water sorption
-Range of RH analysed for water sorption was from 0 to 97%RH, including only part of the over hygroscopic range.
-Water in small pores does not freeze
-Inaccuracy of the baseline calculation by LTC

Fig. 5.84: Total volume of pores (faction) by LTC versus total volume of pores (fraction) by (a)MIP; (b)SEM; (c) water sorption from 0 to 97%RH; (d) estimated porosity for cement pastes with and without slag and slag cured saturated at 20ºC. Days and curing conditions are given in the Table 5.16
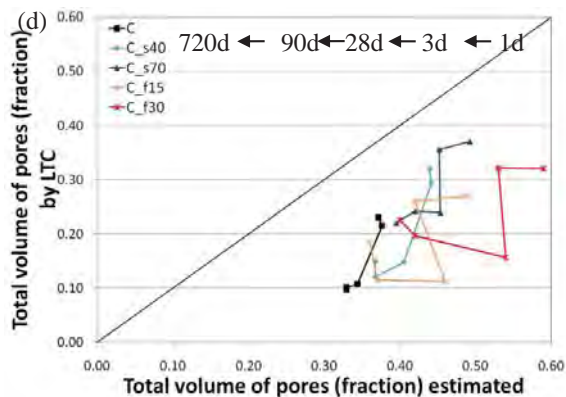
(a)

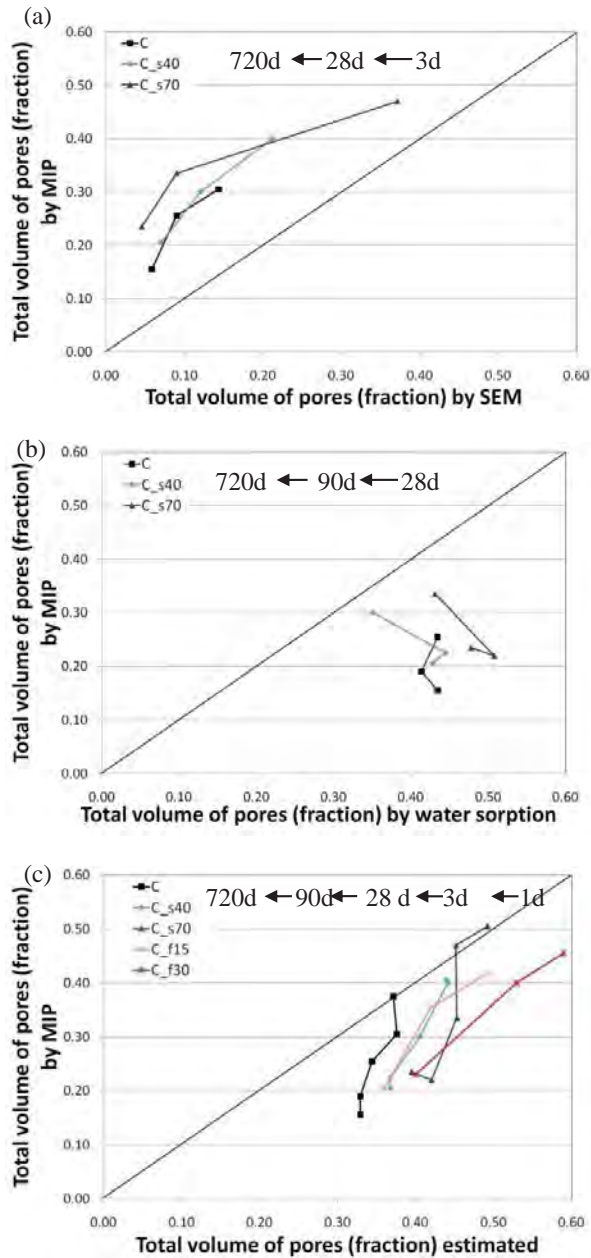| Main remarks: Higher porosity MIP |
|---|
| -Different range of pores measured by LTC and SEM. SEM using the magnification of 1000x, measures the large capillary pores. |
| -Compression of the solid products by MIP |

(b)

Main remarks: Higher porosity water sorption
-Possible carbonation and continuous hydration observed for samples tested by water sorption
-Range of RH analysed for water sorption was from 0 to 97%RH, including only part of the over hygroscopic range.
-Compression of the solid products by MIP
-Dried sample is required for MIP

(c)

Main remarks: Higher for estimated porosity
-Assumptions made by the estimation (e.g. density of the products, degree of hydration etc.)

Fig. 5.85: Total volume of pores (faction) by MIP versus total volume of pores (fraction) by (a) SEM; (b) water sorption; (c) estimated porosity for cement pastes with and without slag and fly ash cured saturated at 20ºC. Days and curing conditions are given in the Table 5.16
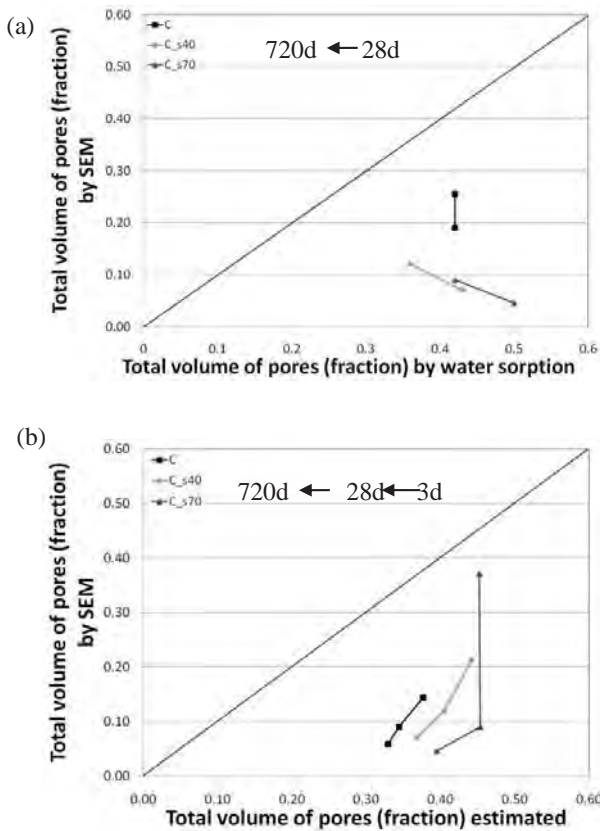
(a)

Main remarks: Higher porosity for water sorption
-Possible carbonation and continuous hydration observed for samples tested by water sorption
-Range of RH analysed for water sorption was from 0 to 97%RH, including only part of the over hygroscopic range.
-Different range of pores measured by SEM and water sorption. SEM using the magnification of 1000x, measures the large capillary pores.

(b)

Main remarks: Higher porosity for estimated
-Assumptions made by the estimation (e.g. density of the products, degree of hydration etc.)
-Limited range measured by SEM at 1000 magnification

Fig. 5.86: Total volume of pores (faction) by SEM versus (a) total volume of pores (fraction) by water sorption and (b) total volume of pores (fraction) estimated for cement pastes with and without slag cured saturated at 20ºC. Days and curing conditions are given in the Table 5.16

Fig. 5.87: Total volume of pores (faction) by water sorption versus total volume of pores (fraction) estimated for cement pastes with and without slag cured saturated at 20ºC. Days and curing conditions are given in the Table 5.16
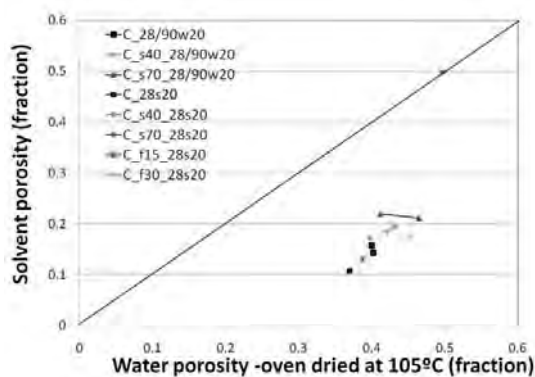
Fig. 5.88: Porosity measurements by solvent exchange versus porosity by oven at 105ºC. Days and curing conditions are given in the Table 5.16
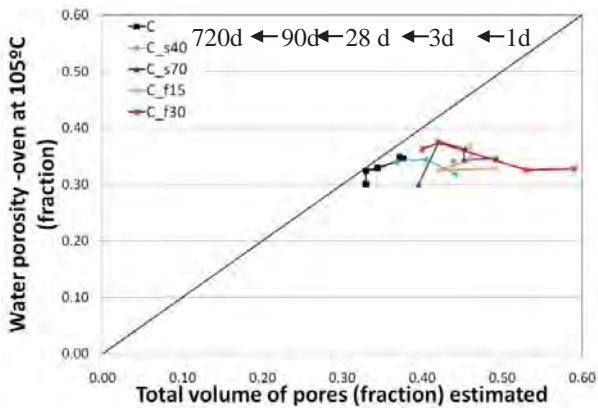
Fig. 5.89: Estimated porosity versus water porosity using oven at 105ºC. Days and curing conditions are given in the Table 5.16

Predictions made by GEMs were also compared with data given by LTC, MIP and SEM for similar pastes cured saturated at 20ºC. Fig. 5.90 show lower values for porosity measured by the selected methods, than predicted by GEMs. It seems that the porosity of SCMs is overestimate by the predictions made by GEMs. A better agreement was found for plain cement paste measured by MIP and predicted by GEMs.
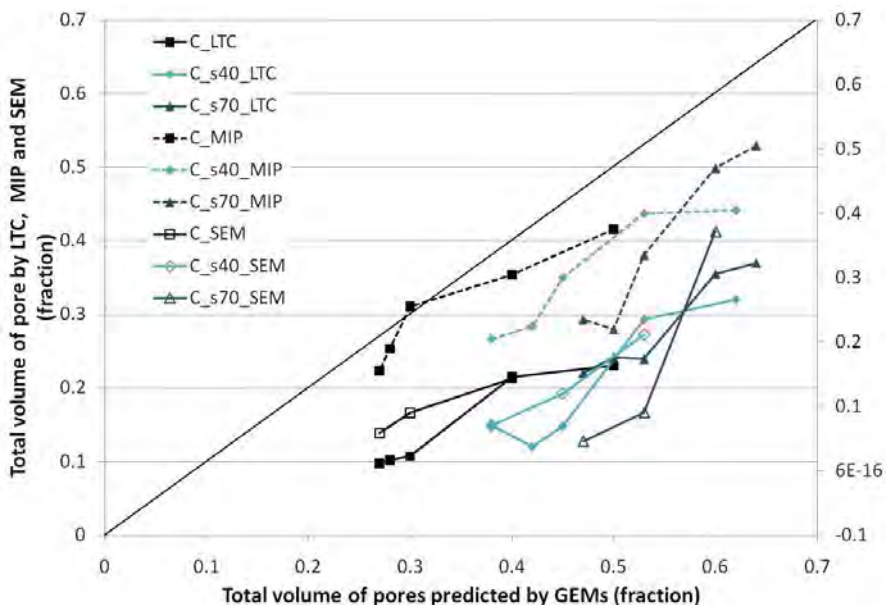
Fig. 5.90: Total volume of pores by LTC (full line with market), MIP (broken line) and SEM (full line without market) versus total volume of pores predicted by GEMs in volume fraction for similar pastes cured saturated at 20ºC

Pore size distribution for similar pastes cured saturated for 28 and 720 days tested using varying methods is shown in the Fig. 5.91 and 5.92.

Figs. 5.91 and 5.92 shows that total volume of MIP and water sorption in the range from 0.3 to 0.004 µm (smaller pores) may be overestimated, especially for samples cured for 28 days. Both methods, MIP and water sorption may be affected by "ink bottle" pores, where the smaller pores can only be entered through larger pores. LTC curves indicated lower values of pores when compared with MIP. This is also showed by Sun and Scherer (2010); the author suggested that the smaller pores are not entered by ice when LTC is used. Moreover, dried sample is used for testing MIP, where a coarsening of the pores may occur. LTC and MIP have a better agreement in the curves of pore size distribution for pastes cured for 720 days than for pastes cured at 28 days. The correction of block temperature (-3°C, see section 5.1.2) due to freezing point depression and non equilibrium of temperature between block and sample may shifted the curves of pore size distribution. It seems that the correction is different from sample to sample. According to Puertas el al.(2004) the effect of freezing point depression may be less for pastes with slag due to the decrease of Na^+ from the pore solution. For water sorption, only a small range of RH humidity (above 50%) where capillary condensation takes place can be relate to the pores size. In the case of the present results, the range from 58% to 97% RH was used. A smaller volume of pore was detected in this range when compared with MIP and LTC (Fig. 5.91 and 5.92).
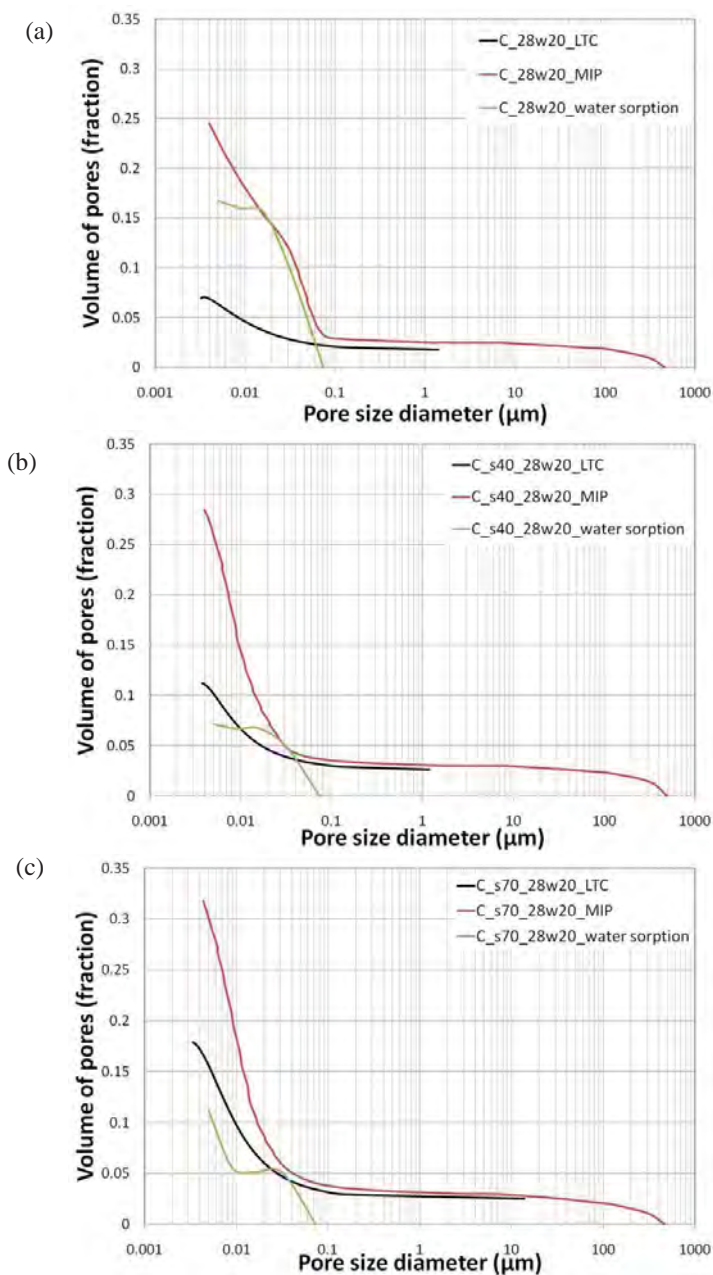
Fig. 5.91: Pore size distribution for pastes with and without slag cured saturated at 20ºC for 28 days using LTC, MIP and water sorption
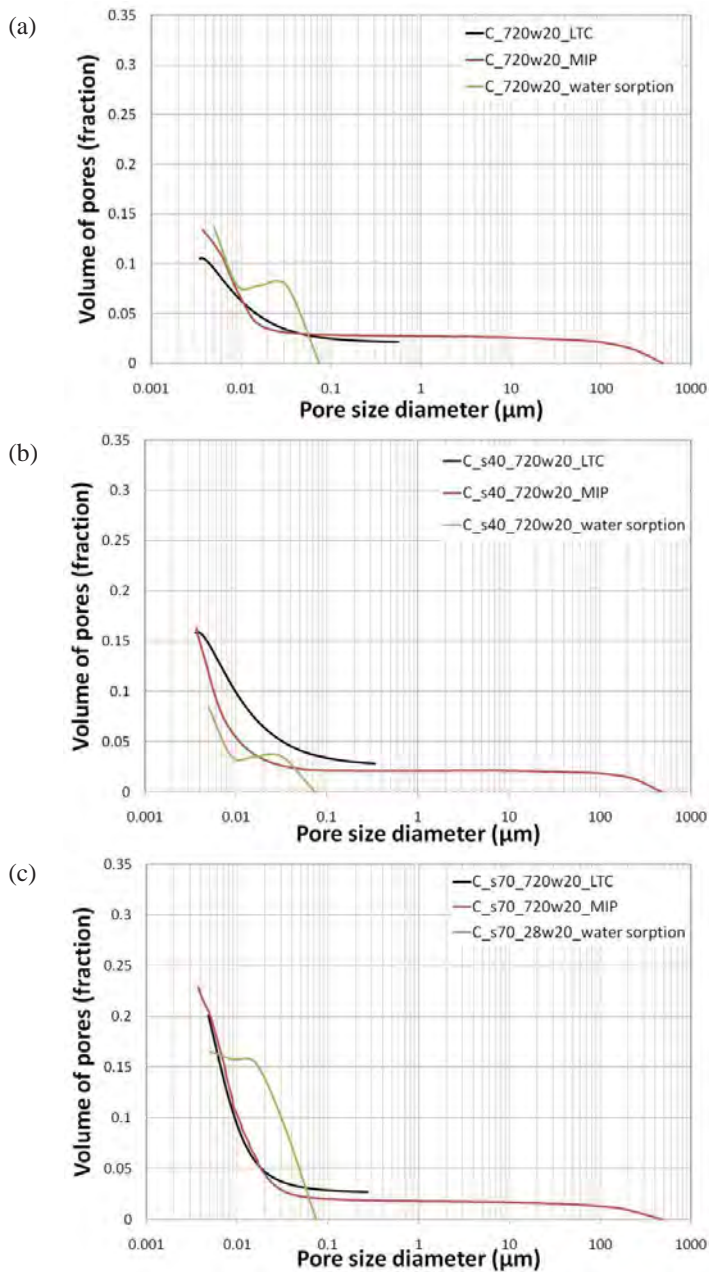
Fig. 5.92: Pore size distribution for pastes with and without slag cured saturated at 20ºC for 28 days using LTC, MIP and water sorption

Based on the data above was possible to draw out some important points for porosity measurements by LTC, MIP, SEM and water sorption regarding to:

- Sample preparation (casting, curing and conditions)
- Measuring
- Assessment of results

Sample preparation
Sample preparation should be carried out using ways to avoid impacts (e.g. bleeding, leaching, and carbonation) on the porosity. Procedure were prepared in the present project describing possible ways to limit the amount of for instances carbonation and leaching on cement pastes, see Appendix II. Proposals to limit effects on the porosity of the tested sample are described in the Table 5.17.

Table 5.17: Proposals to limit the impact of leaching, bleeding, carbonation and drying on the porosity

Effect	Porosity	Proposal
Leaching	Larger	Use of calcium hydroxide saturated solution for during saturated curing Limit the amount of solution during the saturated curing
Bleeding	Larger on the top Lower on the bottom	Use of a lower water/cement ratio Check the porosity of the pastes (top, middle, bottom of the specimen). If there are changes on porosity, remove the affected part (e.g. top and bottom). Use mortar or concrete
Carbonation	Larger	Keep the samples in sealed moulds during the curing Avoid crushing the samples Avoid drying the samples and keep them in desiccators for long time
Drying	Larger	Use solvent (isopropyl) as a drying method

Measuring
For the measurement of the porosity, it is suggested the use of at least two similar samples to evaluate the accuracy of the results. Also the use of more than one porosity method, the methods may to some extend complement each other as different ranges of pores are measured. General proposals are given in the Table 5.18.

Table 5.18: Proposals for the measurements

Method	Matters of consideration	Proposal
LTC	Number of cycles	Use of one freeze/thaw cycle due to the difficulty to control maximum temperature at the end of the first cycle when using large samples (55x ø15 mm) and to limit duration the testing
	Reference cell	Use of empty reference cell.
	Accuracy of the data: first peak of freezing curve (0 to -20ºC) may vary when similar samples are tested	Limit the water evaporation from the samples surface during weighing (before the test) by use of weighing glass and limit the time between weighing and measurement
MIP	Drying of the sample	Use solvent exchange by isopropyl followed by vacuum drying. Gentlest method for drying cementitious materials (Beaudoin et al., 1998, Beaudoin and Tamtsia, 2004, Kocaba, 2009).
	Sample size	Particles larger than 0.5 mm (Bager and Sellevold, 1975)
SEM	Sample preparation	Drying see "MIP". Impregnation and polishing are difficult and time spending steps. They required some experience and good equipments.
	Parameters used for imaging	Walk distance of about 10 mm and voltage of 15kV for images at 1000x
Water sorption	Sample size	Use of samples in slices or larger grains to avoid carbonation and effect of the increased specific surface area
	Sample age	Testing of old samples to avoid continuous hydration
	Time of testing: approx. six months to obtain equilibrium of the samples.	Use of dynamic sorption instead of salt solutions to save time

Assessment of the results

For the assessment of the results, a nomenclature for a given range of pores measured is suggested to be established A broad range of different names and size for pores are found in the literature (IUPAC, 1998, Mehta and Monteiro, 2006, Mindness et al., 2002). The use of the same nomenclature for the size of the pores tested by different methods will avoid misleading of the porosity data. An example of the nomenclature is given in the Table 2.1(e.g. gel pores in the range of 0.001 and 0.004 µm). Proposals for the assessment of the results are described in the Table 5.19.

Table 5.19: Proposals to limit the impact of leaching, bleeding, carbonation and drying on the porosity

Method	Parameter	Proposal
LTC	Sample temperature	Correction of temperature difference between the sample and the block. This correction depends on the amount of water from the samples, the freezing/heating rate and equipment set up
	Parameters for Kelvin Equation	According to e.g. Sun and Scherer (2010)
	Calculation of the baseline	According to e.g. Sun and Scherer (2010)
	Threshold pore size	Temperature of the peak starts from the freezing curve. Block temperature is converted to pore size by Kelvin Equation (assuming cylindrical pore shape) plus the t-layer (adsorbed layer) size (correction of the block temperature is necessary)
	Total pore volume	Total volume of ice formed during freezing multiplied by the bulk density of the material (obtained e.g. by MIP). Calculation of the baseline is proposed according to e.g. Sun and Scherer (2010)
	Pore size distribution	Heating curve of apparent heat capacity versus block temperature. Apparent heat capacity is converted into amount of pores and block temperature into pore size (correction of the block temperature is necessary)
MIP	Contact angle	Use high value (130 to 140º) when gentle drying is applied (Yassin, 2010)
	Results	Use of threshold pore size and not the pore size from the pressure curves.
	Threshold pore size	Intersection of the two tangents to the curve of cumulative pore volume versus pressure. Pressure is converted into pore size by the Washburn Equation (assuming cylindrical pore shape)
	Total pore volume	Highest cumulative pore volume of mercury measured multiplied by the bulk density of the sample.
SEM	Total volume of pores	Total volume of dark pixels from the images compared with the overall number of pixels. Programs (e.g. Ipiwin) can be used for thresholding and calculation of the volume of pores(2010a)
	Thresholding of grey level histogram	If it is made automatically it should be checked for possible mistakes of "thresholding" the pore area (darker pixels) from the grey level histogram.
Water sorption	Total pore volume	Total volume of water desorbed or absorbed multiplied by the bulk density of the material (obtained by e.g. MIP)
	Pore size distribution	Pore size is calculated based on the relative humidity by Kelvin Equation (assuming cylindrical pore shape) plus the t-layer (adsorbed layer) size.

6 Conclusion

The pore structure of hydrated cementitious materials was determined for different cement blended pastes by different methods (low temperature calorimetry (LTC), mercury intrusion porosimetry (MIP), scanning electron microscopy (SEM), water sorption). The main objectives of the thesis were following:

- Determine the porosity in hydrated cement pastes with SCMs;

- Determine the porosity in hydrated cement pastes cured at different moisture and temperature conditions;

- Characterize the porosity in cementitious materials by selected methods;

- Modelling of phase composition for the hydrated pastes;

Moreover to clarify and limit the errors in the interpretation of pore structure often seen in the literature, the presented thesis provides a guideline for porosity measurements and assessment of the data.

The conclusions were drawn according to the three main parts:
- Materials (supplementary cementitious materials)
- Curing conditions (moisture and temperature)
- Methods

Materials (supplementary cementitious materials)
The present work has showed the effect of SCMs (slag and fly ash) in the pore structure of cement pastes by different methods (e.g. LTC, MIP, SEM and water sorption). The data presented here are limited by the physical and chemical properties of the materials used, and the chosen moisture (sealed and saturated) and temperature (20 and 55ºC) curing conditions.

The decrease in both, threshold and total pore volume, with time was observed for pastes cured saturated at 20ºC.Semi quantitative analysis by LTC showed the shift of pore size from capillary to gel for the pastes cured from 3 to up to 720 days. Also, the amount of adsorbed water and gel pores increased with curing time for pastes tested by water sorption.

Type and percentage of SCMs addition contributes to the variance in the pore structure parameters. Results presented here, indicated that slag causes a refinement of pores illustrated by a decreased threshold pore size for a given intruded volume for pastes cured saturated at 20ºC for 28 days or more. SEM showed different morphology for plain cement and slag pastes. For slag pastes, high amount of unhydrated grains was observed at early age (3 days). For older slag pastes (28 and 720 days), a lighter C-S-H from slag reaction and blocked pores were formed. Micro-cracks were found when the pastes cured for 720 days were impregnated to be tested by SEM. The cracks were more evidence for pastes with slag and cured at 20ºC. This may be explained by data from autogenous deformation which indicated that an expansion followed by shrinkage of the volume occurred for pastes with slag addition.

Conclusion

Based on these experimental, the pore structure of slag pastes seems to consist of a new family of rather larger pores with small openings. The particularly benefits of refining of pore threshold showed for slag pastes produce a drive for the use of this material to enhance the durability of concrete structures. Generally, higher threshold pore size was found for fly ash than for plain cement and slag paste.

Curing conditions (moisture and temperature)
The proposed work has evaluated the porosity of the pastes exposed to different moisture (sealed and saturated) and temperature (20 and 55ºC) conditions.

The impact of temperature is clearly seen by the coarsening of the pore structure parameters of the plain pastes cured after 28 days. Important contribution of slag addition was observed at increased temperature, where a reduced total volume of pores is observed as opposed to what is observed for plain cement paste. LTC showed a large peak in the range of capillary pores for plain cement paste cured at 55ºC at 720 days, whereas for slag pastes cured at 55ºC was shown decreased volume and threshold parameters. SEM showed an increase in relative C-S-H brightness indicating a higher C-S-H density for pastes cured at high temperature.

The effect of moisture conditions was mainly accomplished by MIP. The effect of moisture seems to not be clear for pastes cured before 28 days. After 28 days, higher porosity values were found for pastes cured sealed when compared with saturated curing conditions. De-percolation of the pores was found for the pastes cured sealed, it may be caused by self-desiccation. Curing of fly ash paste at sealed conditions caused an increase of total volume (at similar threshold pore size).

Methods
The porosity characterization presented focuses on selected methods often used for hydrated cementitious materials (LTC, MIP, SEM and water sorption).

Important pore structure parameters (e.g. pore volume and threshold pore size) related to mechanical properties and durability of the pastes were determined by the selected methods. Threshold pore size is the size of pores providing entry to the pore network and thus one of particularly importance parameters in the controlling the transport of substance in the material. For pore characterization, it is recommended to use a combination of methods. The assumptions and mechanisms of the tests may have a significant impact on the data and they have been discussed at length in this work: difficulty in precisely defining physical parameters to be applied in the Equations, intrusion of different liquids (water, solvent, mercury), differences caused by the moisture state of the paste and etc.

When testing porosity consideration should be given to possible experimental errors: avoid leaching, bleeding and carbonation of samples during the samples preparation and testing; and if drying is required the use of a more gentle method as solvent exchange by isopropyl is suggested.

There are fundamental differences in the nature of the pores measured by the selected methods; however as the first approximation of porosity the use of a fast, simple and non costly method such as MIP may give the best estimation of the pore system of the paste and it is useful for comparison between samples. The test provides information on the maximum size of the connected pores and the total volume of capillary pores. In the assessment of MIP data the impact of preconditioning the sample, the test conditions, the range of pore sizes measured as well as the assumptions made in the

data analysis should be taken into account. In combination with MIP, other methods such as LTC may be used for semi quantitative characterization of non dried sample. Porosity could be estimated by thermodynamic modelling by GEMs. However, complexities of hydrated system increase when slag is added; predictions showed instabilities for slag system and a significant larger volume of pores when compared with the selected methods.

Noticing the discrepancy in the data showed in the literature and the lack of the standards for porosity measurements. This thesis proposed a guideline with information on sample preparation, measurements and assessment of the data for the selected methods.

7 References

A.C.I., Farzam, H., Bollin, G., Gibbe, F. K., Henry, R. L., Hogan, M. B., Holub, E. P., Howe, R. H., Isabelle, H. L., Kaetzel, L. J., Khan, T. S., Libby, J. R., Luther, M. D., Marin, J., Mather, B., Meseguer, A. G., Mielenz, R. C., Morgan Jr, A. H.and Rutenbeck, T. (2004) Cement and concrete terminology. *ACI Committee 116*, 1-74.

ACI224R-01 (2001) Control of cracking in concrete structures. *American Concrete Institute* 1-46.

Al-Amoudi, O. S. B., Maslehuddin, M.and Abiola, T. O. (2004) Effect of type and dosage of silica fume on plastic shrinkage in concrete exposed to hot weather. *Construction and Building Materials* 18, 737-743.

Aligizaki, K. K. (2006) *Pore structure of cement-based materials: testing, interpretation and requirements*.

Aono, Y., Matsushita, F., Shibata, S.and Hama, Y. (2007) Nano-stuctural changes of C-S-H in hardened cement paste during drying at 50ºC. *Journal of Advanced concrete technology,* 3, 313-323.

ASTM-C1698–09 (2009) Standard Test Method for Autogenous Strain of Cement Paste and Mortar1. *ASTM International*, 1-8.

ASTMC618-08a (2008) Standard Specification for Coal Fly Ash and Raw or Calcined Natural Pozzolan for Use in Concrete. IN INTERNATIONAL, A. (Ed.) West Conshohocken.

Atkins, P. W. (1997) Physical Chemistry. 5.

Atkins, P. W., Bennett, D. G., Glasser, F. P., Kindness, A.and Read, D. (1992) A Thermodynamic model for blended cements. *Cement and Concreat Research,* 22, 497-502.

Atkins, P. W.and Glasser, F. P. (1992) A thermodynamic model for blended cements. II: Cement hydrate phases. *Journal of Nuclear Materials* 190, 315-325.

Atlassi, E. H. (1993) A Quantitative thermogravimetric study on the nonevaporable water in mature silica concrete. *Building Materials.* Goteborg, Chalmers Tekniska Hogskola.

Bager, D. H. (1984) Ice formaiton in hardened cement pastes. *Departament of civil engineering.* Kgs. Lyngby, Technical University of Denmark.

Bager, D. H. (1987) Ice formation in hardened cement paste, Part III - slow resaturation of room temperature cured pastes. *Cement and Concreat Research,* 17, 1-11.

Bager, D. H.and Hansen, T. B. (2000) Influence of water binding on the ice formation and freeze/thaw damage in cement paste and concrete. 1-14.

Bager, D. H.and Sellevold, E. (1986a) Ice formation in hardened cement paste, Part I - room remperature cured pastes with variable moisture contents. *Cement and Concreat Research,* 16, 709-720.

Bager, D. H.and Sellevold, E. J. (1975) Mercury porosimetry of hardened cement paste: The influence of particle size. *Cement and Concrete Research,* 5, 171-178.

Bager, D. H.and Sellevold, E. J. (1986b) Ice formation in hardened cement paste, Part II - drying and resaturation on room temperature cured pastes. *Cement and Concrete Research,* 16, 835-844.

Bakhshi, M.and Mobasher, B. (2011) Experimental observations of early-age drying of Portland cement paste under low-pressure conditions. *Cement & Concrete Composites* 33, 474-482.

Balonis, M. (2010) The Influence of Inorganic Chemical Accelerators and Corrosion Inhibitors on the Mineralogy of Hydrated Portland Cement Systems. *Department of Chemistry.* Aberdeen, University of Aberdeen.

Balonis, M.and Glasser, F. P. (2008) The Density of Cement Substances *Nanocem articles.*

References

Baroghel-Bouny, V. (1994) Caracteérisation des pâtes de ciment et des bétons: Méthodes, Analyse, Interprétations. *Microstructure et Durabilité des Bétons.* Paris, Ponts et Chaussées.

Baroghel-Bouny, V. (2007a) Water vapour sorption experiments on hardened cementitious materials Part I: Essential tool for analysis of hygral behaviour and its relation to pore structure. *Cement and Concrete Research* 37**,** 414-437.

Baroghel-Bouny, V. (2007b) Water vapour sorption experiments on hardened cementitious materials. Part II: Essential tool for assessment of transport properties and for durability prediction. *Cement and Concrete Research* 37**,** 438-454.

Battelle (2002) Toward a sustainable cement industry. *Climate Change substudy Report***,** 25-32.

Beaudoin, J. J., Gu, P., Marchand, J., Tamtsia, B., Myers, R. E.and Liu, Z. (1998) Solvent Replacement Studies of Hydrated Portland Cement Systems: The Role of Calcium Hydroxide. *Advanced Cement Based Materials,* 8**,** 56-65.

Beaudoin, J. J., Tamtsia, B., Marchand, J.and Myers, H. R. (2000) Solvent exchange in partially saturated and saturated microporous systems Length change anomalies. *Cement and Concrete Research,* 30**,** 359-370.

Beaudoin, J. J.and Tamtsia, T. B. (2004) Effect of Drying Methods on Microstructural Changes in Hardened Cement Paste: an A. C. Impedance Spectroscopy Evaluation. *Advanced Concrete Technology,* 2**,** 113-120.

Belie, N. D., Kratky, J.and Vlierberghe, S. V. (2010) Influence of pozzolans and slag on the microstructure of partially carbonated cement paste by means of water vapour and nitrogen sorption experiments and BET calculations. *Cement and Concrete Research* 40**,** 1723-1733.

Bentur, A.and Berger, R. L. (1979) Structural properties of calcium silicate pastes: Effect of curing temperature. *Journal of the American Ceramic Society* 62**,** 362-366.

Bentz, D. P. (1999) Modelling cement microsturcture:Pixels, particles and property prediction. *Materials and Structures,* 32**,** 187-195.

Bentz, D. P. (2007) Internal Curing of High-Performance Blended Cement Mortars. *ACI Materials Journal,* 104**,** 408 -414

Bentz, D. P., Jensen, O. M., Coats, A. M.and Glasser, F. P. (2000) Influence of silica fume on diffusivity in cement based materials I. Experimental and computer modeling studies on cement pastes. *Cement and Concreat Research,* 30**,** 953-962.

Bentz, D. P.and Stutzman, P. E. (2006) Curing, Hydration, and Microstructure of Cement Paste. *ACI Materials Journal,* 103**,** 348-356.

Bentz, D. P.and Stutzman, P. E. (2008) Curing, Hydration, and Microstructure of Cement Paste. *ACI Materials Journal,* 103**,** 348-356.

Bijen, J. (1996) Benefits of slag and fly ash. *Con.wuction and Building Materials,* 10**,** 309-314.

Blachere, J. R.and Young, J. E. (1972) The freezing point of water in porous glass. *American Ceramic Society,* 55**,** 306.

Bogdana, A. (1996) Thermodynamics of the curvature effect on ice surface tension and nucleation theory. IN DEPARTMENT OF PHYSICS, U. O. H. (Ed.) Finland.

Broekhoff, J. C. P. (1969) Sorption and Capillarity.

Brown, M. L., Jennings, H. M.and Ledbetter, W. B. (1990) On the generation of heat during the mixing of cement pastes. *Cement and Concrete Research,* 20**,** 471-474.

Brun, M., Lallemand, A., Quinson, J. F.and Eyraud, C. (1977) A new method for the simultaneous determination of the size and shape of pores: the thermoporometry *Thermochimica Acta* 21**,** 59-88.

Brunauer, S., Mikhail, R. S.and Bodor, E. E. (1967) Some Remarks about Capillary Condensation and Pore Structure Analysis. *Journal of Colloid and Interface Science* 25**,** 353-358.

Byfors, J. (1980) Plain concrete at early ages. *Swedish cement and concrete research institute - Stockholm, Sweden*.

Canada, C. A. o. (2006) Drying Rate of Concrete.

Canut, M. M. (2007) Preliminary guidelines for characterization of porosity of cement based materials. *Nanocem - Task 3.1*. DTU.

Canut, M. M.and Geiker, M. R. (2011) Impact of curing on the porosity development of cement pastes with and without slag *XIII International Congress on the Chemistry of Cement*. Madrid.

Cao, Y., Detwiler, R. J., Cao, Y., Detwiler, R. J., Cao, Y.and Detwiler, R. J. (1995) Backscattered electron imaging of cement pastes cured at elevated temperatures. *Cement and Concrete Research,* 25**,** 627-638.

Carde, C.and Francois, R. (1997) Effect of leaching of calcium hydraoxide from cement paste on mechanical and physical properties. *Cement and Concrete Research,* 27**,** 539-550.

Carlier, J.-P., Yang, H.and Burlion, N. (2009) Experimental and numerical study of water sorption in cementitious materials. *CONCREEP 8 - Creep, Shrinkage and Durability Mechanics of Concrete and Concrete Structures.* Ise-Shima, Japan.

Cebeci, O. Z.and Received June 4, a. M., 1980 (1980) The Intrusion of Conical and Spherical Pores in Mercury Intrusion Porosimetry. *Journal of Colloid and Interface Science* 78.

Chen, W.and Brouwers, H. J. H. (2007) The hydration of slag, part 2: reaction models for blended cement. *Jornal Materias Science,* 42**,** 444-464.

Chini, A. R., Muszynski, L. C.and Hicks, J. (2003) Determination of Acceptance Permeability Characteristics for Performance Related Specifications for Portland Cement Concrete. *Department of Civil Engineering.* University of Florida.

Cobanoglu, I., Celik, S. B., Dincer, I.and Alkaya, D. (2009) Core size and time effects on water absorption values of rock and cement mortar samples. *Bull Eng Geol Environ,* 68**,** 483-489.

Cook, D. J. (1986) Natural pozzolans. IN SWAMY, R. N. (Ed.) *Cement replacement materials.* London, Balckie & Son Ltd - University of Surrey.

Cook, R. A.and Hover, K. C. (1991) Experiments on the contact angle between mercury and hardened cement paste. *Cement and Concrete Research,* 21**,** 1165-1175.

Cook, R. A.and Hover, K. C. (1993) Mercury porosimetry of cement-based materials and associated correction factors. *Construction and Building Materials* 7.

Corr, S. J. L., J. Monteiro, P. M., Bastacky, S. J.and Gartner, E. M. (2002) Air void morphology in fresh cement pases. *Cement and Concrete Research,* 32**,** 1025-1031.

Darquennes, A., Staquet, S., Delplancke-Ogletree, M. P.and Espion, B. (2011) Effect of autogenous deformation on the cracking risk of slag cement concretes. *Cement & Concrete Composites* 33**,** 368-379.

Darquennes, A., Staquet, S.and Espion, B. (2009) Autogenous shrinkage development and setting monitoring of slag cement concrete. *CONCREEP 8 -Creep, Shrinkage and Durability Mechanics of Concrete and Concrete Structures* Ise-Shima, Japan.

Day, R. L.and Marsh, B. K. (1988) Measurement of porosity in blended cement pastes. *Cement and Concrete Research,* 18**,** 63-73.

Defay, R., Prigogine, I., Bellemans, A.and Everett, D. H. (1966) Surface Tension and Adsorption.

Dehoff, R. T.and Russ, J. C. (2000) *Practical Stereology,* New York, Plenum Press.

Dewaele, P. J., J., R. E.and Dayal, R. (1991) Permeability and porosity changes associated with cement grout carbonation. *Cement and Concrete Research,* 27**,** 441-454.

Diamond, S. (1971) A critical comparison of mercury porosimetry and capillary condensation pore distribution of Portland cement pastes. *Cement and Concreat Research,* 1**,** 445-531.

References

Diamond, S. (1995) Pore size distribution in hardened cement paste. *Materials research society symposium proceedings,* 370**,** 217-226.

Diamond, S. (1999) Aspects of concrete porosity revised. *Cement and Concrete Research,* 29**,** 1181-1188.

Diamond, S. (2001) Reply to the discussion by S. Wild of the paper:Mercury porosimetry-an inappropriate method for the measurement of pore size distributions in cement-based materials&quot. *Cement and Concrete Research,* 31**,** 1655-1656.

Diamond, S. (2000) Mercury porosimetry : An inappropriate method for the measurement of pore size distributions in cement-based materials. *Cement and Concrete Research,* 30**,** 1517-1525.

Diamond, S.and Leeman, M. E. (1995) Pore size distribution in hardened cement paste by SEM image analysis. *Materials research society symposium proceedings,* 370**,** 217-226.

Dictionary, W. s. (2010) Capillary tube.

Dorsey, N. E. (1954) Spontaneous Freezing of Water. *The Scientific Monthly,* 78**,** 283-288.

Dufay, R., Prigogine, I., Bellemans, A.and Everett, D. H. (1966) Surface Tension and Adsorption.

Escalante-Garcia, J. I.and Sharp, J. H. (2001) The microstructure and mechanical properties of blended cements hydrated at various temperatures. *Cement and Concreat Research,* 31**,** 695-702.

Espinosa, R. M.and Franke, L. (2006) Influence of the age and drying process on pore structure and sorption isotherms of hardened cement paste. *Cement and Concrete Research,* 36**,** 1969-1984.

Everett, D. H.and Haynes, J. M. (1965) *Bulletin RILEM* 27**,** 31.

Fagerlund, G. (1973) Determination of pore-size distribution from freezing-point depression. *Materials and Structures,* 33**,** 215-225.

Fagerlund, G. (1994) Frost resistance of high perfomance concrete some theoretical consideration. IN RILEM-3C-WORKSHOP (Ed.) *Durability of High Performance Concrete.* Wien.

Feldman, R. (1984) Pore structure damage in blended cements caused by mercury intrusion. *Journal of the American Society,* 67**,** 30-33.

Feldman, R. F. (1981) Pore structure formation during hydration of fly ash and slag cement blend. *Symposium N, materials research society annual metting.*

Feldman, R. F. (1986a) A discussion of the paper.contact angle and damage during mercury intrusion into cement paste by Dexiang Shi and Douglas N. Winslow. *Cement and Concrete Research,* 16**,** 452-454.

Feldman, R. F. (1986b) Pore Structure, Permeability and Diffusivity as Related to Durability. *8th International Congress on the Chemistry of Cement.* Rio de Janeiro, Brazil.

Feldman, R. F. (1987) Diffusion measurements in cement pastes by water replacement using propan-2-ol. *Cement and Concreat Research,* 17**,** 602-612.

Feldman, R. F.and Beaudoin, J. J. (1991) Pretreatment of hardened hydrated cement pastes for mercury intrusion measurements. *Cement and Concrete Research,* 21**,** 297-308.

Feldman, R. F.and Sereda, P. J. (1968) A model for hydrated Porland cement as deduced from sortption length change and mechanical properties *Matériaux et Construction,* 1.

Feldman, R. F.and Sereda, P. J. (1970) A new model for hydrated portland cement and its pratical implications. *Engineering Journal (Canada),* 53**,** 53-59.

Fernandez- Altable, V. (2010) Hydration of slag blended cements - power point presentation. IN ATTACK, M.-R. G. A. S. (Ed.) *Theme coordination Meeting January 2010.* Lausanne.

Fischer, R.and Kuzel, H. J. (1982) Reinvestigation of the system C4A·nH2O–C4A·CO2·nH2O. *Cement and Concrete Research,* 12**,** 517.

Fontenay, C. S.and Sellevold, E. (1980) Ice formation in hardened cement pastes -Durability of Building Materials and Components. *ASTM STP* 691**,** 425-454.

Fraaij, A. L. A., Bijen, J.and Haan, Y. M. (1989) The reaction of fly ash in concrete. A critical examination. *Cement Concr. Res.*

Fridh, K. (2005) Internal frost damage in concrete - Experimental studies of destruction mechanisms. *Division of Building Materials.* Lund, Lund University.

Galle, C. (2001) Effect of drying on cement-based materials pore structure as identified by mercury intrusion porosimetry - A comparative study between oven-, vacuum-, and freeze-drying. . *Cement and Concrete Research,* 31**,** 1467-1477.

Gallucci, E. (2007a) High resolution microscopies SEM, TEM and AFM. *MC-RTN training course 2 - Ljubljana,* Lecture 07.

Gallucci, E. (2007b) Stop hydration of cement paste.

Gallucci, E., Mathur, P.and Scrivener, K. (2010) Microstructural development of early age hydration shells around cement grains. *Cement and Concrete Research* 40**,** 4-13.

Gallucci, E., Scrivener, K., Groso, A., Stampanoni, M.and Margaritondo, G. (2007) 3D experimental investigation of the microstructure of cement pastes using synchrotron X-ray microtomography (μCT). *Cement and Concrete Research* 37**,** 360-368.

Garboczi, E. J.and Bentur, A. (1996) Modelling of the microstructure and transport properties of concrete. *Contruction and Building Materials,* 10**,** 293-300.

Geiker, M. (1983) Studies of Portland cement hydration by measurements of chemical shrinkage and systematic evaluation of hydration curves by means of the dispersion model. *Institut of Mineral Industry.* Kgs. Lyngby, Technical University of Denmark.

Geiker, M. (1999) Effect of temperature and alkali content on the hydration of selected cementitious systems. IN RESEARCH, N. C. (Ed.) *Nordic Miniseminar.* Skagen.

Gervais, C., Garrabrants, A. C., Sanchez, F., Barna, R., Moszkowiscz, P.and Kosson, D. S. (2004) The effects of carbonation and drying during intermittent leaching on the release of inorganic constituents from a cement based matrix. *Cement and Concrete research* 34**,** 119-131.

Gibbs, J. W. (1993) The scientific papers of J. Willard Gibbs. *Thermodynamics 1.*

Goodhew, P. J., Humphreys, J.and Beanland, R. (2000) *Electron Microscopy and Analysis,* London

Goto, S.and Roy, D. M. (1981) The effect of w/c ratio and curing temperature on the permeability of hardened cement paste. *Cement and Concrete Research,* 11**,** 575-579.

Griesel, E. J. M.and Alexander, M. G. (2001) Effect of Controlled Environmental Conditions on Durability Index Parameters of Portland Cement Concretes
23**,** 1-6.

Griesser, A. (2002) Cement-Superplasticizer Interactions at Ambient Temperatures - Rheology, Phase Composition, Pore Water and Heat of Hydration of Cementitious Systems. *Technical Sciences.* Swiss Federal Institure of Technology.

Gutteridge, W. A.and Dalziel, J. A. (1990) Filler cement: the effect of the secondary component on the hydration of Portland cement: part I. A fine non-hydraulic filler. *Cement and Concrete Research,* 20**,** 778-782.

Gutteridge, W. A.and Parrott, L. J. (1976) A study of the changes in weight, length and interplanar spacing induced by drying and rewetting synthetic CSH (I). *Cement and Concrete Research,* 6**,** 357-366.

Haerdlt, R. (2008) Principle of fly ash reaction. *Nanocem articles.*

Hagymassy, J., Brauner, S. J.and Mikhail, R. S. (1969) Pore strucutre by water vapor adsoprtion. *J.Colloid Surface Science,* 29**,** 485.

References

Haha, M. B., Bary, P. B., Gallucci, E.and Scrivener, K. (2009) Quantitative microstructural characterisation of cement paste submitted to different moderate temperature and loading conditions. *CONCREEP 8 - Creep, Shrinkage and Durability Mechanics of Concrete and Concrete Structures* Ise-Shima, Japan.

Halsey, G. D. (1952) On Multilayer Adsorption. *American Chem. Soc.,* 74**,** 1082

Hansen, P. F.and Pedersen, E. J. (1977) Measuring instrument for the control of concrete hardening. *Nord Betong***,** 21-25.

Hansen, T. B., Thrylsøe, J., Simmelsgaard, P. A.and Jespen, M. T. (2000) Experimental characterization of porous materials. *Aalborg Portland Cement***,** 1-100.

Hansen, T. C. (1986) Physical strucutre of hardened cement paste. *Materaux et Constructions,* 19**,** 423-436.

Hansen, W. C. (1963) Porosity of hardened Portland cement paste. *ACI Journal***,** 141-155.

Hansenb, W.and Panea, I. (2005) Investigation of blended cement hydration by isothermal calorimetry and thermal analysis. *Cement and Concrete Research* 35**,** 1155-1164.

Haynes, J. M. (1973a) Determination of pore properties of constructional and other materials – General introduction and classification of methods. . *Rilem Materials and Structural – 15 Rilem Technical Committee,* 6**,** 169-174.

Haynes, J. M. (1973b) Stereological analysis of pore structure. *Rilem Materials and Structural – 15 Rilem Technical Committee,* 6**,** 175-179.

Hedenblad, G. (1993) Moisture permeability of mature concrete, cment mortar and cement paste. *Division of Building Maerials.* Lunds, Institute of Technology.

Hedenblad, G. (1997) Drying of construction water in concrete. *Swedish Council for Building Research.* Stockholm.

Henrichsen, A., Laugesen, P., Geiker, M., Pedersen, E. J.and Thaulow, N. (1997) Hetek - Frostaprøvningsmetoder til bestemmelse af højkvalitetsbetons frostbestandighed. *HETEK - Report n.105*.

Hesstvedt, E. (1964) The interfacial energy ice/water. *Norwegian Geothecnical Institute,* 56**,** 7.

Hooton, R. D. (1986) Permeabilidade and pore structure of cement pastes containing slag. fly ash and silica fume. *ASTM Special Technical Publication***,** 128-143.

Hooton, R. D. (2010 (in press)) Concrete and durability and sustainability as influenced by resistance to fluid ingress and selection of cementitious materials. IN ENVIRONMENTS, C. U. S. (Ed.) *CONSEC 10.* Merida, Mexico.

Horsewell, A. (2010) Electron Microscopy for Materials Science Lesson 2. *Scanning electron microscopy Phd. course / DTU Mechanical Engineering*.

IUPAC (1998) IUPAC Classification. *International Union of Pure and Applied Chemistry*.

Jakob, W. (2011) Introduction to Transmission Electron Microscopy. *DTU / Center for electron nanoscopy (Cen)*.

Jennings, H. M. (1999) A model for the microstructure of calcium silicate hydrate in cement paste. *Cement and Concrete Research,* 30**,** 101-116.

Jennings, H. M. a. T., Jeffrey J. and Gevrenov, Julia S. and Constantinides, Georgios and Ulm, Franz-Josef (2007) A multi-technique investigation of the nanoporosity of cement paste. *Cement and Concrete Research,* 37**,** 329-336.

Jensen, M. M. (2010a) Optimization of sample preparation for SEM and investigation of pore system characteristics in cement paste. *Civil Engineering.* Kgs. Lyngby, Technical University of Denmark.

Jensen, O. M. (2010b) Power´s model -Lecture. *Doctoral course:Durability of concrete RILEM***,** 1-19.

Jensen, O. M.and Hansen, P. F. (1995) A dilatometer for measuring autogenous deformation in hardening Portland cement paste. *Materials and Structures,* 28**,** 406-409.

Jensen, O. M.and Hansen, P. F. (1999) Influence of temperature on autogenous deformation and relative humidity change in hardening cement paste - I. Modelling at macroscopic scale. *Cement and Concrete Research,* 29**,** 567-575.

Jensen, O. M.and Hansen, P. F. (2001) Autogenous deformation and RH-change in perspective. *Cement and Concrete Research,* 31**,** 1859-1865.

Jensen, O. M., Hansen, P. F., Lachowski, E. E.and Glasser, F. P. (1999) Clinker mineral hydration at reduced relative humidities. *Cement and Concrete Research*

29**,** 1505–1512.

Jesser, L. (1927) Zement. *Protokoll der Generalversamrnlungen des Veremes der Osterr-Zementjabrikanten,* 16**,** 741.

Jiang, Z., Sun, Z.and Wang, P. (2005) Autogenous relative humidity change and autogenous shrinkage of high-performance cement pastes. *Cement and Concrete Research,* 35**,** 1539-1545.

Johannesson, B. (2002) Prestudy on diffusion and transient condensation of water vapor in cement mortar. *Cement and Concrete Research* 32**,** 955 - 962.

Johannesson, B. (2010) Dimensional and ice content changes of hardened concrete at different freezing and thawing temperatures. *Cement & Concrete Composites,* 32**,** 73-83.

Johannesson, B.and Janz, M. (2002) Test of four different experimetnal methods to determine sorption isotherms. *Journal of materials in civinl engineering*

Kamali, S., Moranville, M.and Leclercq, S. (2008) Material and environmental parameter effects on the leaching of cement pastes: Experiments and modelling. *Cement and Concrete Research,* 38**,** 575-585.

Khoury, G. A. (1992) Compressive strength of concrete at high temperatures: a reassessment. *Mag. Concr. Res.,* 44**,** 291- 309.

Kjeldsen, A. M. (2002) The effect of layer silicates and silica fume on the micro porosity of cement-based materials. *Construction materials.* kgs. Lyngby, Technical Universiy of Denmark.

Kjeldsen, A. M.and Geiker, M. R. (2008) On the interpretation of low temperature calorimetry data. *Materials and Structures* 41**,** 213–224.

Kjellsen, K. O., Detwiler, R. J.and Gjorv, O. E. (1990a) Pore structure of plain cement pastes hydrated at different temperatures. *Cement and Concrete Research* 20**,** 927-933.

Kjellsen, K. O., Detwiler, R. J.and Gjørv, O. E. (1990b) Backscattered electron imaging of cement pastes hydrated at different temperatures. *Cement and Concrete Research,* 20**,** 308-311.

Kocaba, V. (2006) Procedure for mixing of cement pastes. *Prepared for NanoCem Core project 4: Reactivity of blended cement with SCM.***,** 1-4.

Kocaba, V. (2007a) Particle size distribution selected samples. *Nanocem core project 4.*

Kocaba, V. (2007b) Reactivity of blended cements with Supplementary Cementitious Materials. IN 4, C. P. (Ed.), École Polytechnique Fédérale de Lausanne, Lausanne, Switzerland.

Kocaba, V. (2008) Degree of hydration for selected samples cured at 20ºC. IN 4, N. C. P. (Ed.).

Kocaba, V. (2009) Development and evaluation of methods to follow microstructural development of cementitious systems including slags. *Materials Department.* Lausanne, École Politechnique Fedérale de Lausanne.

Konecny, L.and Naqvi, S. J. (1993) The effect of different drying techniques on the pore size distribution of blended cement mortars. *Cement and Concrete Research,* 23**,** 1223-1228.

Korpa, A.and Trettin, R. (2006) The influence of different drying methods on cement paste microstructures as reflected by gas adsorption: Comparison between freeze-drying (F-

drying), D-drying, P-drying and oven-drying methods. . *Cement and Concrete Research,* 36**,** 634-649.

Kosmatka, S. H., Kerkhoff, B., Panarese, W. C., Macleod, N. F.and McGrath, R. J. (2002) Design and control of concrete mixes. . *Engineering bulletin 101***,** 1-348.

Koster, H.and Odler, I. (1986) Investigation on the structure of fully hydrated Portland cement and tricalcium silicate pastes. Bound water, chemical shirinkage and density of hydrates. *Cement and Concrete Research,* 16**,** 207-214.

Krus, M., Hansen, K. K.and Kiinzel, H. M. (1997) Porosity and liquid absorption of cement paste. *Materials and Structures/Materiaux et Constructions,* 30**,** 394-398.

Kubelka, P.and Wenzel, W. (1931) Equilibrium conditions in action of water vapor on methane. *Metallboerse (Supplement to Chemisch-Metallurgische Zeitschrift)* 21**,** 1421-1422.

Kumar, R.and Bhattacharjee, B. (2003a) Porosity, pore size distribution and in situ strength of concrete. *Cement and Concrete Research,* 33**,** 155-164.

Kumar, R.and Bhattacharjee, B. (2003b) Study on some factors affecting the results in the use of MIP method in concrete research. *Cement and Concrete Research,* 33**,** 417-424.

Kurtis, K. E. (2007) Structure of hydrated cement paste. . *Georgia Institute of Technology.* Power point.

Lamberet, S. (2005) Durability of ternary binders based on portland cement, calcium aluminate cement and calcium sulfate. Lausanne, École Polytechnique Fédérale de Lausanne.

Lange, F., Mortel, H.and Rudert, V. (1997) Dense packing of cement pastes and resulting consequences on mortar properties. *Cement and Concrete Research,* 27**,** 1481-1488.

Langmuir;J.I. (1916) The constitution and fundamental properties of solids and liquids. Part I. *Journal of the American Chemical Society,* 38**,** 2221-2295.

Larsen-Helms, T. (2008) Method development: Continuous measurement of capillary suction for cement pastes. *Civil Enginneering.* Kgs. Lyngby, DTU.

Laugesen, P., Geiker, M., Pedersen, E. J., Thaulow, N., Golterman, P.and Frederiksen, J. O. (1997) Method of the frost restistance of high performance concrete. *Hetek - Report n.86.*

Le Sage de Fontenay, C.and Bager, D. H. (1980) Ice formation in hardened cement paste - I. Mature water saturated pastes. *Durability of Building Materials and Components ASTM STP 691 - american Society for Testing and Materials.***,** 425-438.

Le Saout, G. (2007) Main oxides of selected materials. *Personal reference - EPFL.*

Lea, F. M. (2004) *Chemistry of cement and concrete*, Heinemann.

Lee, S. F.and Jacobsen, S. (2010) Sample preparation, image acquisition and image analysis on interfacial transition zone of steel fiber-reinforced mortar. *Tekna*

Lide, D. R. (2005) *CRC Handbook of Chemistry and Physics*.

Lindgreen, H., Geiker, M., Krøyer, H., Springer, S.and Skibsted, J. (2006) Microstructure engineering of Portland cement pastes and mortars through addition of ultrafine layer silicates. *Cement and Concrete Research*.

Lothenbach, B. (2008) Thermodynamic modelling: Database. *Nanocem articles.*

Lothenbach, B.and De Weerdt, K. (2011) GEMs predictions. Lyngby DK.

Lothenbach, B., Matschei, T., Möschner, G.and Glasser, F. P. (2008) Thermodynamic modelling of the effect of temperature on the hydration and porosity of Portland cement. *Cement and Concrete Research,* 38**,** 1-18.

Lothenbach, B., Scrivener, K.and Hooton, R. D. (2010) Supplementary cementitious materials. *Cement and Concreat Research***,** 13.

Lura, P., Van Breugel, K.and Maruyama, I. (2001) Effect of curing temperature and type of cement on early-age shrinkage of high-performance concrete. *Cement and Concrete Research* 31**,** 1867-1872.

Macaulay, W., DiGiovanni, C. W., Restrepo, A., Saleh, K. J., Walsh, H., Crossett, L. S., Peterson, M. G. E., Li, S.and Salvati, E. A. (2002) Differences in Bone-Cement Porosity by Vacuum Mixing, Centrifugation, and H and Mixing. *Journal of Arthroplasty,* 17**,** 569.

Mackenzie, R. C.and Mitchell, B. D. (1961) Differential Thermal Analysis: A Review. *The Macaulay Institute for Soil Research,* 87**,** 420-435.

Maia, L. M., Geiker, M. R.and Figueiras, J. A. (2008) Hydration of Portugueses cements, measurement and modelling of chemical shrinkage *CCC 2008 - Challenges for Civil Construction***,** 1-12.

Malhotra, V. M. (1993) Fly ash, slag, silica fume and rice husk ash in concrete: A Review. *Concrete International***,** 1-8.

Marchand, J., Bentz, D. P., Samson, E.and Maltais, Y. (2001) Influence of calcium hydroxide dissolution on the transport properties of hydrated cement systems. . *Materials Science of Concrete***,** 113-129.

Marsh, B. K.and Day, L. R. (1985) Some difficulties in the assessment of pore structure of high performance blended cement pastes. *Materials research society symposium proceedings,* 42**,** 113-121.

Martys, N. S.and Ferraris, C. F. (1997) Capillary transport in mortars and concrete. *Cement and Concrete Research,* 27**,** 747-760.

McDonald, P. J., Mitchell, J.and Mulheron, M. (2006) Two-dimensional correlation relaxometry studies of cement pastes performed using a new one-sided NMR magnet. *Cement and Concrete Research***,** 1-7.

McDonald, P. J., Mitchell, J. M.and Mulheron, M. M. (2005) Cement Products: Characterisation by NMR and MRI. *School of Electronics and Physical Sciences, and School of Engineering University of Surrey Guildford***,** 1-33.

McDonald, P. J., Rodin, V.and Valori, A. (2010) Intra-C–S–H sheet pores and inter-C–S–H particle gel pores.

Mehta, P. K. (1981) *Fifth International Symposium on Concrete Technology.* Monterrey.

Mehta, P. K. (1986) Condesed silica fume. IN SWAMY, R. N. (Ed.) *Cement replacement materials.* London, Blackie Group - University of Surrey.

Mehta, P. K.and Gjorv, O. E. (1982) Properties of Portland cement concrete containting fly ash and condensed silica fume. *CEM CONCR RES,* V 12**,** 587-595.

Mehta, P. K.and Monteiro, P. J. M. (2006) *Concrete: Microstructure, Properties, and Materials*

Michler, G. H. (2008) *Electron microscope for polymers,* Heidelberg, Springer-Verlag

Micrometrics, I. C. (2000) Auto pore IV 9500. *Part no.950-42801-01.*

Mikhail, R. S.and Abo-El-Enein, S. A. (1972) STUDIES ON WATER AND NITROGEN ADSORPTION ON HARDENED CEMENT PASTES I : DEVELOPMENT OF SURFACE IN LOW POROSITY PASTES. *Cement and Concreat Research,* 2**,** 401-414.

Mindness, S., Young, J. F.and Darwin, D. (Eds.) (2002) *Concrete,* London.

Mjornell, K. N. (1994) Self dessication in concrete. *Institutionen for Bygnadsmaterial.* Goteborg-Sweeden, Chalmers University of Technology

Mohr, B. J.and Hooda, K. L. (2010) Influence of bleed water reabsorption on cement paste autogenous deformation *Cement and Concrete Research,* 40**,** 220-225

Morioka, Y., Kobayashi, Y.and Higuchi, J. (1973) Colloid interface. 42**,** 156.

Neuwald, A. D. (2005) Supplementary cementitious materials. *MC Magazine.*

Neville, A. M. (2002) *Properties of concrete,* London EN, Prentice Hall.

References

Ngala, V. T.and Page, C. L. (1997a) Effect of carbonation on pore structure and diffusional properties of hydrated cement pastes. *Cement and Concrete Research,* 27**,** 995-1007.

Ngala, V. T.and Page, C. L. (1997b) Effects of carbonation on pore structure and diffusional properties of hydrated cement pastes. *Cement and Concrete Research* 27**,** 995-1007.

Nielsen, A. (1970) Measuremnts of pore size distribution of porous materials. *State Institute for Technical Research,* Finland.

Nielsen, R. P. (2001) Transport mechanisms in cementitious materials. *Department of Civil Engineering.* Lyngby, Technical University of Denmark.

Nilsson, L. O. (2002) *Durability Concept; Pore Structure and Transport Processes,* London.

NTBuild-368 (1991) Concrete repair materials: capillary absorption. . *Nordhest mehtod,* 2**,** 1-3.

NTEnvir002 (1995) Solid waste, granular inorgannic material: column test. *Nordhest mehtod***,** 1-6.

Oatley, C. W., Nixon, W. C.and Pease, R. F. W. (1965) Scanning electron microscopy. *Advances in Electronics and Electron Physics,* 21**,** 181-247.

Odler, I.and Rößler, M. (1985) Investigations on the relationship between porosity, structure and strength of hydrated Portland cement pastes. II. Effect of pore structure and of degree of hydration. *Cement and Concrete Research,* 15**,** 401-410.

Olson, R. A.and Jennings, H. M. (2001) Estimation of C–S–H content in a blended cement paste using water adsorption. *Cement and Concrete Research* 31**,** 351-356.

Panea, I.and Hansen, W. (2005) Investigation of blended cement hydration by isothermal calorimetry and thermal analysis. *Cement and Concrete Research* 35**,** 1155- 1164.

Park, C. Y.and Ihm, S. K. (1990) New hypotheses for mercuty porosimetry with percolation approach. *AIChE Journal,* 36**,** 1642-1650.

Parrot, L. J., Hansen, W.and Berger, R. L. (1980) Effect of first drying upon the pore structure of hydrated alite paste. *Cement and Concreat Research,* 10**,** 647-655.

Parrot, L. J.and Killoh, D. C. (1984) Prediction of cement hydration. *British Ceramic Proceedings***,** 41-53.

Patel, R. G., Killoh, D. C., Parrott, L. J.and Gutteridge, W. A. (1988) Influence of curing at different relative humidities upon compound reactions and porosity in Portland cmenet paste. *Materials and Strucutre,* 21**,** 192-197.

Persson, B.and Fagerlund, G. (2002) SELF-DESICCATION AND ITS IMPORTANCE IN CONCRETE TECHNOLOGY. *Third International Research Seminar* Lund

Powers, T. C. (1939a) The bleeding of Portland cement paste, mortar and concrete. *American Concrete Institute - Bulletin 2,* 10**,** 465-479.

Powers, T. C. (1939b) Bleeding of Portland cement paste, mortar and concrete. *American Concrete Institute -- Journal,* 10**,** 465-479.

Powers, T. C. (1945) A Working Hypothesis for Further Studies of Frost Resistance of Concrete. *American Concrete Institute - Bulletin 5,* 41**,** 245.

Powers, T. C. (1960) Physical properties of cement paste. *Research and Development Laboratories of the Portland Cement Association,* Bulletin 154**,** 577-609.

Powers, T. C. (1975) Freezing effects in concrete. *Durability of concrete aCI SP47***,** 1-11.

Powers, T. C.and Brownyard, T. L. (1947) Studies of the Physical Properties of Hardened Portland Cement Paste. *Journal of the American Concrete Institute - Bulletin 22,* 43**,** 101-992.

Prat, M. (2007) On the influence of pore shape, contact angle and film flows on drying of capillary porous media. *International Journal of Heat and Mass Transfer,* 50**,** 1455-1468.

prEN-ISO12571 (1999) Hygrothermal performance of building materials - Determination of hygroscopic sorption properties. *European Committee for Standardization - CEN/TC89/WG10.*

Puertas, F., Fernández-Jiménez, A.and Blanco-Varela, M. T. (2004) Pore solution in alkali-activated slag cement pastes. Relation to the composition and structure of calcium silicate hydrate. *Cement and Concrete Research,* 34**,** 139-148.

Quantachrome, I. (2007) Autosorb-1 Series surface area and pore size analyzers.

Radjy, F. F., Bogen, T., Sellevold, E. J.and Loeland, K. E. (1986) A review of experience with condensed silica fume concrete and products. 1135-1152.

Radjy, F. F.and E.J., S. (1972) Effect of freezing on the dynamic mechanical response of hardened cement paste down to -60ºC. *Cement and Concreat Research,* 2**,** 697-715.

Ramlochan, T., Thomas, M. D. A.and Hooton, R. D. (2004) The effect of pozzolans and slag on the expansion of mortars cured at elevated temperature Part II: Microstructural and microchemical investigations. *Cement and Concrete Research* 34**,** 1341-1356.

Rarick, R. L., Thomas, J. J., Christensen, B. J.and Jennings, H. M. (1996) Deterioration of the Nitrogen BET Surface Area of Dried Cement Paste with Storage Time. *Advanced Cement Based Materials,* 3**,** 72-75.

Rashed, A. I.and Williamson, R. B. (1991) Microstructure of entrained air voids in concrete. *Journal of Materials Research,* 6**,** 2474 -2483.

Richardson, I. G. (2008) The calcium silicate hydrates. *Cement and Concrete Research,* 38**,** 137-158.

Richardson, I. G.and Groves, G. W. (1997) The structure of the calciumsilicate hydrate phases present in hardened pastes of white Portland cement/blast-furnace slag blends. *Materials Science,* 32.

Rigby, S. P.and Edler, K. J. (2002) The Influence of Mercury Contact Angle, Surface Tension, and Retraction Mechanism on the Interpretation of Mercury Porosimetry Data. *Journal of Colloid and Interface Science,* 250**,** 175-190.

Rigby, S. P.and Fletcher, R. S. (2004) Interfacing Mercury Porosimetry with Nitrogen Sorption. *Part. Part. Syst. Charact. ,* 21**,** 138 - 148.

Roper, H. (1966) Dimensional change and water sorption studies of cement paste. *National Research Council -- Highway Research Board -- Special Reports* 74-83.

Roy, D. M., Brown, P. W., Ski, D., Scheetz, B. E.and May, W. (1993) Concrete Microstructure Porosity and Permeability. IN COUNCIL, S. H. R. P.-N. R. (Ed.) *Materials Research Laboratory.* Washington, DC.

Roy, D. M.and Idorn, G. M. (1982) Hydration, structure and properties of blast furnace slag cements, mortar and concrete. *ACI Journal,* Committe 444**,** 444-457.

Roy, S. K., Poh, K. B.and Northwoo, D. O. (1999) Accelerated carbonation and weathering studies. *Building and Environment* 23**,** 486-595.

Rubner, K.and Hoffmann, D. (2006) Characterization of mineral building materials mercury intrusion porosimetry. *Part.Syst. Characterisation,* 23**,** 20-28.

Ruiza, L. A., Platretb, G., Massieub, E.and Ehrlachera, A. (2005) The use of thermal analysis in assessing the effect of temperature on a cement paste. *Cement and Concrete Research* 35**,** 609-613.

Salmas, C.and Androutsopoulos, G. (2001) Mercury porosimetry: Contact angle hysteresis of materials with controlled pore structure. *Journal of Colloid and Interface Science,* 239**,** 178-189.

SCA (2003) Slag cement and the environment. *Slag Cement Association,* 22**,** 1-4.

Scherer, G. W., Smith, D. M.and Stein, D. (1995) Deformation of aerogels during characterization. *Jornal of Non Crystalline Solids,* 186**,** 309-315.

Scherer, G. W., Valenza, J. J.and Simmons, G. (2007) New methods to measure liquid permeability in porous materials. *Cement and Concreat Research,* 37**,** 386-397.

References

Scrivener, K. (1989) Microstructure of concrete. *Materials Science of Concrete I*, 127-161.

Scrivener, K. L. (1997) Microscopy methods in cement and concrete science. *World cement research and development*, 92-112.

Scrivener, K. L. (2004) Backscattered electron imaging of cementitious microstructures: understanding and quantification. *Cement & Concrete Composites* 26, 935-945.

Scrivener, K. L., Patel, H. H., Pratt, P. L.and Pratt, L. J. (1987) Analysis of phases in cement paste using backscattered electron images, methanol absorption and thermogravimetric analysis. *Mater Res Soc Symp Proc,* 85, 67-76.

Scrivener, K. L.and Pratt, P. L. (1983) Characterisation of portland cement hydration by electron optical techniques. In: Electron microscopy of materials. *Mater Res Soc Symp Proc.*

Scrivener, K. (2010) Microstructural Characterisation Methods for Cementitious Materials. *Durability of concrete -RILEM 2010.*

Sellevold, E.and Bager, D. (1980) Low Temperature Calorimetry as a Pore Structure Probe. *7'th International Congress on the Chemistry of Cements.* Paris.

Sellevold, E. J.and F.F., R. (1983) Condensed silica fume in concrete: water demand and strength development. *ACI SP-79*, 677-694.

Sellevold, E. J.and Radjy, F. F. (1976) Low temperature dynamic mechanical response of porous Vycor glass as a function of moisture content. Part 1- The capillary transition. *Materials Science,* 11, 1927-1938.

Sellevold, E. J.and Radky, F. F. (1983) Condensed silica fume in concrete: water demand and strength development. *ACI SP-79*, 677-694.

Setaram, I. (2005) Manual Calorimeter 1-58.

Setzer, M. J.and Zech, B. (1988) *Materials and Structures* 21, 323.

Shimada, Y.and Young, J. F. (2001) Structural changes during thermal dehydration of ettringite *Advances in Cement Research* 13, 77-81.

Slag Cement Association (2007) Ternary concrete mixtures with slag cement.

Snyder, K. A.and Bentz, D. P. (2004) Suspended hydration and loss of freezable water in cement pastes exposed to 90 % relative humidity. *Cement and Concrete Research,* 34, 2045-2056.

Stefanovic, G., Ojba, L., Sekuli, V.and Matija, S. A. (2007) Hydration study of mechanically activated mixtures of Portland cement and fly ash. *J. Serb. Chem. Soc. ,* 72, 591-604.

Sun, Z.and Scherer, G. W. (2010) Pore size and shape in mortar by thermoporometry. *Cement and Concrete Research* 40, 740-751.

Takemoto, K.and Uchikawa, H. (1980) Hydration of pozzolanic cement. IN IV-2, S.-T. (Ed.) *7th Int. Cong. on the Chemistry of Cements* Paris.

Taylor, H. F. W. (1997) *Cement chemistry*.

Taylor, H. F. W.and Turner, A. B. (1987) Reactions of tricalcium silicate paste with organic liquids. *Cement and Concrete Research,* 17, 613.

Tazawa, E.-i.and Miyazawa, S. (1995) Experimental study on mechanism of autogenous shirinkage of concrete. *Cement and Concrete Research,* 25, 1633-1638.

Thomas, J.and Jennings, H. M. (2008) The science of concrete.

Thomas, J. J., Hsieh, J.and Jennings, H. M. (1996) Effect of carbonation on the Nitrogen BET surface area of hardened Portland cement paste. *Advanced Cement Based Materials,* 3, 76-80.

Thomas, J. J., Rothstein, D., Jennings, H. M.and Christensen, B. J. (2003) Effect of hydration temperature on the solubility behavior of Ca-, S-, Al-, and Si-bearing solid phases in Portland cement pastes *Cement and Concrete Research,* 33, 2037-2047.

Toolbox, T. E. (2009) Isopropanol (2-Propanol) based Water Solutions.

Türkmen, Idotand brahim (2003) Influence of different curing conditions on the physical and mechanical properties of concretes with admixtures of silica fume and blast furnace slag. *Materials Letters,* 57**,** 4560-4569.

Valori, A. (2007) NMR on porous media (cement and concrete). *Presentation of Nanocem Marie Curie RTN 2, Lyublyana, Slovenia,* Department of Physics University of Surrey Guildford (UK)**,** 1-19.

Valori, A. (2009) Characterisation of cementitious materials by ^{1}H NMR. *Department of Physics.* University of Surrey.

Van Gerven, T., Cornelis, G., Vandoren, E.and Vandecasteele, C. (2007) Effects of carbonation and leaching on porosity in cement-bound waste. *Waste Management,* 27**,** 977-985.

Verbeck, G. J.and Helmuth, R. H. (1968) Structure and Physical Properties of Cement Pastes. *Proceedings of the Fifth International Symposium on the Chemistry of Cement.* Tokyo.

Villadsen, J. (1992) Pore structure in cement based materials. . *Technincal report 277.* Kgs. Lyngby, Technical University of Denmark (DTU).

Vodák, F., Trti'k, K., Kapicková, O., Hosková, S.and Demo, P. (2004) The effect of temperature on strength - porosity relationship for concrete. *Construction and Building Materials,* 18**,** 529-534.

Von Ardenne, M.and Beischer, D. (1940) Untersuchung von metalloxyd-rauchen mit dem universal-elektronenmikroskop. *Zeitschrift Electrochemie,* 46**,** 270-277.

Washburn, E. W. (1921) The dynamics of capillary flow. *Physical review,* 17**,** 273-283.

Weeks, W.and Ackley, S. (1986) The Geophysics of Sea Ice. *NATO ASI Series.* New York, chapter The growth structure and properties of sea ice.

Westermarck, S. (2000) Use of mercury porosimetry and nitrogen adsorption in characterization of the pore structure of mannitol and microscrystalline cellulose powders, granules and tablets. *Department of pharmacy.* Helsink, University of Helsink, Finland.

Wikepedia (2010) Silver iodide.

Williams, D. A., Saak, A. W.and Jennings, H. M. (1999) The influence of mixing on the rheology of fresh cement paste - Combined effect of shear rate and coagulation rate on viscosity. *Cement and Concrete Research,* 29**,** 1491-1496.

Williams, P. J. (1967) Properties and behaviour of freezing soils. *Norwegian Geothecnical Institute,* 72.

Winslow, D.and Liu, D. (1990) The pore structure of paste in concrete. *Cement and Concrete Research,* 20**,** 227-235.

Winslow, D. N., Cohen, M. D., Bentz, D. P., Snyder, K. A.and Garboczi, E. J. (1994) Percolation and pore structure in mortars and concrete. *Cement and Concrete Research,* 24**,** 25-37.

Winslow, N.and Diamonds, S. (1970) A mercury porosimetry study of the evolution of porosity in Portland cement. *Journal of Materials Science,* 5**,** 564-585.

Wittmann, F. H. (1973) Interaction of hardened cement paste and water. *American Ceramic Society,* 56**,** 409.

Wong, H. S., Head, M. K.and Buenfeld, N. R. (2006) Pore segmentation of cement-based materials from backscattered electron images. *Cement Concrete Res,* 36**,** 1083–1090.

Yang, M.and Jennings, H. M. (1995) Influences of Mixing Methods on the Microstructure and Rheological Behavior of Cement Paste. *Advanced Cement Based Materials,* 2**,** 70-78.

Yao, N.and Wang, Z. L. (2005) *Handbook of microscopy for nanotechnology,* New York, Springer Science

Yassin, M. (2010) Charecterization of Pozzolana and Its effect on cement properties. 1-55.

References

Yurtdas, I., Peng, H., Burlion, N.and Skoczylas, F. (2006) Influences of water by cement ratio on mechanical properties of mortars submitted to drying. *Cement and Concrete Research,* 36**,** 1286-1293.

Zhang, B. (1998) Relationship Between Pore Structure and Mechanical Properties of Ordinary Concrete Under Bending Fatigue. *Cement and Concrete Research,* 28**,** 699-711.

Zhang, X. (2007) Quantitative microstructural characterisation of concrete cured under realistic temperature conditions. Lausanne, École Polytechinique Fédérale de Lausanne.

Zhou, J., Ye, G.and Van Breugel, K. (2010) Characterization of pore structure in cement-based materials using pressurization-depressurization cycling mercury intrusion porosimetry (PDC-MIP). *Cement and Concrete Research* 40**,** 1120-1128.

Appendixes

Appendix I – Materials characterization

A list of binder combinations to be used in the considered MC RTN projects is listed in Table I.1; comments on selection are given in Table I.2. Lists of all investigated materials and their main characterisation are given in Table I.3,I.4 and I.5.

Table I.1: Updated list of materials combinations (CP4: Part 1 of CP4, new combinations possibly to be tested in Part 2 of CP4).

		Weight percent of binder	Cement					
			A	**B**	**F**	**D**[1)	**E**	**C**
	Ref.		**CP4, M3, M4, M10,**	CP4	M2, M14	(CP4)	PP3	**CP4, M2, M3, M10**
Slag	S01	40	CP4	CP4		(CP4)		**CP4, M2, M3, M10**
	S01	70						M2, M3. M10
Fly ash	FA01	15						M2, M3, M10
	FA01	30						M2, M3, M10

1-2 % CO_3 is expected in the cement; i.e. no need to add.
Note 1:Work on C11 has been discontinued and replaced by C13, see Table I.1b

Table I.2:Comments on materials selection

		EN 197	Special characteristics	Purpose
C	C		High C_3S, high alkali	Standard cement
S01			Normal reactivity	
F01			Normal	Standard

Tale I.3:List of investigated cements and their main characterisation

		Main phases (XRD-Rietveld)								Main oxides (XRF)	
Id.	**Name**	**Alite C_3S (%)**	**Belite C_2S (%)**	**Ferrite C_4AF (%)**	**Aluminate C_3A (%)**	**Lime C (%)**	**Periclase MgO (%)**	**Gypsum + Hemihydrate +Anhydrite (%)**	**Calcite $CaCO_3$ (%)**	**Fe_2O_3 (%)**	**$Na_2O_{equivalent}$ (%)**
Cement	**C**	65.8	16.5	7.2	6.6	0.5	1	2.2	0.0	2.52	?

Table I.4: List of investigated slag and their main characterisation

Name	**Amorphous content**	Main oxides (XRF)						
		SiO_2 (%)	**Al_2O_3 (%)**	**Fe_2O_3 (%)**	**CaO (%)**	**MgO (%)**	**SO_3 (%)**	**$Na_2O_{equivalent}$ (%)**
Slag 01	>99%	36.45	11.59	1.4	40.78	7.45	2.1	0.50

Table I.5: List of investigated SCMs and their main characterisation

Name	Main oxides (XRF)						
	SiO_2 (%)	**Al_2O_3 (%)**	**Fe_2O_3 (%)**	**CaO (%)**	**MgO (%)**	**SO_3 (%)**	**$Na_2O_{equivalent}$ (%)**
Fly ash 01	51.7	25.5	5.7	3.1	2.7	0.8	3.99

Appendix II-Materials proportion

Constituent material	Density (g/cm³)	A Weigh	A Volume	A_SF10 Weigh	A_SF10 Volume	C Weigh	C Volume	C_S1-40 Weigh	C_S1-40 Adj.W	C_S1-40 Volume	C_S1-70 Weigh	C_S1-70 Adj.W	C_S1-70 Volume	C_FA1-15 Weigh	C_FA1-15 Volume	C_FA130 Weigh	C_FA130 Volume	C_SF-10 Weigh	C_SF-10 Volume
Water/Binder		0.40		0.42		0.40		0.43	0.43		0.46	0.46		0.42		0.45		0.41	
V_{water}/V_{binder}		1.26	1.26	1.26	1.26	1.26	1.26	1.26	1.26	1.26	1.26	1.26	1.26	1.26	1.26	1.26	1.26	1.26	1.26
		g	cm³	g	cm³	g	cm³	g	g	cm³	g	g	cm³	g	cm³	g	cm³	g	cm³
Water	1.000	64.00	64.00	66.74	66.74	63.31	63.31	68.94	68.94	68.94	73.15	66.84	73.15	67.53	67.53	71.75	71.75	66.12	66.12
Cement A*	3.143	160.00	50.90	144.00	45.81					0.00			0.00		0.00		0.00		0.00
Cement B	3.180																		
Cement C*	3.178					160.00	50.35	96.00	93.08	30.21	48.00	43.86	15.11	136.00	42.80	112.00	35.25	144.00	45.32
Cement D	3.183																		
Slag 1*	2.6							64.00	62.05	24.62	112.00	102.33	43.08						
Slag 8	2.6																		
Fly ash 1*	2.2													24.00	10.91	48.00	21.82		
Fly ash 2	2.2																		
Silica fume	2.2			16.00	7.27		0.00			0.00			0.00					16.00	7.27
Sum			114.90		119.83		113.67			123.76			131.34		121.24		128.82		118.72

* Materials proportion adjusted to 120 cm³ batch

Appendix III- Procedure for mixing cement pastes
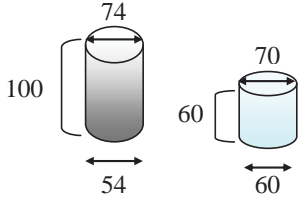
Purpose
Mixing of cement paste in batches of approximately 120 cm^3.

Equipment
- Mixer equipped with a paddle, see Figure III.1 and III.2. Such mixer may be obtained from IKA – Weke GMBH & CO.KG (www.ika.net);
- Paddle, diameter of 44.5 mm. This paddle is custom made at EPFL; contact Emmanuel Gallucci;
- Scale (accuracy 0.01 g.)
- Plastic containers with lid for weighing and mixing, see Figure III.3:
    - Binder: conical cylindrical cup approx. diameter 54 mm at bottom and 75 mm at top and 100 mm high;
    - Water: e.g. conical cylindrical cup approx. diameter 60 mm at bottom and 70 mm at top and 60 mm high;
    Such cups may be obtained from Semadeni (www.semadeni.com);
- Moulds (size and amounts depends on your purpose);
- Room of ambient temperature.

Possible additional equipment
- A powder mixer for blending of powder; capacity 0.5 litres, maximum speed of rotation 60 rpm (adjustable), e.g. a TURBULA model T2 F shaker mixer from Glen Mills Inc. (www.glenmills.com), see Figure III. The powder mixer container is set into three-dimensional movement that exposes the product to always changing, rhythmically pulsing motion.
- If the control of the mixer is analog an instrument to check the rotational speed of the paste mixer; e.g. JAQUET type DMR 903.

Fig. III. 1: Paste mixer (LABORTECHNIK RW 20.n)

Fig. III.2: Custom made paddle

Fig. III.3: Containers for weighing and mixing, dimensions in (mm)

Fig. III.4: Powder mixer (TURBULA shaker-mixer)

Materials
- Cement
- Distilled water (20^oC)
- Possible supplementary materials
- Possible chemical admixtures
- Saturated calcium hydroxide for possible saturated curing

The size of container and paddle for mixing is suitable for pastes from 160 g powder. The mix proportions are based on a constant volume water to volume binder ratio and w/c=0.4 of the paste with cement A. The need for use of superplasticizer when mixing pastes with silica fume is to be discussed with Elkem and Sika.

Procedure
Blending of binders
Either use a powder blender
1. Weighed out the cement and the supplementary cementitious materials in amounts to fit the volume of the powder mixer.
2. Blend the binders in the TURBULA shaker-mixer for minimum 5 hours
3. Weighed out the exact amount of binders

or blend binders in "binder container"
4. Weighed out the exact amounts of cement and the supplementary cementitious materials in the "binder container" and blend by shaking the container with two 15-20 mm glass balls in for 5 min.

Mixing
5. Adjust the rotational speed of the mixer to 500 rpm (if analog check rotational speed)
6. Add the water to the cement and immediately after mix the paste at a rotational speed of 500 rpm for 3 minutes.
7. Stop the mixing for 2 minutes, and cover the paste during this period. If analog check rotational speed adjust the rotational speed of the mixer to 2000 rpm
8. Mix at a rotational speed of 2000 rpm for 2 minutes.

Casting
Cast your samples, ensure proper compaction.
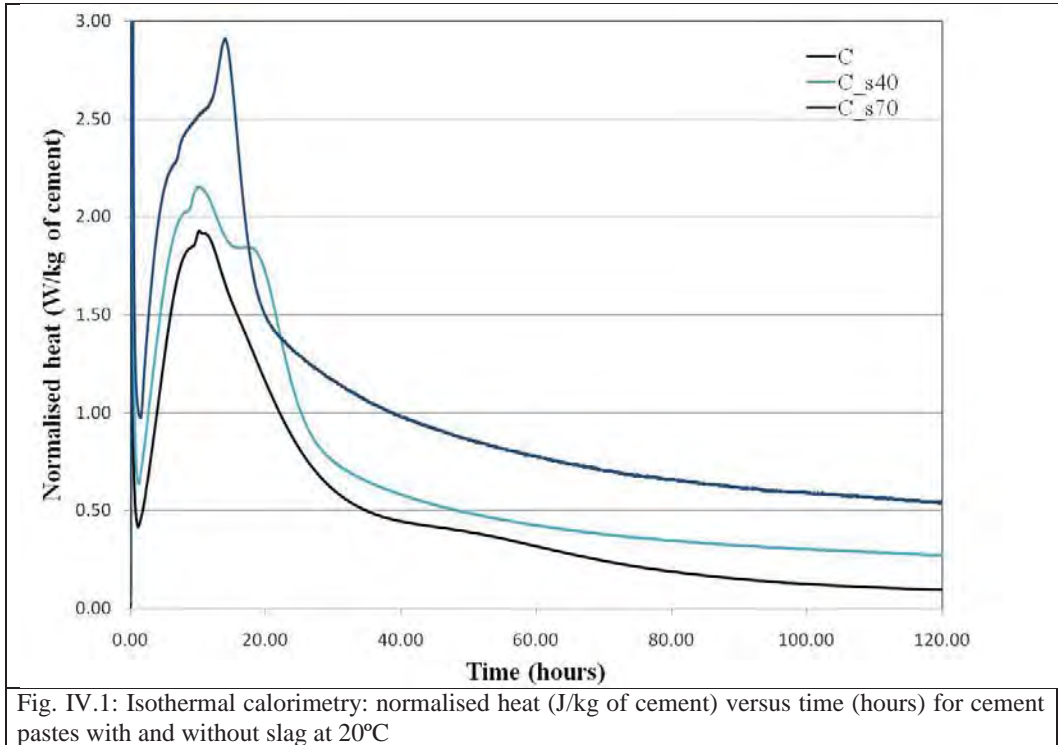
Curing
Either sealed curing
9. Close the flask with the paste and put on the date and time when the hydration cement paste started. Keep sealed to restrict evaporation and ingress of CO_2.

or saturated curing
10. The samples should not dry at any time. Add a few drops of saturated calcium hydroxide right after casting and add additional saturated calcium hydroxide to keep the sample saturated (minimum the amount which will be imbibed (sucked in) due to 6 ml/100 g cement and 18g/100 silica fume). The sample size should be limited to ensure transport of water to the center of the sample; i.e. high samples should be de-moulded and kept submerged in saturated calcium hydroxide in a slightly larger container. Keep sealed to restrict evaporation and ingress of CO_2.

Appendix IV- Development of heat of hydration by isothermal calorimeter

Development of heat of hydration for pastes with and without fly ash and slag cured at 20 and 55ºC is showed in the Figs IV.1,IV.3,IV.5 and IV.7. The cumulative heat evolution curves of pastes blended with slag and fly ahs at 20ºC over a period of 120 hours are illustrated by the Figs. IV.2,IV.4,IV.6 and IV.8.
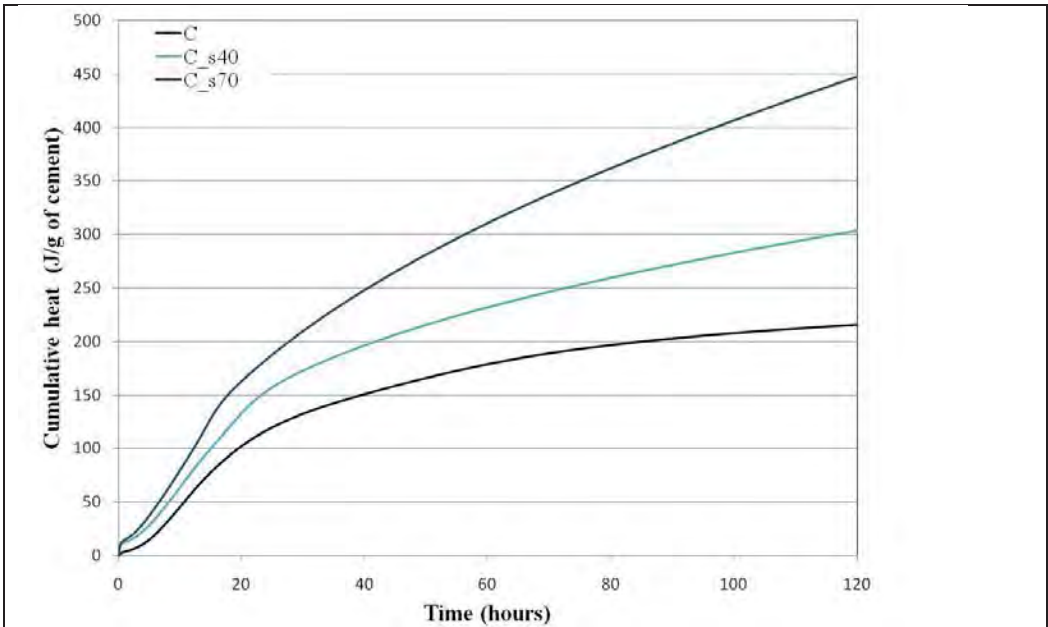

Fig. IV.1: Isothermal calorimetry: normalised heat (J/kg of cement) versus time (hours) for cement pastes with and without slag at 20ºC

Fig. IV.2: Isothermal calorimetry: cumulative heat (J/kg of cement) versus time (hours) for cement pastes with and without slag at 20ºC.
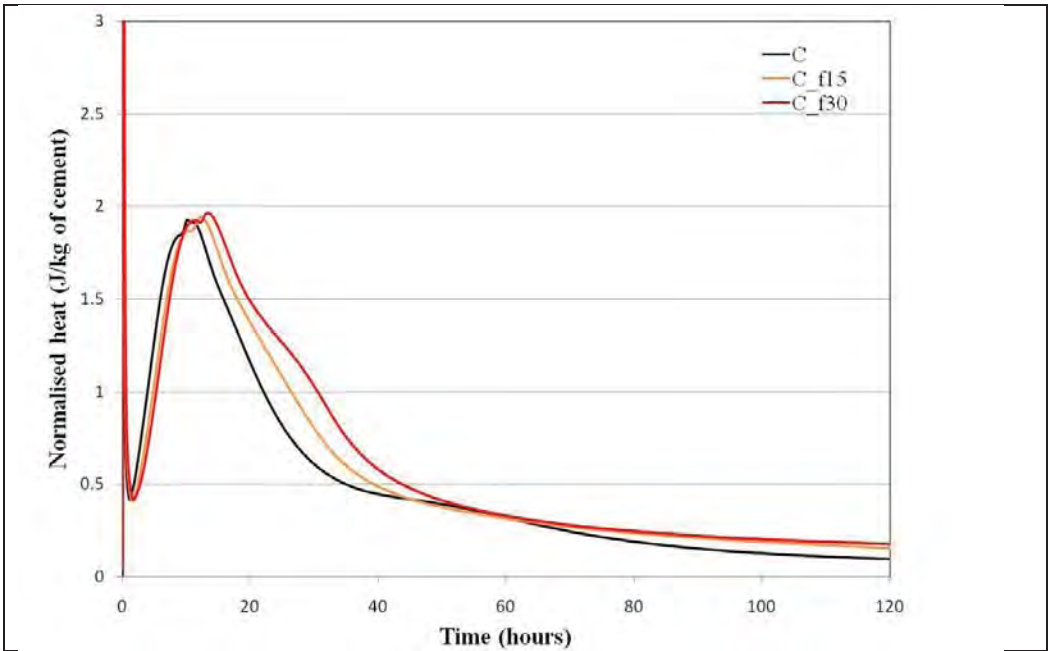
Fig. IV.3: Isothermal calorimetry: normalised heat (J/kg of cement) versus time (hours) for fly ash pastes at 20ºC
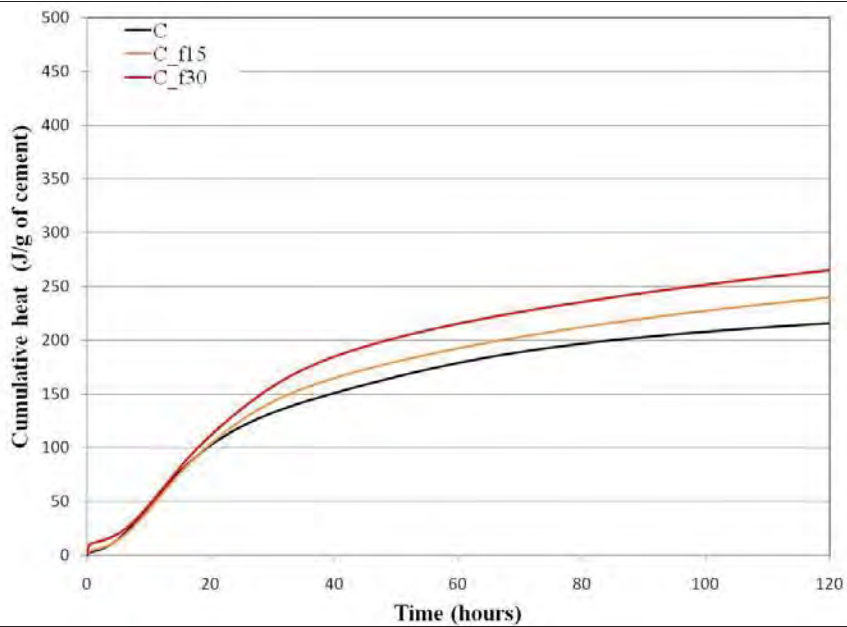
Fig. IV.4: Isothermal calorimetry: cumulative heat (J/kg of cement) versus time (hours) for cement pastes with and without fly ash at 20ºC.
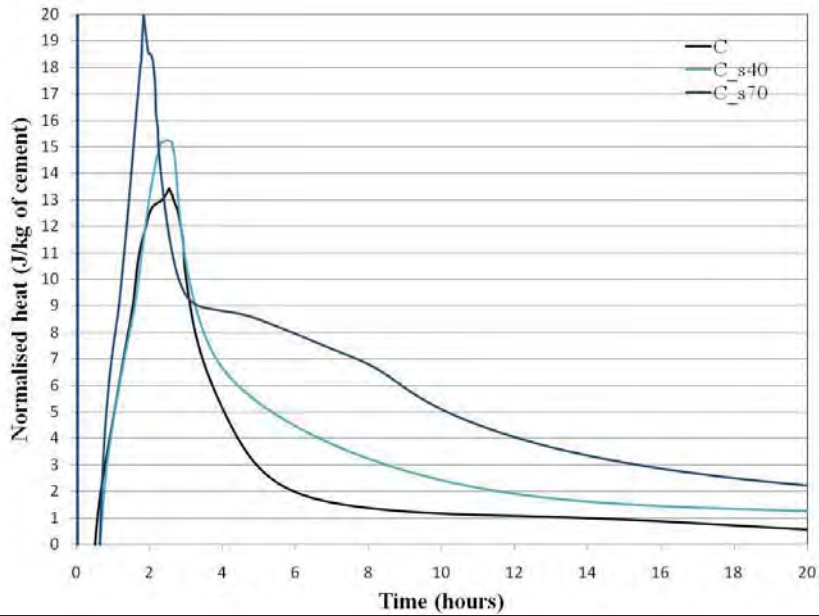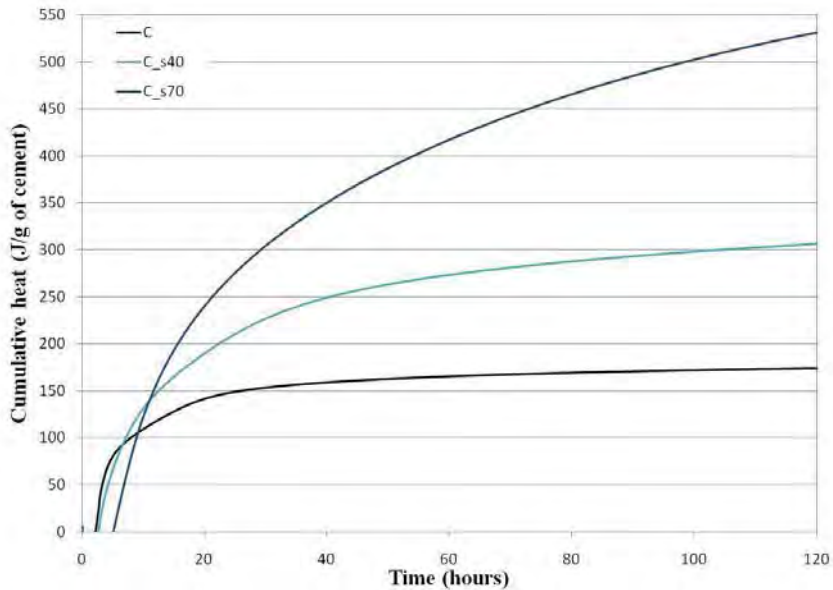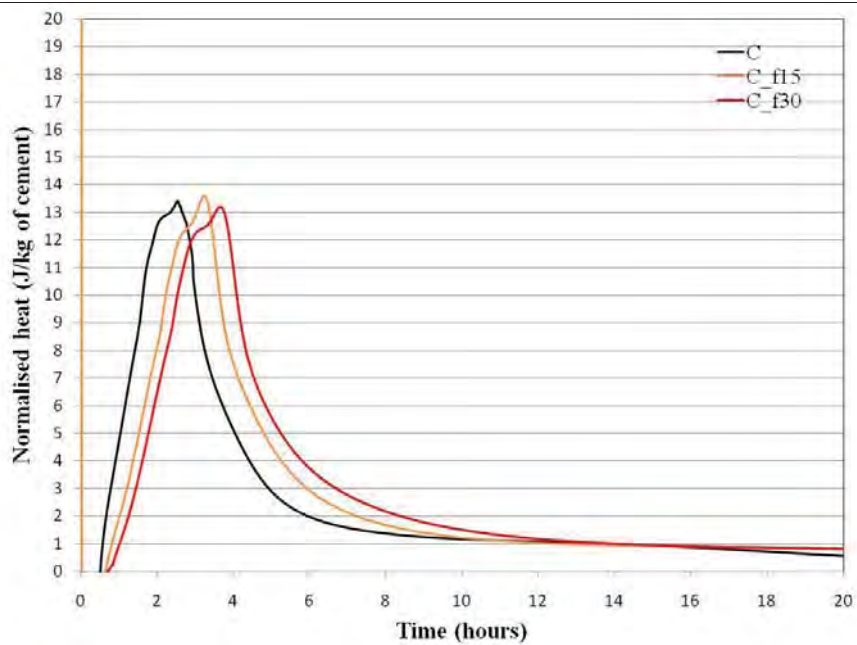
Fig. IV.5: Isothermal calorimetry: normalised heat (J/kg of cement) versus time (hours) for cement pastes with and without slag at 55ºC

Fig. IV.6: Isothermal calorimetry: cumulative heat (J/kg of cement) versus time (hours) for cement pastes with and without slag at 55ºC.

Fig. IV.7: Isothermal calorimetry: normalised heat (J/kg of cement) versus time (hours) for cement pastes with and without fly ash at 55ºC
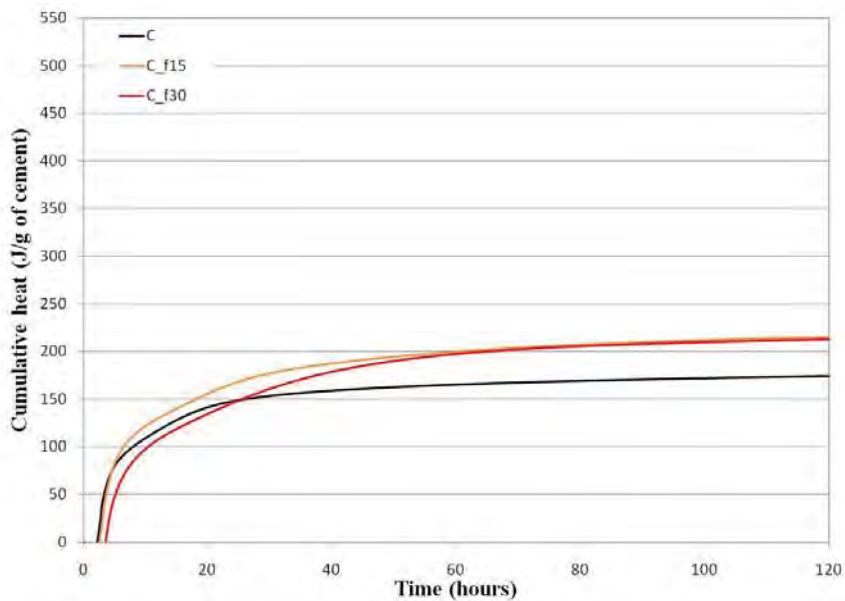

Fig. IV.8: Isothermal calorimetry: cumulative heat (J/kg of cement) versus time (hours) for cement pastes with and without fly ash at 55ºC.

Appendix V- Procedure for bleeding

Purpose
Measure the amount of bleed water of the cement pastes

Procedure
At the present work, bleeding is evaluated by three different methods. The adopted mix procedure and materials were used at the tests are given in Appendix II and III.
- Method 1 - Constant measurements of the cement paste level varying the water/binder ratio (0.45, 0.50, 0.55) using graduated glasses
- Method 2 - Weight the sample before and after removing the bleeding water on the top of the pastes
- Method 3 - Measuring height of paste in plastic moulds after casting and 2 hours

Method 1 - Constant measurements of the cement paste level varying the water/binder ratio (0.40, 0.50, 0.55) using graduated glasses

In this method, bleeding is measured as the ratio of water that bleeds (bd) by gram of cement (c), also the percentage of bleeding water is given.

bleeding is given as the ratio of water that bleeds (bd) by gram of cement (c). This means, that where bd/c may be understood as the ratio w/c that changes in paste because of bleeding. Applying this method a prediction of bleeding may also be found. Steinour (1945) studies suggest by the Equation V.1 to predict bleeding of paste samples above a critical size:

$$\frac{bd}{c} = k \cdot (w/c - (w/c_0)^2 \qquad \text{(Equation V.1)}$$

Where
bd/c	bleeding per gram of cement, g/g
w/c	water/cement ratio
w/c_0	highest water cement ratio for a paste without bleeding
k	constant, for spheres particles k=4; irregular particles k= 4.05

For the modeling of the system, the Equation 15 is rewritten and expressed by Equation V.2.

$$\sqrt{\frac{bd}{c}} = \sqrt{k} \cdot (w/c - (w/c_0)) \qquad \text{(Equation V.2)}$$

A chart of $\sqrt{bd/c}$ versus w/c is a linear correlation which may be used for the bleeding estimation.

For this method, two different graduated glasses (25.8 and 15.35mm of diameter) were used varying the height of the cement pastes:
- 25.8x55 mm (diameter x height)
- 13.35x45 mm (diameter x height)

Purpose
Determine the amount of bleeding of cement paste as a function of water/binder ratio (w/b-ratio) and sample height. Bleeding is water that is separated from the cement paste before setting.

Water/ binder ratio of:
-0.40 (approx., see the table of the mixes composition at next page); 0.50 and 0.55.

Materials and Equipment
- Scale (accurate to 0.01 g.);
- 2 graduated glass, 25 ml with 15.35 mm of diameter;
- 2 graduated glass, 100 ml with 25 mm of diameter;
- Plastic film;
- Watch(es);
- Distilled water.

Specimens
Cement pastes

Procedure
For each w/b:
1. Calculate and weighed out the needed amount of water.
2. Mix the paste (see Appendix III).
3. The graduated glasses are filled with paste at different heights (45 and 55 mm). It is important to keep the side of the glasses clean.
4. Cover the glasses with a plastic film to limit evaporation.
5. The first measurement (0 min.) is taken when the sample is placed in the graduated glass.
6. Record the paste level each 10 min.

Weight measurements
After the previous test (approximately 2 hours after casting), weight measurements are carried out:

7. Take off the plastic film
8. Weight the samples within the graduated glasses
9. Carefully, take off the water from the surface of the samples, if it is necessary use a paper.

Method 2 - Weight the sample before and after removing the bleeding water on the top of the pastes

The second method is based on weight measurements of sample with and without bleeding. The sample weight is measured 2 hours after casting the samples (assuming the bleeding has stopped at this time) with the bleed water and without the bleed water. This method may not be precise, because some of paste may be removed with bleeding, however it allows finding bleeding in samples with different shapes. This method is reported as a overestimated method (Maia et al. 2008, Powers 1960, Steinour 1945).

Method 3 - Measuring height of paste in plastic moulds after casting and 2 hours later

The samples were cast in plastic container with 30mm of diameter at 2 different heights (60 and 30 mm approx.) and left for 2 hours at room temperature (20 ± 2°C). At this method bleeding was based on the height measurements right after the cast and after 2 hours.

Appendix VI- Results of bleeding

Method 1 - Constant measurements of the cement paste level varying the water/binder ratio (0.45, 0.50, 0.55) using graduated glasses

The used water/binder ratio was the original one (0.40 for cement A), and 0.50, 0.55 were also used. After casting the samples following the procedure in the Appendix III, they were placed in a graduated glass and sealed with a plastic cover. Measurements of the cement paste level were carried out from 10 to 10 minutes. Knowing the amount of paste and cement, it is possible to evaluate the bleeding evolution by time from the decrease of the paste level. The maximum value of bleeding is found when the level of paste stops to decrease, approximately 90 minutes after the casting of the sample. The bleeding is given from the % of bleeding water from the total water of the pastes and bleeding water by gram of cement and the results are compared.

Trough graphic below is possible to observe the average of the amount of bleeding water (%) versus time (min) (Fig. VI.1) for the w/b ratio of 0.45, 0.5 and 0.55. Linear estimation of bleeding is given trough the average of bleeding by w/b ratio see Fig. VI.2.
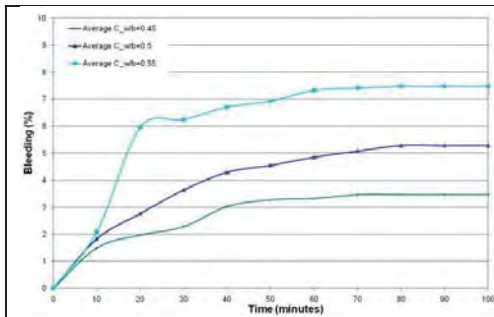

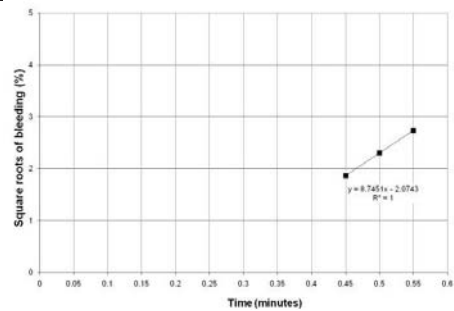| Fig. VI.1: Percentage of bleeding versus time (min) for cement C varying the w/b ratio (0.45, 0.50, 0.55)	Fig. VI.2: Estimation of % of bleeding by height measurements for cement C varying the w/b ratio (0.45, 0.50, 0.55)

The evolution of bleeding by the amount of bleeding water (g) by gram of cement (g) versus time (min) at 0.45, 0.50 and 0.55 w/b ratio is shown in the Fig. VI.3. To predict the bleeding varying the w/b ratio the linear relation of $(bd/c)^{1/2}$ versus w/b ratio is given in the Fig. VI.4.
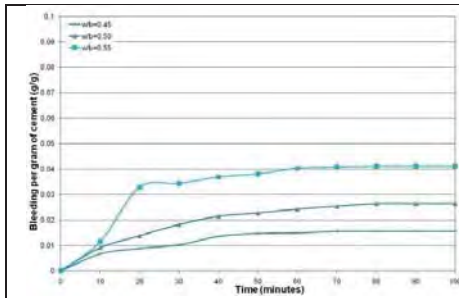
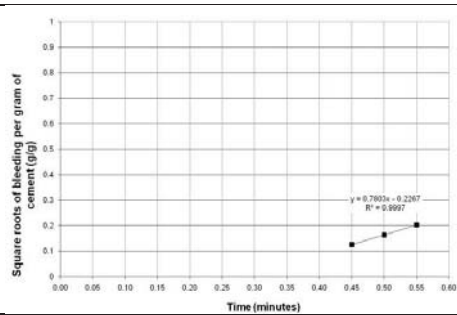| Fig. VI.3: Bleeding per gram of cement (g/g) versus time (min.) for cement C varying the w/b ratio (0.45, 0.50, 0.55).	Fig. VI.4: Estimation of bleeding per gram of cement by height measurements for paste C varying the w/b (0.45, 0.50, 0.55)

As expected, over time the amount of bleeding with high w/b ratio is larger. So far, there is a good linear correlation between % of bleeding and bd/c versus w/b. Trough these correlations; one can estimate the amount of bleeding water for other w/b ratios as show in the Table VI.1 and VI.2.

Table VI.1:Estimation of % of bleeding for plain cement paste at varying w/b ratio

w/b	% of bleeding
0.25	0.01
0.30	0.30
0.35	0.97
0.40	2.03
0.45	3.46
0.50	5.28

Table VI.2: Prediction of bleeding per gram of cement for plain cement paste at varying w/b ratio

w/b	Bleeding per gram of cement (g/g)
0.25	0.00
0.30	0.00
0.35	0.00
0.40	0.01
0.45	0.02
0.50	0.03

Trough the predictions is possible to observe that the estimations of bleeding for cement paste C at w/b ratio of 0.40 are about 2% or 0.01g per gram of cement. These results may explain the amount of bleed water found during the casting of the paste. It may also be observed that for w/b ratio estimated of 0.30 not significant rate of bleeding is found. Comparing the results of the present method with the first method (Measuring height of paste in plastic moulds after casting and 2 hours later) the amount of bleeding water is underestimated. Maia et al. (2008) reported that the estimation of bleeding by gram of cement underestimate the final results.

Method 2 - Weight the sample before and after removing the bleeding water on the top of the pastes

The second method is based on weight measurements of sample with and without bleeding. This method may not be precise, because some of paste may be removed with bleeding; however it allows finding bleeding in samples with different shapes. This method is reported as a overestimated method (Maia et al. 2008, Powers 1960, Steinour 1945).

By the weight measurement right after the casting and after 2 hours approximately, it was possible to estimate the bleeding water of cement paste C at varying w/b (0.45, 0.50 and 0.55) and size (diameter and height) of specimens. In the Table VI.3, it is given the results of the weight measurements before and after bleeding of the pastes. The estimation of %bleed water was also undertaken by the correlation line form % of bleeding water/binder ratios, see Fig VI.5.

Table VI.3:Weight measurement of bleeding test for cement paste C.

| Sample size (mm)	flask weight	Weight (g)											
		0.45				0.5				0.55			
		with water	without water	total water	% of bd*	with water	without water	total water	% of bd*	with water	without water	total water	% of bd
ø25.8 x0.80	119.80	202.69	201.39	37.30	3.49	193.82	191.63	37.01	5.92	202.07	197.41	45.25	10.30
ø25.8 x0.50	119.80	177.59	176.73	26.01	3.31	174.61	172.36	27.41	8.21	145.81	143.01	14.31	19.57
ø15.3 5.80	54.93	96.72	95.80	18.81	4.89	93.46	92.22	19.27	6.44	82.32	80.35	15.06	13.08
ø15.3 5.50	54.93	77.37	76.91	10.10	4.56	73.97	72.95	9.52	10.71	75.83	74.37	11.50	12.70

*bd = bleeding water from the total amount of water
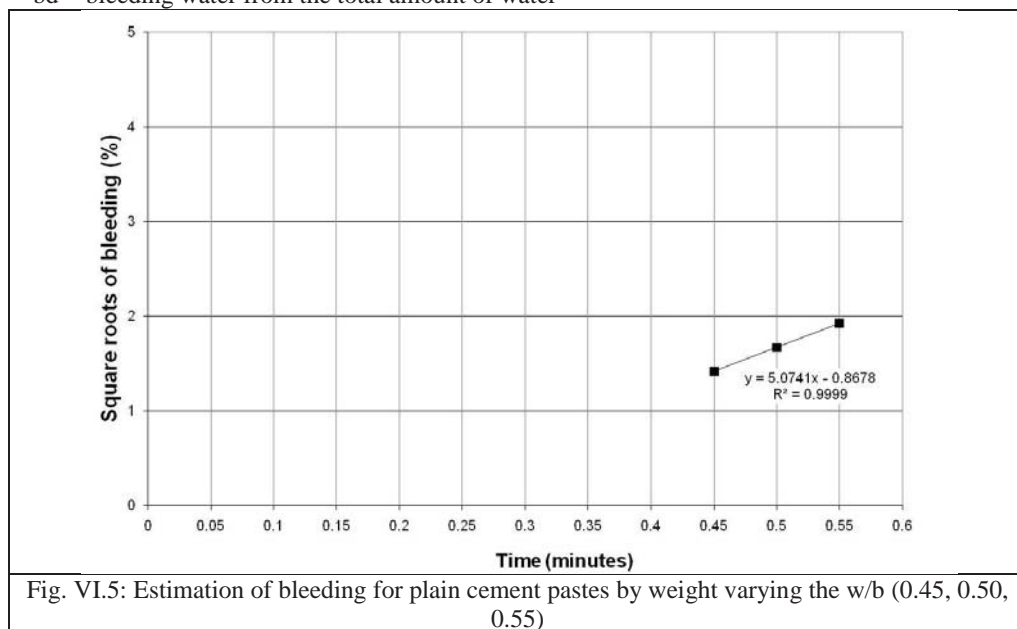
Fig. VI.5: Estimation of bleeding for plain cement pastes by weight varying the w/b (0.45, 0.50, 0.55)

Table VI.4:Estimation of amount of bleeding (%) for cement paste C by weight measurements

w/b ratio	% bleeding
0.25	0.16
0.30	0.43
0.35	0.83
0.40	1.35
0.45	2.00
0.50	2.79

A good correlation was found for the bleeding test using weight measurements. However the results show lower results of bleeding comparing with the method 1 and 2. Lower value of bleeding may be found at the w/b ratio of 0.25 and 0.30.

Method 3 - Measuring height of paste in plastic moulds after casting and 2 hours later
The samples were cast in plastic container with 30mm of diameter at 2 different heights (60 and 30 mm approx.) and left for 2 hours at room temperature ($20\pm2^{\circ}$C). At this method bleeding was based on the height measurements right after the cast and after 2 hours, see Table VI.5.

Table VI.5: Bleeding test (measured by height) in the selected samples

Material	w/b	Sample (after casting)				Bleeding (water)			Sample (after bleeding)					
		height	d	Total volume	volume of water	height	d	Vol.	height	d	volume of water	w/b	Vol % of water	Water to solid vol
	-	cm	cm	cm^3	cm^3	cm	cm	cm^3	cm	cm	cm^3	-	cm^3	cm^3
C	0.40	6.25	2.80	38.47	21.53	0.45	2.8	2	5.80	2.80	20	0.36	0.54	1.16
		2.90	2.80	17.85	9.99	0.2	2.8	1	2.70	2.80	9	0.36	0.54	1.16
C_s40	0.43	6.35	2.80	39.08	21.75	0.4	2.8	2	5.95	2.80	20	0.40	0.54	1.15
		2.9	2.80	17.85	9.93	0.15	2.8	1	2.75	2.80	9	0.40	0.54	1.17
C_s70	0.46	5.95	2.80	36.62	20.45	0.3	2.8	1	5.65	2.80	19	0.43	0.54	1.18
		2.8	2.80	17.23	9.63	0.15	2.8	1	2.65	2.80	9	0.43	0.54	1.18
C_f15	0.42	6	2.80	36.93	20.53	0.45	2.8	2	5.55	2.80	19	0.38	0.53	1.13
		3.55	2.80	21.85	12.15	0.2	2.8	1	3.35	2.80	11	0.39	0.54	1.16
C_f30	0.45	6.25	2.80	38.47	21.46	0.55	2.8	2	5.70	2.80	19	0.40	0.53	1.12
		3.85	2.80	23.69	13.22	0.35	2.8	2	3.50	2.80	12	0.40	0.53	1.12
A	0.40	5.05	2.80	31.08	17.40	0.05	2.8	0	5.00	2.80	17	0.40	0.56	1.26
		3.15	2.80	19.39	10.85	0	2.8	0	3.15	2.80	11	0.40	0.56	1.27

It may be seen that a large amount of bleeding water was found for selected pastes. The results showed a reduction of the water/ binder ratio for selected cement pastes due the bleeding, except for sample A (100% of white cement). A reduction of about 12% of mixed water was observed for pastes C_f30 (70% of cement "C" and 30% of fly ash).

Appendix VII- Procedure for evaporable and non evaporable water

Purpose

The purpose of the investigation is to estimate the degree of hydration based on determinations of the relative amount of chemically bound water. Evaporable water is measured as the weight loss when 105ºC. The non evaporable water is measured as the weight loss due to heating from 105^0C to 1000^0C.

Materials and equipment
- Scale (accurate to 0.0001g)
- Crucibles, for heating to 1000^0C
- Kiln (1000^0C) gloves and tong
- Oven (105^0C) and gloves
- Desiccators with silica gel

Specimens

Cement pastes

Procedure
1. Weight the sample.
2. Place the sample to a 105ºC.
3. After that, place the samples in a desiccator for 15 minutes.
4. Write down the weight of the sample and calculate the amount of evaporable water following the Equation VII.1.
5. Place the crucibles to a 1000ºC kiln.
6. After 1 hour the samples are cooled in the desiccator for 15 minutes, and then weighed it.
7. Write down the weight and calculate the amount of non evaporable water following the Equation VII.2.

Data analyses

Evaporable and non evaporable water are given by the Equations VII.1 and VII.2.

Evaporable water	Non-evaporable water
$$E_w = \frac{w_{20} - w_{105}}{w_{20}}$$ where E_w Evaporable water, fraction w_{20} Sample weight at 20ºC,kg w_{105} Sample weight at 105ºC,kg	$$E_w = \frac{w_{105} - w_{1000}}{w_{105}}$$ where E_w Evaporable water, fraction w_{105} Sample weight at 105ºC, kg w_{1000} Sample weight at 1000ºC, kg
Equation VII.1 – Evaporable water	Equation VII.2: Non evaporable water

References

Design and Control of Concrete Mixtures, Portland Cement Association, EB001, 14 edt. 2002

Appendix VIII- Procedure for solvent exchange (stop hydration)

Purpose

The purpose of the method is to stop the hydration of cementitious and subsequently dry them before, e.g. impregnation or testing of properties of dried material.

The hydration should have passed the acceleration period, corresponding to maturity (age at 20°C) at 1 day.

Principle

The water in the sample is exchanged with isopropyl alcohol, which only to a limited degree react with cement (Zhang 2007).

Materials and equipments

- Scale(e.g. Accutom-2 from Struers)
- Isopropyl alcohol, 99.9 %
- Flasks with a flask volume to sample volume higher than 50/1
- Desiccator
- Vacuum pump (less than 10 mbar)

Specimens

Cement pastes

Procedure

1. Slices of a size approximately at 3 mm are cut using water cooling (the slices should preferably be 3 mm thick to allow for rapid exchange)
2. The slices are submerged in isopropyl alcohol.
3. The specimen is cut to a size with the minimal dimension at 5 mm or less (preferably 3 mm) using water cooling
4. The specimen is submerged in isopropyl alcohol (solvent / specimen volume > 50) and left for 7 days
5. The isopropyl alcohol is discharged and the specimen is left for 3 days in a desiccator, which is evacuated (<10 mbar), or for 1 day if the pump is turned on.

References

- Zhang, Z.: Quantitative microstructural characterisation of concrete cured under realistic temperature conditions. PhD thesis No. 3725 EPFL, Suisse (2007)

Appendix IX - Procedure for vacuum saturation and pressure saturation

Purpose

The purpose of the saturation method is to estimate the amount of entrapped air voids of the samples. Also when the re-saturation of the sealed samples are required

Principle

The sample is re-saturated applying vacuum or pressure.

Materials and equipments

- Scale (e.g. Accutom-2 from Struers)
- Water with calcium hydroxide (saturated)
- Desiccator
- Vacuum pump
- Pressure apparatus (see NTBuild-368 (1991))

Procedure

Firstly, the sample is weighted (0.0001g), placed in desiccator and evacuated for one hour. Subsequently solution of water saturated with calcium hydroxide is introduced in the desiccator. The sample is kept in desiccator in the calcium hydroxide solution for 24 hours. After that the sample was saturated surface dried (SSF) and weighted. Thus, the same sample is placed in a pressure cell with calcium hydroxide saturated water, and a pressure of 15MPa was applied for 24 hours. The weight was measured right after the test. The measurement of volume of entrapped are calculated based on the weight measurements of before and after pressure saturation. Pressure saturation is described in the standard NTBuild-368 (1991). The air void volume is expressed by the Equation IX.1.

$$V_{av} = (V_{ps} - V_{ws})$$ (Equation IX.1)

where

V_{av} volume of air voids (cm³)
V_{ps} volume of water after water pressure test (cm³)
V_{ws} volume of water after vacuum saturation test (cm³)

Some authors suggested the use of image analyses. Thin section methos may be performed in optical of electronic microscopy acquiring the volume of the spaces with diameter greater than 2 mm (NTBuild-381 1991).

Appendix X- Procedure for low temperature calorimetry (LTC)

Purpose
Low temperature calorimetry (LTC) is proposed to examine the pore thresholds (connectivity) and size distribution of water filled pores in cement based materials by the measurements of heat flow during the freezing of cement pastes. Set up of the equipment are illustrated in the Figs. X.1 and X.2.

Equipment:
1. Micro Calorimeter: Temperature Calvet Micro Calorimeter
   Model: BT 2.15 Setaram

2. Thermojet: ThermoJet TM Precision Temperature Cycling System
   Model: THJ-TC1, from FTS

3. Data Acquisition/Switch Unit
   Model: 34970A, from Agilent

4. Heat control system

5. Manometer (control for the gas circulation in the Micro Calorimeter)
   From Setaram

6. Central manometer(on the wall)

7. Duct heater (Lindab)
   Model: KVU 160, from Lindab

8. Computer program Labview 8.5 – "Calorimeter (Main)v2."

Material
Samples with 55x15Ø mm (approx).
Approximately 10 mg of silver iodide;
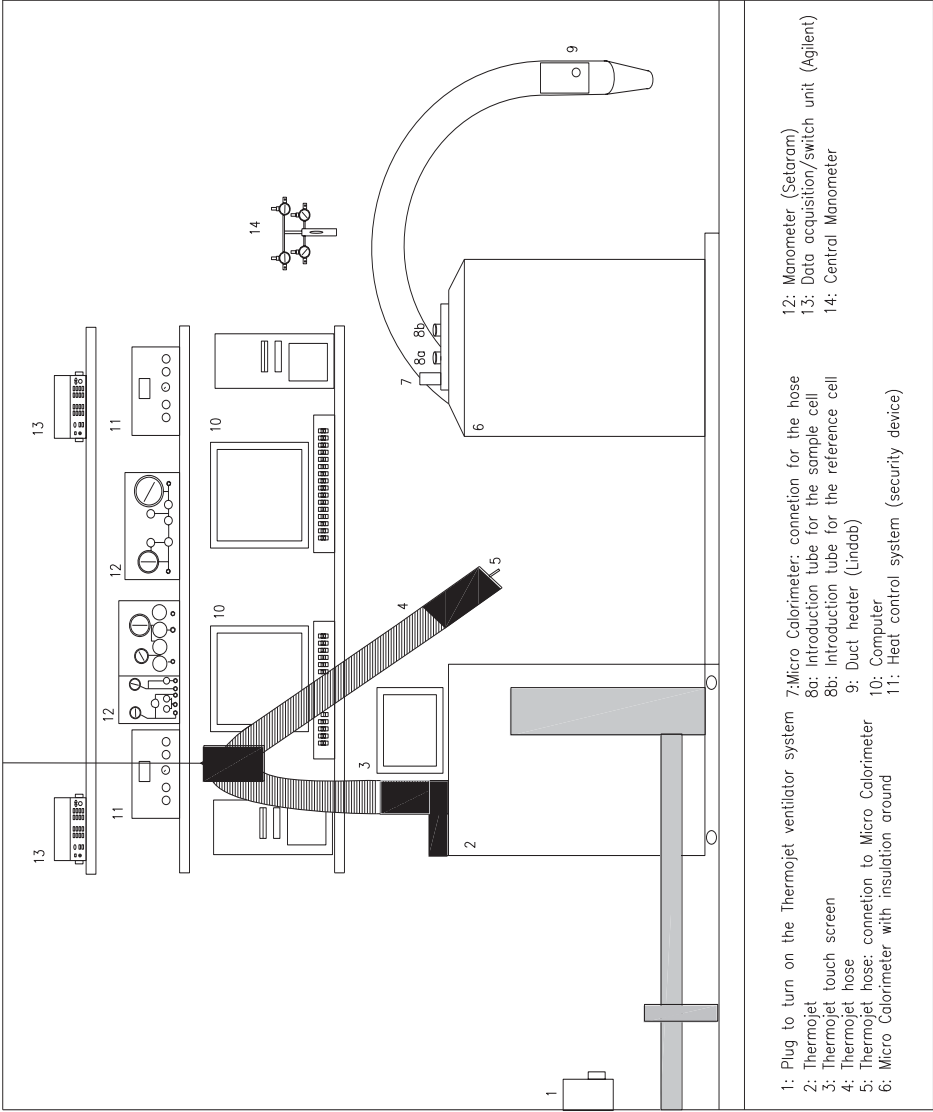
Fig. X.1: Set up of the Micro calorimeter 1

1: Plug to turn on the Thermojet ventilator system
2: Thermojet
3: Thermojet touch screen
4: Thermojet hose
5: Thermojet hose: connetion to Micro Calorimeter
6: Micro Calorimeter with insulation around

7: Micro Calorimeter: connetion for the hose
8a: Introduction tube for the sample cell
8b: Introduction tube for the reference cell
9: Duct heater (Lindab)
10: Computer
11: Heat control system (security device)

12: Manometer (Setaram)
13: Data acquisition/switch unit (Agilent)
14: Central Manometer

1: Connetion for the hose
2a: Introduction tube for sample cell
2b: Introduction tube for reference cell
3: Aluminim stopper
4: Sample cell
5: PT 100
6: PT 200
7: Over heat Thermostat

8: Duct heater 220V (Lindab)
9: Micro Calorimeter insulation (3 layers)
10: Plastic hose
11: Hose insulation
12: Sortie GAZ ENCIENTE (gas outlet)
13: SORTIE GAZ CELLULE (cell gas outlet)
14: ENTREE GAZ (gas inlet)
15: Air outlet

16: Metallic bar

Fig.X.2 : Micro calorimeter details

1. Procedure

The procedure consists of five different stages: "Place the sample into the calorimeter, Cooling process; Turning the process; Heating process and End of the process".

1.1 Place the samples into the Calorimeter
1.1.1. Opening of the introduction tubes
1.1.2 Sample preparation

1.2 Cooling process
1.2.1 Connect the Thermojet to the Micro Calorimeter
1.2.2 Start the heating devices (heat control system and duct heater)
1.2.3 Start the Thermojet
1.1.4 Start the PC program

1.3 Turning the process (Cooling to heating process)
1.3.1. Stop the PC program
1.3.2 Turn off the Thermojet

1.4 Heating process
1.4.1 Input for the PC program
1.4.2 Start the PC program

1.5 End the process
1.5.1 Stop the PC program
1.5.2 Stop the heating devices (heat control system and duct heater) and dry air flow
1.5.3. Remove the sample from the Micro Calorimeter
1.5.4 Clean the sample cell

1.6 Data analysis
1.6.1 Collect of data
1.6.2 Calculation

1.1 Cooling process
1.1.1 Opening of introduction tubes
The steps below have to be followed when the sample cell introduction tubes have to be opened to avoid moisture inside the calorimetry.

1. Open the valve in the manometer to increase N_2 gas pressure from 0.5 to 1 bar. Check the pressure at manometer MM1 (Fig.X.1:12);
2. Fully open the valve "GROS DEBIT" (Fig.X.3) in the manometer. It is normal for the pressure to drop off on MM1(26) at this moment;
3. Close the "SORTIE GAZ ENCEINTE"(Fig. X.4) in the microcalorimeter using the screw.
4. Remove the screw from the "SORTIE GAZ CELLULE" (Fig. X.4);

5. Place the sample and reference sample in the proper places in the microcalorimeter, follow the steps proposed at "*2.1.2 Sample preparation"*
6. After that: close the screw of the "SORTIE GAZ CELLULE" (Fig.X.4);
7. Open the "SORTIE GAZ ENCEINTE"(Fig.X.4) in the microcalorimeter by removing the screw;
8. Close the valve "GROS DEBIT" in the manometer (Fig.X.3);
9. Open the valve to decrease N_2 gas pressure from 1 to 0.5 bar. Check the pressure at MM1 (Fig.X.3)

Fig. X.3: Gross debit valve in the manometer	Fig. X.4: Lid of calorimeter
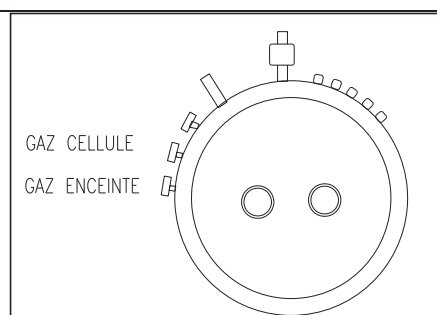
1.1.2 Sample preparation
A small amount (usually around 10 mg) of silver iodide, AgI, is sprinkled upon the sample surface. The silver iodide is added to reduce the super cooling of the water at the sample surface. It is necessary to obtain the weight of the:

- Sample holder + spring + lid (empty cell);
- Sample;

Close the sample holder as showed in the Fig.X.5, it should be well locked using the lid and the spring around the lid and weight:

- Sample holder + spring + lid (empty cell)+ sample +AgI as shown in the Table X.1.

Table X.1: Sample weight

Material	Weight (in grams)
Sample holder +spring + lid (empty cell)	
*Sample	
Sample holder + spring + lid + sample +AgI	

*Use always the weight of the sample as input in the computer program.
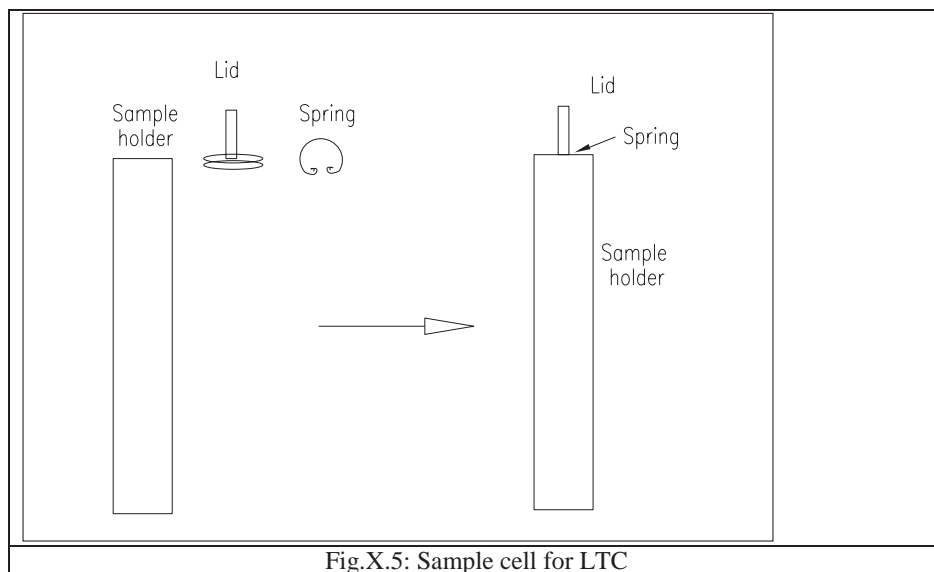
Fig.X.5: Sample cell for LTC

Place the sample cell in the sample cell introduction tube (Fig X.6 -22) of the calorimeter using the metallic bar (Fig. X.6 -23), as shown in the Figure X.6. After that, place the "aluminium stopper" in the same introduction tube.

Sample cell introduction tube: 22
Reference cell introduction tube: 22a
Connection for nozzle: 19
Metallic bar: 23

Fig. X.6: Schematic drawing of LTC
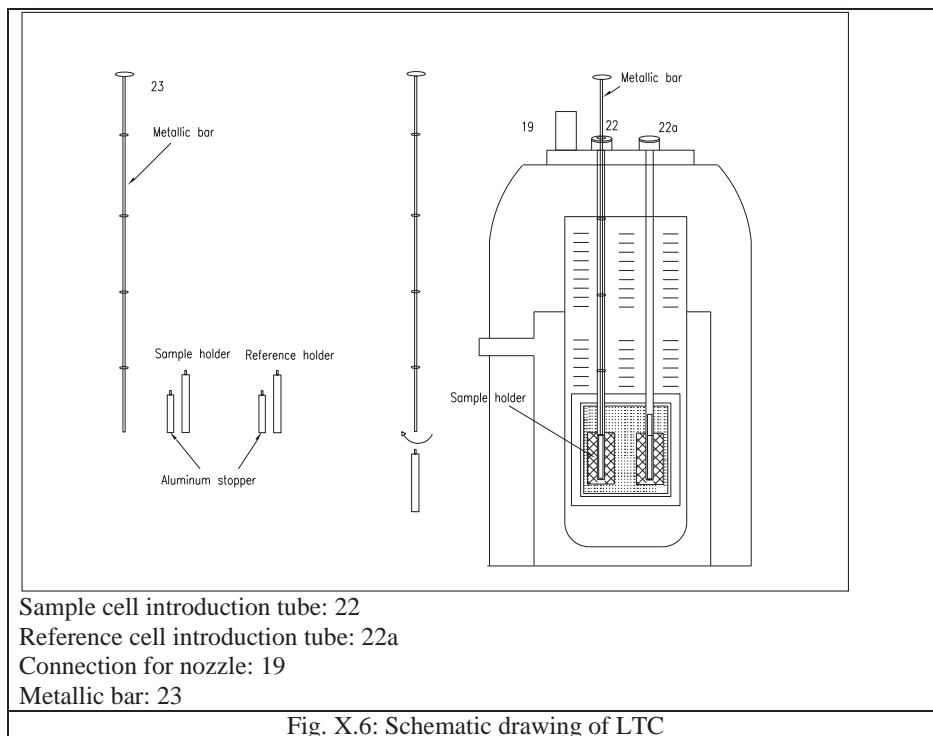
1.2 Cooling process of LTC

Turn on the plug to activate the ventilation system (red light on) for the Thermojet. It is located on the wall. The plug should always be on.

1.2.1 Connect the Thermojet to the Micro Calorimeter

1. Remove the metallic protection from the calorimeter (see Fig.X.7);
2. Open the screw in the calorimeter using the "hex key";
3. Open the screw in the nozzle holder;
4. Connect the ThermoJet nozzle to the calorimeter;
5. Fasten the screw in the calorimetry using the "hex key";
6. Place an extra black insulation; use the duct tape to close it. Close the screw in the nozzle holder.
7. Turn on the calorimetry in the illuminated bottom in the calorimeter control
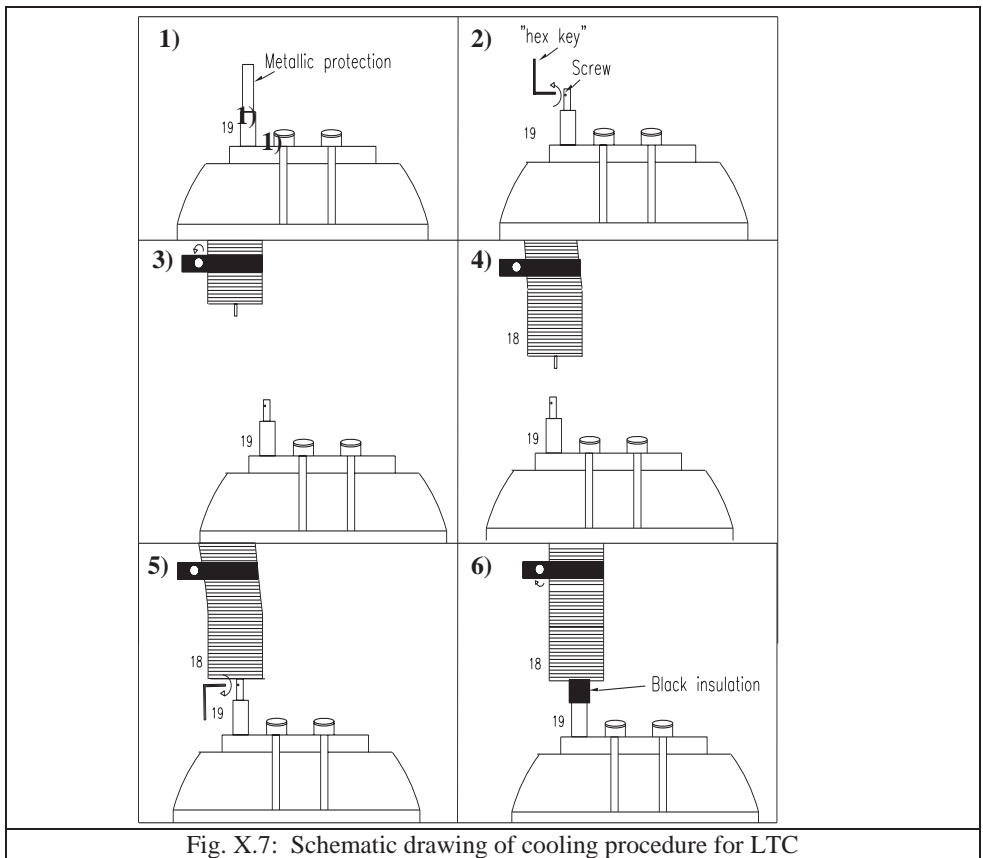
Fig. X.7: Schematic drawing of cooling procedure for LTC

1.2.2 Start the heating devices

1. Turn on the heat control system (Fig X.8);
2. Turn on the plug on the wall to activate the duct heater (Lindab) of the Micro Calorimeter hose (Fig X.9).
3.
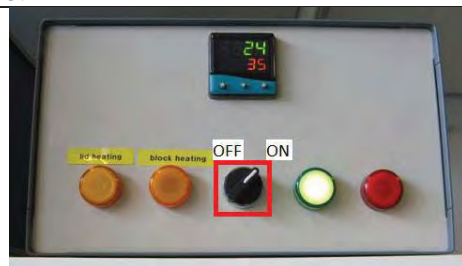
| Fig. X.8: Heating control system | Fig. X.9: Plug to activate the duct heater |

1.2.3 Start of ThermoJet

1. Touch the screen of the equipment to turn it on, see Fig. X.10;
2. Press "restart" on the screen of Thermojet;
3. Wait 5 minutes until the machine shows idle in the screen (upper right);
4. Activate the SET 3, -85ºC touching the screen on the Thermojet screen; check the air flow of 13 scfm;
5. Wait for 25 minutes to turn on the computer.

	Off				
	Set 1	25.00			Air
	Set 2	5.00			
5)			6)		Air flow
	Set 3	-85.00	13		
	Manual	Program 1-4	Trending	Utilities	

Fig.X.10: Thermojet screen
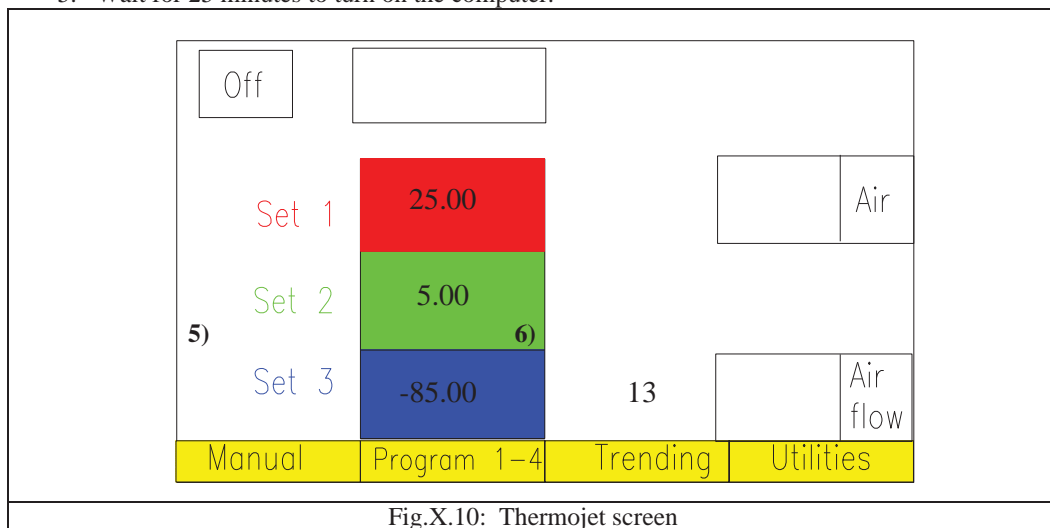
2.2.4 Start of the PC program

Switch on the computer using the program CalBYGall.1v.proj.

Press the arrow in the right upper of the computer screen ➡

Fill up the fields: "Number", "Sample description", "Type of sample holder", "Sample preparation", "Weight".

On the right of the screen fill up the fields, as shown Table X.12.

Logger Timing	
1000	Time Between datalogger run
60	Time between write to file
50	Log at voltage jumps
Temperature Control	
▷	**Control Temp. Block (False)**
-55	Desired Temperature
3.3	Temperature gradient
0	Temperature Band-Block
1	Aggressiveness - Block
▷	**Control Temp. Lid (False)**
25	Desired Lid temperature
0	Temperature Band-Lid
1	Aggressiveness - Lid
500	Offtime for lidheat
Size of Running Mean	
1	Heatflow
1	PT 100
1	PT 200
1	Lid Temperature

Fig. X.11: Screen of the program	Fig. X.12: Example of test parameters for cooling process

"Control temperature of the lid" in the arrow at the left part of the computer screen, see Figure X.8. Make sure the arrow is green.

Press save the data in the green arrow in the lower part of the computer screen.

1.3 Turning the process
1.3.1 Stop the program

At the main screen of the PC program check the PT100. If Pt100 is below the cooling set temperature (Ex:– 55 ºC), press "Stop Program" in the lower left corner of the PC screen.

1.3.2 Turn off the Thermojet
On the screen of ThermoJet (see Fig X.10)
- − Activate the SET 2, 5ºC pressing the screen of the ThermoJet,
- − Decrease the gas flow to 5, pressing screen of the ThermoJet;

After that:
1. Unfreeze the black insulation (sponge) using a hair drier. After that, take off the duct tape and the black insulation from the calorimeter, see Fig. X.13;
2. Open the screw in the calorimeter using the "hex key" and open the screw in the Thermojet nozzle holder;
3. Move the ThermoJet nozzle gently upwards. Fasten the screw in the nozzle holder;
4. Fasten the screw in the calorimeter using a "hex key";

5. Take place the metallic protection on the calorimeter air inlet;
6. Use the styrofoam board between the ThermoJet nozzle and the calorimeter. Fix it with duct tape.
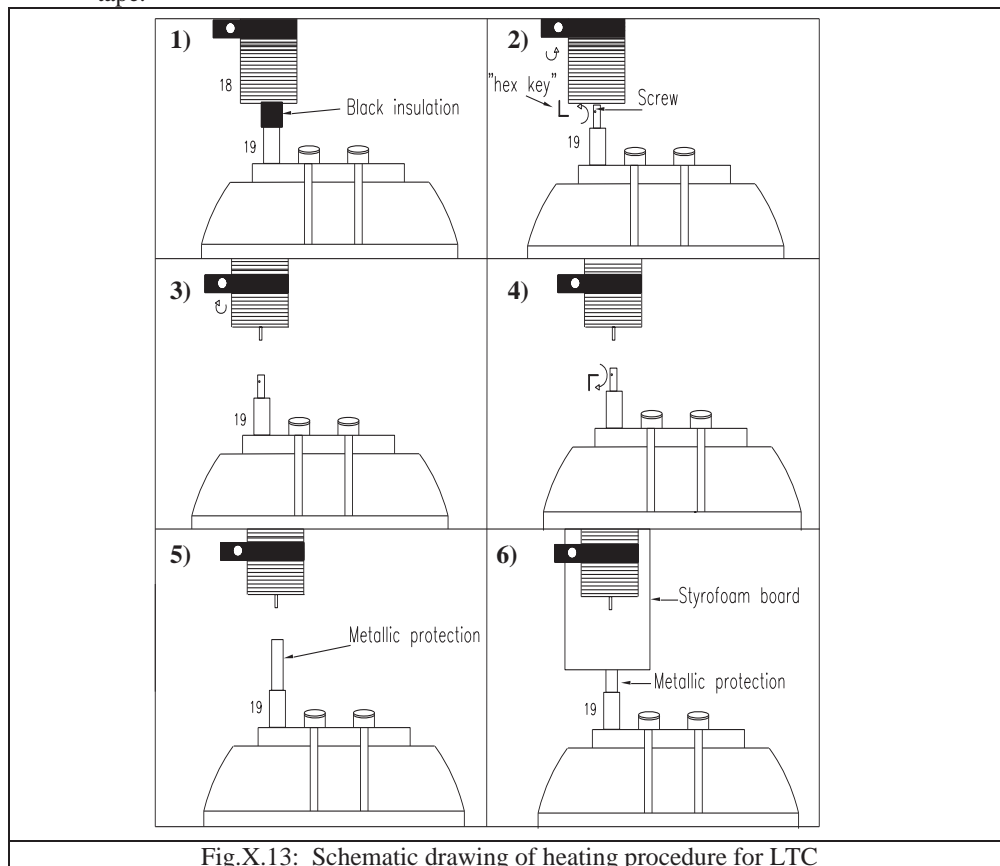
Fig.X.13: Schematic drawing of heating procedure for LTC

Switch off the ThermoJet by pressing "off" in the upper left corner of the screen. Confirm the next step by pressing "yes". The ThermoJet now performer an automatic shut down procedure (about 10 minutes). After the screen turns black and the airflow the stops the styrofoam board can be removed.

1.4 Heating process
1.4.1 Input of data and control parameters
Change the parameters on the right of the screen, see Table X.2:

Table X.2: Parameters for heating process of LTC

1000	Time
300	Time between measurements
20	Log at voltage jumps
1	Size of running mean heat flow
1	Size of running
1	Size of running
1	Size of running
▷ Control block temperature	
20	Desire temperature
4.1	Temperature gradient
0	Temperature band block
1	Aggressiveness
▷ Control lid temperature	
30	Lid temperature
0	Temperature band lid
1	Aggressiveness

Press "Control temperature of the block" and "Control temperature of the lid" in the arrow at the left part of the computer screen, see table 3. Make sure the arrow is green.

Press save the data in the green arrow in the lower part of the computer screen to start to save the data

1.5 End the process

1.5.1 Stop the PC program
When Pt100 is about the heating set temperature (Ex: 20ºC), press "Stop Program" on the bottom left corner of the PC screen. Press "File" and "Exit" to shut down the PC program. Remember to transfer the saved files from both the cooling and the heating process to a USB storage device or upload it to CampusNet.

1.5.2 Stop the heating devices (heating control system and duct heater) and dry air flow

1. Turn off the heat control system;
2. Turn off clockwise the dry air valve at the Central manometer;
3. Turn off the plug on the wall to shut down the duct heater (Lindab) of the Micro Calorimeter

1.5.3 Remove sample from the Micro Calorimeter
1. Turn clockwise the regulation valve at the Central Manometer. The N_2 pressure manometer will increase from 0.5 to 1 bar;
2. Check the pressure at theMM1 from the Manometer (from Setaram). The pressure must be around 1 bar;
3. Fully open counter clockwise the valve "GROS DEBIT" at the Manometer. The pressure at the manometer MM1 is decreased to 0.
4. Close the screw of the "SORTIE GAZ ENCEINTE" at the top of the Micro Calorimeter
5. Open the screw from the "SORTIE GAZ CELLULE" on the top of the Micro calorimeter.

6. Open the sample cell introduction tube on the top of the Micro Calorimeter
7. Use the metallic bar to remove the aluminum and sample cell trough the introduction tubes of the Micro Calorimeter.
8. Close the lid of the introduction tube at the Micro Calorimeter. Press the lid on with a screwing motion.

1.5.4 Clean the sample cell
1. To open the sample cell: using a pincers to remove the z-ring from the top of the sample cell. Open the lid of he sample cell using a screw.
2. Remove the sample from the sample cell. Place the sample in the weighing glass to limit evaporation.
3. Weigh the sample within the weighing glass using an accurately scale (0.0001).

1.6 Data analysis
1.6.1 Collect the data

The final data is collected trough the computer and analyzed and discussed trough graphics and values. The heat flow is measured as a differential output signal, q (µV) and it is converted to Dq/Dt (mcal/sec/g$_{sample}$) and then converted to a heat flow, see Section 2.3.2.1 of the thesis

Table X.3 shows the adopted values for the determination of threshold pore size.

Table X.3: Parameters used for the threshold pore size determination for LTC (Sun and Scherer, 2010).

Description	Symbol	Addopted value	Unit
Heat of fusion of ice (heating and melting)	ΔH_{fus}	332.4	J/g$_{ice}$
Surface tension liquid-solid	$\sigma_{l\text{-}s}$	0.0409+3.9·10^{-4}ΔT	N/m
Density of the ice	P_{ice}	$(0.9167 - 2.053 \cdot 10^{-4} \cdot T - 1.357 \cdot 10^{-6} \cdot T^2) \cdot 10^{-3}$	g/cm³
Freezing temperature of the pore	T_o	273	K
Molar mass of the liquid	M	18.10^{-3}	Kg/mol

1.6.2 Calculation of the apparent heat capacity

Correlated data on time, temperature and heat flow are measured and processed to provide the output given in Table X.4.

Table X.4: Output from low temperature calorimeter test of a 14.9506 g cement paste sample (not all decimals shown). Text in italic and bold is added for explanation of equations

	Registered	Cal.	Registered				Temp		Calculated		
	Time	Elapsed time	Heat flow	Pt100	Pt200	Lid temp.	Setpo int	dT/dt	Cpa. norminal	Cpa. true	Integrated qi
i		t_i	E_i	T_c				dT/dt		$C_{pa,true}$	q_i
		s	µV	°C	°C	°C	°C	m °C /s	J/ °C /g	J/ °C /g	
		s	V 10⁻⁶	°C				°C /s 10⁻³	J/(°C kg) 10⁻³	J/(°C kg) 10⁻³	
1	08-04-2008 18:52	43.37	-5.542	19.65	20.14	34.08	0	0	0	0	0
2	08-04-2008 18:52	45.39	-4.846	19.79	20.20	34.36	NaN	68.70	-0.00479	-7.9E-05	-1.1E-05
3	08-04-2008 18:52	47.39	-4.792	19.93	20.07	34.64	NaN	69.24	-0.00474	-7.8E-05	-2.2E-05

The following equations are used (Equations X.1 to X.5). :

$$C_{pa,true} = \frac{E_i}{\frac{dT}{dt} \cdot S_M \cdot w} \text{ ,J/(°C·kg)} \qquad \text{(Equation X.1)}$$

where

w is the sample weight in kg

$$\frac{dT}{dt} = \frac{T_{c,i} - T_{c,i-1}}{t_i - t_{i-1}} \text{ , °C /s} \qquad \text{(Equation X.2)}$$

$$S_{M,cal-1} = 58.845 + 0.03642 \cdot T_c - 0.000454 \cdot T_c^2 \text{ [V/W 10}^{-3}] \text{ (T}_c \text{ in °C)}$$

$$q_i = \frac{E_i \cdot (t_i - t_{i-1})}{S_M \cdot w} + \sum q_{i-1} \text{ , J/kg} \qquad \text{(Equation X.3)}$$

$$C_{pa,nominal} = \frac{dq}{dt} \cdot \frac{1}{A} \cdot \frac{1}{w} \text{ , J/ °C·kg)} \qquad \text{(Equation X.4)}$$

where

$$\frac{dq}{dt} = \frac{E_i}{S_M} \text{ [J/s] (heat flux)} \qquad \text{(Equation X.5)}$$

$$A = -0.355 \cdot 10^{-6} \cdot T_c - 0.00093 \text{ during cooling and}$$

$$A = 0.001147 \text{ during heating}$$

Example (line 2):

$$C_{pa,true} = \frac{-4.846 \cdot 10^{-6}}{0.0687 \cdot 59.388 \cdot 14.95} = -79.43 \cdot 10^{-6} \qquad [J/(°C·kg)] \qquad \text{(Equation X.1)}$$

where

w = 0.01495 [kg]

$$\frac{dT}{dt} = \frac{19.79 - 19.65}{43.37 - 45.39} = 0.0687 \text{ [°C /s]}$$

(equation 2)

$$S_M = 58.845 + 0.3642 \cdot 19.79 - 0.000454 \cdot 19.79^2 = 59.388 \text{ [V/W 10}^{-3}] \qquad \text{(Equation X.2)}$$

$$q_i = \frac{-4.846 \cdot 10^{-6} \cdot (43.37 - 45.39)}{59.388 \cdot 0.01495} + 0 = 11.00 \cdot 10^{-6} \text{ ,J/kg} \qquad \text{(Equation X.3)}$$

(equation 4)

$$C_{pa,no\min al} = \frac{-4.846 \cdot 10^{-6}}{(43.37 - 45.39)} \cdot \frac{1}{0.355 \cdot 10^{-6}} \cdot \frac{1}{0.01495} = 5.847 \cdot 10^{-3} \text{ [J/(}^o\text{C} \cdot \text{kg)]} \qquad \text{(Equation X.4.)}$$

1.6.3 Calculation of the ice formation (proposed by Sun and Scherer (2010))- used for the present work

```
clear all

time=xlsread('LTC_6w55.xlsx','C_6w55_dried','B:B');
temp=xlsread('LTC_6w55.xlsx','C_6w55_dried','E:E');
heat=xlsread('LTC_6w55.xlsx','C_6w55_dried','T:T');

lheat=length(heat);
ltime=length(time);
ltemp=length(temp);

Pice1=250; Pice2=750; Pice3=880; Pice4=1000; Pice5=1420; korr=0.00070;
totwe=10.9803;

  % J/s
initial heat flux before bulk water freezes
% for the freezing circle, give the calculate range:
PQ1=250; PQ2=750;
q1=-0.000916; %(q=dT/dt,cooling rate)
Q10= -0.0015;    % heat flux befor bulk water freezes
mc1=0;           % inital ice content
Wthfreeze=332.4; %J/g solidification energy for freezeing
h=0;
for i=PQ1:1:PQ2-1
h=h+1;
Cw=4.222;
Ci=2.114;

X1(h)=exp((Cw-Ci)*(temp(i+1)-temp(i))/Wthfreeze);

mc1(h+1)=mc1(h)+0.5*(temp(i+1)-temp(i))*(heat(i)-Q10)/(q1*Wthfreeze)*...
    X1(h)+0.5*(temp(i+1)-temp(i))*X1(h)*(heat(i+1)-Q10)/(q1*Wthfreeze);

temp1(h)=temp(i);
end

% for the melting circle, give the calculate range:

Pice3=880; Pice4=1000; Pice5=1410;
q2=0.00113;    %%(q=dT/dt,heating rate)
Q20= 0.0015;   %% heat flux before ice melts
mc2m=0;        %% inital melted ice
```

```matlab
h=0;
for i=Pice4:1:Pice5-1
h=h+1;
Cw=4.222;
Ci=2.114;
%solidification energy for melting
Wthmelt(h)=(333.8+1.797*(temp(i)));%J/g
X2(h)=exp((Cw-Ci)*(temp(i+1)-temp(i))/Wthmelt(h));
mc2m(h+1)=mc2m(h)+0.5*(temp(i+1)-temp(i))*(heat(i)-Q20)/q2/Wthmelt(h)*...
    X2(h)+0.5*(temp(i+1)-temp(i))*X2(h)*(heat(i+1)-Q20)/q2/Wthmelt(h);
temp2(h)=temp(i);
end
mc2mstop=mc2m(Pice5-Pice4-1);
mc2=mc2m-mc2mstop;

hold on

figure(1)

plot(temp1,mc1(:,1:length(mc1)-1))
plot(temp2,mc2(:,1:length(mc2)-1),'r')
hx=xlabel('Calorimetric block temp. [^oC]')
hy=ylabel('Mass of ice [g]')
set([hx,hy,gca],'fontsize',14)
title('Mass of ice ')
axis([-50 10 0 2])
grid on
hold off
```

Appendix XI - Procedure for mercury intrusion porosimetry (MIP)

Purpose
Determination of threshold (or characteristic) pore sizes and total assessable porosity. A broad range of pores can be measured starting from a radius of approximately 2 nm (pressure = 400 MPa) up to approximately 100 µm (Micromeretics 2000).

Materials
- 4.8 mm sieve
- Grease
- Liquid mercury
- Gloves
- Proper containers for mercury discharge
- Penetrometer for solid sample, see Table XI.1

Table XI.1: Penetrometer selected guide (Autopore IV 9500 Micrometrics, 2000).

Bulb Volume (cc)	Sample Type	Maximum Measurable Volume (cc)	Total Stem Volume (cc)	Maximum Head Pressure (psia)	(kPa)	Penetrometer Constant (µL/pF)	Physical Dimensions I (mm)	H (mm)	D (mm)	Part Number
3	Solid	0.387	0.412	4.68	32.3	10.79	227	242	1.473	950-61713-00
3	Solid	1.116	1.190	4.68	32.3	21.63	227	242	2.502	950-61715-00
3	Powder	0.387	0.412	4.68	32.3	10.79	227	242	1.473	950-61714-00
3	Powder	1.116	1.190	4.68	32.3	21.63	227	242	2.502	950-61716-00
5	Solid	0.366	0.392	4.45	30.7	10.79	215	230	1.473	950-61707-00
5	Solid	1.057	1.131	4.45	30.7	21.63	215	230	2.502	950-61709-00
5	Solid	1.716	1.836	4.45	30.7	27.82	215	230	3.188	950-61711-00
5	Powder	0.366	0.392	4.45	30.7	10.79	215	230	1.473	950-61708-00
5	Powder	1.057	1.131	4.45	30.7	21.63	215	230	2.502	950-61710-00
5	Powder	1.716	1.836	4.45	30.7	27.82	215	230	3.188	950-61712-00
15	Solid	0.366	0.392	4.45	30.7	10.79	215	230	1.473	950-61701-00
15	Solid	1.057	1.131	4.45	30.7	21.63	215	230	2.502	950-61703-00
15	Solid	1.716	1.836	4.45	30.7	27.82	215	230	3.188	950-61705-00
15*	Solid	3.007	(3.263)	4.45	30.7	33.13	215	230	4.813	950-61724-00
15*	Solid	3.857	(4.185)	4.45	30.7	34.48	215	230	4.813	950-61725-00
15	Powder	0.366	0.392	4.45	30.7	10.79	215	230	1.473	950-61702-00
15	Powder	1.057	1.131	4.45	30.7	21.63	215	230	2.502	950-61704-00
15	Powder	1.716	1.836	4.45	30.7	27.82	215	230	3.188	950-61706-00

Equipments
- Autopore IV 9500 "*Micromeritics Instruments*"

Specimens
Cement paste. Sample piece size minimum 5 mm (confirmation from literature to be obtained), max 10 mm (depends on penetrometer size).

Procedure

Selection of penetrometer

According to Auto Pore IV Micrometrics Manual, the maximum (total) intrusion volume of the sample should not exceed 90% nor be less than 25% of the total Stem volume of the penetrometer (see Table XI.1, column 4). The Stem volume is the capacity of the penetrometer and calculated according to Equation XI.1.

$$Stem = \left(\frac{3.14 \cdot D^2 \cdot H}{4} \right) \cdot 0.001 cm^3/mm^3$$	
Equation XI.1: Total Stem volume	Fig. XI.1: Penetrometer
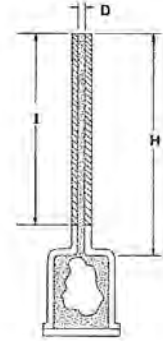
The maximum intrusion volume required by the sample cell is given by the Equation XI.2:

$$V_{max} = \frac{P_{vol}}{STEM_{vol}} \cdot 100 \qquad \qquad \text{(Equation XI.2)}$$

Where
$P_{vol} = Fractional\ pore\ volume\ \cdot sample\ volume$
$STEM_{vol}$ given in Equation 1

Selection of pressure range and steps

The selection of a pressure table is required for the starting of the test, see Table XI.2. The pressure increases according with the values chosen for the table and it may reaches the maximum pressure of the equipment is 414 MPa (approx.).

Table XI.2: Adopted pressure for MIP

MIP adopted pressure (MPa)			
0.003	4.301	90.789	18.192
0.005	4.394	109.977	17.921
0.010	5.374	112.849	14.074
0.014	5.496	136.877	13.805
0.021	6.650	137.548	10.665
0.028	6.812	170.275	10.333
0.038	8.105	172.282	8.552
0.041	8.258	206.732	8.262
0.052	10.176	241.271	6.490
0.059	10.320	275.713	6.217
0.072	12.874	310.181	5.067
0.090	13.073	344.581	4.837
0.110	15.993	378.976	3.646
0.138	16.168	412.461	3.464
0.172	19.709	317.711	2.916
0.207	19.955	244.744	2.763
0.250	24.124	188.232	2.260
0.326	24.777	144.882	2.082
0.394	29.329	110.424	1.780
0.495	30.926	85.623	1.674
0.590	36.520	66.334	1.463
0.773	38.456	50.781	1.322
0.940	44.776	50.505	1.022
1.184	47.410	39.633	0.775
1.495	55.670	39.415	0.594
1.839	59.137	30.000	0.474
2.247	70.080	29.680	0.360
2.896	72.905	23.052	0.224
3.567	87.762	22.788	0.120

Sample preparation
1. Crush the sample in pieces of 5 mm (approx.) using a porcelain mortar.
2. A sieve is used to verify the size of the particles;
3. Crashed sample is weighted and placed in a sample cell, called as penetrometer (Fig.XI.1).
4. Use grease around the lid of the penetrometer and then close the penetrometer and fast it using a screw.

Test
The tests are carried out in agreement with the manual for the equipment.

5. Place the penetrometer at the vacuum pressure chamber where it is evacuated, see Fig. XI.2.
6. Wait the sample cell filling by mercury (approximately 1 hour). When it is ready the screen shows "idle".
7. Transfer the penetrometer to the high pressure chamber (approximately 2 hours).

Fig. XI.2: MIP equipment

Parameters
-   Parameters adopted in the MIP test are:
-   Hg contact angle = 141.30 degrees
-   Hg surface tension = 485x10^{-7} MPa
-   Hg density = 13.5335 g/cm³
-   Reached pressure= 414MPa (maximum pressure of the MIP equipment)

Collect data
The final data is collected trough the computer and analyzed and discussed trough graphics and values:

The pore threshold size is calculated based on the pressure value obtained by the computer by the Washburn equation (see Equation XI.3).

$$r_W = \frac{-2 \cdot \gamma_{s-l} \cdot \cos\theta}{p}$$ (Equation XI.3)

where

r_w	pore radius (Washburn Equation), m
γ_{s-l}	surface tension solid-liquid, N/m
θ	contact angle between the liquid and the pore wall, degrees,
p_w	pressure applied on mercury to intrude the pore, N/m².

The total porosity is measured when the volume of mercury measured is reached at the highest pressure and it is given by the Equation XI.4

$$P = V_{MIP} \cdot D_{bulk}$$ (Equation XI.4)

where
P porosity,
V_{MIP} specific volume of pores given by MIP, cm³/g
D_{bulk} bulk density, cm³/g

Safety use
Mercury
After the test, the used tools should be carefully cleaned (mainly concern to the penetrometer). The mercury should be removed and storage in special flasks which keeps it closed and distant of people contact.

A special discharge of the sample containing mercury is also required.

Use of solvents (Isopropanol)
Isopropanol bottles must be store in a cool and well ventilation place, way from areas where the fire may be acute. The empty bottles of isopropanol must be placed in the fume cabinet for 24 hours and then discharged in proper recycle containers.

The use of solvents including isopropanol should be undertaken always inside a fume cabinet. Protection masks are also available in the market.

Appendix XII - Procedure for SEM

Procedure for SEM is divided in sample preparation data acquisition in SEM for determination of porosity

Sample preparation is carried out in 3 steps:
- Impregnation of the samples for SEM
- Polishing of the samples for SEM
- Carbon coating for SEM samples

Procedure for impregnation of samples for SEM
Purpose
The purpose of the method is to impregnate dry samples of cementitious materials for subsequent polishing.

Principle
The dry specimen is evacuated in a desiccator (an impregnation unit) and epoxy is poured over (see Fig.XII.1).

Specimen
The specimen should be dry (see method for hydrations stop and drying) and fit into the mould, i.e. have max size 2 mm less than the diameter of the mould, see Fig.XII.2.

Fig. XII.1 : Impregation unit with molds and tube for inlet of epoxy	Fig. XII.2: Silicone mould with sample
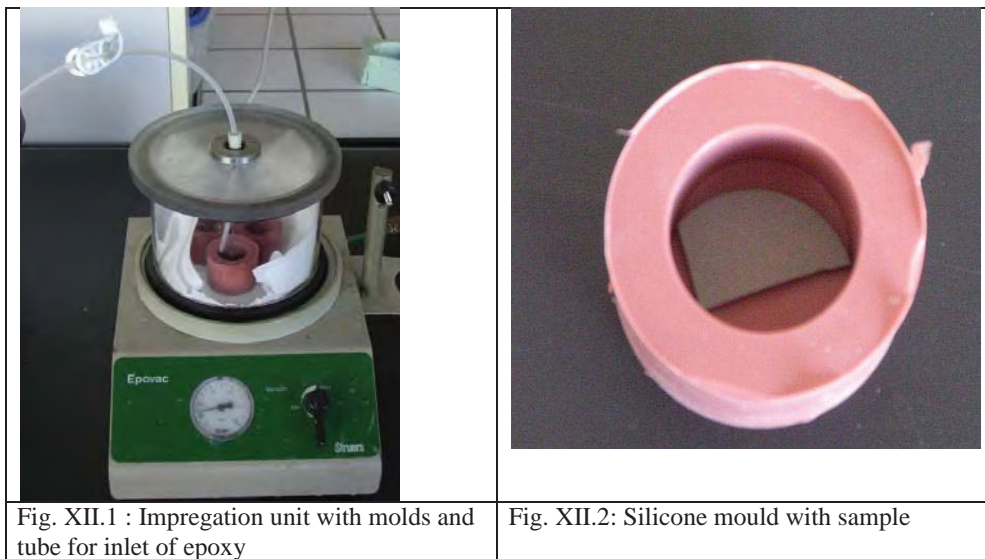
Materials and equipment
- Silicone/plastic moulds (ϕ=30mm)
- Silicone grease for **lubrication of moulds ("form oil")**
- Impregnation unit from Epovac (10-20 mbar) (or desiccator) , Fig. XII.1

- Impregnation kit: Disposable tube, φ of 2 mm, length 30 cm, disposable beaker and spatula (for mixing epoxy) from Struers
- Epoxy (Epo-Tek 301-1 from Epoxy Technology, www.epotek.com)
- Hardener (Epo-Tek 301-2 from Epoxy Technology, www.epotek.com)
- Scale (precision of 0.01 g)
- Gloves and safety glasses
- Fume cabinet

Safety requirements
All work including weighing of materials is to be undertaken in a fume cabinet
Personal training: Epoxy course
Personal protection: Lab coat, plastic apron, gloves 4H, safety glasses
Waste: Bucket with a plastic bag placed in the fume cabinet

Procedure
1. Mount a tube with a cover at the end through the top of the desiccator
2. Lubricate the moulds
3. Place the specimen in a mould with the picture side up (the sample is flipped over, see step 11). The mould is placed at the centre of the desiccator
4. Close the desiccator and lower the cover over the mould
5. Evacuated the desiccator is to 20-10 mbar and keep the vacuum for approximately 30 minutes
6. Weigh out 25 g epoxy and 3 g of hardener and mix it for 20 seconds
7. Mix the epoxy and led it into the desiccator through the tube controlled by the clips. Fill the moulds with epoxy
8. Keep the evacuation until entrapped air has left the epoxy (changing colour from white to transparent)
9. Open the valve of the desiccator to let the air in
10. Remove the samples mould from the desiccator
11. Flip the specimen to place the picture side downwards and press the sample against the bottom using the spatula
12. Dismount the desiccator and place the mould with epoxy to harden for 24 hours in a closed box to control the hardening process.

Possible re-impregnation
See "***Procedure for polishing of samples for SEM***"

Procedure for polishing of samples for SEM

Purpose
The purpose is to polish impregnated samples for SEM. The procedure of polishing may change according to the sample used (age, material etc.)

Principle
Use of diamond discs to polish the surface of the impregnated samples.

Specimen
Cement pastes impregnated by resin (see "*Procedure* **for impregnation of samples for SEM**").
Select specimens with similar abrasion resistance to be polished at the same time. Up to six samples may be polished at the same time.

Materials and Equipments
- Polish machine - Abramin 03946146 from Struers A/S (see Fig.XII.3)
- Sample holder
- MD Piano 80, 600, and 1200 from Struers
- MD Pan (named 6 μm) and 6 µm DP spray from Struers A/S
- MD Pan (named 3 μm) and 3 µm spray from Struers A/S
- DAC (named 1 μm) and 1 µm spray from Struers A/S
- Butandiol
- Ultrasound bath from VWR
- Isopropanol
- Pressurized air

Fig.XII.3 :Polish machine Abramin 03946146 from Struers A/S

The steps in the polishing procedure are summarized in Table XII.1.

Table XII.1: Steps in polishing procedure

Step	Purpose	Grinding or polishing plate	Spray	Solution for lubrication	Approximate load and duration1	Accept criteria
1	Removal of excess epoxy and planing	MD Piano 80	-	Water		Epoxy free surface and perpendicular
2	Removal of water exposed surface	MD Piano 80	-	Butandiol 2	10-20 N, ½ min	50-100 µm is to be removed3. In total 0.5 mm should be removed after cutting.
3	Possible re-impregnation		-			
4	Polishing, removal of coarse scratches	MD Piano 600	-	Butandiol	10-20 N (½ - 4 min)	Removal of coarse scratches
5	Polishing, removal medium of scratches	MD Piano 1200	-	Butandiol		Removal of medium sized scratches
6	Polishing, removal fine of scratches	MD-Pan (6)	6 µm	Butandiol	3 min	Removal of fine scratches
7	Polishing, removal fine of scratches	MD-Pan (3)	3 µm	Butandiol	3 min	Removal of fine scratches
8	Polishing, removal very fine of scratches	Dac	1 µm	Butandiol	3 min	Removal of very fine scratches

Step 1 -Removal of excess epoxy and planning
1. Place specimens in sample holder
2. Place MD Piano 80 in the polishing machine
3. Wet plate with water
4. Lower samples when the plate is wet and keep wetting
5. Grind until all excess epoxy is removed and the plane and cylindrical surfaces are perpendicular
6. Remove sample holder and dry specimens (in holder) by pressurized air
7. Turn plate to remove excess water and dry by pressurized air

Step 2 - Removal of water exposed surface
1. Wet plate with butandiol
2. Lower samples when the plate is wet and keep wetting

---

[1] Load and duration to be determined based on a trail. Michal Dissing suggest 15 kg for 6 specimens
[2] or glycerine (or "blue or brown) polishing solution from Struers)
[3] measure thickness of trail sample before and after and determine combination of load and duration

3. Lower samples when the plate is wet and keep wetting
4. Grind until 50-100 μm is removed (measure thickness of trail sample before and after and determine combination of load and duration).
5. Remove sample holder and clean samples 10 s in ultrasonic bath with isopropanol
6. Remove plate and clean it by water and soft brush, leave to dry in vertical position
7. Clean under plate with a cloth and water (the plate must be fully clean)

In total 0.5 mm should be removed after cutting. If the new surface is fully impregnated go to step 4, else proceed with Step 3.

Step 3 - Possible re-impregnation
1. Dry the specimens at a desiccator with silica gel until the next day or evacuate for three hours
2. Place specimens in beaker with face down and lifted slightly by rubber bands
3. Evacuate and add epoxy, which will form foam
4. Take out the specimens, place them on plastic with face up and place small pieces of plastic (diameter 10 mm larger than specimen) on picture side. Press down the plastic to remove all air possible bobbles
5. Leave for 24 hours
6. Remove excess epoxy by grinding manually on Piano 80 (if flouorescence in epoxy check in stereo microscope with blue/yellow filter and UV light)
7. Remove sample holder and clean samples 10 s in ultrasonic bath with isopropanol

Steps 4 and 5 Polishing, removal of coarse and medium scratches
1. Place MD Piano 600 / MD Piano 1200 in the polishing machine
2. Wet plate with butandiol
3. Lower samples when the plate is wet and keep wetting
4. Polish until coarse /medium sized scratches are removed (check in stereo microscope)
5. Remove sample holder and clean samples 10 s in ultrasonic bath with isopropanol
6. Remove plate and clean it by water and soft brush, leave to dry in vertical position
7. Clean under plate with a cloth and water (the plate must be fully clean)

Step 6-8 Polishing, removal of fine and very fine cracks
1. Place MD-Pan 6μm / MD-Pan 3μm / Dac 1μm in the polishing machine
2. Wet plate with butandiol
3. Lower samples when the plate is wet and keep wetting
4. Spray with diamond spray 6μm / 3μm / 1μm
5. Polish until fine /very fine scratches are removed (check in stereo microscope)
6. Remove sample holder and clean samples 10 s in ultrasonic bath with isopropanol
7. Remove plate, store finest plate in top shelf. (Only clean with detergent and hard brush after x number of samples, leave to dry in vertical position)
8. Clean under plate with a cloth and water (the plate must be fully clean)
9. Wash hands

Procedure for carbon coating for SEM samples

Purpose
Cover a sample with carbon layer to be tested at SEM.
Principle
Evaporate a carbon thread on the top of the impregnated samples at vacuum.

Specimen
Impregnated and polished samples.

Materials and equipment
- Carbon evaporation unit Emitech K450x
- Carbon thread l=3.5m from Axlab
- Carbon tape from Axlab

Procedure
1. Place carbon tape from bottom side to picture side to improve the electrical contact between specimen and stage
2. Take place the samples at the position about 3-4mm (working distance) in the plastic glass (chamber) from the carbon evaporator
3. Prepare the double carbon thread as show the Fig.XII.4
4. Close the chamber and switch the power on
5. Evacuate the sample for 10 minutes (approx.) until a pressure of 0.02mbar is reached

Fig.XII.4Carbon thread

6. Close the shutter at the top of the chamber lid
7. Apply tension in the carbon thread pressing UP key. When it is become orange wait 10 seconds and press DOWN key
8. Open the shutter at the top of the chamber lid
9. Evaporate the carbon thread by pushing the HIGH CURRENT key. Keep the key pressed until it burns (6 seconds approx.)
10. Switch the power off.
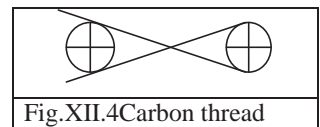
Procedure for data acquisition in SEM

Purpose
Obtain images with reasonable contrast and brightness to analyse the pore structure of impregnated and polished cement paste using back scattered electrons of SEM

Principle
Incident electrons get in touch with the sample surface which emits electron and the output signal from the samples is visualised on a monitor.

Specimen
Impregnated and polished cement pastes.

Materials and equipment
- SEM equipment – FEI Quantum 2000

Procedures
1. Tuned off the vacuum to put the sample in the SEM (press venting).
2. Take place the sample inside the equipment at a distance of 10mm from the beam using the "elephant".
3. Set the HV for about 15 kV and turn it on pressing HV key. HV is the filament responsible for the acceleration of the electrons. (This filament has to be changed after 200-400 hours of use.)
4. Set the spot size to 5 (approx.). Spot size is the diameter of the beam. At high magnification the spot size has to be decreased and at low magnification it is increased.
5. There are two ways to refine the focus of the image: moving the sample and move the beam. First move the sample up and down using the bottom indicate in the Fig. 1. After that move the beam to right or left pressing the right of the mouse. The best focus is always at the walking distance (WD) of 10mm.
6. Use a higher magnification ("videoscoppe" key) and increase the speed of the beam ("+"key) to improve the focus.

Technical terms used for SEM

This section focuses on the definitions of technical terms applied for microscopy analyses, which are important to understand the technique and its parameters.

Resolution

SEM´s resolution is dependent upon the size of the area from which signal is emitted from the sample. The size of this area is influenced by many factors including size of the primary beam, the composition of the specimen, the energy of the primary beam, and the type of signal (Michler, 2008).

Contrast

Contrast refers to the distribution of brightness in an image. An image with good contrast should have all 256 gray levels represented somewhere in the image reflecting the natural distribution all the way from black to white. A low contrast image has only middle gray tones present and appears washed out (Egerton, 2005).

Brightness

Brightness is also known as a black level of an image. Raises or lowers of the brightness will affect the light output of the image.

Signal to Noise (S/N) ratio

Signal to noise ratio is defined as the ratio of signal power to the noise power corrupting the signal (Egerton, 2005, Shields, 2010). The noise introduced to the final image is influenced by such factors as primary beam brightness, condenser lens strength, and detector gain. The resolution is also affected by the signal to noise ratio. When the resolution of a picture is increased its brightness decreases; thus the operator must balance all the competing factors to maximize the S/N ratio by increasing the total number of electrons recorded per picture point, see (Shields, 2010).

Aberrations

Aberration is an imperfection in image formation by the optical system of the microscope. There are a variety of abnormalities or aberrations that must be corrected for in an electron microscope: spherical (monochromatic), chromatic, astigmatism. Spherical aberration is common in SEM images because all electro-magnetic lenses are bi-convex converging lenses. If spherical aberration is present the electrons will pass along the axis of the electron beam and refract less than electrons passing through the periphery of the electron beam creating more than one focal point and therefore resulting in a large and unsharp spot, see Fig.XII.5(a).

Fig. XII.5: (a) Spherical aberration, and (b) Non spherical aberration
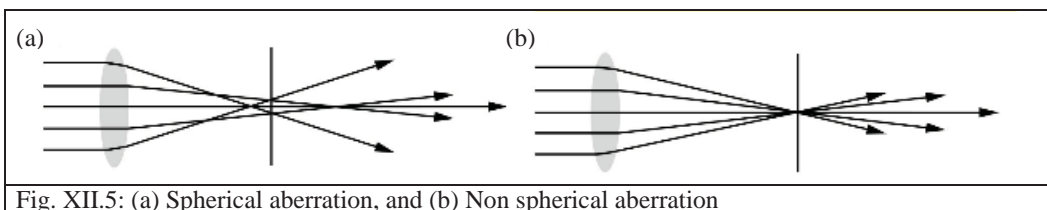
Depth of field and depth of focus

Depth of field is the range of positions where the eye can detect no change in the sharpness of the image. Depth of field may be acquired adjusting the working distance or using a flat sample (Michler, 2008). The sharpness of the image is not affected if the sample is anywhere within the range of depth of focus (h) (Goodhew et al., 2000) (Fig, XII.6).
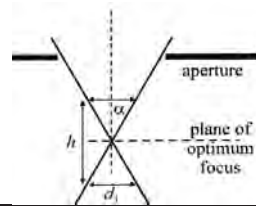
Fig.XII.6: Depth of focus, h (Goodhew et al., 2000).

Appendix XIII - Procedure for water desorption

Purpose
Obtain the sorption isotherms of the cement pastes.

Equipment: sample preparation
- Aquarium pump
- Glove cabine
- Calcium hydroxide
- Porcelain mortar
- 0.25 and 0.15mm sieve
- Weighing glasses
- Scale

Equipment: test
- Scale (0.001g)
- Dessicator
- Vacuum pump
- Water bath at constant temperature of 20^oC ($\pm 2^oC$)
- Temperature control
- Saturated salt solution (see Table XIII.1) for humidity control
- Magnetic stirrer
- Gloves

Material
Crushed cement paste. Pieces from 150 to 250µm (approx.1 gram).

Procedure
Bath and desiccators preparation
1. Check level of the water bath (see the mark in the bath) and the cooling water level (50ml). Turn on the water agitator control.
2. Open the program CR10.vi to check the temperature of the bath. Check the temperature of the chosen bath.
3. Prepare saturated solutions using chosen salts for the humidity control (see Table XIII.1). Seven dessicator with seven different salt solutions are possible to be tested at the same time (Fig. XIII.1).
4. Place the saturated salt solution and a magnetic stirrer in desiccators.

Table XIII.1 : Saturated salt solution for humidity control

Salt	Used	mbar	Equilibrium humidity (%)
LiBr		3	6.5
LiCl	X	4	11
CH$_3$COOK		7	23
MgCl$_2$	X	10	33
K$_2$CO$_3$		13	44
NaBr	X	17	59
NaNO$_3$		21	65
NaCl	X	23	75
KBr	X	25	83
KNO$_3$	X	29	92
K$_2$SO$_4$	X	31	97
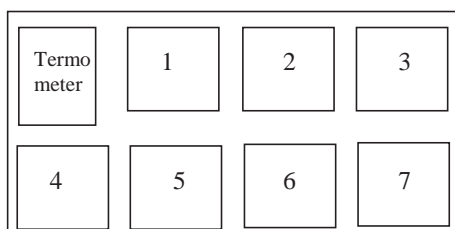
Fig. XIII.1: Number and place of the dessicators in the water bath

Weigh the weighing glasses by computer program
1. Open the program BathMonitor.vi and chose the file BathMonitor.vi
2. Fill in the screen of computer the "Promp User for Input" with your enter name (experiment name), bath number, user (your name), exicator (how many desiccator are you going to use- maximum of 7 desiccator), salt solution, temperature (of the water bath), RH, containers (how many sample cell in the desiccator) (Fig. XIII.2).
3. Press "Done" when you finish

Fig.XIII. 2: Data screen of BathMonitor.vi

4. Press the green arrow on the left of the screen "Start weighing", see Fig. XIII.3
5. Make a note of the name and save the file
6. Turn on the scale.
7. Calibrate the scale by pressing "Tare" and then "Calibrate" in the screen of the computer.
8. Place the empty weighing glass with the lid in the scale. Each weighing glass has a number, it is necessary to type the name of the sample together with the name of weighing glass to identify them in the desiccator. Use gloves to weigh the samples.
9. Record the weight of the empty weighing glass pressing the green arrow below the "Containers".
10. After weighting all the empty weighing glass. Press "Save weighting" and "Update graph" the upper right side of the screen
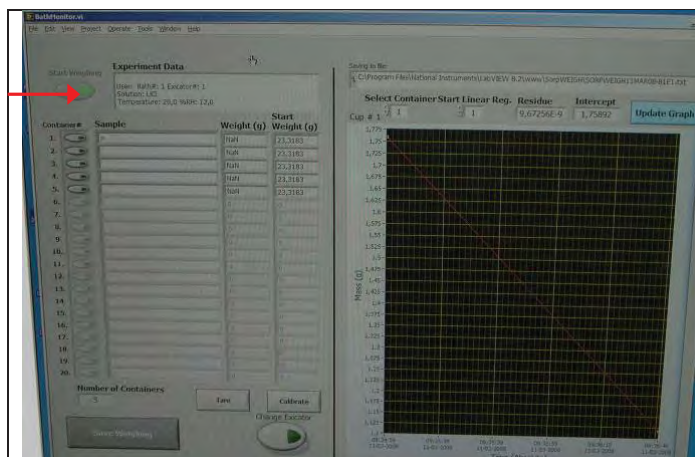
Fig. XIII.3 :BathMonitor.vi screen (red arrow – "Star weighing")

Sample preparation
1. Weigh all the weighing glasses
2. Place all the material (mortar, sieve, scale) weighing glasses and sample inside of a glove cabin.
3. Prepare a saturated solution with calcium hydroxide to create an environmental with high relative humidity (RH). Place inside the glove cabin.
4. Turn on an aquarium pump to produce bubbles in the saturated calcium hydroxide water. Close the glove cabin avoiding any air inside the cabin.
5. Wait for 15 minutes to reach a high RH inside the closed glove cabin
6. Crush and sieve (particles from 150 to 250µm) the sample using a porcelain mortar inside the closed glove cabin.
7. Weigh approximately 1 gram of samples and place them at selected weighing glasses.
8. Sealed the weighing glass with the proper lid.

Sample weight by computer program
1. Weight the sealed weighing glasses with samples inside using the same file from the previous file (empty weighing glasses)
2. Record the weigh pressing the green arrow
3. After weighting all the samples. Press "Save Weighting" and "Update graph" the upper right side of the computer screen.

Placing the sample at desiccator
1. Place the weighing glasses with samples with the lid as showed in the Fig. XIII.4 in the desiccator with the respective saturated salt solution.
2. Evacuate the desiccator to a equilibrium water vapour pressure of the salt solutions, as shown in the Table 1, 2nd column.
3. Place the desiccator in the water bath (Fig.XIII.5) and close the external lid of the bath.
4. The procedure above "Sample weight by computer program" has to be repeated for each desiccator. For that purpose, Select "Change exicator" and "Start weighing".

Fig. XIII.4 :Position of the lid of the sample cell
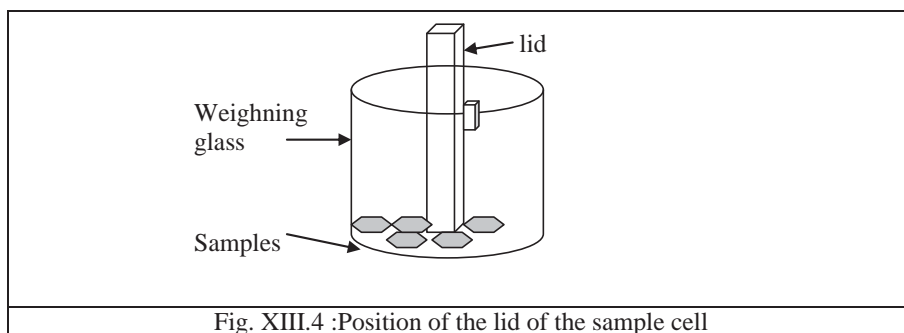
Fig. XIII.5: Desiccator in the water bath.

Second weight

Every two week the samples should be taken out from the desiccator and weighted until the sample reaches a constant weigh. For that the following procedure is proposed:

1. Slowly and carefully, let the air out from the desiccator. Use the finger in the outlet of the desiccator.
2. Take off the samples from the desiccator.
3. Press "Start weighing" in the computer screen. Automatically a window will be opened with the computer files. Choose the one you have used to save the first data (weight).
4. Turn on the scale.
5. Calibrate the scale by pressing "Tare"on the screen and then "Calibrate".
6. Place your sample within the sample cell and sealed it with the lid. Record the weigh pressing the green arrow
7. After weighting all the samples. Press "Save Weighting" and "Update graph" the upper right side of the computer screen.
8. Place the samples cell in the desiccator and evacuate the desiccator to a equilibrium water vapour pressure of the salt solutions, as shown in the Table XIII.1, 2nd column.
9. Place the desiccator in the water bath and close the external lid of the bath.

Appendix XIV - Procedure for isothermal calorimeter

Purpose
Development of hydration using and determination of activation energy of cement based materials.

Equipment
3114/3236 TAM Air Isothermal calorimeter by Thermometric
The software used by the calorimeter is IsoCal Data Logger version 4.5 by Solidus.

The calorimeter has eight channel with one side for the sample (side A) and the other side for a static reference (side B), as showed in the Figs.XIV.1 and XIV.2.
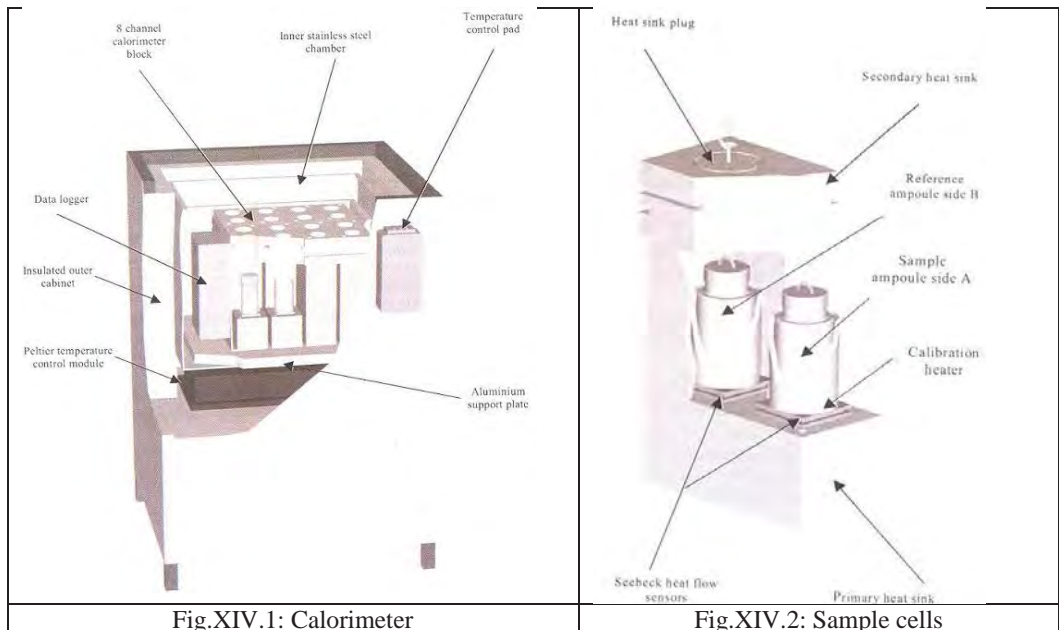
| Fig.XIV.1: Calorimeter | Fig.XIV.2: Sample cells |

Material
Cement paste and static reference sample. The samples are held in 20 ml sealed ampoules (sample cell), see Figure XIV.3. However the amount of cement paste introduced in the sample cell is about 6-8 ml (1/3 of the flask).The reference sample must be an inert material with approximately the same heat capacity as the sample in the reference ampoule. Sand is often used as the reference sample.

Fig. XIV.3:Thermal calorimeter and the ampoules

Procedure

Set up of the temperature
The desired temperature is set on the temperature control pad located on the front of the instrument. The control panel has two temperatures indicators: red digitals show the actual temperature and green digitals show the set temperature. Generally one day is required to reach the desired temperature.

Calibration
According with the equipment manual, calibration is carried out to calculate a calibration constant for each individual twins (side A and B) calorimetric channel. Calibration is performed with empty calorimetric channels. Once a stable baseline has been achieved, a known voltage is applied over the calibration heater by switching the toglle switch.

Sample preparation
- weight the empty ampoule;
- introduce the sample in the ampoule. Take care to do not spill any material on the neck or over the outer of the ampoule;
- weight the loaded ampoule. Record the sample weight (loaded ampoule – empty ampoule)
- Seal the lid onto the ampoule using the cap crimping tool;
- In the center of the aluminium lid screw a lifting eyelet into the indentation, see Fig. XIV.3

Programming the tests

Open Isocal Logger program.
Select "Edit field" in the main screen.
The "Edit field names" screen is opened and the information about the sample and test are required: "Sample id", Duration , hrs", "Date /time".

Loading the sample and reference

The same and reference ampoules should be loaded into TAM Air at the same following the procedure bellow:

- Remove the top lid from side A and side B of the channel to be used. Channel A should be used for the sample ampoule and channel B for the reference ampoule.
- Use the lifting tool to lift our the heat sink plug (blocker);
- Pick up the sample ampoule using the lift tool and slowly lower the ampoule down within the selected channel. Next step is to replace the heat sink plug and refit the top lid.

With the ampoules at the measuring position they will take 30 minutes to equilibrate, or longer when working in high temperature e.g. 50 degrees. During this time the thermal disturbance caused by the introduction of the ampoules is eliminated.

Start the test and exporting the data using the computer software

Open the data file to be exported. Selected File, Save as. File format menu select Text Files and click OK. The data is saved as Excel file.

Reference
Instruction Manual 3114/3236 TAM Air Isothermal – Termometric p.1-40

Appendix XV - Procedure for capillary suction method

Purpose
The purpose of this method is to give a continuous measurement of capillary suction and avoid some of the main uncertainties and sources of error associated with the common test methods.

Principle
The sample is suspended from a scale down to a reservoir of deionised water. A computer previously programmed to take continuous records every minute will write down the weight and time. This continues until a specified time have been acquired.

Specimen
Cement paste samples of sizes, Ø = 21.5 mm, height 25-30 mm

Materials and equipment
- Scale (0.0001g)
- Cask
- distillate water
- Steel wire, length accordingly to test arrangement
- PVC
- Tape

Procedure
- The test specimen is wrapped with PVC secured with tape to avoid evaporation, only the area intended for exposure to water is left free. The area kept free is a couple of mm up the height. This is to prevent that the surface tension of water causing meniscus to rise, comes into contact with the plastic wrapped around the test specimen, as additional suction can occur here. Around the tape steel wires is attached and it is important to secure that the exposed surface area of the test specimen is level. A picture of a wrapped test specimen is shown below.
- The specimen is then suspended from the scale down into the cask.
- When the specimen is completely level and still the deionised water is slowly added until 1-2 mm of the test sample is submerged.
- Hereafter the cask is covered with PVC to prevent further evaporation (see Fig. XV.1) of the cask given rise to loss in buoyancy and therefore a weight gain not caused by the capillary suction. The Fig. XV.2 shows the test arrangement.

-

Fig. XV.1: Sample with plastic around to prevent evaporation.	Fig. XV.2: Set up for capillary suction test.

Appendix XVI- Parameters used for NMR relaxation

Table XVI.1 : Parameter used for H^{1}NMR relaxation

CPMG		T1	
Frequency	2.01E+16	Frequency	2.01E+16
Filter	1.00E+09	Filter	1.00E+09
Points	1024	Points	512
Scans	512	Scans	8
P90	2.30E+09	P90	2.30E+09
P180	4.60E+09	P180	4.60E+09
PW	1.00E+09	PW	1.00E+09
Dead1	7.00E+09	Dead1	1.50E+09
Dead2	1.00E+10	Dead2	1.00E+10
Dwell	1.00E+09	Dwell	1.00E+09
RD	2.00E+12	RD	2.00E+12
Tau	4.00E+10	Tau	4.00E+10
D1	3.00E+10	D1	1.50E+10
D2	4.90E+13	D2	2.50E+13
D3	6.40E+10	D3	3.50E+10
D4	1.00E+11	D4	1.00E+11
D5	1.00E+15	D5	1.00E+15
Gain	8.00E+09	Gain	8.00E+09
NumT1FIDs	20	NumT1FIDs	20
T1Spacing	1.00E+11	T1Spacing	1.00E+11
T1Low	2.00E+07	T1Low	2.00E+07
T1High	1.00E+12	T1High	1.00E+12
NumEchoes	64	NumEchoes	64
EchoPoints	8	EchoPoints	8

Appendix XVII– Results of LTC

To observe the accuracy of the measurements of SSD (saturated surface dried), a similar sample were measure 10 times. Fig. XVII.1 illustrated the variance between the weight measurements.
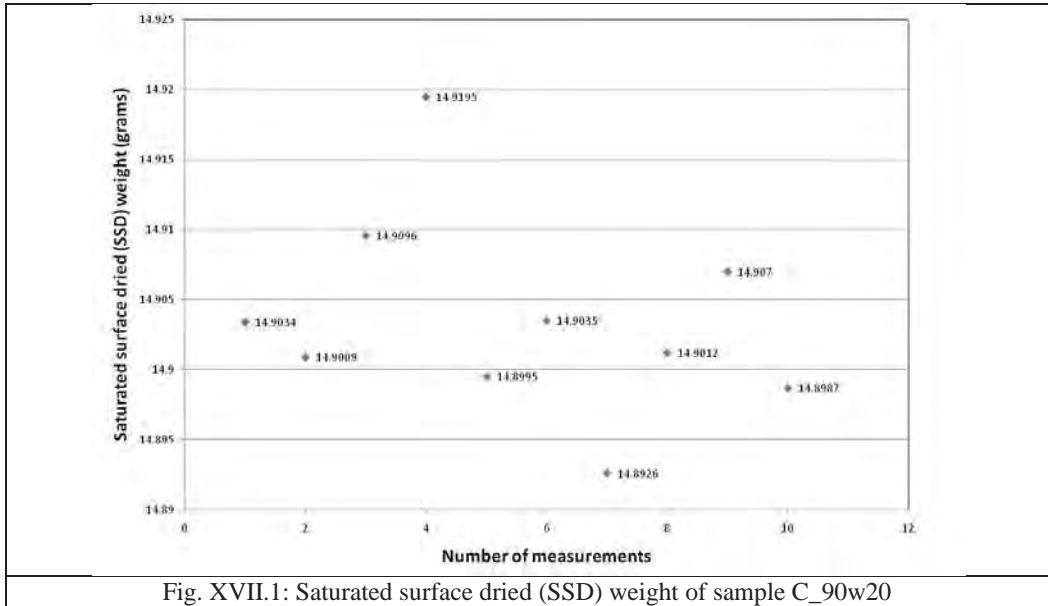
Fig. XVII.1: Saturated surface dried (SSD) weight of sample C_90w20

Apparent heat capacity for pastes with and without slag and fly ash cured at 20ºC for 1 days I sigven in the Fig. XVII.2.Volume of the pores for melting curves calculated by Sun and Scherer (2010)is given in the Fig. XVII.3. and XVII.4.
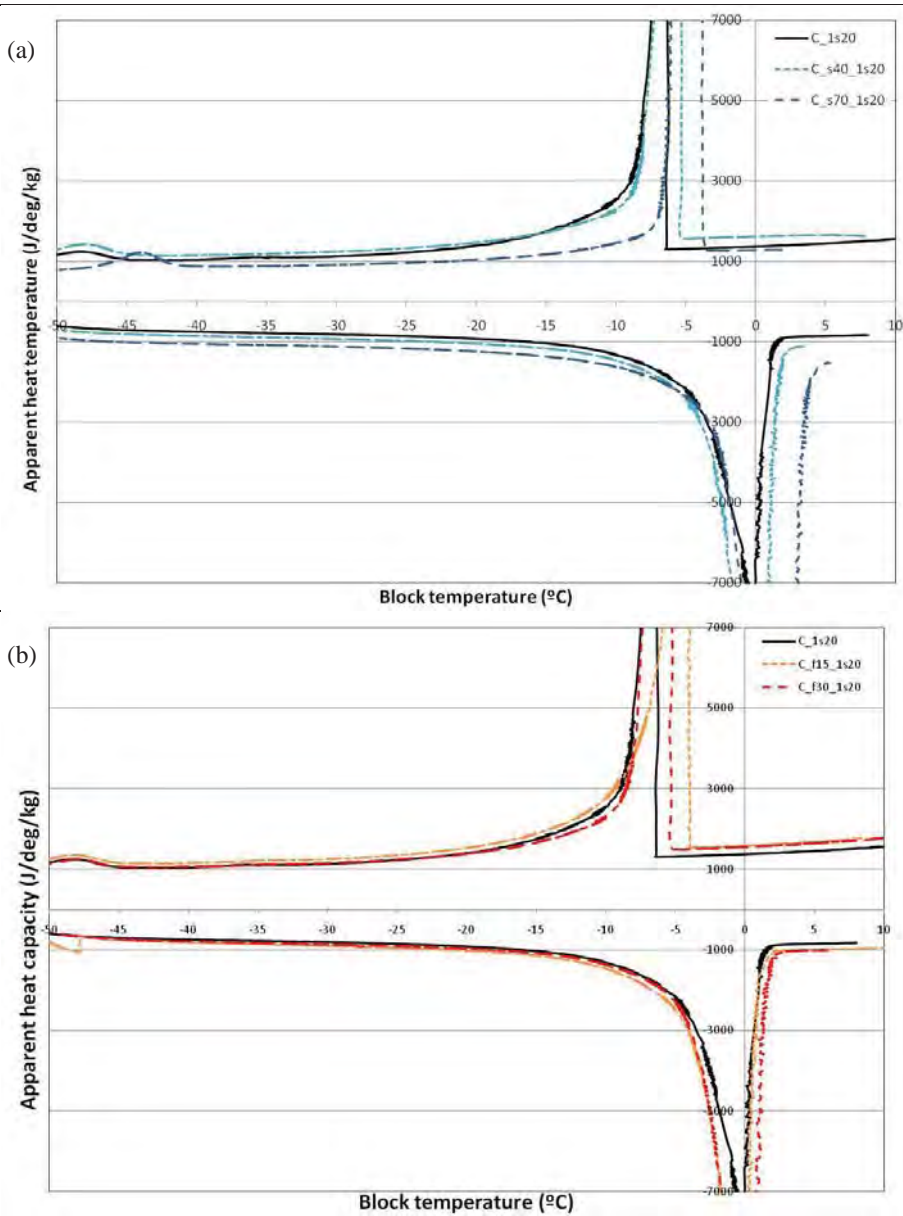
Fig XVII.2: Apparent heat capacity (J/deg/kg) versus block temperature (ºC) of pastes with and without (a) slag and (b) fly ash cured saturated at 20ºC for 1 day

(a) 1 day

Volume of pores from melting curve, cured saturated at 20oC for 1 day

Legend:
- C-1w20
- Cs40-1w20
- C-s70-1w20
- C-f15-3w20
- C-f30-1w20

Volume of pores (fraction) vs Block temperature (°C)

(b) 3days

Legend:
- C_3w20
- C_s40_3w20
- C_s70_3w20
- C_f15_3w20
- C_f30_3w20

Total pore volume (fraction) vs Block temperature (ºC)

(c) 28 days

Legend:
- C_28w20
- C_s40_28w20
- C_s70_28w20
- C_f15_28w20
- C_f30_28w20

Total pore volume (fraction) vs Block temperature (ºC)
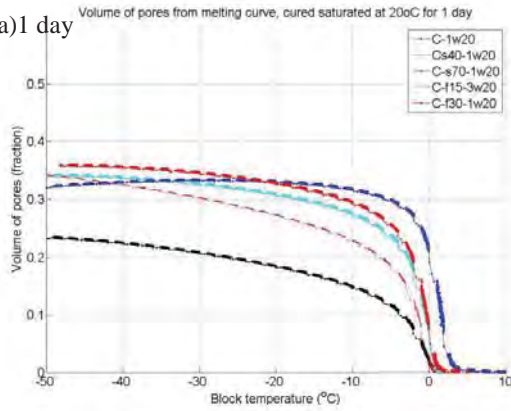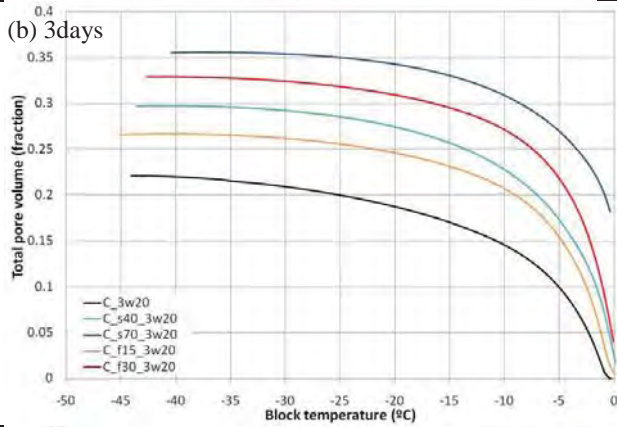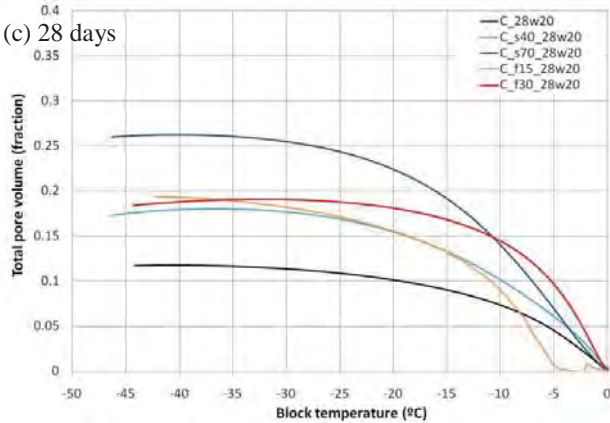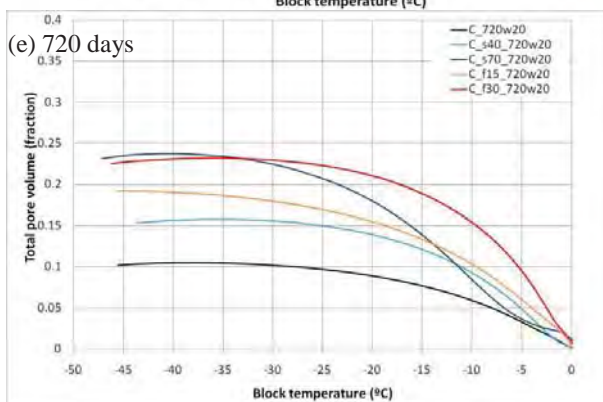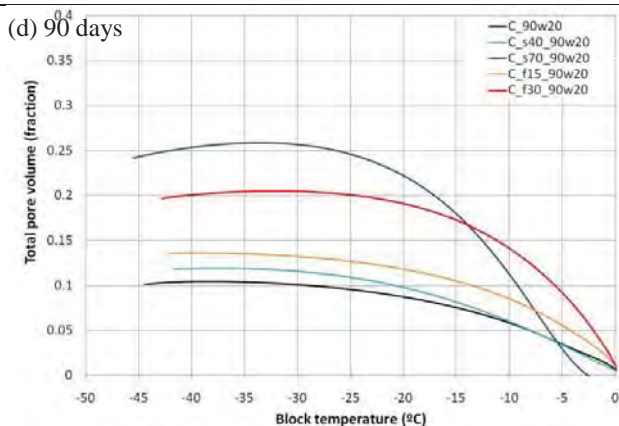
(d) 90 days

(e) 720 days

Fig. XVII.3 Pore size distribution: volume of pores melted (fraction) versus block temperature (ºC) for pastes cured saturated at 20ºC for (a) 1 day, (b) 3 days, (c) 28 days, (d) 90 days and (e) 720 days. Reference-plain paste (black); 40% of slag (light blue),70% of slag; (dark blue)15% of fly ash (light red); and 30% of fly ash (dark red).

(a)
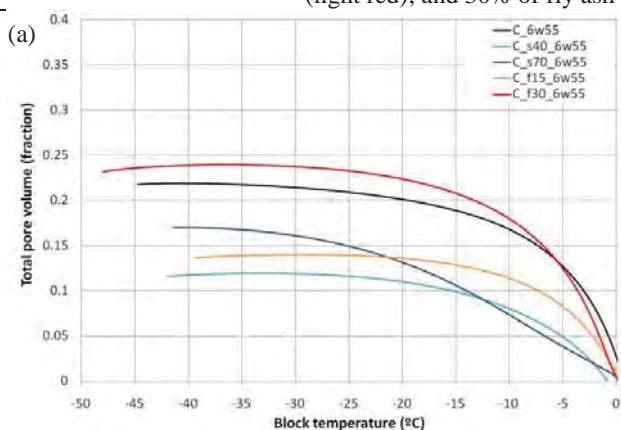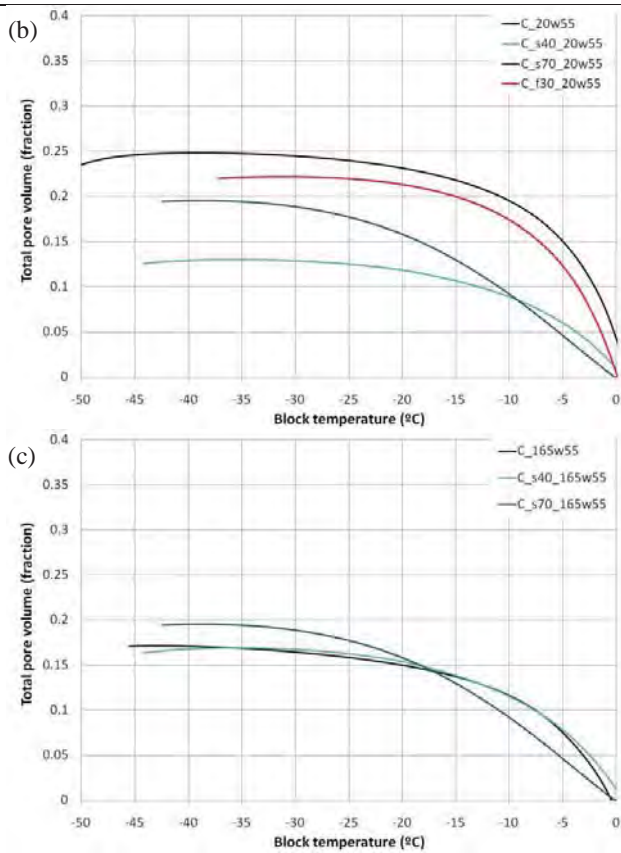
Fig. XVII.4: Volume of pores (fraction) versus block temperature (ºC) pastes with and without slag cured saturated at 55ºC for a) 6.5 days (28 maturity days); b) 20.7 days (90 maturity days); c)165 days(720 maturity days).

Appendix XVIII – Results of MIP

Curves of intrusion and extrusion of mercury versus pore diameter are given in the Figs. XVIII.1 to XVIII.15.
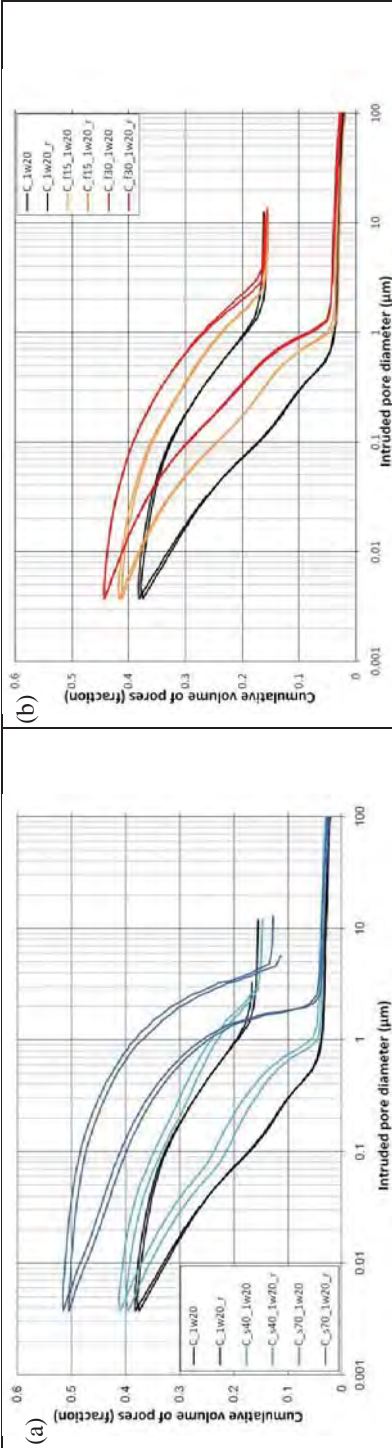
Fig.XVIII.1: Cumulated pore volume versus intruded pore diameter for pastes with and without (a) slag and (b) fly ash cured saturated at 20°C for 1 day .
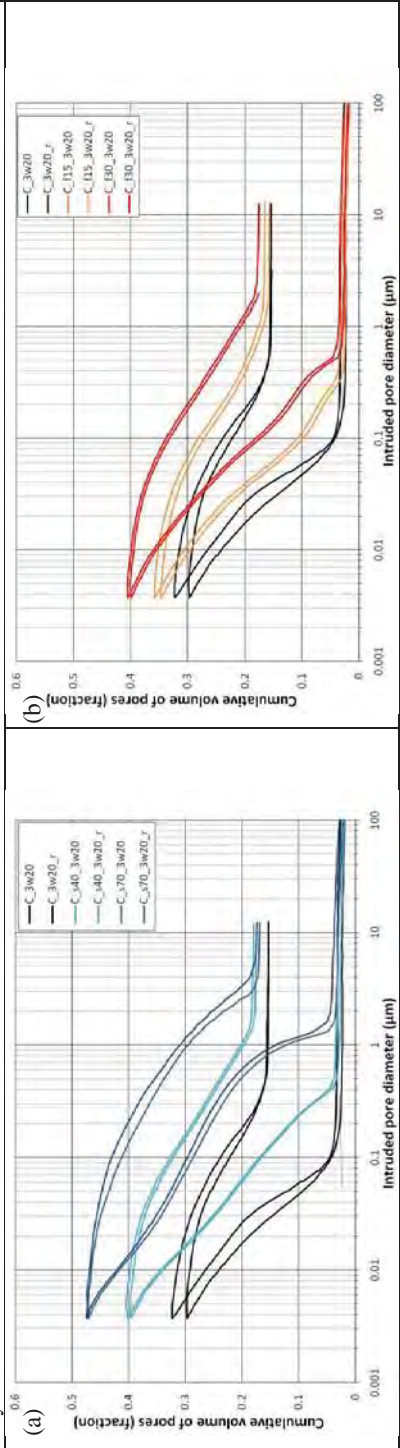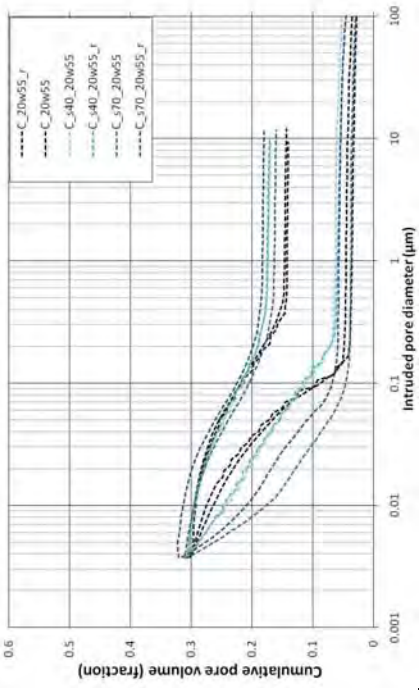
Fig.XVIII.1 : Cumulated pore volume versus intruded pore diameter for pastes with and without (a) slag and (b) fly ash cured saturated at 20°C for 3 days .
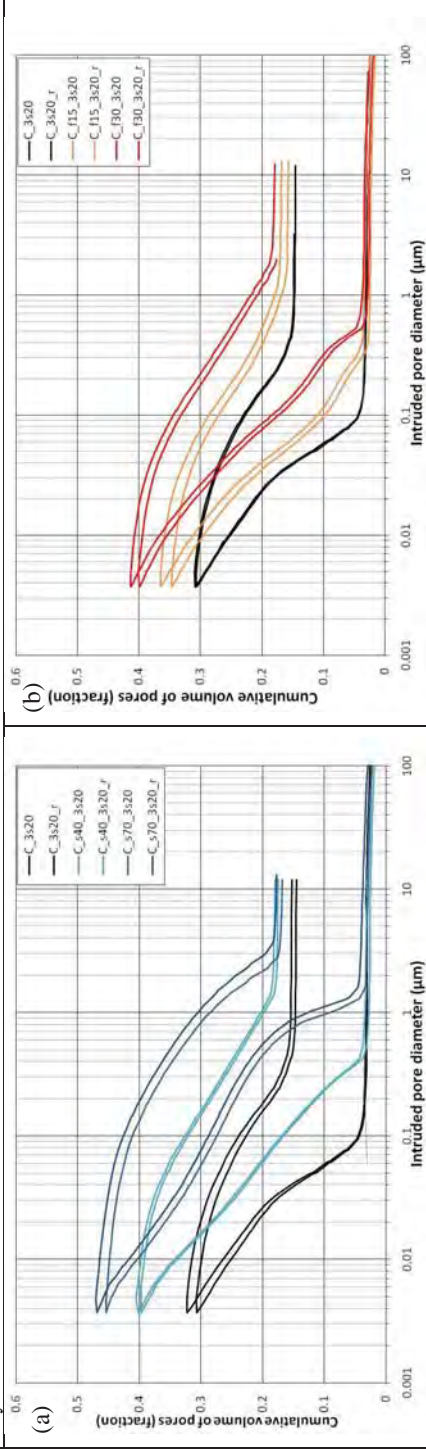
Fig.XVIII.2 : Cumulated pore volume versus intruded pore diameter for pastes with and without (a) slag and (b) fly ash cured sealed at 20°C for 3 days .
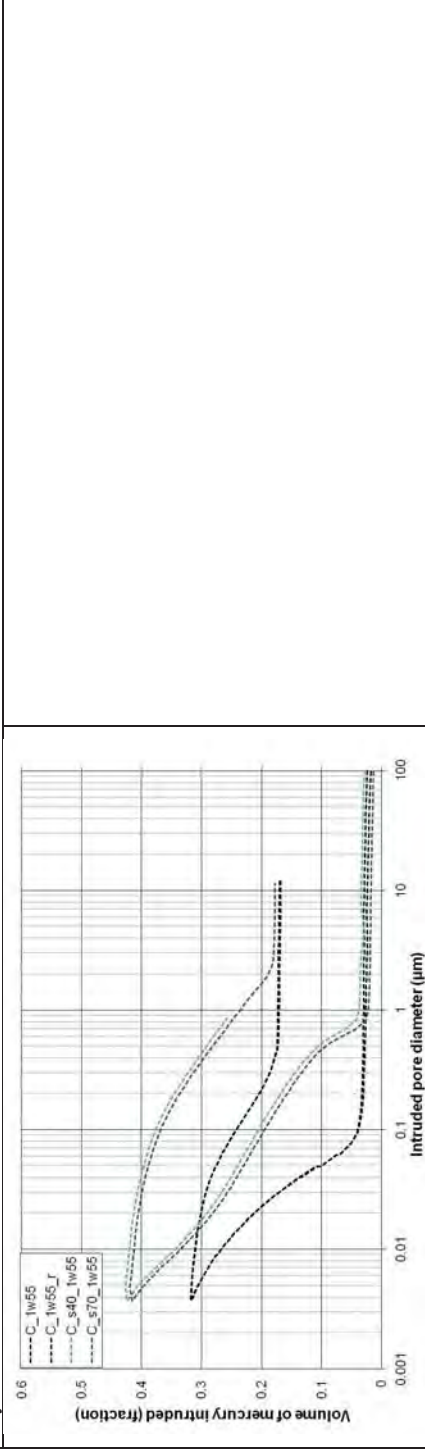
Fig.XVIII.3 : Cumulated pore volume versus intruded pore diameter for pastes with and without slag cured saturated at 55°C for 3 maturity days .
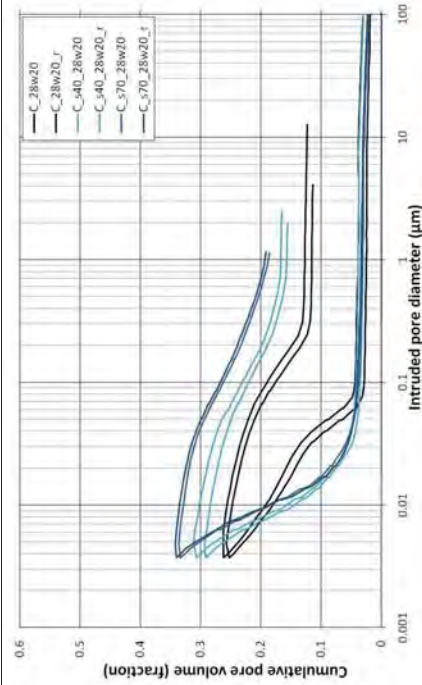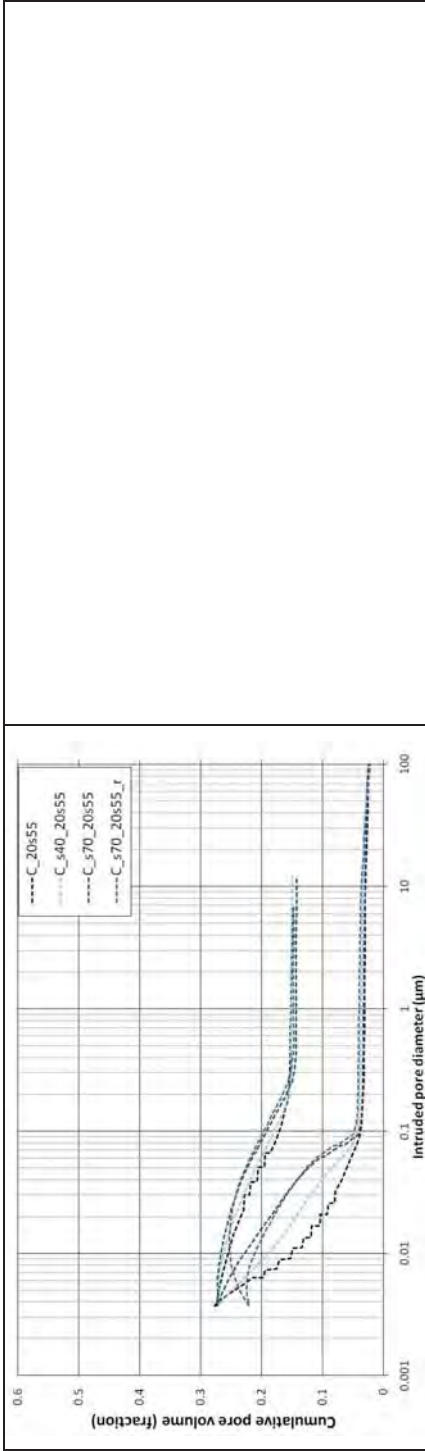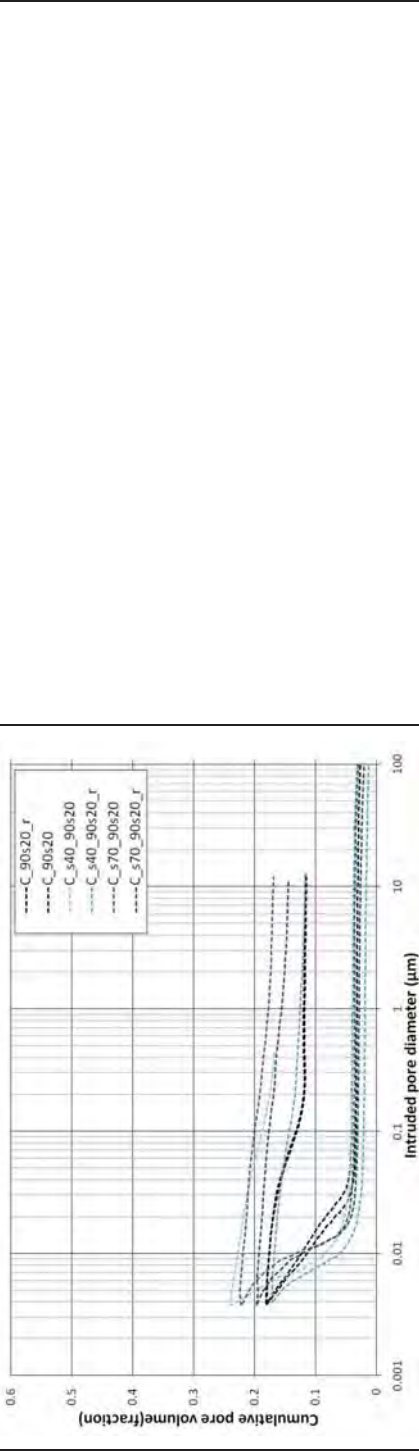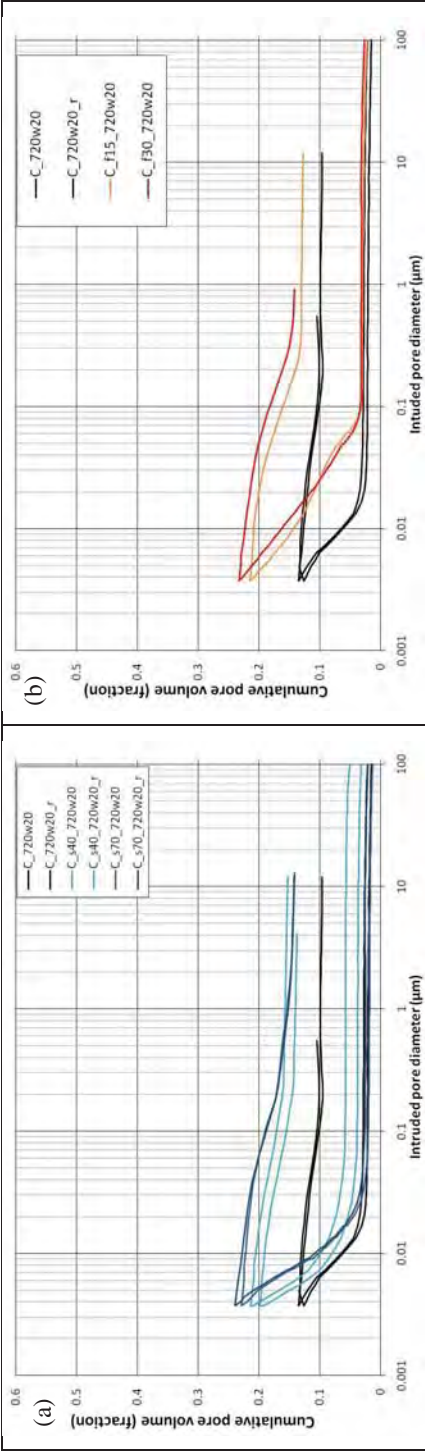
Fig.XVIII.4: Cumulated pore volume versus intruded pore diameter for pastes with and without slag cured saturated at 20°C for 28 days .
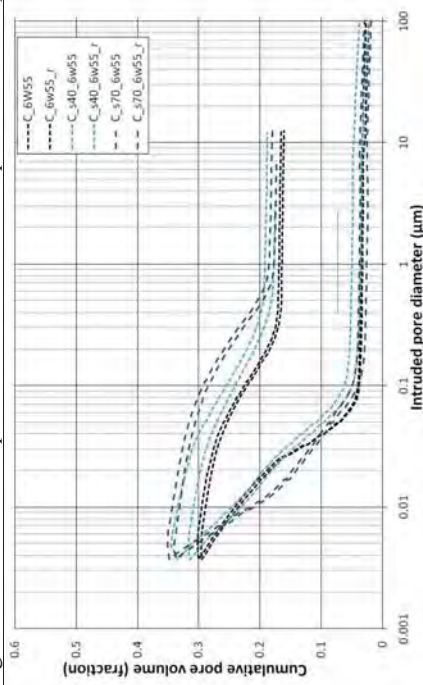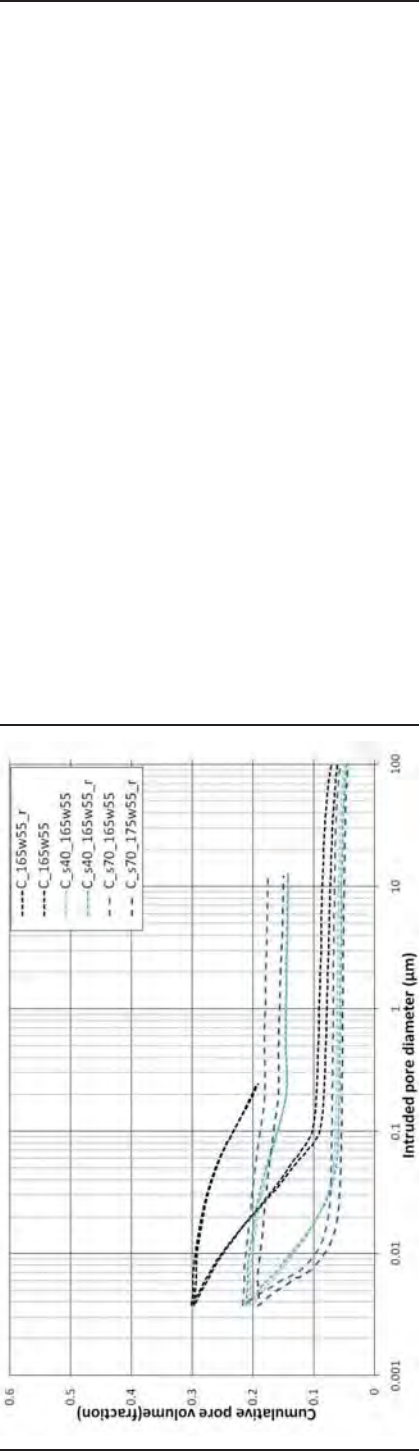

Fig.XVIII.5: Cumulated pore volume versus intruded pore diameter for pastes with and without slag cured saturated at 55°C for 28 maturity days .
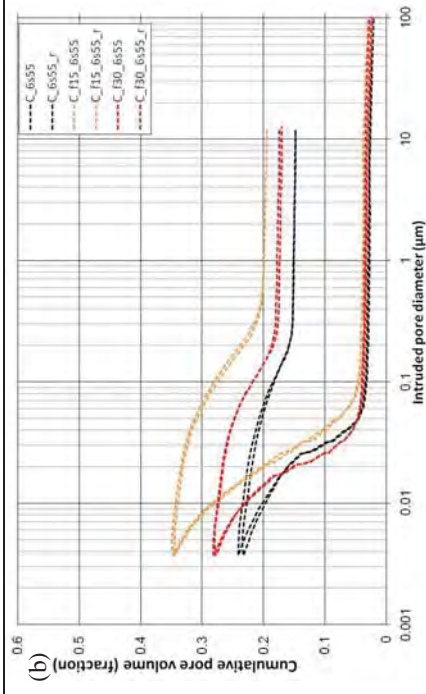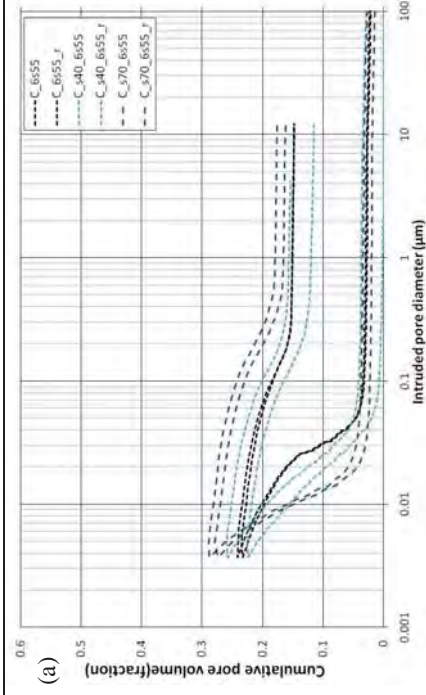
Fig.XVIII.6: Cumulated pore volume versus intruded pore diameter for pastes with and without (a) slag and (b)fly ash cured sealed at 55°C for 28 maturity days .
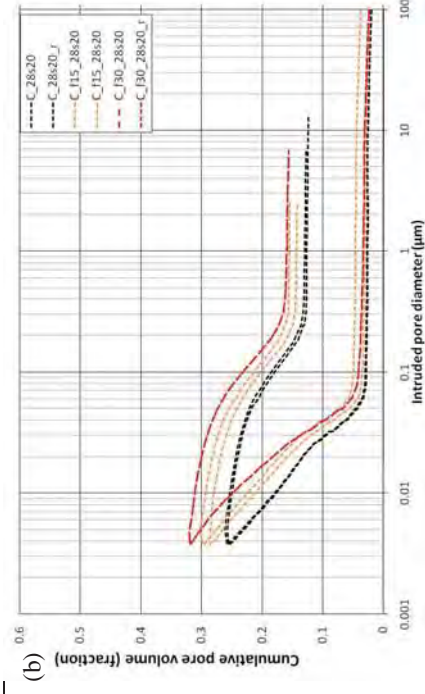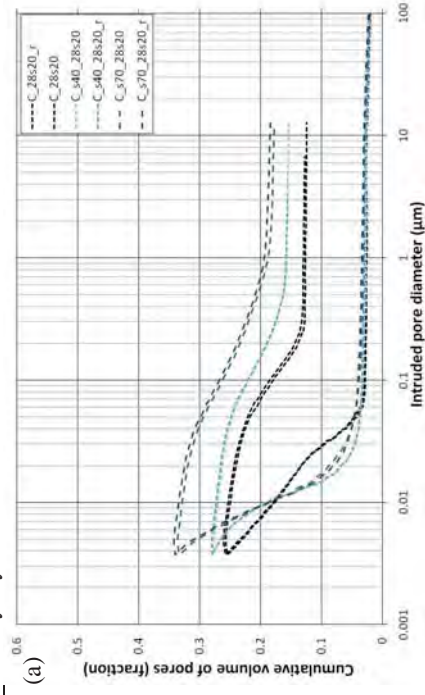
Fig.XVIII.7: Cumulated pore volume versus intruded pore diameter for pastes with and without (a) slag and (b)fly ash cured sealed at 20°C for 28 maturity days .
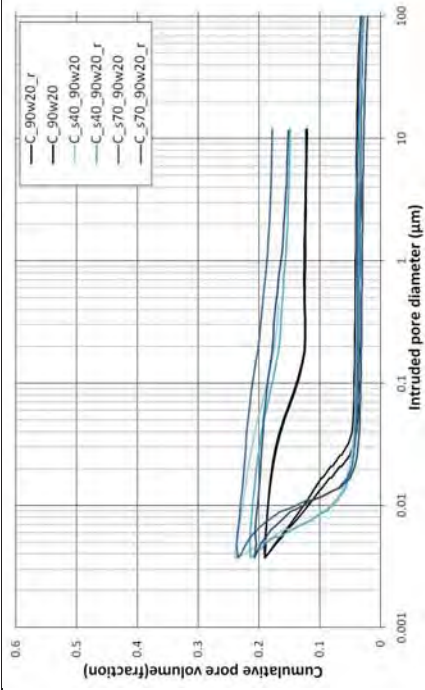
Fig.XVIII.8: Cumulated pore volume versus intruded pore diameter for pastes with and without slag cured saturated at 20°C for 90 days .

Fig.XVIII.9: Cumulated pore volume versus intruded pore diameter for pastes with and without slag cured saturated at 55°C for 90 maturity days .
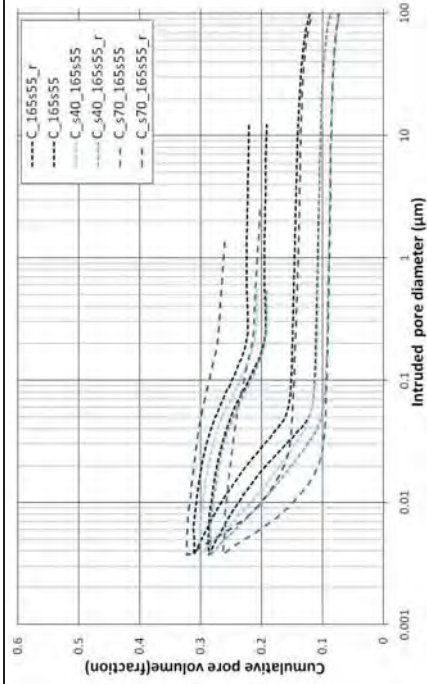
Fig.XVIII.10: Cumulated pore volume versus intruded pore diameter for pastes with and without slag cured saturated at 55°C for 90 maturity days

Fig.XVIII.11: Cumulated pore volume versus intruded pore diameter for pastes with and without slag cured sealedat 20°C for 90 days .
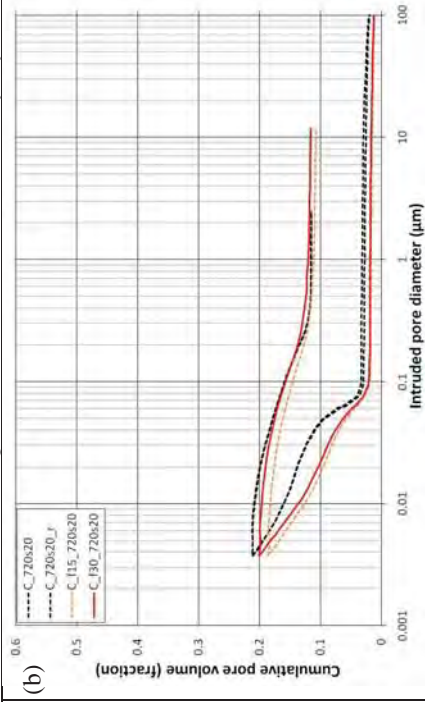
Fig.XVIII.12: Cumulated pore volume versus intruded pore diameter for pastes with and without (a) slag and (b) fly ash cured saturated at 20°C for 720 days .

Fig.XVIII.13: Cumulated pore volume versus intruded pore diameter for pastes with and without slag cured saturated at 55°C for 720 maturity days.

Fig.XVIII.14: Cumulated pore volume versus intruded pore diameter for pastes with and without slag cured sealed at 55°C for 720 maturity days .
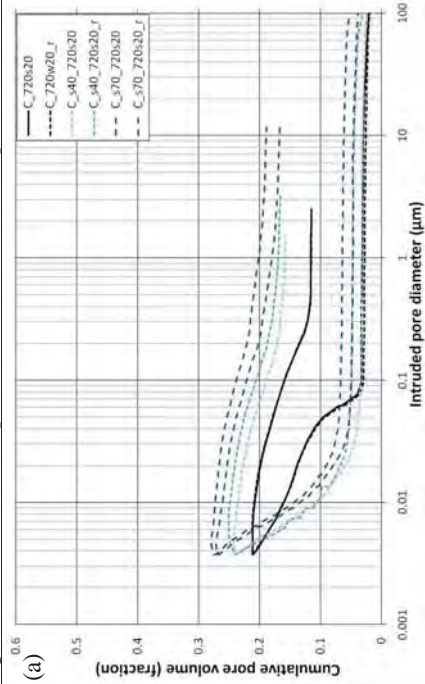
Fig.XVIII.15: Cumulated pore volume versus intruded pore diameter for pastes with and without (a) slag and (b) fly ash cured sealed at 20°C for 720 days .

MIP density for pastes cured saturated or sealed at 20ºC is illustrated in the Fig. XVIII.16(a). For samples cured saturated at 55ºC, the densities are illustrated in the Fig. XVIII.16(b).
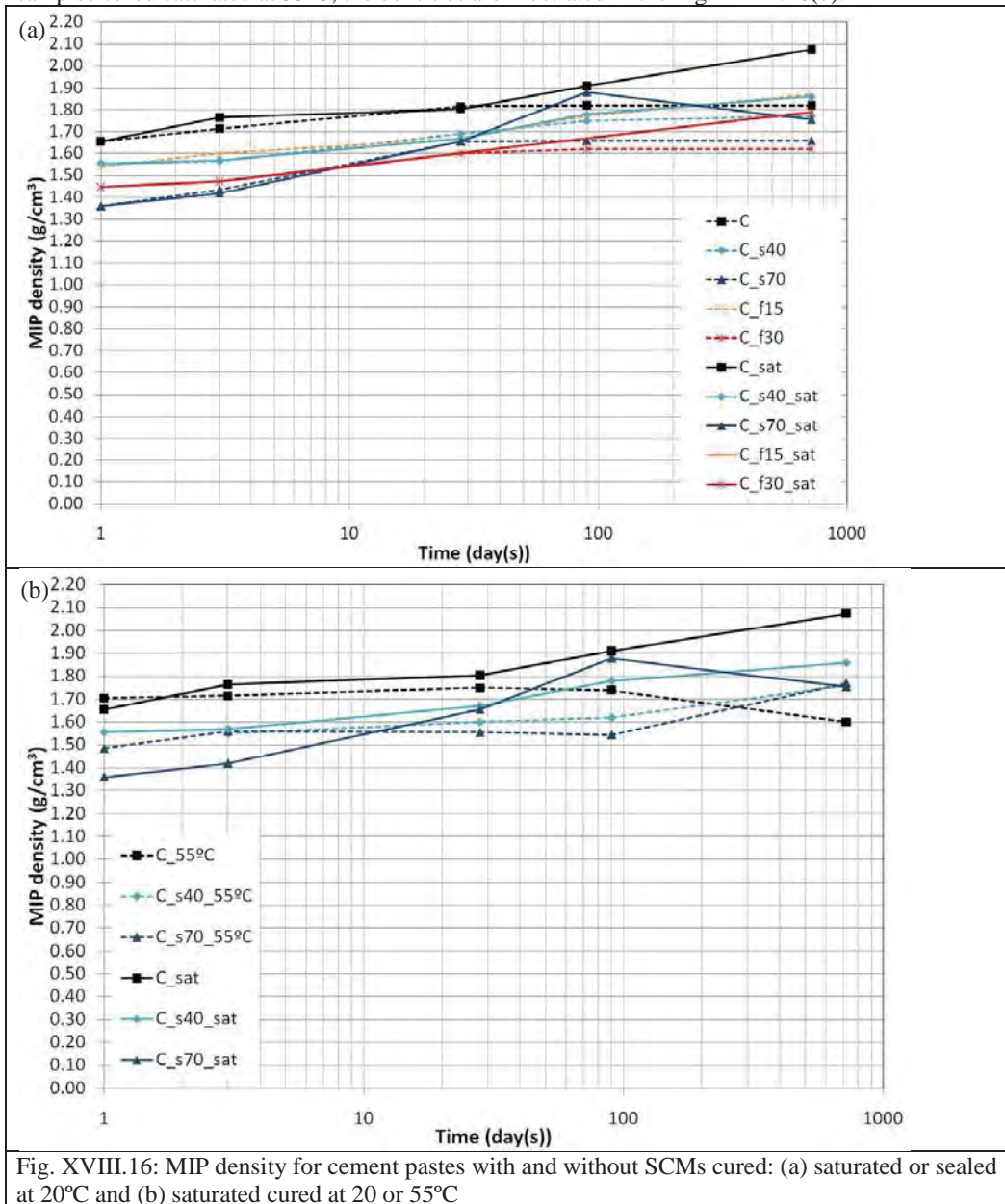

Fig. XVIII.16: MIP density for cement pastes with and without SCMs cured: (a) saturated or sealed at 20ºC and (b) saturated cured at 20 or 55ºC

Appendix XIX - Results of SEM

Parameters analysed for SEM images

Working distance (WD)

The working distance is the distance between the final condenser lens and the specimen (Michler, 2008). The working distance leads to a spherical aberration and it also may interfere on the depth of field of the imaging system. At a short working distance the sample will be scanned with a wide cone of electrons resulting in an image with little depth of focus. According to Shields (2010), if a sample with large topographical variation needs to be scanned it may be important to use a longer working distance to bring as much of the image into focus as possible; however, some of the resolution will be lost. This effect may be observed in the Fig. XIX.1, at higher working distance (13mm) an image with better sharpness is acquired when compared with a lower working distance (3.3mm).

Fig. XIX.1: Zeolite, working distance of 3.3mm and (b) 13 mm
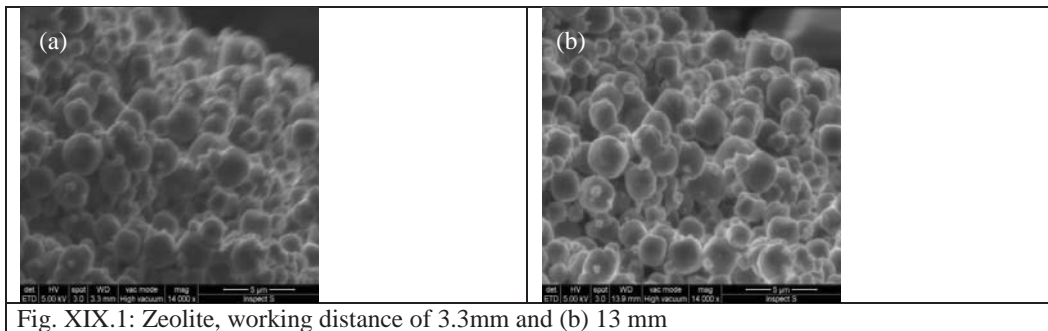
Accelerating voltage

The accelerating voltage is the high voltage applied to the filament. At low accelerating voltage (e.g. ≤ 5 kV), the beam interacts with the region very close to the surface of the specimen. Therefore, the image detected carries information mainly on surface details. At high accelerating voltage (e.g. 15-30 kV), the beam penetrates and interacts deep into the surface of the sample (Michler, 2008). Increasing the accelerating voltage will also decrease the spherical aberration of the system and therefore increase the resolution. However, the increase of accelerating voltage may generate unnecessary signals from within the specimen which may compromise the contrast of the image. This effect will be much less in a sample with high atomic numbers. Fig. XIX.2(a) and XIX.2(b) shows the images acquired using low (5keV) and high (15keV) values for accelerating voltage (the other parameters were constant). A better contrast and resolution were obtained when 15keV is used when compared to 5keV. However, it is possible to observe undesirable effects of high accelerating voltage such as charging and edge effect (lighter part of the image), see Fig. XIX.2(b) and XIX.2(c). As the sample charging tends to accumulate, after a while it is possible to observe the damage of the samples, see Fig. XIX.2(c). To avoid the charging of the samples, their surfaces are usually coated by conducting layers of gold (Au) or carbon (C) and then connected to the ground potential (Jeol, 2010). Also, the edge effect is more pronounced when a higher accelerating voltage is used. Edge effect is largely depended on the incident beam angle and the sample surface (conductive or not) and it may be limited by the coating of the sample.
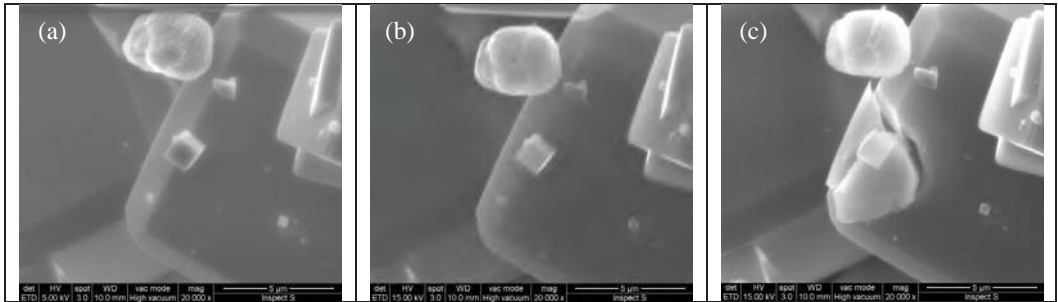
Fig. XIX.2: Accelerating voltage of (a)5kV, (b)15kV and (c) 15kV (damage of the particle)

Probe size and current

Image resolution depends on the size of the electron probe, which in turn depends on both the wavelength of the electrons and the electron-optical system (Michler, 2008, Shields, 2010). Usually, an increased current will produce a smaller probe size. In the Figs. XIX.3(a) and XIX.3(b), two values of beam size were used for a similar image using a magnification of 20000x. It is possible to observe that image with smaller probe size (Fig.XIX.3) has a higher resolution and sharpness. Goodhew et al. (2000) reported that if the probe is larger than the specimen pixel then the signal from the adjacent pixels is merged and the resolution is degraded.
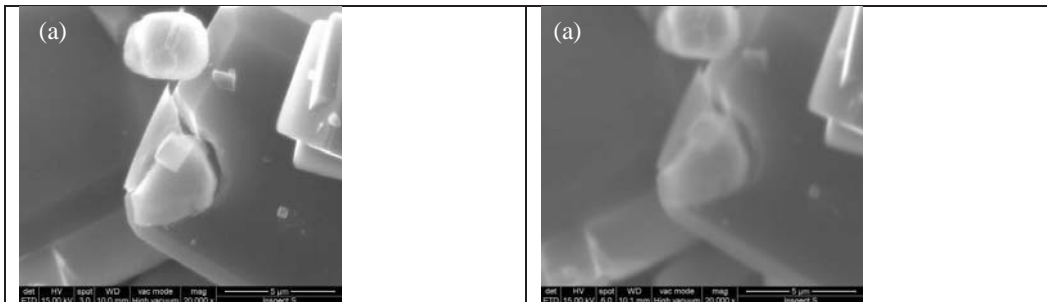

Fig. XIX.3 : Zeolite using probe size of (a)3mm and (b) 6mm

Contamination

Contamination may also affect the sharpness and brightness of the picture, see Fig. XIX.4(a) (darker stripes). It happens due to the residual gas in the vicinity of the specimen being struck by the electron probe (Egerton, 2005, Michler, 2008). The gas may be from instrument or from the sample. The effect of the contamination may be minimized scanning the same area more than once, see Fig.XIX.4(b).
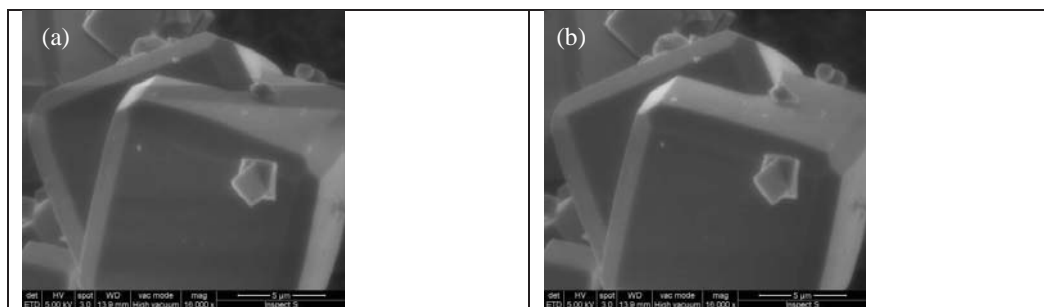
Fig. XIX.4: Zeolite (a) darker stripes are reported as contamination of the image (b) improved by several scanning.

Appendix XX- Results of water sorption

An example of volume of pore versus pore size for pastes with and without slag cured saturated at 28 and 90 days, see the Figs. XX.1.
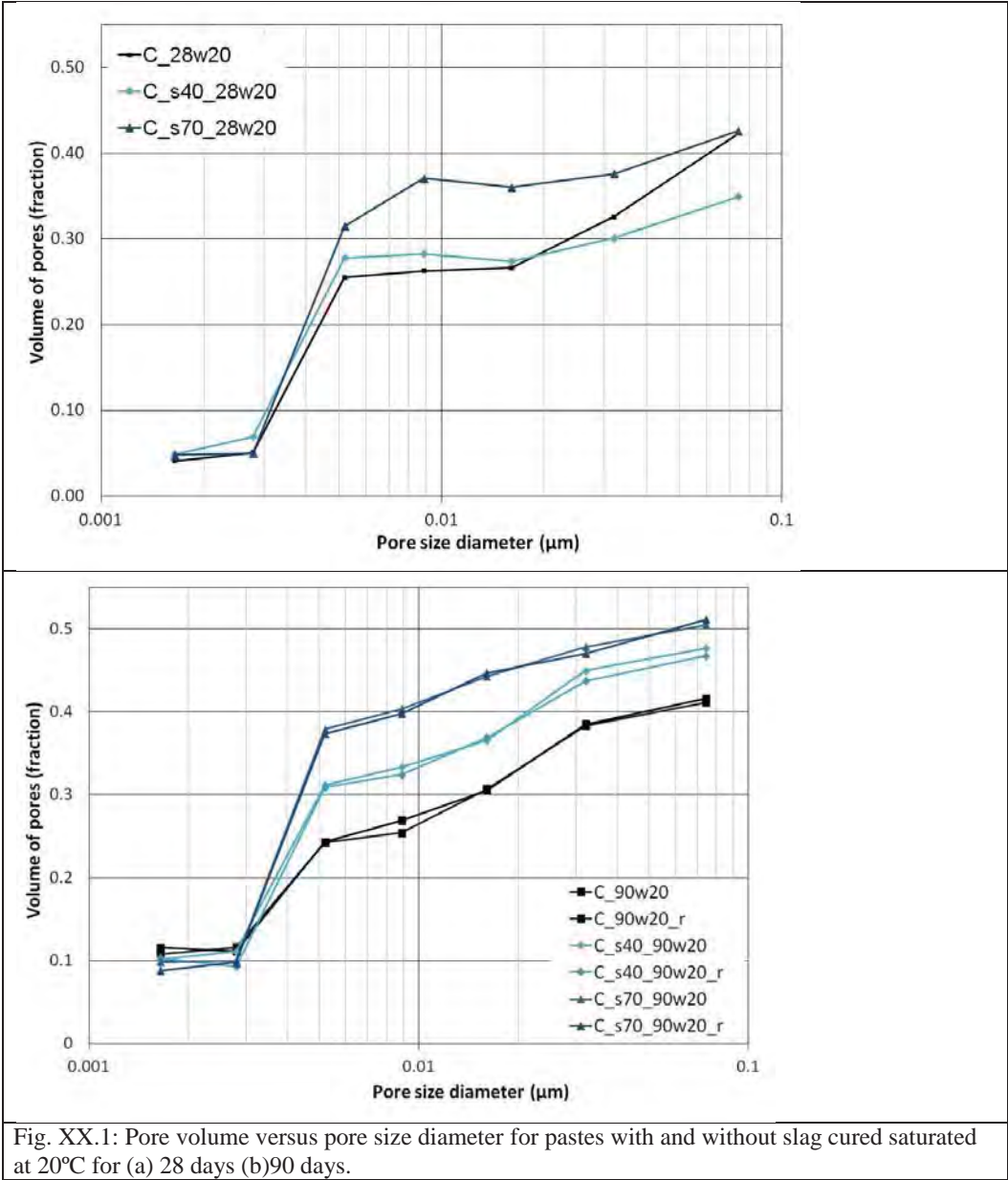

Fig. XX.1: Pore volume versus pore size diameter for pastes with and without slag cured saturated at 20ºC for (a) 28 days (b)90 days.

Appendix XXI –Non evaporable and evaporable water measurements

The weight change measurements for cement pastes at varying sample size (powder, slice of 0.5x3Øcm and slice of 5.5x1Ø cm) oven at 105ºC (evaporable water) and 1000ºC (non evaporable water) at varying time is given in the Tables XXI.1 and XXI.2.

Table XXI.1: Effect of sample size on evaporable and non evaporable water measurements for sample C cured saturated at 20ºC for 3 days: powder; slices of 0.5x3Øcmcm and 5.5x1.5Øcm

Sample id.	Powder (particles < 5mm)						Slices (5x3.0ømm aprox.)						LTC samples (5.5x1.5øcm aprox.)					
	W evaporable g/g$_{105°C}$			W non evaporable g/g$_{105°C}$			W evaporable g/g$_{105°C}$			W non evaporable g/g$_{105°C}$			W evaporable g/g$_{105°C}$			W non evaporable g/g$_{105°C}$		
	Time (days)			Time (hours)			Time (days)			Time (hours)			Time (days)			Time (hours)		
	1	3	10	1	4	24	1	3	10	1	4	24	1	3	10	1	4	24
C	0.24	0.25	0.25	0.12	0.12	0.13	0.24	0.25	0.25	0.12	0.11	0.11	0.23	0.24	0.24	0.12	0.12	0.12
	0.25	0.25	0.26	0.13	0.13	0.13	0.24	0.25	0.25	0.12	0.12	0.12	0.24	0.25	0.25	0.12	0.12	0.12
	0.24	0.25	0.25	0.12	0.12	0.12	0.23	0.24	0.24	0.12	0.13	0.12	0.24	0.24	0.24	0.11	0.11	0.12
Av.	0.24	0.25	0.25	0.12	0.13	0.13	0.24	0.25	0.24	0.12	0.12	0.12	0.24	0.24	0.24	0.12	0.12	0.12
std.	0.00	0.00	0.01	0.00	0.00	0.00	0.00	0.00	0.00	0.00	0.01	0.01	0.00	0.00	0.00	0.00	0.00	0.00

Table XXI.2: Effect of sample size on evaporable and non evaporable water measurements for sample with 40% of slag cured saturated at 20ºC for 3 days: powder; slices of 0.5x3Øcmcm and 5.5x1.5Øcm

Sample id	Powder (particles < 5mm)						Slices (5x30ømm aprox.)						LTC samples (50x15ømm aprox.)					
	W evaporable g/g$_{105°C}$			W non evaporable g/g$_{105°C}$			W evaporable g/g$_{105°C}$			W non evaporable g/g$_{105°C}$			W evaporable g/g$_{105°C}$			W non evaporable g/g$_{105°C}$		
	Time (days)			Time (hours)			Time (days)			Time (hours)			Time (days)			Time (hours)		
	1	3	10	1	4	24	1	3	10	1	4	24	1	3	10	1	4	24
C_s40	0.30	0.31	0.31	0.09	0.09	0.09	0.23	0.24	0.24	0.09	0.09	0.09	0.30	0.30	0.30	0.09	0.09	0.09
	0.28	0.29	0.30	0.17	0.18	0.18	0.24	0.26	0.25	0.09	0.09	0.09	0.25	0.26	0.25	0.09	0.09	0.09
	0.28	0.30	0.29	0.10	0.10	0.10	0.25	0.26	0.25	0.09	0.09	0.09	-	-	-	-	-	-
Av.	0.29	0.30	0.30	0.12	0.12	0.13	0.24	0.25	0.25	0.09	0.09	0.09	0.28	0.28	0.28	0.09	0.09	0.09
std.	0.01	0.01	0.01	0.04	0.04	0.04	0.01	0.01	0.01	0.00	0.00	0.00	-	-	-	-	-	-

Evaporable and non evaporable water measurements were carried out for cement pastes with and without slag and fly ash cured saturated at 20 and 55ºC for 1, 3, 28 and 90 maturity days see Fig.XI.1 and XXI.2.
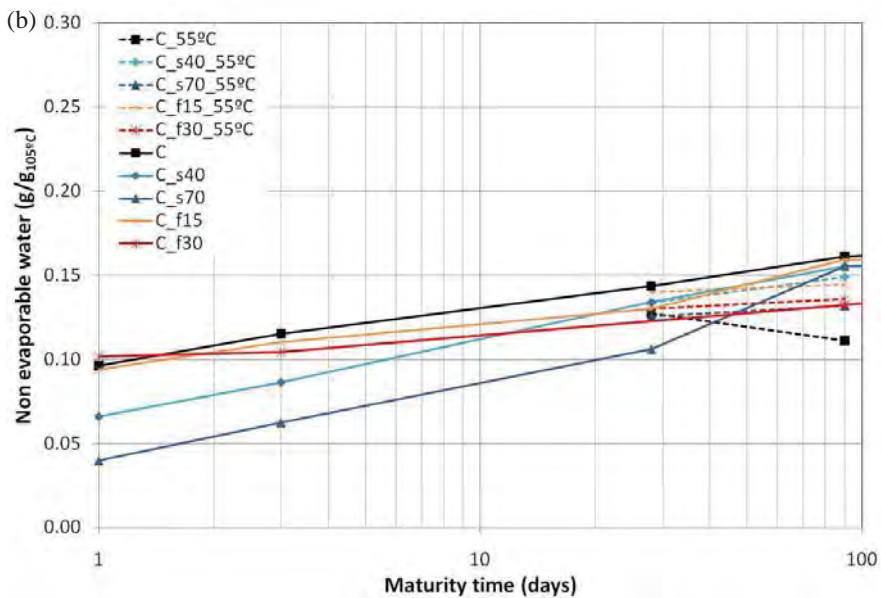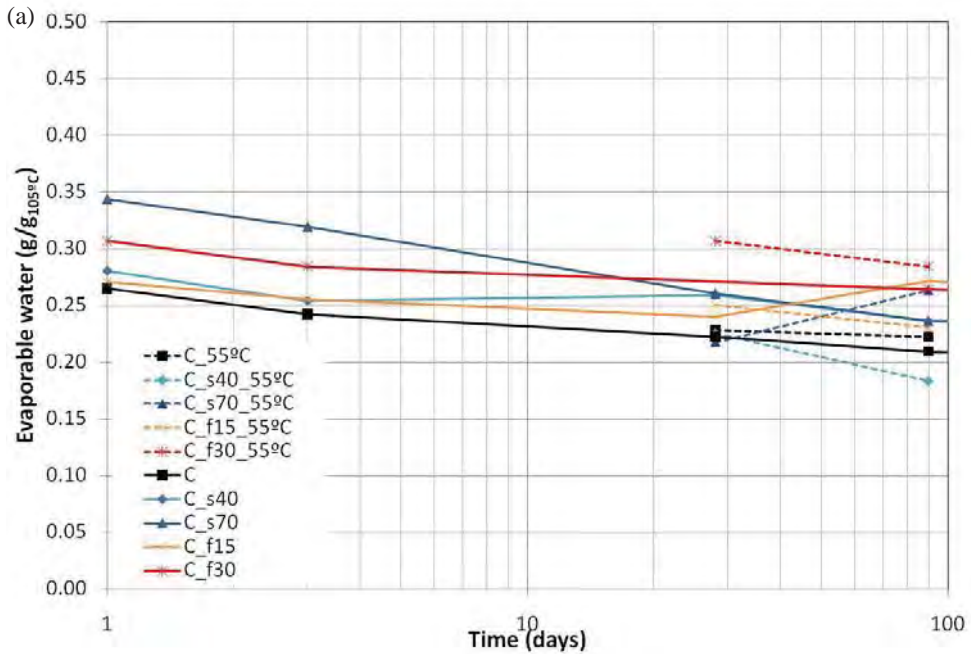
Fig. XXI.1(a) Evaporable water (g/g105°C) versus time, and (b) non evaporable water (g/g105°C) versus time(days) for cement pastes with and without slag and fly ash cured saturated at 20°C (full line) for 1, 3,28, 90 days and 55°C (broken line) 28 and 90 maturity days
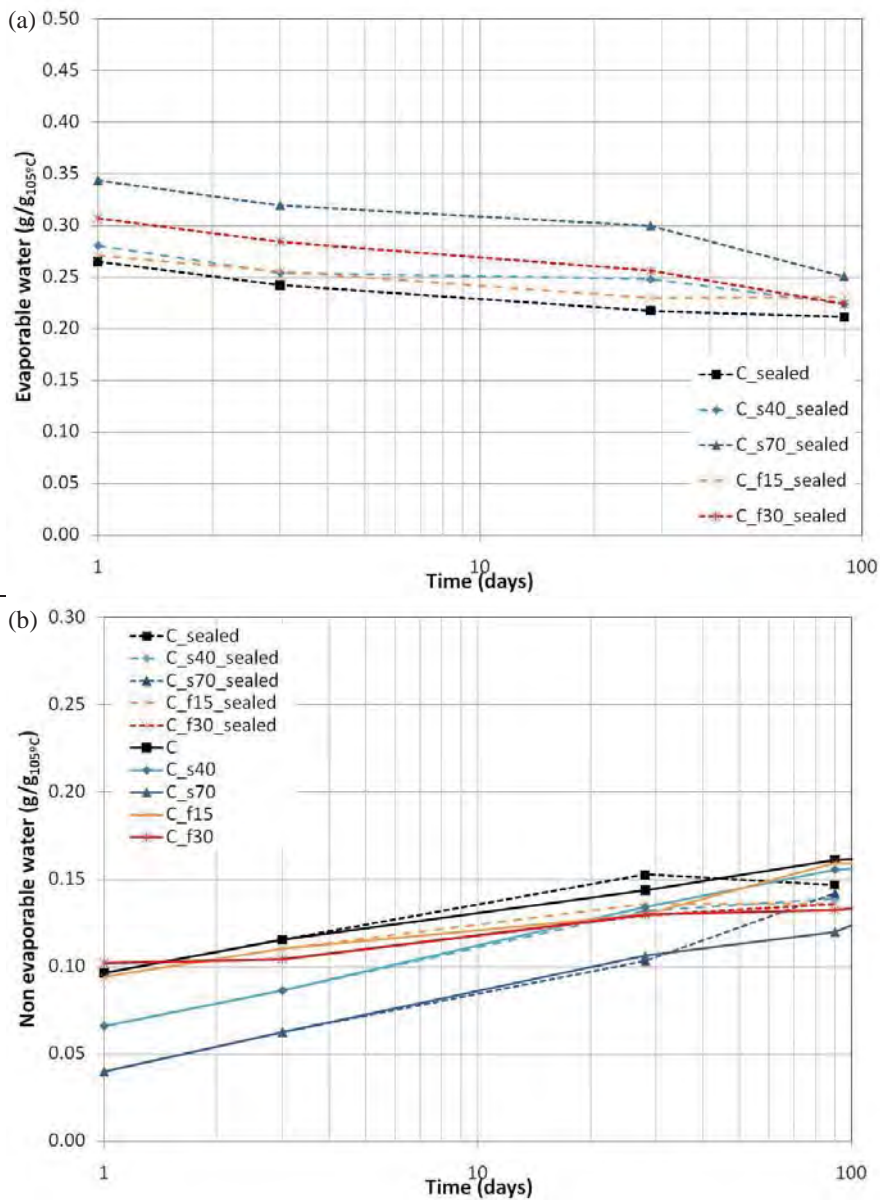
Fig. XXI.2 (a) Evaporable water (g/g105ºC) versus time, and (b) non evaporable water (g/g105ºC) versus time(days) for cement pastes with and without slag and fly ash cured saturated (full line) and sealed (broken line) at 20ºC for 1, 3, 28 and 90 days.

Appendix XXII –Capillary suction measurements

Capillary suction test was carried out to determine the ingress of water on dried cement pastes. Weight gain versus time for cement pastes with and without slag cured sealed at 20ºC for 28 days is given in the Fig. XXII.1. The test was carried out twice for similar samples. The slope of the curves was calculated at the end of the curves weight gain versus sqrt time and it indicates the sorptibility of the pastes see Table XXII.1. Three regimes of the curves are expected: first the water absorbed by the surface of the sample with a large slope of the curves weight gain versus time. The weight change in this regime is very fast (high rate of absorption by the sample surface) which makes the automatic read of the scale difficult, see in (Larsen-Helms, 2008). After that, the ingress of the water with a decline of the slope of the curves may be observed, and at the end of the curves the saturation state of the sample with lower slope of the curves. Larger values of sorptivity were found for pastes with slag when compared with the plain cement pastes. It may indicate a higher porosity of the pastes with slag.

Two regimes were observed in the Fig. XXII.1(a): the absorption of the water on the surface of the samples and followed by the ingress of the water on the pastes. It was observed large variance between the data for similar pastes with 40% of slag, see Fig. XXII.1. The difference between bottom and top of the pastes was also noticed, where a higher water absorption was observed for the top of the pastes. It may be due to the bleeding observed for the pastes and documented in the section 4.2.

Errors were observed during the test following the procedure: high suction rate for some of the cement pastes making the first part of the weight gain difficult to be measured by automatic scale. An exponential weight gain curve was observed for pastes cured for 28 days. Studies have been carried out using capillary suction on mortar and concrete see in (Martys and Ferraris, 1997, Morin et al., 2002, Zhang, 2007). The use of mortar and concrete may limit the leaching and a more accurate picture of the water transport may be obtained by capillary suction.

The capillary suction method was proposed as additional method to obtain information for capillary transport and water ingress on the selected pastes. However the method seems to be not suitable when automatic measurement is used for cement pastes.
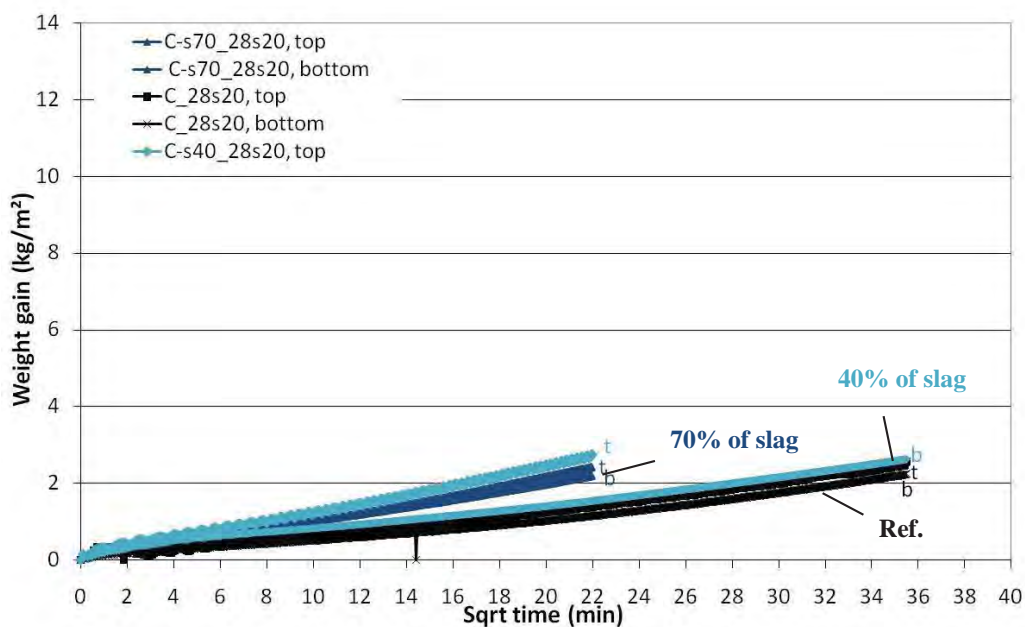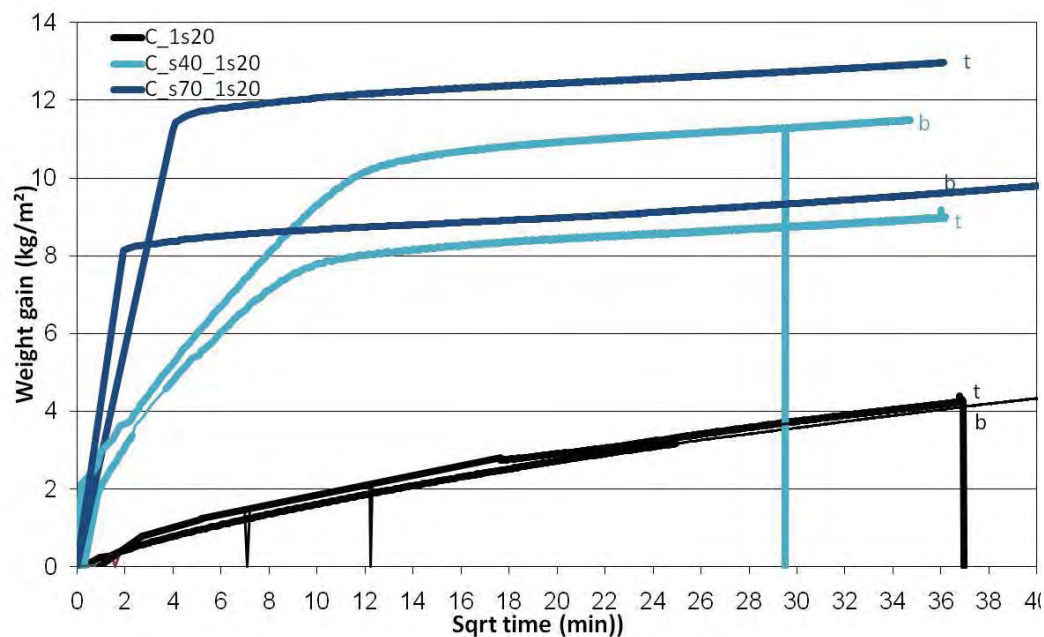
Fig. XXII.1 Weight gain (kg/m²) versus sqrt time (min) for cement pastes with and without slag cured sealed at 20ºC for (a) 1 day and (b) 28 days

The project was motivated by the need for low-CO2 materials for concrete and the correlation between pore structure and engineering properties. Pore structure of cement pastes with and without slag and fly ash cured at different curing conditions (temperature and moisture) for up to two years was characterize by various methods. Results showed that slag caused a refinement of pores. Temperature and moisture affected porosity parameters of all pastes. A beneficial effect of slag addition for pastes cured at high temperature was observed. Differences in porosity were measured by the methods. This is expected as the methods are limited to a certain range of pore size and they are based on principles and assumptions.